ADVANCED ELECTROSTATIC ION THRUSTER FOR SPACE PROPULSION

(NASA-CR-159406) ADVANCED ELECTROSTATIC ION THRUSTER FOR SPACE PROPULSION Final Report, 21 May 1976 - 21 Jan. 1978 (Hughes Research Labs.) 400 p HC A17/MF A01 CSCL 21C

N79-14153

G3/20 Unclas 41026

Final Report

NAS 3–20101

21 May 1976 through 21 January 1978

April 1978

by

Ion Physics Department Staff

of

Hughes Research Laboratories

3011 Malibu Canyon Road

Malibu, CA 90265

Prepared for

NASA LEWIS RESEARCH CENTER

21000 Brookpark Road

Cleveland, OH 44135

ADVANCED ELECTROSTATIC ION THRUSTER FOR SPACE PROPULSION

Final Report

NAS 3–20101
21 May 1976 through 21 January 1978

April 1978

by
Ion Physics Department Staff
of
Hughes Research Laboratories
3011 Malibu Canyon Road
Malibu, CA 90265

Prepared for
NASA LEWIS RESEARCH CENTER
21000 Brookpark Road
Cleveland, OH 44135

TABLE OF CONTENTS

LIST OF ILLUSTRATIONS

FOREWORD

The work described herein was performed primarily by personnel of the Hughes Research Laboratories. Assistance with mission analysis and thrust system modeling was supplied by personnel of the Space and Communications Group of the Hughes Aircraft company. The program was organized and directed by Mr. Tommy Masek,* Head of the Thruster Systems Section in the Ion Physics Department of the Hughes Research Laboratories. The key technical contributors were

Tommy D. Masek	-	Study manager and principal investigator
Duncan MacPherson	-	Mission Analysis and Thrust System Modeling (Space and Communications Group)
Walter Gelon	-	Mission Analysis (Space and Communications Group)
Seiji Kami	-	Mechanical Design
Robert L. Poeschel	-	Thruster Technology
James W. Ward	-	Mission Cost Model

*Mr. Masek is presently associated with Hughes Aircraft Company on a consulting basis only.

SECTION 1

INTRODUCTION AND SUMMARY

Electric propulsion (EP) mission studies are usually conducted on the basis that thruster characteristics are given. The objective is to define the best mission using these characteristics. Over the past decade, the 30-cm electron bombardment thruster using mercury propellant has been the primary candidate for EP mission studies. The bulk of near-term mission possibilities could be accomplished relatively well with the 30-cm thruster.[1-17]

Within the last few years, several new high energy mission possibilities have been suggested. These include transportation of large space systems from low Earth orbit (LEO) to geosynchronous Earth orbit (GEO), stationkeeping and attitude control of large space systems,[18-22] and planetary sample returns.[23] For these missions, the 30-cm thruster operating at baseline conditions (i.e., 3,000-sec specific impulse (I_{sp}), 3 kW into the power processor) may not result in optimum mission performance. Considerations such as propellant type, number of modules, power level, and I_{sp} suggest that a different thruster operating point would benefit several missions.

This study of advanced electrostatic ion thrusters for space propulsion was initiated to determine the suitability of the baseline 30-cm thruster for future missions and to identify other thruster concepts that would better satisfy mission requirements. In developing advanced thruster concepts, scaling and performance assumptions must include technological realities. Thus, the general scope of the study was to review mission requirements, select thruster designs to meet these requirements, assess the associated thruster technology requirements, and recommend short- and long-term technology directions that would support future thruster needs. Preliminary design concepts for several advanced thrusters were developed to assess the potential practical difficulties of a new design.

A. OBJECTIVES

The overall objective of this program was to develop recommendations for future ion thruster technology directions. Three specific objectives guided the study: (1) identification of the probable useful mission range of the existing 30-cm thruster, (2) investigation of methods and benefits of expanding the 30-cm thruster mission capabilities, and (3) investigation of methods and benefits of developing new thruster concepts (e.g., another size thruster) for those missions for which the 30-cm thruster is not well suited.

To carry out the investigation implied by these guiding objectives, several detailed objectives were established, including (1) selection and analysis of a representative set of potential ion propulsion missions, (2) assessment of mission performance as a function of thruster capability, (3) assessment of thruster technology boundaries, (4) identification of thruster or system parameters that strongly influence mission design, and (5) development of a cost modeling technique to investigate the relationship between thruster parameters and overall mission cost. Relative to the last objective, only Earth orbit missions were considered, although, with minor modification, planetary missions could also be accommodated by the computer model.

B. STUDY PLAN

The study plan follows rather directly from the stated objectives. However, at the beginning of the study, the "working level" objectives had not yet been so clearly defined; they were, in fact, partially developed during the study. The thruster technology assessment task was clear from the start. Mission set selection was reasonably clear but of rather broad scope. Since the analysis of the missions was dependent on the mission set selected, the exact analytical approach was initially difficult to define. Similar to the mission analysis task, the process of defining important parameters was not straightforward because of the wide range of mission possibilities and mission objectives. The cost modeling task was developed during the study as the result of attempts to develop a generalized approach to Earth orbit missions. A logic

diagram of the various study tasks and their interrelationships is shown in Figure 1-1; included in the diagram are the numbered tasks called for under the contract. Although the contract tasks were not necessarily performed in the sequence originally planned, all contract objectives were satisfied.

After a period that included data collection, selection of a preliminary mission set, analysis of several missions, and the start of the technology assessments, two significant study approaches became apparent. The first, a generalized mission analysis approach, allowed a wide variety of available mission results to be displayed in a common format and provided a straightforward method for evaluating the sensitivity of "mission performance" to thruster characteristics. With the adoption of this technique, the mission set final selection process was greatly simplified since many missions could be handled easily and the problem of arbitrarily selecting or eliminating missions was essentially eliminated. The output of the generalized mission analysis approach is an estimate of the degree to which a given thruster technology could support the selected mission.

The second approach that provided significant direction to the study evolved from an Earth orbit mission cost model technique. A computer program was developed to include cost models, mass models, thrust system performance models, and approximate relations for mission performance (i.e., "rocket equation"). For a given set of mission parameters (e.g., velocity requirement (ΔV), vehicle total mass, flight time), costs are computed as a function of specific impulse. This cost model approach provides a simple method for evaluating the relative sensitivity of total mission cost to a large number of thruster and system parameters (≈ 100). Most efforts during the last half of the study concentrated on the development and use of the cost model program.

As Figure 1-1 indicates, both the generalized analysis and the cost model approaches were supported by the technology assessment task. Performance scaling relations, physical scaling experience, and operating limits (e.g., perveance, thermal) were incorporated into the

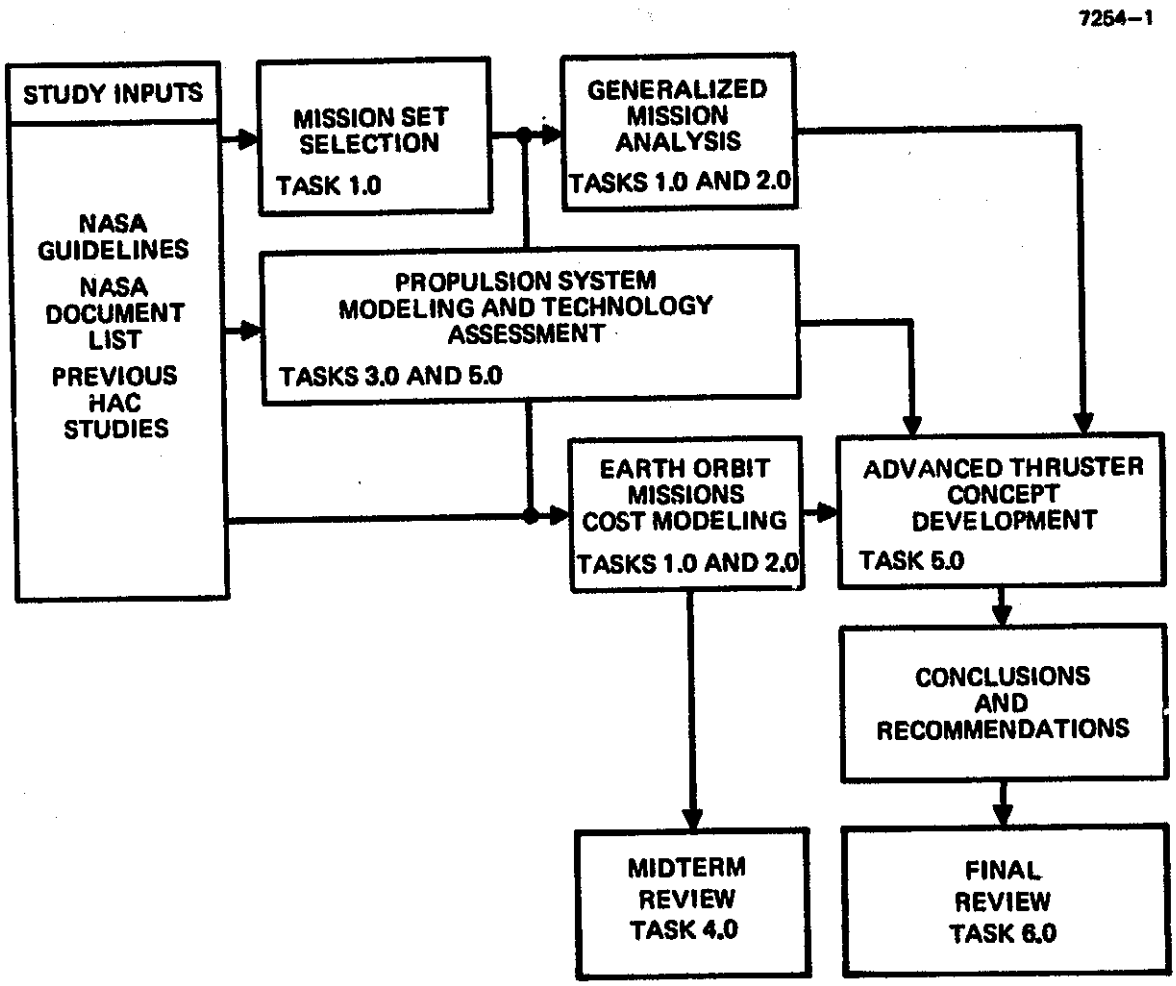

Figure 1-1. Study logic diagram.

analytical approaches and into advanced thruster design concepts. Several design concepts for thrusters with larger beam areas were prepared and analyzed in terms of technology advancement requirements.

C. MISSION SET SELECTION AND ANALYSIS

Initial efforts under the study were directed toward preparing a mission set to be used as the basis for the remainder of the work. The selection process, described in detail in Section 2, resulted in the following set of missions:

- Earth orbit transportation
- Earth orbit stationkeeping
- Earth observatory
- Outer planets (composite of seven missions)
- Solar system escape
- Mercury orbiter
- Close solar probe
- Comet Encke rendezvous/flyby
- Comet Halley rendezvous/flyby
- Asteroid rendezvous
- Asteroid sample return
- Mars sample return
- Out-of-ecliptic.

A generalized analytical approach was developed to assess the capabilities of several levels of thruster technology to perform these missions. The analytical approach utilizes mission trajectory calculation results obtained from the literature and from work done under this contract. For each mission, characteristics such as ΔV, initial acceleration (A_o), initial mass, and payload mass were determined. These characteristics and an analytical formulation based on the rocket equation were then used to develop sets of curves in a ΔV vs A_o coordinate system using payload mass fraction (MF, payload mass divided by vehicle initial mass) as a parameter. Part of the analytical formulation required models of thrust system performance and mass. Thruster and thrust system technology enter the analysis through these models. An example of the ΔV vs A_o curve set format is shown in Figure 1-2.

By entering a given curve set (i.e., a set based on a given technology) with mission data for ΔV and A_o, the payload mass fraction required to perform a specific mission (MFR) can be compared with the mass fraction

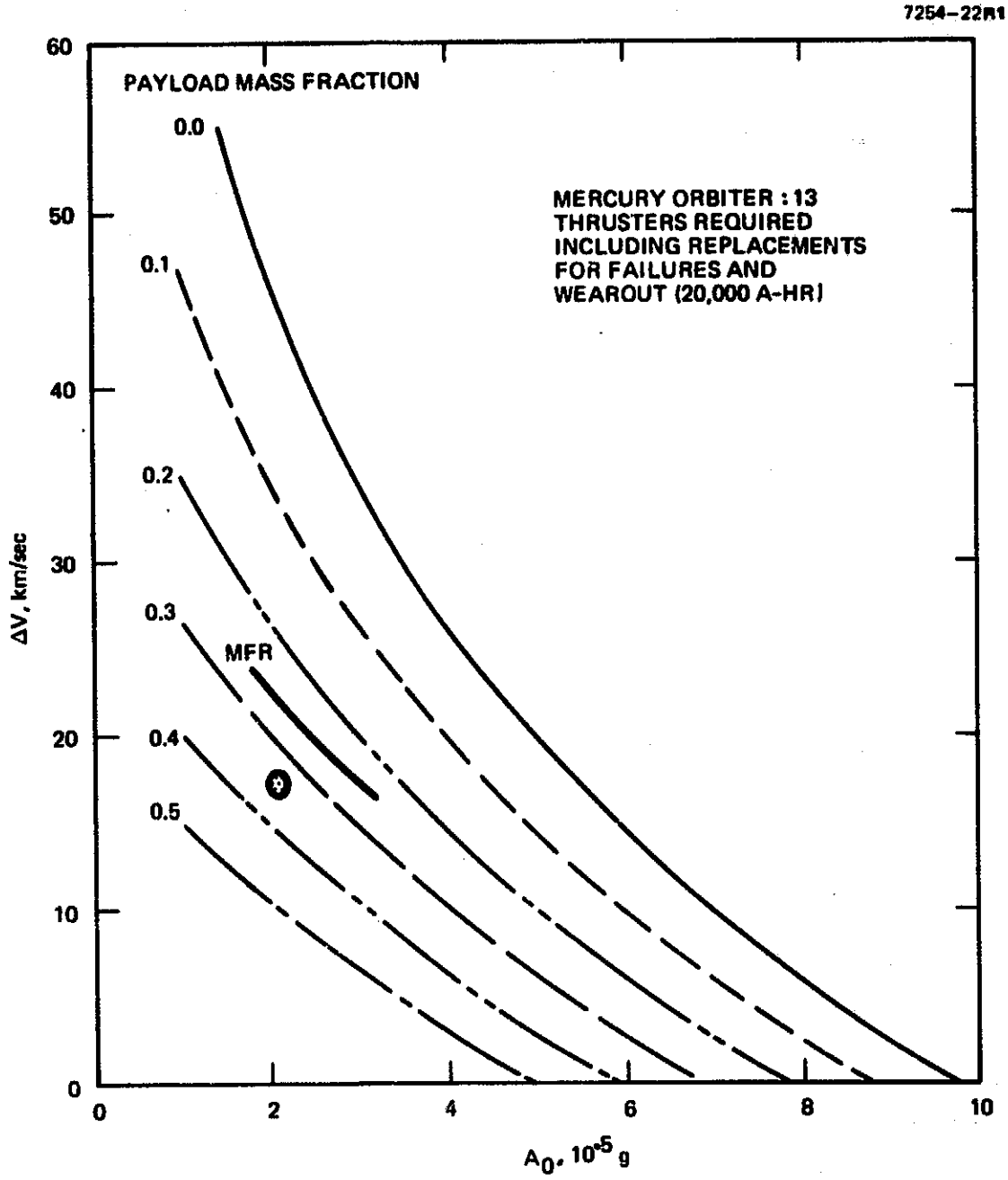

Figure 1-2. Example of ΔV vs A_o format and results.

capability of the assumed technology. The required mass fraction is imposed on the curve map as indicated. Thus, if the ΔV vs A_o coordinate point occurs at a mass fraction higher than that required, the mission can be accomplished with the assumed technology. If the point falls at a lower mass fraction, the assumed technology level is not adequate. Since this approach involves several approximations, the conclusions are not necessarily quantitatively accurate. When the results show a definite capability margin or a definite inability to perform the mission, a relatively firm conclusion is possible. However, when the results are close, slight variations in assumptions could change the conclusion. Such precise interpretation of the results is not warranted. Analysis details and results are presented in Section 3.

D. EARTH ORBIT COST MODELING

The generalized analysis approach provides a relatively simple method of gauging the ability of a given technology to perform a mission. However, several technologies potentially could satisfy the mission technical requirements and remain within the boundaries of technology projections. The selection of one technology direction over another will certainly involve cost (technology development cost and recurring mission cost).

Although this study does not attempt to predict technology development cost, significant effort was devoted to modeling the relationship of "transportation" cost to numerous technology-related thruster and system parameters. Since this study was primarily directed toward ion thruster technology, the scope of the cost modeling was limited to the propulsion function of a given mission.

The cost model work was applied to several earth orbit missions. Earth orbit missions were selected because of the future potential of electric propulsion in the transportation and on-orbit support of large space systems. Selection of a propulsion system type (i.e., electric or chemical) will probably be strongly influenced by total system cost. Therefore, this cost model work was directed toward determining those

factors that significantly affect system cost and toward determining the sensitivity of system cost to variations in thruster, system, and mission parameters.

The cost modeling analysis approach is illustrated qualitatively in Figure 1-3. The objective of the calculations is to obtain total propulsion cost (transportation or on-orbit) as a function of various parameters. With total cost and various mass breakdowns, cost per unit of payload mass (transportation) or cost per unit of net satellite mass per year (on-orbit stationkeeping and attitude control) are program outputs. A convenient format for displaying the results is shown in Figure 1-4. Specific cost ($/kg of payload) is plotted as a function of specific impulse (I_{sp}), with module power as a parameter. The number of modules needed to perform a given mission varies with I_{sp} and module power. Details of the analysis method and extensive results are presented in Section 4.

E. SUMMARY OF CONCLUSIONS

This study produced useful general methodologies for assessing both planetary and Earth orbit missions. For planetary missions, the assessment is in terms of payload performance as a function of propulsion system technology level. For Earth orbit missions, the assessment is made on the basis of cost (cost sensitivity to propulsion system technology level).

The selection of the 30-cm thruster for near-term missions (for power levels below 100 kW) was reinforced by this work. Except for high-power missions or those requiring a propellant other than mercury, the 30-cm engineering-model thruster (EMT) is a good choice. However, for systems larger than about 100 kW (Earth orbit or planetary), a larger thruster size would be advantageous in terms of cost and payload performance.

Based on the mission studies, cost modeling, and technology assessments, a 50-cm-diameter thruster is suggested as the next step in

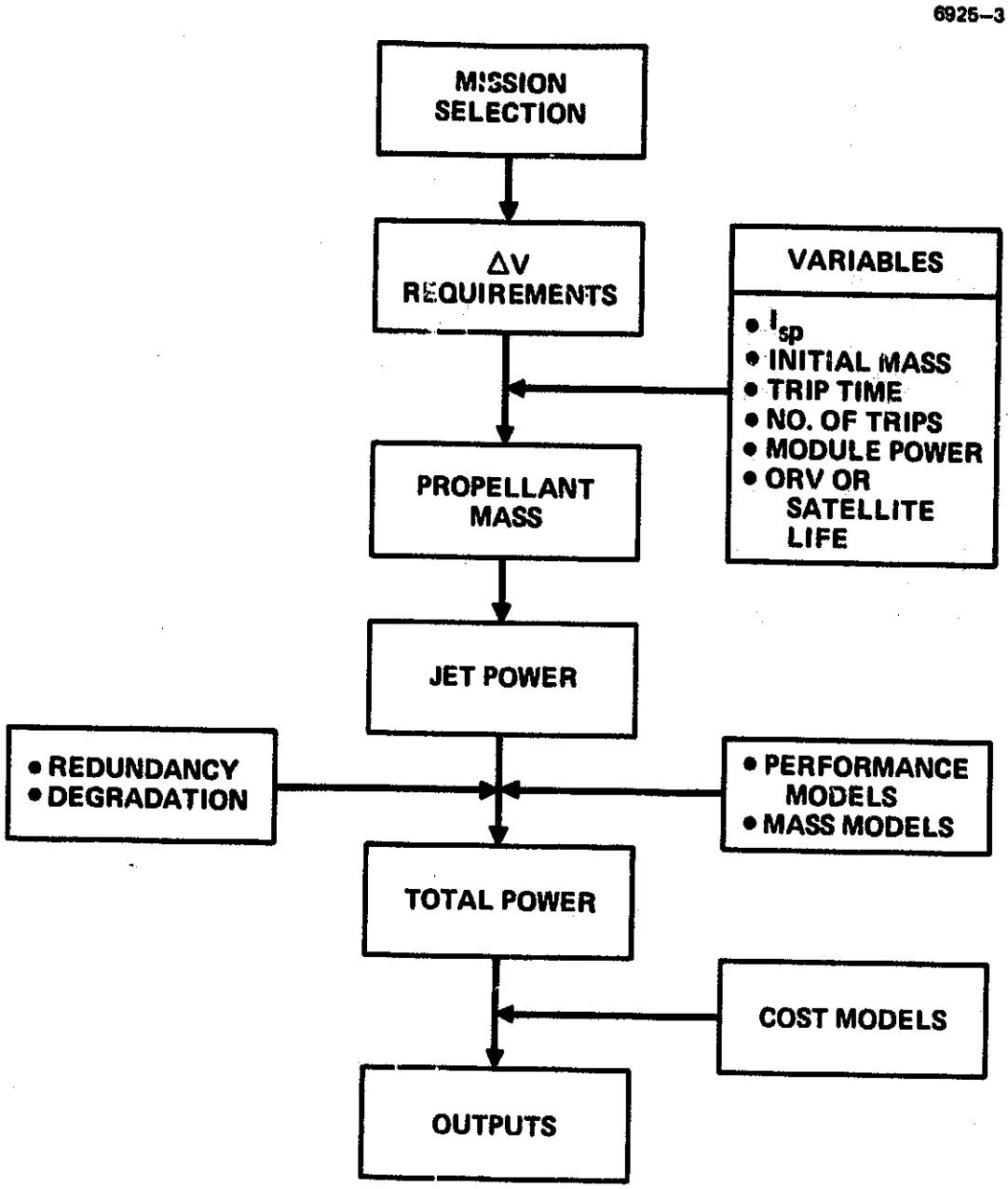

Figure 1-3. Earth orbit mission cost modeling, simplified block diagram.

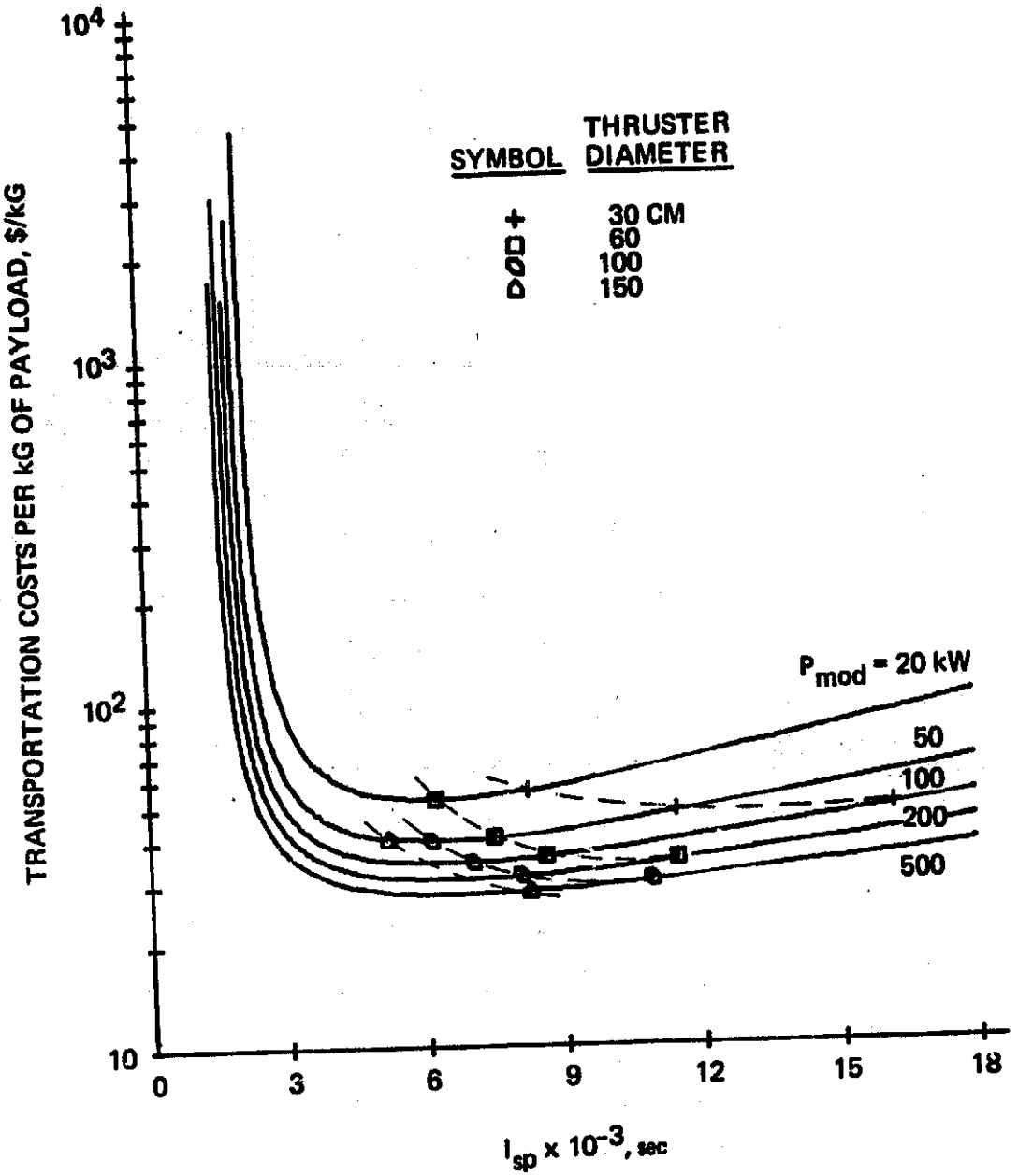

Figure 1-4. Example of cost modeling results.

thruster technology development. By proper selection of propellants and beam currents, a 50-cm thruster designed to operate with a beam voltage of about 2400 V would satisfy most of the requirements of future missions. Thruster concepts, including an oval cross section, were developed to illustrate design techniques for thrusters with larger beam areas.

SECTION 2

MISSION SET SELECTION

The goal of the mission set selection process was to establish a representative set of 10 missions that would fairly reflect the range of future electrostatic ion thruster requirements. These requirements provided direction and motivation for future thruster technology development. The general selection process followed is illustrated in Figure 2-1.

A. CONTRACT GUIDELINES

Guidelines for selecting 6 of the 10 missions were provided in the contract. Specifically, the mission set was to include:

- Transportation of large space systems from LEO to GEO
- Stationkeeping and attitude control of large space systems in GEO
- A mission to less than 0.7 AU
- A solar system escape mission
- At least two missions between 0.7 and 5.0 AU.

These mission categories indicated the desired scope of the study without being overly restrictive.

To aid in the mission selection process, NASA provided several reports on previous electric propulsion studies and a list of documents to be considered in establishing the mission set. The document list used is presented in Appendix A. This background information provided results of trajectory calculations for various missions, system concepts, and designs and the general sensitivities between thruster requirements and mission objectives. Although a certain amount of mission/trajectory analysis was anticipated, it was assumed that the bulk of the mission data needed in the study would be obtained from existing literature.

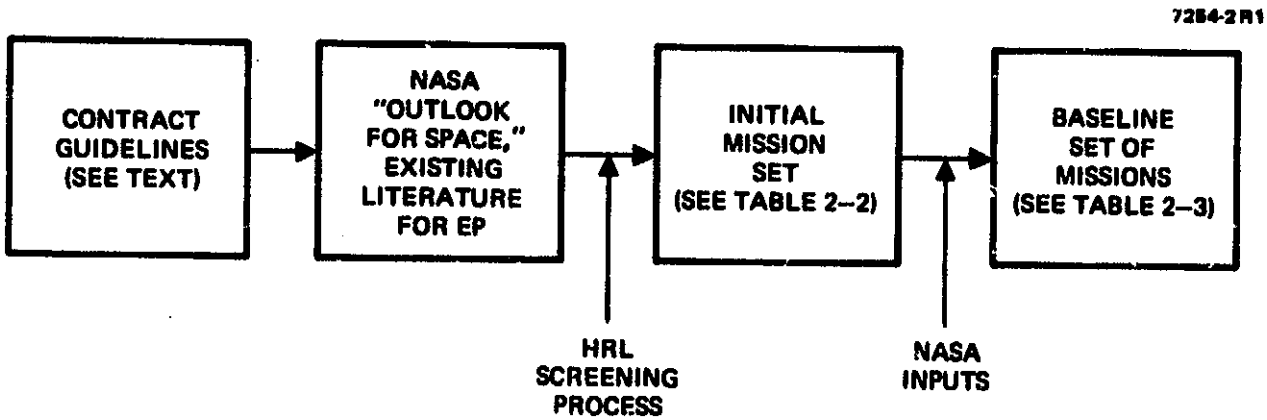

Figure 2-1. Mission set selection process flow diagram.

B. MISSION CANDIDATES

The missions initially considered for selection are shown in Table 2-1 and are characterized in terms of payload mass range and ΔV range. The relatively wide spread in the parameters of Table 2-1 reflects the flexibility of mission requirements, mission design, and utilization of electric propulsion. Clearly, a specific mission design would require defining many other factors. However, ΔV and payload mass tend to allow a first-order examination of propulsion system requirements. Candidate missions are summarized briefly here to provide a basis for evaluation.

1. Transportation of Large Masses

The types of missions that could be considered in this category include transportation of full Shuttle-size payloads, portions of large space power generation satellites from LEO to GEO, transportation of space stations, or recovery of large satellites for repair or disposal.[18-23] Propulsion requirements might include single one-way-trip-to-orbit, single round trips with refueling, or multiple round trips with and without refueling. In some cases, power might be provided by the payload, while in others (e.g., a return to LEO) the EP transportation vehicle would require its own power source. EP is a prime candidate for this category of missions and will probably benefit from advanced technology.

2. Stationkeeping and Attitude Control of Large Systems

Massive and/or large-surface-area systems in Earth orbit will experience large torques and disturbance forces.[18-21] Correcting these attitude and orbit perturbations could require a significant propulsion capability on-orbit. The specific mission of the satellite will dictate the detailed requirements in terms of allowable eccentricity change or pointing variations. However, propulsion system hardware and propellant for on-orbit operations represent a penalty to the satellite since this material must be transported to and stored on orbit. In addition,

Table 2-1. Candidate Missions and Characteristics

Mission	Approximate ΔV,[a] km/sec	Payload Range, kg	Comments
Earth orbit			
Transportation of large masses	4-8	10^4-10^7	
Stationkeeping and attitude control of large systems	1-10	10^4-10^7	
Multimission modular spacecraft missions	0.1-4	10^3	
Earth observatory	4-6	10^4	
Planetary			
Out-of-ecliptic	20-50	$5x10^2$-10^3	
Close solar probe	10-15	10^3	Thermal constraints
Solar system escape	4-5	10^3	Jupiter swingby
Mercury orbiter	10-20	10^3-$2x10^3$	Thermal constraints
Mercury lander	10-20	10^4	Thermal constraints
Mercury sample return	20-40	10^5	Thermal constraints
Venus orbiter			EP has little advantage over ballistic mission
Venus lander			
Venus sample return			
Mars sample return	15-20	$3-5x10^3$	
Jupiter orbiter	4-5	10^3-$2x10^3$	
Jupiter satellite orbiter	4-5	10^3-$2x10^3$	
Saturn flyby	3-4	10^3	

6119

Table 2-1. Candidate Missions and Characteristics (Continued)

Mission	Approximate ΔV,[a] km/sec	Payload Range, kg	Comments
Planetary (Continued)			
Saturn orbiter	3-4	10^3	
Titan orbiter	3-4	10^3	
Uranus flyby	4-5	10^3	
Neptune flyby	4-5	10^3	
Asteroid rendezvous	6-1[illegible]	5×10^2-10^3	
Asteroid sample return	10-15	10^3-3×10^3	
Comet Encke rendezvous	10-15	5×10^2-10^3	
Comet Halley flyby	20-60	5×10^2-10^3	Flyby velocity dependent
Waste disposal	5-10	10^3-10^5	Nuclear, using payload as power source

[a]Applicable to an electric propulsion system.

6119

multi-decade operating lives will probably significantly affect design philosophy, redundancy, and net useful satellite mass. EP has characteristics that should minimize the on-orbit propulsion penalties. Large vehicles may require advanced thruster technology for cost-effective operation.

3. Multimission Modular Spacecraft

The multimission modular spacecraft (MMS) will provide a basic satellite bus that, with certain mission-independent modules, has the potential for significantly reducing satellite development costs.[24] Although EP could be beneficially applied as a module, the propulsion system requirements can be adequately supplied by existing 30-cm or 8-cm thrusters. Because of the relatively low ΔV requirements and mass, the MMS is unlikely to require advanced thrusters.

4. Earth Observatory

This category represents a composite of various earth science desires.[21] Satellite measurements might include Earth's magnetic field, crystal dynamics, ocean dynamics, and atmospheric dynamics. A satellite of this type might also include "space"-oriented instruments. The orbit would probably be synchronous for stationary local measurements; a satellite capability for orbit position adjustment would probably be included. Thus, it is likely that such an observatory satellite, capable of operating for many years with a broad range of instruments, would be substantially larger than ordinary single-purpose satellites. EP should be well suited for orbit raising, stationkeeping, and positioning.

5. Out-of-Ecliptic

Transfers out of the ecliptic plane up to 90° are of interest to space scientists because of the new perspective on the solar system that such an orbit would provide.[1,25-28] EP is ideally suited to this mission because of the high ΔV, the unconstrained flight time, and the gradual inclination change (as opposed to an impulsive chemical transfer). The power level and satellite size depend largely on the instrument complement.

6. Close Solar Probe

The close solar probe is a good EP mission candidate because of the relatively high ΔV and the effective reduction in propulsion system specific mass resulting from increased solar intensity.[7-11] Such a satellite is expected to be relatively small, requiring a propulsion power level in the range of 15 to 25 kW (1 AU). However, "advanced" thruster requirements might result from thermal constraints.

7. Solar System Escape

The degree to which EP is needed for this mission depends on payload mass. Using a Jupiter swing-by trajectory and relatively long flight times, a reasonable payload could be transported ballistically. Electric systems in the 15- to 25-kW range improve payload capability and/or reduce flight time. However, since solar power is drastically reduced beyond 5 AU, larger EP systems probably would not be required unless a nuclear power source was used.

8. Mercury Orbiter

This mission is similar to the close solar probe mission, with somewhat relaxed thermal constraints.[1,8,29-31] Typical payloads of a few hundred kilograms will require propulsion power levels of 20 to 25 kW. Thus, except for possible thruster thermal limitations, existing technology is probably adequate.

9. Mercury Lander

The payload (transported by an EP system) for a Mercury lander mission probably would be about an order of magnitude greater than that for an orbiter mission. An electric propulsion system power level of 100 to 150 kW would be needed to transport such a vehicle (initial mass $\sim 4 \times 10^4$ kg). Existing 30-cm thruster technology could be applied to such a large system, but it would probably be less effective than a system using a higher power thruster.

10. Mercury Sample Return

This mission would need about two orders of magnitude more payload than an orbiter mission. Thus, the EP system would be propelling a vehicle having an initial mass in the range of 2 to 4 x 10^5 kg and would require a power level on the order of 10^3 kW. Such a system, which is in the range of "large space systems" being considered under Mission 1, would probably benefit significantly from the use of an advanced thruster.

11. Venus Orbiter

The relatively short transfer time to Venus reduces the usual potential advantages of EP. If the mission were performed with EP, the existing 30-cm thruster would probably be sufficient.

12. Venus Lander

The increased payload required for a lander would make EP more advantageous, but probably not mandatory.

13. Venus Sample Return

With the increased flight time demanded by a return flight and possible maneuvers in orbit at Venus, an EP system would probably be beneficial. The large mass and high power level might require an advanced thruster.

14. Mars Sample Return

Compared with a ballistic approach to this mission, EP can increase the payload returned to Earth from a few hundred grams to several kilograms.[22] Typical missions would use a shuttle launch, EP for Earth/Mars transfers, and chemical systems for Mars descent and ascent maneuvers. Mission times of three to four years and power levels of 50 to 100 kW would be needed.

15. Jupiter Orbiter

If performed using EP, this mission would require power levels of 15 to 25 kW for typical payloads.[1-17] Larger payloads (for instance,

if surface probes were included) might require higher power levels. Thus, conventional mission approaches of the type considered in many EP studies would require only existing technology. More aggressive missions might benefit from advanced technology.

16. Jupiter Satellite Orbiter

Limited reconnaissance of Jovian satellites will probably be performed as part of Jupiter orbiter missions. However, more extensive satellite investigations could require larger payloads. For such vehicles, advanced EP systems would be beneficial.

17. Saturn Fly-By

EP improves the payload capability or reduces flight time for missions of this type with only modest power levels (15 to 25 kW).[1-17] However, with solar-powered systems, propulsion is limited to distances of 4 to 5 AU. Significant payload improvements will occur when space nuclear power sources become available. Such systems in the multi-100-kW range would benefit from advanced technology thrusters with long life at high power levels.

18. Saturn Orbiter

See comments on Mission 17.

19. Titan Orbiter

See comments on Mission 17.

20. Uranus Fly-By

See comments on Mission 17.

21. Neptune Fly-By

See comments on Mission 17.

22. Asteriod Rendezvous

Several asteriod missions have been studied by others and found to be well within existing EP technology capabilities.[1,2,29,32-35] Because of the high ΔVs associated with asteriod missions and the reasonable AU distances, EP is ideally suited to such missions.

23. Asteriod Sample Return

The higher ΔV associated with such a mission improves the advantage of an EP system.[36-38] The larger masses and higher power levels required, compared with a rendezvous, would increase the size of the propulsion system, but would probably not require advanced thruster technology.

24. Comet Encke Rendezvous/Fly-By

This mission is typical of several cometary missions, but is of particular interest because of its three year orbital period and near earth passages.[1,2,7-10,29,32-34,39-42] Encke is a good EP mission because of the high ΔV. However, various navigation errors might make a true rendezvous rather difficult. With typical science payloads, propulsion power levels of 20 to 25 kW would be adequate for this mission. Advanced thruster technology should not be needed.

25. Comet Halley Rendezvous/Fly-By

Comet Halley is of both scientific and popular interest.[13-16] Because the comet's orbit is retrograde, the mission is essentially impossible chemically. It would, however, be quite possible with EP. Significant factors in evaluating EP system requirements are flight time and fly-by velocity. Given some flexibility in these parameters, existing technology would be adequate for the comet Halley mission. Unfortunately, the time available to develop a spacecraft for the 1986 passage is very short.

26. Nuclear Waste Disposal

Strictly from an EP point of view, the nuclear waste mission is technologically feasible. Since power would be derived from the payload and flight time would be unconstrained, the existing 30-cm thruster would probably be adequate.

C. MISSION SELECTION

Based on considerations of the type presented in Section 2.B, discussions with the NASA LeRC study manager, and contract guidelines, a

set of missions was selected for analysis. The initial set, shown in Table 2-2, generally satisfied all requirements. However, improvements were recommended as the study progressed. Although the final mission set, shown in Table 2-3, includes more than the 10 missions required, it is more representative of the study goals than was the initial set.

In the final mission set, the various outer planet missions were taken as a group because their requirements are similar. The multi-mission modular spacecraft was eliminated from the set because the bulk of the payloads represented by this category require low ΔVs, have low mass, and would most likely use existing thruster technology. The Mars sample return mission and the comet Halley mission were added because both were of current interest and both might require an advance in thruster technology. The close solar probe was added because it was an extension of the mercury orbiter mission.

Each mission selected was analyzed from the standpoint of its demands on thruster and propulsion system technology. These demands, which may properly be considered to be requirements, indicate the degree and direction of technological change needed. At various points in the analyses, technology assessments were included to assure that technology extrapolations were not unreasonable.

Table 2-2. Initial Mission Set

Mission	Comment
Earth orbit	
EO transportation	Contract requirement
EO stationkeeping	Contract requirement
Multimission modular spacecraft missions	
Earth observatory	
Planetary	
Out-of-ecliptic	Contract requirement
Solar system escape	Contract requirement
Mercury orbiter	Contract requirement
Neptune flyby or orbiter	
Asteroid rendezvous	Contract requirement
Comet Encke rendezvous	

6119

Table 2-3. Final Mission Set Used in Study

Mission	Comment
Earth orbit	
LO transportation	Contract requirement[a]
EO stationkeeping	Contract requirement
Earth observatory	
Planetary	
Outer planets	Considered as a single type of mission
Jupiter orbiter	
Jupiter satellite orbiter	
Saturn flyby	
Saturn orbiter	
Titan orbiter	
Uranus orbiter	
Neptune flyby	
Solar system escape	Contract requirement
Mercury orbiter	Contract requirement
Close solar probe	
Comet Encke rendezvous	
Comet Halley rendezvous	
Asteroid rendezvous	Contract requirement
Asteroid sample return	
Mars sample return	
Out-of-ecliptic	Contract requirement

[a]See Section 2.A for discussion of requirements.

6119

SECTION 3

MISSION SET ANALYSIS

To use the information gathered from the various reference sources and the trajectory data generated by this study, a generalized analysis technique was developed. All the pertinent data was converted to a common format to provide a uniform basis for comparison. The technique is discussed in Section 3.A. Section 3.B presents propulsion system performance and mass models used in the analysis, including estimates for several technology levels. Section 3.C summarizes the mission characteristics required for the generalized approach, including ΔV, initial acceleration, payload, and initial mass. Section 3.D discusses the generalized analysis. In addition, results for specific missions analyzed in detail (e.g., trajectory calculations) are summarized. Detailed information that does not fall in the "generalized analysis" category is included in the Appendix B. Conclusions from this portion of the study are presented in Section 3.E.

The generalized mission analysis technique was applied to the total mission set, including the Earth orbit missions. However, the transportation and stationkeeping of large systems, Missions 1 and 2, were not clearly defined. That is, since wide ranges of mass, size, and power level were to be considered, with only broad mission objectives, the generalized analysis could not provide all the desired results. In particular, large-scale operation in Earth orbit will require cost-effective propulsion systems. The economic tradeoffs related to Missions 1 and 2 were developed through cost modeling techniques (discussed in Section 4).

A. GENERALIZED ANALYSIS APPROACH

1. Results Format Basis

Mission analysis results obtained from various studies are generally somewhat difficult to compare because of the multitude of assumptions required in the basic calculations. However, by distilling the pertinent

information and displaying it in a common format, as illustrated in Figure 3-1, approximate comparisons can be made. The basis of this format is derived from the rocket equation with an appropriate use of EP system definitions.

The rocket equation has the form

$$\Delta V = g_o I_{sp} \ln\left(\frac{M_o}{M_f}\right), \tag{3-1}$$

where

ΔV = velocity change characterizing the mission

g_o = gravitational constant

I_{sp} = true specific impulse (corrected for multiply charged ions, beam divergence, and propellant utilization efficiency)

M_o = initial mass of the vehicle

M_f = final mass of the vehicle.

The initial mass can be written as

$$M_o = M_f + M_p \tag{3-2}$$

or

$$M_o = M_{p\ell} + M_{ps} + M_p , \tag{3-3}$$

where

M_p = propellant mass

$M_{p\ell}$ = payload mass

M_{ps} = propulsion system mass.

A simple rearrangement of Eqs. 3-2 and 3-3 yields

$$\frac{M_f}{M_o} = \frac{M_{p\ell}}{M_o} + \frac{M_{ps}}{M_o} \tag{3-4}$$

or

$$\frac{M_f}{M_o} = MF + \frac{M_{ps}}{M_o} , \tag{3-5}$$

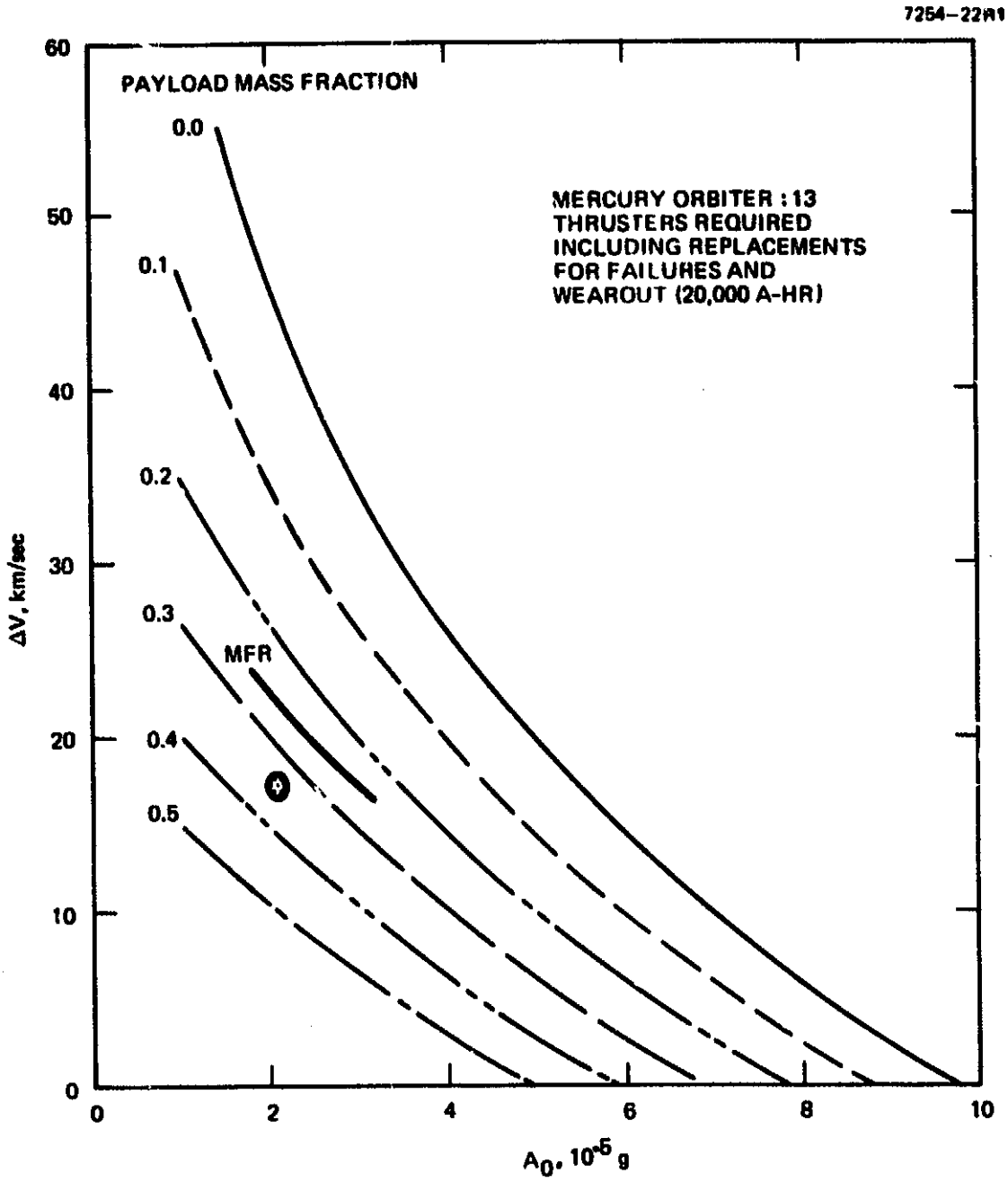

Figure 3-1. Generalized mission analysis results format.

where MF = payload mass fraction.

EP system parameters are related to propulsion system mass as follows:

$$\alpha_{ps} = \frac{M_{ps}}{P_{ps}}, \tag{3-6}$$

where P_{ps} = propulsion system input power, or

$$\frac{M_{ps}}{M_o} = \frac{P_{ps}\,\alpha_{ps}}{M_o}. \tag{3-7}$$

Power is related to other parameters by means of the energy equation:

$$P_{ps} = \frac{TI_{sp}\,g_o}{2\eta_{ps}}, \tag{3-8}$$

where

T = True thrust (corrected for multiply charged ions and beam divergence)

η_{ps} = True propulsion system total efficiency (corrected for multiply charged ions and beam divergence).

This allows us to write

$$\frac{M_{ps}}{M_o} = \frac{TI_{sp}\,g_o\,\alpha_{ps}}{2M_o\,\eta_{ps}}. \tag{3-9}$$

In terms of vehicle initial acceleration,

$$A_o = \frac{T}{M_o g_o}. \tag{3-10}$$

For convenience in using mission analysis literature, A_o has the units of "g's." Eqs. 3-8 and 3-9 become

$$P_{ps} = M_o\left(\frac{A_o I_{sp}\,g_o^2}{2\eta_{ps}}\right) \tag{3-11}$$

$$\frac{M_{ps}}{M_o} = \frac{A_o I_{sp}\alpha_{ps}\,g_o^2}{2\eta_{ps}}. \tag{3-12}$$

If α_{ps} is expressed in conventional units of kg/kW, then

$$\frac{M_{ps}}{M_o} = \frac{A_o I_{sp} \alpha_{ps}}{20.79\ \eta_{ps}} . \qquad (3\text{-}13)$$

Substituting Eq. 3-5 into Eq. 3-1 and using Eq. 3-13 yields

$$\Delta V = g_o I_{sp} \ln \left(MF + \frac{A_o I_{sp} \alpha_{ps}}{20.79\ \eta_{ps}} \right)^{-1} . \qquad (3\text{-}14)$$

As illustrated in Figure 3-1 for a given set of propulsion system parameters that are technology-level related, lines of constant payload mass fraction can be defined in a ΔV vs A_o coordinate system. To use this format, propulsion system models were developed for the desired technology level and were used in displaying Eq. 3-14 graphically. The result is a graph having lines of constant mass fraction that represent a given propulsion technology level. Mission data is then used to obtain typical values of ΔV, A_c, and MFR.

The mission study value of MFR is then imposed as a line on the appropriate graph. This line represents the payload mass fraction typically required to satisfactorily perform the mission. Then, the study values of ΔV and A_o are located on the graph. If the ΔV vs A_o point is at higher mass fraction than that required, the mission probably can be performed with the assumed technology. If the ΔV vs A_o point is at a lower mass fraction than required, the mission probably cannot be accomplished with the assumed technology.

2. Number of Thrusters

An estimate of the number of thrusters required for a given mission and an assumed technology level can be obtained as follows. The maximum number of operating modules (one thruster and power processor combination) is approximately the ratio of propulsion system input power to the total power per module (i.e., power into a power processing unit (PPU)):

$$N_{mod} \cong \frac{P_{ps}}{P_{pp}} , \qquad (3\text{-}15)$$

where P_{pp} = power per power processor and

$$P_{PP} = \frac{P_t}{\eta_{pp}\eta_c} = \frac{I_b V_b}{\eta_e \eta_{pp}\eta_c} \quad , \tag{3-16}$$

where

P_t = thruster input power

I_b = beam current per thruster

V_b = beam voltage

η_{pp} = power processor efficiency

η_e = thruster electrical efficiency

η_c = cabling efficiency.

The beam parameters are determined by the technology choice since I_b depends on thruster design, and V_b depends on I_{sp} from

$$V_b = \left(\frac{m_i}{2e}\right)\left(\frac{g_o}{\eta_u \gamma}\right)^2 I_{sp}^{\ 2} \quad , \tag{3-17}$$

where

m_i = ion mass

e = electronic charge

η_u = measured propellant utilization efficiency

γ = thrust loss parameter.

Combining Eqs. 3-11, 3-15, and 3-16 yields

$$N_{mod} \cong \left(\frac{M_o}{I_b V_b}\right)\left(\frac{\eta_e \eta_{pp}\eta_c}{2\eta_{ps}}\right)\left(A_o I_{sp}\ g_o^{\ 2}\right) ;$$

because

$$\eta_{ps} = \eta_e \eta_u\ \eta_{pp}\eta_c \gamma^2 \quad ,$$

it follows that

$$N_{mod} = \left(\frac{M_o A_o}{I_b}\right)\left(\frac{e}{m}\right)\left(\frac{\eta_u}{I_{sp}}\right) . \tag{3-18}$$

This is the approximate number of operating modules needed to utilize the propulsion system power.

Two additional conditions must be satisfied: (1) there must be enough modules provided to account for wearout, and (2) standby redundancy must be provided independently of wearout. The total number of modules required for wearout (now) can be estimated from total propellant requirements. Using Eqs. 3-2, 3-5, and 3-13, the propellant mass is

$$M_p = M_o \left[1 - \left(MF + \frac{A_o I_{sp} \alpha_{ps}}{20.79 \eta_{ps}} \right) \right] \tag{3-19}$$

and

$$M_p = \int \dot{M} dt \simeq \frac{1}{\eta_u} \left(\frac{m_i}{e} \right) \int I_b(t)\, N_{ot}(t) dt \ , \tag{3-20}$$

where $\dot{M}$ = total mass flowrate.

The value of the integral in Eq. 3-20 is simply the total number of ampere-hours of operation required to use the propellant. If a thruster is characterized by a wearout life in ampere-hours, independent of throttling, the total propellant mass can be simply divided by the mass equivalent of the ampere-hour life. Thus,

$$N_{ow} = \left(\frac{M_p}{AH} \right) \left(\frac{e \eta_u}{m_i} \right) \ , \tag{3-21}$$

where AH = thruster life in ampere-hours.

To establish the total number of thrusters required, N_{ot} and N_{ow} must be scaled up to account for redundancy/reliability. To first order, a simple redundancy factor, R_t, can be used. Then, the approximate number required is the larger of

$$N_{ot} \cong \text{No. of thrusters required} = \begin{cases} (1 + R_t) \left[\dfrac{M_o A_o}{I_b} \left(\dfrac{e}{m_i} \right) \left(\dfrac{\eta_u}{I_{sp}} \right) \right] \\ \text{or} \\ (1 + R_t) \left[\dfrac{M_p \eta_u}{(AH)} \left(\dfrac{e}{m_i} \right) \right] \end{cases} . \tag{3-22}$$

B. PROPULSION SYSTEM MODELS

The generalized analysis technique discussed above requires models for propulsion system specific mass α_{ps} and total efficiency η_{ps}, as indicated by Eq. 3-14. Models for these parameters are presented below.

1. Performance Models

Although the desired final result of this section is a model for η_{ps}, several other relationships must also be defined. Total efficiency, as illustrated in Eq. 3-8, originates from the energy equation and is a product of all thruster, power processor, and cabling efficiencies:

$$\eta_{ps} = \eta_t \eta_{pp} \eta_c , \tag{3-23}$$

where

η_t = thruster total efficiency

η_{pp} = power processor efficiency

η_c = cabling efficiency.

Thruster total efficiency includes electrical efficiency, propellant utilization efficiency, and factors to account for ion beam divergence and multiply charged ions:

$$\eta_t = \eta_u \eta_e \gamma^2$$

η_u = measured propellant utilization efficiency

$= \eta_1 + 2\eta_2$

η_1 = mass fraction flowrate of singly charged ions

η_2 = mass fractional flowrate of doubly charged ions

η_e = thruster electrical efficiency

$$= \frac{V_b I_b}{P_t}$$

γ = experimentally determined correction factor for beam divergence and multiply charged ions

V_b = beam voltage

I_b = beam current per thruster

P_t = thruster input power.

Beam voltage is related to other parameters through the definition of ion beam energy:

$$eV_b = \frac{1}{2} m_i v_i^2 \tag{3-24}$$

$$= \frac{1}{2} m_i \left(\frac{\bar{v}}{\eta_u \gamma}\right)^2 \tag{3-25}$$

since

$$I_{sp} = \frac{\bar{v}}{g_o} \tag{3-26}$$

$$V_b = \left(\frac{m_i}{2e}\right)\left(\frac{I_{sp}\, g_o}{\eta_u \gamma}\right)^2 , \tag{3-27}$$

where

m_i = ion mass

e = electronic charge

v_i = ion velocity due to acceleration through V_b

$\bar{v}$ = average exhaust velocity

= $V_i \eta_u \gamma$.

Beam current can be related to flowrate through

$$I_b = \dot{m}_i \left(\frac{e}{m_i}\right) = \left(\dot{M}\eta_u\right)\left(\frac{e}{m_i}\right) , \tag{3-28}$$

where

$\dot{m}_i$ = ion mass flowrate

Calculations made for the generalized analysis utilized the following empirical relationships associated with the 30-cm-diameter Hg ion thruster (in mks units):[43,59,60]

$$P_t = I_b \left(V_b + 180 + \frac{20}{I_b^2} \right) \tag{3-29}$$

$$\eta_u = \left(\frac{1}{\beta} \frac{I_b}{I_b + I_n} \right) \tag{3-30}$$

I_n = neutral atom flowrate (equivalent amperes)

$$= 0.24 + 0.032\ I_b \tag{3-31}$$

$$\beta = 1 - 0.08 \left[\frac{I_b + I_{bx}^2}{2.2 + I_{bx}^2} \right] \quad \begin{array}{l} I_{bx} = I_b - 1 \text{ for } I_b \geq 1 \\ I_{bx} = 0 \text{ for } I_b \leq 1 \end{array} \tag{3-32}$$

$$\gamma = 0.942 - 0.005\ I_b + \frac{0.025}{I_b + 0.6} \tag{3-33}$$

$$(\eta_{pp}\ \eta_c) = 1 - \frac{0.13}{I_b^{0.5}} . \tag{3-34}$$

Substituting these terms into Eq. 3-23 is omitted since the equation would be somewhat awkward. But, to summarize, η_{ps} can now be evaluated for a given I_b as follows:

- η_u from Eqs. 3-30, 3-31, and 3-32
- η_e from the definition and Eq. 3-29
- γ from Eq. 3-33
- $\eta_{pp}\ \eta_c$ from Eq. 3-34.

Propulsion system total efficiency is plotted in Figures 3-2 and 3-3. The apparent slight decrease in efficiency that occurs at high beam current is a consequence of the increased influence of multiply charged ions as modelled in equation 3-33. It should be noted that equation 3-33 has been formulated to fit data in the 1- to 4-A beam current range and the accuracy of the expression for 10A has not been verified.

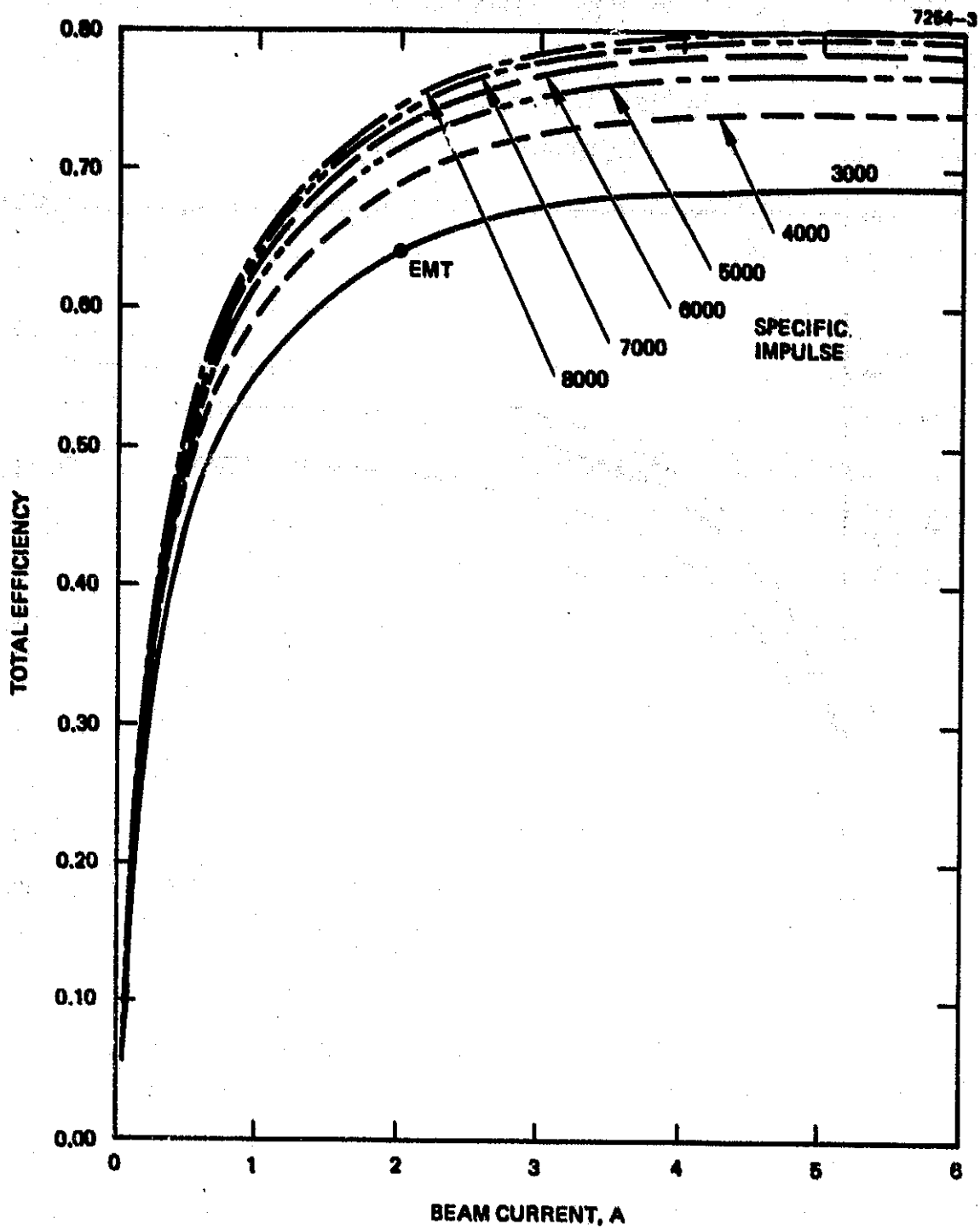

Figure 3-2. Propulsion system total efficiency for 30-cm-diameter mercury thruster as a function of beam current.

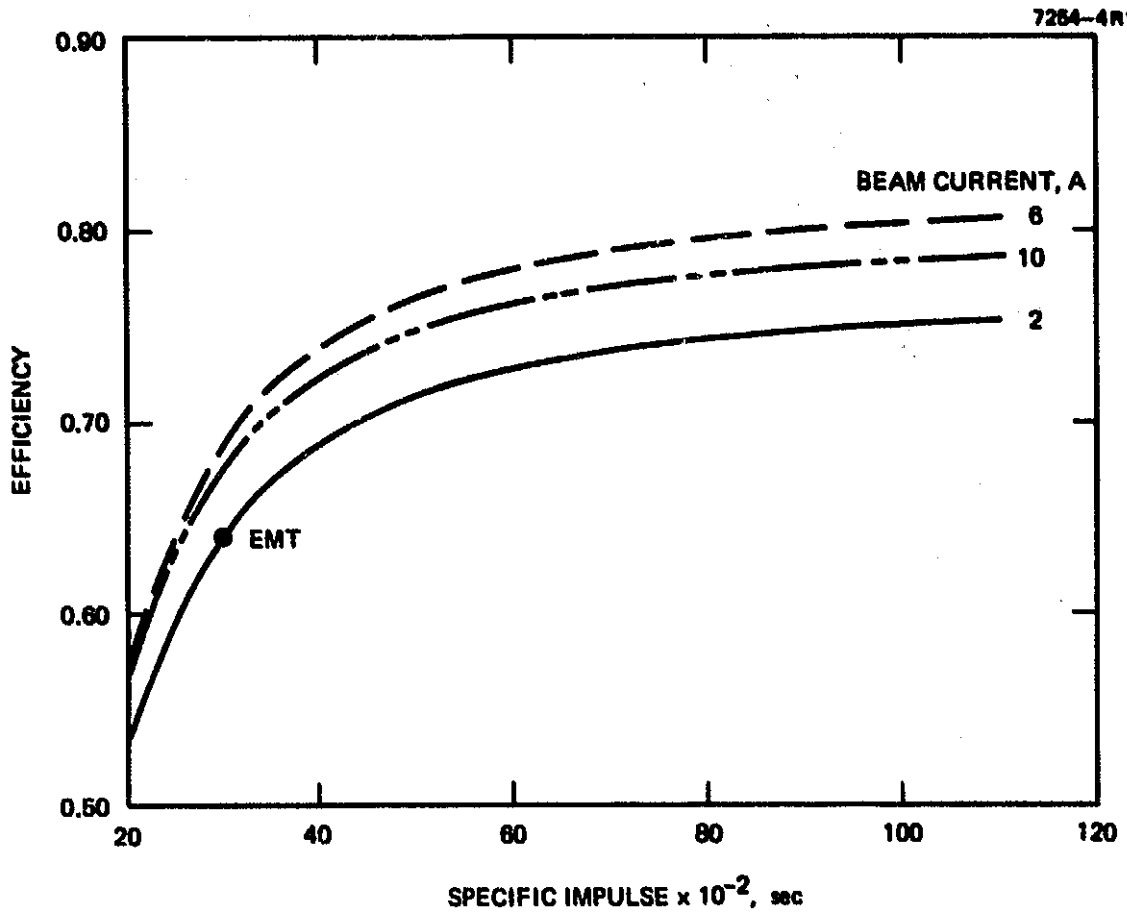

Figure 3-3. Propulsion system total efficiency as a function of I_{sp}.

Although the efficiency calculations are based on data obtained from operation of 30-cm thrusters on Hg.[43,59,60], using these equations for describing thruster performance using other propellants or for other size thrusters can be expected to produce relatively accurate results. More specifically, thruster electrical efficiency will scale exactly; utilization efficiency may be somewhat in error but not seriously; γ should scale roughly as defined by Eq. 3-33 for other propellants, but for other sizes an equivalent 30-cm beam current should be used; and power processor efficiency (Eq. 3-34) is probably reasonable for beam voltages greater than 1 kV.

The general dependence on propellant type is through atomic mass. By normalizing the atomic mass to mercury, the V_b and I_b relationships can be written in the form

$$V_b = \frac{\mu W}{2e}\left(\frac{\bar{v}}{\eta_u \gamma}\right)^2 = \frac{\mu W}{2e}\left(\frac{I_{sp} g_o}{\eta_u \gamma}\right)^2 \qquad (3\text{-}35)$$

$$= \lambda \left(\frac{I_{sp}}{100.02\ \eta_u \gamma}\right)^2 \qquad (3\text{-}36)$$

$$I_b = \dot{M}\eta_u \left(\frac{e}{\mu W}\right) = 481004 \left(\frac{\dot{M}\eta_u}{\lambda}\right), \qquad (3\text{-}37)$$

where

μ = atomic mass unit = $1.6605655 \times 10^{-27}$

W = atomic mass

$\mu W = m_i$

$\lambda = \dfrac{\text{atomic mass of propellant}}{\text{atomic mass of mercury}}$

λ_{Hg} = 1 (mercury)

$\lambda_A = \dfrac{39.948}{200.59} = 0.19915$ (argon)

$\lambda_{Kr} = \dfrac{83.8}{200.59} = 0.41777$ (krypton)

$\lambda_{Xe} = \dfrac{131.3}{200.59} = 0.65457$ (xenon).

Additional relationships that are of use in various calculations include thrust T and vehicle acceleration A:

$$T = \dot{M}\bar{v} = \left(\frac{\dot{M}}{g_o I_{sp}}\right)\bar{v}^2$$

$$= 0.203943\, V_b I_b \left(\frac{\eta_u \gamma}{I_{sp}}\right)^2 \qquad (3\text{-}38)$$

$$= 0.203943 \left(\frac{P_{ps}\eta_{ps}}{I_{sp}}\right)$$

$$A_o = \frac{T}{M_o g_o} = 0.020794 \left(\frac{P_{ps}\eta_{ps}}{M_o I_{sp}}\right),$$

where M_o is the vehicle initial mass and all values are in mks units, except A_o, which is expressed in "g's."

2. Mass Models

Propulsion system specific mass α_{ps} is assumed to include all the elements required to produce thrust, including a power source (e.g., solar array). Historically, α's of 30 kg/kW were used in mission studies based on optimistic technology goals. Generally, these α's included only the element masses and not system considerations such as thermal control and vehicle structure required for support. Depending on the particular study, such system factors may or may not have been included in the overall mass accounting.

The mass models discussed in this section include allowances for the major system factors assuming certain design approaches. Models for present technology are based on hardware currently under development[43,44] (specifically, the 30-cm EMT and its corresponding power processor). For the generalized analysis, advanced technology was modeled by projecting the capability of the 30-cm mercury thruster to higher beam current and voltage.

The mass models used to define present and advanced thruster technology are shown in Table 3-1. Although many system designs exist, these models were based on typical values used in the various reference documents and should be reasonably representative.

Table 3-1. Propulsion System Mass Model Used in Generalized Mission Analysis

Sub-Assembly	Present Technology Mass, kg
Solar array[a]	$18\ P_0$
Power conditioning panel[b] (Including structure and thermal control)	$42 + 3\ P_{pp}$
Thruster (Includes gimbals and structure)	17
Tankage, structure, and miscellaneous[c]	$5\ P_0$
Redundancy factors	
Power conditioning panels	1.2
Thrusters	1.4
Lifetime	c

a. P_0 is solar panel power at 1 AU after degradation.

b. P_{pp} is input power to power conditioning panel (maximum).

c. Constant A-hr wearout.

6119

The solar array specific mass is based on the assumption that all degradation occurs early in the mission. The 18 kg/kW assumes approximately a 15 to 20% degradation of the original installed power (15 kg/kW). Since solar array studies indicate that specific masses on the order of 5 kg/kW may be feasible with present technology,[45,46] the results of the work discussed here are probably conservative.

Power processor mass was modeled using historical data for PPUs alone, and current design data for the series resonant inverter (SRI) concept being developed by NASA LeRC, which includes thermal control and structure.[44,47,48] The basis for the equation used in Table 3-1 is indicated in Figure 3-4. The "historical" curve was obtained as shown in Figure 3-5 using data for various PPUs without structure and thermal control. Since the mass of the packaged PPU is dependent on many vehicle design factors, the straight line shown in Figure 3-4 was assumed as a reasonable estimate.

Thruster mass, as used in the model, includes an allowance for gimbals and miscellaneous structure associated with the thruster. Typically, the total "thruster array" is about twice the weight of the thrusters.[25,49] All remaining propulsion system elements (such as tanks, valves, structure, miscellaneous hardware) are assumed to be proportional to power at the rate of 5 kg/kW.

As Table 3-1 indicates, thruster mass is constant in this formulation. However, since it is assumed that higher power can be obtained, thruster lifetime and the required number of modules plays a strong role in modeling propulsion system specific mass. Figure 3-6 illustrates the influence of lifetime on mission performance. In the first example, the EMT operates at 2 A. The total mass of two thrusters and their individual power conditioners is about 136 kg. Modifying the propulsion system to use a 4-A beam current, but keeping specific impulse at 3000 sec (modified EMT), yields a total mass of 77 kg without considering thruster lifetime (i.e., if no wearout of the thruster occurs). This large decrease in mass is mainly due to the lower specific mass of the PPU at the higher power levels. The trajectory dynamic performance is unchanged for this second example, since running fewer thrusters at higher current can produce the same acceleration time profile with no increase in system propellant or

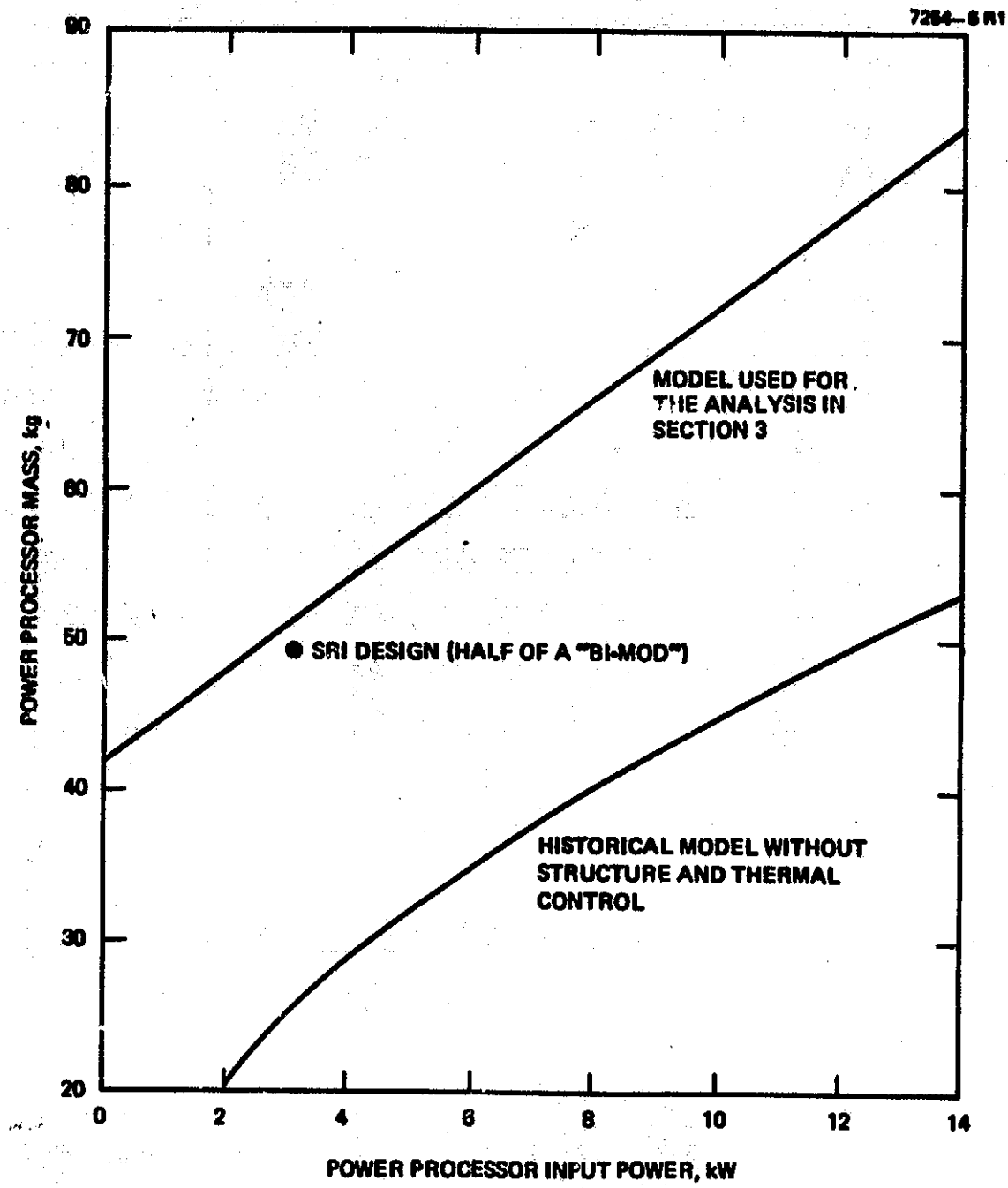

Figure 3-4. Power processor mass model.

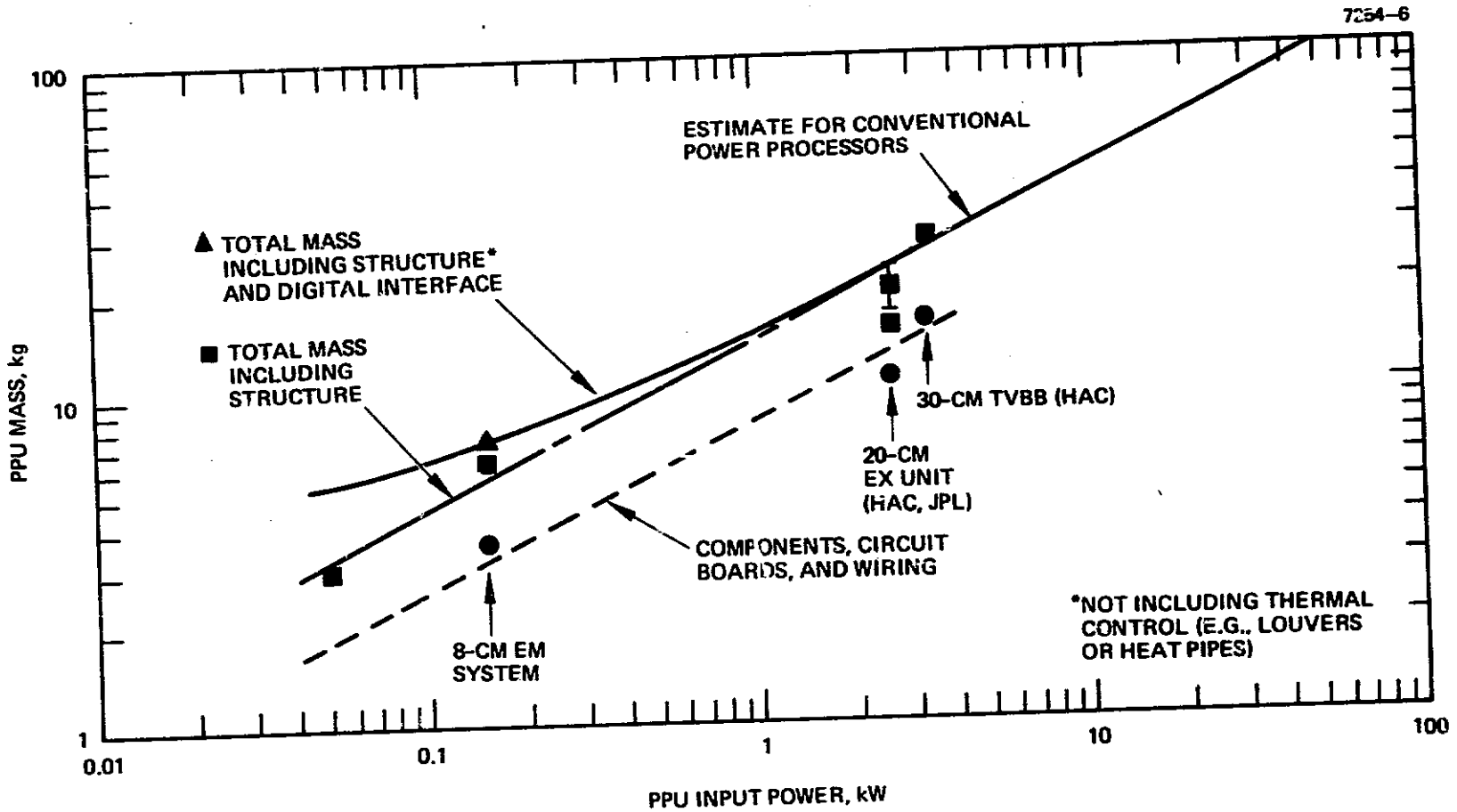

Figure 3-5. Power processor historical mass data.

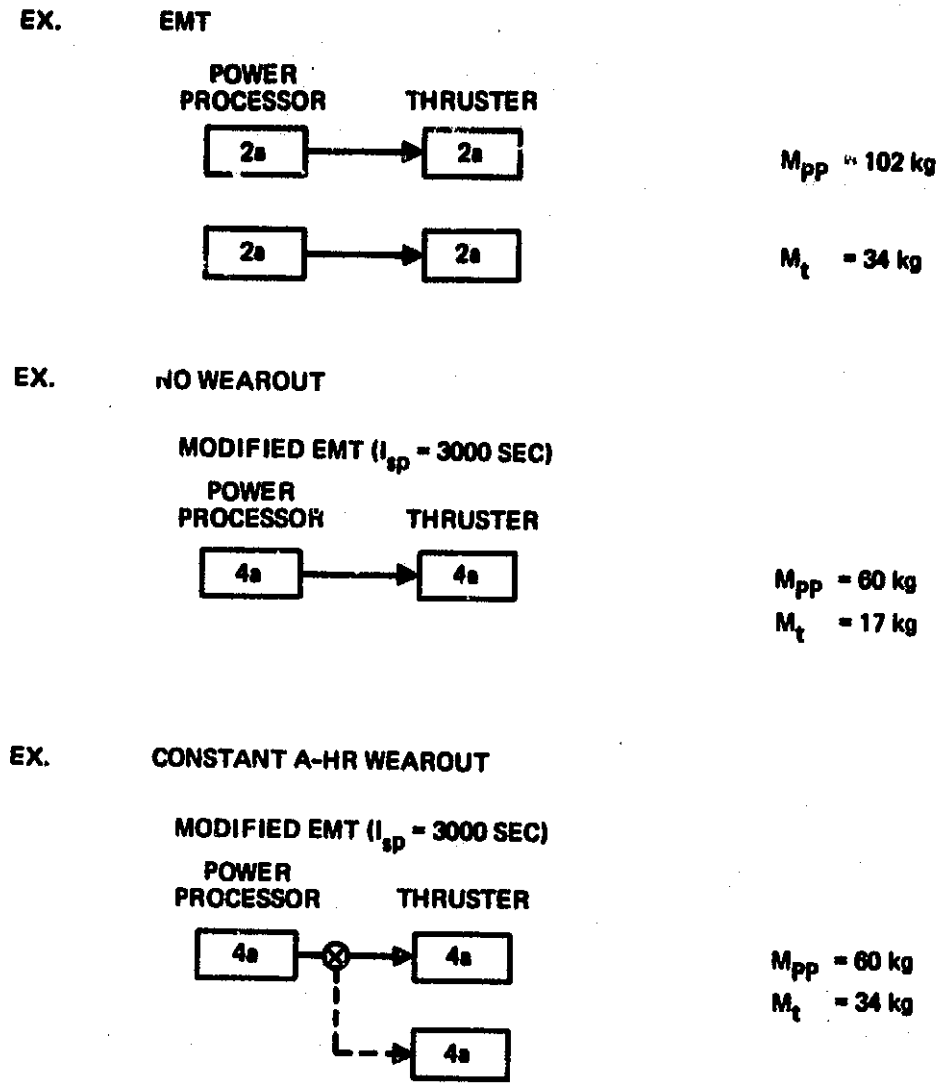

Figure 3-6. Example of mass modeling philosophy applied in generalized analysis.

power requirements. The only change is a lighter propulsion system with potentially improved payload.

The mass modeling of thruster wearout lifetime is assumed to occur at constant ampere-hours. That is, if the thruster lasts for a given duration at 2 A, it will wear out in half that time when operated at 4 A. As in the third example of Figure 3-6, a spare thruster must then be carried. Switching occurs for wearout in a manner analogous to switching for thruster failures. The total number of thrusters is the same as in the first example, but a significant mass savings accrues from raising module power. Total mass would then be 94 kg, a savings of 42 kg. Furthermore, even if a third thruster were necessary to complete the mission (as a result of a variable thruster lifetime in ampere-hours), it would still only add 17 kg, and net savings would then be 25 kg.

Savings in propulsion system mass thus can apparently be achieved by increasing beam current, permitting wearout to occur, and saving power processing mass. Even if the constant ampere-hour wearout assumption is not completely accurate the effect tends to be balanced by reliability considerations. A favorable reliability interaction results at higher beam currents because the total thruster hours are reduced and, consequently, there will be fewer failures and fewer thrusters required for reliability purposes. Based on typical system studies, redundancies of 20% and 40% for the PPU and thrusters, respectively, were selected.

Using the models in Table 3-1 and the previous philosphy for thruster wearout, propulsion system specific mass curves were developed. For the simplified example shown in Figure 3-7, mission thrust time is less than thruster lifetime (i.e., no thruster wearout occurs). The trends caused by increasing beam current and specific impulse are then divorced from lifetime considerations. As is seen for present technology, modifying the EMT from its nominal value of 2 A to around 6 A will generate significant decreases in specific mass. On the other hand, holding beam current constant and increasing the specific impulse from 3000 to 4500 sec will accomplish approximately the same decrease in specific mass (10 kg/kW). Simultaneously increasing both beam current and specific impulse would only further improve specific mass by 5 kg/kW. The

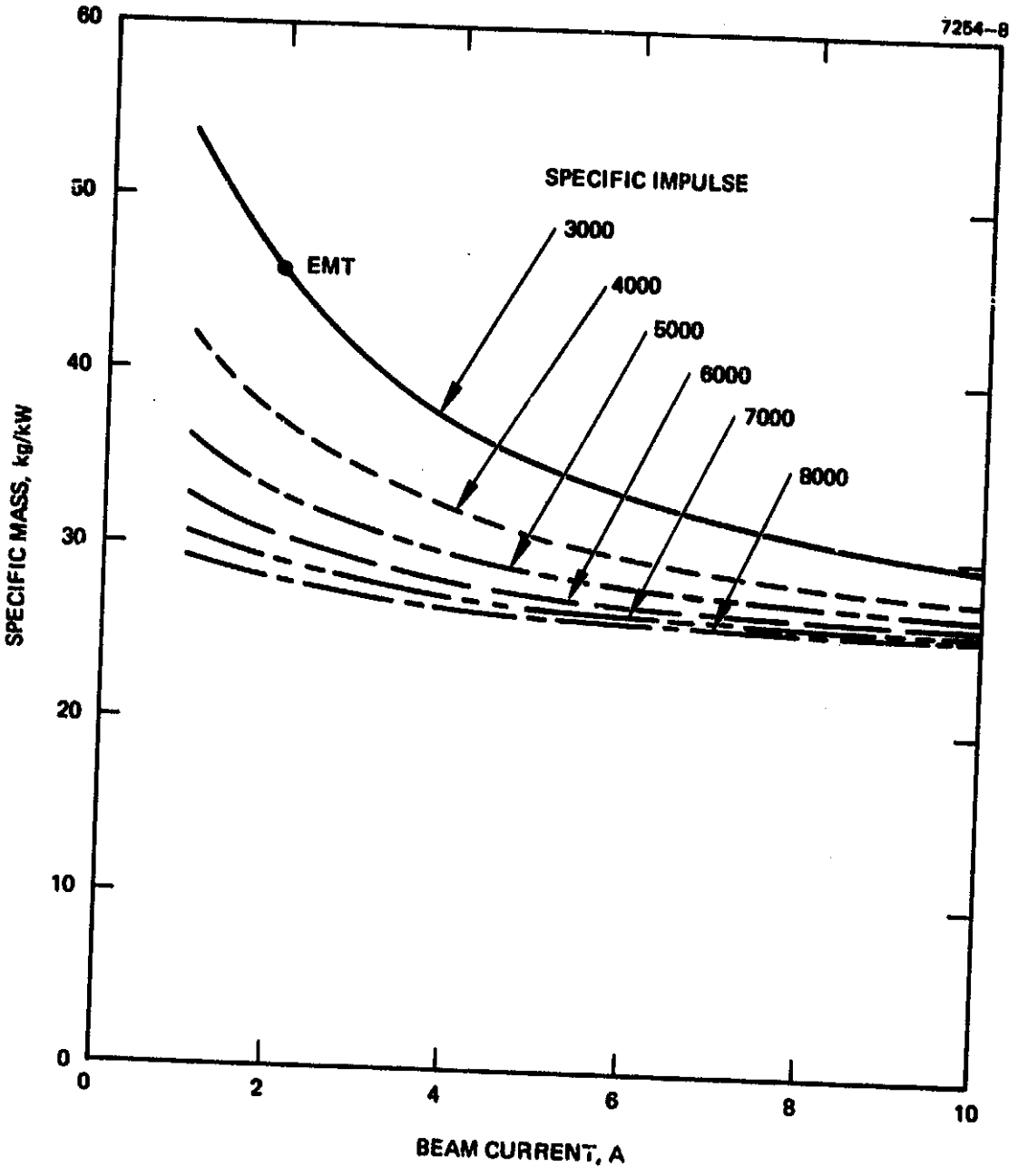

Figure 3-7. Propulsion system specific mass; no wearout.

change is relatively small because the bulk of the benefit comes from the initial increase of module power, which may be accomplished by changing either variable separately.

The specific results used for the generalized analysis presented in this report are shown in Figure 3-8. These curves include wearout on the basis of a 20,000 A-hr thruster life. A break point occurs at 2 A because additional thrusters are required at higher current levels to maintain a constant mission life. The α_{ps} data needed in Eq. 3-14 was obtained from Figure 3-8.

C. MISSION CHARACTERISTICS

Referring to Eq. 3-14, the generalized analysis approach requires mission information on mass fraction (MF), initial acceleration (A_o), and ΔV. Representative data for each of the missions included in the mission set was obtained from the literature and from trajectory calculations made under this study, as indicated in Tables 3-2 and 3-3. Payload mass data and references for each mission are shown in Table 3-2. This data was used to select a maximum payload mass for computing MFR.

The summary of mission requirements presented in Table 3-3 was distilled from the referenced literature. The parameters of interest, MFR, A_o, and ΔV, were calculated from the results presented in those studies. ΔV and A_o were obtained using Eqs. 3-1 and 3-11, respectively. MFR is based on the maximum payload values indicated in Table 3-2.

D. RESULTS OF THE GENERALIZED ANALYSIS

The results of the generalized analysis were derived from Eq. 3-14 and based on the performance models, mass models, and mission characteristics discussed above. A general example of the relationships involved is shown in Figure 3-9. The legend on top of Figure 3-9 describes the technology of the particular low thrust propulsion system being considered. ("Present power technology" refers to the use of the relations in Table 3-1.) First, the level of power system technology (existing hardware or present power) is chosen. Then, for a modified EMT within the

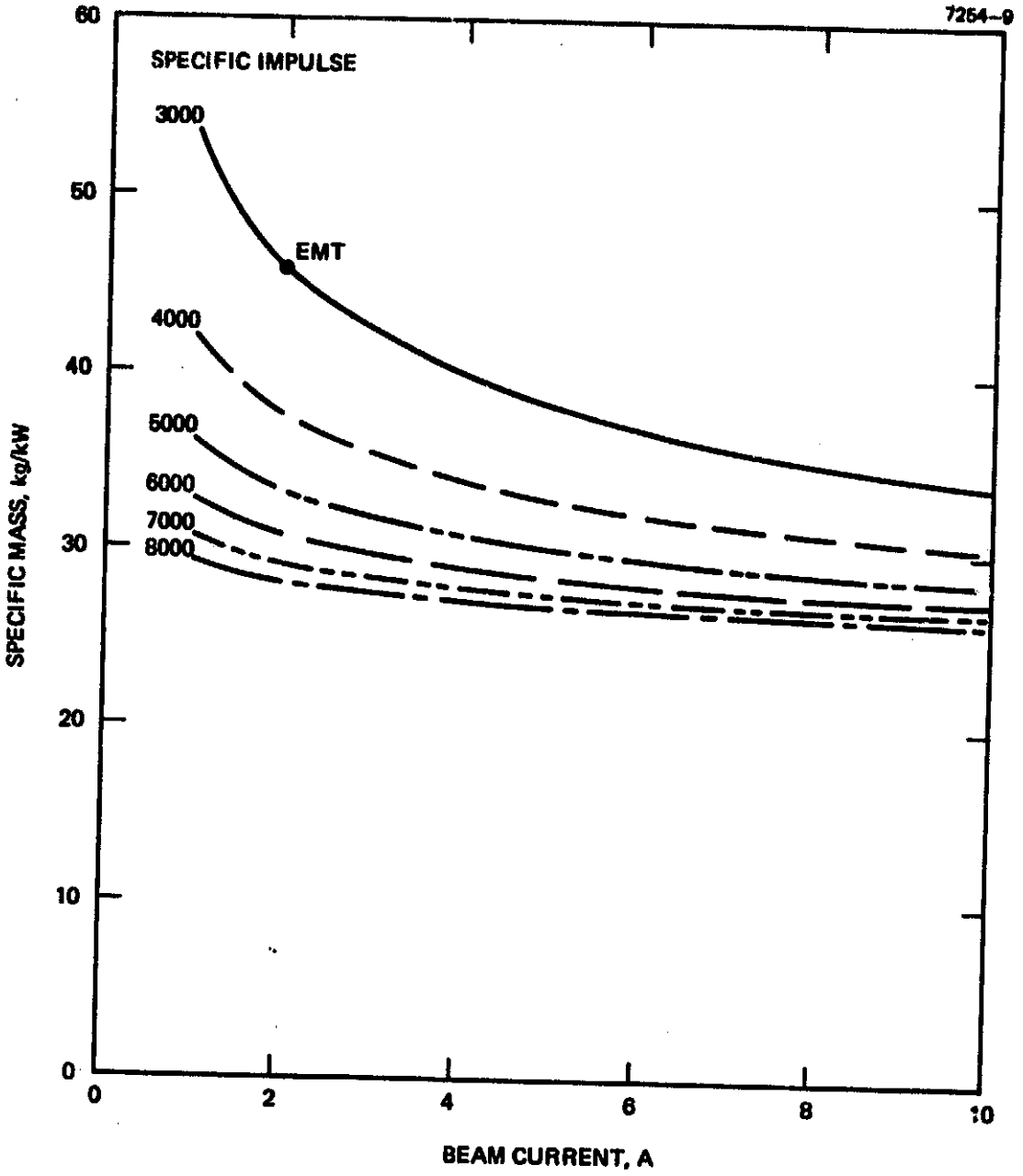

Figure 3-8. Propulsion system specific mass; with wearout.

Table 3-2. Mission Payload Mass Summary and References

Mission	Payload Mass, kg	References	Remarks
Outer planets			
Jupiter orbiter	982	8, 29	570 kg MJS[a] + retro
	1282	50	Same as above but includes 150-300 kg entry probe
	1360	51	MJO[b] design
Jupiter satellite orbiter	1265	52	Pioneer Venus Module includes: 150 kg probe; retro, lower orbit fuel for satellite explorations
	1100	53	Pioneer class; includes: 150 kg probe; Type I retro fuel; lower orbit fuel for satellite explorations
Saturn flyby	840	51	Uses Jupiter flyby
Saturn orbiter	1031	8, 29	Includes 570 kg MJS and retro fuel; add 150-300 kg for probe
	1016	54	HAC study for technical proposal
Titan orbiter	1096	54	Scaled from HAC study for technical proposal
Uranus flyby	750	8	750 kg MJS for Uranus/Neptune flyby
	825	51	Mariner class, uses Jupiter flyby, includes probe
Neptune flyby	750	8	750 kg MJS uses Uranus flyby

[a]Mariner class, Jupiter swingby (MJS).
[b]Mariner class, Jupiter Orbiter (MJO).

6119

Table 3-2. Mission Payload Mass Summary and References (Continued)

Mission	Payload Mass, kg	References	Remarks
Outer planets (Continued)			
Solar system escape	320	8	Helios class
Mercury orbiter	1335	30	HAC study; Pioneer Venus Module (793 kg); includes retro; drop propulsion system before injection
	1480	31	Drops propulsion system before injection
	824	8, 29	350 kg Helios
	1317	51	Mariner class (775 kg) plus retro
Close solar probe (0.1 AU)	465	55	Solar probe uses Venus swingby
	1000	55	Low cost (heavy) payload
Earth observatory	8000-10,000	11, 18, 21	Shuttle class maximum payloads
Comet Encke			
Slow flyby	113	8	Small science package
	508	56	JPL Mariner Encke study; 4 km/sec
	358-608	33	Pioneer 10/11 class and Advanced Pioneer
	450	13, 15	Representative payload for flyby opportunity and background for comet missions

6119

Table 3-2. Mission Payload Mass Summary and Reference (Continued)

Mission	Payload Mass, kg	References	Remarks
Comet Encke (Continued)			
Slow flyby (Continued)	400	38	
	533	25	
	350	32	
Rendezvous	635	41	
	545	51	Mariner class
	500	38	
Asteroid rendezvous	350	8	HAC/Metis (Pioneer class)
	500	34	Eros
	500	35	Eros
	635	34	Ceres
	500	38	Various
	350	32	Various
Asteroid sample return (Eros)	940	37	Return capsule, leave stage at Eros
	1000	38	
Out-of-ecliptic (1 AU)	600	11	
	391	51	Includes science package of 31 kg
	200-400	2	Inclination dependent payload
	200	27	

6119

Table 3-3. Mission Characteristics

Mission	C_3, km^2/sec^2	M_o, kg	M_{pl} Conservative Payload, kg	MFR	A_o, $10^{-5}g$	ΔV, km/sec	Reference	Remarks
Outer planets								
Jupiter Orbiter	37	3050	1360	0.45	3.4	4.3	8,29	
Jupiter satellite orbiter	37	3050	1265	0.41	3.4	4.3	8,29	
Saturn flyby	64	2320	840	0.36	3.4	3.6	8,29	
Saturn orbiter	64	2320	1031	0.44	3.4	3.6	8,29	
Titan orbiter	64	2320	1096	0.47	3.4	3.6	8,29	
Uranus flyby	42	2920	825	0.28	3.8	4.5	8	Jupiter swingby
	72	2120	825	0.39	3.8	3.8	8	Uranus flyby to Neptune
Neptune flyby	72	2120	750	0.35	3.8	3.8	8	Uranus swingby
Solar system escape	37	3050	450	0.15	3.4	4.3	8,29	Jupiter swingby
Mercury orbiter	4	5720	1480	0.26	2.1	17.4		HAC trajectory studies; thermal constraints, payload is approach mass

Table 3-3. Mission Characteristics (Continued)

Mission	C_3, km^2/sec^2	M_o, kg	M_{pl} Conservative Payload, kg	MFR	A_o, $10^{-5}g$	ΔV, km/sec	Reference	Remarks
Mercury orbiter (Continued)	25	3827	1480	0.39	1.6	10.9		HAC trajectory studies, thermal constraints, payload is approach mass
	25	3827	1480	0.39	1.7	13.1	31	
Close solar probe (0.1 AU)	20	4260	1000	0.23	2.9	14.1		HAC trajectory studies; thermal constraints, (Sun angle > 90°)
Earth observatory	-	27,215	10,000	0.37	2.-4.	6.0		HAC trajectory studies to sync. eq.
Comet Encke								
Slow flyby	55	2560	608	0.24	4.1-4.7	8.8		HAC studies; approach = 4.5 km/sec
	54	2600	608	0.23	4.6	9.5	8	4 km/sec
	77	1970	608	0.31	3.1	11.2	39	4 km/sec
	49	2720	608	0.22	2.7	8.7	39	Venus gravity assist

Table 3-3. Mission Characteristics (Continued)

Mission	C_3, km^2/sec^2	M_o, kg	M_{pl} Conservative Payload, kg	MFR	A_o, $10^{-5}g$	ΔV, km/sec	Reference	Remarks
Comet Encke (Continued)	55	2560	608	0.24	3.4	11.3	29	
Slow flyby (Continued)	54	2600	608	0.23	2.5	10.4	2	
Rendezvous	49	2720	635	0.23	4.4-4.5	9.1-9.8	41	Different opportunities
	54	2600	635	0.24	4.0	11.1	41	
	42	2920	635	0.22	4.1	9.5	8	Long flight time
	44	2860	635	0.22	4.2	14.3	8	Short flight time
	51	2680	635	0.24	4.2	10.4	2	
Asteroid rendezvous	25	3827	635	0.17	3.3	8.5	8,29	Metis
	3	5840	635	0.11	3.6	8.1	34	Eros
	4	5720	635	0.11	4.2	5.9	32	Eros
	56	2530	635	0.25	4.6	7.8	34	Ceres
Asteroid sample return (Eros)	4	5720	1000	0.17	4.2	12.0	36	Return capsule, leave stage at Eros

Table 3-3. Mission Characteristics (Continued)

Mission	C_3, km^2/sec^2	M_o, kg	Mpl Conservative Payload, kg	MFR	A_o, $10^{-5}g$	ΔV, km/sec	Reference	Remarks
Out-of-ecliptic (1 AU)	1	6040	600	0.10	2.-3.	20-55		HAC trajectory studies; inclination dependent
	1	6040	600	0.10	2.2-3.8	22-38	2	

6119

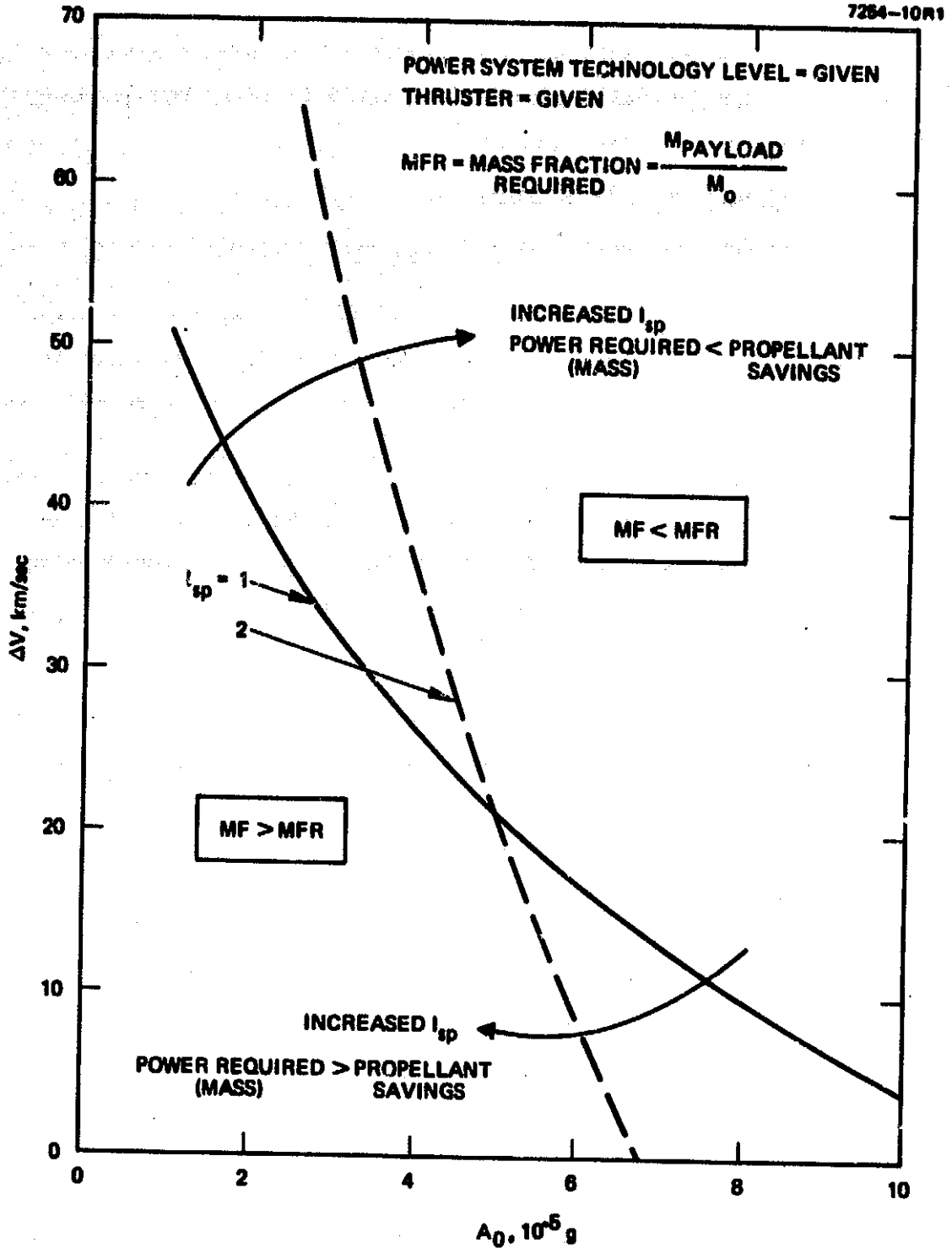

Figure 3-9. Example of the influence of I_{sp} on ΔV vs A_o format results.

selected power technology, one must choose thruster operating conditions in terms of beam current and specific impulse. These choices will serve to describe the propulsion system according to the modeling in Sections 3.A and 3.B. Mission requirements are defined by the payload (MFR) for mission success.

1. Specific Impulse Considerations

The dependence of performance on I_{sp} is illustrated in Figure 3-9. Any mission can be categorized in terms of an initial acceleration A_o and a velocity ΔV required to be delivered by the propulsion system. The spectrum of A_o and ΔV combinations for all missions is shown in Figure 3-9 for a constant (MFR). The solid line on the curve corresponds to a particular propulsion system (system technology level, thruster operating conditions) that can deliver the specified MFR. To the left of these curves, the propulsion system performs the mission with an MF greater than that required; to the right, it performs the mission with the inadequate MF (or payload). The effect of increasing I_{sp} is shown by arrows. In the region of higher ΔV and lower A_o, where correspondingly less thrust is needed, the preference is to keep the propellant mass as small as possible, and increasing I_{sp} helps to do this. On the other hand, when higher thrust is needed at low ΔV, increasing I_{sp} causes a decrease in performance. The reason is that the power required, in terms of mass, when increasing I_{sp} is greater than the propellant savings that would result from the higher I_{sp}.

Figure 3-10 outlines the tradeoffs between I_{sp} and various thruster modifications and MFRs. These charts also show equivalent thrust time, which is the mission duration parameter used to characterize the required thruster lifetime for any mission. This equivalent thrust time is actually the time it would take to expel all of the propellant with the power available at 1 AU. For orientation, the Halley's comet mission, which is a relatively long thrusting mission, requires only about one year of equivalent thrust time.

The trends, as far as I_{sp} is concerned, show a very flat optimal. Considering Figure 3-10(a), for example, for very high accelerations

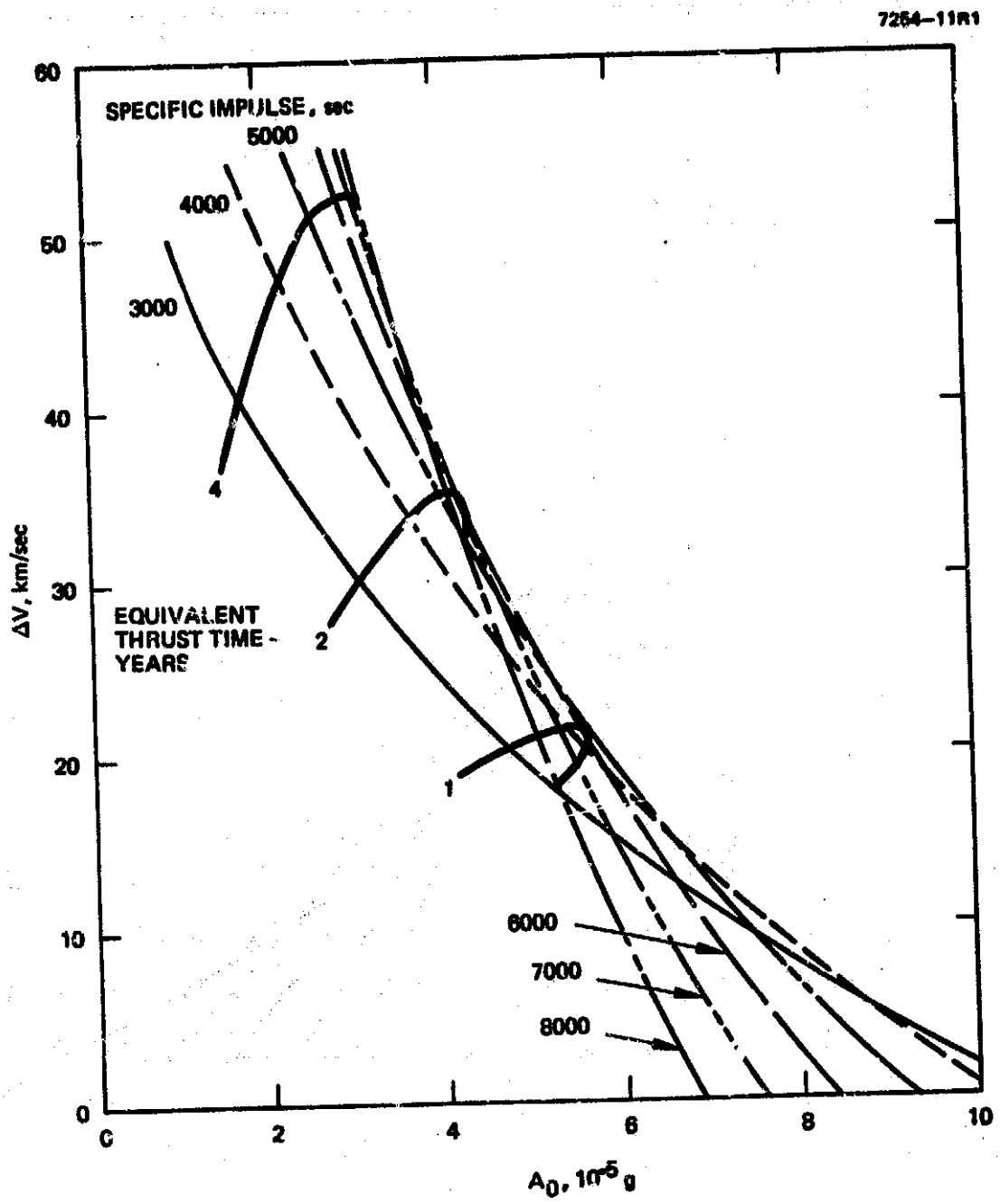

Figure 3-10(a). ΔV vs A_0 format for present power technology with modified EMT; MF = 0.1.

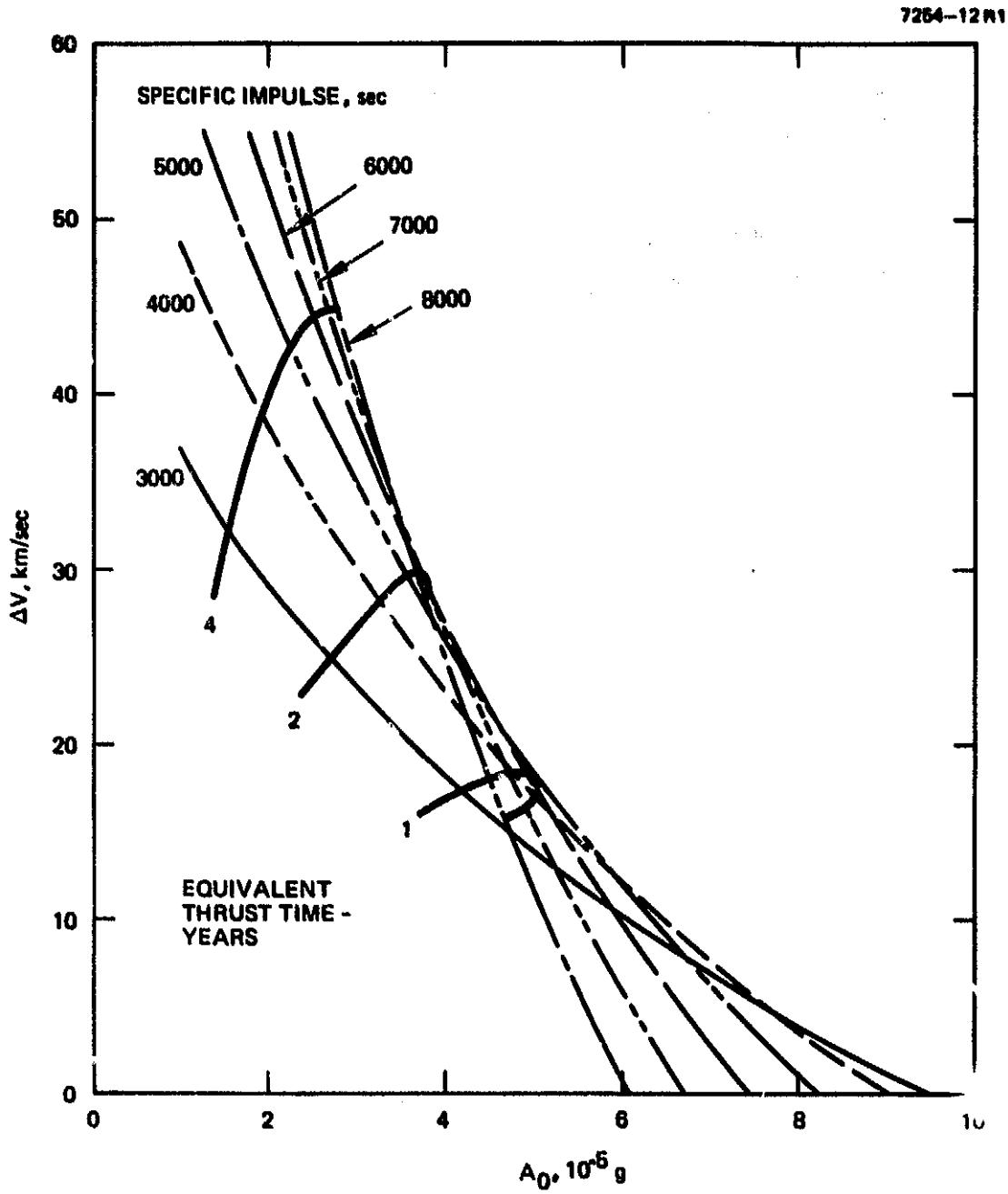

Figure 3-10(b). ΔV vs A_o format for present power technology with modified EMT; MF = 0.2.

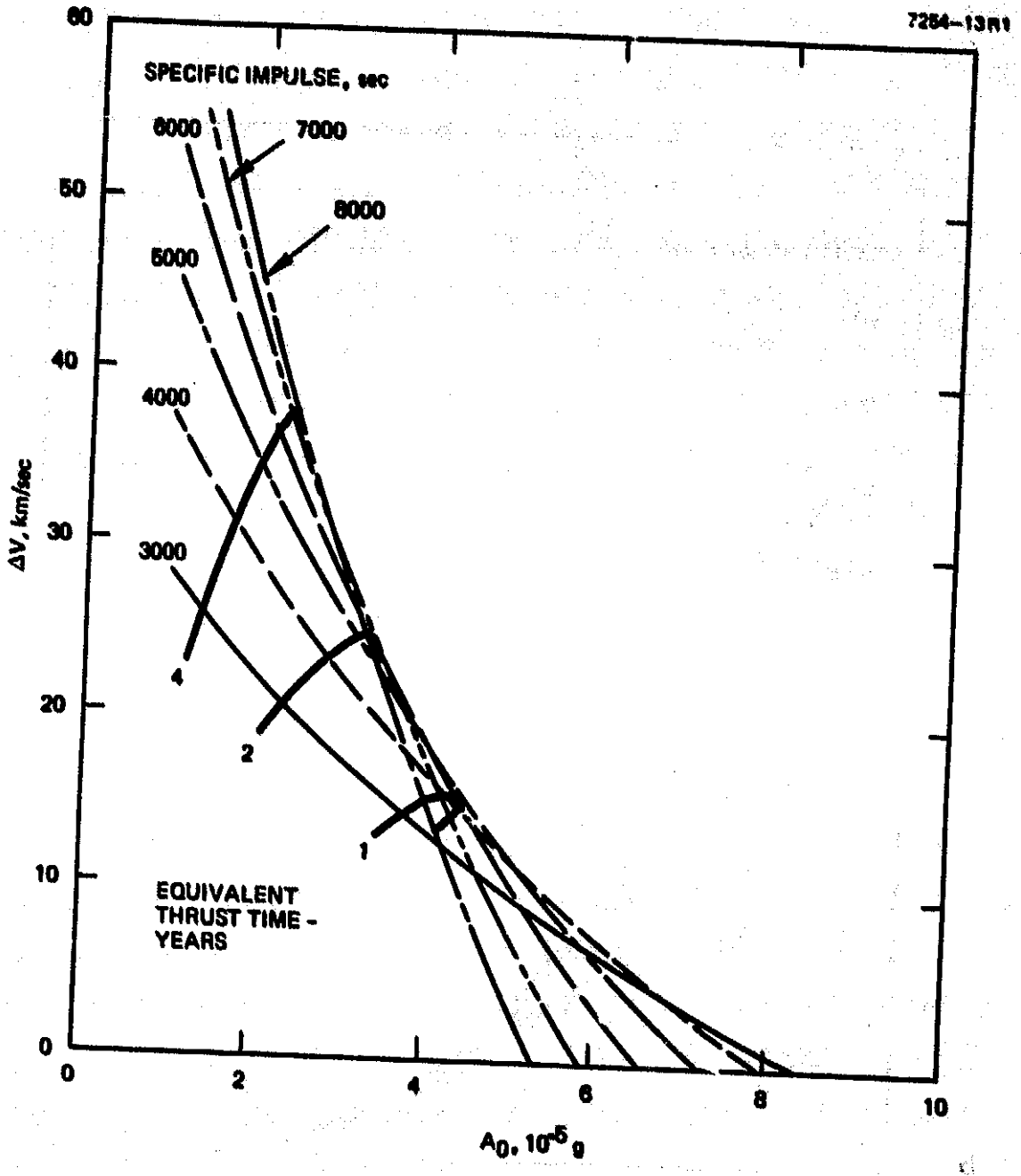

Figure 3-10(c). ΔV vs A_o format for present power technology with modified EMT; MF = 0.3.

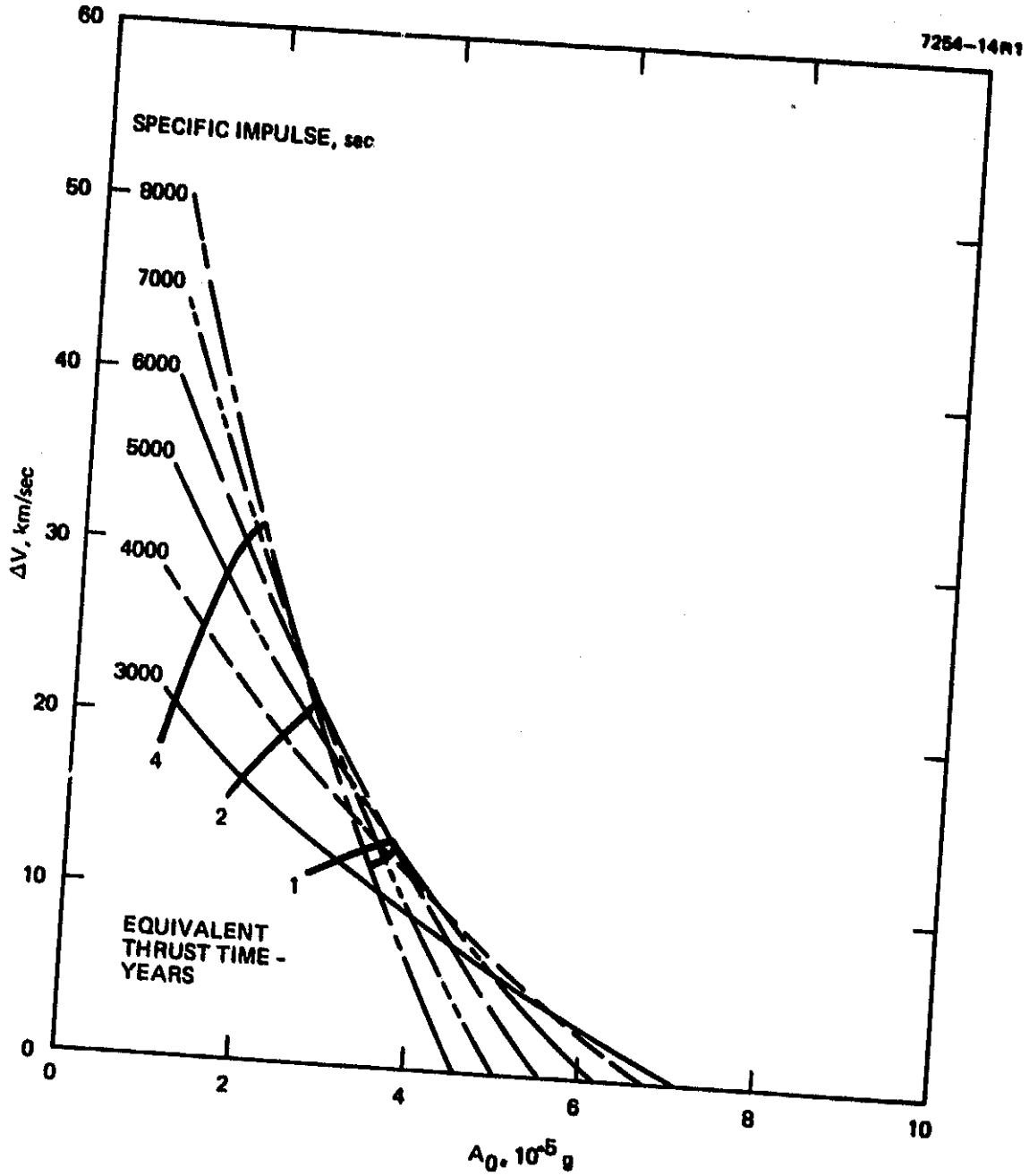

Figure 3-10(d). ΔV vs A_o format for present power technology with modified EMT; MF = 0.4.

(6 to 8 x 10^{-5} g) and low ΔV (10 to 15 km/sec), the performance resulting from an I_{sp} up to 5000 sec is relatively constant. The fact that there is not much difference indicates the very flat optimal. At the extreme right (the envelope of maximum performance), little variation occurs in I_{sp} over a great range of A_o and ΔV combinations. The message of these curves is that, since increasing I_{sp} may not significantly increase mass performance, the higher cost of higher power may not be justified.

The other parts of Figure 3-10 have the same propulsion system with increased MFs. Since the particular propulsion system now has all of the curves moved over to the left and down, fewer potential missions can be captured by the particular technology level and thruster modifications because of the higher MFR. The trends, as far as I_{sp} is concerned, are basically the same. Since these missions are characterized by rather flat optimals, the basic I_{sp} considerations become a cost tradeoff: increasing I_{sp} to improve performance, although sometimes possible, is expensive.

In summary, the above considerations suggest that I_{sp} should be raised only after other alternatives have been examined. It is generally better to first attempt to lower the specific mass of the propulsion system by raising beam current.

2. Mission Performance Results

The space shuttle was assumed available as a launch vehicle for these advanced missions (Table 3-3). The major implication of the shuttle is that larger injected mass and larger propulsion systems are possible as compared to earlier launch vehicles (e.g., Atlas Centaur). Figure 3-11 shows the assumed capability of the Shuttle. The two-stage IUS is assumed for the lower launch energy missions and a three-stage concept for the higher values of C_3.[57,58]

The mission performance comparison curves used in the remainder of this analysis are shown in Figures 3-12 through 3-16. These figures display lines of constant mass fraction in the ΔV vs A_o format for various technology assumptions. Given a particular mission, specified in terms of A_o and ΔV, any propulsion system (power technology level,

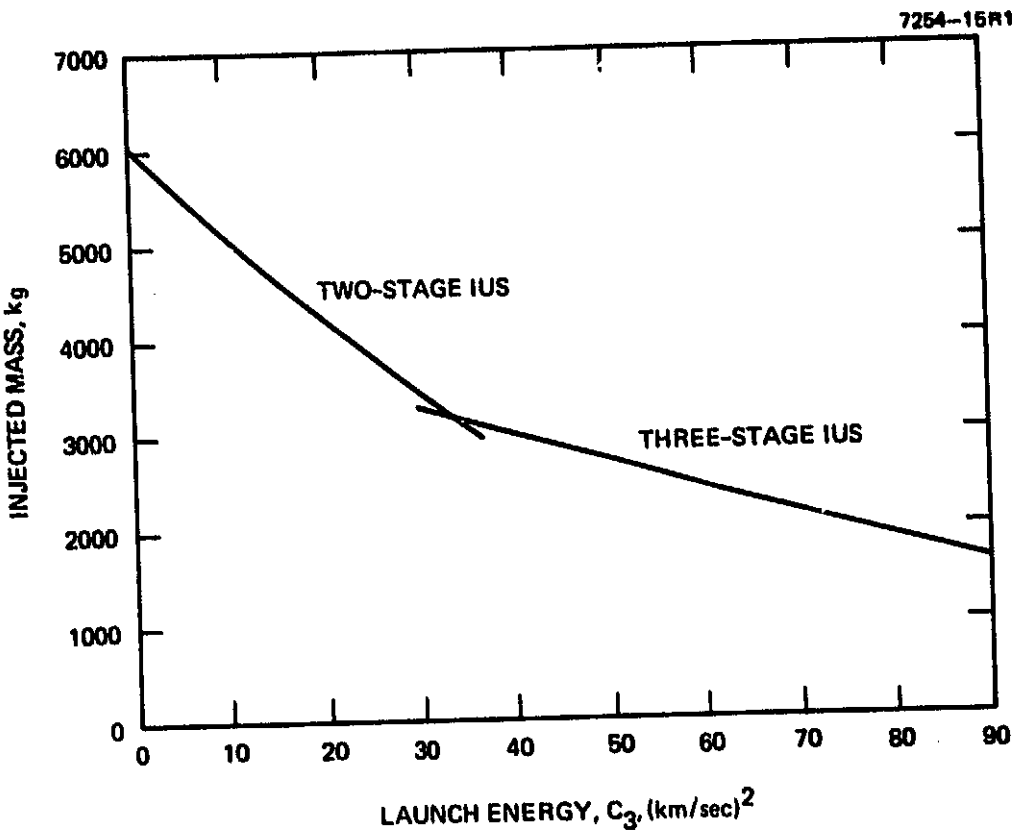

Figure 3-11. Interim upper stage (IUS) capability with Shuttle.

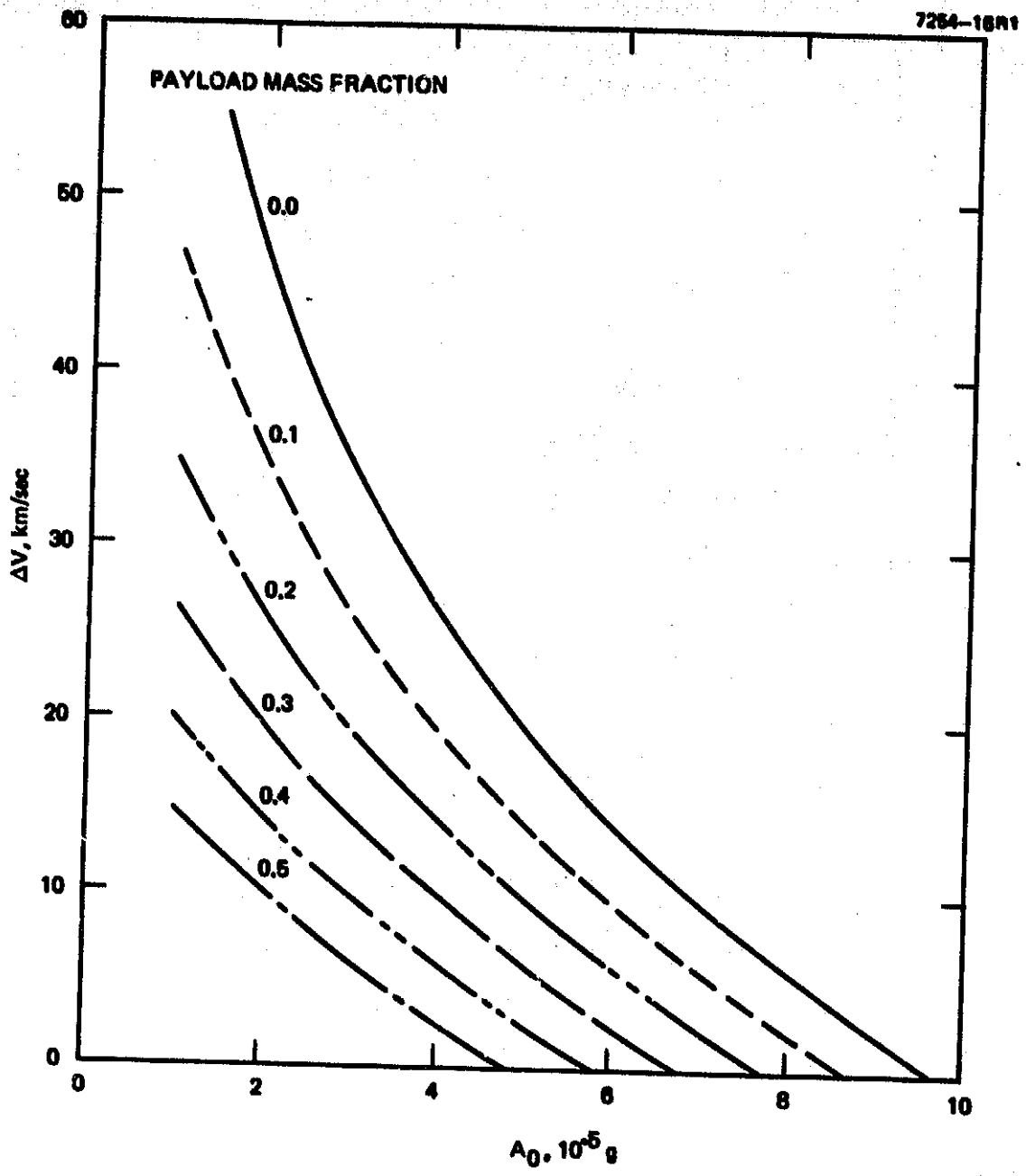

Figure 3-12. ΔV vs A_o format; EMT, existing power subsystems.

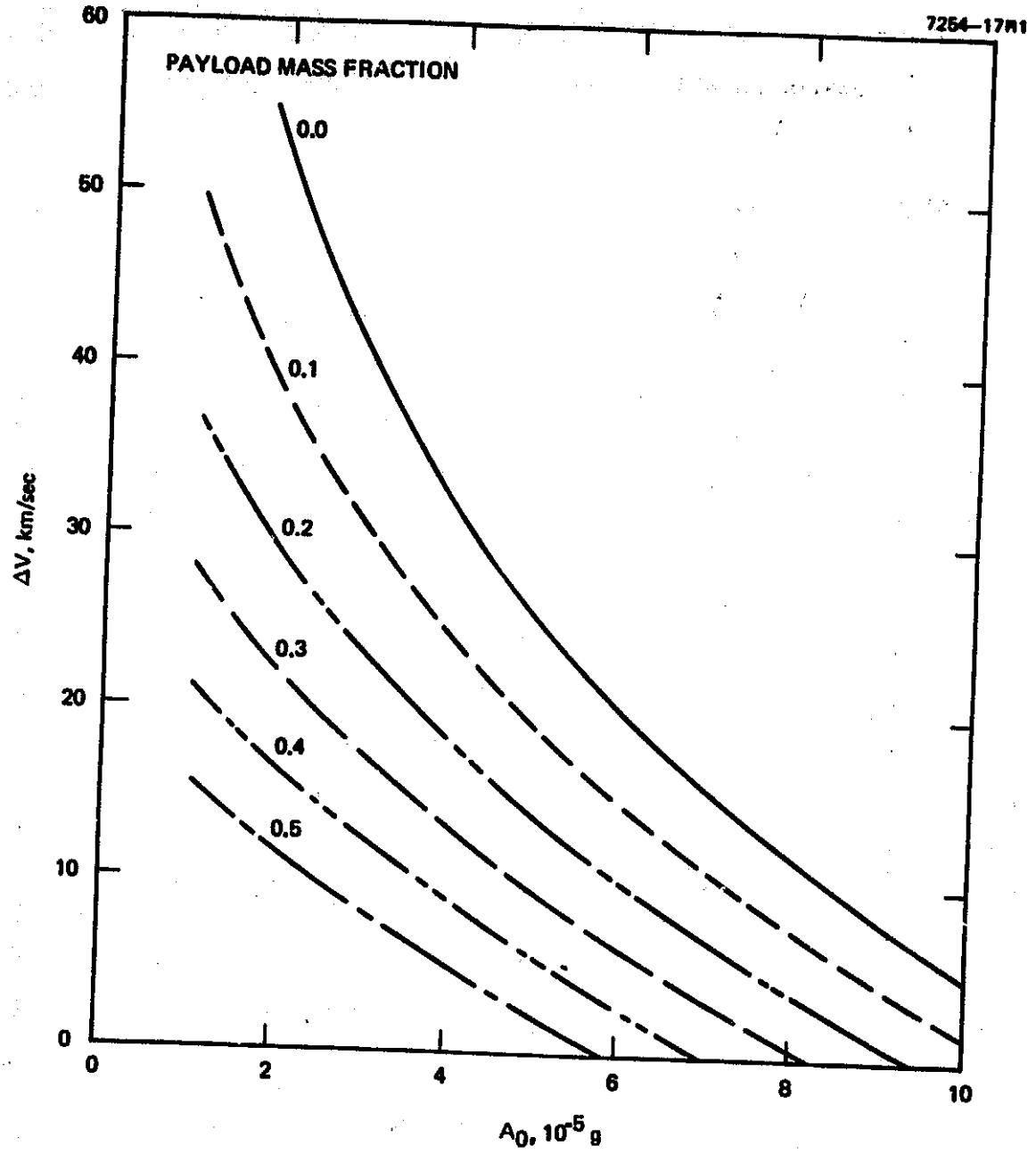

Figure 3-13. ΔV vs A_o format; modified EMT (4 A), present power technology, 3000 sec I_{sp}.

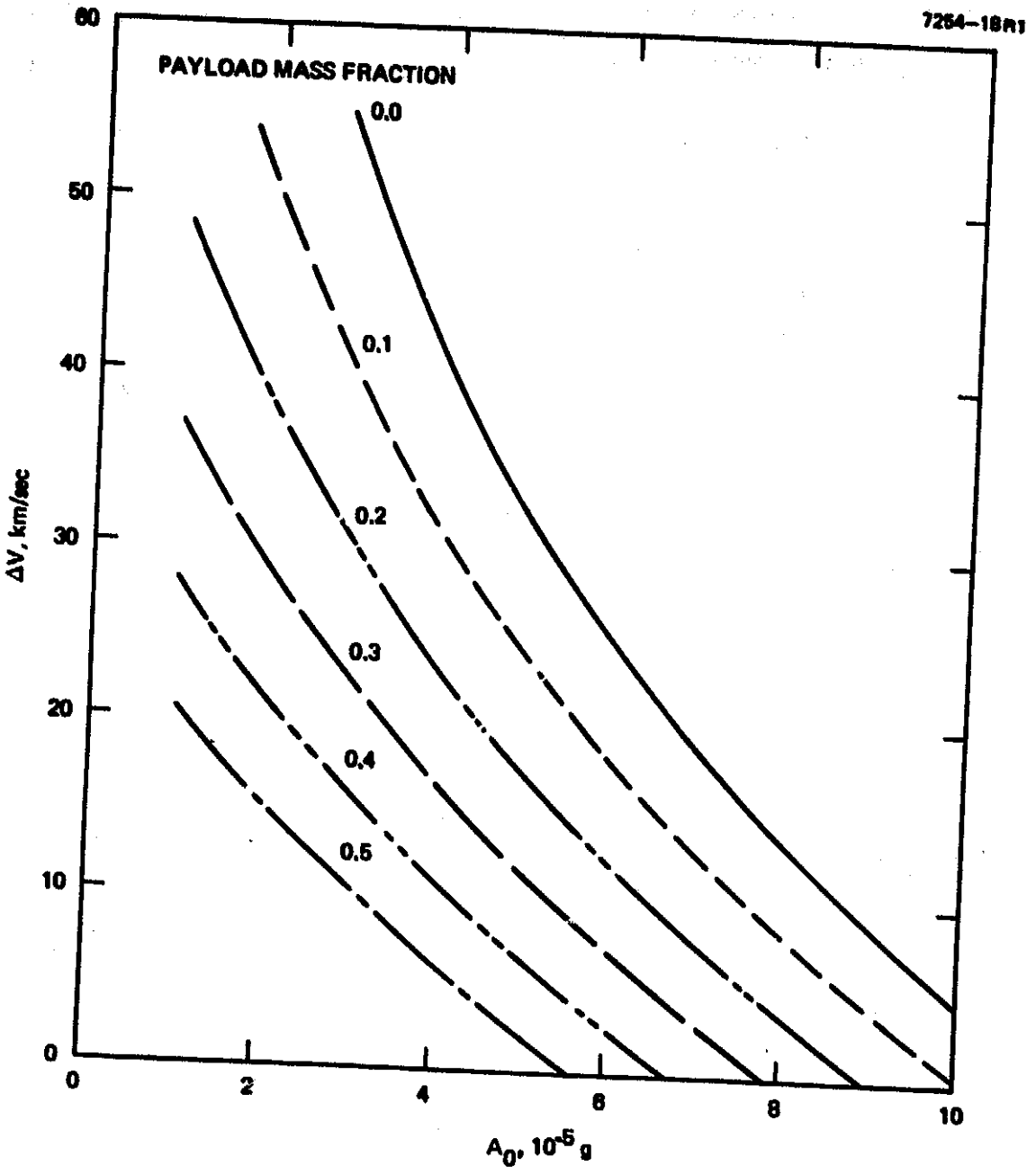

Figure 3-14. ΔV vs A_o format; modified EMT (4 A), present power technology, 4000 sec I_{sp}.

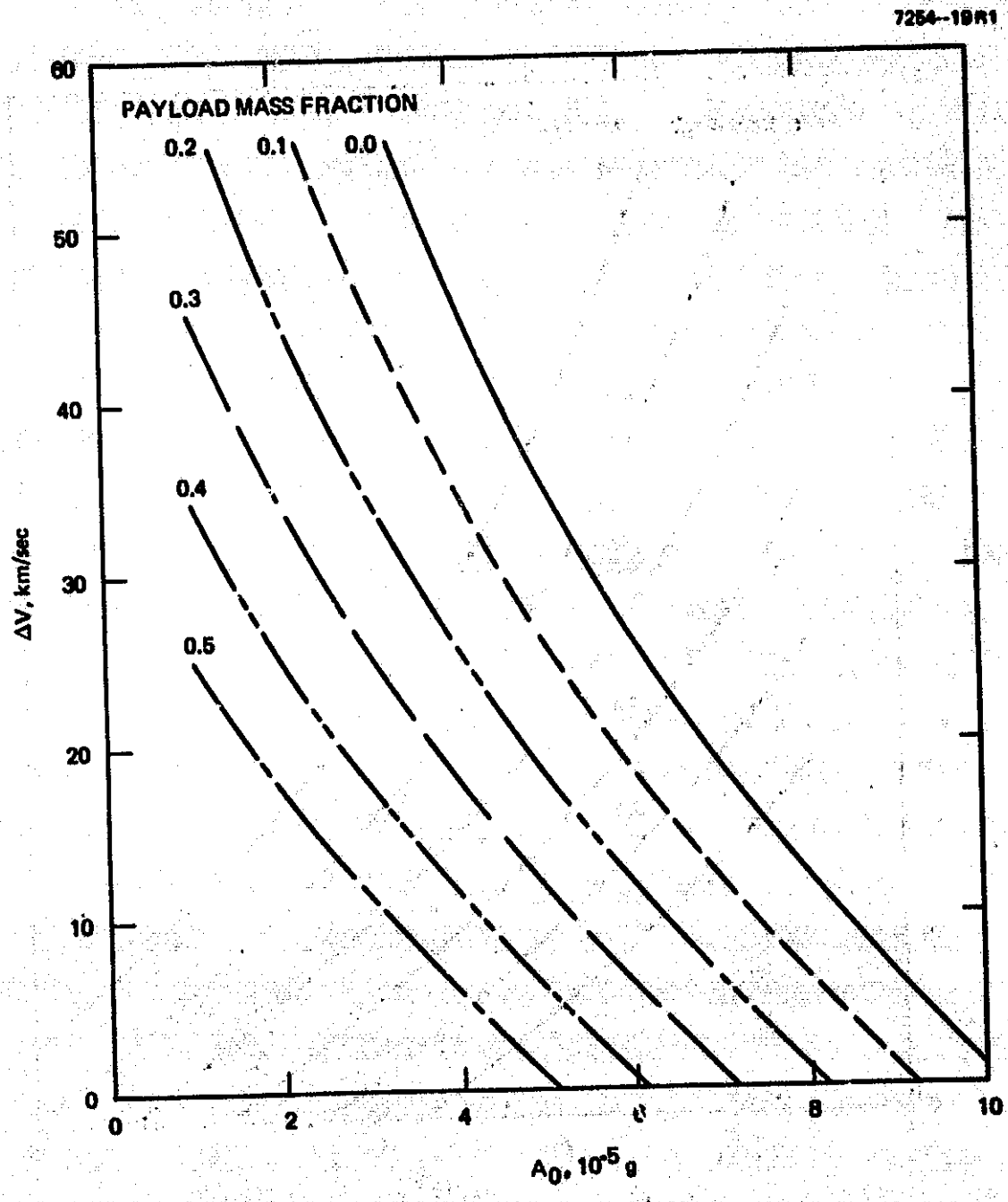

Figure 3-15. ΔV vs A_o format; modified EMT (4 A), present power technology, 5000 sec I_{sp}.

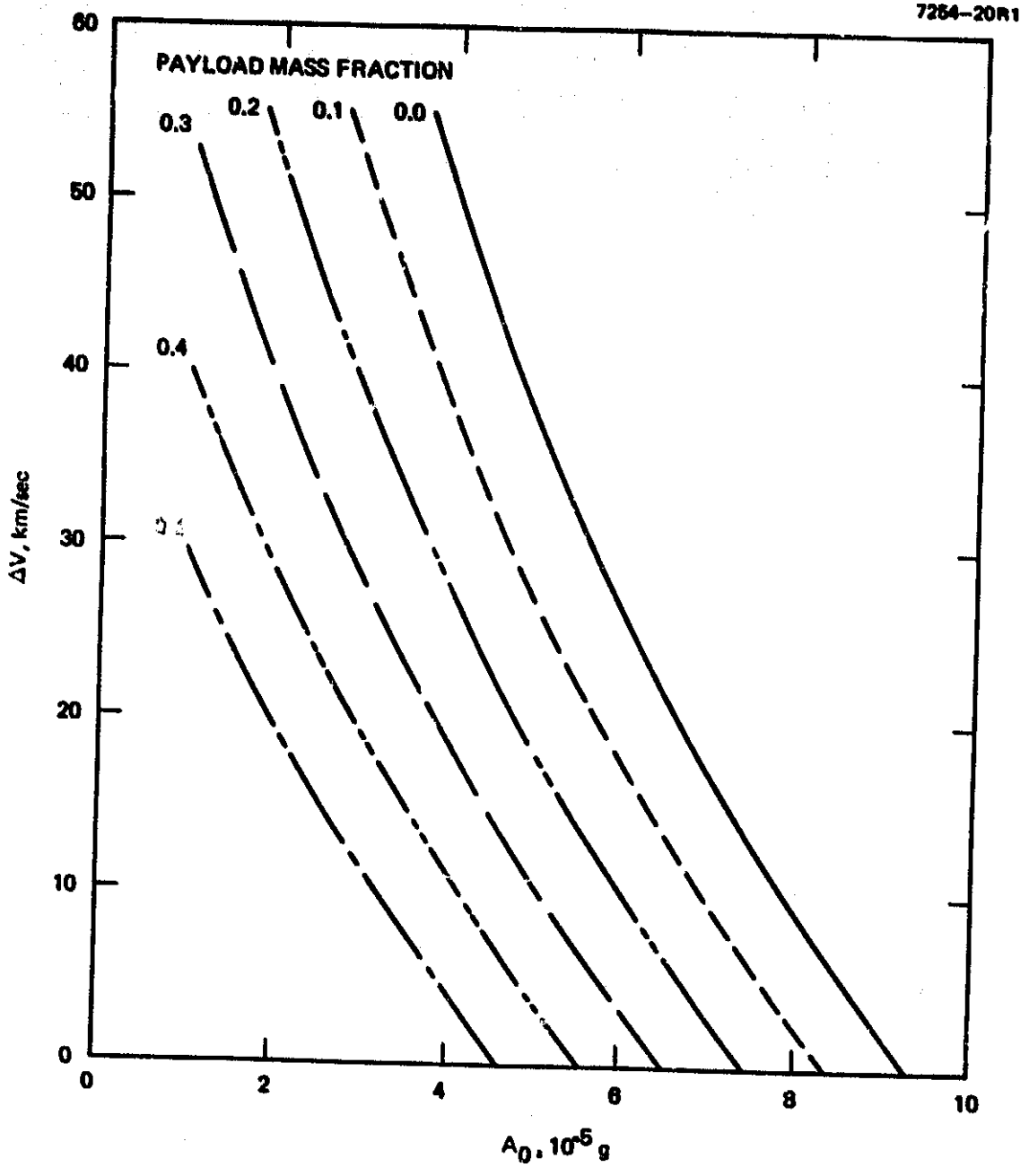

Figure 3-16. ΔV vs A_o format; modified EMT (4 A), present power technology, 6000 sec I_{sp}.

thruster operating characteristics) can deliver a characteristic MF. This MF must be greater than MFR if the propulsion system is to deliver an adequate payload.

Figure 3-12 presents the generalized performance of the existing hardware (EMT); Figures 3-13 through 3-16 present the results for present power technology and a modified EMT (4 A) with a range of specific impulse (3000 to 6000 sec). A comparison of Figure 3-13 with 3-16 shows that the higher I_{sp} can capture more missions (MF) for low A_o and high ΔV but has a low capability for high A_o and low ΔV.

a. Outer Planets

Missions to the outer planets are depicted in Figure 3-17, which is Figure 3-12 replotted with the mission requirements superimposed. The small elliptical area bounds the range of accelerations and velocities in Table 3-3 for the outer planet missions. Also shown is a line representing the largest MFR in Table 3-3 (0.47 for the Titan orbiter). Obviously, since the EMT can deliver the largest MF, it can also perform the remaining outer planet mission. Another piece of information in Figure 3-17 is the number of thrusters required for thrust and redundancy. Thruster wearout does not occur because of the short mission equivalent thrust time (EMT life was assumed to be 20,000 A-hr).

b. Mercury Orbiter

The results of the detailed trajectory studies of the Mercury orbiter mission are shown in Figure 3-18. The areas indicated on the curves are the different trajectory classes investigated: low launch energy with high propulsion system power requirements (MF = 0.26) and high launch energy with low propulsion power requirements (MF = 0.39). The EMT with existing hardware and a moderate number of thrusters calculated from actual trajectory runs easily meets the requirements of both classes of trajectories.

The generalized plots in Figures 3-12 and 3-17 include the assumption that wearout occurs for the mission thrust duration at 2 A. The Mercury orbiter is one of the few missions that has a thrust duration longer

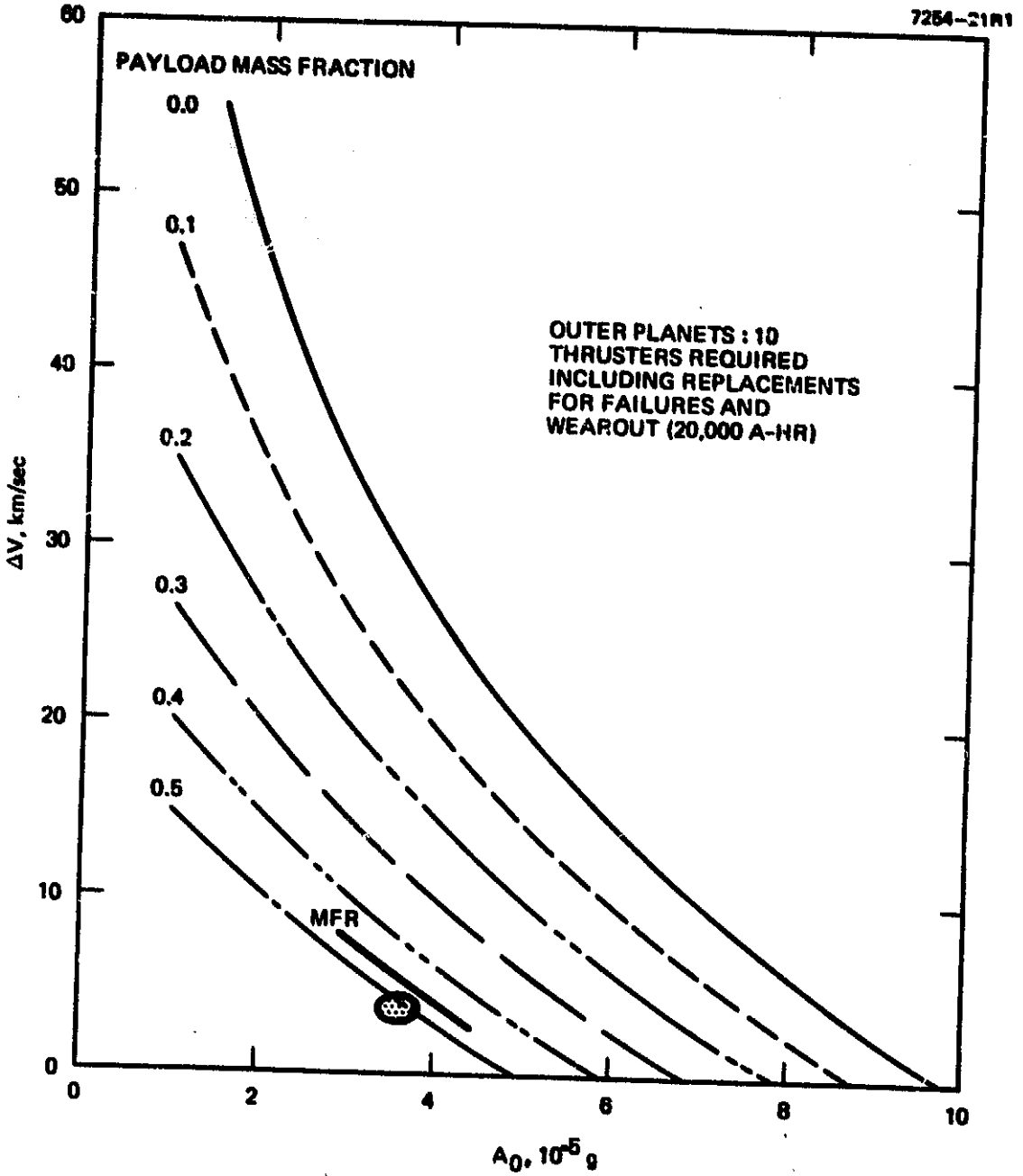

Figure 3-17. Outer planets mission results; EMT, existing power subsystems.

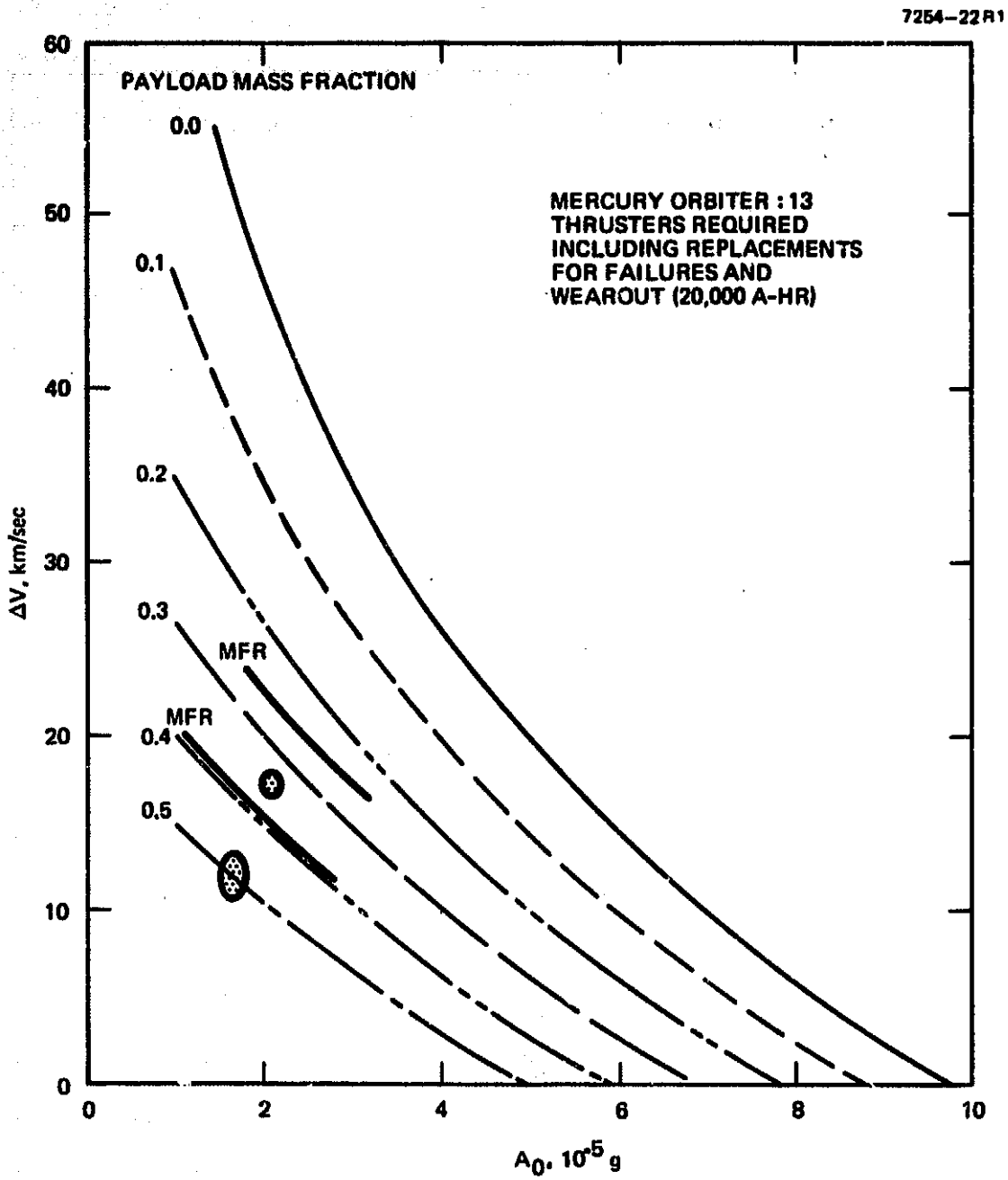

Figure 3-18. Mercury orbiter mission results; EMT, existing power subsystems.

than 20,000 A-hr. Its equivalent thrust time is 16,000 hr (32,000 A-hr). Thus, four thrusters were included in the maximum of 13 required for the high-power case to compensate for wearout (assuming a 20,000 A-hr lifetime). The HAC trajectory studies of the mercury orbiter included thermal constraints which kept the thrust attitude 90° from the sunline.

c. Close Solar Probe

The close solar probe (0.1 AU) was also analyzed using HAC trajectory programs with conservative MFs (Table 3-3). As Figure 3-19 shows, the EMT adequately performs this mission with a moderate number of thrusters using existing hardware. This mission has a relatively long equivalent thrust time compared to other missions, but it is still only 10,400 hr, which is just slightly more than the assumed 20,000 A-hr lifetime of the EMT. The HAC trajectory studies again included thermal constraints that kept thrust attitude 90° from the sunline.

d. Earth Observatory

Figure 3-20 shows that the conservative payload mass fraction (0.37) required for the Earth observatory mission could be easily accomplished with existing hardware, but the number of thrusters might be too large for the Shuttle bay. To decrease the number of thrusters, present power technology could be used with a modification of the beam current. For example, if beam current were increased to 4 A, a reasonable number of thrusters for the very large payload results (as shown in Figure 3-21). Increasing the beam current also increases the already adequate payload. More performance and a further decrease in the number of thrusters could be achieved by raising I_{sp}, but this is not required to perform the Earth observatory mission. In addition, advanced power system technology is not required to perform this mission.

e. Comet Encke Missions

The comet Encke slow flyby missions are depicted by the shaded areas indicated in Figure 3-22 (see Table 3-3). Existing hardware is

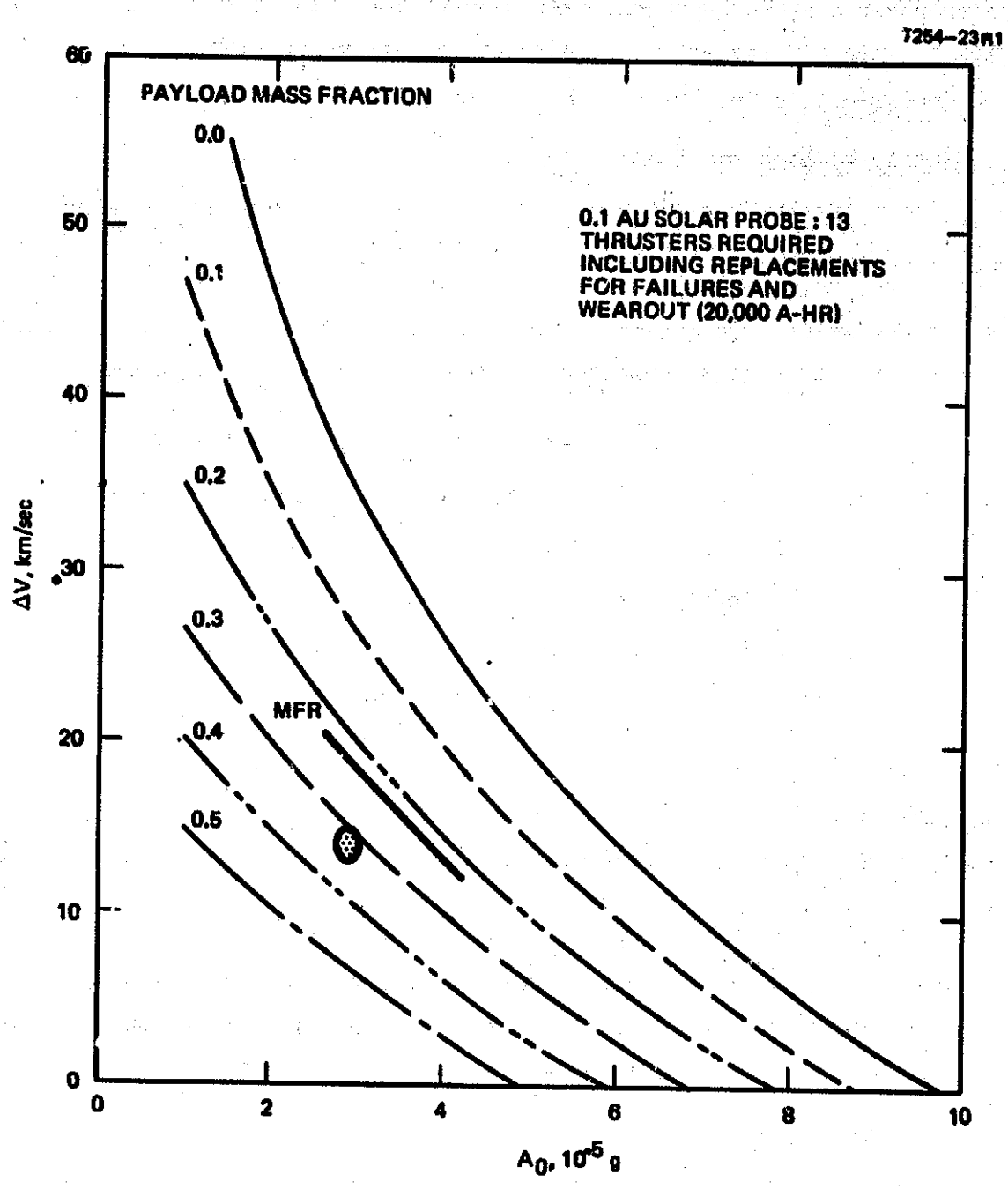

Figure 3-19. Close solar probe (0.1 AU) mission results; EMT, existing power subsystems.

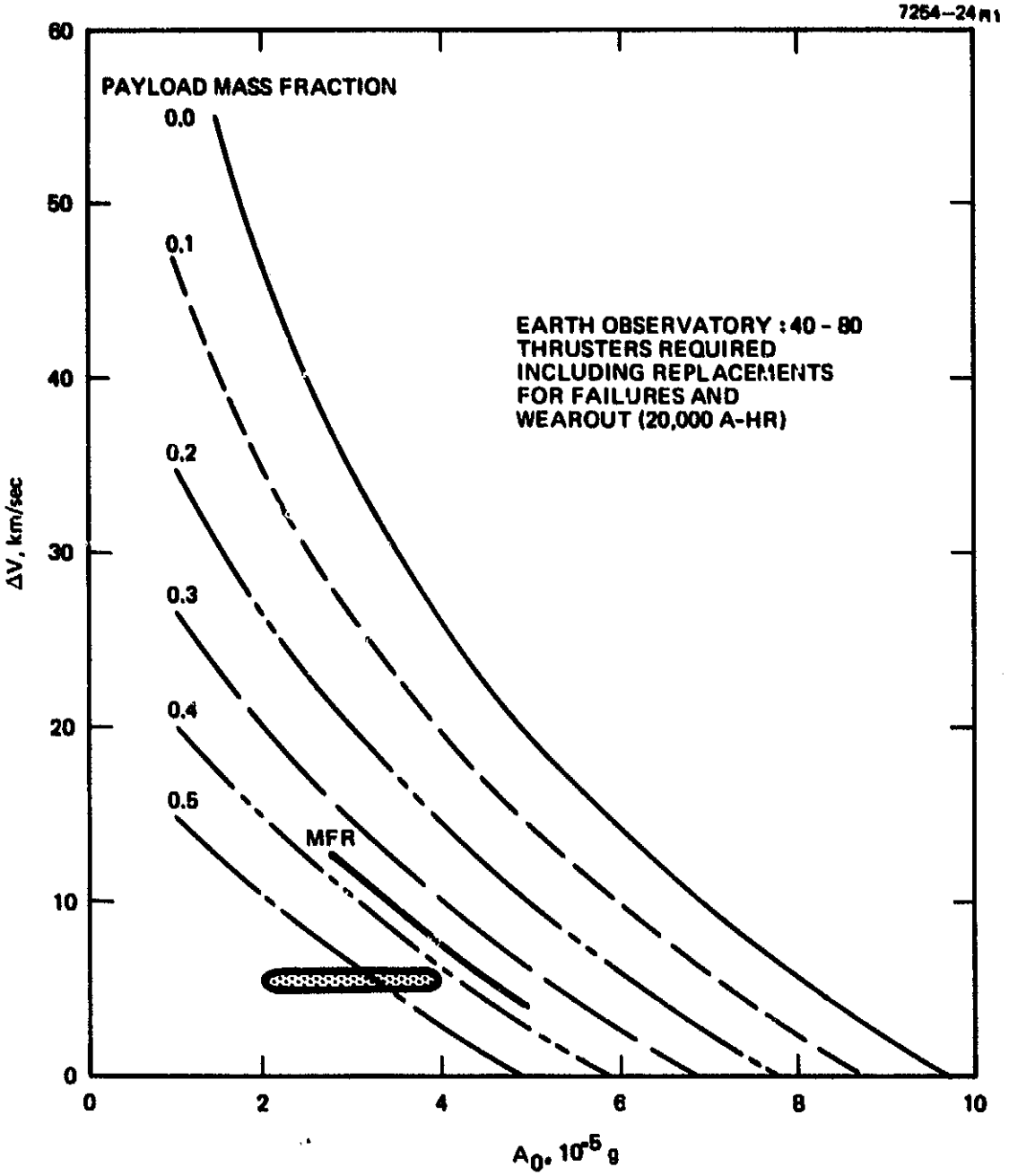

Figure 3-20. Earth observatory mission results; EMT, existing power subsystems.

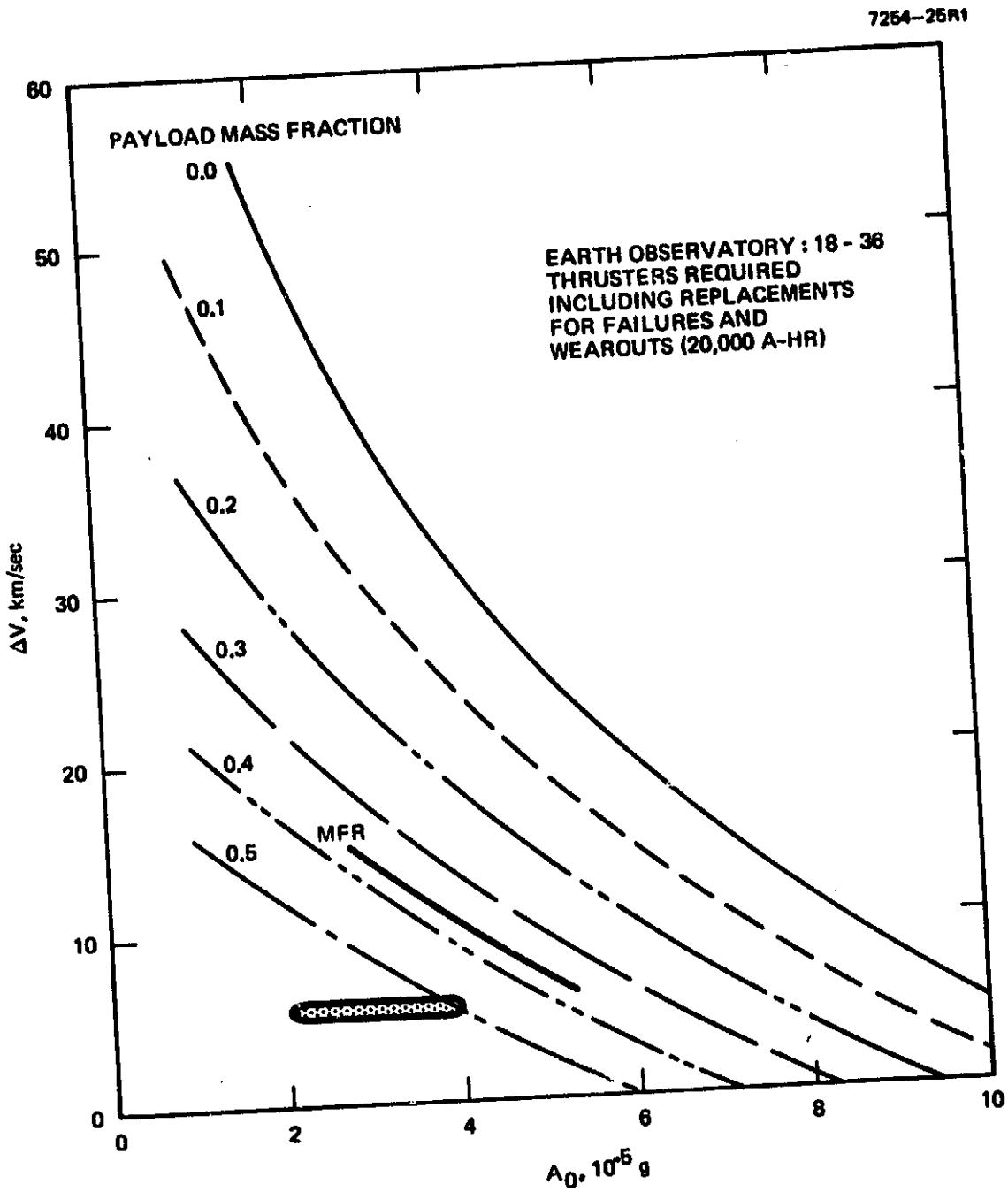

Figure 3-21. Earth observatory mission results; modified EMT (4 A, 3000 sec), present power technology.

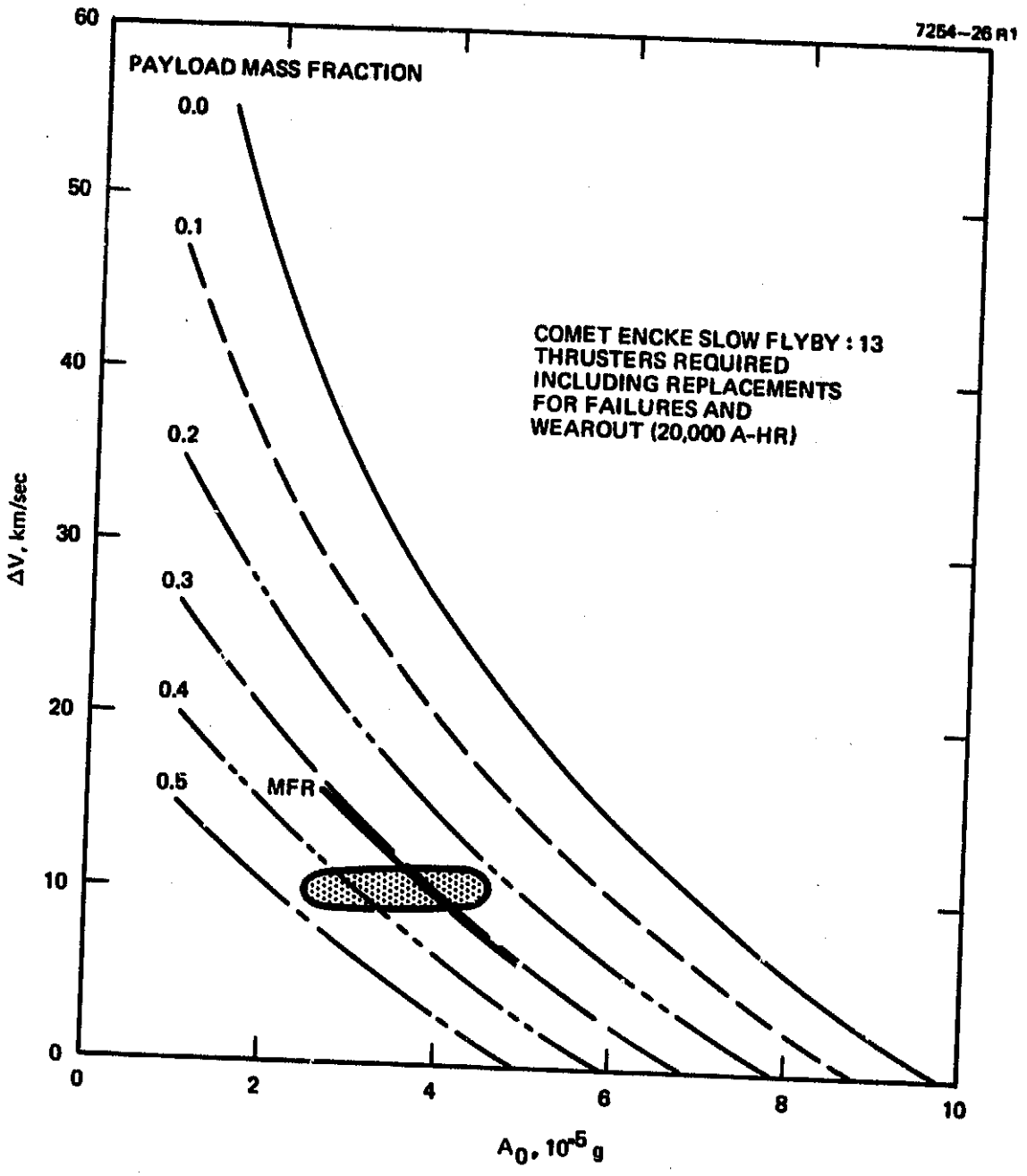

Figure 3-22. Comet Encke slow flyby mission results; EMT, existing power subsystems.

not adequate to perform all missions but, as Figure 3-23 shows, all proposed Comet Encke slow flyby missions can be performed with adequate payload, using a small number of thrusters and a modified EMT.

Similar results hold for the comet Encke rendezvous missions, as shown in Figures 3-24 and 3-25. Modifying the EMT to operate with a 4-A beam current with present power technology yields an adequate payload MF.

f. Asteroid Rendezvous

The asteroid rendezvous mission requirements for Eros, Metis, and Ceres are plotted in Figure 3-26 from the data in Table 3-3 using the conservative payload of 635 kg. The existing hardware (EMT) easily meets the payload requirements. The 17 thrusters required is a reasonable bound for the most conservative payload and acceleration but can be decreased, if desired, by increasing beam current.

g. Asteroid Sample Return

The asteroid sample return (Eros), with its somewhat higher payload and velocity requirements may need a modified thruster to obtain additional performance depending on launch opportunity (as indicated in Figures 3-27 and 3-28). Changing the beam current to 4 A provides this extra performance with present power technology.

h. Out of Ecliptic

Figure 3-29 depicts the performance for the existing hardware from the HAC trajectory runs as a function of the out-of-ecliptic inclination angle. Existing hardware can provide up to 50° with a payload mass fraction of 0.1. Raising the beam current to 4 A increases maximum inclination to about 60°. In addition to using a 4 A thruster, it is necessary to increase I_{sp} to obtain a 90° inclination because the very high velocity requirements for 90° inclination can only be met by reducing propellant mass. Trajectory results for a 6000-sec I_{sp} are given in Figure 3-30. If 90° inclination is required, then I_{sp} and cost will be higher.

Out of ecliptic missions can also have very long equivalent thrust times. Acceleration increases as propellant is consumed, but the average time is about 11,000 hr for each 30° of inclination. Thus, the

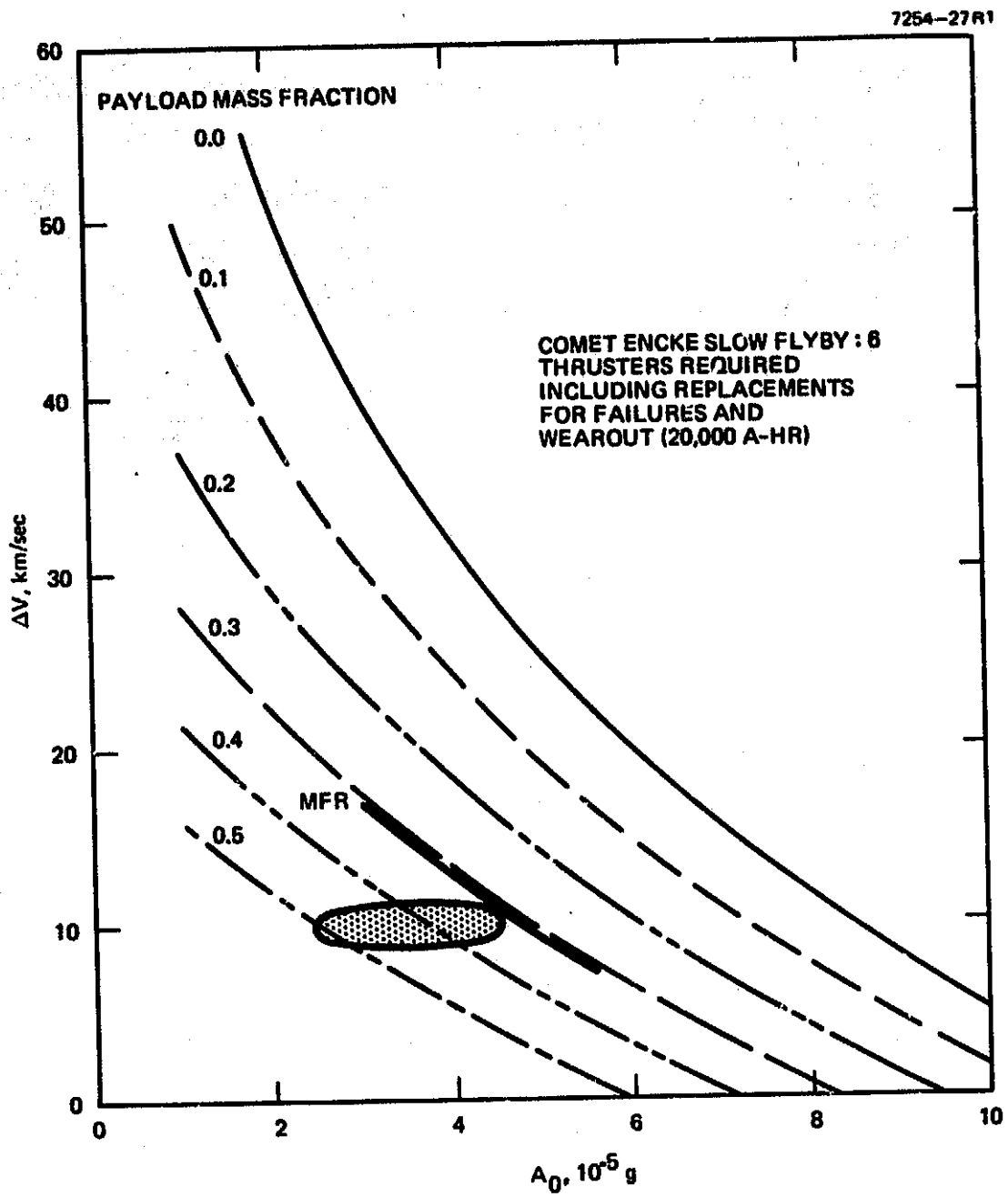

Figure 3-23. Comet Encke slow flyby mission results; modified EMT (4 A, 3000 sec), present power technology.

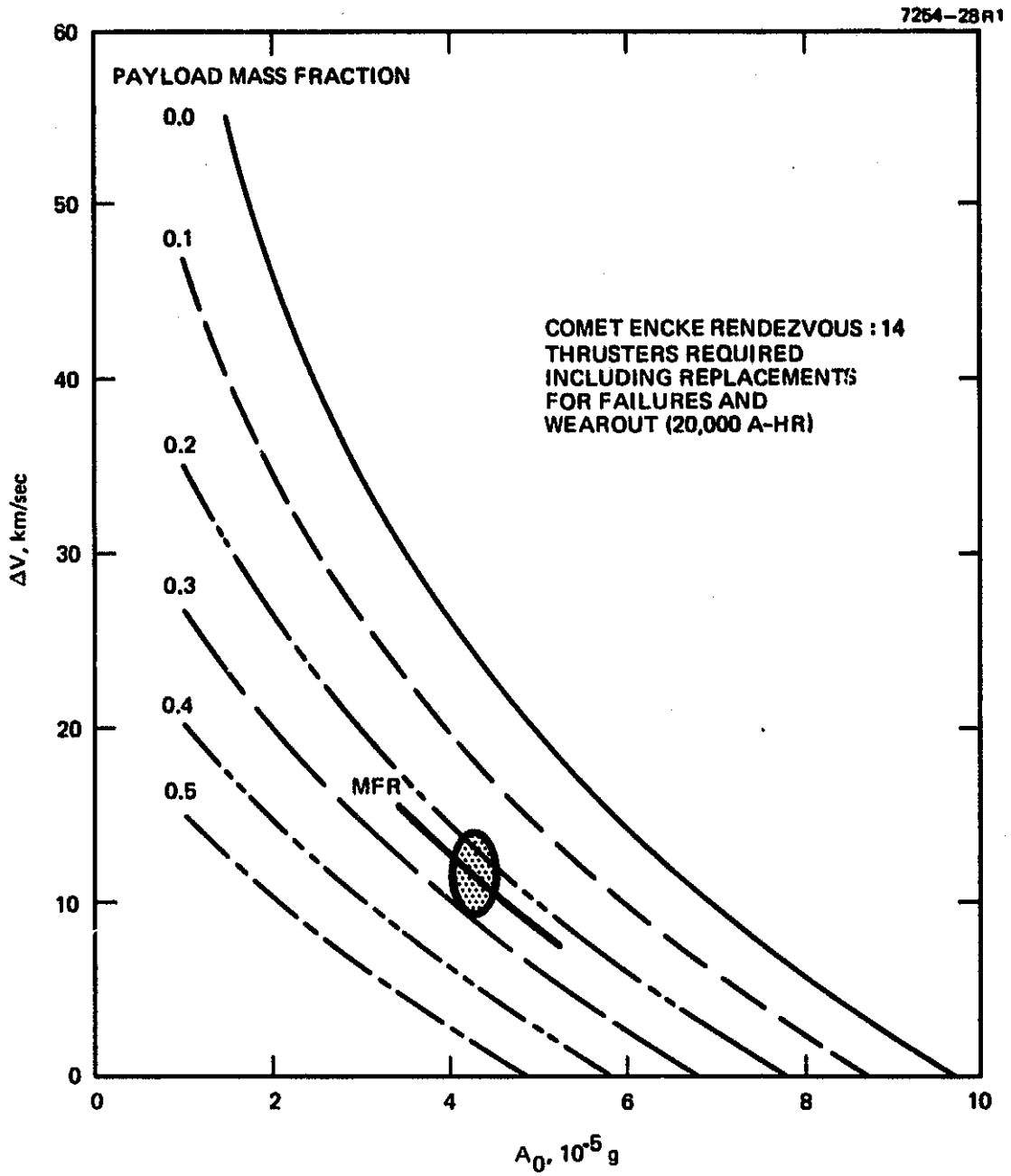

Figure 3-24. Comet Encke rendezvous mission results; EMT, existing power subsystems.

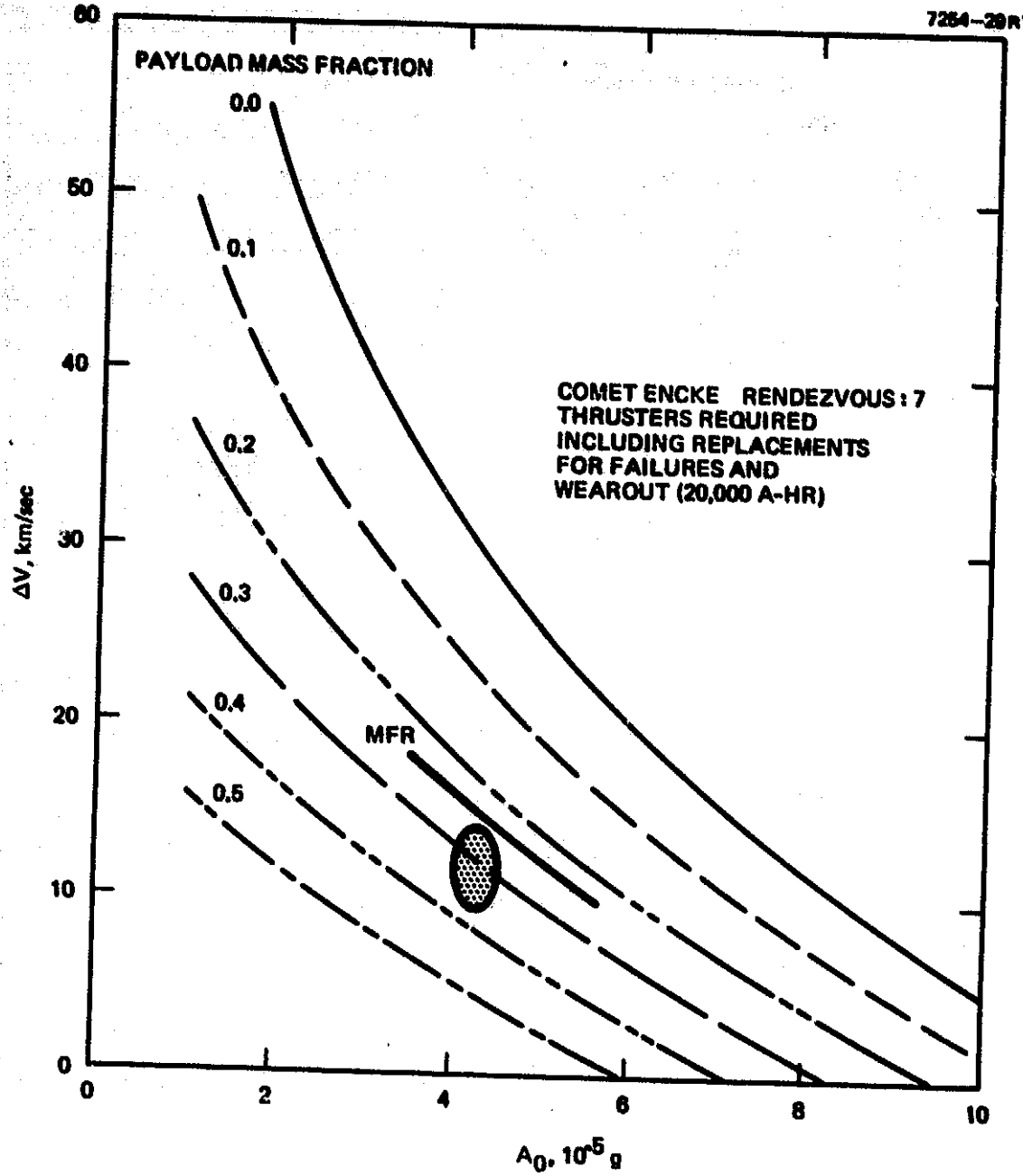

Figure 3-25. Comet Encke rendezvous mission results; modified EMT (4 A, 3000 sec), present power technology.

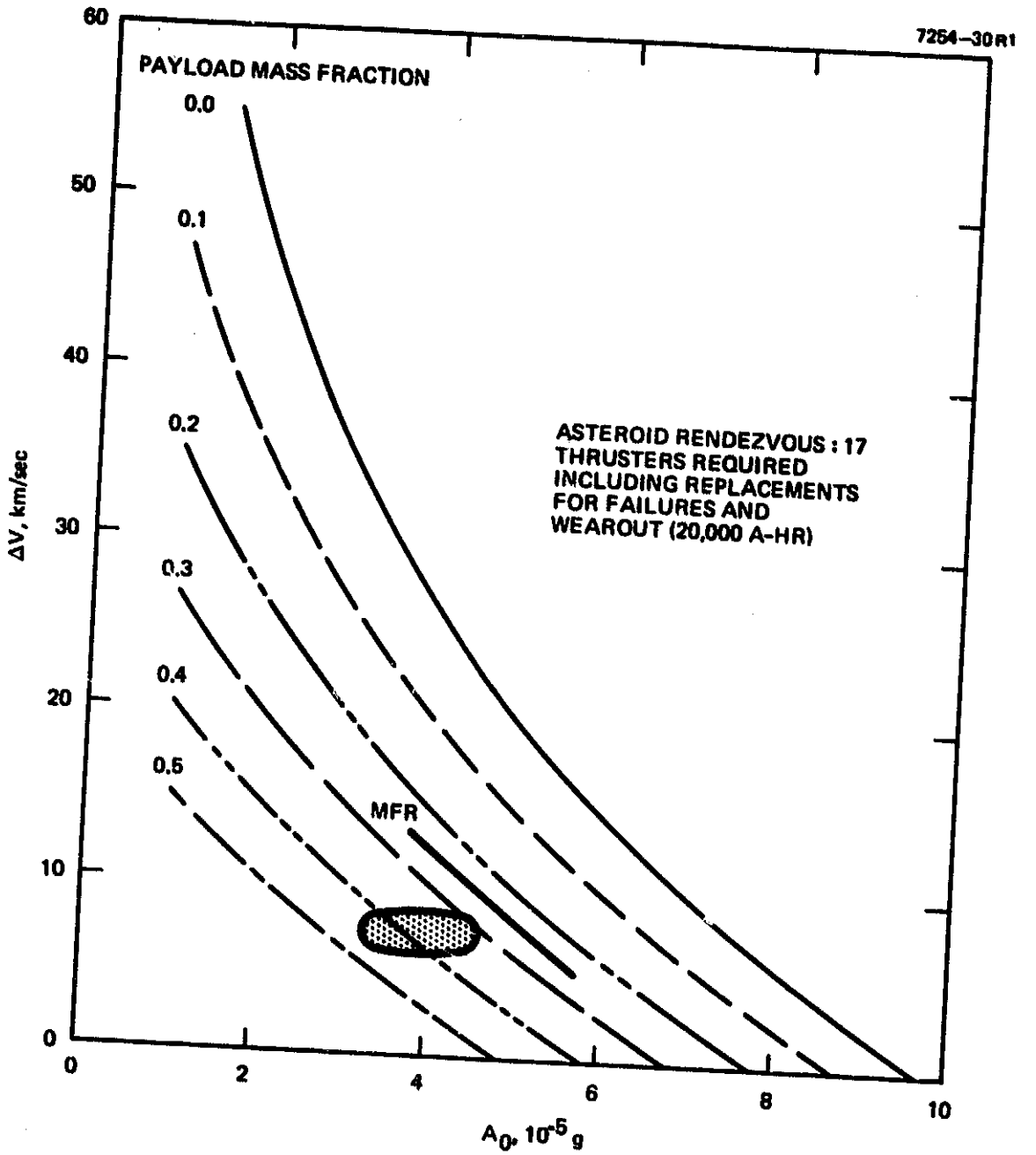

Figure 3-26. Asteroid rendezvous mission results; EMT, existing power subsystems.

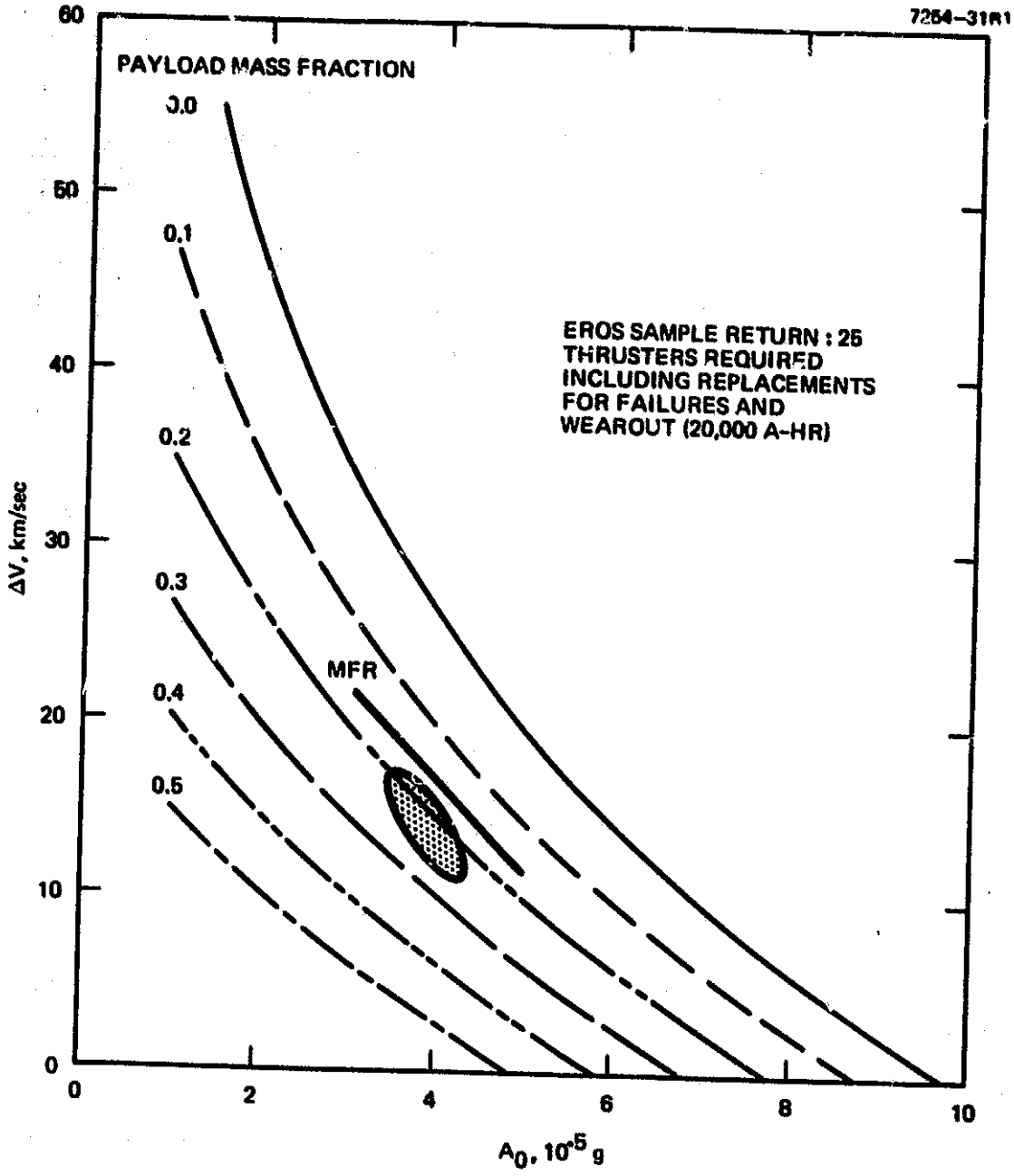

Figure 3-27. EROS sample return mission results; EMT, existing power subsystems.

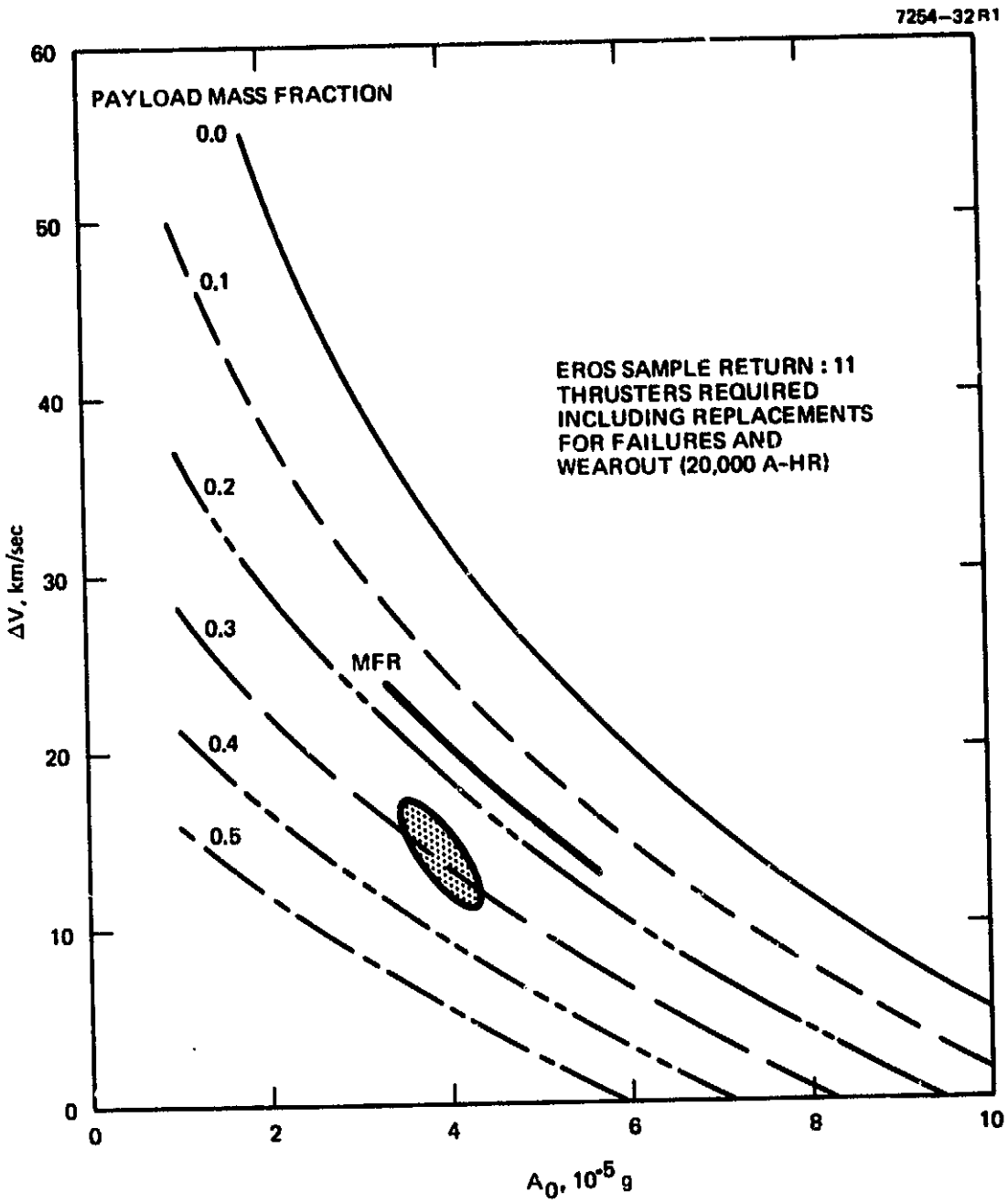

Figure 3-28. EROS sample return mission results; modified EMT, present power technology.

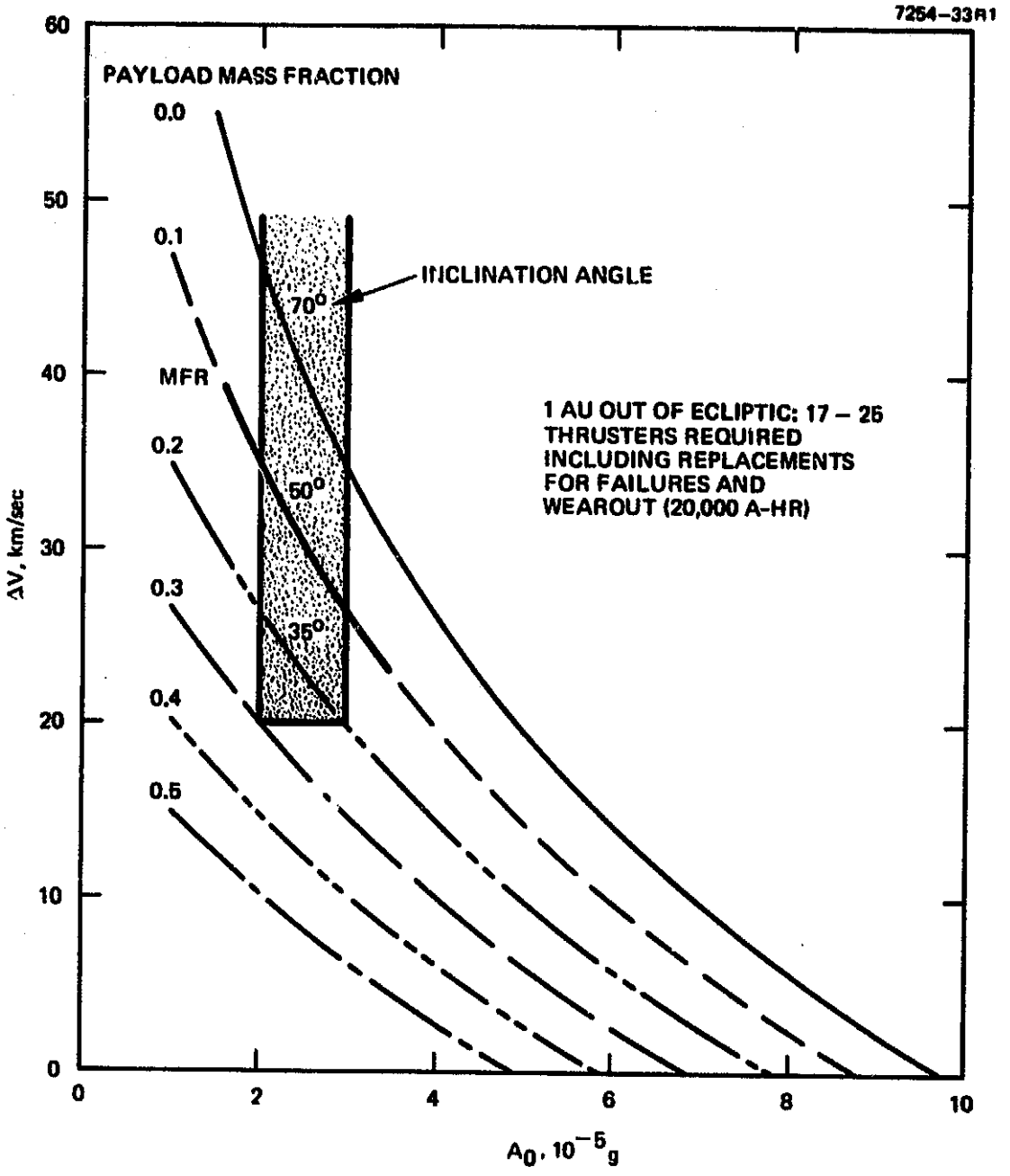

Figure 3-29. 1 AU out-of-the-ecliptic mission results; EMT, existing power subsystems.

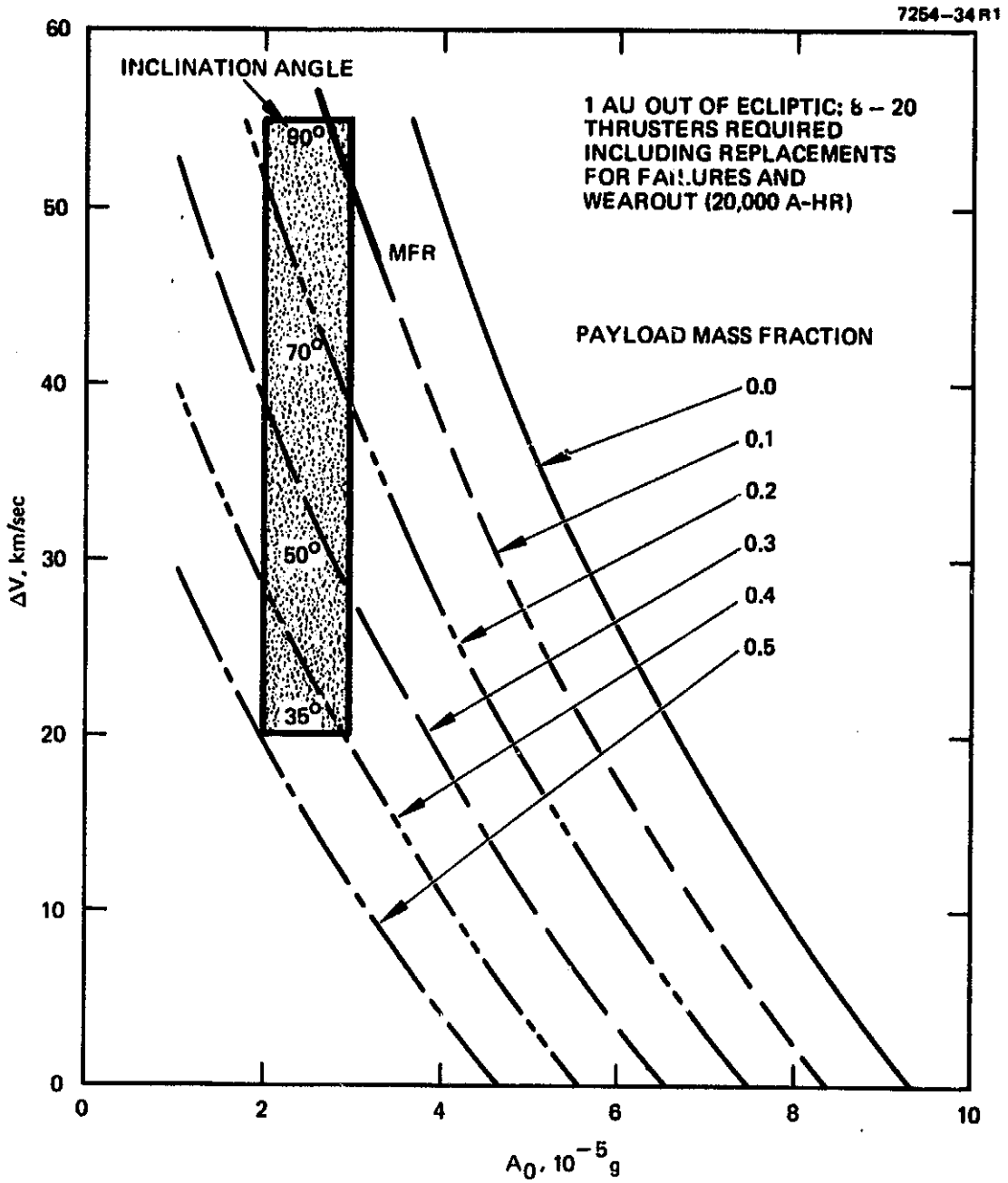

Figure 3-30. 1 AU out-of-the-ecliptic mission results; modified EMT, (4 A, 6000 sec) present power technology.

thrusters required (in Figures 3-29 and 3-30) are mainly for wearout replacement. In fact, the modified EMT (4 A, 3000 sec) requires only four operating thrusters to provide the highest acceleration. Thus, for the highest inclination case (90°), eight thrusters are required for wearout and another eight for failure for the conservative payload and maximum acceleration. The equivalent thrust time compensation provided in the propulsion system assumed in Figure 3-30 results in an increased mass fraction of less than 0.05 for the 6040 kg injected mass in this worst case.

3. Conclusions from the Generalized Analysis

In summary, the EMT can perform a large fraction of the missions analyzed. Development of a thruster (modified EMT) capable of 4-A or higher beam current at 3000-sec specific impulse will provide the capability to perform all the missions considered, with the possible exception of the out-of-ecliptic mission. Increasing I_{sp} is generally good from a performance viewpoint because it improves the payload and reduces the number of thrusters required, but it could increase mission cost because of higher power. Similarly, the 90° out of ecliptic mission can be accomplished with present power technology (solar array and PPU) by increasing specific impulse. Advanced lightweight power technology would improve performance, but it is not required to perform any of these missions and may not be economically justifiable.

This analysis did not consider Earth orbit missions involving large space systems. This subject is discussed in Section 4. In addition, the generalized analysis did not consider other thruster sizes since the existing EMT or a modified EMT could adequately accomplish all the missions considered.

SECTION 4

COST MODELING FOR EARTH ORBIT MISSIONS

The generalized analysis approach, discussed in Section 2, is an efficient means for assessing the first-order impact of various missions on thruster technology. However, the generalized approach omits cost, which, under certain circumstances, may be decisive in the use of EP. Although cost is an important factor in planetary and small body missions, for these the use of EP will probably rest on the tradeoff of mission risk against technical advantage, with cost as a secondary factor.

With new large space systems, for which most elements will have limited bases for assessing reliability/risk, EP will be judged largely on its merits as a cost-effective propulsion system. This section describes cost models developed for several Earth orbit missions to indicate where ion thruster technology would best satisfy selected cost-effectiveness criteria. In general, the goal is the technology that would produce the lowest mission cost consistent with the reality of developing such technology. In other words, from a mission standpoint, the goal is to determine the thruster (and possibly other) parameters that would minimize mission cost, and then, through an understanding of technology limits, recommend a direction that has a reasonable probability of success.

Two general types of Earth orbit missions were considered: (1) orbit raising (transportation) of large masses from low (altitude) Earth orbit (LEO) to higher altitude orbit and (2) stationkeeping and attitude control of large masses in Earth orbit. Details of the assumed missions are discussed in "mission description" sections. The computer models developed are presented in the "general model" sections, which include descriptions of the mission analysis portions of the models. Propulsion system performance models, which apply to both types of missions, are discussed in the orbit raising mission section. Similarly, power source degradation and redundancy models, which also apply to both types of missions, are discussed in a single section. Mass and

cost models are discussed separately for each type of mission because the models and terminology vary somewhat. Results of each model are grouped into two categories: (1) baseline results using model parameter values selected as being reasonable compromises between 1977 technology and future technology and (2) sensitivity results obtained by varying each major parameter over a wide range of values. Certain combination sensitivities, obtained by varying two or more parameters, are also presented in the latter category.

The basic graphical format presents cost as a function of specific impulse. This format was selected because I_{sp} is one of the most fundamental parameters in thruster technology. For orbit raising missions, the cost scale is in terms of cost per unit mass of net payload delivered to the destination (i.e., $/kg of payload). For on-orbit missions, the cost scale is in terms of cost per unit mass of net satellite maintained on orbit per year ($/kg/yr). Other plots are also presented to aid in understanding the results and the various relationships.

A. ORBIT RAISING (TRANSPORTATION) MISSIONS

To carry out the economics analysis with the cost modeling program described in this section, a relatively large number of assumptions and detailed models were required. The orbit raising mission work was generally oriented toward the transportation of masses from LEO to GEO. However, this particular transfer is only representative, and other transfers can be simply handled by the model through the specification of ΔV. To further clarify assumptions, two baselines were considered: (1) matured Shuttle era and (2) large space systems era. Such a distinction was made to identify differences in thruster technology requirements that might result from different launch vehicle sizes and levels of activity in space. For instance, the matured Shuttle era baseline assumes a payload size of 25,000 kg, a launch cost to LEO of $300/kg, solar power cost of $100/W, and a solar power specific mass of 6 kg/kW. The magnitude of these factors significantly influences the results of the cost analysis.

For the large space systems baseline, it is assumed that the applications being considered are in the area of highly expanded use of space, the masses of interest are larger than those of current-day satellites, launch costs are lower, and power sources are lighter and cheaper. Specifically, masses in the range of 10^4 to 10^7 kg are considered. Such masses would be delivered to LEO by new launch vehicles (e.g., a heavy lift launch vehicle) at relatively low cost ($10 to 50/kg).[18-21] Power sources are projected to weigh 3 kg/kW at a cost of $0.5/W. Other differences in these two baselines are discussed in conjunction with the results.

Once in LEO, the payload must be placed in another orbit. An electrostatic ion propulsion system, using a solar source, transports the mass to the specified orbit. Except for characterizing this transfer by ΔV, the details of the transfer were not considered in this study. Clearly, many factors must be considered in designing such a transfer from LEO (e.g., occultation, attitude control, solar array orientation and vehicle maneuvers). However, the impact of most of these factors on propulsion system design is through ΔV. The mission options considered (such as one-way or round trips) are discussed in Section 4.A.1.

For the orbit raising mission, the propulsion system is part of an orbit raising vehicle (ORV), shown schematically in Figure 4-1, which contains the subsystems (e.g., computers, data handling, communications) necessary to operate with only limited ground interfacing. Models of the various elements of the ORV used in this study are described in Sections 4.A.6 and 4.A.7. As mentioned earlier, the analysis of the sensitivity of the cost results to the various models was a significant part of the work.

1. Mission Descriptions

The three types of orbit raising missions considered are shown schematically in Figure 4-2; they include:

- Self-powered round trip — ORV contains the power source to supply the necessary propulsion power. On the "down trip," the full power is used. Power source mass and cost are charged to the ORV.

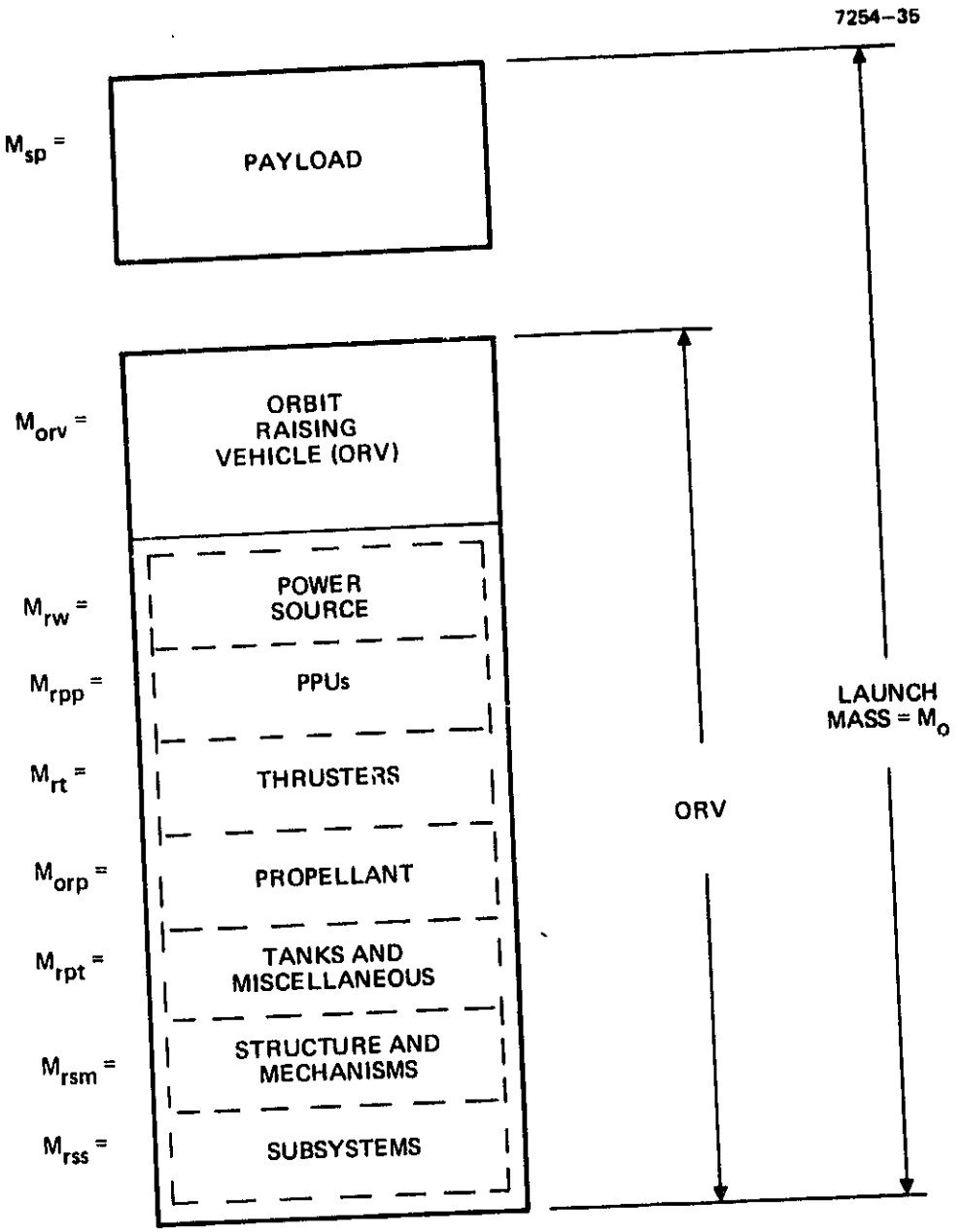

Figure 4-1. ORV block diagram.

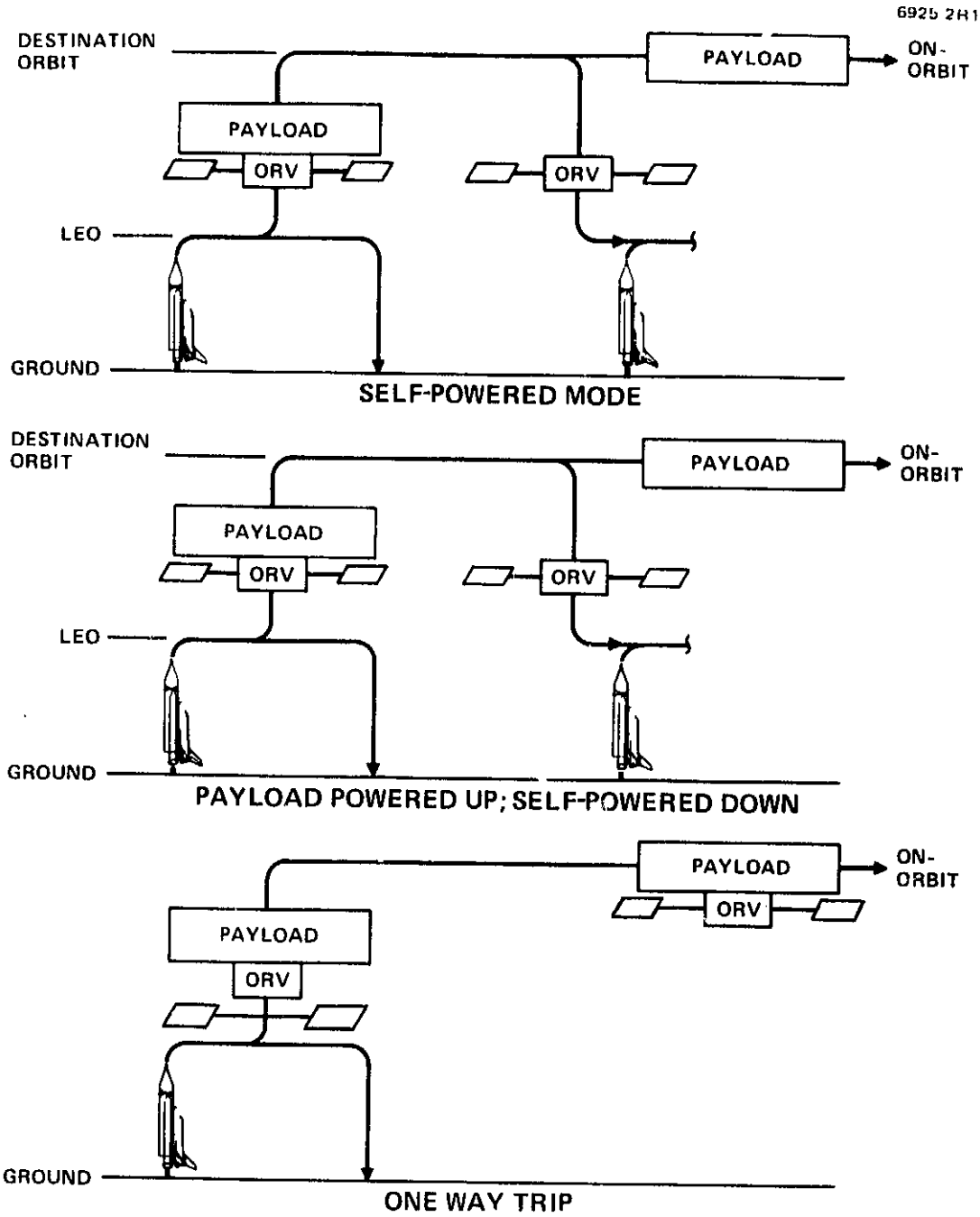

Figure 4-2. Orbit raising mission scenarios.

- Payload powered up; self-powered down — payload is, or contains, a power source capable of supplying the propulsion power during the up trip. On the down trip, the ORV provides its own power. Up trip power source mass and/or cost may be charged to payload.

- One-way trip (up) — ORV contains the power source, but stays with the payload on-orbit.

Although many other mission options can be defined, these three should be representative of a wide range of mission requirements.

a. Self-Powered Mode

In this mode, the ORV may make a given number of round trips from LEO to a destination orbit (defined by ΔV) consistent with the specified ORV life. Propulsion power for both the up and down trips is provided by the ORV, and the power source mass and cost are charged against the ORV. The number of thrusters required per trip is based on the number operating, wearout rate, and redundancy for random failures.

Assuming that the use of the ORV for a given transfer is paid for by a "user," the fraction of the worn out thrusters must be taken into account. This is done by subtracting from the cost to the user the fraction of unused thruster life and adding the cost for refurbishment. In this way, each user effectively only pays for the fraction of the ORV worn out. This approach also eliminates the need to transport a large number of spare thrusters through many round trips before they are needed. In addition, propellant for only one round trip is carried for the same reason. More specific details of this mode are discussed in the "general model" section.

b. Payload Powered Up-Trip; Self-Powered Down-Trip Mode

Since the ORV mass is generally only a fraction of the payload mass, and down-trip time may be less critical than up-trip time, significantly less power may be needed for the down-trip. In addition, many future payloads may contain large power sources that could be used on the up-trip. For such missions, the cost charged to a user might be reduced since a smaller power source would be paid for as part of the transportation cost, and the net payload delivered on-orbit is increased.

c. One-Way Trip (Up)

In certain cases, it might be advantageous to leave the ORV with the payload on orbit. For this assumed mode, the power source is charged to the ORV. The cost results will be conservative if the payload can make use of this power on orbit. Propellant is sized only for the up-trip, and operation of the ORV on orbit would require using part of the payload for propellant.

2. General Model: Orbit Raising

A logic diagram for the orbit-raising cost model program is shown in Figure 4-3. This diagram correctly indicates the functional form of the program, but does not necessarily correspond identically with the computer program listing. Efficient coding and the many details not shown in this general diagram introduce format variations. A typical program listing and a discussion of the listing are included in Appendix C.

Mission mode selection indicated in Figure 4-3 is actually accomplished by selecting a few parameters within the program (see the listing discussion in Appendix C). For a given set of mission variables, the mission computations are started. Propellant mass is obtained from the rocket equation (see Eqs. 3-1 and 3-2). Although this equation is not strictly accurate for low-thrust propulsion, conservatism in selecting ΔV tends to compensate.

Propellant mass can be related to ion beam "jet power" as follows. The ion beam energy is

$$eV_b = E_j = \frac{1}{2} m_i v_i^2 \quad , \tag{4-1}$$

or, in terms of beam power,

$$\dot{E}_j = \frac{1}{2} \dot{m}_i v_i^2 \quad , \tag{4-2}$$

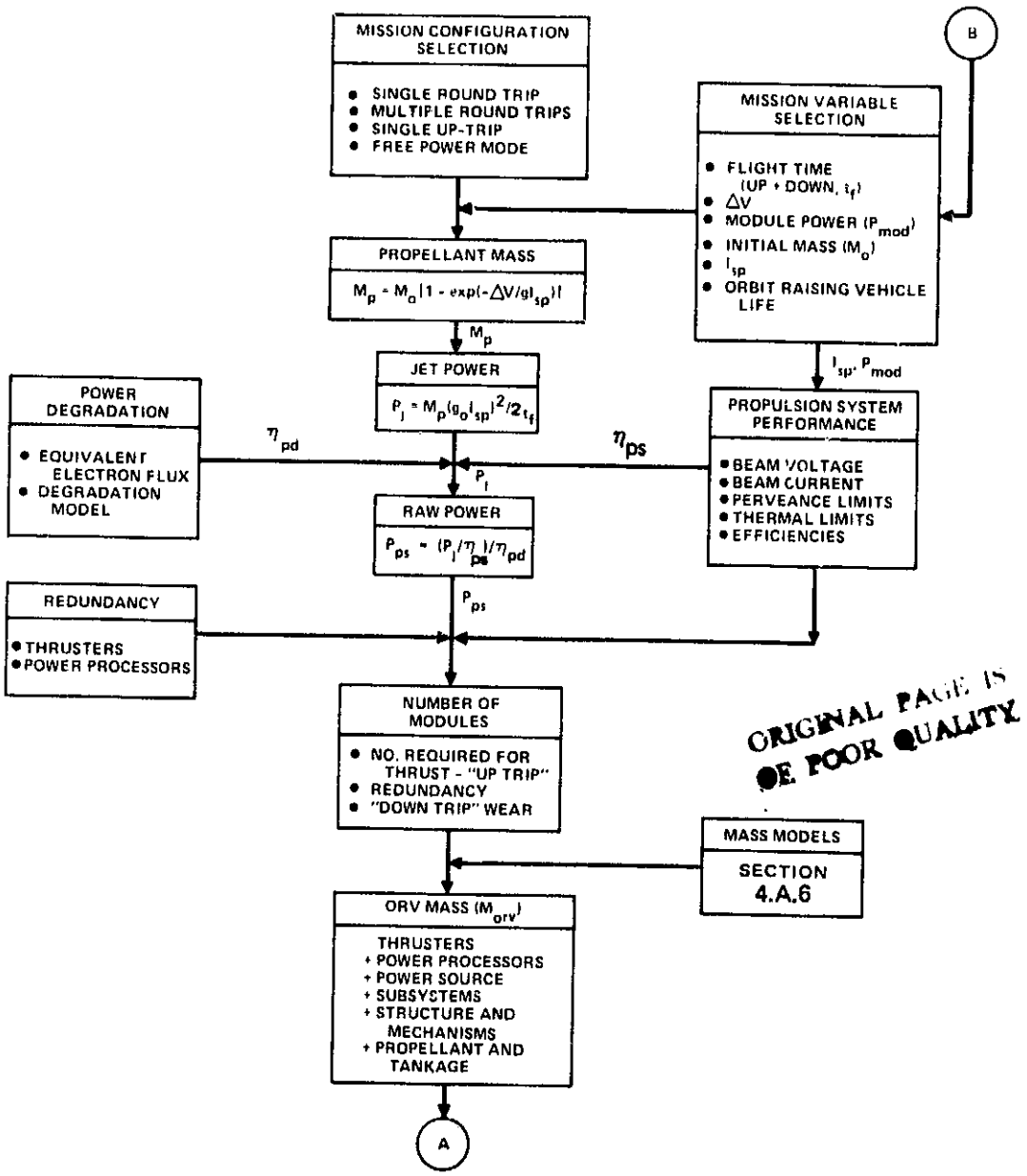

Figure 4-3. Orbit raising cost model logic diagram.

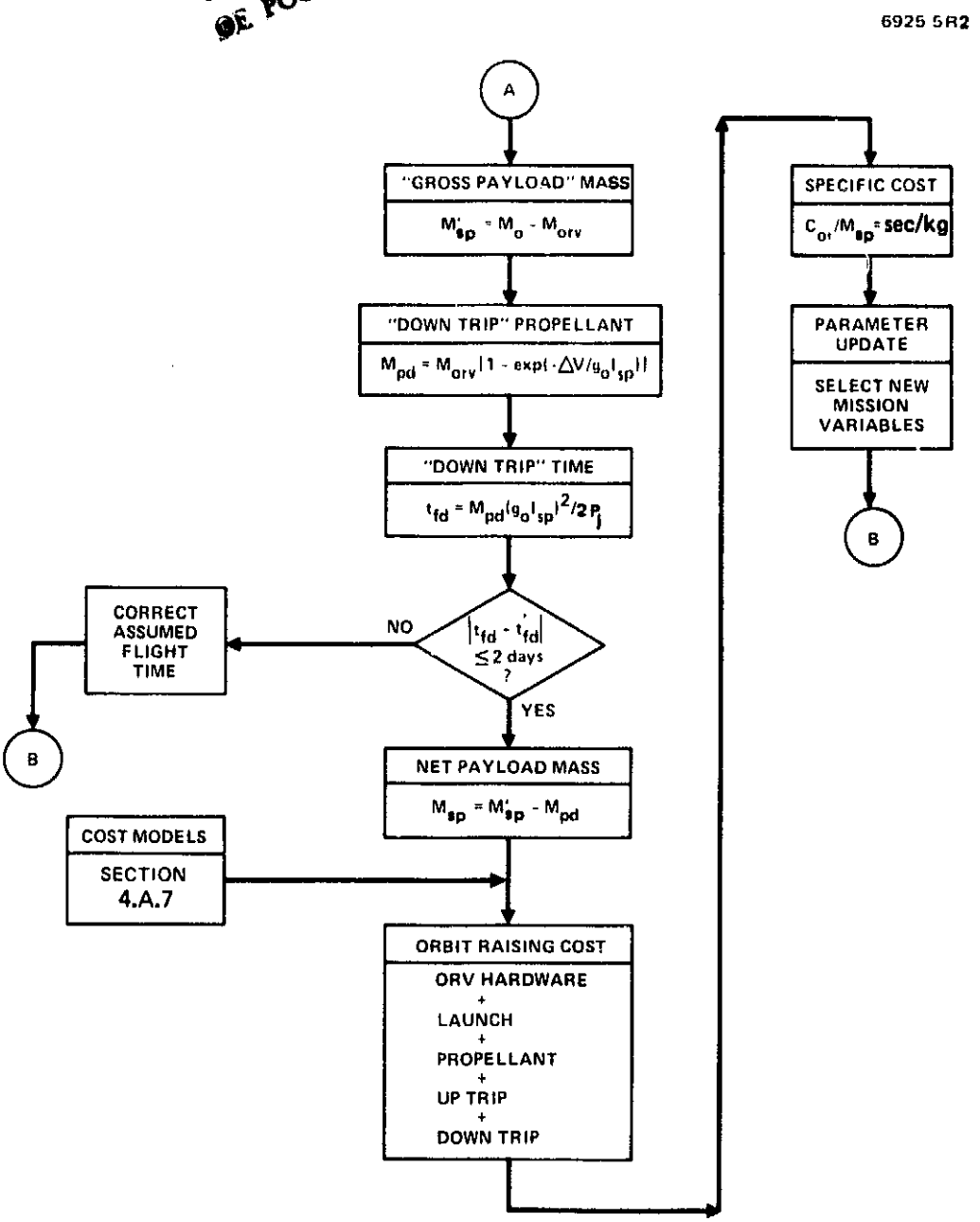

Figure 4-3. Continued.

where

E_j = ion beam kinetic energy

$\dot{E}_j$ = rate derivative of E_j

P_j = total jet power

v_i = ion velocity

m_i = ion mass

$\dot{m}_i$ = total ion flowrate.

Total propellant mass flowrate is related to total ion flowrate by

$$\dot{m}_i = \dot{M}_p \, \eta_u \tag{4-3}$$

$$M_p = \dot{M}_p \, t_f \, , \tag{4-4}$$

where t_f is the flight time appropriate to the mission being considered (self-powered, one-way, etc).

$$v_i = \frac{I_{sp} g_o}{\eta_u \gamma} \, , \tag{4-5}$$

where η_u and γ are as defined in Section 3.A.2. Substituting Eqs. 4-3, 4-4, and 4-5 into 4-2 yields

$$P_j = \frac{M_p \, (I_{sp} g_o)^2}{2 t_f \, (\eta_u \gamma 2)} \, . \tag{4-6}$$

To simplify the jet power computations, the quantity $\eta_u \gamma^2$ was assumed equal to one. This approximation, at this point in the calculation, introduces an error of 5 to 10 percent in P_j. However, since the rocket equation for computing M_p is approximate, ΔV can be adjusted for conservatism, and thruster and PPU redundancy can be adjusted, the approximation will not significantly affect the results. (P_j is used only in computing the number of operating modules; P_j is divided by P_{mod}, where $P_{mod} = I_b V_b$.)

The next step in Figure 4-3 is to calculate total propulsion system input power according to

$$P_{ps} = \frac{M_p (g_o I_{sp})^2}{2 t_f \eta_{ps}} \quad , \tag{4-7}$$

where η_{ps} is as defined in Eq. 3-8. With the use of η_{ps} in Eq. 4-7, the approximation made in computing P_j is not included in P_{ps} since η_{ps} includes $\eta_u \gamma^2$ as well as other efficiencies. Total propulsion system power is used for sizing the solar power source, as explained in Section 4.A.5.

The total number of modules needed for the ORV for one trip includes those operating, redundant modules for random failures, and spares for wearout if required:

$$N_{ot} = N_{mod} \left(\frac{TOTRIP}{L_t}\right) \left(1 + R_t\right) \tag{4-8}$$

$$N_{op} = N_{mod} \quad (1 + R_p) \quad ,$$

where

N_{ot} = total number of thrusters installed in ORV

N_{mod} = P_j/P_{mod} = number of operating thrusters

N_{op} = total number of power processors

P_{mod} = selected module power (beam power)

TOTRIP = selected up-trip time plus down-trip time

R_t = thruster redundancy

R_p = PPU redundancy

L_t = thruster life.

If TOTRIP is $< L_t$, then $TOTRIP/L_t = 1$. PPU life is assumed to be long compared with trip time, and wearout can be neglected. Only enough thrusters are carried to support one round trip. Those used during the mission are assumed to be replaced.

The round-trip models require an iterative procedure such as illustrated in Figure 4-3. Initially, the down-trip time is assumed to be half the up-trip time. Since the down-trip time depends on the down propellant, which is not known until M_{orv} is found, the calculations proceed until the correct down-trip times are found (typically three iterations). The net payload is obtained by subtracting the down propellant as indicated in Figure 4-3. Mass models used to define the ORV are discussed in Section 4.A.7.

Once a solution to the trip time and payload mass calculations is obtained, cost models are applied to determine the total cost. Details of the cost models are presented in Section 4.A.6. Total cost divided by net payload mass is the basic answer sought for each data point. Generally, this calculation cycle is repeated for a range of I_{sp}'s and for a series of values of a selected parameter (e.g., P_{mod}, M_o, flight time).

Since down propellant is not used for a one-way up-trip, the iterative procedure is not required, and net payload is calculated directly. The other difference for one-way trips is the lack of amortization of the ORV. For multiple trips, a user is charged for only a fraction of the ORV life. However, for a one-way trip, the total cost is charged for the one trip. The specifics of the cost allocation are given in Section 4.A.7.

3. Propulsion System Performance

The various general equations defining the performance of an EP system are presented in Section 3.2. The purpose of this section is to define the assumptions used in simplifying and applying the general equations to the Earth orbit cost modeling analysis. Since the cost modeling includes several approximations, simplifications of the performance models are believed to be consistent with the overall modeling accuracy.

Propulsion system total efficiency (Eq. 3-23) can be written in the form

$$\eta_{ps} = \eta_u \eta_e \eta_{pp} \eta_c \gamma^2 \quad . \tag{4-9}$$

In the cost model analysis, the following assumptions were made to simplify the computations:[59,60]

$$\begin{aligned} \eta_u &= 0.95 \\ \eta_{pp}\,\eta_c &= 0.95 \\ \gamma &= 0.95 \\ \eta_e &= \frac{V_b}{V_b + 220} \quad . \end{aligned} \tag{4-10}$$

These values are representative of highly developed components (e.g., the 30-cm Hg thruster and PPU) as might be expected from a development program.[59,60] These values are assumed to apply to all propellants considered (Hg, Xe, Kr, Ar). (This assumption will be shown to be justified by the lack of sensitivity of cost to minor variations in performance.) Using the values defined by Eq. 4-10, Eq. 4-9 becomes

$$\eta_{ps} = 0.80 \left(\frac{V_b}{V_b + 220} \right) . \tag{4-11}$$

Total propulsion system input power, Eq. 4-7, is determined using this relationship. The relationship between V_b and I_{sp}, Eq. 3-35, can now be simplified to

$$V_b \cong \lambda \left(\frac{I_{sp}}{90} \right)^2 \tag{4-12}$$

or

$$\begin{aligned} V_b &= \left(\frac{I_{sp}}{90} \right)^2, \ (\text{Hg}) \\ &= \left(\frac{I_{sp}}{110} \right)^2, \ (\text{Xe}) \\ &= \left(\frac{I_{sp}}{140} \right)^2, \ (\text{Kr}) \\ &= \left(\frac{I_{sp}}{200} \right)^2, \ (\text{A}) \quad . \end{aligned} \tag{4-13}$$

These relationships (solid lines) are plotted in Figure 4-4. Also shown are lines of constant thruster diameter for a module power of 100 kW.

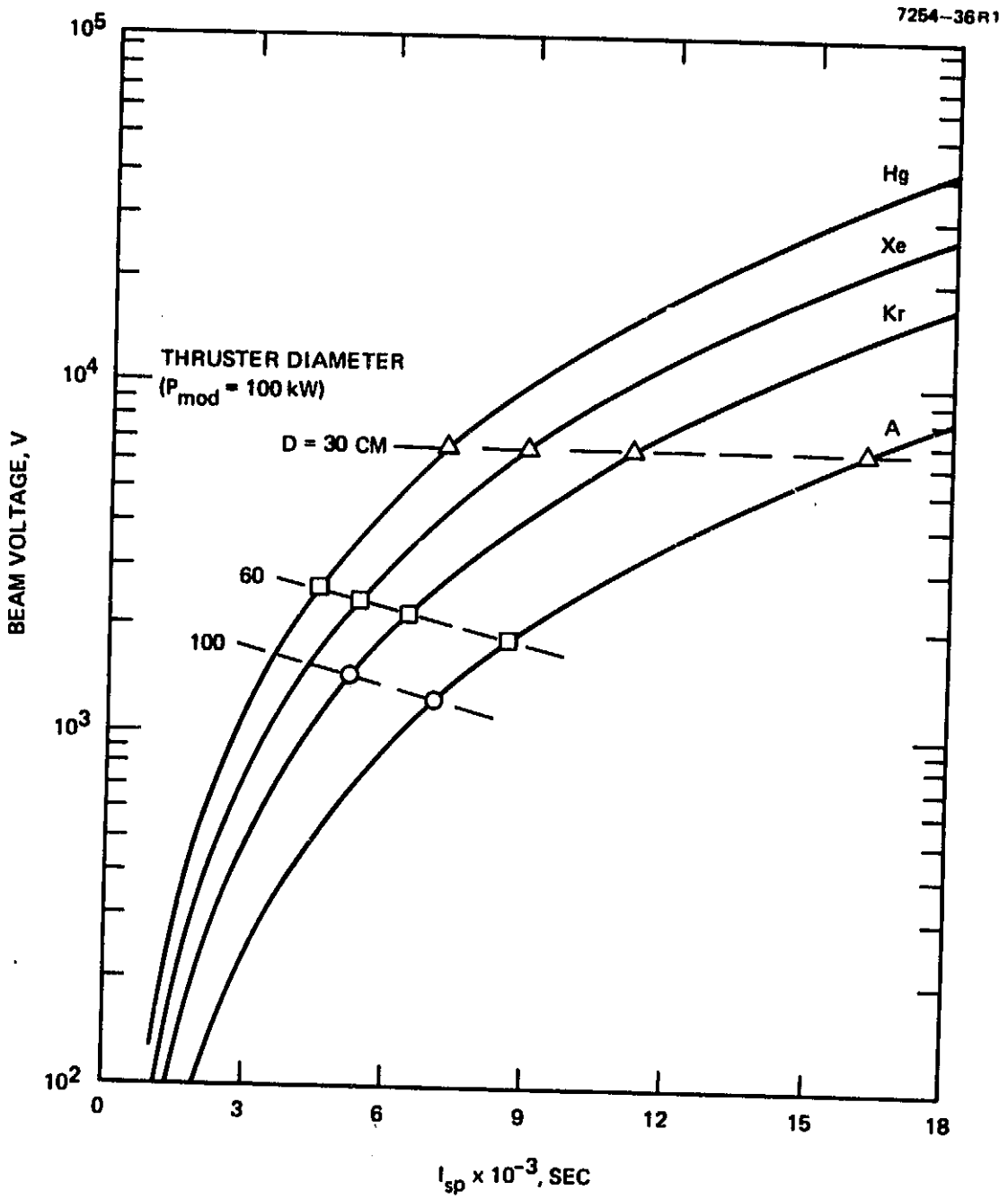

Figure 4-4. I_{sp} versus V_b for various propellants.

To determine thruster size for given beam current and beam voltage requirements, the considerations illustrated in Figure 4-5 must be addressed. Perveance, the proportionality between beam current and beam voltage, is discussed in Section 5.A. The result of that technology assessment was used in the cost modeling analysis in the form

$$I_b = 8.19 \times 10^{-8} D^2 \lambda^{-1/2} V_b^{3/2} , \qquad (4\text{-}14)$$

where

D = thruster beam diameter, cm

λ = ratio of atomic mass of propellant to Hg,

or, normalized to the 30-cm thruster,

$$\begin{aligned} I_b &= 2.33 \left(\frac{D}{30}\right)^2 \left(\frac{V_b}{1000}\right)^{3/2} \lambda^{-1/2} \\ &= 2.33 \left(\frac{D}{30}\right)^2 \left(\frac{V_b}{1000}\right)^{3/2} , \text{(Hg)} \\ &= 2.88 \left(\frac{D}{30}\right)^2 \left(\frac{V_b}{1000}\right)^{3/2} , \text{(Xe)} \qquad (4\text{-}15) \\ &= 3.60 \left(\frac{D}{30}\right)^2 \left(\frac{V_b}{1000}\right)^{3/2} , \text{(Kr)} \\ &= 5.22 \left(\frac{D}{30}\right)^2 \left(\frac{V_b}{1000}\right)^{3/2} , \text{(A)} \ . \end{aligned}$$

As shown in Section 5.A, Eq. 4-14 assumes a net-to-total accelerating voltage ratio, "R", of 0.7.

Thermal limits are established by thruster maximum operating temperatures. Results of the thermal analysis, presented in Section 5.D, show that the thermal limit can be expressed in the form

$$(I_b)_{max} = 15 \left(\frac{D}{30}\right)^2 . \qquad (4\text{-}16)$$

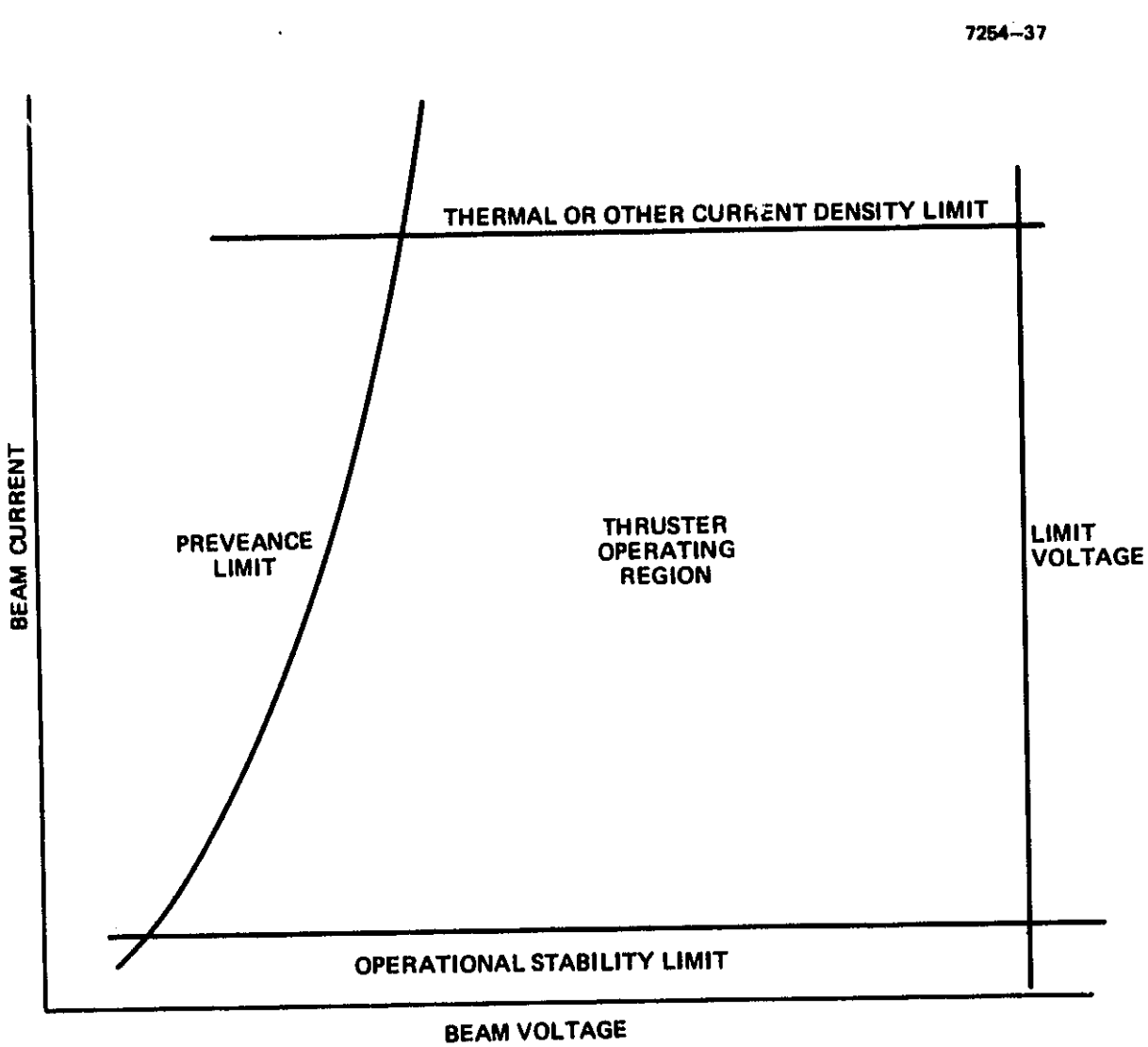

Figure 4-5. Thruster operating limits.

Thus, in the process of calculating the size of modules required to use the selected power, Eq. 4-15 is used if the current is less than the thermal-limited value. For example, the cost model calculations select a module power and an I_{sp} for each data point. Thus, I_b and V_b are established. If the beam current found from Eq. 4-15 satisfies the inequality

$$2.33 \left(\frac{V_b}{1000}\right)^{3/2} \lambda^{-1/2} \leq 15 \quad ,$$

then the perveance equation is used to determine beam diameter. If the inequality is not satisfied, thruster diameter is determined from the thermal limit equation. Thruster diameter as a function of I_{sp} and module power is shown for argon in Figure 4-6.

The maximum voltage limit indicated in Figure 4-5 is of practical significance in developing a thruster. As shown in Figure 4-4, the maximum beam voltages are below 7 kV for thruster diameters larger than 30 cm. In terms of breakdown, this voltage level may be slightly inconsistent with the close grid spacing assumptions used to develop Eq. 4-14. However, most of the calculations for the cost model involve lower voltages and should not produce breakdown concerns.

The lower limit shown in Figure 4-5 is of little practical importance here since maximum power per module is of interest. At very low beam currents, thruster stability must be considered.

Thruster life is affected by several operating conditions (e.g., beam current density, discharge voltage, propellant utilization efficiency). However, in developing a new thruster for a specific application, a given life could probably be achieved by selecting operating conditions, materials, and designs.[61,64] Conversely, present knowledge of thruster wearout life could be extrapolated to larger diameters by normalizing to the 30-cm beam current density. For cost model program purposes, two thruster life models that assume either constant life or a life

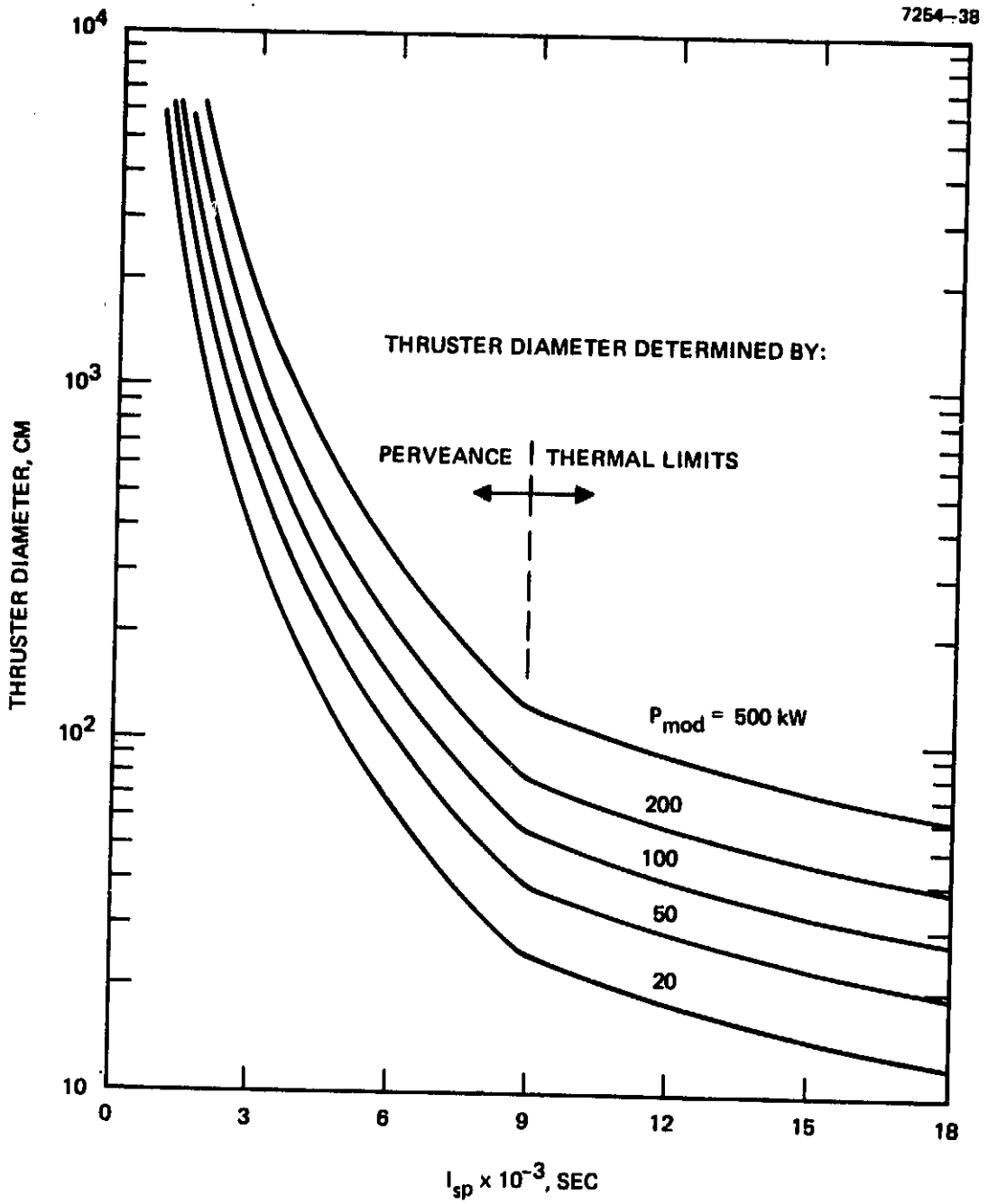

Figure 4-6. Thruster diameter versus I_{sp} for argon.

proportional to beam current density have been formulated and described in the relationship

$$L_t = 10^{\omega} \quad , \tag{4-17}$$

where

$$\omega = \omega_c = 4 \text{ or } 5 \text{ for constant life}$$

or

$$\omega = \omega_v = 4.4 - 1.27 \log (I_{eq})$$

where

I_{eq} = equivalent 30-cm thruster beam current

$$I_{eq} = I_{mod} \left(\frac{900}{D^2} \right) \quad .$$

The model for ω_v was based on 30-cm thruster life test results. A third life model that assumes constant ampere-hour life (as used in Section 3) would predict lives intermediate between the constant life and the beam current dependent models.

4. Redundancy

In a typical set of cost model calculations (e.g., cost versus I_{sp} as a function of module power), the number of thruster and PPU modules varies from point to point. To be consistent, each point in this map should have the same reliability. Since reliability calculations are somewhat more complicated than simply adding redundancy, an analysis was performed to assess the error introduced by using a fixed redundancy. Details of that analysis are included in Appendix D. The basic result of the analysis is illustrated in Figure 4-7.

For reasonable assumptions on failure rate, standby redundancy, and operating time, reliability becomes relatively high for large numbers of modules. Thus, if a redundancy is selected that makes the reliability

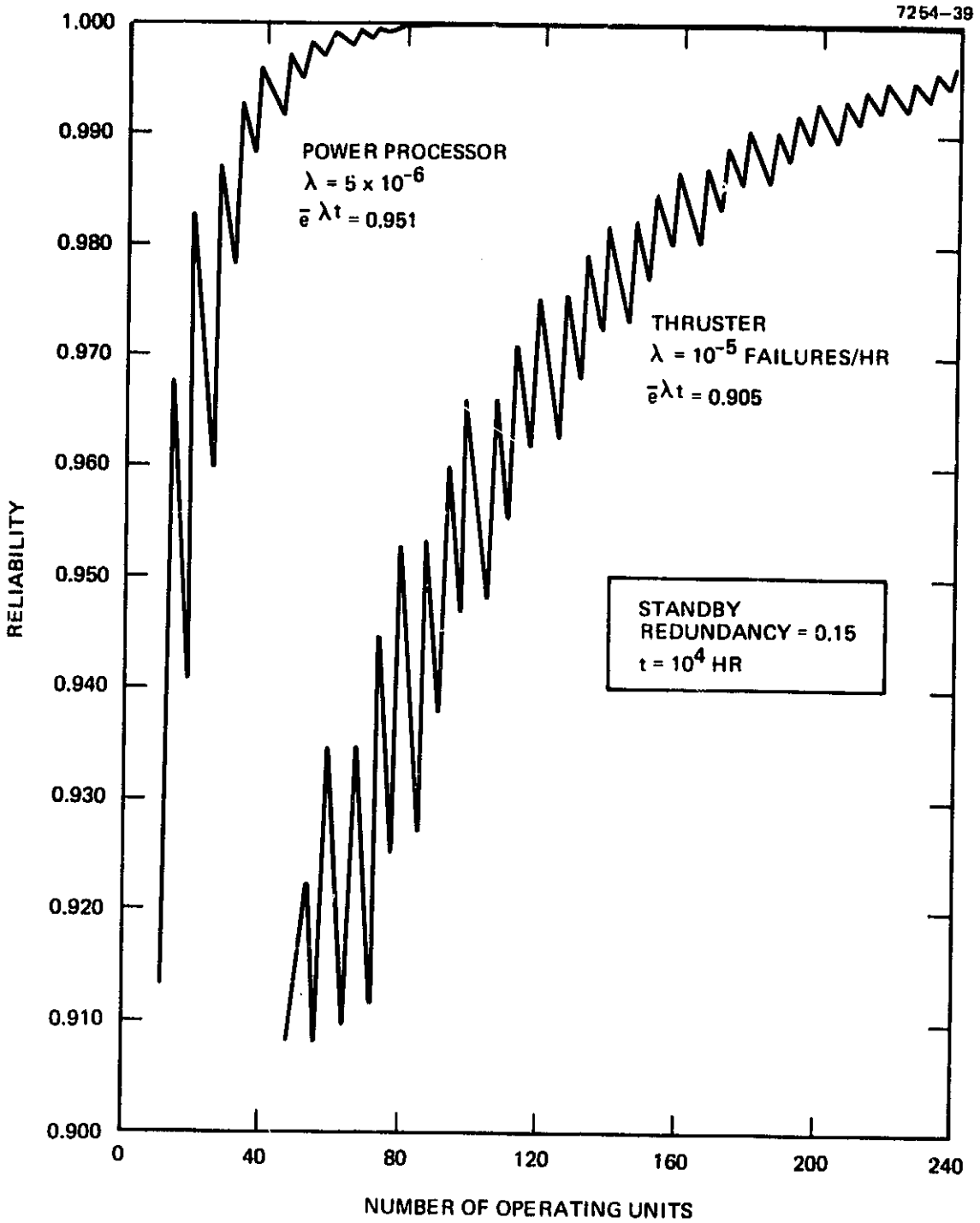

Figure 4-7. Reliability/redundancy results.

high for any number of modules, little error will be introduced by assuming fixed redundancy. Based on these results, a redundancy factor of 20 percent was used for both PPUs and thrusters. Other results shown in Appendix D illustrate that, even for small numbers of modules (e.g., 25) and lower redundancy for which the reliability would be reduced, the final transportation cost is not significantly affected.

5. Degradation

The mission approach used in the orbit-raising mission cost modeling assumes low thrust propulsion through the Van Allen Belt. The degradation model used in sizing the solar power source is shown in Figure 4-8. The model was based on published degradation factors used for silicon P/N solar cells (curve A).[65] Typically, low-thrust missions are expected to incur degradations in solar array output on the order of 25 percent to 50 percent depending on the trajectory.

Since future solar cell or design improvements may reduce degradation, two additional curves (B and C) were added to Figure 4-8 to reflect 10 percent degradation in array output with equivalent 1 MeV electron fluxes of 10^{15} and 10^{16} cm^{-2}, respectively. This model is also included in the on-orbit calculations since the long operating times may accumulate large dosages even though the flux rate is low.

The power degradation factor used in the model is viewed as an efficiency:

$$\eta_{pd} = \frac{\text{final power}}{\text{initial power}} .$$

Thus, the power used for sizing the power source is

$$P_{tot} = P_{ps}/\eta_{pd} . \qquad (4\text{-}18)$$

6. Mass Models

Mass models for the propulsion system and ORV, as defined in Figure 4-1, are summarized in Table 4-1. In the cost model program (see Figure 4-3), net payload is obtained by subtracting the ORV mass from

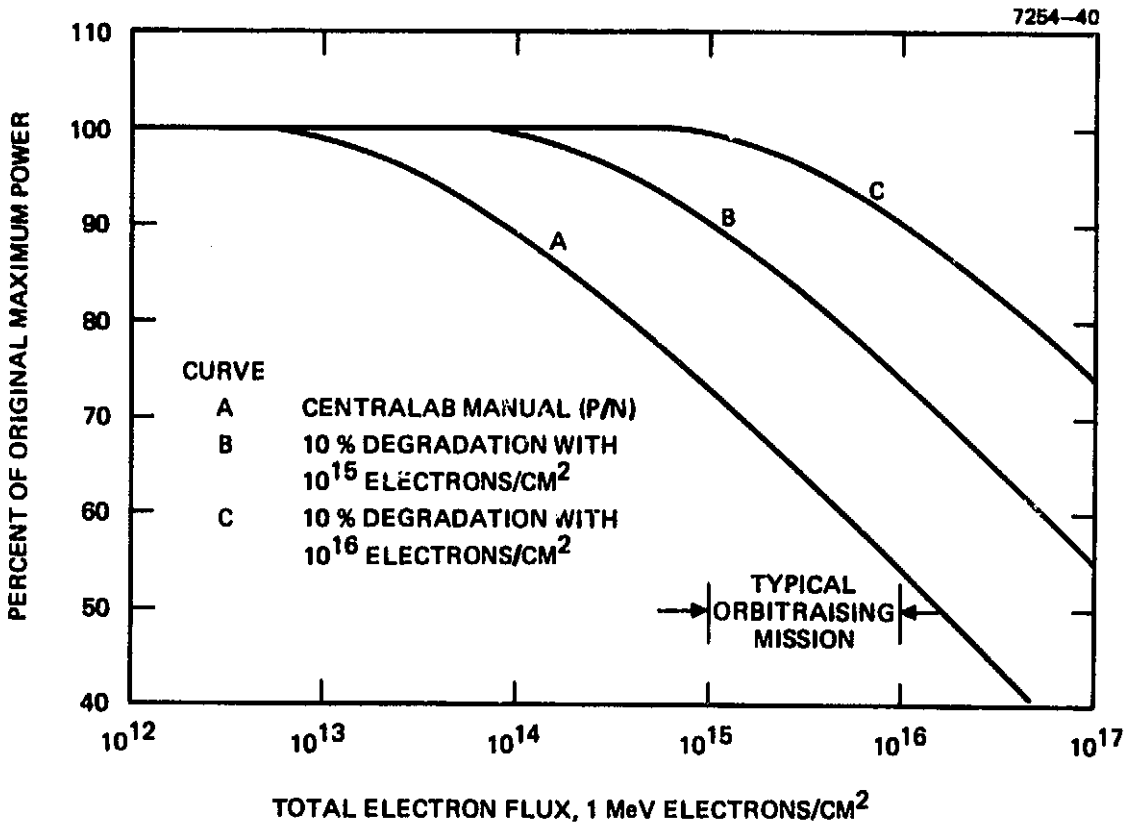

Figure 4-8. Solar cell degradation model.

Table 4-1. Mass Models Used in Orbit-Raising Cost Model

$$M_{sp} = M_o - M_{orv}$$

$$M_{ORV} = M_{rt} + M_{rpp} + M_{orp} + M_{rpt} + M_{rsm} + M_{rss} + M_{rw}$$

$$M_{rt} = 2M_t N_{ot} = 2\ (0.078\ D^{1.35})\ N_{ot}$$

$$M_{rpp} = 0.001\ \alpha_{pp}\ P_{ps}\ (1 + R_p)$$

where,

$$\alpha_{pp} = 10^{[-0.503\ \log\ (P_{pp}) + 1.153]}$$

$$M_{orp} = M_o \left[1 - \exp\ (-\Delta V/g\ I_{sp})\right]$$

$$M_{rpt} = \alpha_{rpt}\ M_{orp}$$

$$M_{rw} = \alpha_{rw}\ (0.001\ P_{tot})$$

$$M_{rsm} = 0.2 \left[M_{rt} + M_{rpp} + M_{orp} + M_{rpt} + M_{rss} + M_{rw}\right]$$

$$M_{rss} = 100 \left[1 + 10^{-6}\ P_{tot} + (N_{ot}/N_{op} - 1)\right]$$

6119

the initial mass. Except for determining total propellant mass, the calculations do not require iteration.

a. Thruster Mass

The mass assigned to each thruster in the system model makes an allowance for gimbals and miscellaneous structures by doubling the thruster individual mass. The model for the individual thruster mass as a function of diameter is shown in Figure 4-9. A reasonable fit to the data points is provided by

$$M_t = 0.078\ D^{1.35}\ (D \text{ in cm}) \quad .$$

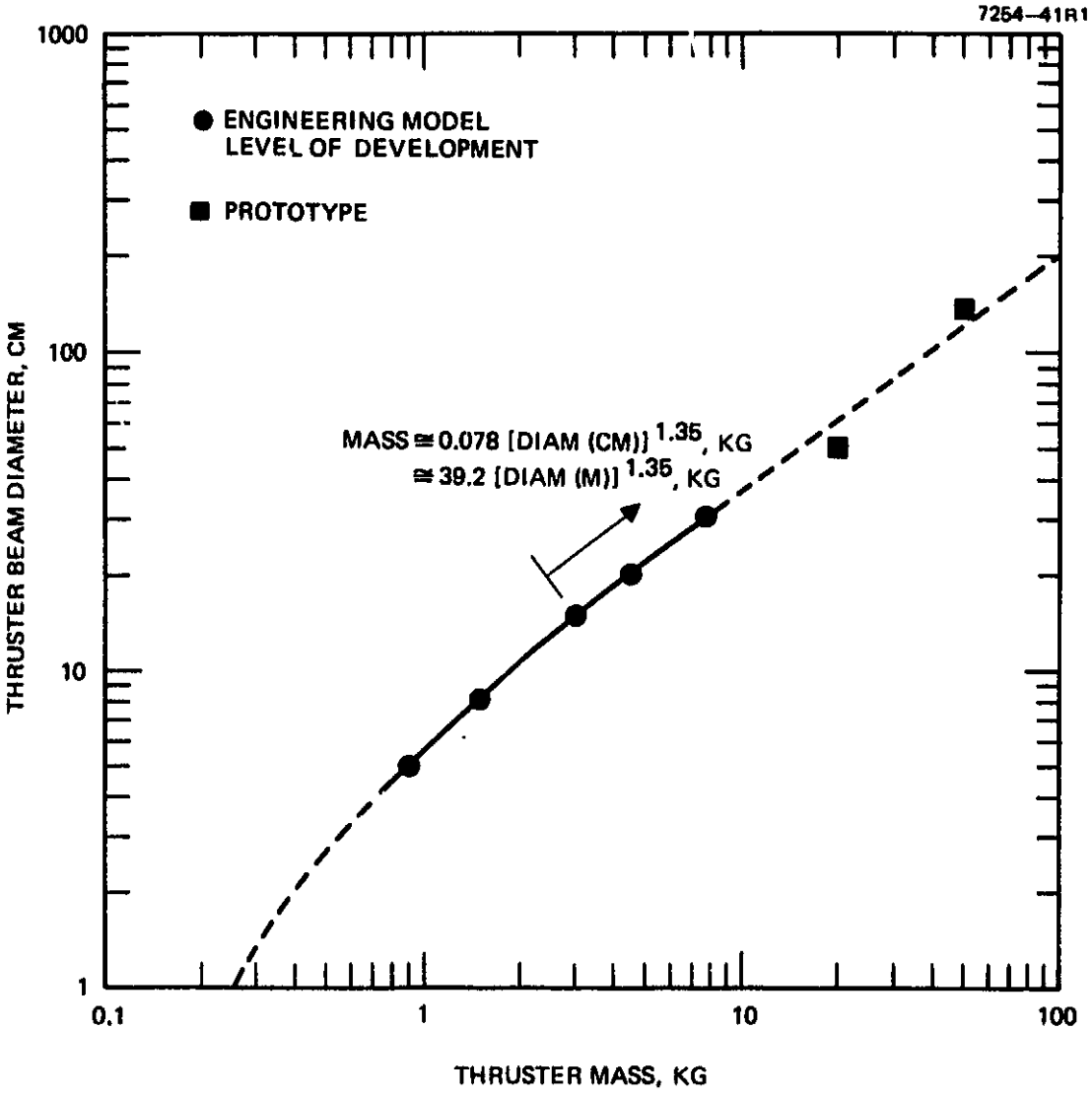

Figure 4-9. Thruster mass versus diameter.

Thruster total mass is estimated by assuming items such as gimbals and thruster "array" structure double the thruster effective mass.

$$M_{rt} = 2(0.078\ D^{1.35})\ N_{ot} \quad . \tag{4-19}$$

b. PPU Mass

The historical curve for total PPU mass plotted in Figure 3-4 was converted to specific mass, as shown in Figure 4-10. This curve is represented by the equation

$$\alpha_{PP} = 10^{[-0.503\ \log\ (P_{PP}) + 1.153]}\ (kg/kW) \quad , \tag{4-20}$$

where

P_{PP} = power processor input power (kW) .

Since the model is only approximate, the computer program assumes module power, P_{mod}, is equal to P_{PP} for convenience. These powers are actually related by

$$P_{mod} = \eta_{PP}\eta_e P_{PP} \quad , \tag{4-21}$$

but P_{PP} is not calculated in the program. This results in a more conservative estimate for α_{PP} than would be obtained if P_{PP} were actually used in Eq. 4-20. Power processor total mass is then obtained from

$$M_{rpp} = 10^{-3}\ \alpha_{PP}\ P_{ps}\ (1 + R_p) \quad , \tag{4-22}$$

where α_{PP} is in kilograms per kilowatt, P_{ps} is in watts, and R_p is the PPU redundancy factor.

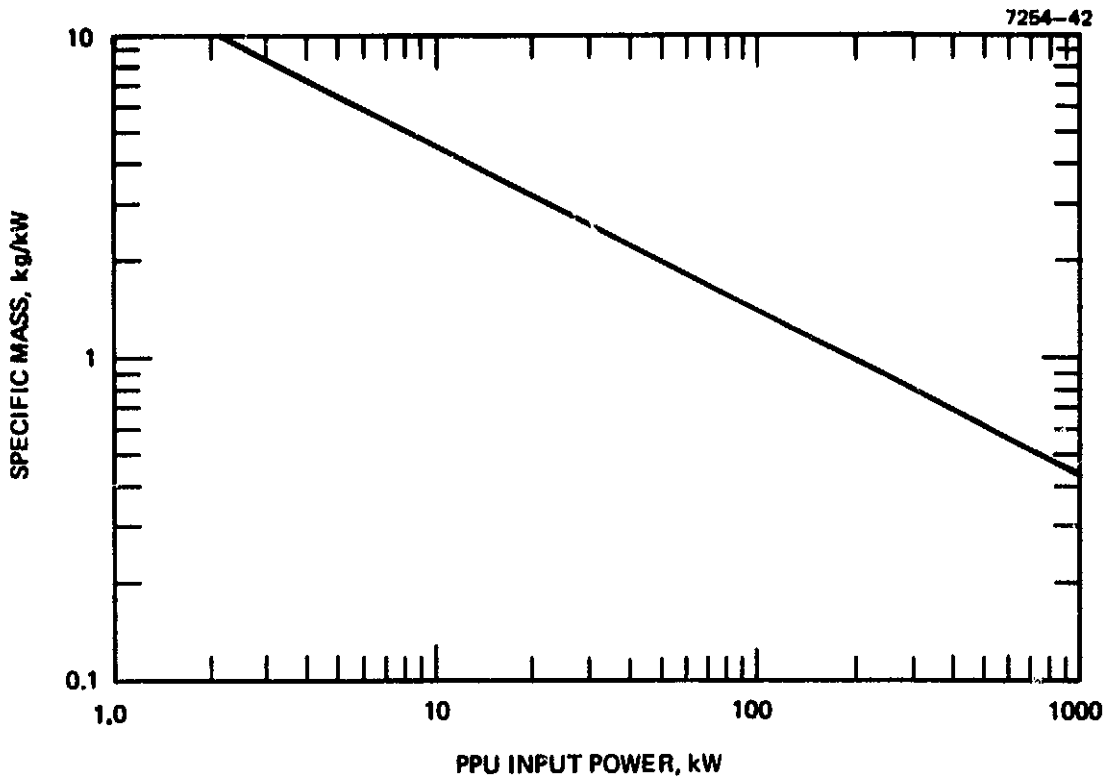

Figure 4-10. Power processor specific mass versus input power.

c. Propellant Tankage

Propellant tankage, including valves, lines, and miscellaneous hardware, is modeled as a fixed fraction of the propellant mass:

$$M_{rpt} = \alpha_{rpt} M_{orp} \quad , \tag{4-23}$$

where

$$M_{orp} = M_o \left[1 - \exp\left(-\frac{\Delta V}{g_o I_{sp}}\right)\right]$$

α_{rpt} = tankage fraction .

The baseline cases use $\alpha_{rpt} = 0.1$. Sensitivity studies show that cost results are not sensitive to the reasonable variations in α_{rpt}.

d. Power Source

Power source mass is typically considered in terms of specific mass (kilograms per kilowatt). Thus,

$$M_{rw} = 10^{-3} \alpha_{rw} P_{tot} \quad , \tag{4-24}$$

where

P_{tot} = total installed solar power (W)

α_{rw} = power source specific mass (kg/kW) .

For the matured Shuttle era and large space systems era baselines, α's of 6 kg/kW and 3 kg/kW, respectively, were assumed.

e. Subsystems

The model used for ORV subsystem mass is

$$M_{rss} = 100\left[(1 + 10^{-6} P_{tot}) + \left(\frac{N_{ot}}{N_{op}} - 1\right)\right] \quad , \tag{4-25}$$

where the first term in brackets represents the dependence on power level, and the second term accounts for complexity added by PPU/thruster switching. In the baseline cases, N_{ot}/N_{op} equals 1.0 because total trip time is less than the thruster lifetime, and no switching is assumed.

f. Structure and Mechanisms

The mass of ORV structure and mechanisms is modeled as a fraction of the sum of the other ORV component masses, including propellant:

$$M_{rsm} = \alpha_{sm} \left(M_{rt} + M_{rpp} + M_{orp} + M_{rpt} + M_{rss} + M_{rw} \right) . \quad (4\text{-}26)$$

The baseline value of 0.2 was assigned to α_{sm} throughout this study.

7. Cost Models

Cost models for the ORV are summarized in Table 4-2. The overall objective of these cost equations is to obtain total orbit-raising cost, C_{or}. This total cost divided by the net delivered payload M_{sp} is the basic final product of each calculation.

The total cost to launch and transport a given payload mass to orbit is expressed in the form

$$C_{or} = C_{oef} C_1 + C_{rt} + C_{opf} + C_{opt} + C_{\ell} + C_{orp} , \quad (4\text{-}27)$$

where

C_{oef} = ORV utilization cost factor

C_1 = ORV hardware cost

C_{rt} = cost of thrusters

C_{opf} = fixed cost of flight operations

C_{opt} = time-dependent cost of flight operations

C_{ℓ} = launch cost to LEO

C_{orp} = cost of propellant .

Each of these terms is defined quantitatively in Table 4-2, and each is discussed below. Many of the subscripts are defined in Figure 4-1.

Table 4-2. Cost Models Used in Orbit-Raising Cost Model

$$C_{or} = C_{oef}\, C_l + C_{rt} + C_{opf} + C_{opt} + C_{\ell} + C_{orp}$$

$$C_{oef} = \left(\frac{TOTRIP}{L_{orv}}\right) + r\ TOTRIP$$

$$C_l = C_{ori} + C_{rp} + C_{rpt} + C_{rsm} + C_{rss} + C_{rw} + C_{ord}$$

$$C_{ori} = C'_{ori}\ (M_{orv} - M_{orp} + T_{used})$$

$$T_{used} = M_t\ N_{mod} \left(\frac{TOTRIP}{L_t}\right)\ 1 + R_{ot}$$

$$C_{rt} = 2\left[42 \times 10^3 \log D\right] \left(\frac{TOTRIP}{L_t}\right) \left(1.47\ N_{ot}^{0.68}\right)$$

$$C_{rp} = 1.88 \times 10^5 \left(P_{PP}\right)^{0.12} \left(1.47\ N_{op}^{0.68}\right)$$

$$C_{rpt} = M_{orp}\ \alpha_{pt}\ C_{rpt}$$

$$C_{orp} = M_{orp}\ C'_{orp}$$

$$C_{rsm} = C'_{rsm}\ \left(M_{rsm}\right)^{0.3}$$

$$C_{rss} = C'_{rss}\ \left(M_{rss}\right)^{0.9}$$

$$C_{rw} = C'_{rw}\ P_{tot}$$

$$C_{ord} = C'_{ord}\ \left(M_{orv} - M_{orp}\right)^{0.3}\ \ N_r^{-1}$$

$$C_{opf} = 10^5$$

$$C_{opt} = C'_{opt}\ TOTRIP$$

$$C_{\ell} = C'_{\ell}\ (M_o + T_{used})$$

$$\bar{C}_{or} = C_{or}/M_{sp}$$

6119

a. ORV Utilization Factor (C_{oef})

The ORV is considered to be a reusable vehicle that is rented to a "user" for payload transport. A user utilization factor has been included in the form

$$C_{oef} = \left(\frac{TOTRIP}{L_{orv}}\right) + r\ TOTRIP \quad , \qquad (4\text{-}28)$$

where

TOTRIP = flight time per trip

L_{orv} = ORV useful life

r = interest rate .

Part of C_{oef} represents the fraction of ORV useful life (L_{orv}) charged to the user. The second part represents interest on the cost of the ORV during the flight. An ORV life of 2000 days and an interest rate of 10 percent per year were used throughout this study.

b. ORV Hardware Cost (C_1)

This factor includes recurring costs and development costs amortized over a given fleet of ORVs.

$$C_1 = C_{rp} + C_{rpt} + C_{rsm} + C_{rss} + C_{rw} + C_{ori} + C_{ord} \quad , \qquad (4\text{-}29)$$

where

C_{rp} = cost of PPUs

C_{rpt} = cost of propellant tankage

C_{rsm} = cost of structure and mechanisms

C_{rss} = cost of subsystems

C_{rw} = cost of power source

C_{ori} = cost of ORV integration and testing

C_{ord} = cost of design, development, test, and evaluation (DDT&E) .

Thrusters, propellant, and operations are not included in C_1 because they are the components that are worn or fully used each trip. These costs are calculated separately.

c. Thruster Cost (C_{rt})

The relatively large systems being considered require a large number of thruster and PPU modules. The thruster cost model assumes that a mass-production type fabrication approach will be used to reduce costs. Furthermore, thruster costs are modeled by a learning curve, in which the unit cost decreases as quantity increases in the form

$$C_{rt} = 2C'_{rt}\left[1 + \frac{1}{2^{\alpha}} + \frac{1}{3^{\alpha}} + \ldots + \frac{1}{N_{ot}^{\alpha}}\right]\left(\frac{TOTRIP}{L_t}\right) , \qquad (4\text{-}30)$$

where

C'_{rt} = first unit cost

α = learning curve parameter

L_t = thruster life (hours) .

$\left(\frac{TOTRIP}{L_t}\right) = 1$ if $\left(\frac{TOTRIP}{L_t}\right) < 1$

The last term in Eq. 4-30 is the fraction of thrusters worn out although this wear is distributed among many thrusters. A user only pays for those used. The factor of 2 in Eq. 4-30 is included to account for gimbals, structure, and other miscellaneous costs associated with the thrusters. All results were obtained using an 80 percent learning curve, giving $\alpha = 0.34$. This means that the unit cost is reduced by 20 percent each time the quantity doubles. For instance, if the 100th unit costs \$100, the 200th unit will cost \$80. Since the summation in Eq. 4-29 is inconvenient, an approximate equation was derived in the form

$$C_{rt} = 2C'_{rt}\frac{N_{ot}^{2\alpha}}{2^{\alpha}}\left(\frac{TOTRIP}{L_t}\right) . \qquad (4\text{-}31)$$

Thruster first unit cost was obtained from Figure 4-11, which displays current thruster costs and a projection for future costs. The rationale used for reducing costs is that future systems for Earth orbit missions will allow reduced fabrication tolerances and greater performance dispersions. The close tolerances of present thrusters contribute significantly to cost. Using the equation that fits the projected thruster cost in Figure 4-11, Eq. 4-31 becomes

$$C_{rt} = 2\,(4.2 \times 10^{4} \log D)\,(1.47\, N_{ot}^{0.68}) \left(\frac{TOTRIP}{L_t}\right) , \qquad (4\text{-}32)$$

where D is in cm.

d. Power Processing Unit Cost (C_{rp})

PPU cost is modeled similarly to the thruster using an 80 percent learning curve. The first unit cost was derived by fitting a curve to cost data for 8-cm and 30-cm PPUs. The PPU cost is then expressed as

$$C_{rp} = 1.88 \times 10^{5}\,(P_{pp})^{0.12}\,(1.47\, N_{op}^{0.68}) , \qquad (4\text{-}33)$$

where

P_{pp} = power processor input power.

e. Propellant Cost (C_{orp})

Propellant costs are assumed to be proportional to propellant mass:

$$C_{orp} = C'_{orp}\, M_{orp} , \qquad (4\text{-}34)$$

where

C'_{orp} = cost per unit mass

= \$0.4/kg for baseline .

f. Propellant Tankage Cost (C_{rpt})

Tankage costs are assumed to be proportional to tankage mass using Eq. 4-23

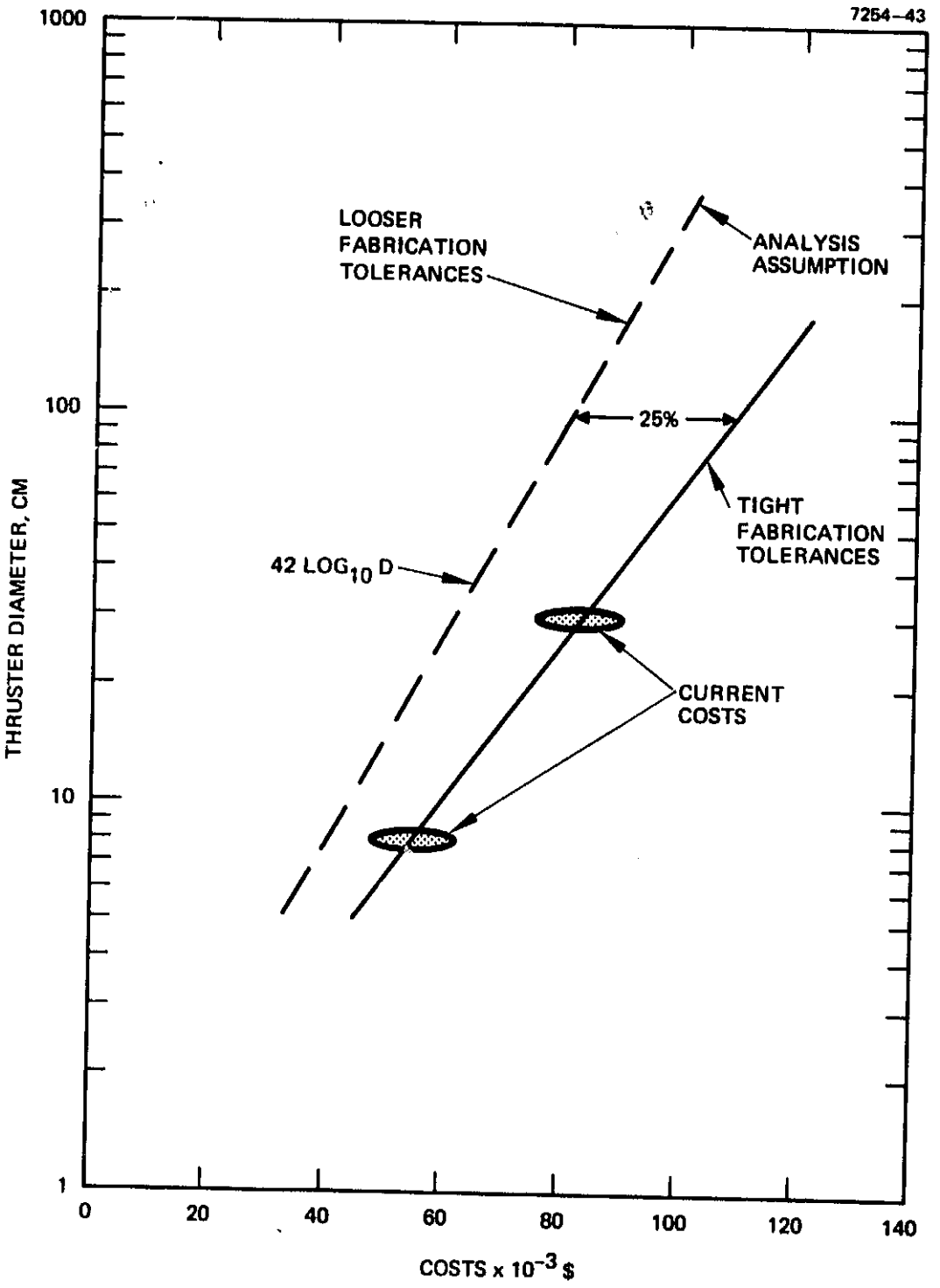

Figure 4-11. Thruster first unit cost.

$$C_{rpt} = C'_{rpt}\, \alpha_{pt}\, M_{orp} \quad , \tag{4-35}$$

where

C_{rpt} = tankage cost per unit mass

= \$100/kg for baseline

α_{pt} = tankage factor

= 0.1 for baseline .

g. Structure and Mechanisms Cost (C_{rsm})

The structure and mechanisms cost model was derived from consideration of past vehicle costs and has the form

$$C_{rsm} = C'_{rsm}\, (M_{rsm})^{0.3} \quad , \tag{4-36}$$

where

C'_{rsm} = 10^4 \$/kg for both baselines.

Since the details and complexity of these elements would affect their costs, any general model necessarily must be rather arbitrary. However, using the model, the sensitivity of overall transportation cost to variations in structure and mechanisms cost can be evaluated.

h. Subsystems Cost (C_{rss})

As with structure and mechanisms, the ORV subsystem cost will be highly dependent on design details. Again, through discussions of various programs, the following model was assumed:

$$C_{rss} = C'_{rss}\, (M_{rss})^{0.9} \quad , \tag{4-37}$$

where

C'_{rss} = 10^4 \$/kg for both baselines.

Compared with Eq. 4-35, the difference in the exponents reflects the differences in complexity. If the size of a structure is increased, the cost is probably not too strongly affected. However, with electronics, increased mass certainly means increased cost.

i. Power Source Cost (C_{rw})

Power costs are modeled in the conventional form

$$C_{rw} = C'_{rw} P_{tot} \quad , \tag{4-38}$$

where

C'_{rw} = cost per unit of power
= \$0.5/W (large system baseline)
= \$100/W (Shuttle era baseline) .

The \$100/W value is only a slight reduction from present technology and is consistent with goals for solar power source development. The \$0.5/W is about three orders of magnitude less than current technology. However, such low power costs will probably be necessary to make a large space system economically viable (independent of SEP).

j. Integration and Test Cost (C_{ori})

This factor is intended to account for ORV recurring costs for assembly and testing. It is assumed that a fleet of ORVs would be produced in a time scale consistent with production-line assembly. The cost of such assembly is modeled in the form

$$C_{ori} = C'_{ori} \left(M_{orv} - M_{orp} + T_{used} \right) \quad , \tag{4-39}$$

where

C'_{ori} = cost of integration per unit of ORV dry mass

T_{used} = mass of thrusters worn out during one round trip

$$= M_t N_{mod} \left(\frac{TOTRIP}{L_t} \right) \left(1 + R_t \right) \quad .$$

By including factors for thruster wearout, the user pays only for the thrusters used (see Eq. 4-30), but must pay for the future installation of new thrusters.

k. Design, Development, Test, and Evaluation (C_{ord})

Design, development, test, and evaluation (DDT&E) costs are included in the model for completeness in the sensitivity analysis. The form of the relationship,

$$C_{ord} = \frac{C'_{ord}}{Nr}\left(M_{orv} - M_{orp}\right)^{0.3} \quad , \qquad (4\text{-}40)$$

is similar to that used for structure and mechanisms. Using the relatively small exponent seems appropriate since C_{ord} should depend on mass and complexity, but significant non-engineering costs should be largely independent of mass. The other parameters in Eq. 4-40 are defined as follows:

C'_{ord} = DDT&E cost coefficient

= $\$10^5$ \$/kg for both baselines

N_r = number of ORVs over which DDT&E costs should be amortized

= 10 for both baselines .

l. Flight Operations Costs (C_{opp}, C_{opt})

These cost factors arise from the philosophy that an SEP ORV flight would incur both fixed costs (similar to those for a ballistic transfer) and time-dependent costs due to the multi-month duration of the flight. For both factors, it is assumed that only the efforts directly related to the ORV (i.e., not the payload or launch vehicle) should be charged to ORV cost. Thus, the following values were used throughout:

$$\begin{aligned} C_{opf} &= 10^5 \\ C_{opt} &= 10^3 \ \text{TOTRIP} \ . \end{aligned} \qquad (4\text{-}41)$$

m. Launch Cost (C_ℓ)

This element accounts for the cost of launching the initial mass from Earth to LEO and thruster refurbishment. The model for C_ℓ has the form

$$C_\ell = C'_\ell \left(M_o + T_{used}\right) \quad , \qquad (4\text{-}42)$$

where

C'_ℓ = cost per unit mass

= \$300/kg for Shuttle era baseline

= \$15/kg for large system baseline

For the multiple round trip mode, the results are conservative because the full launch cost was charged to each launch. The \$300/kg value is based on a possible reduction in current Shuttle projections of \$500 to \$800/kg. The \$15/kg is based on launch cost estimates developed for heavy lift launch vehicles. Overall cost sensitivity studies for each of these quantities are presented in Section 4.A.8.

8. Orbit Raising Large System Baseline Mission Results

Cost model program results are structured around the two baselines selected to represent near future applications (matured Shuttle era) and late 20th century applications (large space systems era). For each baseline, a set of parameters required by the computer model was selected. Computer runs using variations around this baseline set of parameters were then performed to study the sensitivity of the results to various assumptions.

Recall that the goal of this part of the work is to identify thruster characteristics and thruster technology options that have significant impact on transportation system overall cost. Although the model incorporates many anticipated technology limits (e.g., thermal, ion optics), the sensitivity studies also include parameter variations that might require violation of presently expected limits. Thus, interpretation of the final results in terms of new directions in technology will require certain qualitative judgements to temper the "black or white" computer answers.

Initially, the cost model analysis was directed only toward large space systems. Later, the Shuttle baseline was included to provide a link between the present potential applications of the 30-cm thruster to relatively small satellites and to far future systems of the solar power satellite type. Many of the parameters studied in the large system baseline sensitivity analysis proved to be relatively unimportant. Thus,

the number of runs needed for the Shuttle baseline analysis was significantly reduced. For convenience in presenting the results, the large-system baseline is discussed first; the Shuttle baseline follows, drawing on similarities with the large system baseline to reduce duplication.

To simplify the designation of the baselines and to distinguish between various orbit raising and on-orbit missions, the following abbreviations are used:

OR = orbit-raising (transfer) mission
ORS = self-powered orbit-raising mission
ORP = payload powered orbit
ORO = one-way orbit-raising mission
OO = on-orbit mission
LS = large space system era baseline
MS = matured Shuttle era baseline.

Within the OR/LS category, there are three modes (see Section 4.A.1): self-powered, payload powered, and one-way. For these, an additional descriptor is used, as indicated above. The self-powered mode is used as the baseline, and most sensitivities were investigated using this mode.

a. Large Space Systems Era Baseline

A summary of the large system baseline parameter values is shown in Table 4-3 for use with the mass and cost equations listed in Tables 4-1 and 4-2, respectively. All of these parameters were presented in previous sections. The selection of these particular values was accomplished through discussions with NASA LeRC personnel and reviews of preliminary results. Argon propellant was assumed because of the large quantities required.

The results obtained with the computer cost model are categorized as indicated in Table 4-4. The general category presents the baseline results and several breakdowns of mass and cost to show the contributions of the various model elements. The other categories were selected for the sensitivity studies. In each case, the parameter of interest is varied about the baseline value with all other parameters fixed. The results are presented below by category.

Table 4-3. OR/LS Baseline Cost Model Parameters

Argon Propellant

P_{mod} = 100 kW		Module power (beam)
L_t = 10^4 hr		Thruster life
ΔV = 6 km/sec		Velocity change
t_f = 150 days		Up trip flight time
M_o = 10^6 kg		Initial mass in LEO
Flux = 10^{15}		Radiation flux
Curve = "C"		Radiation model
L_{ORV} = 2000 days		Life of ORV
C'_{ori} = \$10/kg		ORV integration and testing
C'_{rw} = \$0.5/W		Cost of ORV associated power
C'_{rt} = \$4.2 x 10^3 log (D)		First unit thruster cost
C'_{rp} = \$4.3 x 10^5 $(P_{pp})^{0.12}$		First unit PPU cost
R_{ot} = 0.2		PPU redundancy
R_{op} = 0.2		Thruster redundancy
C'_{rpt} = \$100/kg		Cost per kg of tankage
α_{pt} = 0.10		Tankage factor
C'_{orp} = \$.40/kg		Propellant cost per kg
C'_{opt} = \$$10^3$/day		Time-dependent cost
C_{rsm} = \$$10^4$ $\left(M_{rsm}\right)^{0.3}$		Cost of ORV structure and mechanisms
C_{ord} = $\frac{\$4 \times 10^6}{10}$ $\left(M_{orv}-M_{orp}\right)^{0.3}$		DDT&E cost amortized over 10 ORVs
C_{rss} = 1 x 10^4 $\left(M_{rss}\right)^{0.9}$		Cost of ORV subsystems

6119

Table 4-3. OR/LS Baseline Cost Model Parameters (Continued)

C_{opf}	= $\$10^5$	Cost not associated with electric ORV
α_{ps}	= 3 kg/kW	Specific mass for power
C_{ℓ}'	= \$15/kg	Launch cost per kg to LEO
r	= 10%/yr	Interest rate

6119

b. OR/LS General Results

The typical data format and results for the baseline conditions are presented in Figure 4-12. The 100-kW curve represents the baseline case, while the other module power curves show the general cost trends with module power. Lines of constant thruster diameter imposed on the power curves indicate the general relationship of size to cost and I_{sp}. Unless otherwise marked, all data was developed using the baseline parameters.

The shape of the curves in Figure 4-12 is the result of changes in many parameters. Figures 4-13 through 4-16 are provided to aid in the interpretation. Breakdowns of the cost model and mass model elements as a function of I_{sp} are shown in Figures 4-13 and 4-14, respectively. In addition, plots of total cost and of cost per kilogram as a function of payload mass are presented in Figure 4-15. An additional aid in interpreting Figure 4-12 is the number of thruster modules (N_{ot}) required, as shown in Figure 4-16.

At low I_{sp}, the steep slope of all the curves in Figure 4-12 is primarily due to the rapidly increasing payload. Since, as shown in Figure 4-15, total cost is relatively constant, the reduction in payload, due to increases in other masses as I_{sp} decreases dominate the low I_{sp} region. (Payload is derived by subtracting the ORV mass and propellant from the initial mass in LEO.) The mass elements that increase with decreasing I_{sp} are, as shown in Figure 4-14, thrusters, propellant (up and down), and structure and mechanisms. Structure increases because

Table 4-4. Data Run and Sensitivity Study Categories, OR/LS Baseline

1. General

   Cost/kg versus I_{sp}; P_{mod}
   Cost breakdown
   Mass breakdown
   Cost/kg versus payload mass
   Number of modules

2. Mission design sensitivites

   ΔV
   Trip time (up-trip)
   Initial mass
   Launch cost

3. Thruster sensitivities

   Life
   Efficiency
   Mass
   First unit cost
   "R" ratio
   Redundancy

4. Propellant sensitivities

   Type
   Cost

5. PPU sensitivities

   Mass
   First unit cost
   Redundancy

6. Power source sensitivities

   Mass
   Cost
   Degradation

7. ORV system design sensitivities

   Structure and mechanisms
   Subsystems
   Integration and testing
   DFT&E
   Flight operations

8. Payload powered options (ORP)

   Power fraction

9. One-way trip options (ORO)

   ΔV
   Trip time
   Initial time
   Launch cost

6119

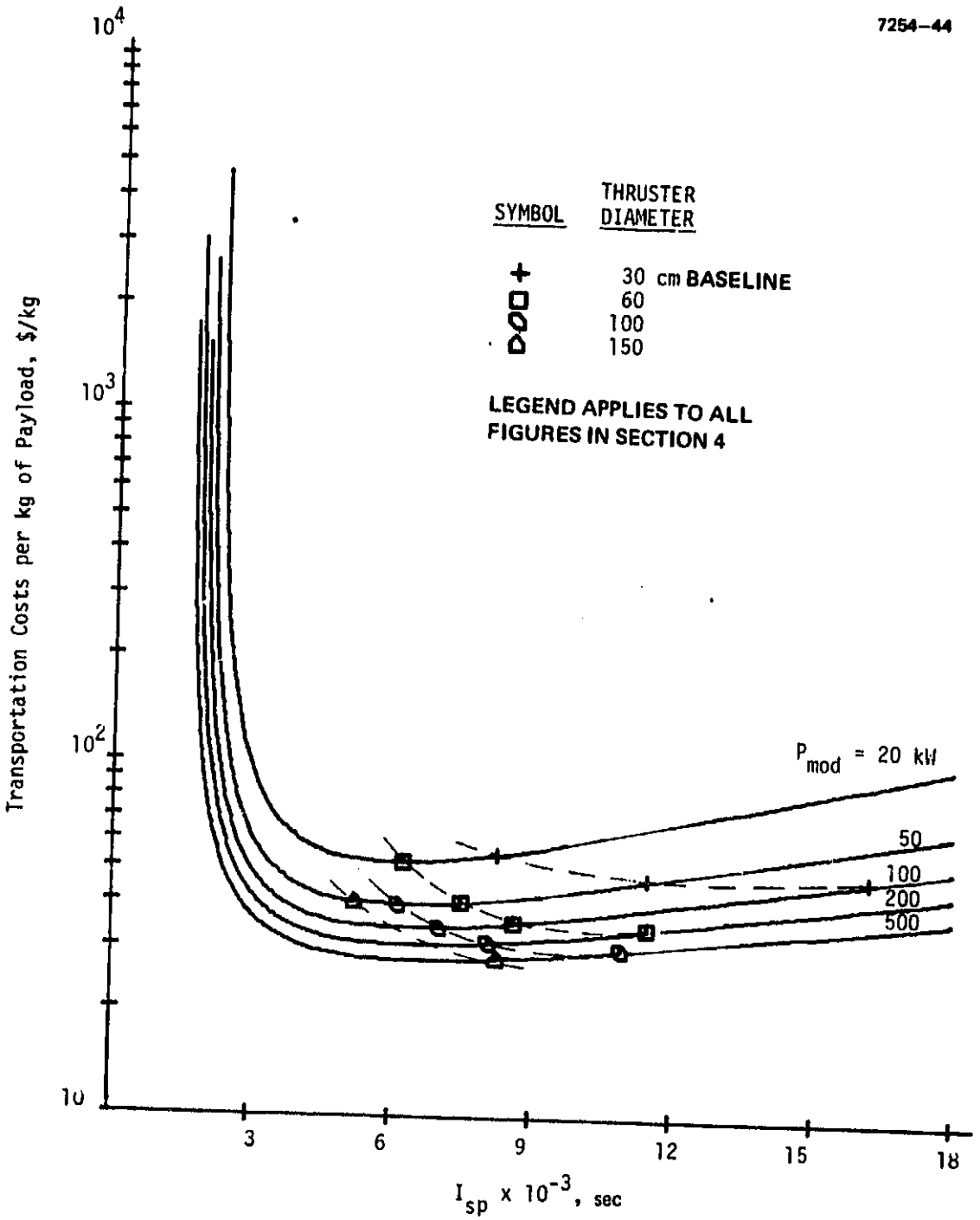

Figure 4-12. ORS/LS effect of module power.

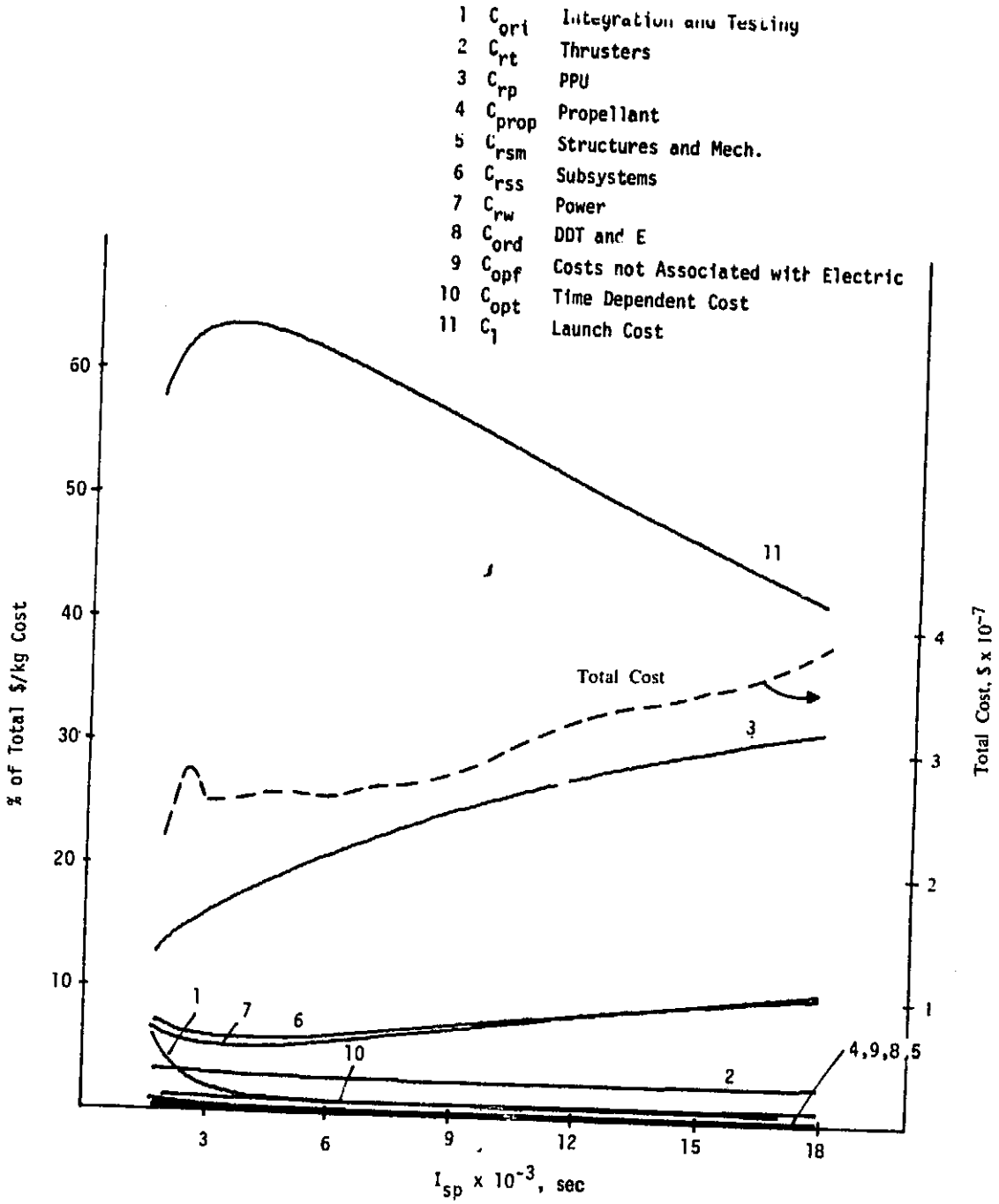

Figure 4-13. ORS/LS cost element breakdown.

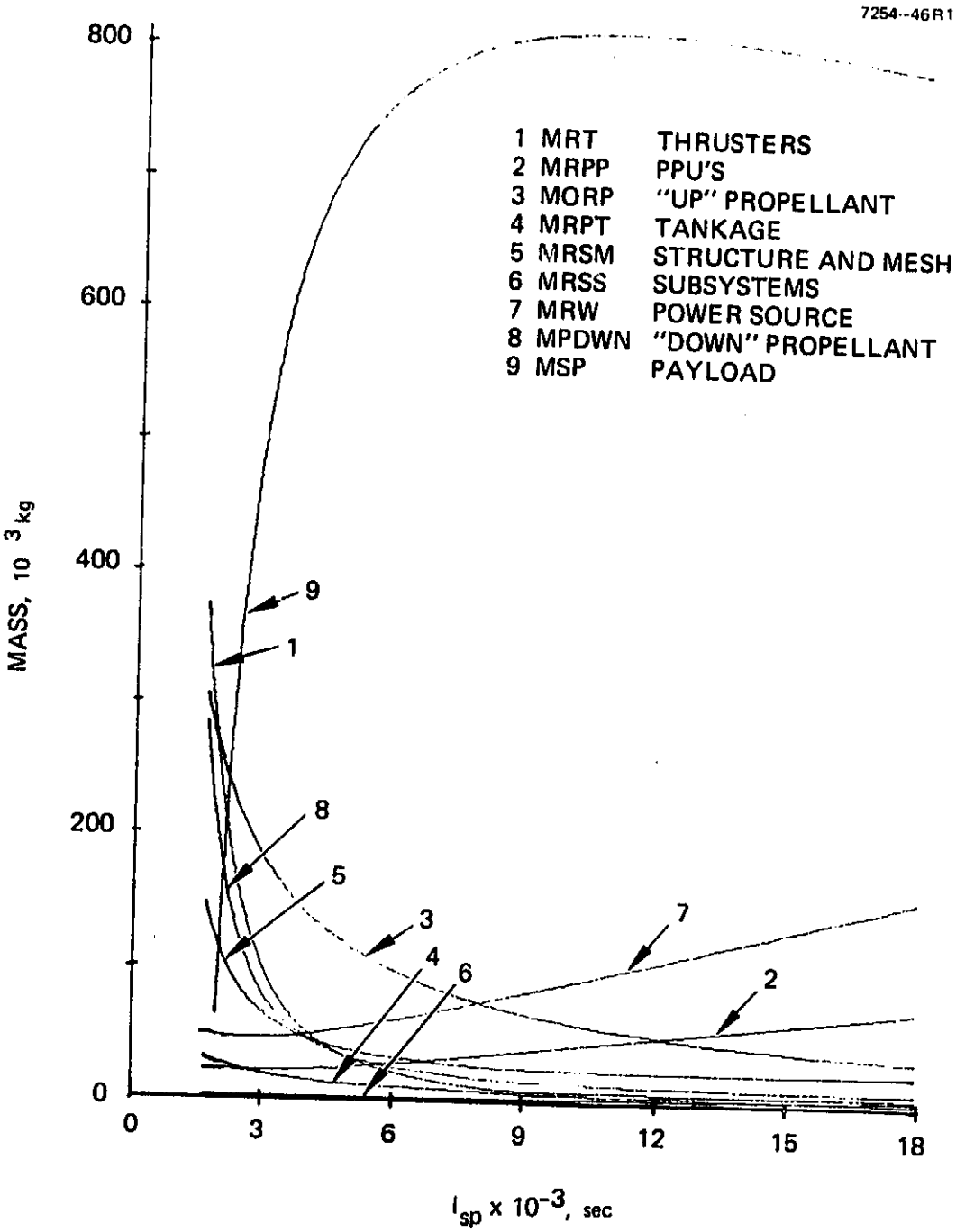

Figure 4-14. ORS/LS mass element breakdown.

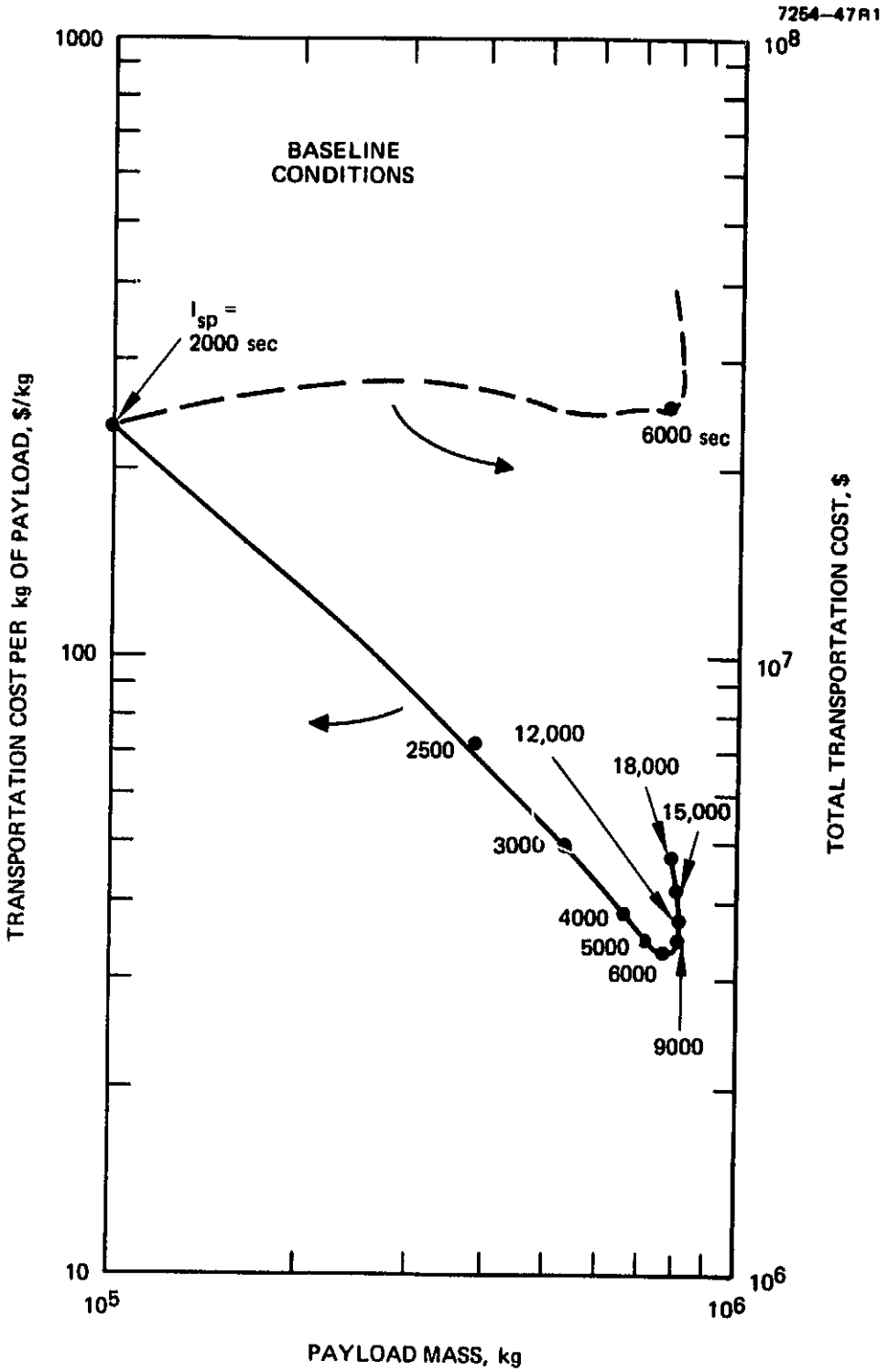

Figure 4-15. ORS/LS total cost and cost/kg versus payload.

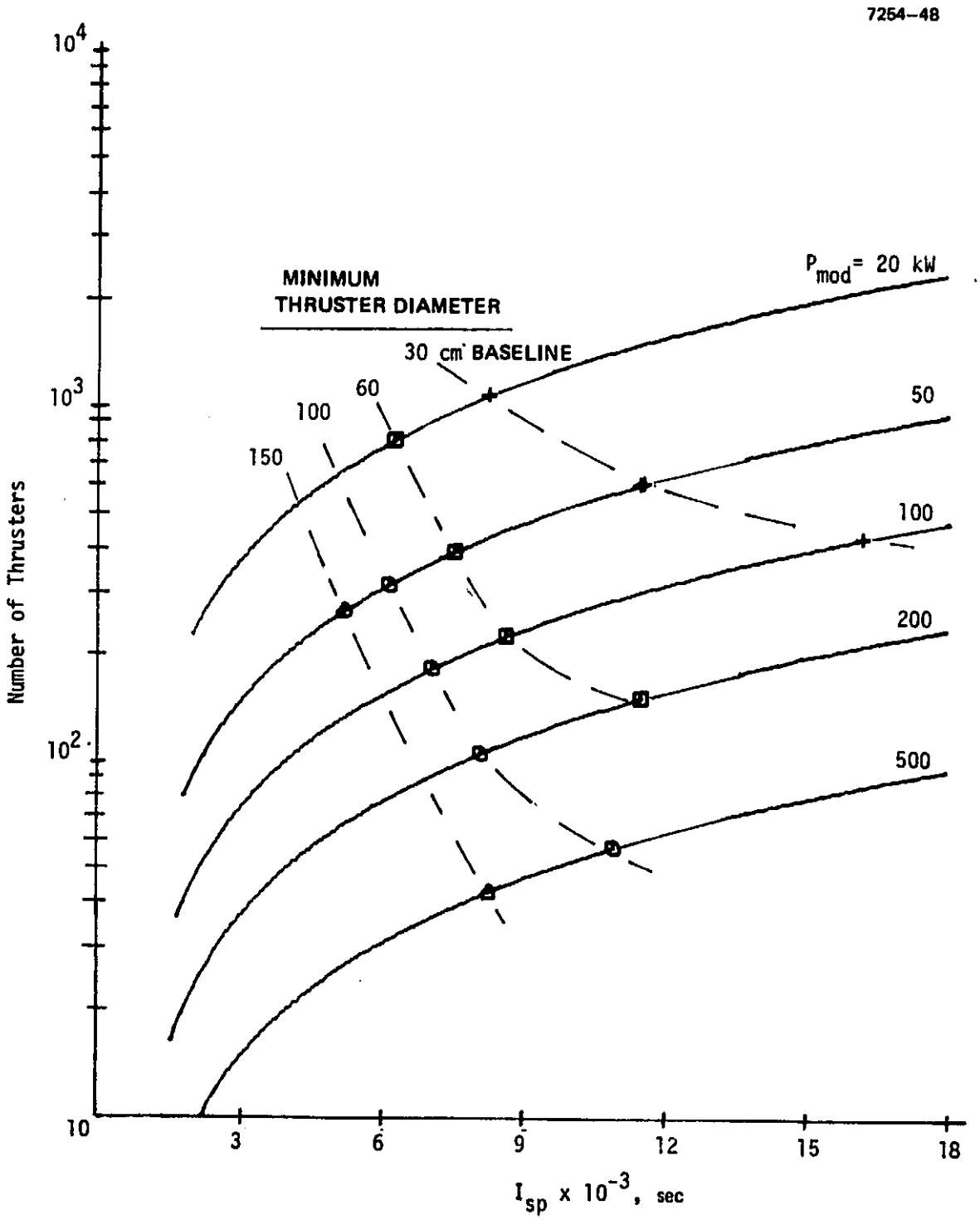

Figure 4-16. ORS/LS total number of thrusters versus I_{sp}.

the model assumes a proportionality to total ORV mass which increases rapidly as I_{sp} decreases. Another significant point is illustrated in Figure 4-16. In the low I_{sp} area, large thruster diameters are required, even for the 20-kW and 40-kW modules. Since a thruster diameter of less than 100 cm would be desirable, and since the number of modules is high (500 to 1000) for low module power, a 100-kW module for the baseline is reasonable.

Moving to the high I_{sp} end of Figure 4-12, total cost (Figure 4-13) is increasing while payload mass (Figure 4-14) is decreasing. The basic cause of both of these changes is the increased power associated with higher I_{sp}. Even with the low cost of power assumed for the baseline, raw power and PPU costs are important at high I_{sp}.

The most cost-effective range of I_{sp} for the ORS/LS baseline is from about 4,000 to 10,000 sec (Figure 4-15). The transportation cost per kg of payload decreases rapidly as I_{sp} increases to 6000 sec. As explained above, this occurs because payload mass is increasing rapidly. At higher values of I_{sp}, the specific cost increases again. This occurs because the payload mass is nearly constant while the costs, mainly for power and PPU, are increasing. Similar comments apply to the total cost as a function of payload mass. At the low end of this range, relatively large diameter thrusters or low-power modules would be needed. However, substantial cost penalties are incurred at low module power. The region around 8,000 to 9,000 sec I_{sp} and a module power of 100 kW provides a good compromise between low cost and thruster diameter. Lower module power would allow smaller diameters, but at a higher cost. Higher module power would reduce costs, but would require larger diameters; modules of even 100 kW will present a challenge for test facilities. These preliminary conclusions will be discussed further in light of the sensitivity results presented below.

c. Mission Design Sensitivities

The sensitivities reported in this section are for variations around the baseline self-powered round-trip mission. Other mission options are presented in Section 4.A.8.i. The sensitivities to mission ΔV, trip time initial mass in LEO, and launch cost can be summarized as follows:

- ΔV Sensitivity. The transportation cost sensitivity to variations in mission velocity requirements (ΔV) is shown in Figure 4-17 to be about $5/kg per km/sec at 9000 sec. This translates into a cost of $4 x 10^6 per km/sec for a payload of 8 x 10^5 kg.

- Trip Time (Up-Trip) Sensitivity. As Figure 4-18 shows, transportation cost is relatively insensitive to trip times longer than 100 days. Short trip times require that a larger fraction of the initial mass be devoted to propulsion and cost per kilogram of payload increases. In the 50 to 100 day interval, at 9000 sec, the sensitivity is approximately 0.2 $/kg day. With a payload of 8 x 10^5 kg, the cost of reducing trip time below 100 days would be about $1.6 x 10^5/day. There is obviously a large incentive for allowing more leisurely trips.

- Initial Mass (in LEO) Sensitivity. The rather significant effect of initial mass is illustrated in Figure 4-19. Quantitative sensitivities will not be assigned for this case because of the nonlinear variations. This behavior occurs because of certain fixed costs and costs that do not scale linearly with mass. However, it can be shown that the absolute cost sensitivity (i.e., $/kg of payload) to variations in initial mass increases with decreasing payload.

- Launch Cost Sensitivity. A major cost sensitivity factor is the cost of launch from Earth to LEO. As Figure 4-20 shows, the sensitivity to variations in C_ℓ is about 1.3 $/kg (payload) per $/kg (initial mass) of launch cost. Since launch cost is a dominant factor, as shown in Figure 4-13, the results will be extremely sensitive to this value. Although increasing C_ℓ shifts the curves to higher levels, the basic curve shape changes only slightly. (This is also generally the case for ΔV, M_o, and t_f.) This fact is important in assessing the impact on thruster technology (i.e., recommended thruster size).

d. Thruster Sensitivities

The factors listed in Table 4-4 represent the major variables related to thruster technology. Note that all the parameters in the cost model are fixed, while the variable being considered is changed. Thus, all the perturbations (except for category 8 in Table 4-4) are relative to the 100-kW curve in Figure 4-12. Sensitivity to thruster related variables are summarized below:

- Thruster Life. This sensitivity is shown in Figure 4-21 for two constant life models and a beam current density dependent model (see Eq. 4-17). Changes from the 10^4 hr baseline to longer life have essentially no effect on cost; shorter lives, as implied by the beam current dependent model, have an effect above 6000 sec.

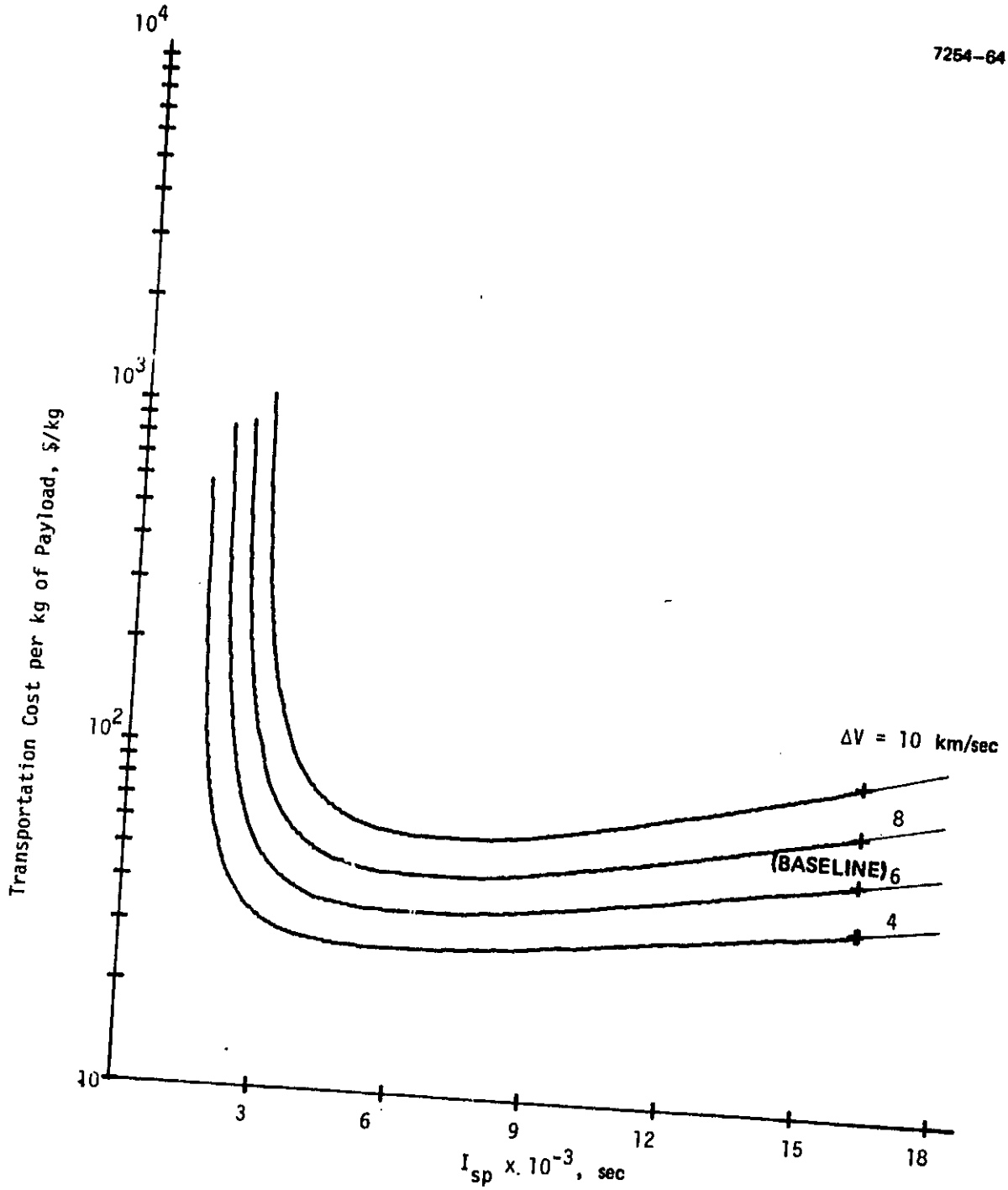

Figure 4-17. ORS/LS effect of mission velocity requirement (ΔV).

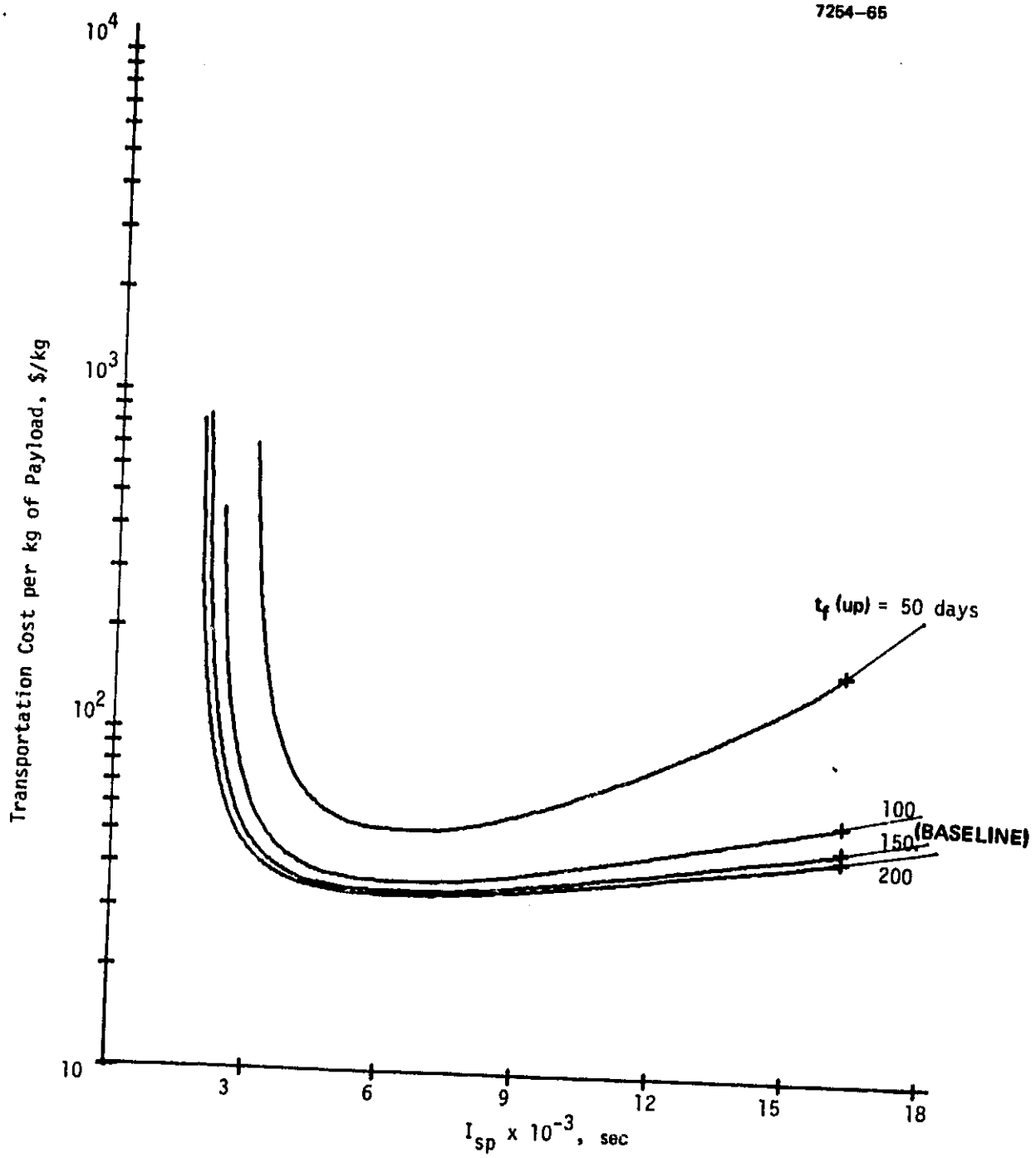

Figure 4-18. ORS/LS effect of trip time (up trip).

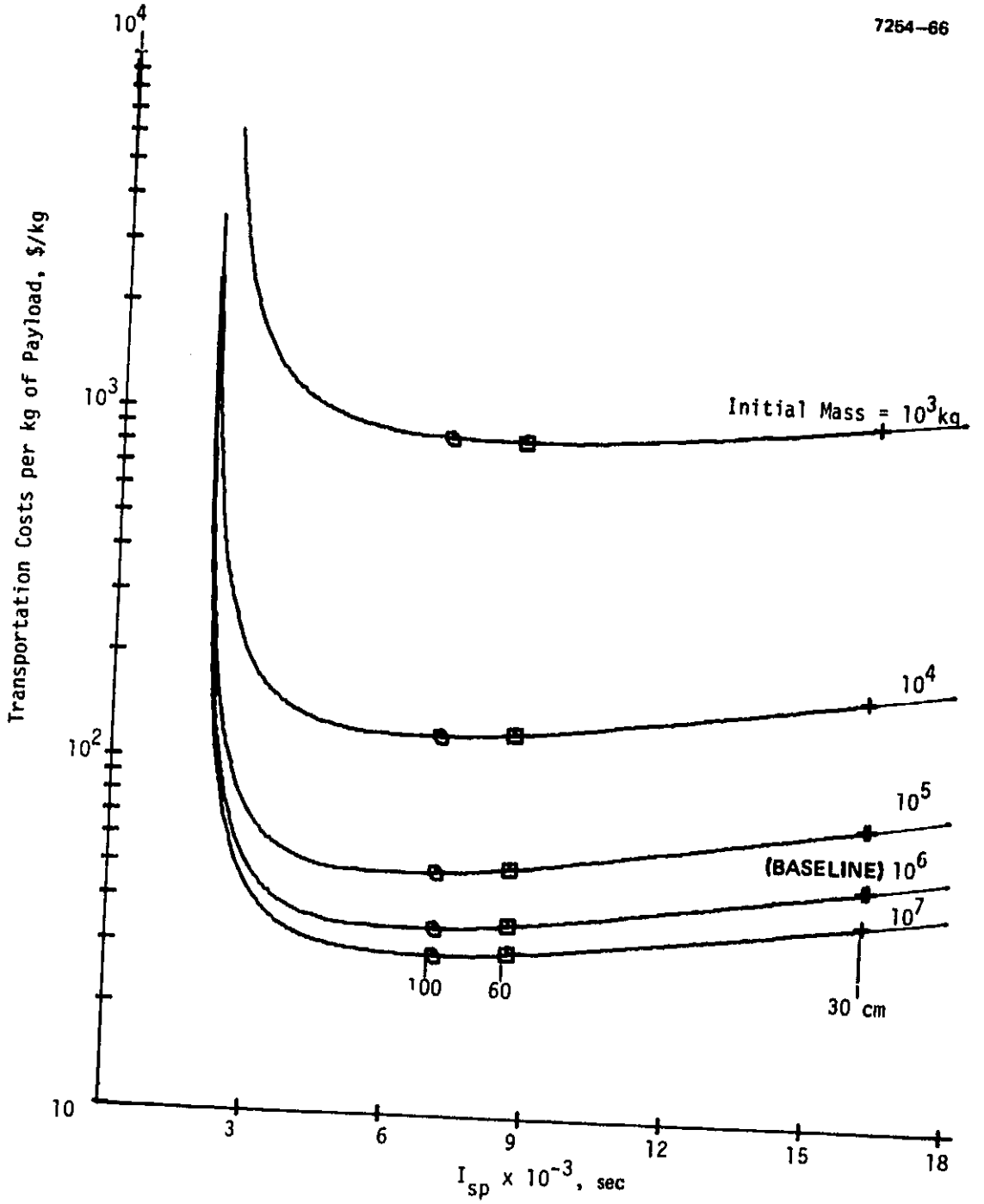

Figure 4-19. ORS/LS effect of initial mass.

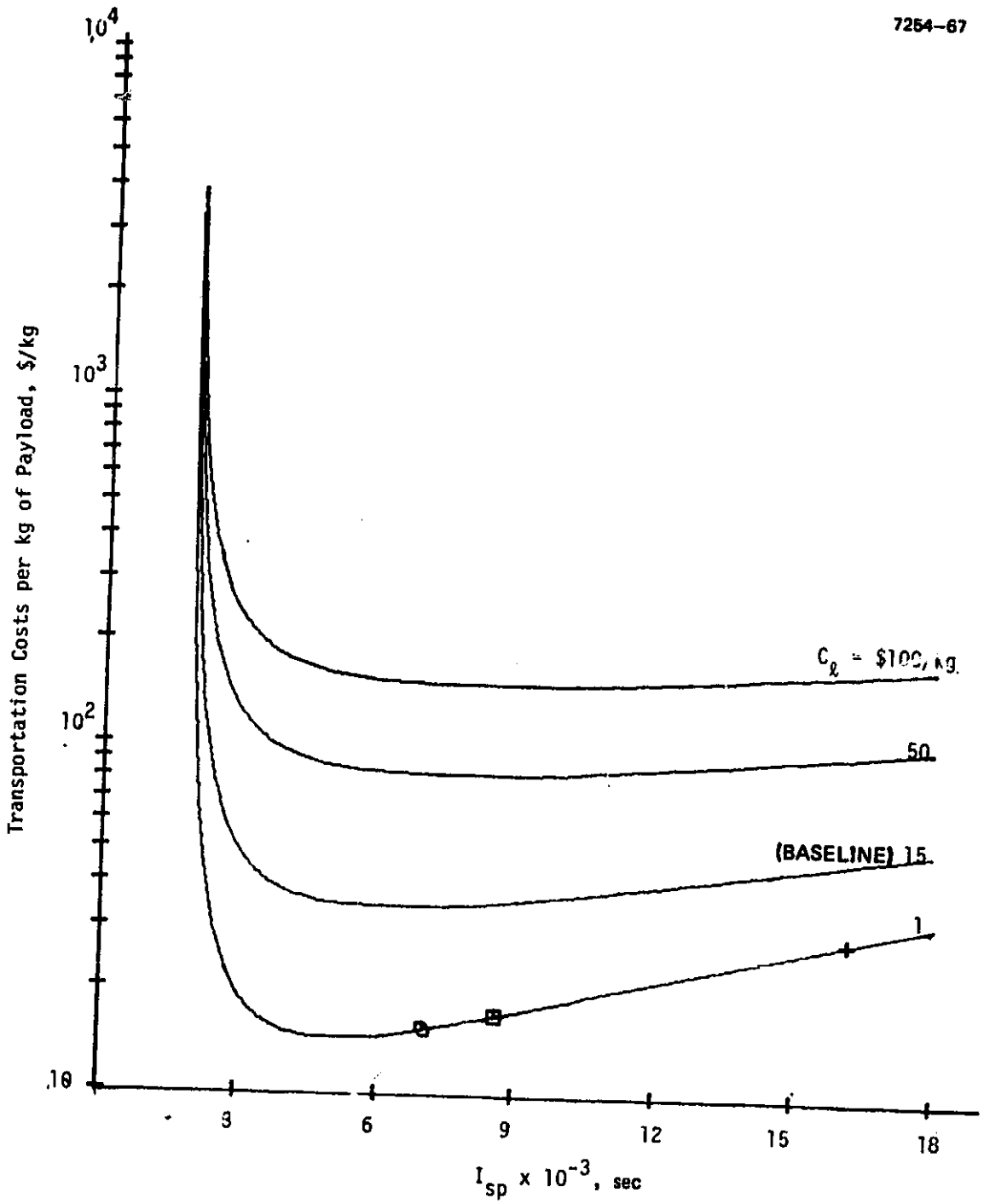

Figure 4-20. ORS/LS effect of launch cost.

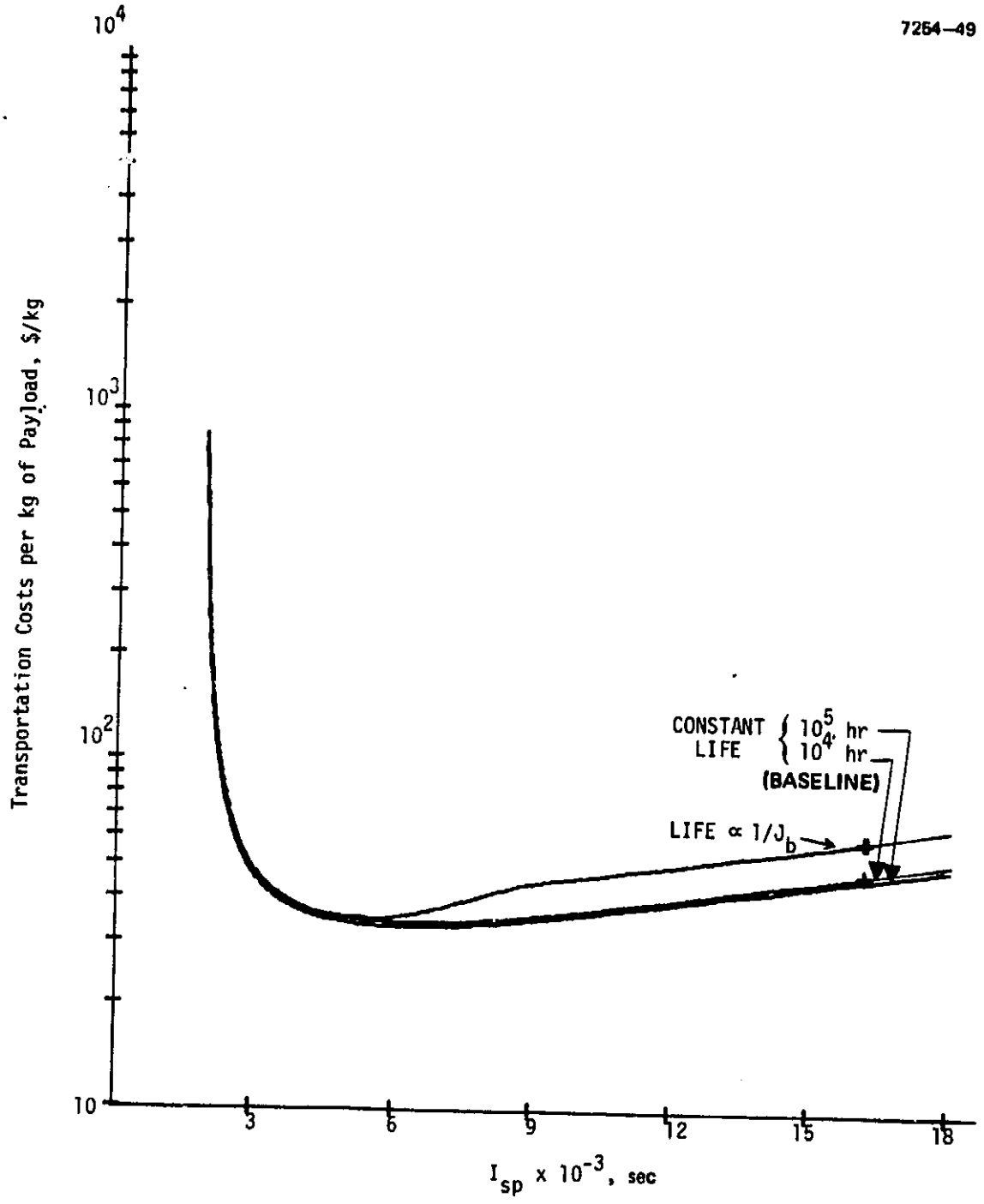

Figure 4-21. ORS/LS effect of thruster life.

As an example of the sensitivity of cost to lives shorter than 10^4, consider the baseline region discussed in Section 4.A.8.b. At 9000 sec, the 100-kW module has a diameter of about 55 cm and beam conditions of 50 A at 2000 V (see Figure 4-4). With the beam current dependent model, a life of about 815 hr is predicted. Since the cost difference is about \$8/kg, the ratio of cost change to life change is approximately 9×10^{-4} \$/kg/hr of life. Thus, for a typical payload of 8×10^5 kg, the absolute ratio would be $\sim$ \$700/hr. In other words, in developing a new thruster for the ORL/LS application, if the cost to achieve thruster lives longer than $\sim$ 1000 hr is less than \$700/hr, the increase would be cost effective. Since this ratio is nonlinear and is probably substantially less near 10^4 hr, a life goal of a few thousand hours would probably be reasonable. The main point to be made is that thruster lives of a few thousand hours are quite acceptable for the assumed application.

- Thruster Efficiency. Cost sensitivity to thruster (or system) efficiency is shown in Figure 4-22. The baseline efficiency, as discussed in Section 4.A.3, is only moderately optimistic. It assumes that electrical losses, utilization efficiency, and correction factors can be maintained at the same values as for the present 30-cm thruster with a 2 A beam. At higher beam current densities, measured utilization increases while the correction factors decrease, tending to produce a constant total efficiency. The probability is low for achieving efficiencies higher than the model predicts. The probability is moderate for slight reductions in the model predictions. But the probability is low for efficiencies significantly lower than predicted.

  Thus, the results indicated in Figure 4-22 show that system cost should not be too sensitive to reasonable changes in efficiency. More specifically, efforts to increase efficiency are not warranted, and minor reductions from the predicted values will not substantially affect cost.

- Thruster Mass. Cost sensitivity to thruster mass is shown in Figure 4-23. Except at low I_{sp}, thruster mass variations from 0 to 200 percent of the baseline value have little impact on total cost. Such an effect is explained by the small fraction thrusters contribute to ORV total mass. In developing a new thruster, mass could be traced for other factors such as larger fabrication tolerances, lower cost, or increased life.

- Thruster Cost. The sensitivity to thruster first unit cost is shown in Figure 4-24. Small variations around the baseline have little impact on transportation cost, although significant increases in cost would begin to be important.

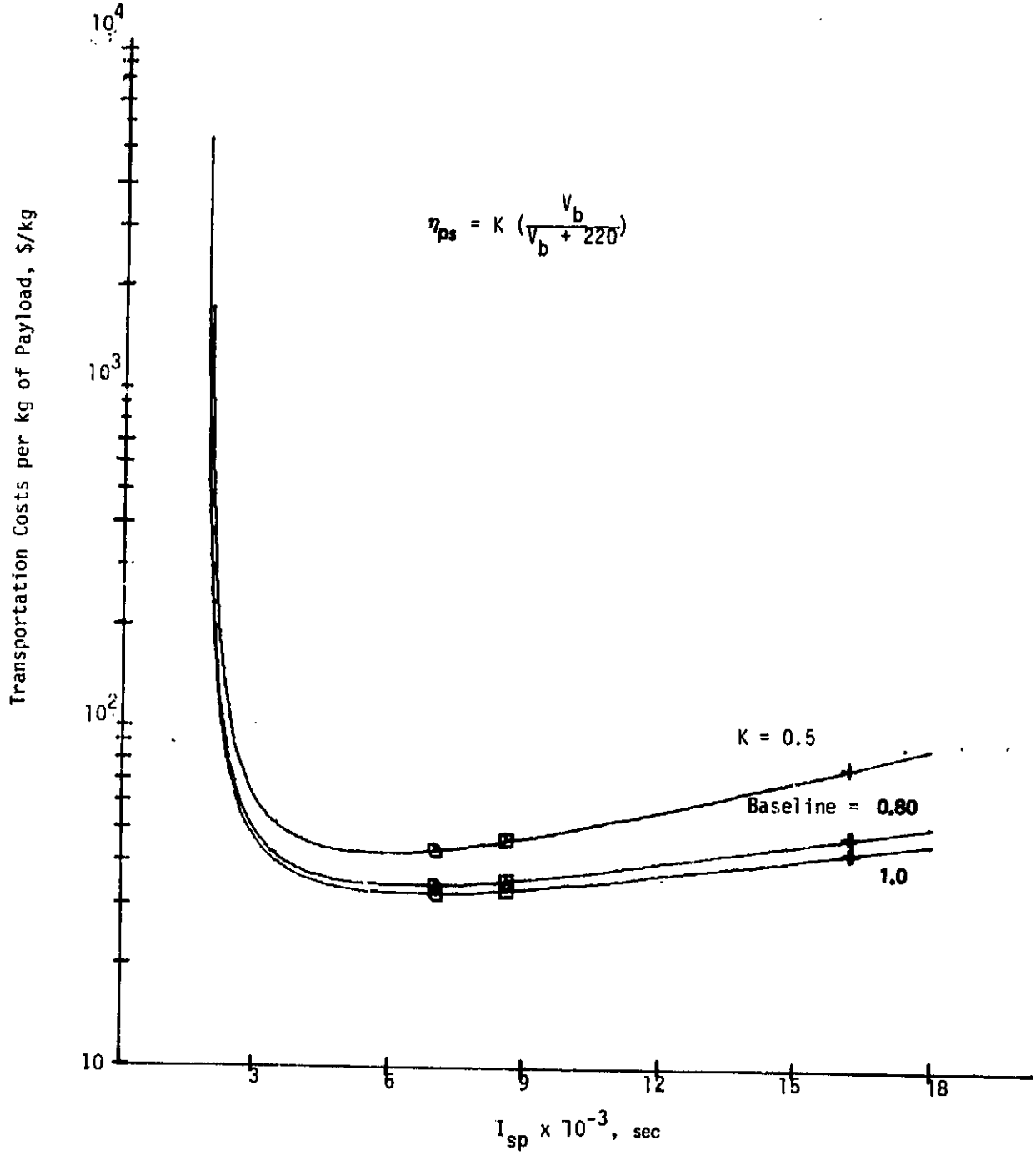

Figure 4-22. ORS/LS effect of thruster or propulsion system efficiency.

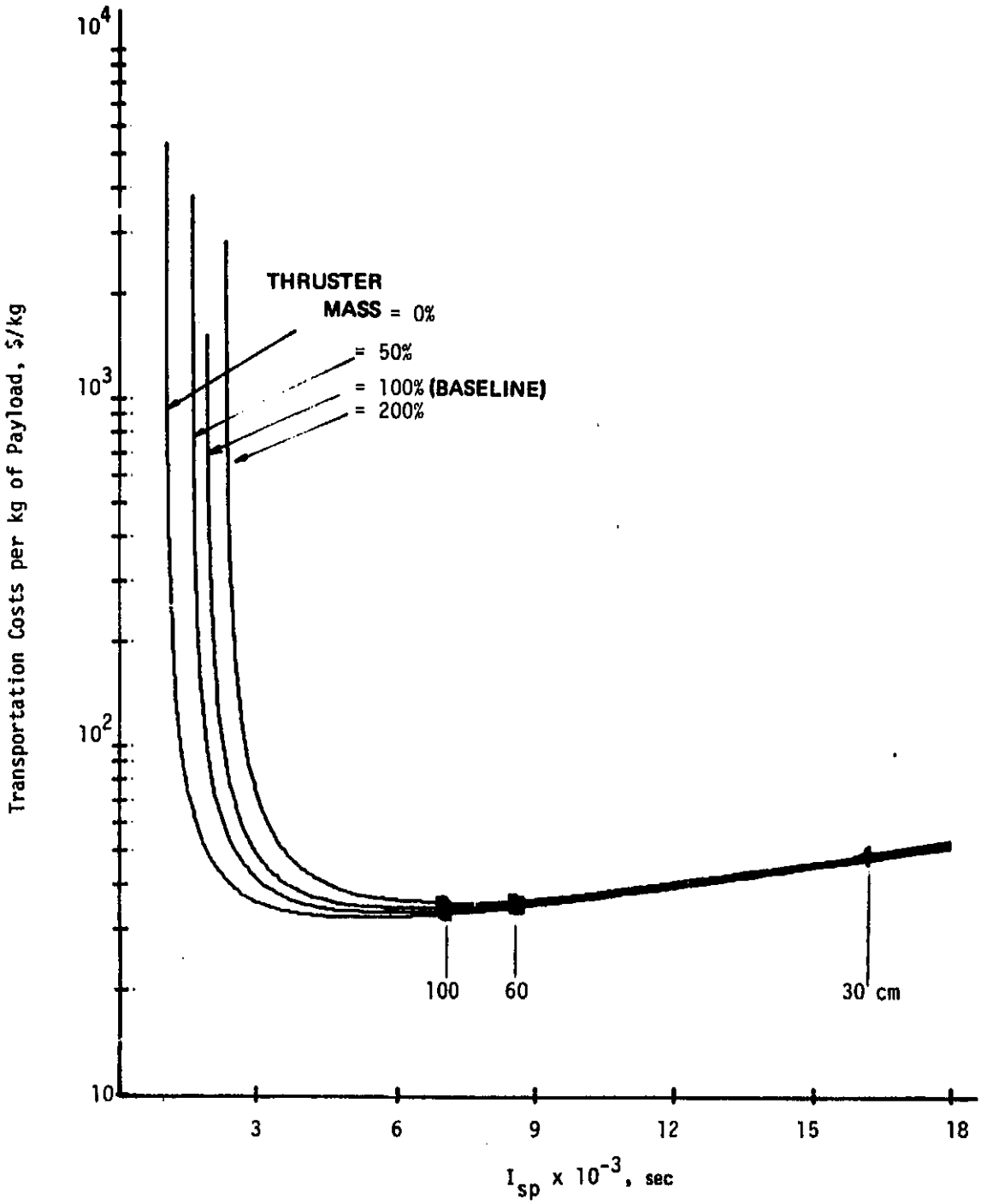

Figure 4-23. ORS/LS effect of thruster mass.

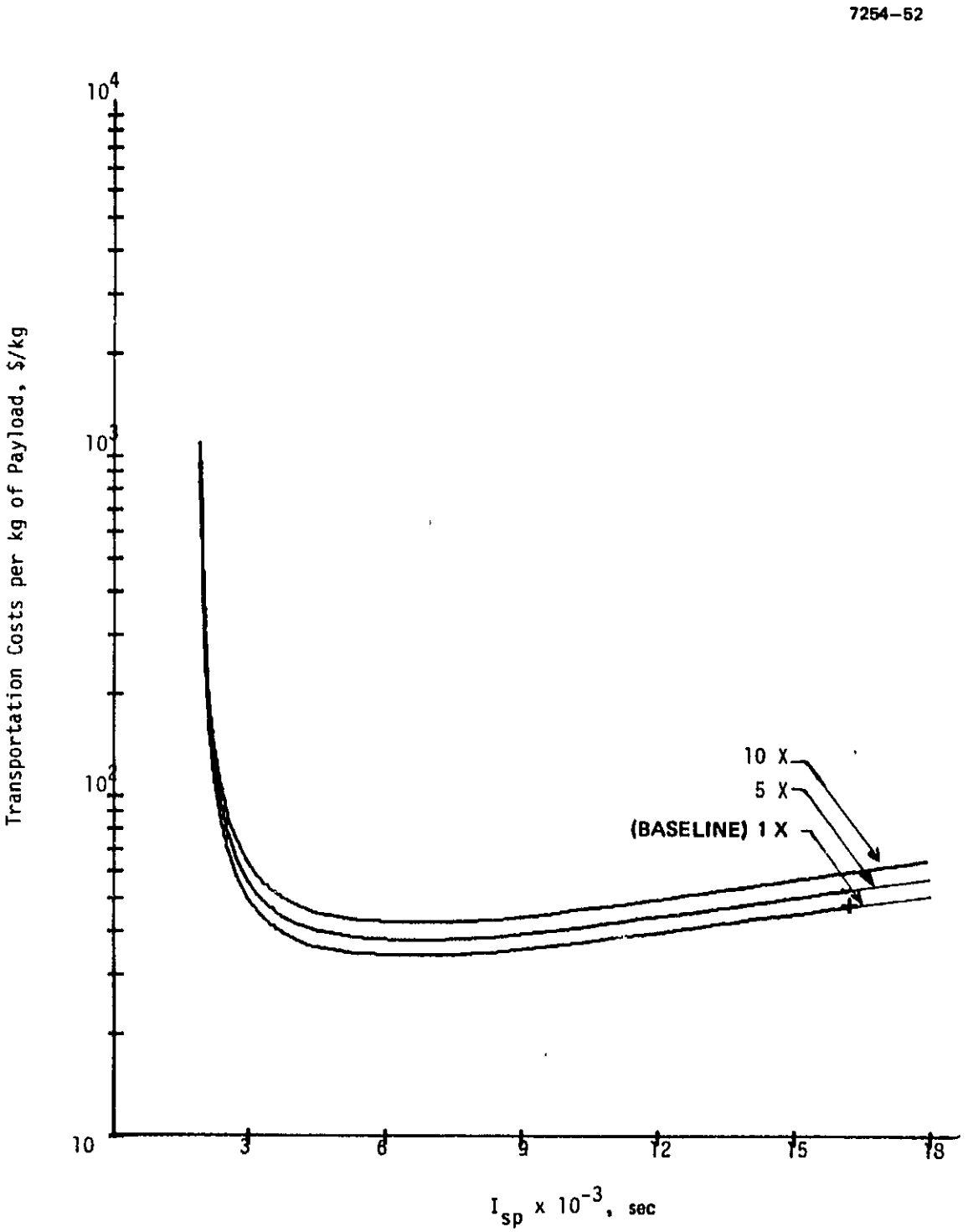

Figure 4-24. ORS/LS effect of thruster cost.

- Ion Optics "R" Ratio. The R ratio, defined as the ratio of beam voltage to total voltage, plays a role in defining perveance. At a fixed beam voltage and thruster diameter, the beam current that can be drawn from a given thruster varies inversely with the R ratio to the 3/2 power. As shown in Figure 4-25, even with ratios as low as 0.4 (0.7 is typical), transportation costs are not strongly affected. The major effect is in thruster diameter, since the power (thrust) per unit area also varies inversely with the R ratio to the 3/2 power.

- Thruster Redundancy. The baseline redundancy used in the cost model is 0.2. Variations from 0 to 2.0 (200 percent redundancy) have, as illustrated in Figure 4-26, only a minor effect on cost. Thus, the ORV can be designed to meet any given reliability requirement with little impact on cost (particularly since 0.2 provides good reliability).

e. Propellant Sensitivities

Two propellant parameters were investigated: propellant type and propellant cost. Propellant tankage mass and tankage cost sensitivities were omitted because tankage mass is such a small fraction of ORV mass (see Figure 4-14) that even large variations would not affect transportation cost.

(1) Propellant Type – Four propellants (argon, krypton, xenon, and mercury) were considered, as shown in Figure 4-27. Although the same cost was used for all propellants in Figure 4-27, the lack of sensitivity to type is valid. The $0.4/kg cost is representative of argon but is low for the other propellants. With higher costs for He, Xe, and Kr, the cost curves will compact even more. The primary difference between the various propellants is thruster diameter at a given I_{sp} if module power is fixed. For a constant module power of 100 kW, the I_{sp} for a 30-cm thruster would range from about 16,000 sec with argon to about 7,000 sec with Hg as shown in Figure 4-4. Propellant choice must be made on a basis other than its impact on transportation cost (e.g., environment, availability, thruster development, or packaging).

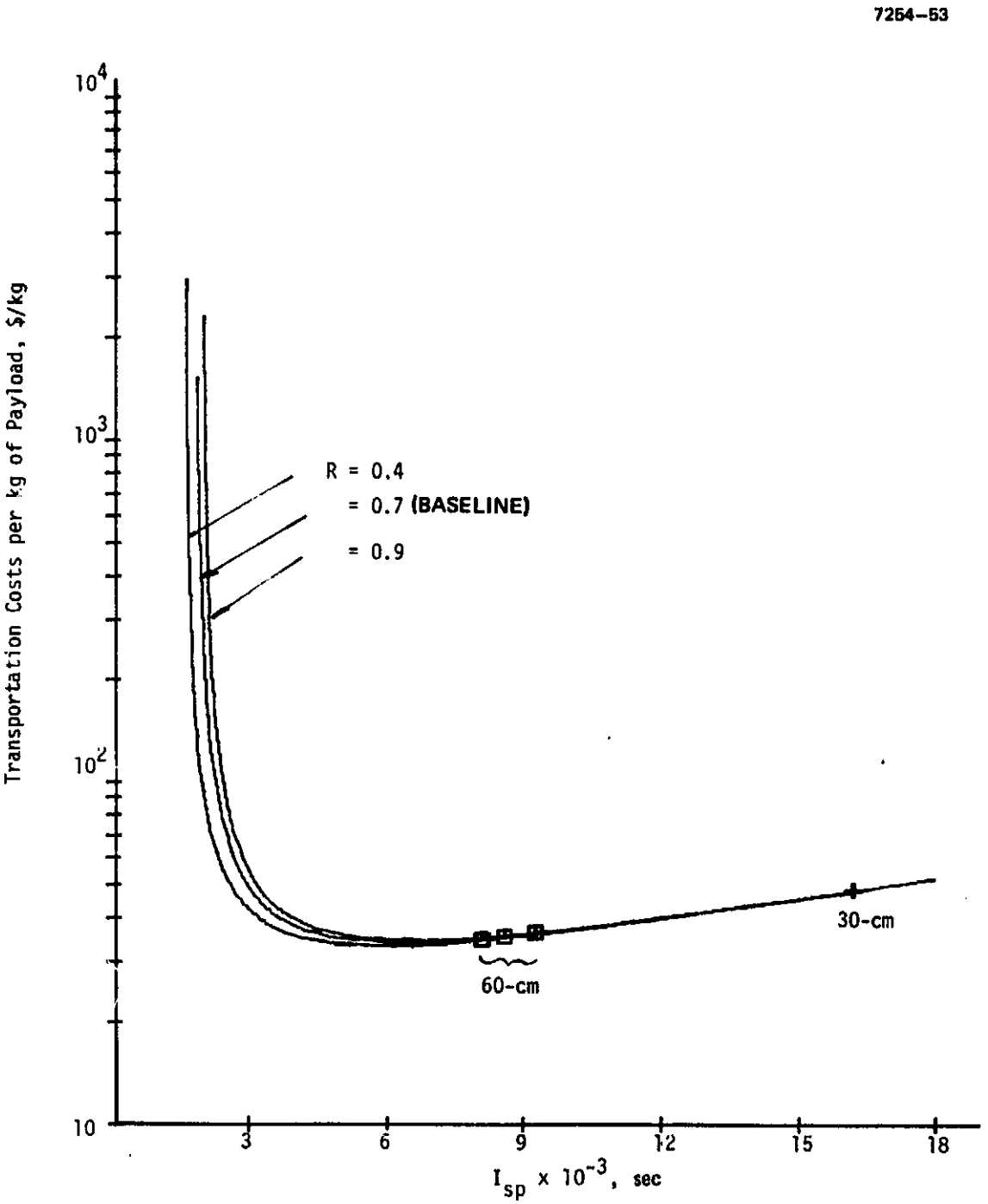

Figure 4-25. ORS/LS effect of "R" ratio.

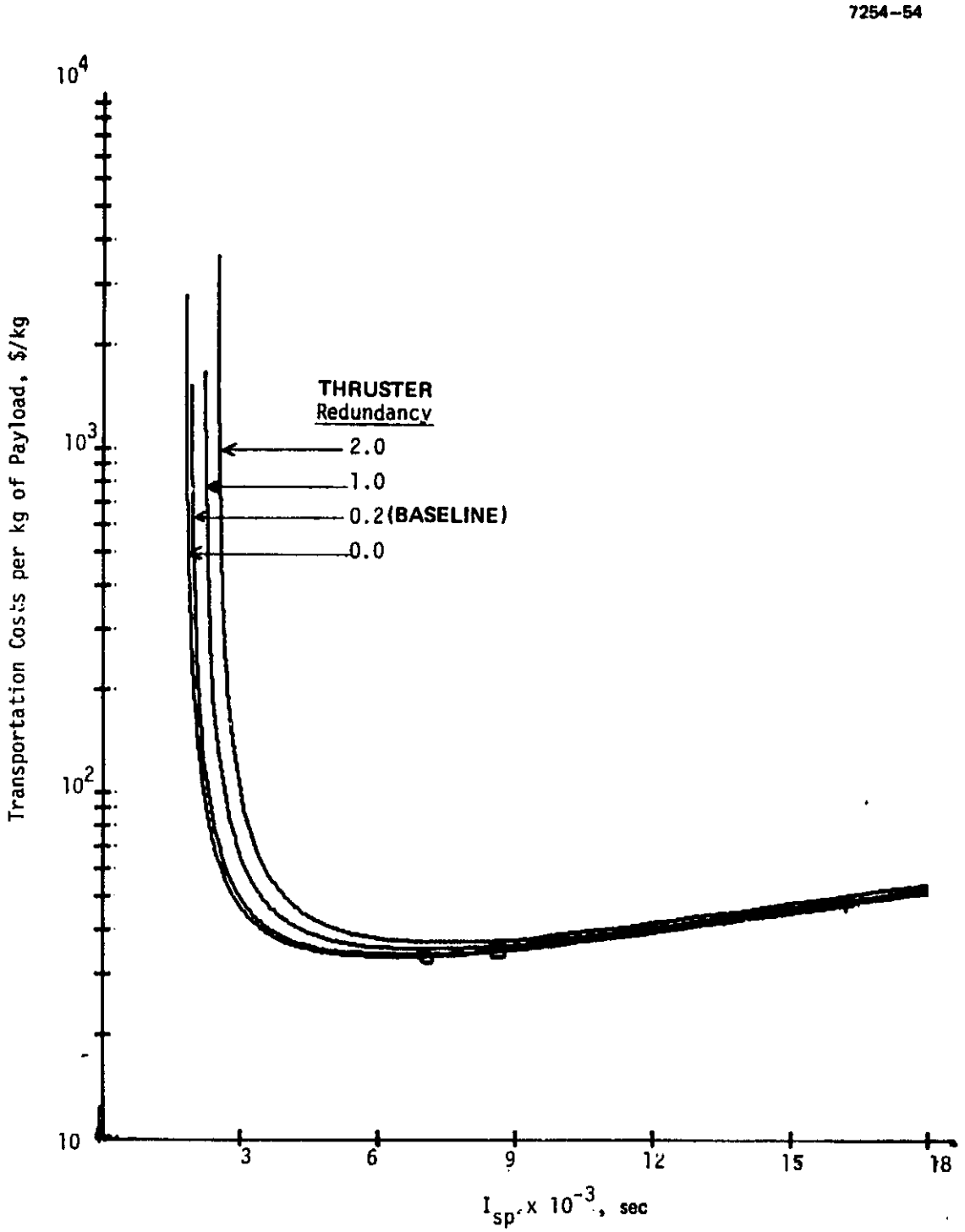

Figure 2-26. ORS/LS effect of thruster redundancy.

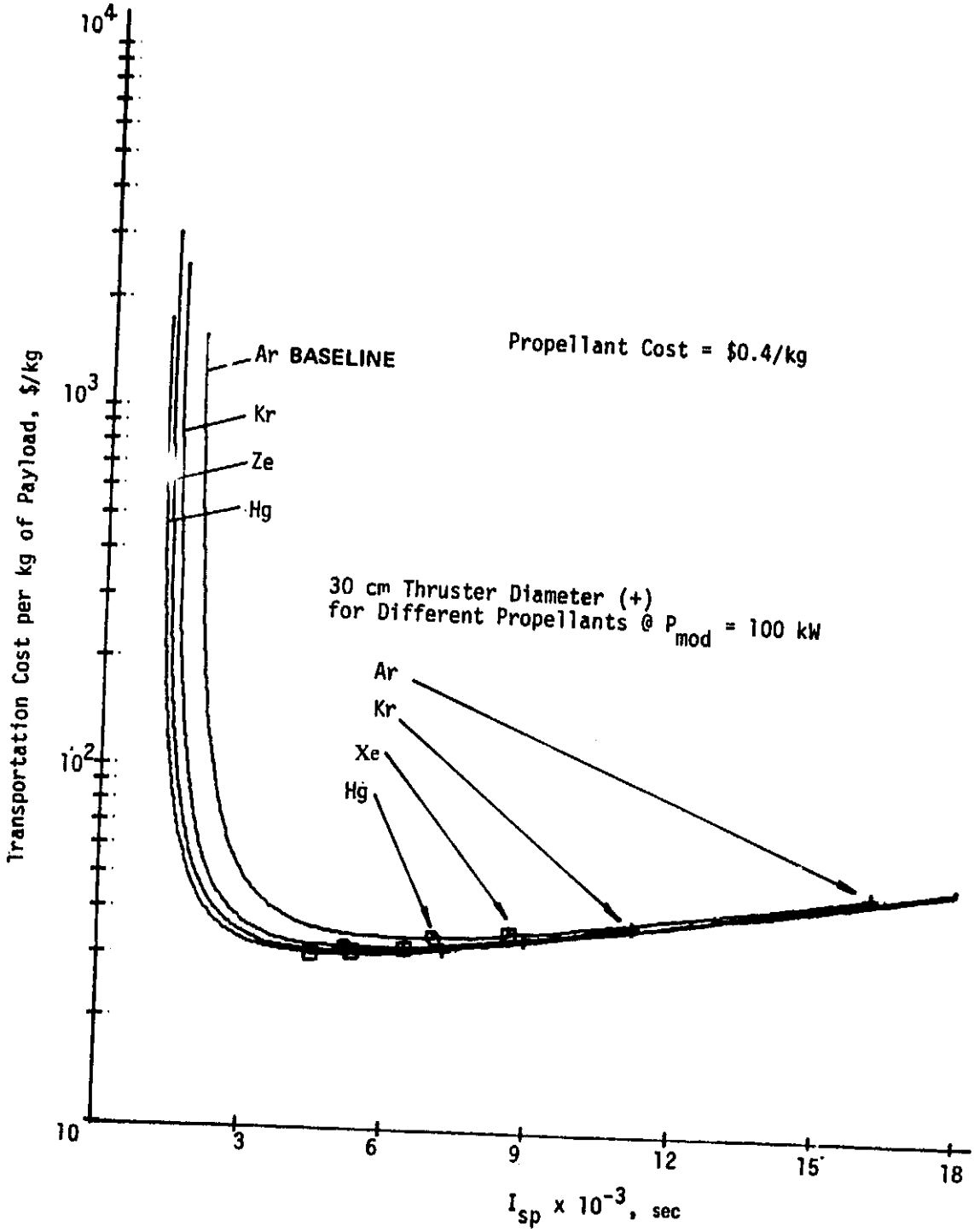

Figure 4-27. ORS/LS effect of propellant type.

(2) Propellant Cost — The transportation cost sensitivity to propellant cost per kilogram is shown in Figure 4-28 for argon. For I_{sp}'s in the range of 3,000 to 9,000 sec, propellant cost can affect transportation cost. However, for I_{sp}'s greater than 9,000 sec, the dependence on propellant cost is rather small and should not influence ORV or propulsion system design.

f. Power Processing Unit Sensitivities

The variables considered in the PPU study include specific mass, cost, and redundancy. PPU life was assumed to be long compared with ORV life, and wearout is negligible. In addition, PPU efficiency was omitted since the sensitivity result would be similar to that shown in Figure 4-22.

(1) PPU Specific Mass — The results presented in Figure 4-29 indicate that mass decreases from the baseline would not significantly reduce transportation costs. However, large increases in mass from the baseline would have a major impact. In the region of 9,000 sec, the transportation cost sensitivity is about \$3/kg/unit change in α_{pp} (baseline value at 100 kW is 1.4 kg/kW). Thus, with a payload of 8×10^5 kg, the sensitivity is about $\$2.4 \times 10^6$ per unit change in α_{pp}. Such sensitivity would probably provide incentive to maintain low specific mass or to reduce specific mass if initial developments are significantly higher than the baseline.

(2) PPU Cost — The importance of PPU first unit cost is shown in Figure 4-30. At 9,000 sec the sensitivity of transportation cost to PPU cost is about \$0.07/kg/percent change in PPU unit cost. In absolute terms with 8×10^5 kg of payload the sensitivity is about $\$5.6 \times 10^4$ per 1 percent change in PPU cost. Since the PPU cost model is probably accurate only within a factor of two (i.e., from 1/2 to 2 times the model estimate), a 100 percent increase in PPU cost would be quite significant.

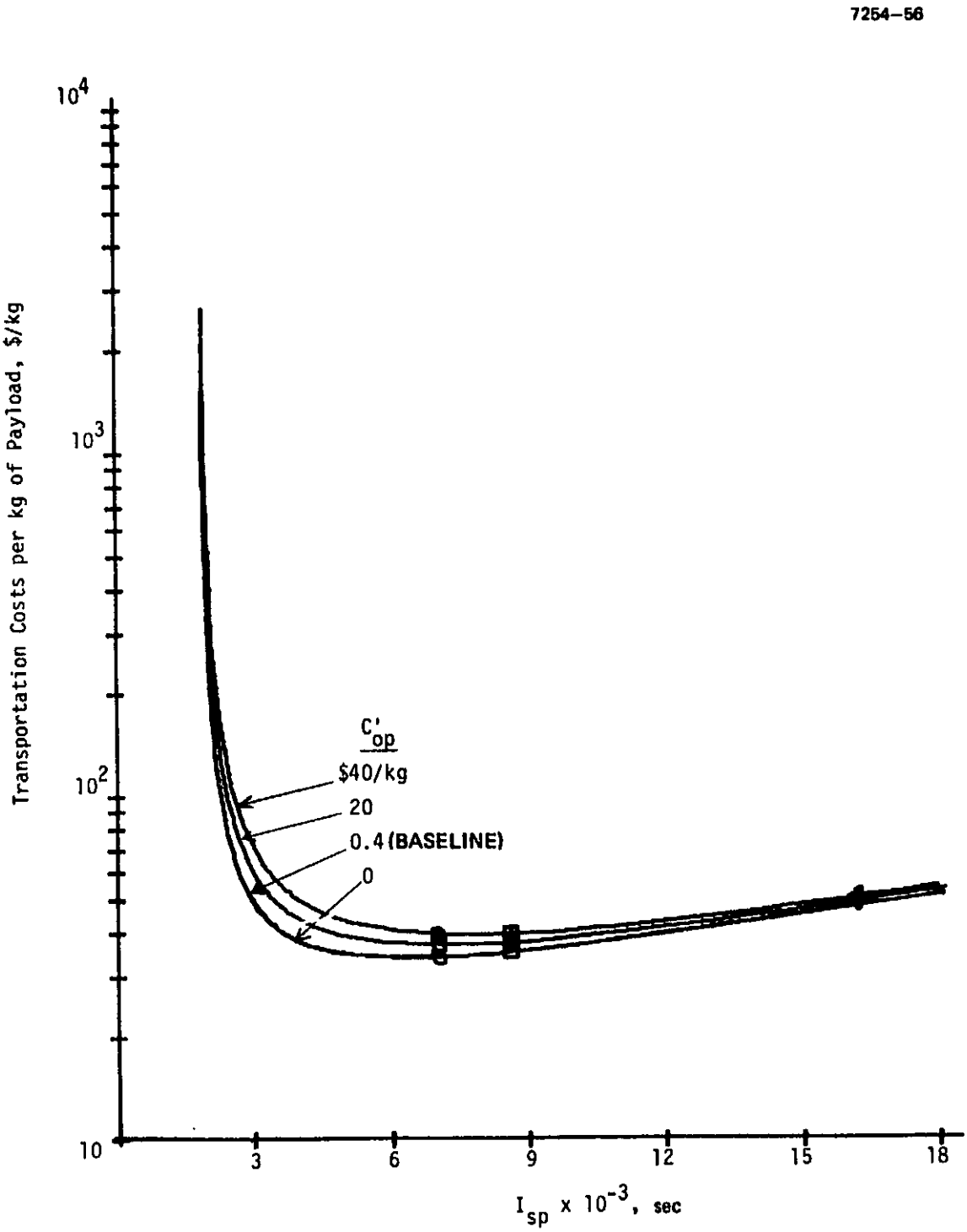

Figure 4-28. ORS/LS effect of propellant cost.

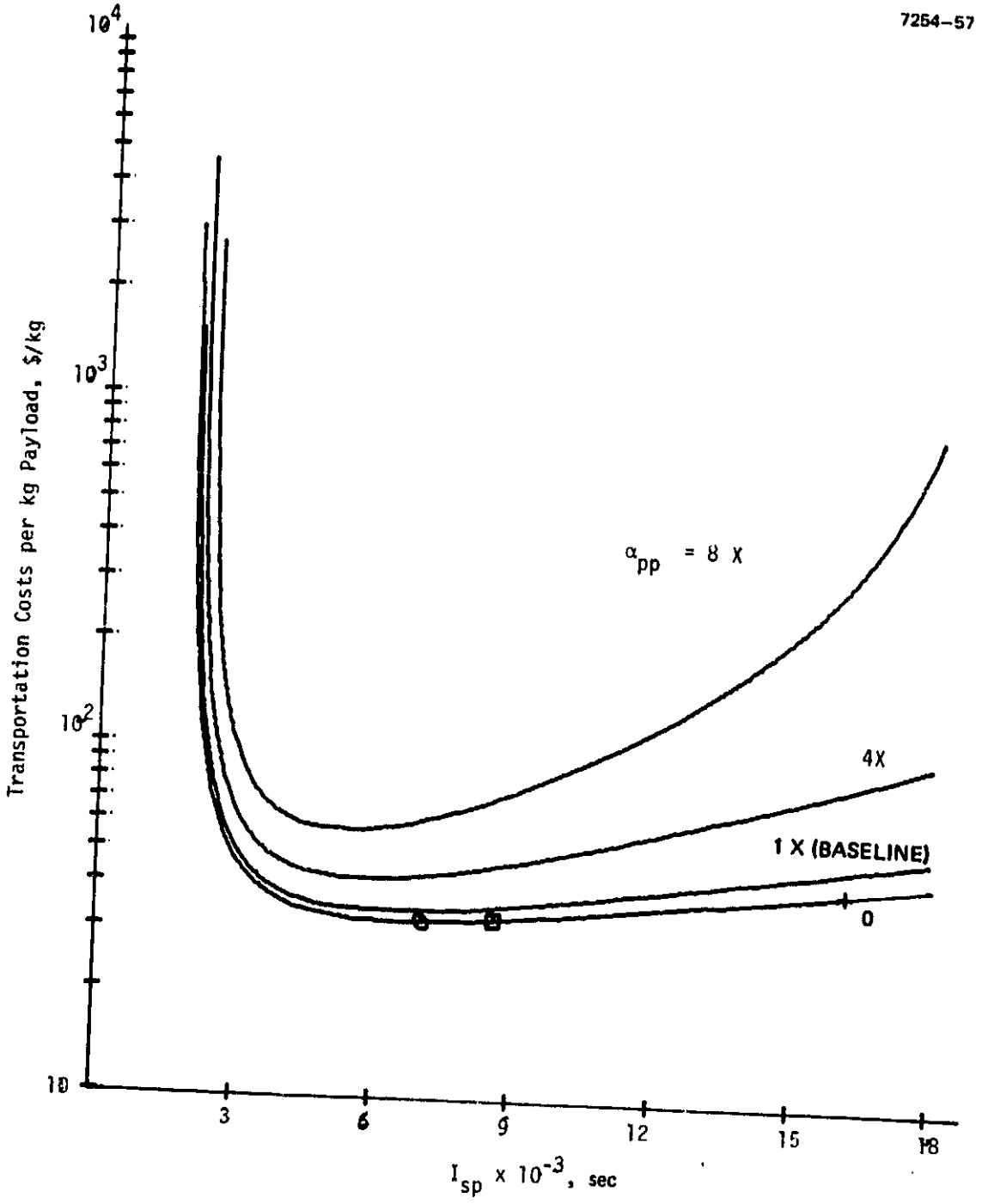

Figure 4-29. ORS/LS effect of power processor specific mass.

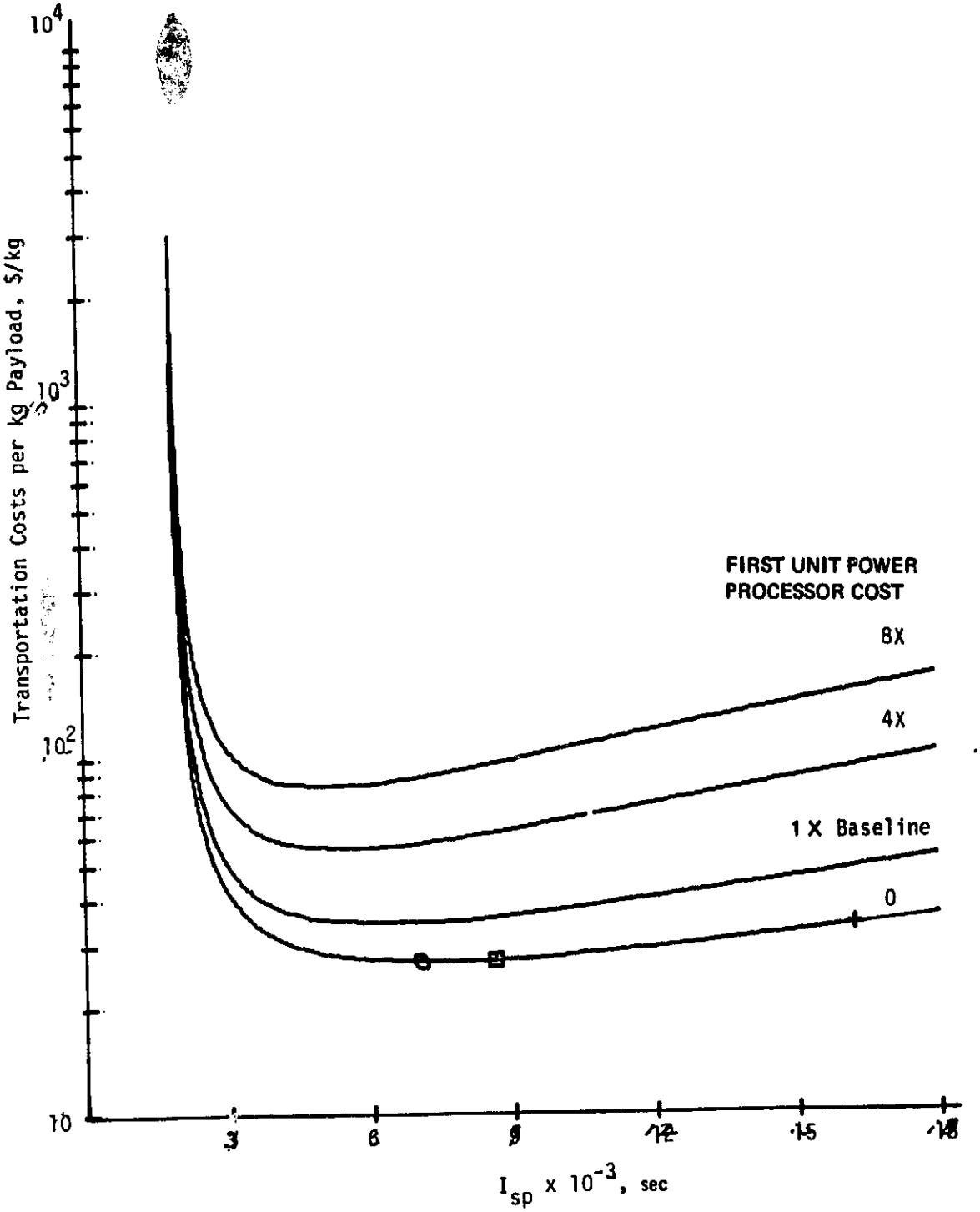

Figure 4-30. ORS/LS effect of power processor first unit cost.

(3) PPU Redundancy — The effect of PPU redundancy is more dramatic than for the thruster, as shown in Figure 4-31, since PPU cost represents a larger fraction. However, with reasonable redundancy factors (i.e., less than 1.0), transportation cost will not be affected significantly.

g. Power Source Sensitivity

Power source mass and cost are among the most sensitive parameters in the present cost model as well as in essentially all SEP applications. These factors and degradation are considered here. However, under category 6 in Table 4-4, other power sensitivities are presented.

(1) Power Source Specific Mass — As indicated in Eq. 4-24, solar power source mass is the product of specific mass (kg/kW) and total installed power (for propulsion). Transportation cost sensitivity to specific mass is shown in Figure 4-32. Current technology is about 15 kg/kW, but projected advances from the literature were assumed in selecting the 3 kW/kg baseline. Using the 9,000 sec point again as a reference point, the transportation cost sensitivity is about 4 to 5 $/kg per unit increase is specific mass. With a payload of 8×10^5 kg, the sensitivity is \$30 to 40 $\times 10^6$ per kg/kW. Clearly, there is a strong incentive to minimize power source specific mass.

(2) Power Source Specific Cost — Sensitivity to power source specific cost ($/kW) is shown in Figure 4-33. Although the baseline of \$0.5/W is about a factor of 10^3 less than current costs, studies of large power systems project such substantial reductions in the next few decades. The sensitivity at 9,000 sec is about 5.5 $/kg per unit change in power cost, or \$44 $\times 10^6$ per $/W of power. This extreme sensitivity places a large premium on low-cost power for this application.

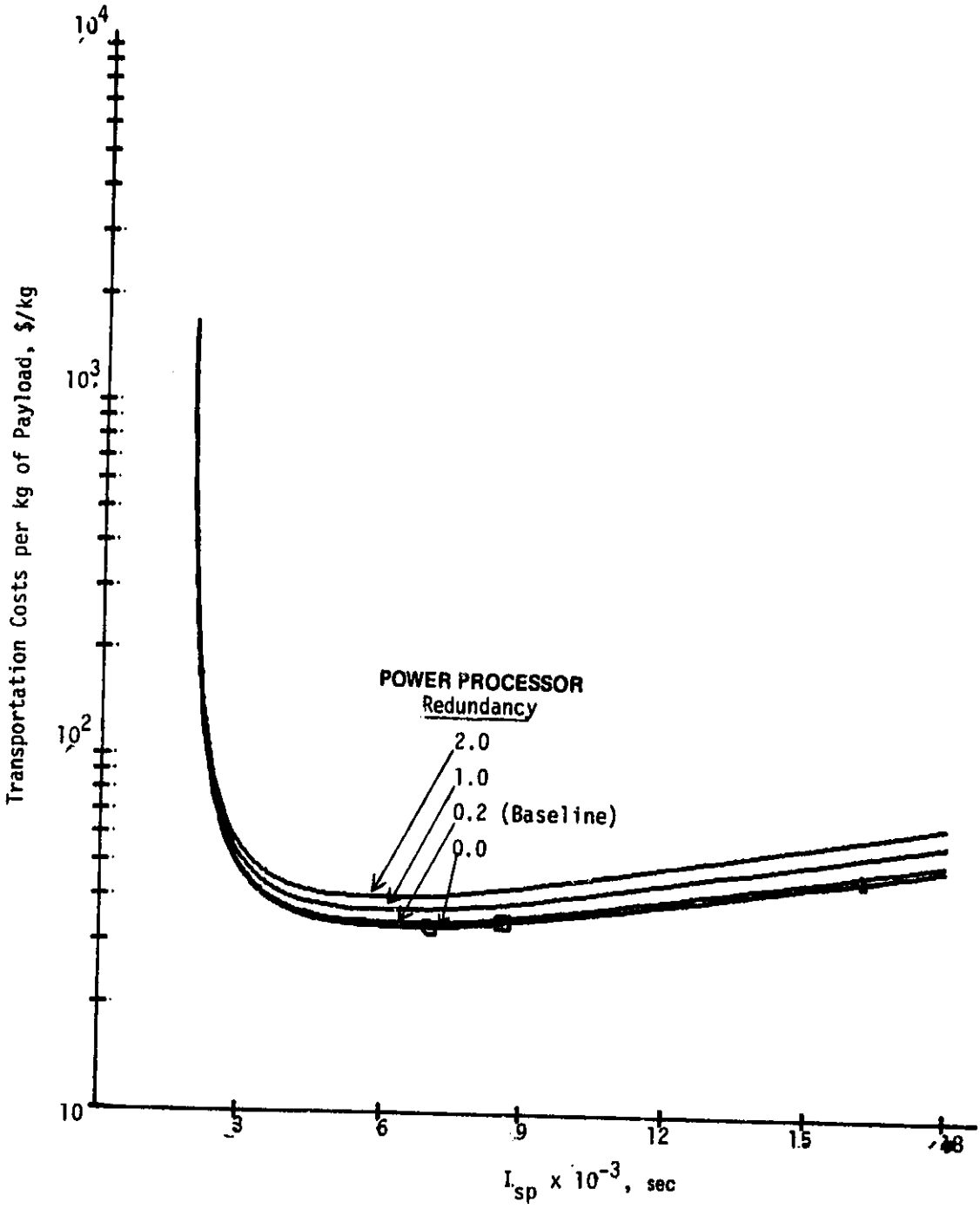

Figure 4-31. ORS/LS effect of power processor redundancy.

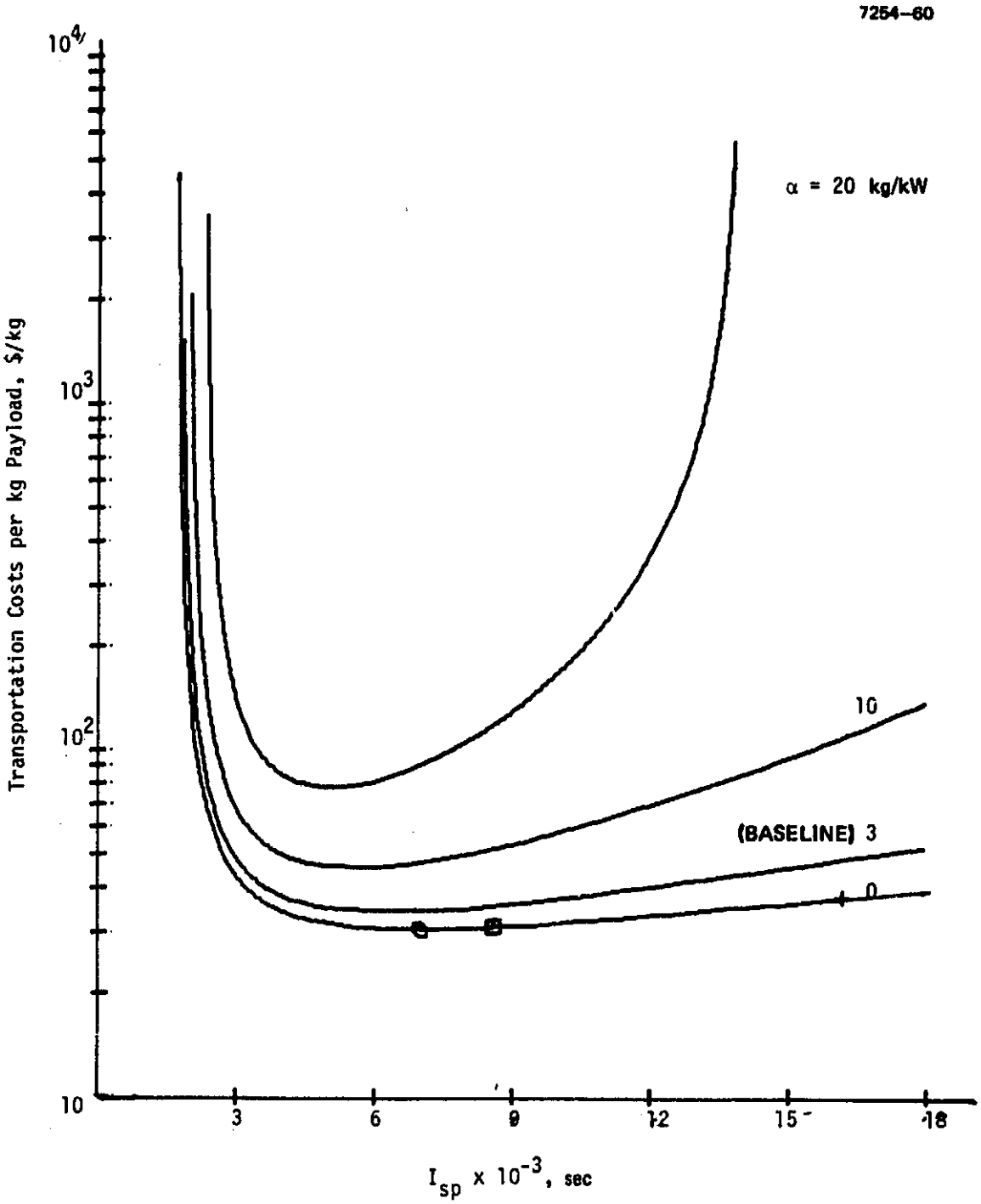

Figure 4-32. ORS/LS effect of power source specific mass.

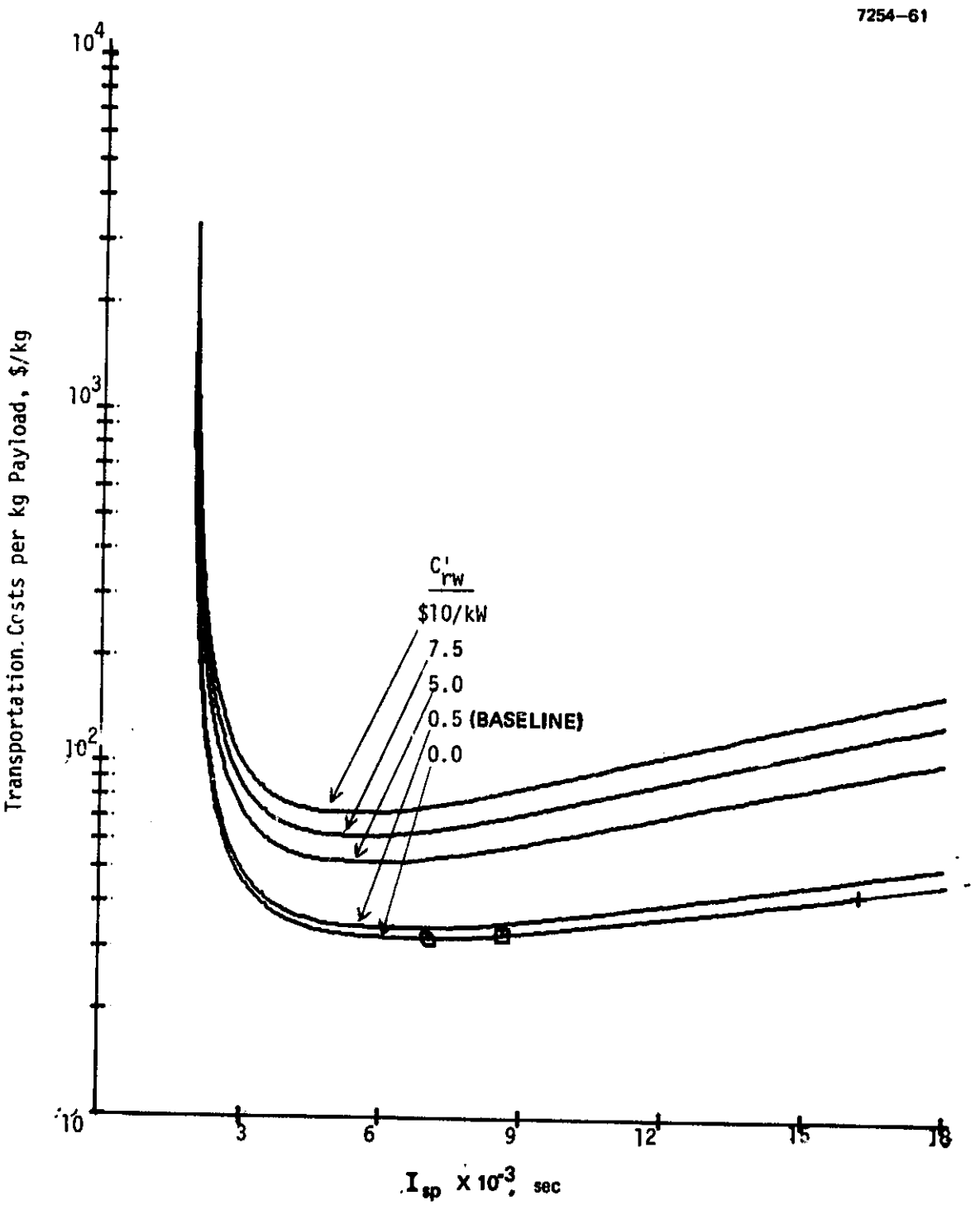

Figure 4-33. ORS/LS effect of power source specific mass.

(3) Power Source Degradation — It is assumed that the power source utilizes some form of photovoltaic conversion. In raising the orbit through the Van Allen belt, degradation may occur depending on the array design and on projected improvements in cell technology. The impact of degradation for two equivalent flux levels is shown in Figures 4-34 and 4-35. As defined in Section 4.A.5, curve A is representative of current technology, while curves B and C are assumed parametric improvements. At the 9,000 sec point, the sensitivities are about 0.3 and 0.5 \$/kg per 1 percent change in degradation at 10^{15} and 10^{16} equivalent flux, respectively. These convert to absolute sensitivities of \$2.4 x 10^5 and \$4 x 10^5, respectively, per 1 percent change in degradation. Although improvements in degradation are not quite as beneficial as cost or mass improvements, costs in the range of \$2 to 8 x 10^6 would be incurred if degradation followed curve A or B rather than the assumed baseline.

h. ORV System Design Sensitivities

This category includes some of the system factors that would go into developing and building an ORV, as indicated in Table 4-4. Since most of the values selected for these factors are rather arbitrary, the main importance of this particular set of results is in assessing which factors might have the most influence. With such sensitivity information, a more logical or balanced direction of thruster technology can be chosen.

(1) Structure and Mechanisms Sensitivity — As Figures 4-36 and 4-37 show, within reasonable bounds, structure and mechanisms parameters (C'_{rsm} and α_{sm}) have little effect on transportation cost. Combining high mass fraction and high specific cost would have a greater effect but would not greatly influence the curve shape or thruster selection.

(2) Subsystems Sensitivity — Because of the large exponent used in the subsystems cost model (see Eq. 4-37), subsystem cost can strongly affect transportation cost, as shown in Figure 4-38. Again, the shape of the curves is not greatly affected over a rather large

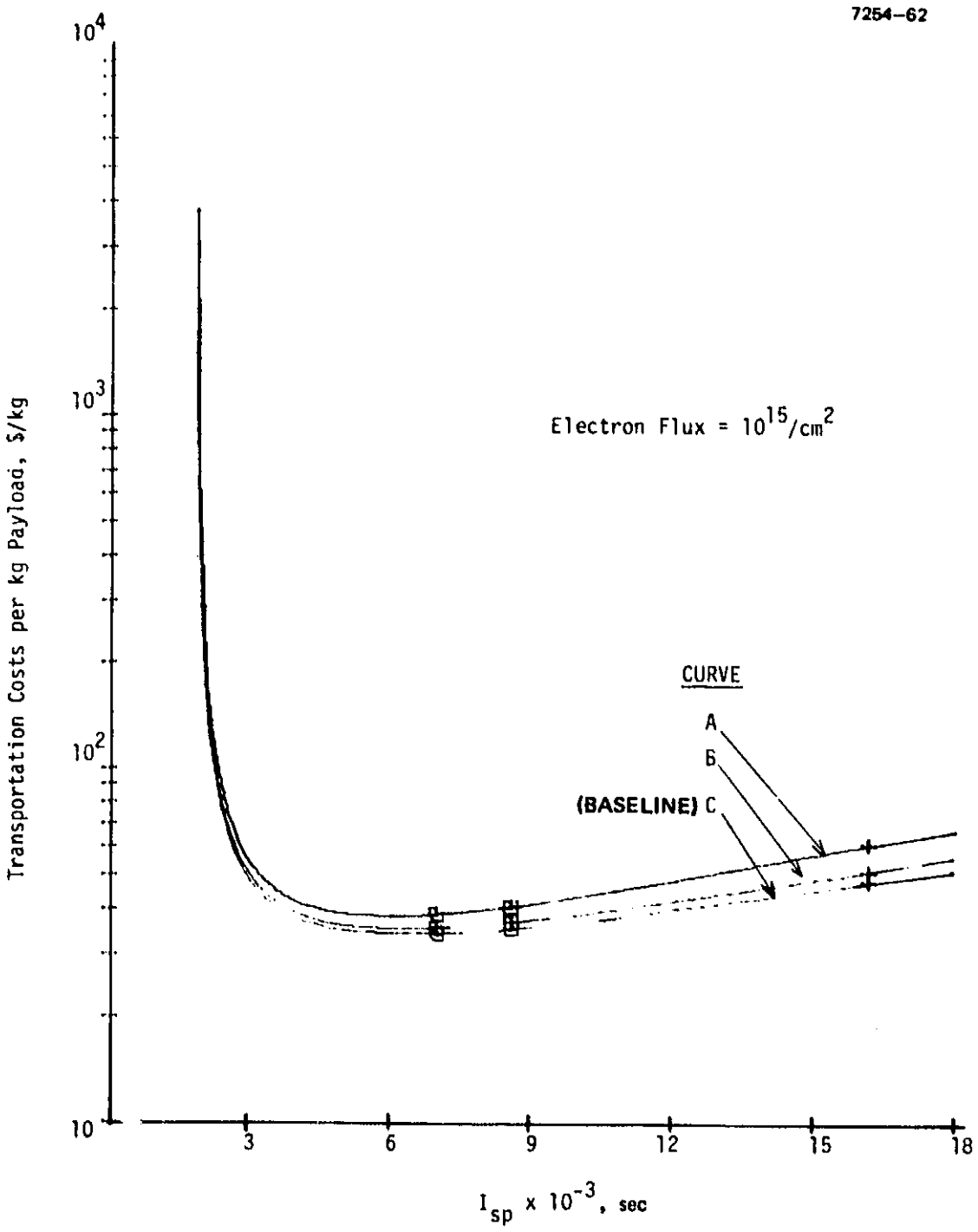

Figure 4-34. ORS/LS effect of power source degradation.

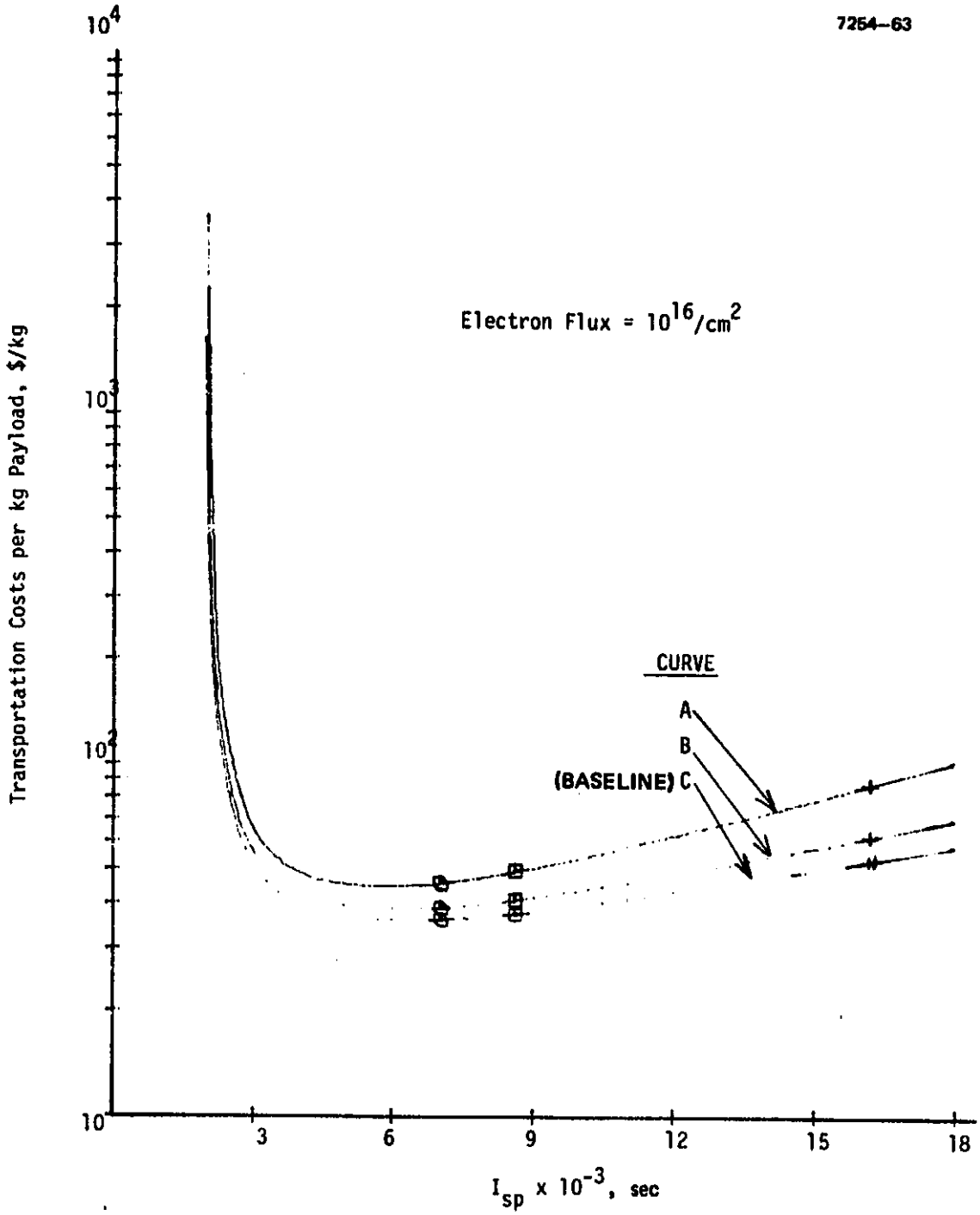

Figure 4-35. ORS/LS effect of power source degradation.

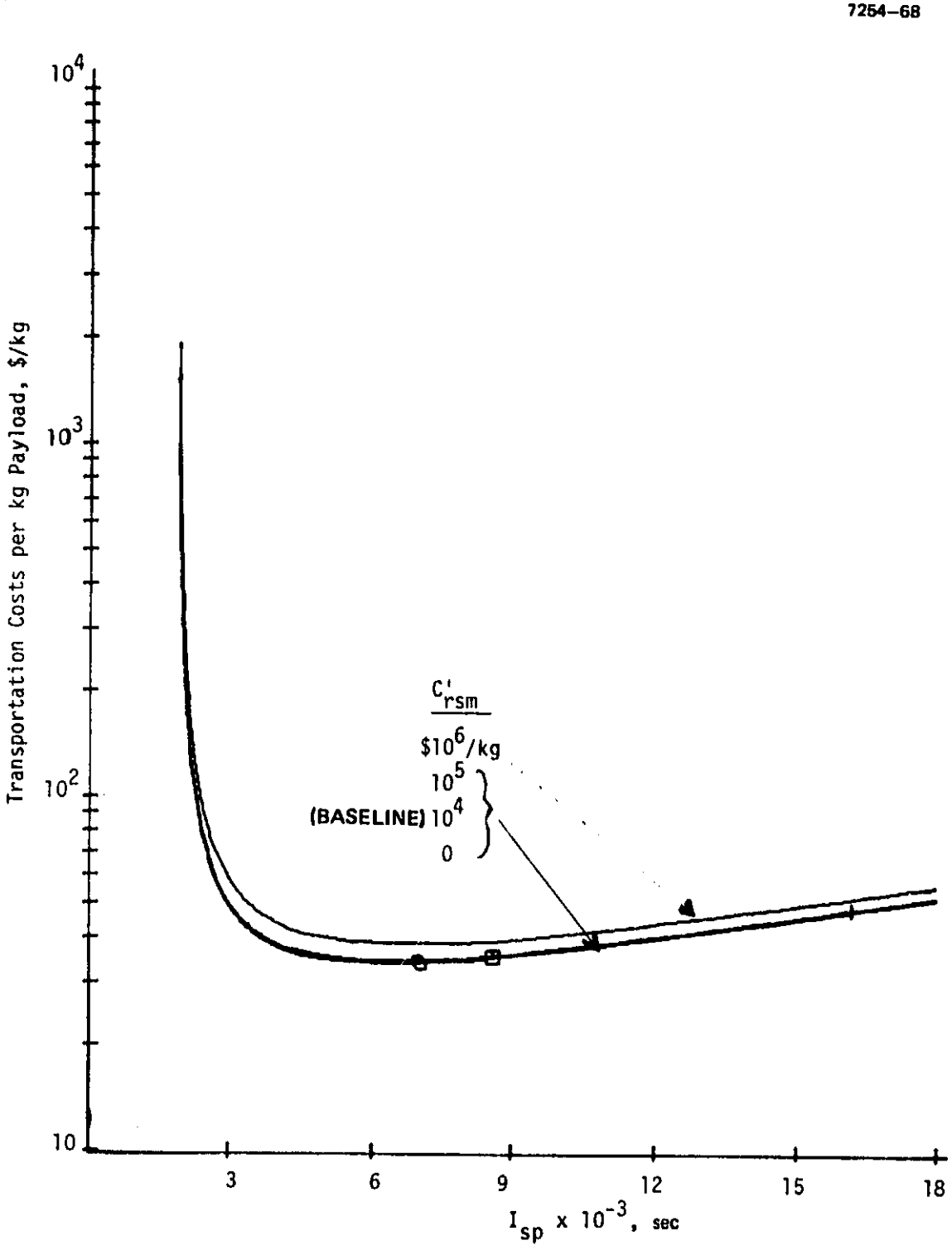

Figure 4-36. ORS/LS effect of specific cost of structure and mechanisms.

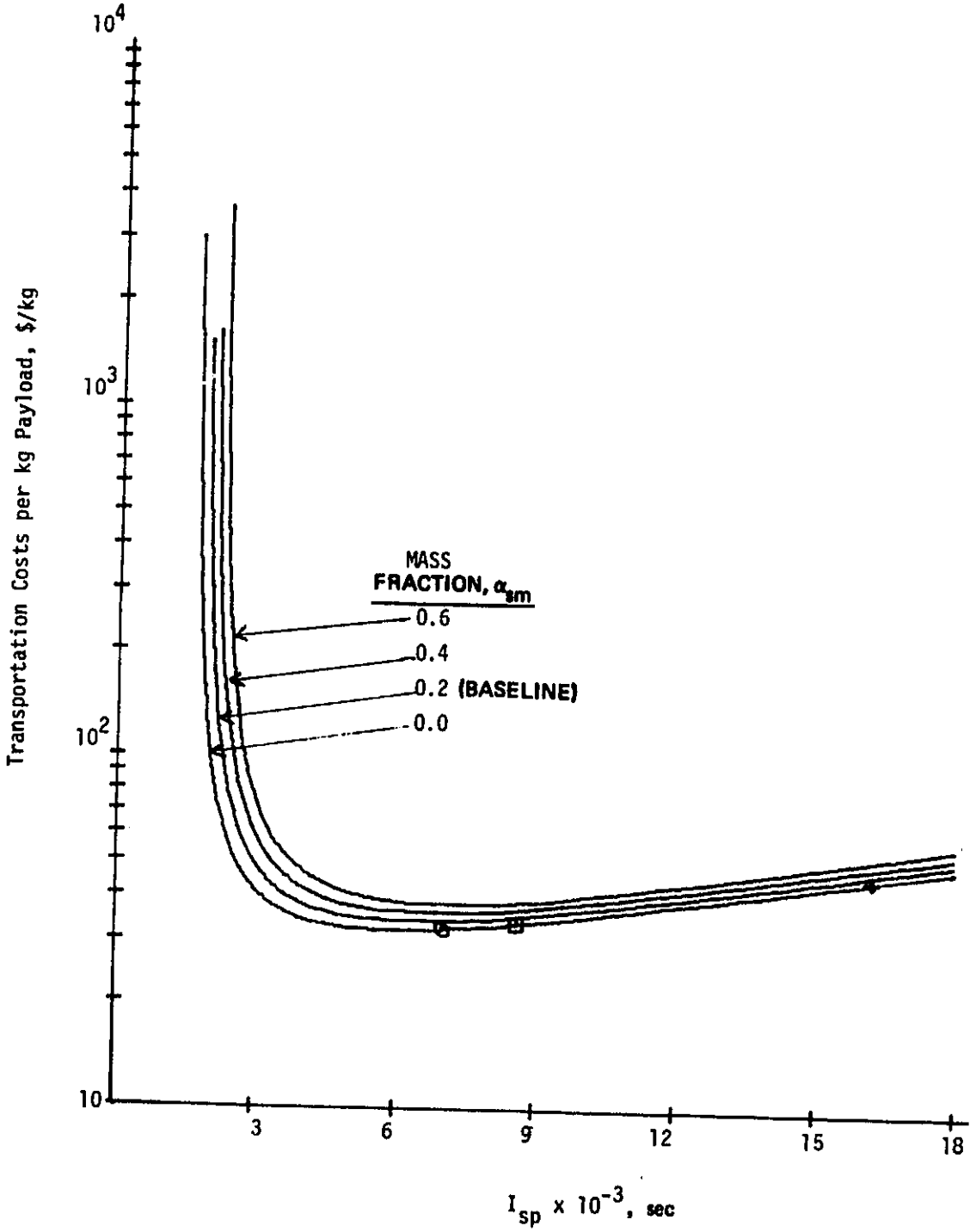

Figure 4-37. ORS/LS effect of mass fraction of structure and mechanisms.

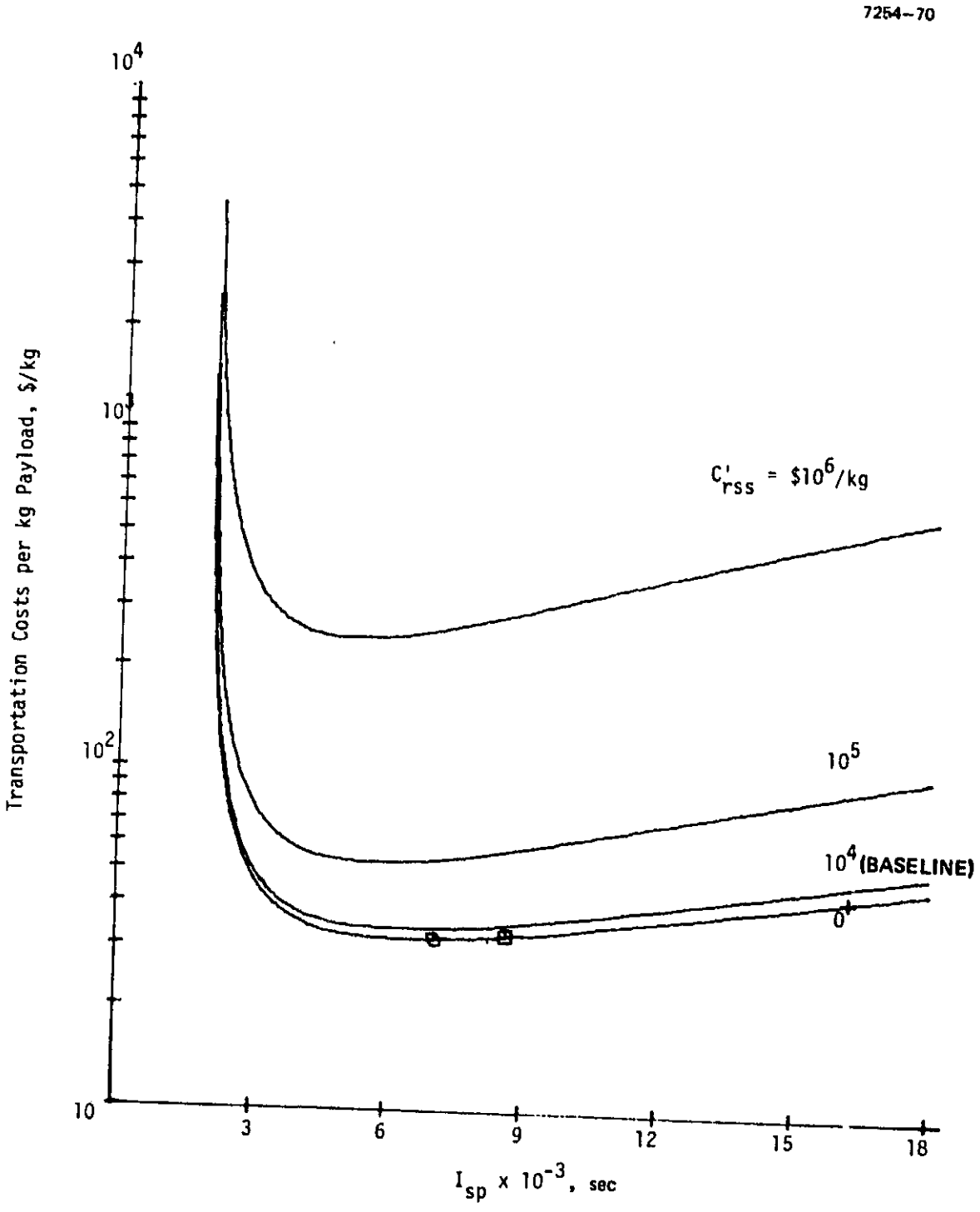

Figure 4-38. ORS/LS effect of specific cost of subsystems.

range of specific costs (C'_{rss}), and thruster selection will not be influenced. However, this sensitivity shows that ORV electronics complexity should be minimized.

(3) ORV Integration Sensitivity — In the range of C'_{ori} from 0 to \$100/kg, transportation cost is not strongly affected, as Figure 4-39 shows. As a figure of merit for assembly-line-type operations, automobiles are probably assembled for about \$1/kg. The baseline selected was an order of magnitude greater, but even costs up to \$100/kg would have only a minor effect on total cost. However, a more significant impact would be introduced if integration and testing exceeded \$100/kg.

(4) DDT&E Sensitivity — Design, development, test, and evaluation are always a large program cost factor. However, as shown in Figure 4-40, unless the coefficient C'_{ord} is raised, and the number of vehicles is reduced, each by an order of magnitude, DDT&E is not a large influence on overall transportation cost.

(5) In-Flight Operations Sensitivity — Operations cost parameter results are shown in Figures 4-41 and 4-42. As Figure 4-41 shows, fixed operations costs above $\$10^6$ would be needed to greatly change the results. For time-dependent costs, the daily rate would have to exceed $\$10^4$ to have an impact. Since a man-day might conservatively cost \$400, $\$10^4$ would imply 25 people/day or about 8 people on 3 shifts. It seems unlikely that a significantly greater number would be necessary on a continuous basis.

i. Payload Powered Option Sensitivities

The results presented thus far have assumed the self-power (ORS) option discussed in Section 4.A.1. The option considered here involves using power from the payload (e.g., a power satellite segment) for the up-trip, but using ORV power for the down-trip (ORP option). In this option, a fraction of the up-trip power (calculated as before) is assumed for the down-trip. The ORV was charged (mass and cost) only for this fraction. Then, the down-trip time is dependent on the available power. Three cases for this option follow.

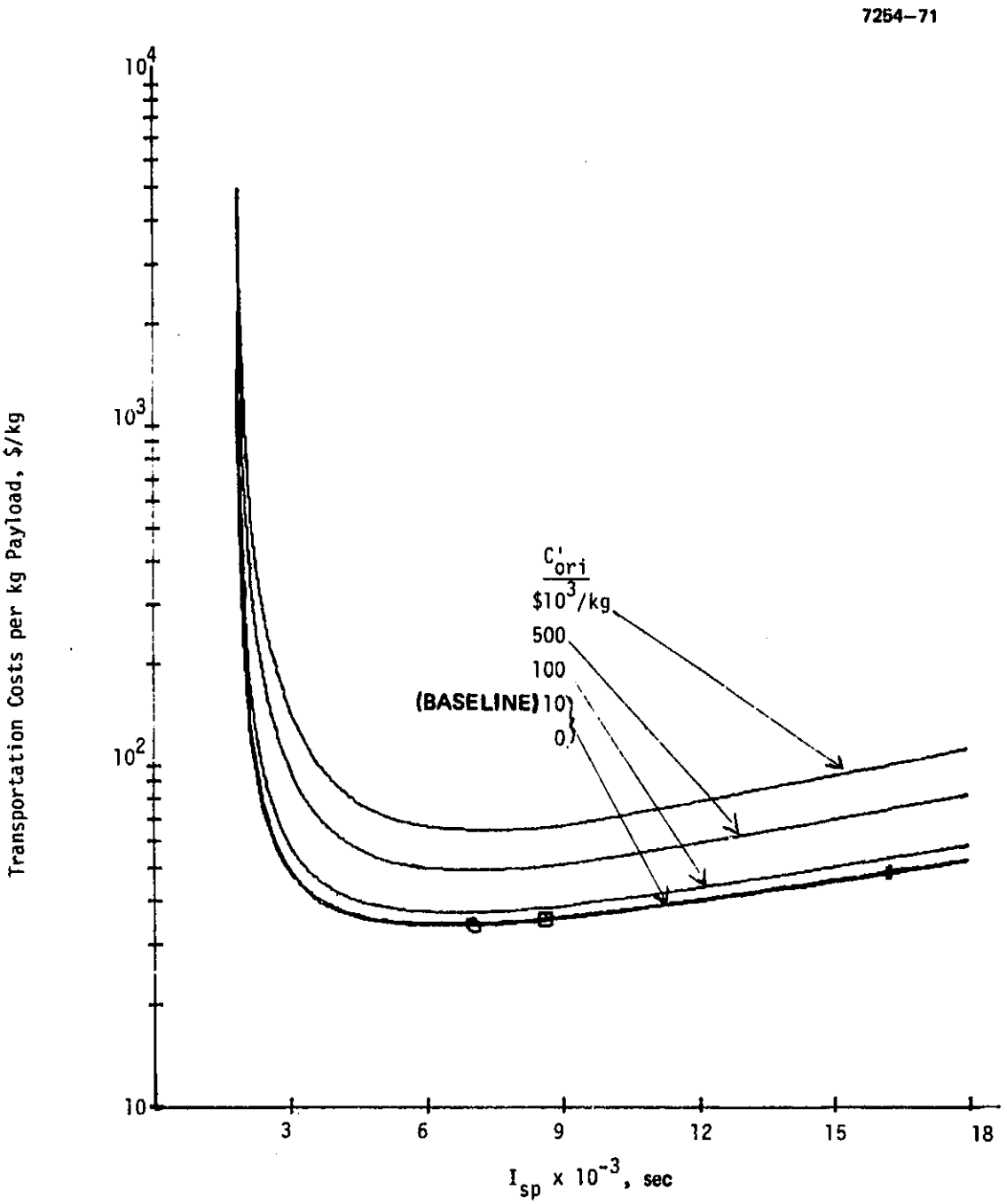

Figure 4-39. ORS/LS effect of specific cost of integration and test.

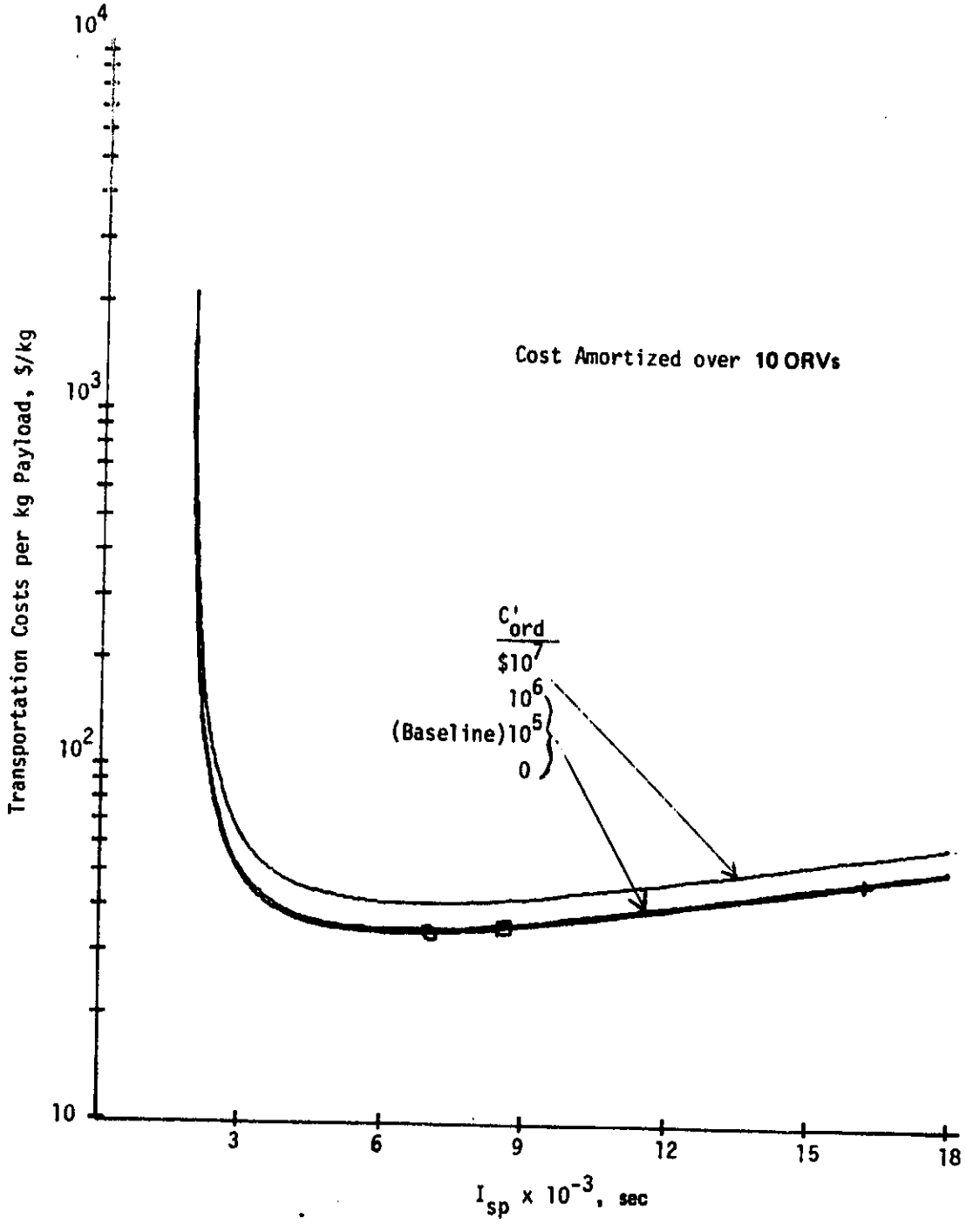

Figure 4-40. ORS/LS effect of specific cost of design, development, test, and evaluation (DDT&E).

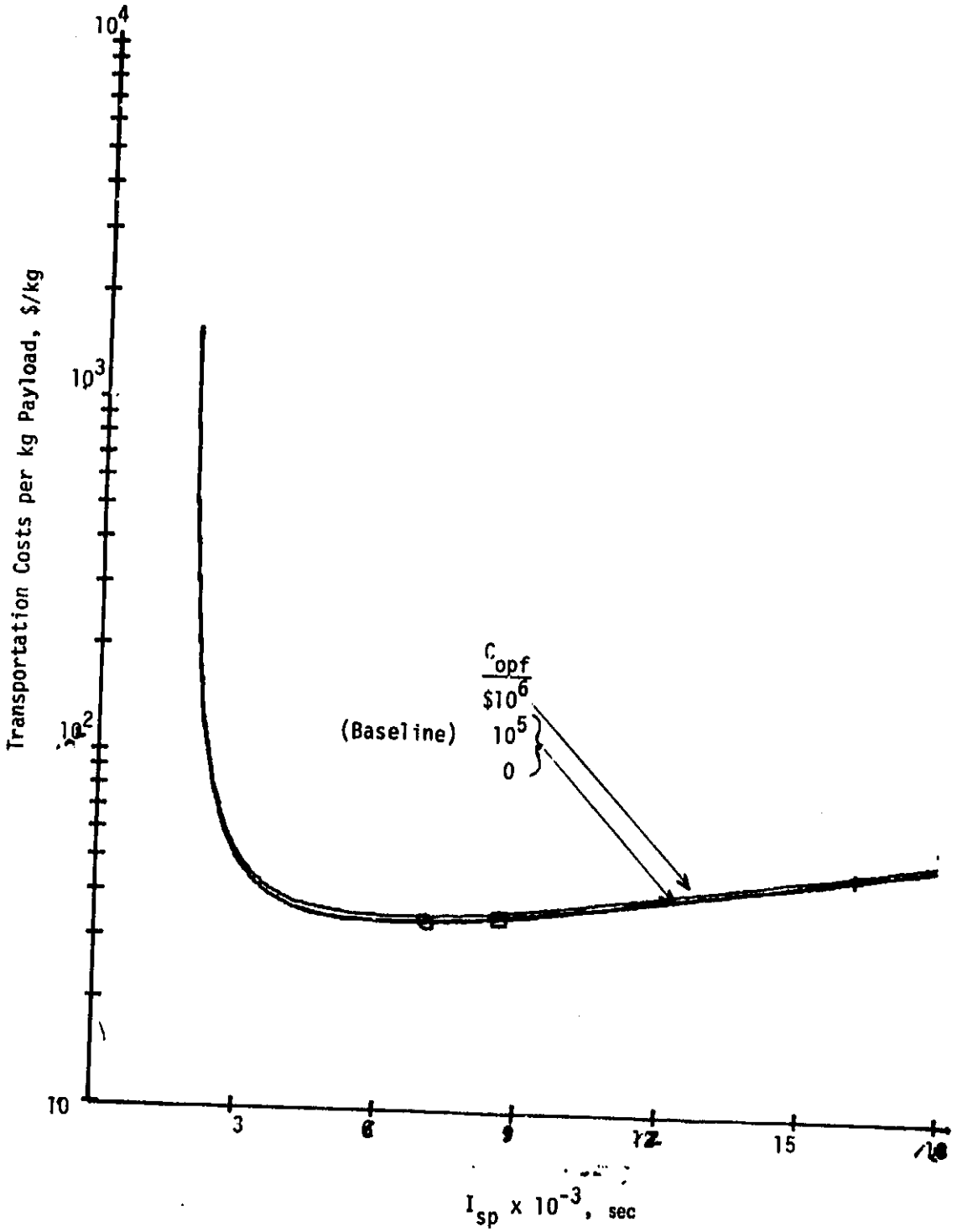

Figure 4-41. ORS/LS effect of fixed operations costs.

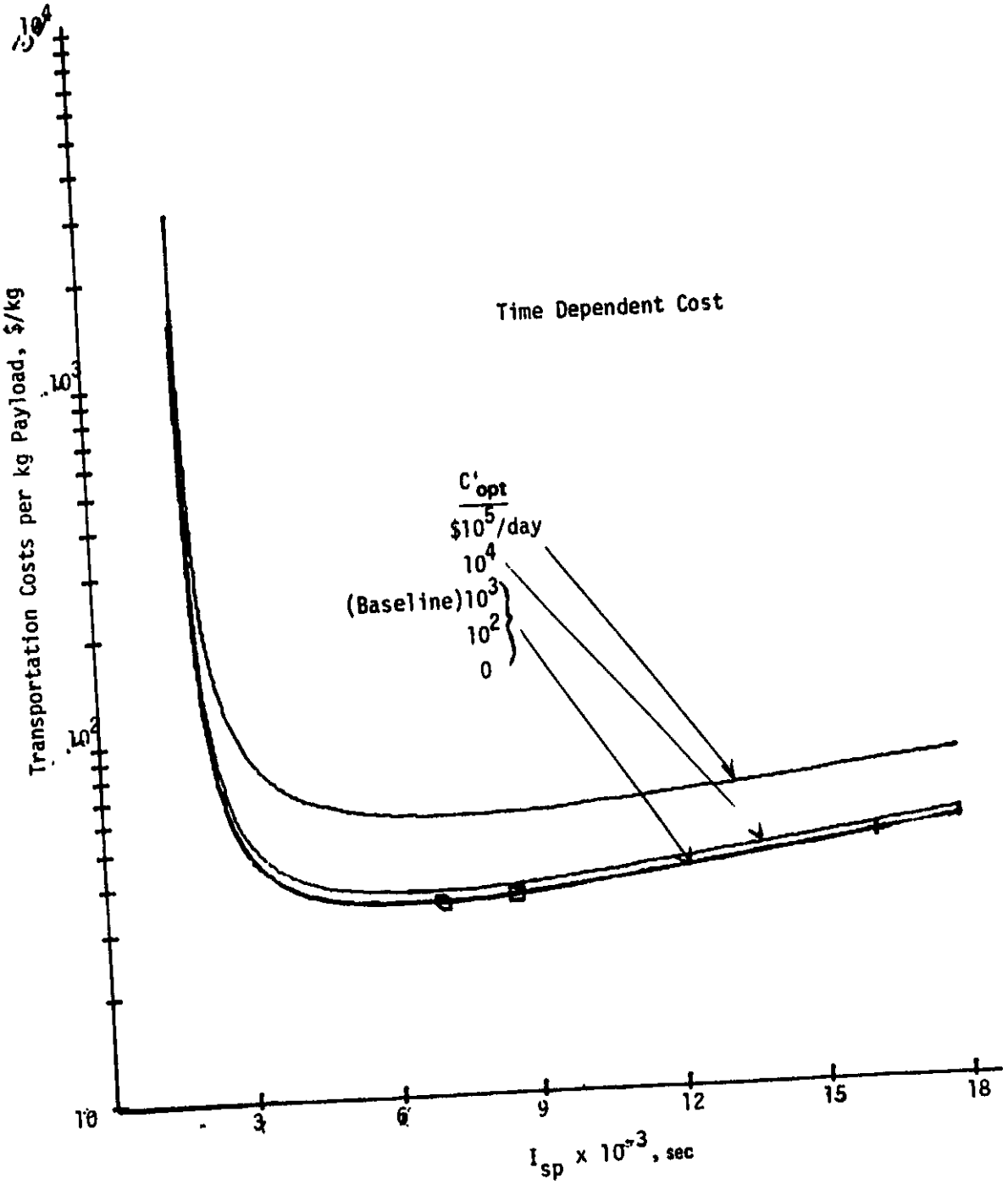

Figure 4-42. ORS/LS effect of time dependent operations on specific costs.

(1) Baseline ORP Power Fraction Sensitivity – Results for the ORP baseline conditions are shown in Figure 4-43. Down-trip powers from 10 percent to 100 percent (ORS baseline) of the up trip were assumed. The total transportation cost is minimized with a fraction of about 50 percent, and is highest at 10 percent. The 50 percent fraction reduces the ORV power source mass and cost, and increases payload. Down-trip time increases, but only about 50 percent. At low fractions, down-trip time becomes extremely long, and so time-dependent factors become important. In the I_{sp} range of interest (8,000 to 12,000 sec), this option has only a slight advantage (1 to 2 percent) over the ORS option.

(2) ORP Power Fraction Sensitivity with Heavy Power Source – In this case, the power source mass is assumed to be 10 kg/kW compared with 3 kg/kW in the baseline. The results shown in Figure 4-44 indicate a slight shift from the results in Figure 4-43. The benefit to the ORV of not being charged for the heavy power source shifts the "optimum" fraction toward the 25 percent level. However, except at low I_{sp}, all fractions reduce transportation cost, particularly at high I_{sp}.

(3) ORP Power Fraction Sensitivity with High-Cost Power Source – Results similar to those in previous figures are presented in Figure 4-45 for power costs of \$5/W (10 times the baseline cost). The minimum transportation cost occurs with a fraction of about 50 percent, but all fractions reduce cost compared to the baseline. Considering the results of Figures 4-43 through 4-45, higher costs would tend to make the ORP option even more cost effective than the ORS option.

j. One-Way Trip Option Sensitivities

The third mission option (ORO), one-way trips from LEO to higher orbit, allows the ORV to remain with the payload on orbit. Since the ORV cost is then charged to a single trip, the transportation cost is higher than for multiple trips. One-way trip sensitivities are presented for ΔV, trip time, initial mass, and launch cost; in each case, the benefit of including the power source in the payload is assessed.

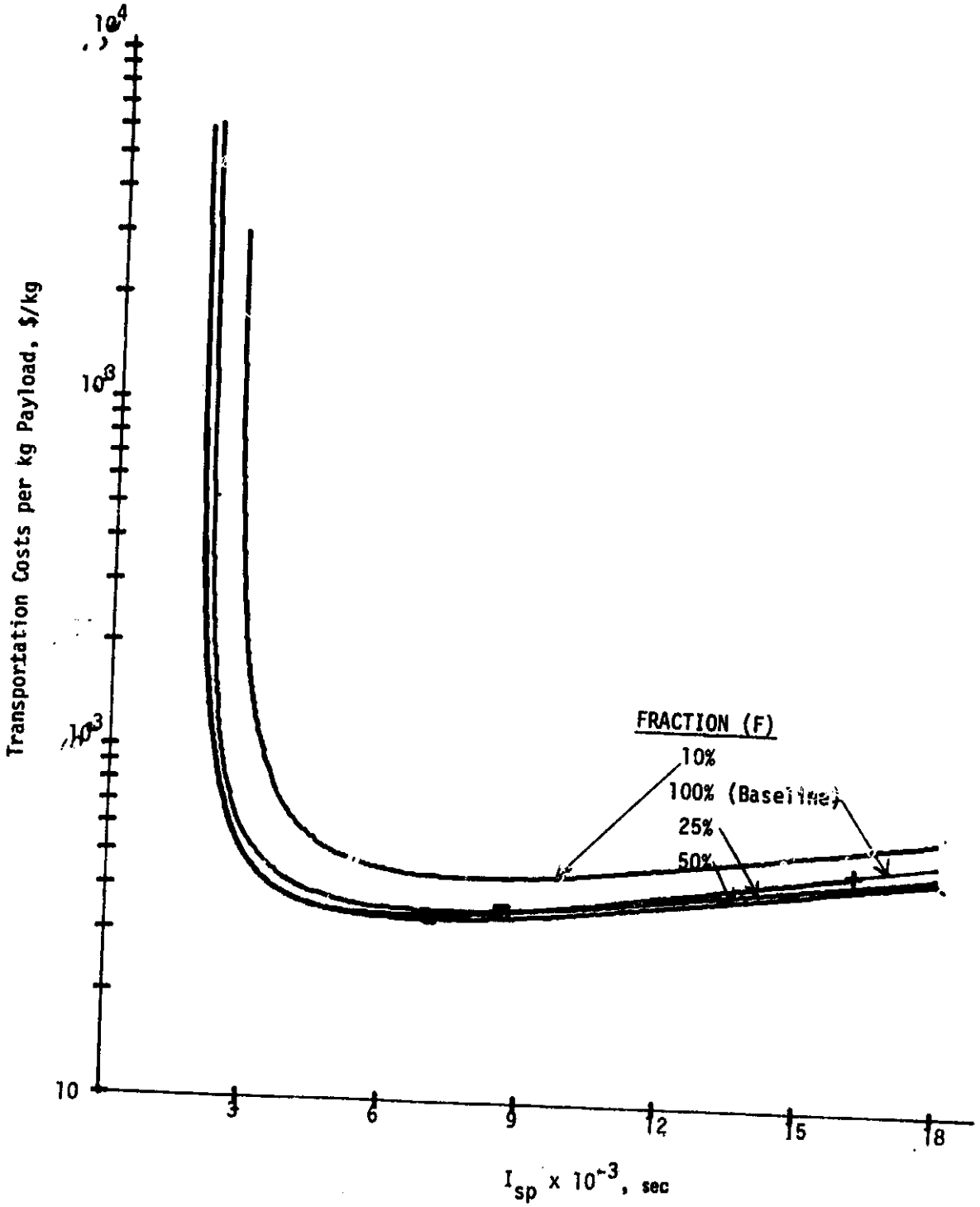

Figure 4-43. ORP/LS effect of fraction of ORS baseline power for down trip power (α_{rw} = 3 kg/kW).

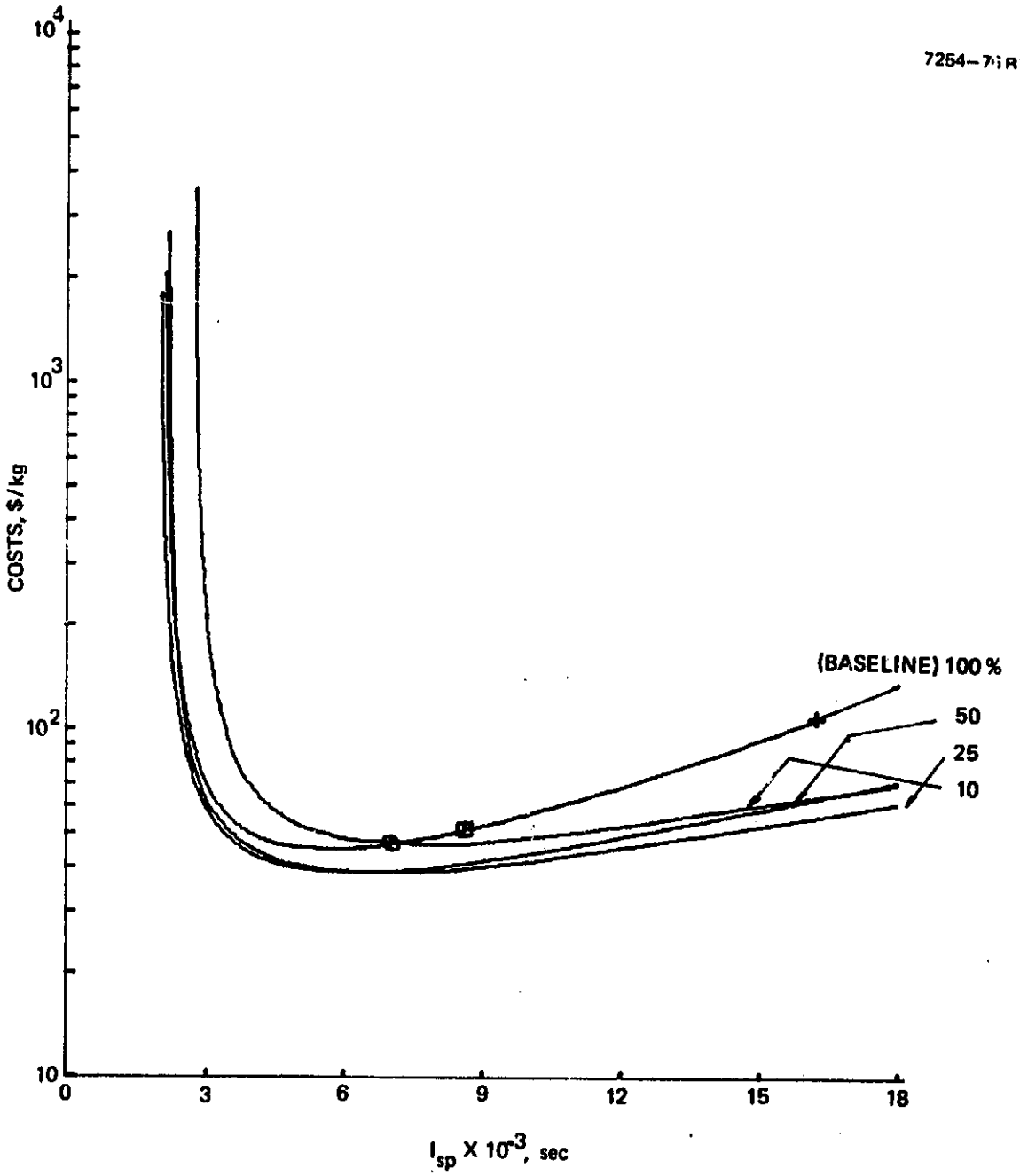

Figure 4-44. ORP/LS effect of fraction of ORS baseline power for down trip power (α_{rw} = 10 kg/kW).

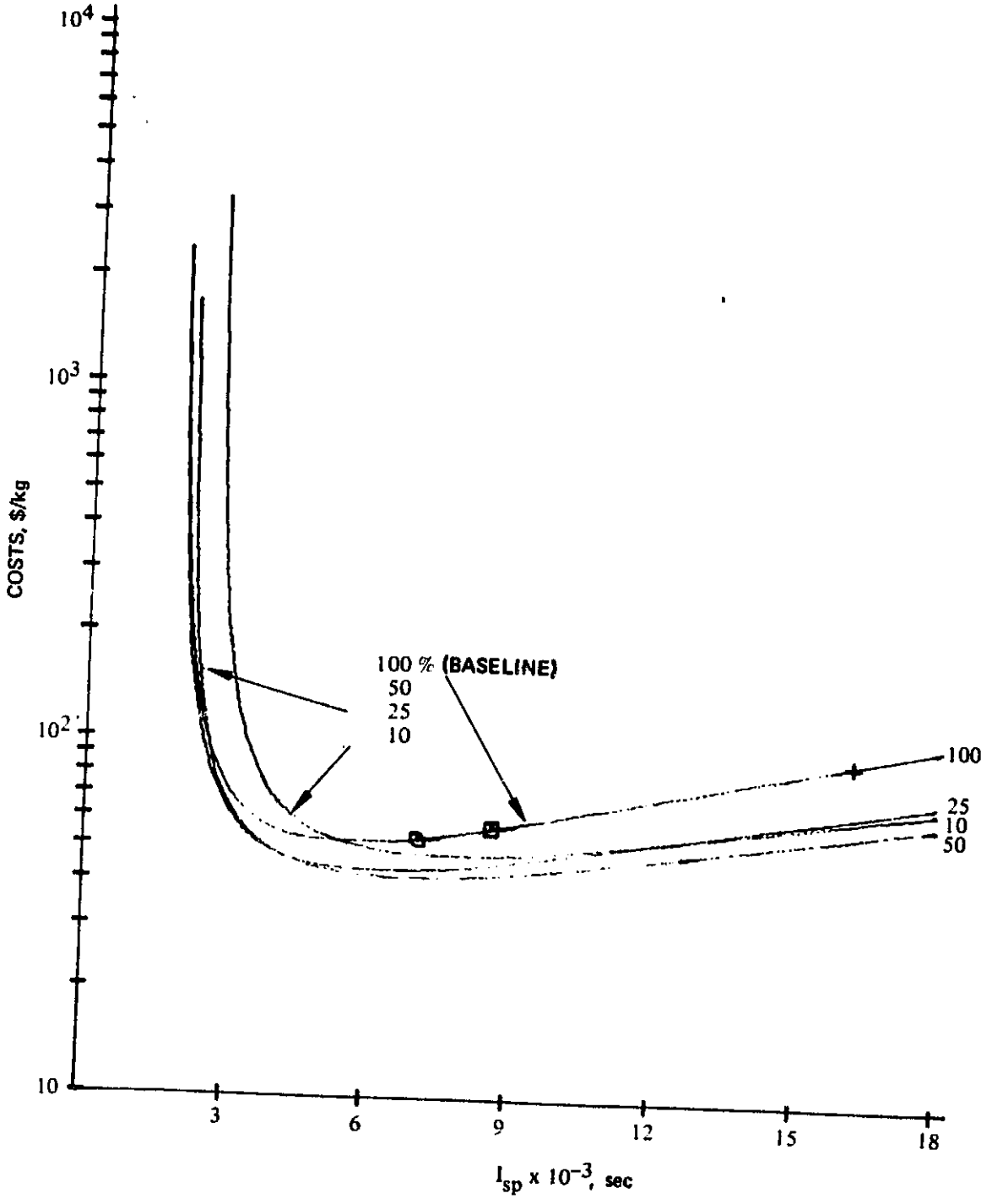

Figure 4-45. ORP/LS effect of fraction of ORS baseline power for down trip power (C'_{rw} = \$5/W).

(1) ORO ΔV Sensitivity -- Cost sensitivities are presented in Figures 4-46 and 4-47 for ΔV for ORV-supplied power and payload-supplied power, respectively. The difference between the two ORO modes varies from about 20 percent at 4 km/sec to about 50 percent at 10 km/sec, with the self-powered costs being greater. The difference between the ORS option (Figure 4-17) and the ORV-powered ORO option is about a factor of 3.5 in transportation cost. Thus, the reuse capability of ORS has a substantial cost benefit.

(2) ORO Trip Time Sensitivity – Cost sensitivities to trip time for the two power source cases are shown in Figures 4-48 and 4-49. For trips of 100 days or more, the differences are of the same magnitudes described for ΔV sensitivity. However, for a 50-day trip time, in the ORV-powered mode, the one-way trip cost increases significantly (to $\sim$ 7.5 times the ORS cost of Figure 4-18). This different nature for low trip times is associated with power, as illustrated by the comparison between Figures 4-48 and 4-49.

(3) ORO Initial Mass Sensitivity -- The cost sensitivity to initial mass variations for the two ORO-powered modes are presented in Figures 4-50 and 4-51. The difference between the ORS option (Figure 4-19) and the ORO ORV-powered option is about 3.5 to 4.0. However, between the ORO modes, the payload-powered mode is only about 10 percent cheaper at 10^4 kg, but is about 40 percent less at 10^7 kg.

(4) ORO Launch Cost Sensitivity - Cost sensitivity to launch cost is shown in Figures 4-52 and 4-53 for the ORV-powered and payload-powered modes, respectiviely. A comparison of Figures 4-20 and 4-52 shows that the one-way trip becomes about 3 times more expensive for the baseline value. If power is charged to the payload (Figure 4-53), the transportation cost will be about 10 percent less at $100/kg and 30 percent less at $1/kg than the self-powered mode (Figure 4-52).

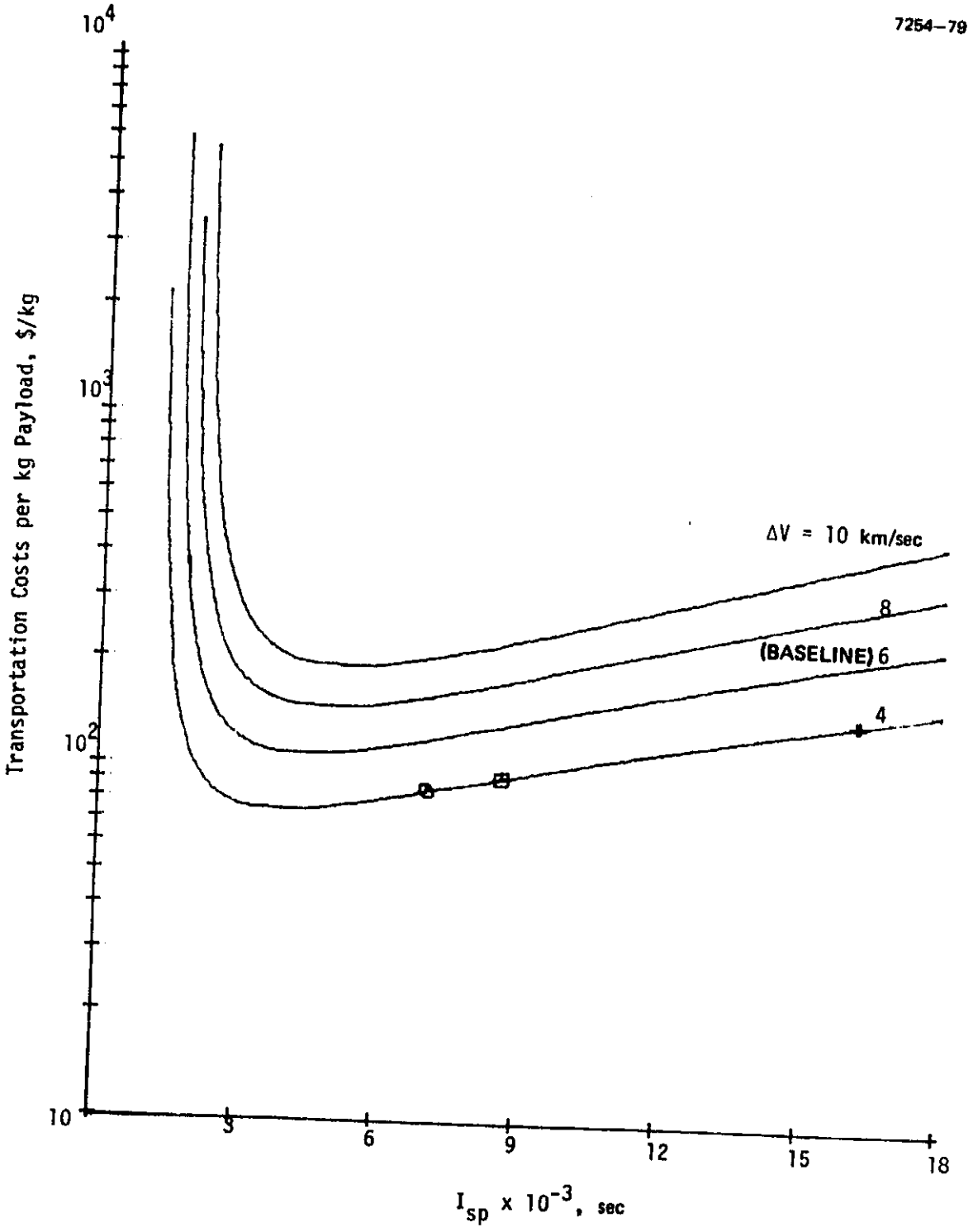

Figure 4-46. ORO/LS effect of ΔV, self-powered.

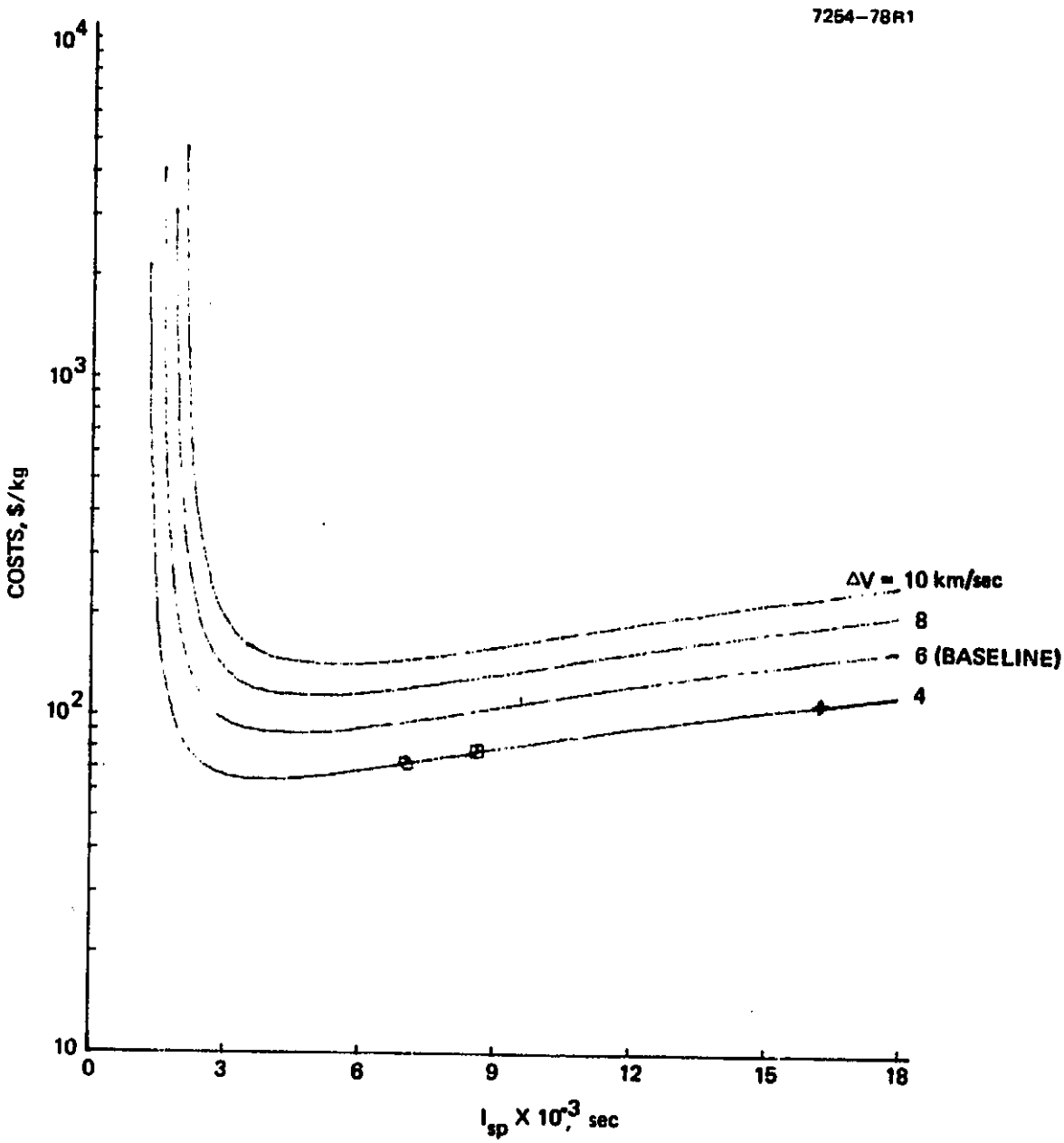

Figure 4-47. ORO/LS effect of ΔV, payload powered (C_{rw} = 0, M_{rw} = 0).

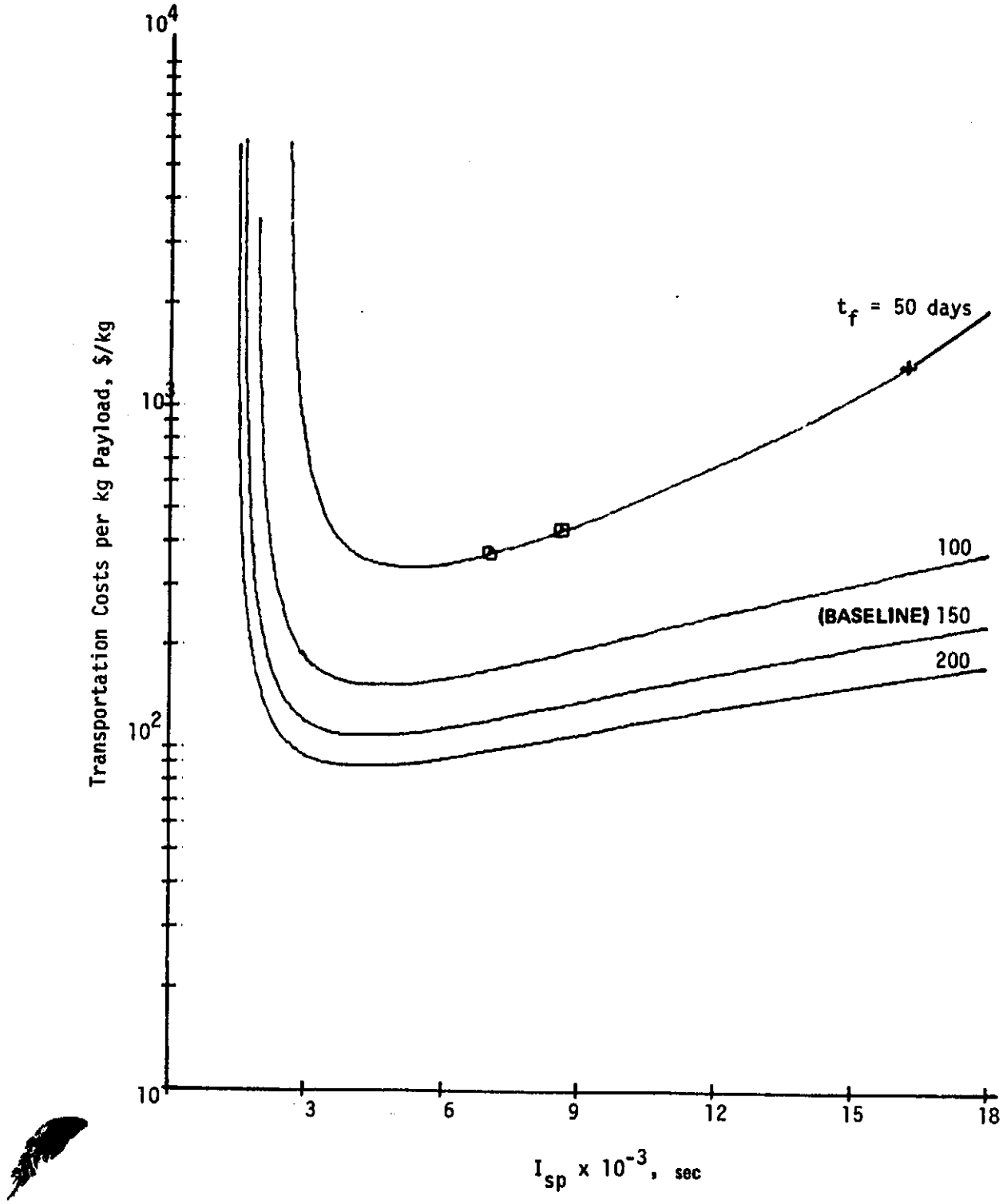

Figure 4-48. ORO/LS effect of trip time, self-powered.

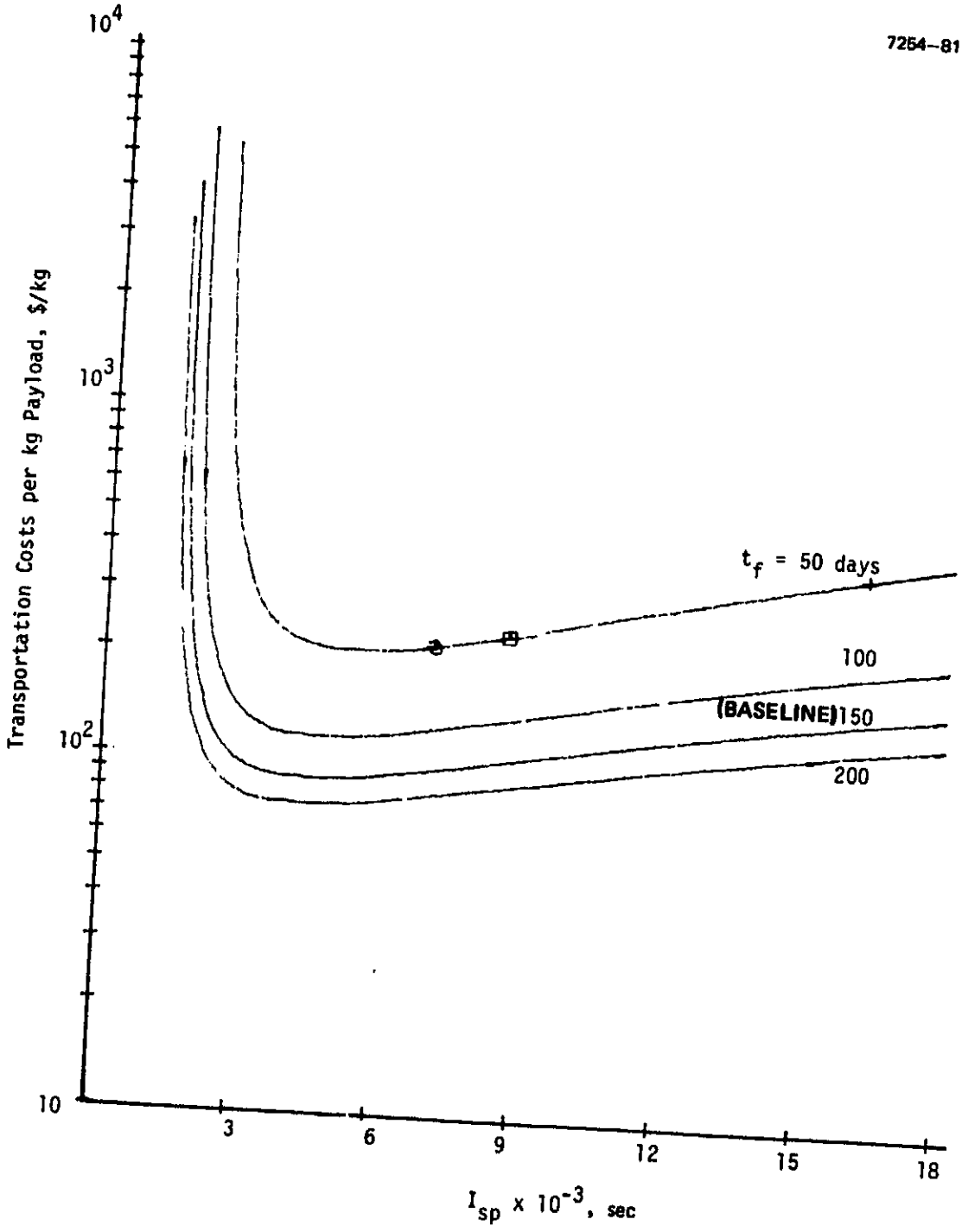

Figure 4-49. ORO/LS effect of trip time, payload powered ($C_{rw} = M_{rw} = 0$).

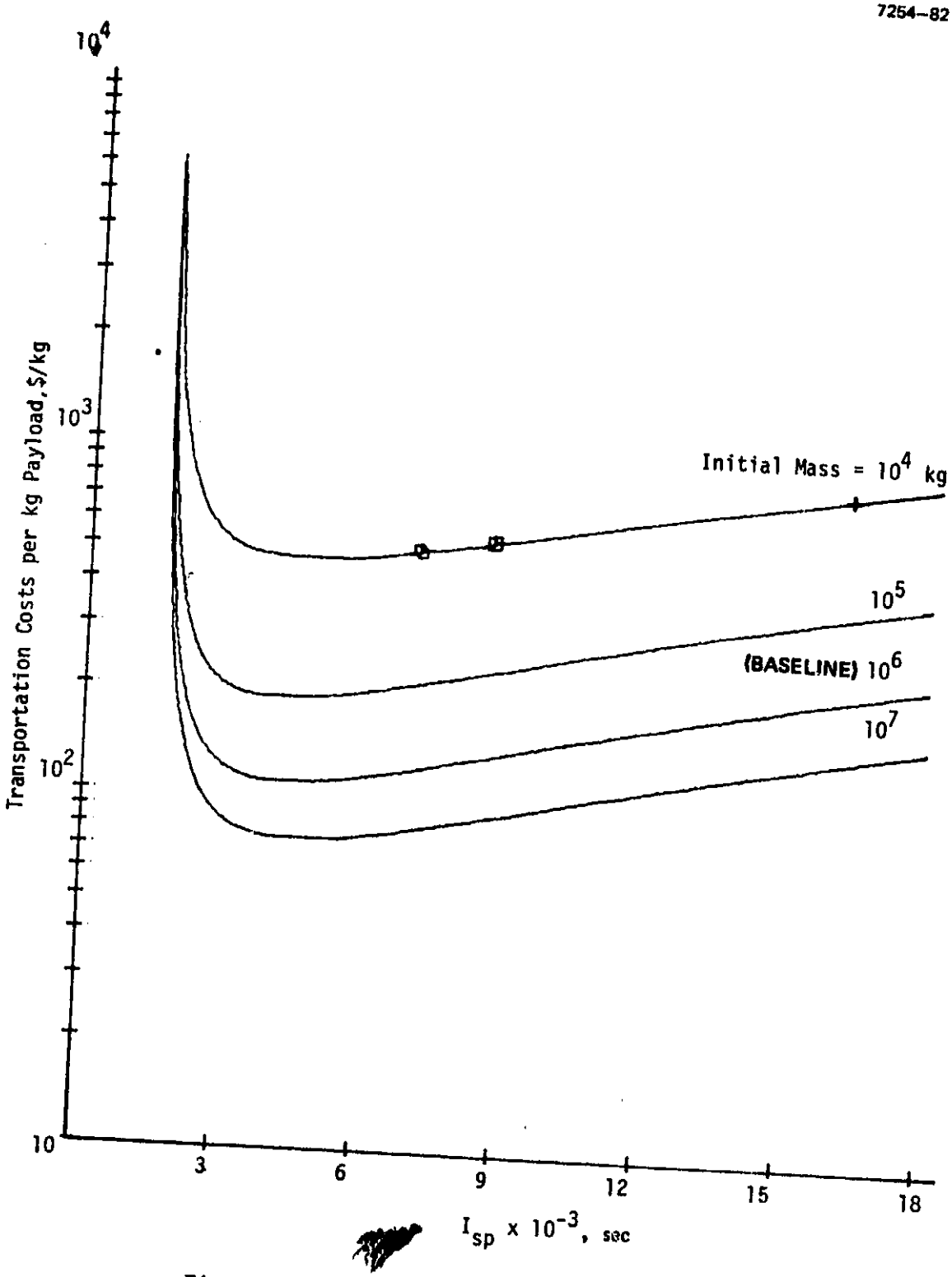

Figure 4-50. ORO/LS effect of initial mass, self-powered.

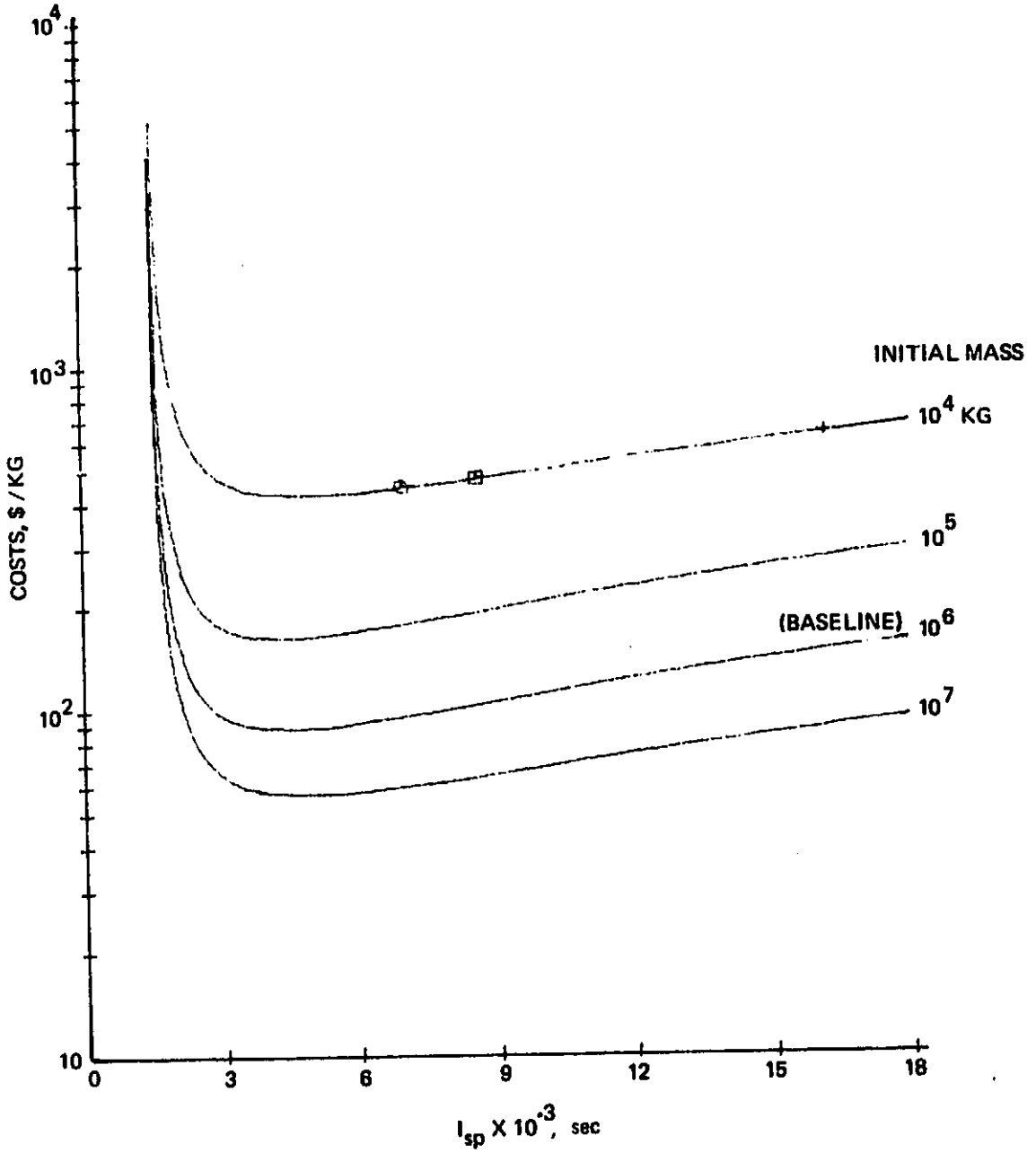

Figure 4-51. ORO/LS effect of initial mass, payload powered ($C_{rw} = M_{rw} = 0$).

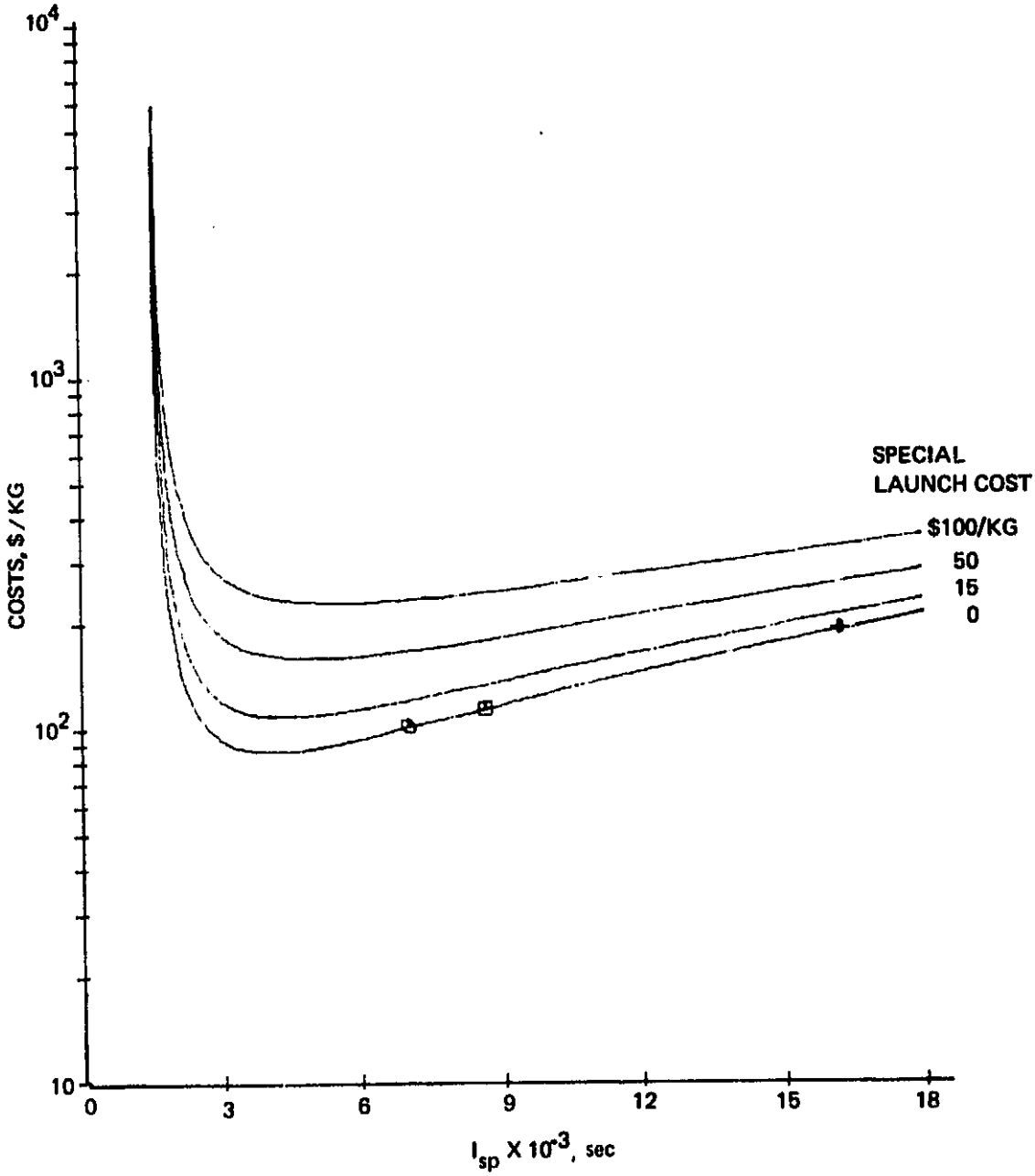

Figure 4-52. ORO/LS effect of specific launch cost, self-powered.

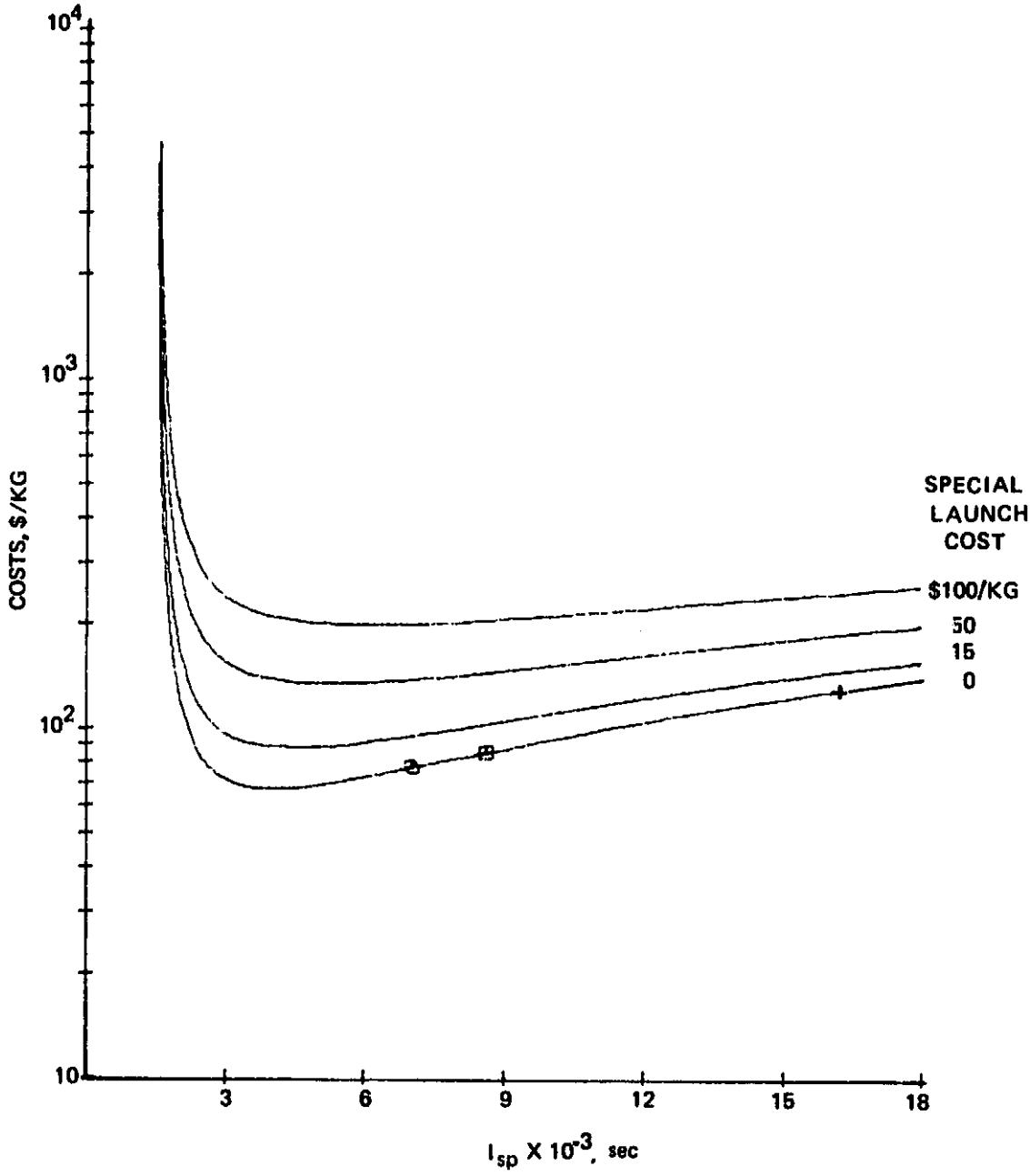

Figure 4-53. ORO/LS effect of specific launch cost, payload powered ($C_{rw} = M_{rw} = 0$).

9. Orbit Raising/Shuttle Era Baseline Mission Results

The MS era baseline is intended to provide a link between present 30-cm projected applications and LS applications, which are probably several decades away. The differences between the LS and MS baselines are characterized by the seven parameters listed in Table 4-5 with all other values as defined in Table 4-3. The new values were selected on the basis that (1) power technology would be less advanced than that projected for the LS baseline, (2) launch would utilize the shuttle (this limits the initial mass to about 25,000 kg and increases the specific launch cost), (3) for smaller systems, lower power modules should be considered, and (4) the ORV fleet size would not allow production-line assembly, which would raise integration costs.

a. OR/MS General Results

The general characteristics of the OR/MS baseline results are shown in Figures 4-54 through 4-58. The effect of module power is shown in Figure 4-54 for the range from 5 to 80 kW. The most obvious change from the OR/LS results shown in Figure 4-12 is the order of magnitude shift in transportation cost to about \$1,000/kg. Other differences include reduced sensitivity to module power level and increased slope to the right of the cost minima. With Xe for a propellant, reasonably sized thrusters (i.e., diameters of less than 100 cm) are closer to minimum cost than with argon. At about 5,000 sec, a 80-kW, 60-cm thruster would be close to optimum. Although the sensitivity to module size appears to be small, the compressed logarithmic scale is deceiving. In the region of minimum cost, the sensitivity is about \$0.44/kg per cm of thruster diameter. For a payload of 18,000 kg (Figure 4-56), the absolute cost is about $\$8 \times 10^4$/cm. Thus, the difference between a 30-cm and a 60-cm thruster produces a transportation cost difference of $\$2.4 \times 10^6$; the cost difference is about $\$5.4 \times 10^6$ for a 30-cm to 100-cm

Table 4-5. OR/MS Baseline Cost Model Parameters[a]

P_{mod}	=	20 kW	Module power
M_o	=	25×10^3 kg	Initial mass in LEO
C'_{ori}	=	\$40/kg	ORV integration and testing
C'_{rw}	=	\$100/W	Cost of ORV associated power
α_{ps}	=	6 kg/kW	Power source specific mass
C_ℓ	=	\$300/kg	Launch cost to LEO
Propellant	=	Xenon	

[a]All other model parameters are the same as those in Table 4-3.

6119

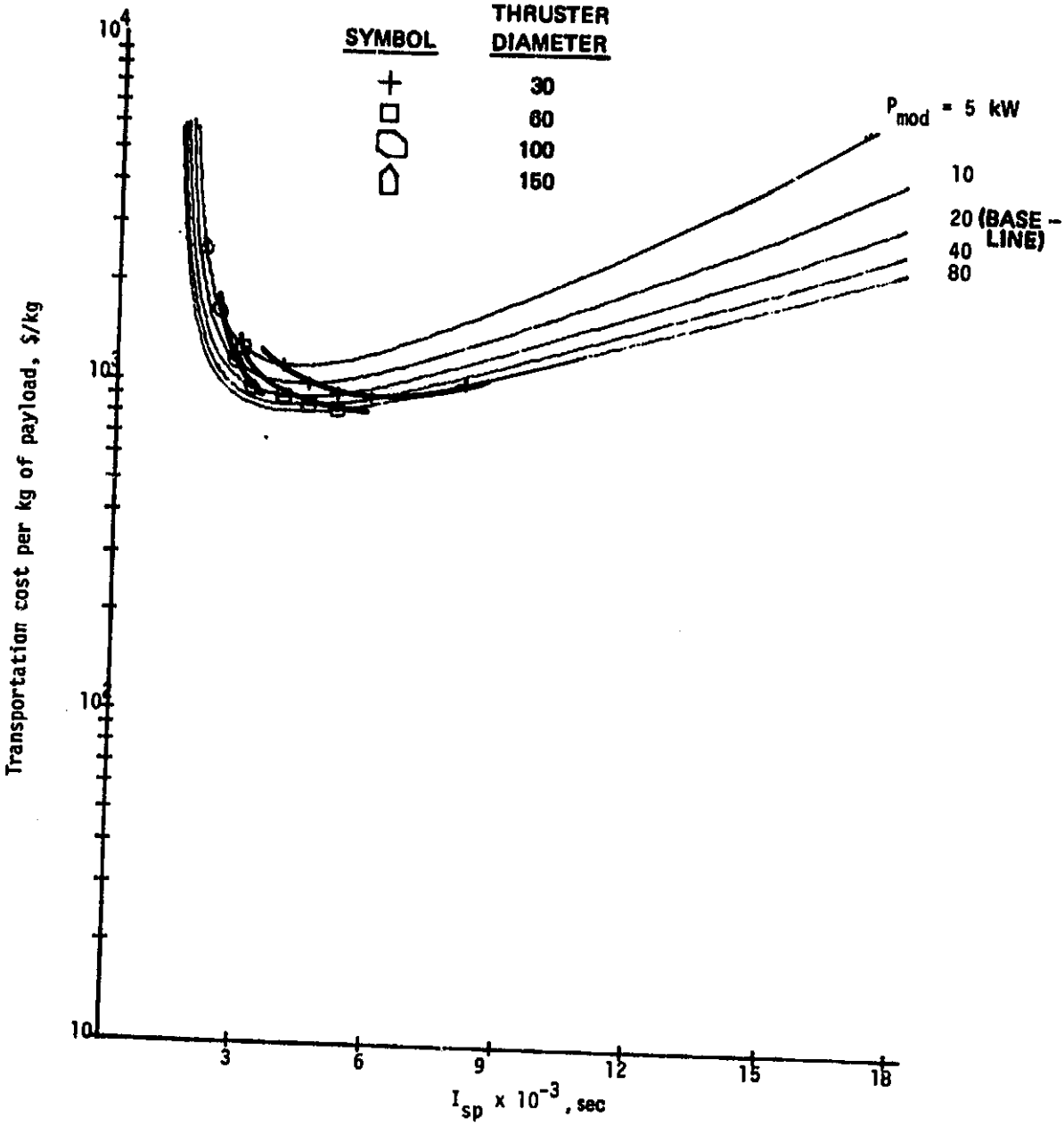

Figure 4-54. OR/MS effect of module power.

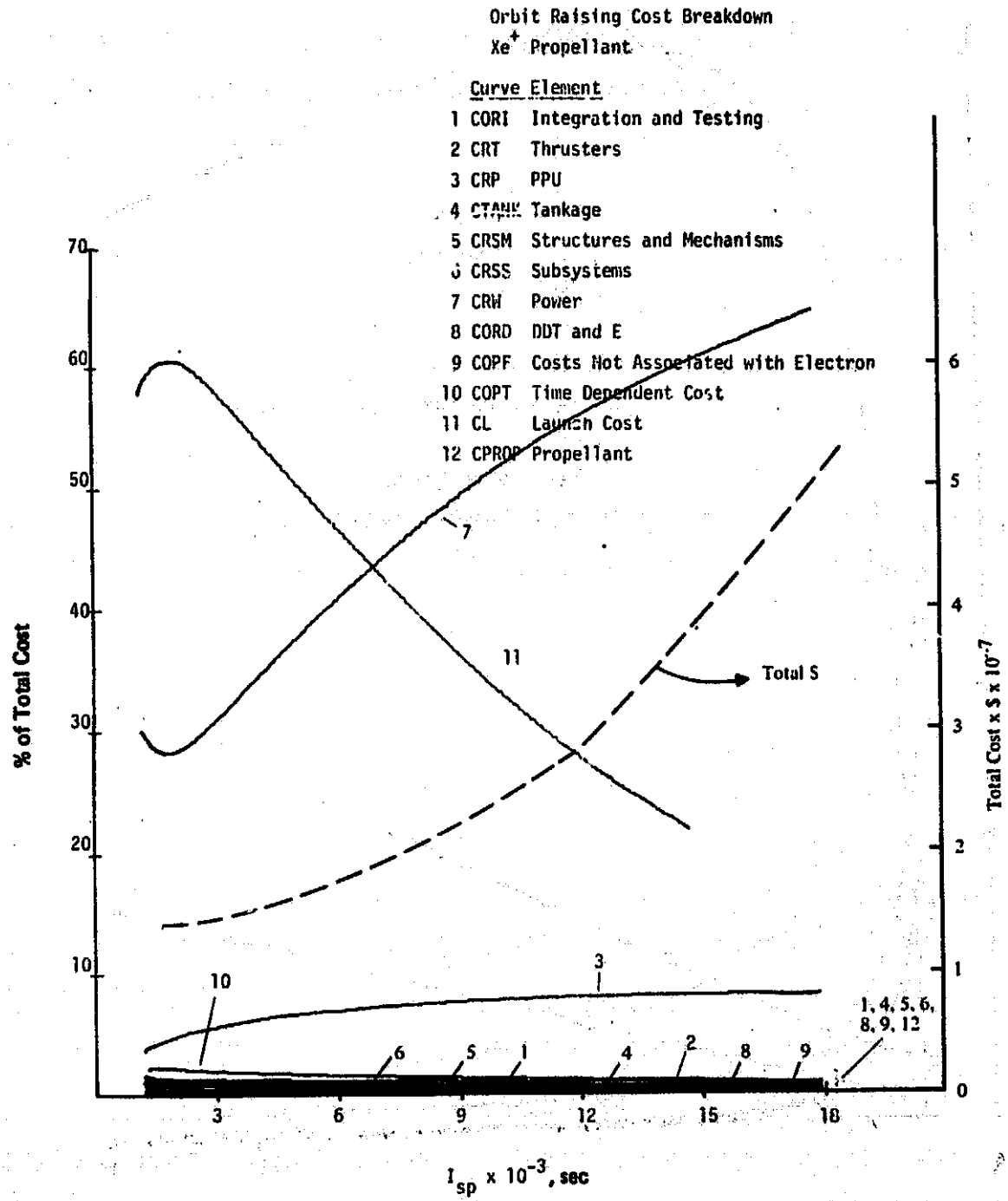

Figure 4-55. OR/MS cost reakdown.

C-3

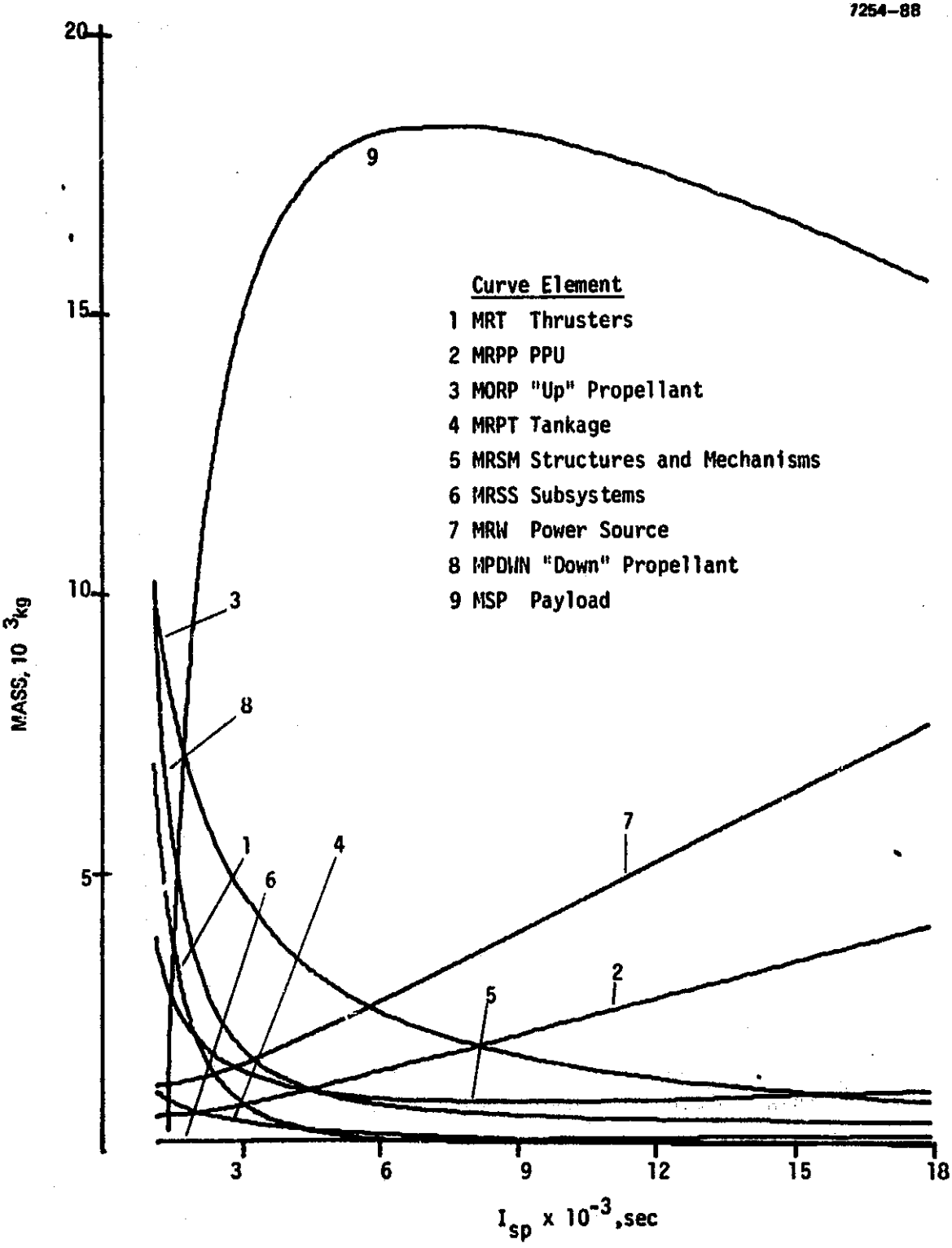

Figure 4-56. OR/MS mass breakdown.

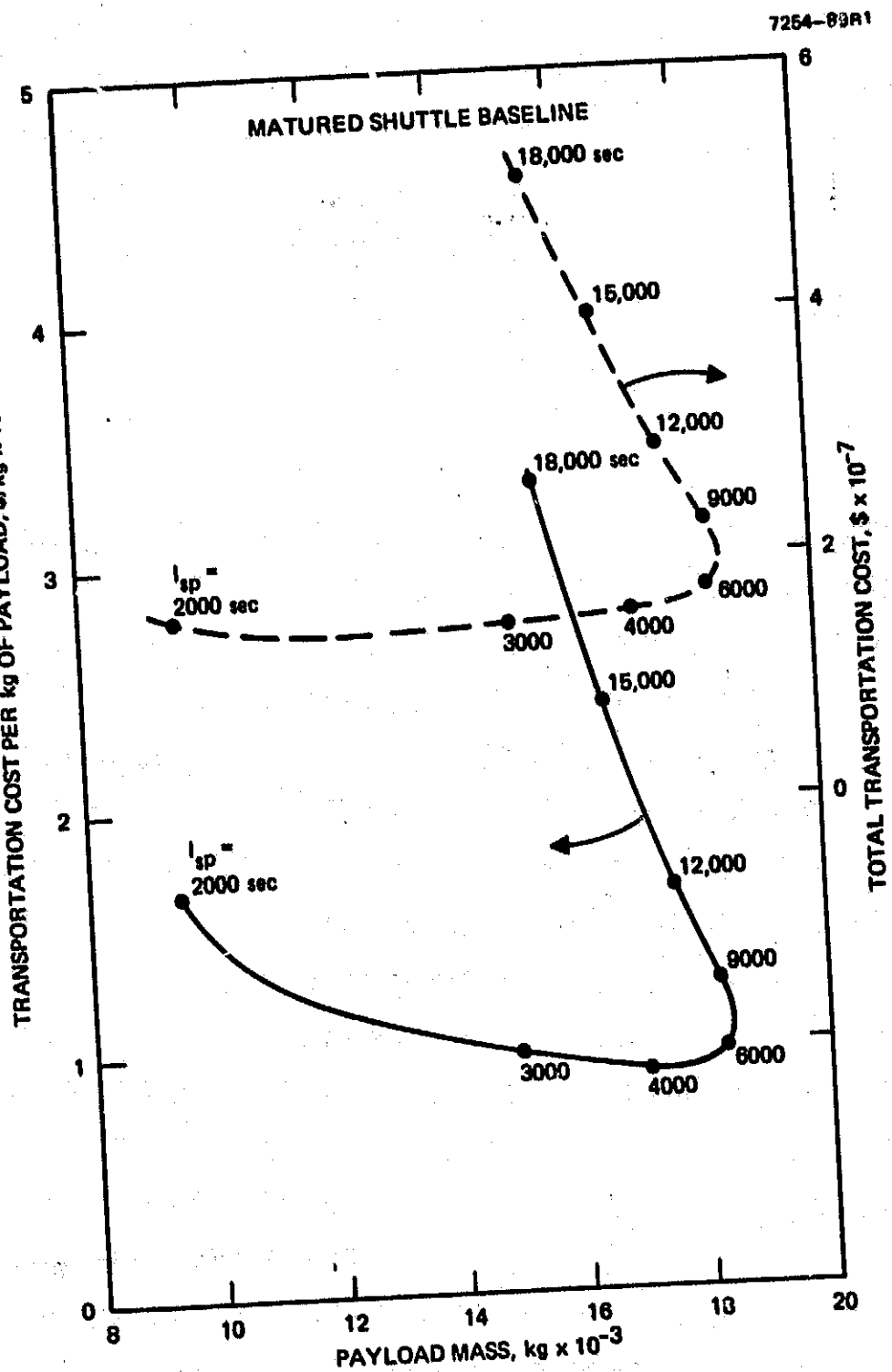

Figure 4-57. OR/MS cost/kg versus payload.

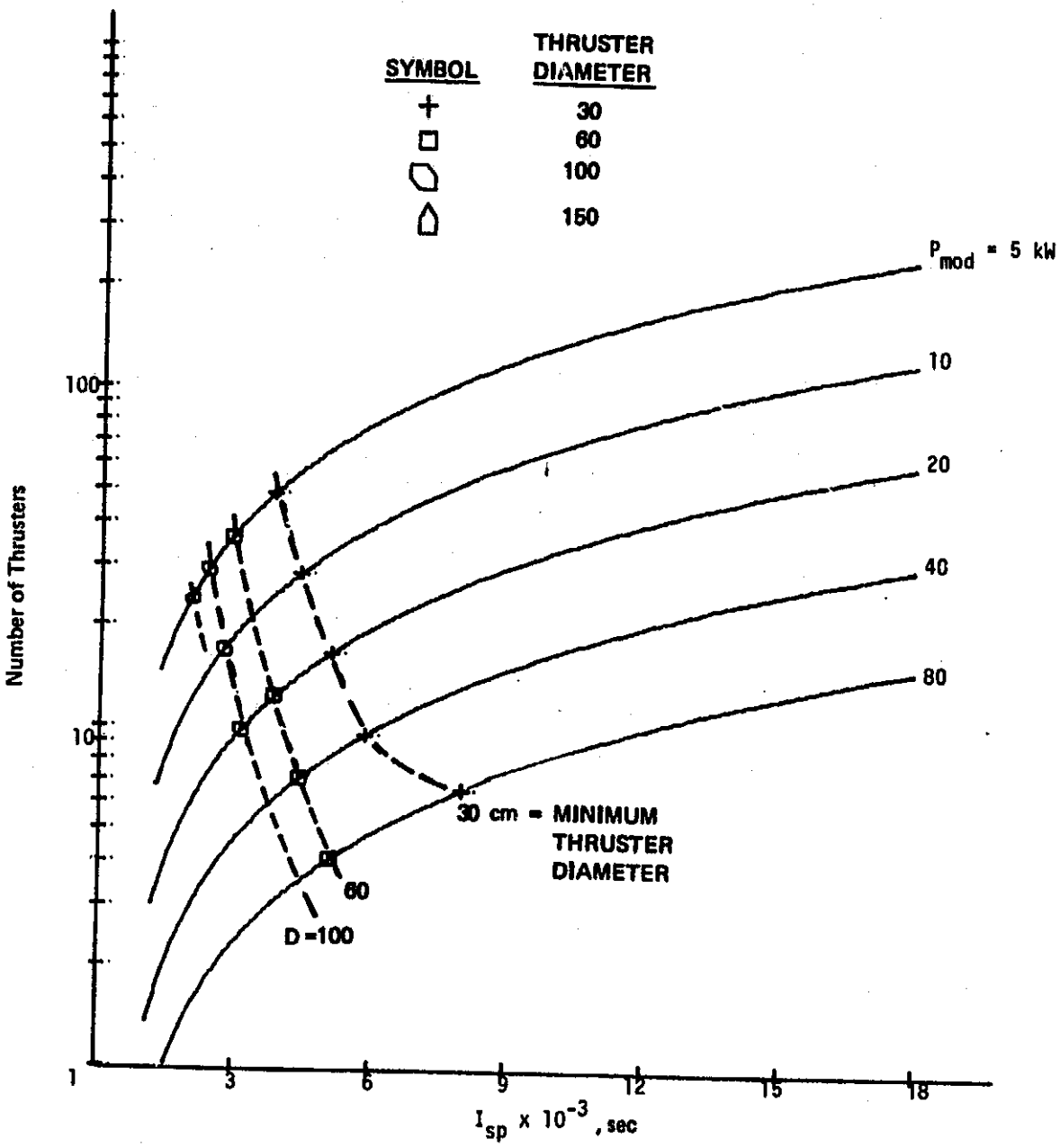

Figure 4-58. OR/MS number of thrusters versus I_{sp}.

difference. Since this cost is per roundtrip, the investment in developing a larger thruster would be well rewarded.

Cost and mass breakdowns are presented in Figures 4-55 and 4-56 for the OR/MS baseline. Transportation cost is now dominated by launch cost and power cost with PPU cost third. Total cost is of the same magnitude ($\$2 \times 10^7$) as for larger payloads in the OR/LS baseline. The mass breakdown is similar to the OR/LS case with propellant and thruster mass dominating at low I_{sp}, and power and PPU masses dominating at high I_{sp}. Cost as a function of payload mass, shown in Figure 4-57, indicates the most cost-effective region to be around 5000 sec. As a reference for thruster requirements, Figure 4-58 shows the number of thrusters required as a function of I_{sp} and module power. Also shown are lines of constant minimum thruster diameter.

b. Power Source Sensitivities

Since power is a major contributor to cost and mass, variations in these areas are also significant, as shown in Figures 4-59 and 4-60. The relative cost sensitivity to changes in specific power costs, at 5000 sec, is about \$3.5/kg per \$/W. With an 18,000-kg payload, the sensitivity is $\$6.3 \times 10^4$ per \$/W. Thus, if the power cost uncertainties were on the order of \$50/W, the transportation cost would be uncertain by about $\$3 \times 10^6$ (i.e., ±15 percent of the total cost).

Specific mass sensitivity, at 5000 sec, is about \$3/kg per kg/kW of specific mass. Thus, an uncertainty of 2 kg/kW with an 18,000 kg payload results in a transportation cost uncertainty of about $\$1 \times 10^5$. In this case, specific mass is probably not as important as power cost.

c. Initial Mass Sensitivities

In the range of 10^4 to 10^5 kg, as might be provided by one or a few Shuttles, the transportation cost is only moderately sensitive to initial mass as shown in Figure 4-61. At 5000 sec, the cost sensitivity is about \$0.002/kg per kg of initial mass. With an 18,000 kg payload, this translates into a sensitivity of about \$30/kg of initial mass. Thus, if a Shuttle could deliver only 2.5×10^4 kg per trip, a cost-effective

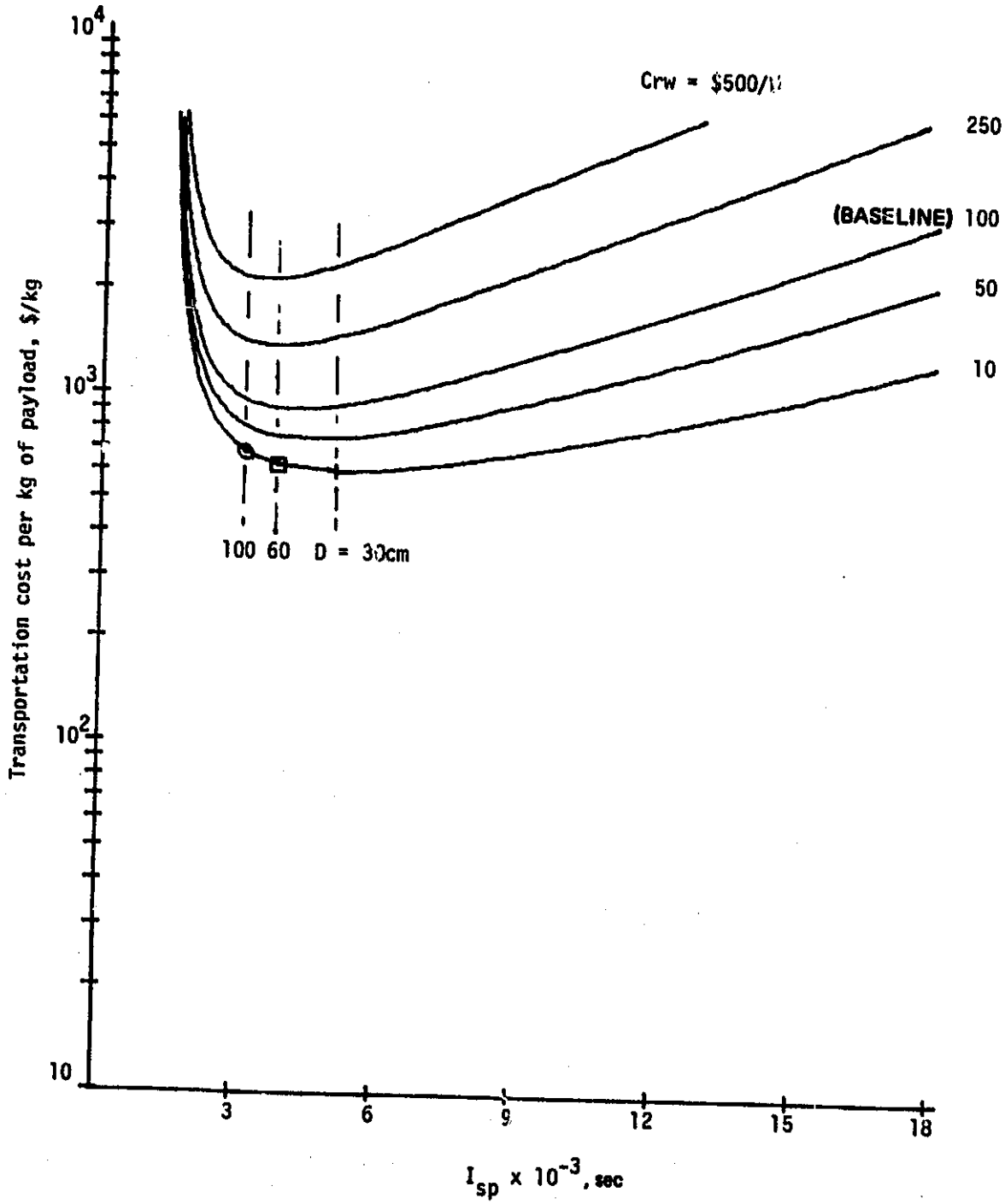

Figure 4-59. OR/MS effect of power specific cost.

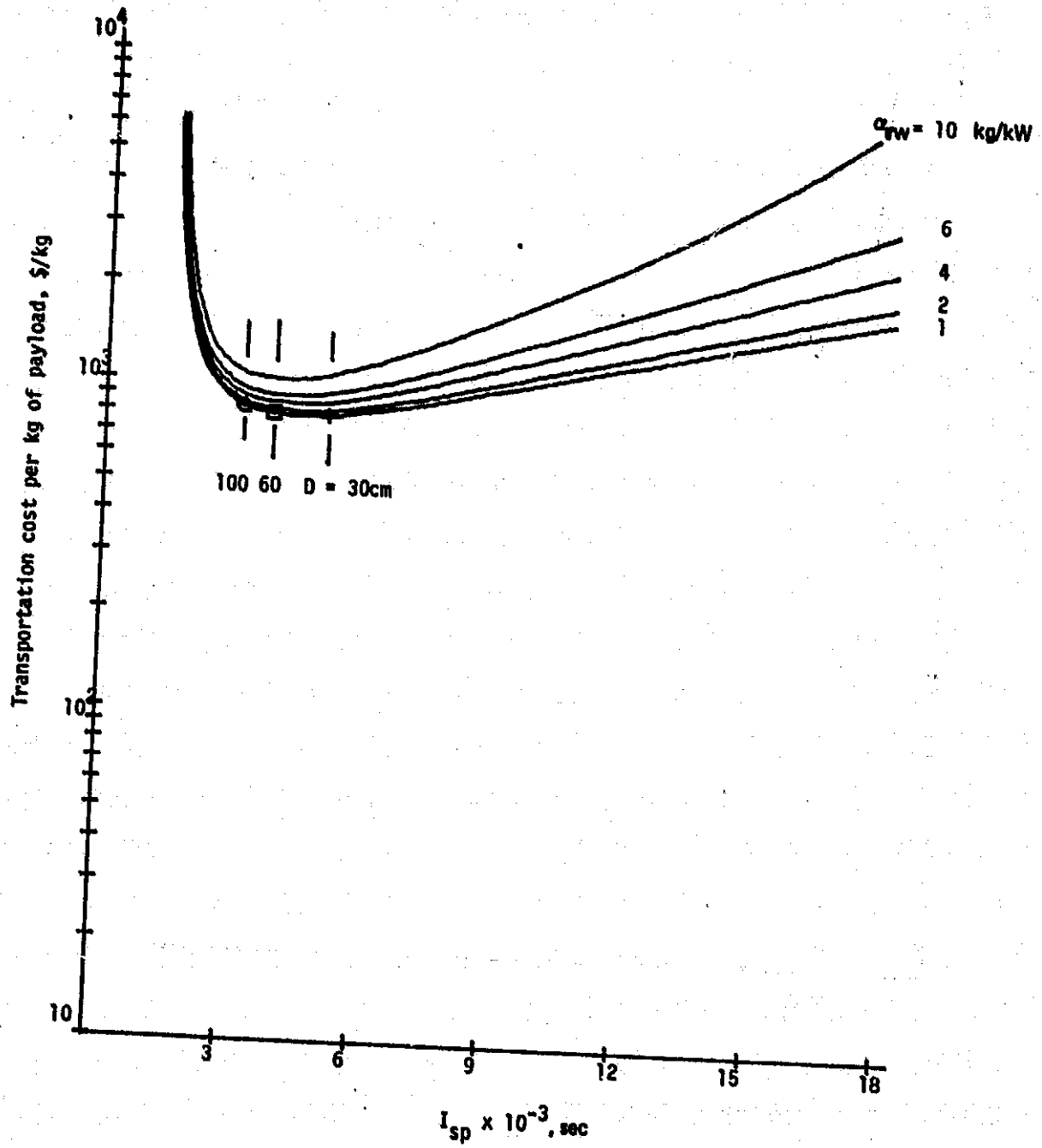

Figure 4-60. OR/MS effect of power specific mass.

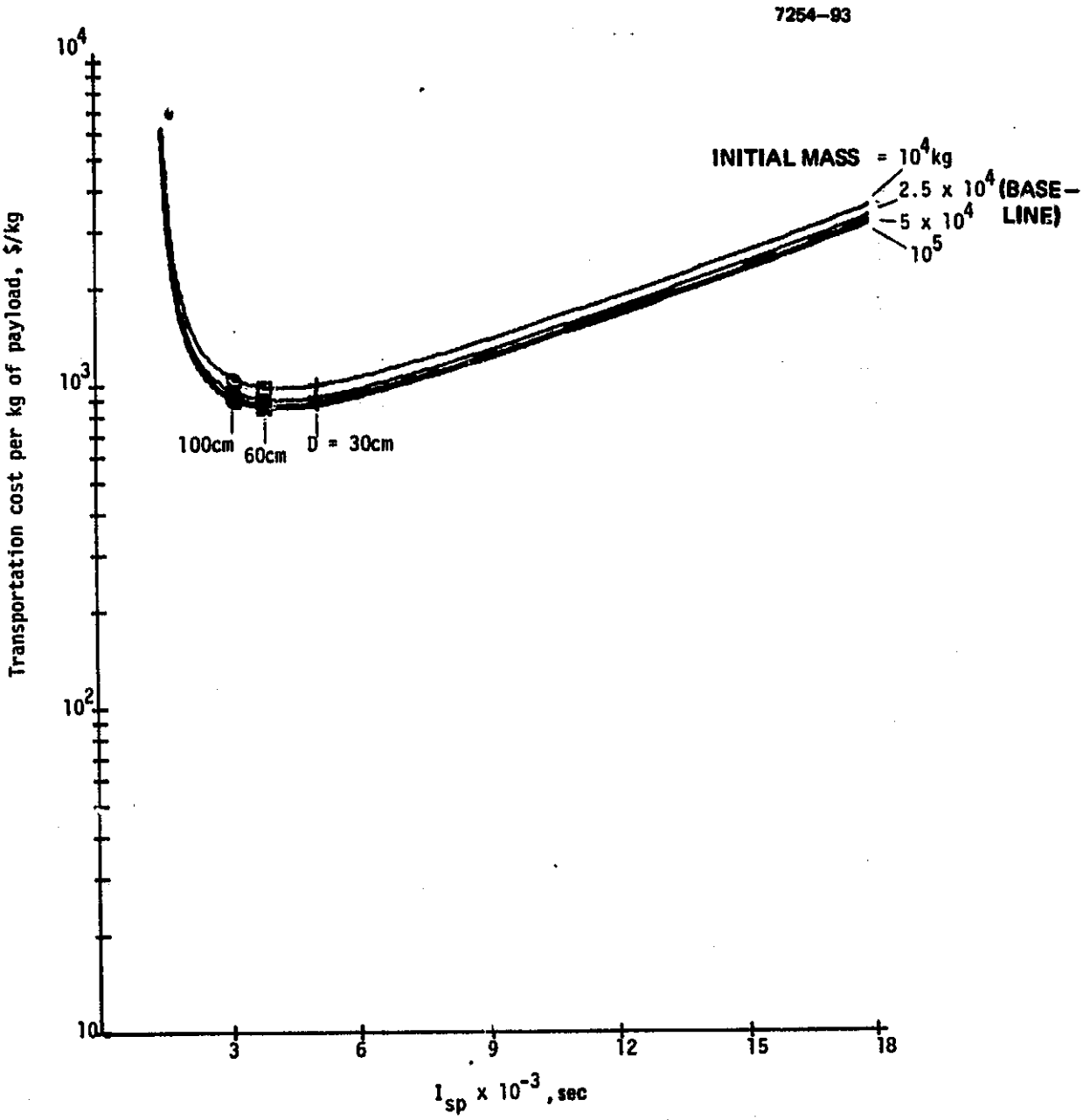

Figure 4-61. OR/MS effect of initial mass.

approach would be to deliver several Shuttle loads to LEO before transport. Using the above values, transporting four 2.5×10^4 kg loads in one ORV trip would effectively reduce the total trip cost by \$30/kg or by $\$3 \times 10^6$.

d. Launch Cost Sensitivities

The effect of launch cost on total transportation cost is shown in Figure 4-62 to be quite significant. The sensitivity around the baseline at 5000 sec is about \$1.6/kg per \$/kg of launch cost. With an uncertainty of 100 \$/kg in launch costs, transportation costs for an 18,000 kg payload would be uncertain by about $\$3 \times 10^6$.

e. Integration and Testing Sensitivity

With the higher baseline values for power and launch cost and the low initial mass, variation of integration costs become relatively insignificant, as Figure 4-63 shows. Integration costs significantly above \$100/kg would be required to affect overall transportation cost.

B. ON-ORBIT MISSION

The basic philosophy used in the orbit-raising analysis is applied to the on-orbit mission cost modeling. With only minor exceptions, the mathematical formulation follows the orbit-raising equations. However, the results of the on-orbit modeling are expressed in terms of the total cost of providing propulsion per unit of satellite mass per year. This figure-of-merit, which includes the cost of transportation from Earth to GEO, produces a convenient normalization and a final number of tractable size (typically in the range of 5 to 500 \$/kg/yr).

Applicable portions of the orbit-raising analysis are not repeated in this section. Specifically, the propulsion system performance, redundancy, and degradation sections are not duplicated. In addition, in describing the on-orbit computer model logic, the mathematical portions are referred to the corresponding relations in Section 4.A.

Terminology and general definitions used in the on-orbit analysis are presented in Figure 4-64. This diagram is identical with that shown in Figure 4-1 except for terminology. For the on-orbit mission, the satellite stationkeeping and attitude control functions are provided by the EP system (i.e., the OOP). A power source mass allocation

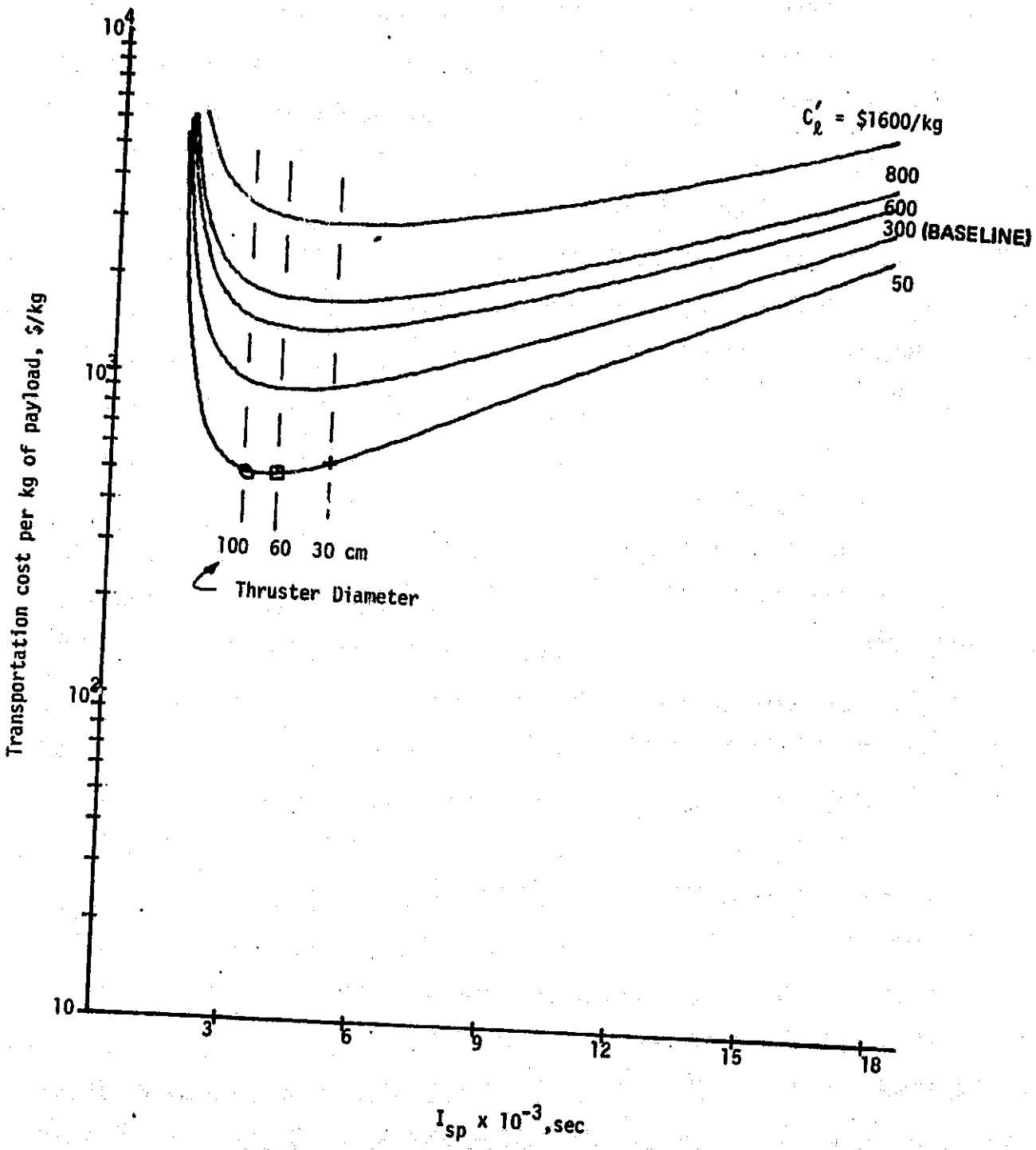

Figure 4-62. OR/MS effect of specific launch cost.

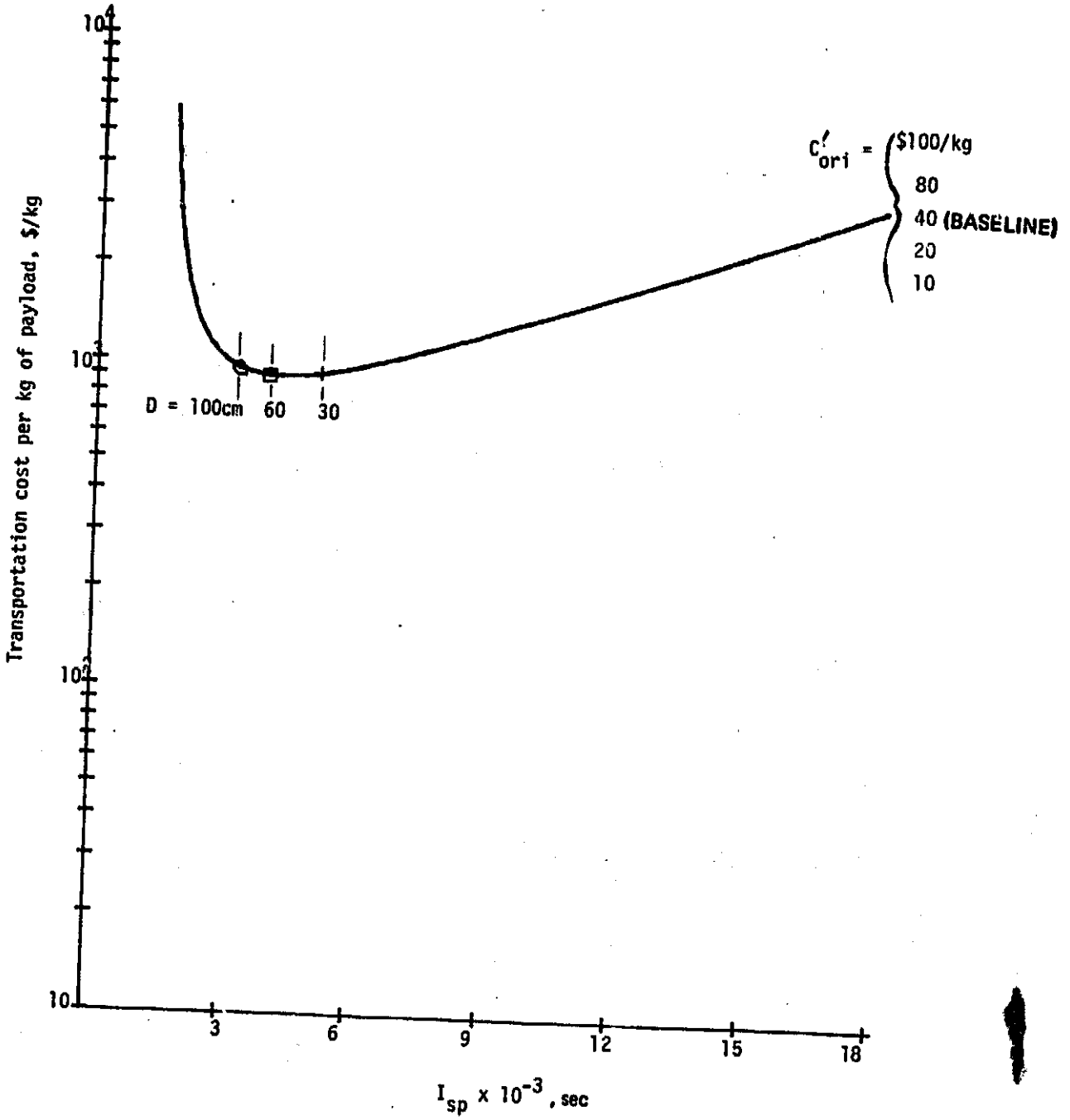

Figure 4-63. OR/MS effect of specific integration cost.

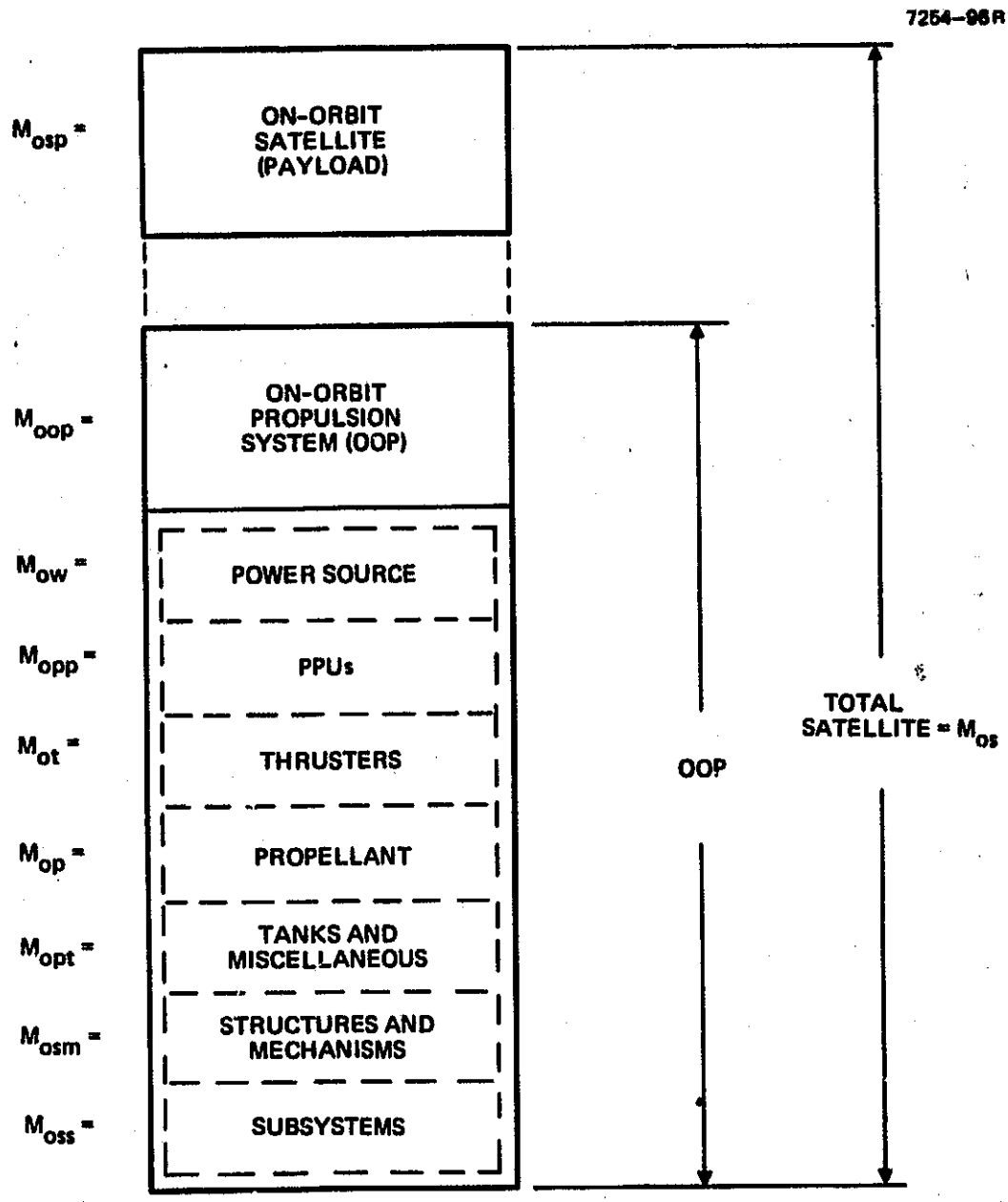

Figure 4-64. OOP block diagram.

is applied to the OOP, although in most cases the power source physically would be part of the basic satellite. Depending on the satellite design, the power source might be required only part of the time and could be used by the satellite during non-propulsion periods.

1. Mission Description

The on-orbit mission is illustrated conceptually in Figure 4-65. The OOP is shown as a unit, but in most applications thrusters would be placed at widely separated locations to provide moment arms for attitude control. In general, the number and location of thrusters installed would depend on satellite size and control requirements. Since such satellite design variables cannot be easily modeled, an alternate approach using estimated ΔV requirements is included in the on-orbit cost model, as discussed in Section 4.B.2.

As in the orbit raising analysis, specific details of the orbit (such as altitude, inclination, or eccentricity) are not directly included in the model. It is assumed that the ΔV selected will adequately characterize mission requirements. The sensitivity of results to ΔV is discussed in Section 4.B.5. Choosing a conservative ΔV should produce a conservative final result since the total propulsion system and propellant scale with ΔV. For large satellites, the forces and torques illustrated in Figure 4-65 are significant contributors to ΔV. An on-orbit ΔV model is discussed in Appendix E.

2. On-Orbit Mission General Model

The logic diagram for the on-orbit mission is shown in Figure 4-66. Comparing Figure 4-66 with Figure 4-3 indicates that the only significant difference in logic is the down trip option included in the orbit-raising analysis. The mathematical formulation, except for details of the cost and mass models, is the same as that presented in Section 4.A.2.

The starting point is the definition of the mission in terms of mission life, ΔV, and satellite mass. Satellite mass and size (area) must be considered in estimating ΔV (see Appendix E). The basic variable, I_{sp}, is used in a looping process to develop cost results as a

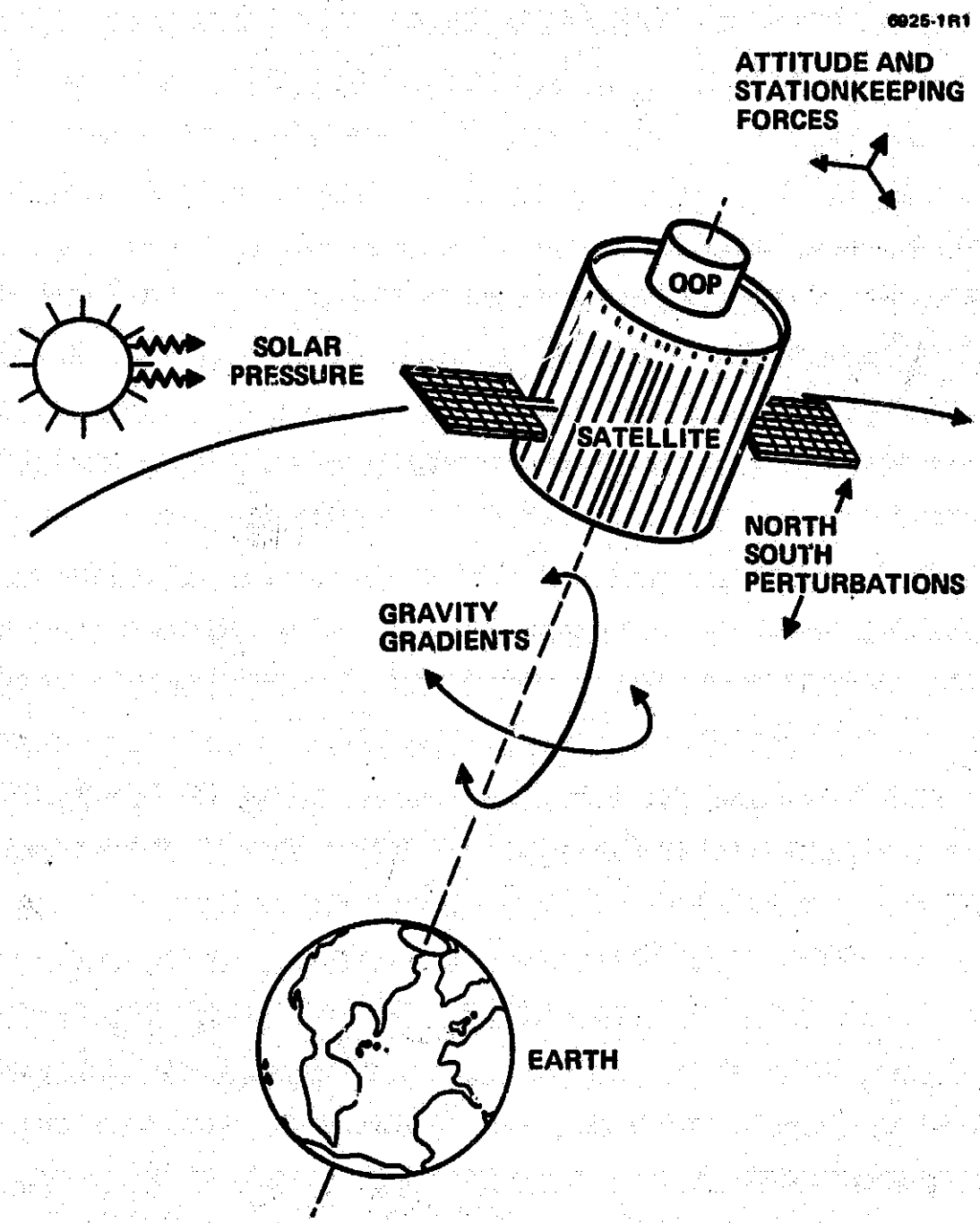

Figure 4-65. On-orbit mission concept.

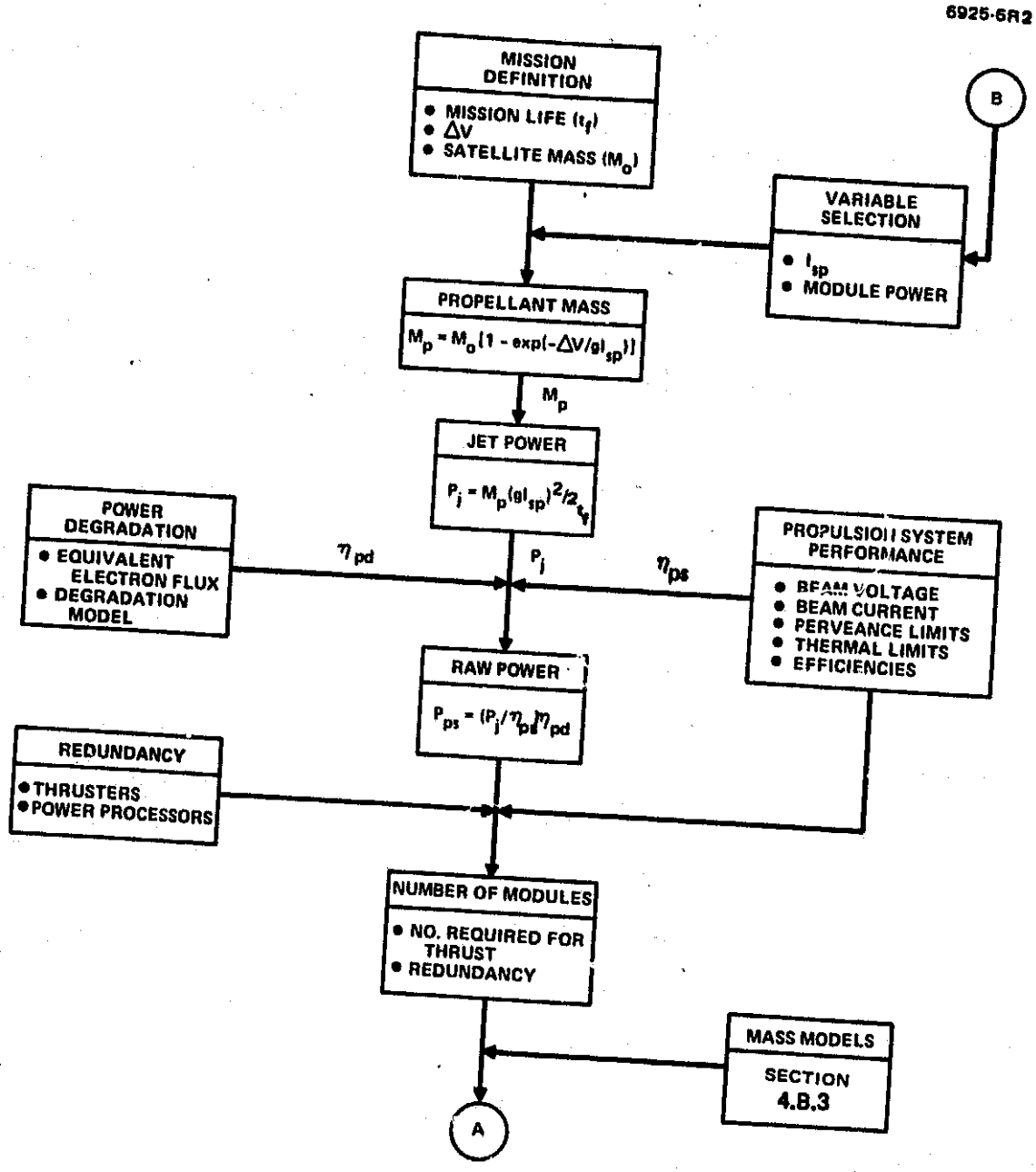

Figure 4-66. On-orbit model logic diagram.

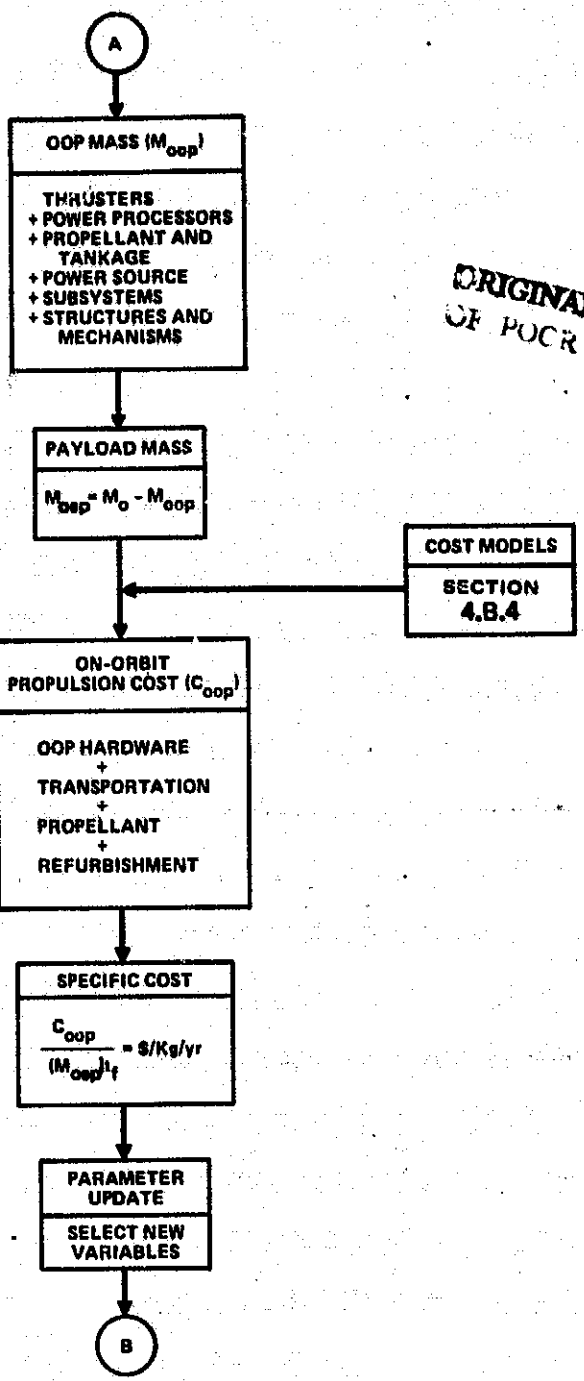

Figure 4-66 (Continued)

function of I_{sp}. Various parameters defining the mission (life, ΔV, M_{os}, etc.), propulsion system performance, cost, and mass are then individually selected for sensitivity analysis.

Payload mass is considered to be the difference between satellite total (initial) mass and OOP mass. Total cost of providing propulsion for the satellite is then divided by mission life and payload mass to obtain costs in terms of $/kg/yr.

3. Mass Models

Mass models for the on-orbit mission are summarized in Table 4-6. With minor exceptions, these terms (defined with ORV subscripts) are identical to those discussed in Section 4.A.6. A brief review is presented here to indicate the equation used for model calculations. (The program listings can also be consulted as a simple reference.) Total OOP mass is defined by

$$M_{oop} = M_{ot} + M_{opp} + M_{op} + M_{opt} + M_{ow} + M_{oss} + M_{osm}, \qquad (4\text{-}43)$$

where

M_{ot} = mass of thrusters (Eq. 4-19)

M_{opp} = mass of PPUs (Eq. 4-22)

M_{op} = propellant mass

$= M_{os}\left[1 - \exp\left(-\Delta V/g_o I_{sp}\right)\right]$

M_{os} = satellite initial mass

M_{opt} = propellant tankage mass (Eq. 4-23)

M_{ow} = power source mass (Eq. 4-24)

M_{oss} = subsystems mass (Eq. 4-25)

M_{osm} = structure and mechanisms mass (Eq. 4-26).

4. Cost Models

Cost models for the OOP are summarized in Table 4-7. As with the mass models, the OOP individual element cost models are essentially identical in form to the ORV models. However, since the OOP is not

Table 4-6. Mass Models Used in On-Orbit Cost Model

$$M_{oop} = M_{ot} + M_{opp} + M_{op} + M_{opt} + M_{oss} + M_{osm} + M_{ow}$$

$$M_{ot} = 2\left(0.078\ D^{1.35}\right) N_{ot}$$

$$M_{opp} = 0.001\ \alpha_{pp}\ P_{ps}\ (1 + R_p)$$

Where,

$$\alpha_{pp} = 10^{[-0.503\ \log\ (P_{tot}) + 1.153]}$$

$$M_{op} = M_o\ [1 - \exp\ (-\Delta V/g_o I_{sp})]$$

$$M_{opt} = \alpha_{rpt}\ M_{op}$$

$$M_{oss} = 100\ \left[(1 + 10^{-6} P_{tot}) + (N_{ot}/N_{op}) - 1\right]$$

$$M_{osm} = \alpha_{sm}\left[M_{ot} + M_{opp} + M_{op} + M_{opt} + M_{oss}\right]$$

$$M_{ow} = \alpha_{rw}\ (0.001\ P_{tot})$$

6119

Table 4-7. Cost Formulae Used in On-Orbit Cost Model

$$C_{oop} = C_{ot} + C_{opp} + C_{opt} + C_{osm} + C_{oss} + C_{to} + C_{oi} + C_{ow} + C_{ops} + C_{odd}$$

$$C_{ot} = 2\,[(42 \times 10^3)\ \log\,(D)]\ \left(1.47\ N_{ot}^{0.68}\right)$$

$$C_{opp} = 4.3 \times 10^5\ P_{pp}^{\ 0.12}\ \left(1.47\ N_{op}^{0.68}\right)$$

$$C_{opt} = M_{op}\ (C'_{op} + \alpha_{pt}\ C'_{opt})$$

$$C_{osm} = C'_{osm}\ (M_{osm})^{0.3}$$

$$C_{oss} = C'_{oss}\ (M_{oss})^{0.9}$$

$$C_{to} = C'_{to}\ M_o$$

$$C_{oi} = C'_{oi}\ M_{oop} - M_{op}$$

$$C_{ow} = C'_{ow}\ P_{tot}$$

$$C_{ops} = C'_{ops}\ t_f$$

t_f = mission time

$$C_{odd} = C'_{ord}/N_{ov}\ (M_{oop} - M_{op})^{0.3}$$

$$\overline{C_{oop}} = C_{oop}/M_{osp}/t_f$$

6119

"rented" to a user for a given trip, the utilization factor (C_{oef}) is not involved. Additional model differences (besides subscripts) are defined here; the costs that are similar are referenced to equations defined for the orbit-raising model. Total propulsion cost for the on-orbit mission is defined by

$$C_{oop} = C_{ot} + C_{opp} + C_{opt} + C_{ow} + C_{oss} + C_{osm} + C_{to} + C_{oi} + C_{ops} + C_{odd}, \quad (4\text{-}43)$$

where

C_{ot} = cost of thrusters (Eq. 4-32 without last term)

C_{opp} = cost of PPUs (Eq. 4-33)

C_{opt} = propellant and tankage (Eqs. 4-34 and 4-35)

C_{ow} = power source cost (Eq. 4-38)

C_{oss} = subsystems cost (Eq. 4-37)

C_{osm} = structure and mechanisms cost (Eq. 4-36)

C_{to} = transportation cost

$= C'_{to} M_{os}$

C'_{to} = transportation cost from Earth to orbit per kg

C_{oi} = integration and testing cost

$= C'_{oi} (M_{oop} - M_{op})$

C'_{oi} = integration cost per kg of dry OOP

C_{ops} = operations cost

$= C'_{ops} t_f$

t_f = mission time

C_{odd} = DDT&E cost (Eq. 4-40)

N_{ov} = number of on-orbit vehicles over which DDT&E costs are amortized

5. On-Orbit/Large System Baseline Mission Results

In a fashion similar to the orbit-raising mission, two baseline sets of parameters are used in developing on-orbit results: large space system era (OO/LS) and matured Shuttle era (OO/MS). Again, for each baseline, general results are presented to illustrate the characteristics. Overall cost sensitivities for selected variables are then analyzed to assess the importance of various parameters, particularly thruster parameters.

a. Orbit/Large System Baseline Parameters

The large system baseline (OO/LS) parameter set is shown in Table 4-8. The parameters that are different from the OR/LS baseline require some discussion and include ΔV, mission time, and transportation cost.

An analysis for estimating ΔV is presented in Appendix E. Clearly, without a specific satellite design, such an analysis is extremely approximate. However, since the primary purpose of the analysis was to determine the order of magnitude of ΔV to be considered, the absolute accuracy is relatively unimportant. A baseline ΔV of 1.65 km/s/yr was selected.

A baseline mission time of 10 years was chosen, based on several factors. Although longer times may be needed to make certain satellites (e.g., solar power satellite) cost effective, it is probably unreasonable to store the necessary propellant for such periods. Thus, if propellant is replenished, propulsion system modules could be replaced. These additional concept variables would substantially complicate the present problem. Mission times of 5 to 10 years are currently being achieved with existing satellites. However, since current satellites are relatively simple compared to those imagined in the large system baseline, a nominal 10 year mission is a reasonable compromise.

Transportation cost, as it is used in the on-orbit cost analysis, includes all costs from Earth to the satellite orbit. This cost is just the value computed in the orbit raising mission. A value of \$50/kg was selected for the OO/LS baseline based on typical OR/LS baseline results.

Table 4-8. OO/LS Baseline Cost Model Parameters

Argon Propellant

P_{mod} = 100 kW

Thruster Life = 10^4 hr

ΔV = 16.5 km/sec

t_f = 10 years

Initial mass = 10^6 kg

Electron flux = 10^{15} electrons/cm^2, using curve "C"

C'_{oi}	= \$10/kg	OOV Integration and Testing
C'_{ow}	= \$500/kW	Cost of OOP Associated Power
C'_{ot}	= $\$4.2 \times 10^3 \cdot \log(D)$	First Unit Thruster Cost
C'_{op}	= $\$4.3 \times 10^5 \ (kW)^{0.12}$	First Unit PPU Cost
R_t	= 0.2	PPU Redundancy
R_p	= 0.2	Thruster Redundancy
C'_{opt}	= 0.4 (1 + 0.1 x 100)	Propellant at \$0.4/kg Tankage at \$100/kg with Tankage factor = 0.1
C'_{ops}	= $\$10^3$/day	Time Dependent Cost
Y_{rs}	= 10	Life of OOV
C_{osm}	= $\$10^4 \ (M_{osm})^{0.3}$	Cost of OOV Structure and Mechanisms
C_{odd}	= $\frac{1 \times 10^5}{10} \ (M_{oop}-M_{op})^{0.3}$	DDT&E Cost Amortized over 10 OOPs
C_{oss}	= $\$1 \times 10^4 \ (M_{oss})^{0.9}$	Cost of COP Subsystems
α_{ps}	= 3 kg/kW	Specific Mass for Power
C'_{to}	= \$50/kg	Orbit Raising Cost per kg

b. 00/LS Baseline, General Results

The general results of the 00/LS baseline are shown in Figures 4-67 through 4-71. Specific cost ($/kg/yr) as a function of I_{sp} for a range of module power is shown in Figure 4-67. At low I_{sp}, these data have a shape similar to the orbit raising results. However, at high I_{sp}, the curves continue to decrease or just flatten out. The explanation for this behavior is illustrated in Figures 4-68 and 4-69, which show cost and mass breakdowns. At low I_{sp}, cost is high (due to the large transportation cost) and payload mass is low (due to large propellant, thruster, and structure masses). At high I_{sp}, propellant and most other masses are decreasing. Power source mass is increasing but is a small fraction of the total. Although total cost is increasing at high I_{sp}, its influence on specific cost is offset by the increasing payload mass.

Specific cost and total cost as a function of the payload mass are shown in Figure 4-70. For the baseline conditions, minimum specific cost, as well as minimum total cost, occurs in the region of 12,000 sec. The sensitivity of specific cost to module power at this point, as found from Figure 4-67, is about 0.013 $/kg/yr per kW. With the 8×10^5 kg payload, the cost/yr is about $\$10^4$ per kW of module power. The cost difference between a 50-kW (30-cm) module system and a 200-kW (60-cm) module system would be about $\$1.5 \times 10^6$/yr or $\$15 \times 10^6$ over the mission life. The benefit of larger modules is clear. The number of thrusters required as a function of I_{sp} is shown in Figure 4-71. The dashed lines show minimum thruster diameter.

Using the baseline results as a starting point, several sensitivity studies were performed to assess the importance of various parameters. These study topics, discussed in the following sections, are shown in Table 4-9.

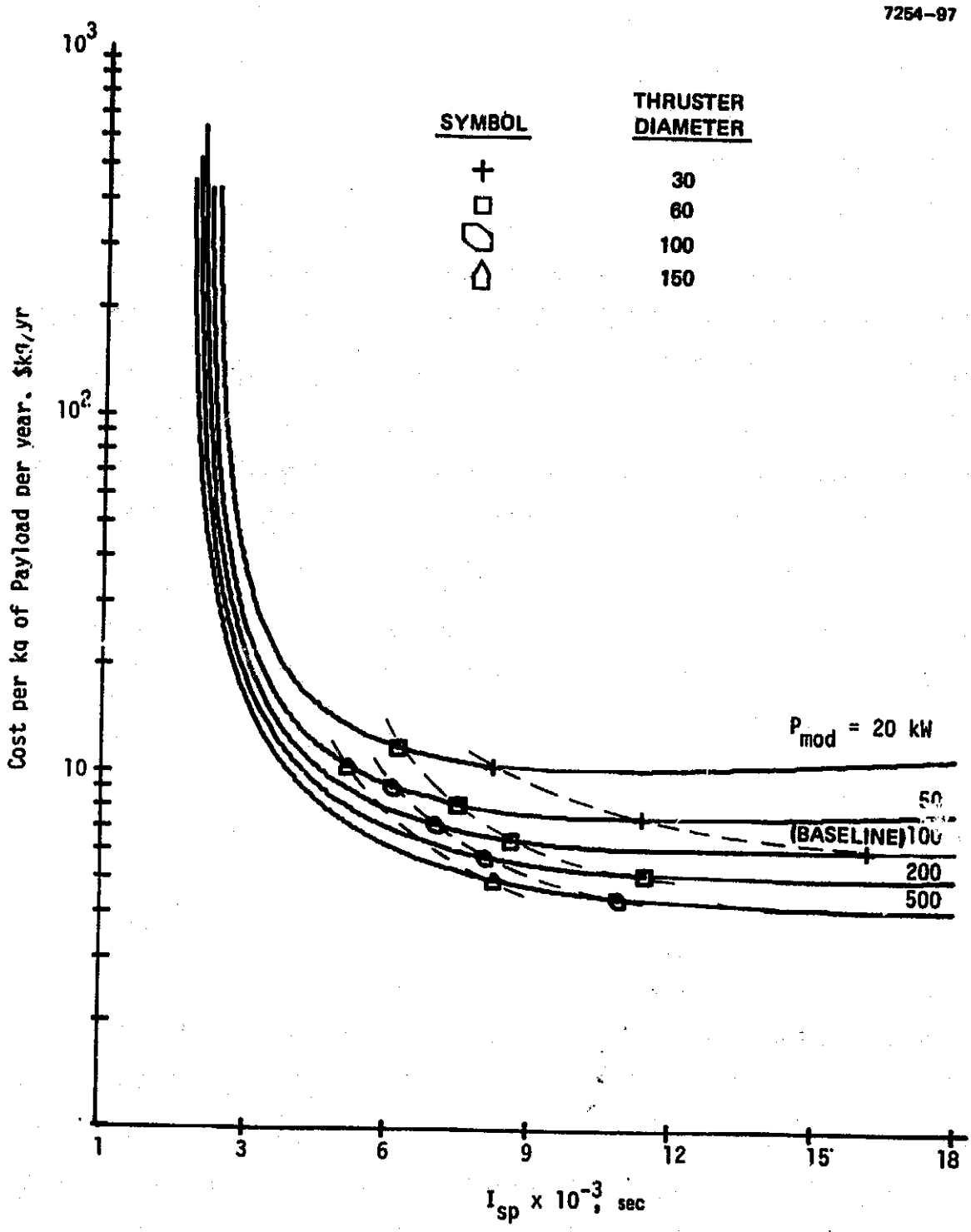

Figure 4-67. OO/LS effect of P_{mod}.

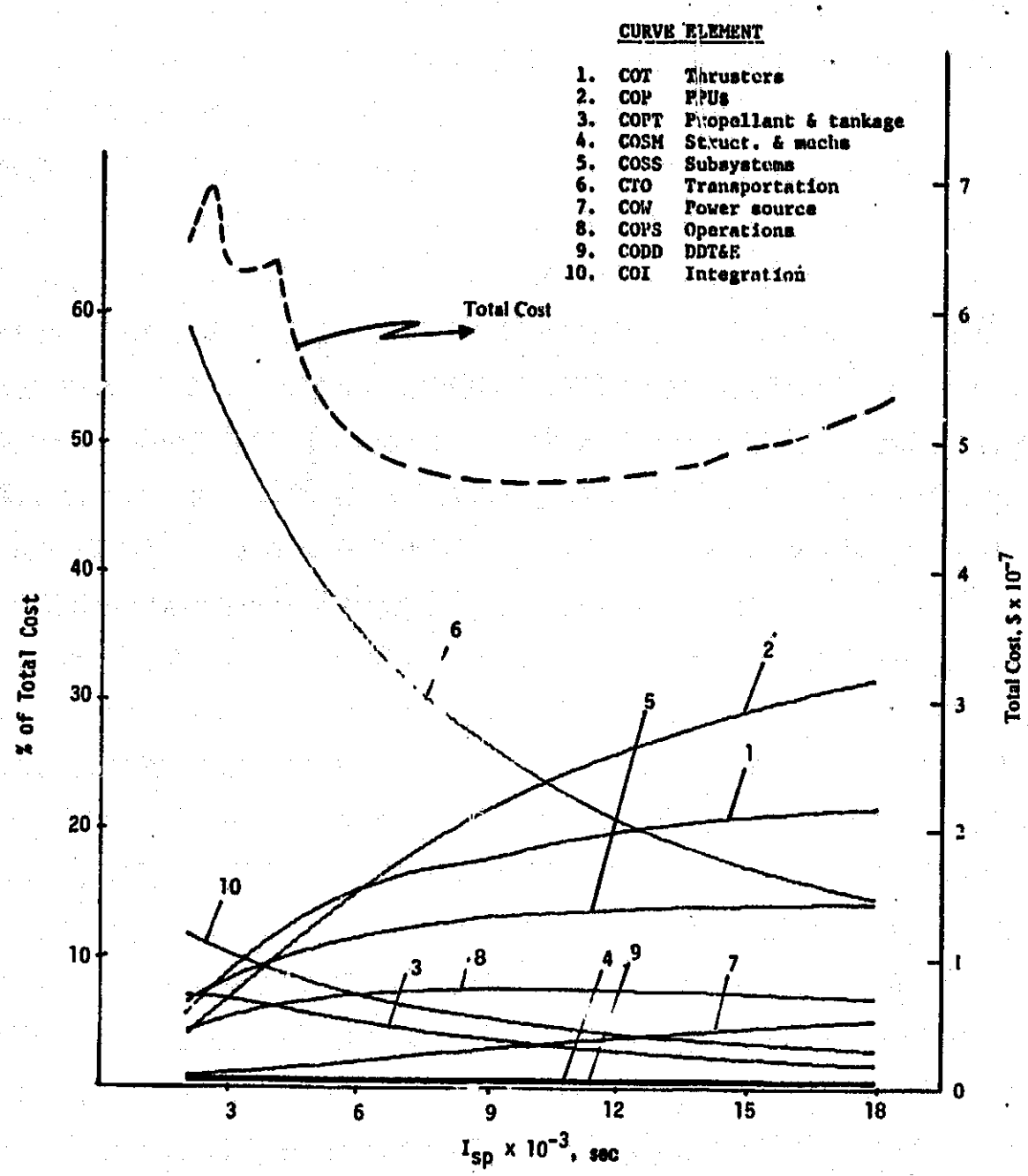

Figure 4-68. OO/LS cost breakdown.

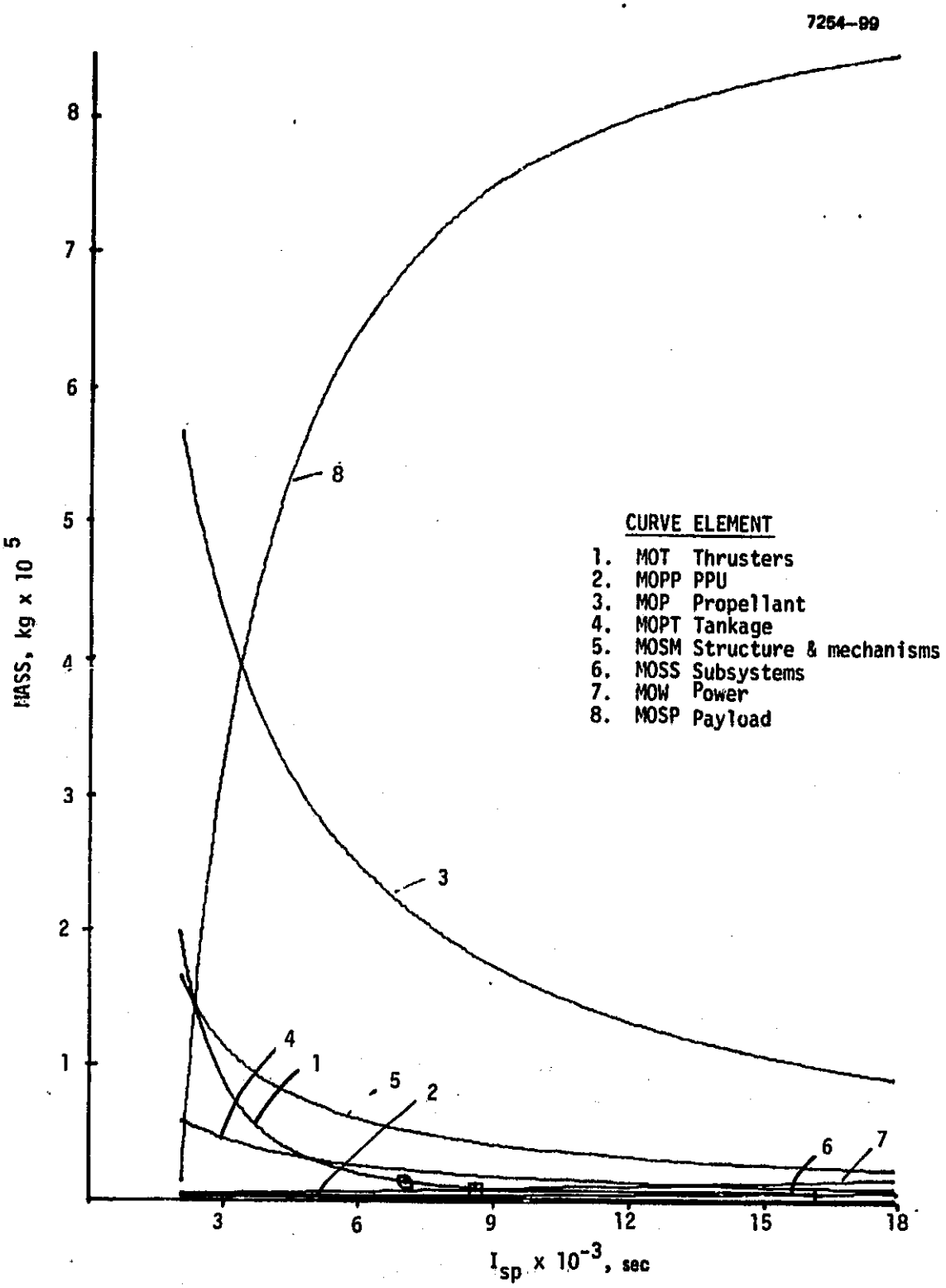

Figure 4-69. OO/LS mass breakdown.

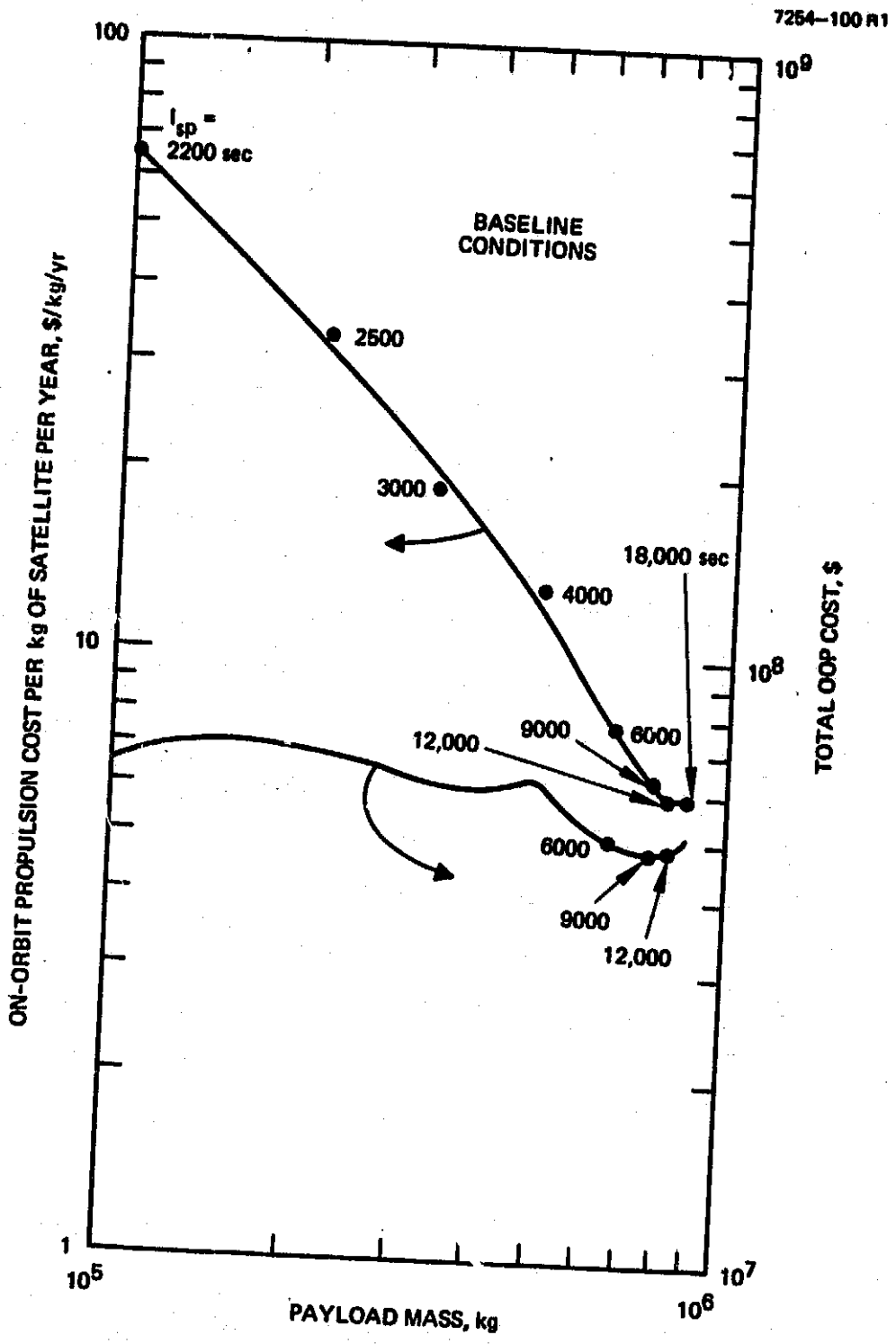

Figure 4-70. OO/LS cost/kg versus payload mass.

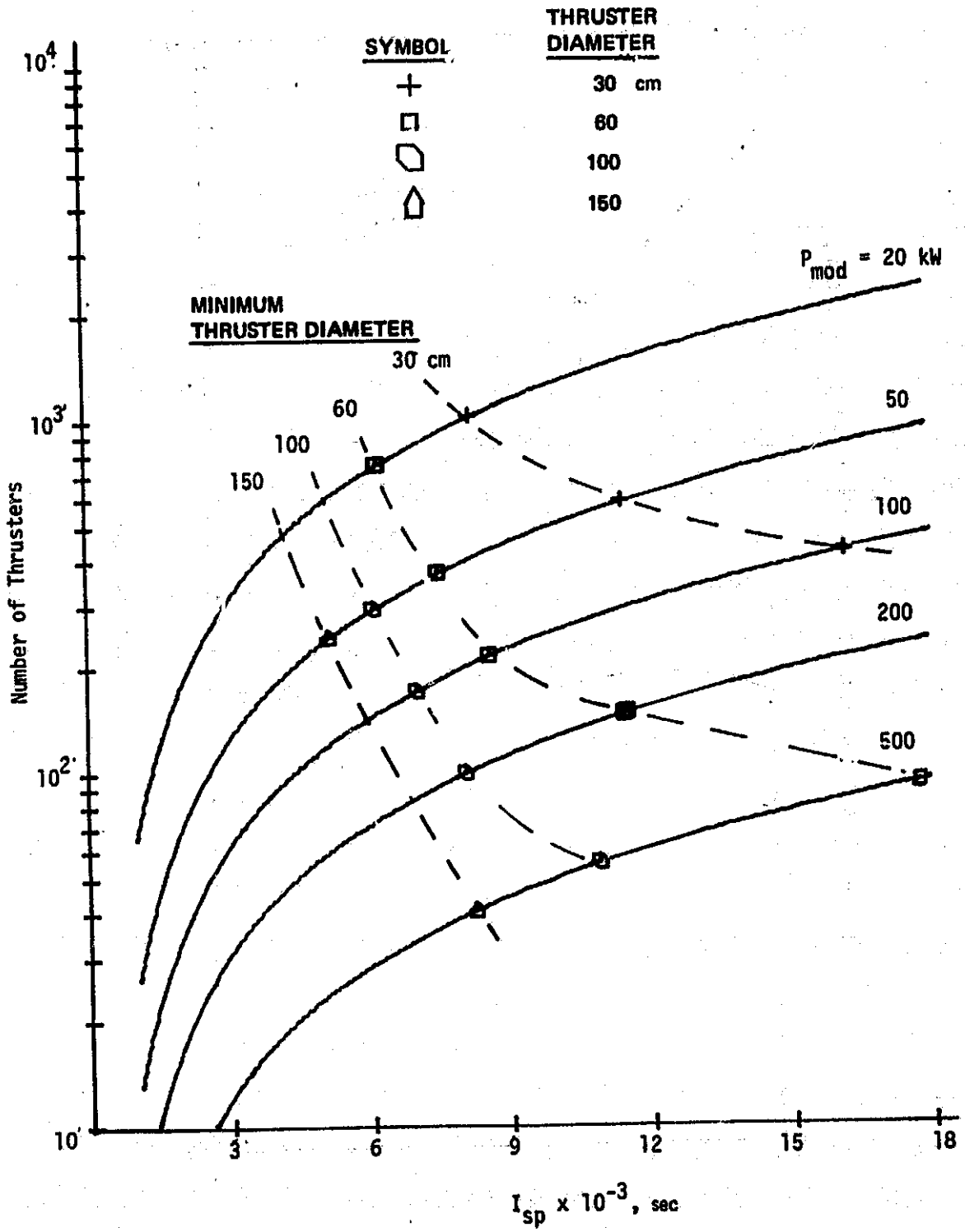

Figure 4-71. OO/LS number of thrusters.

c. Mission Design Sensitivities

Four general mission factors affecting cost are discussed in this section: ΔV, mission time, initial mass, and transportation cost. Although each has a significant impact on cost and could influence mission design, none appears to substantially change the general shape of the curves or thruster considerations.

Table 4-9. OO/LS Data Run and Sensitivity Study Categories

1. General Cost/kg/yr versus I_{sp}; P_{mod} Cost breakdown Mass breakdown Cost/kg/yr versus payload Number of modules	4. Propellant sensitivity Cost
2. Mission design sensitivities ΔV Mission time Initial mass Transportation cost	5. PPU Sensitivities Mass First unit cost Redundancy
3. Thruster sensitivities Life Efficiency Mass First unit cost Redundancy	6. Power source sensitivities Mass Cost Degradation
	7. OOP system design sensitivities Structure and mechanisms Subsystems Integration and testing DDT&E

6119

(1) ΔV Sensitivity — Results for a range of ΔV requirements are shown in Figure 4-72. For a given mission time and initial mass, such a range implies a range of satellite area-to-mass ratios or uncertainty in the ΔV estimate. The minimum cost region around 12,000 sec should not be significantly shifted over this ΔV range.

(2) Mission Time — The effect of mission time on on-orbit propulsion costs is shown in Figure 4-73. Mission times significantly shorter than 10 yr increase special costs dramatically and tend to reduce the optimum I_{sp}. Times longer than 10 yr will decrease the specific costs almost linearly.

(3) Initial Mass — The initial satellite mass, including the OOP and propellant, has a large impact on specific cost, as shown in Figure 4-74. Although this effect is accentuated by the constant ΔV used in producing these curves, the general sensitivity is still significant. The reason for this trend is that, since a reasonable fraction of the OOP costs are independent of mass, specific costs increase as initial mass decreases.

(4) Transportation Cost — The sensitivity of specific cost to transportation specific cost is presented in Figure 4-75. Transportation cost begins to have a significant effect on specific cost above about $10/kg. As discussed in Section 4.A.8, transportation will probably be in the $30 to $50/kg region for the large system baseline, and on-orbit costs will certainly be influenced over this range.

d. Thruster Sensitivities

The thruster sensitivity factors considered for the OO/LS baseline are shown in Table 4-9. Since it was found in the OR/LS cases that the "R" ratio has only a minor impact on cost, this parameter was omitted for the on-orbit work.

(1) Thruster Life — Two models of thruster life, constant and beam dependent, were evaluated as shown in Figure 4-76. Constant life greater than about 10^4 hr has a relatively small impact on cost. However,

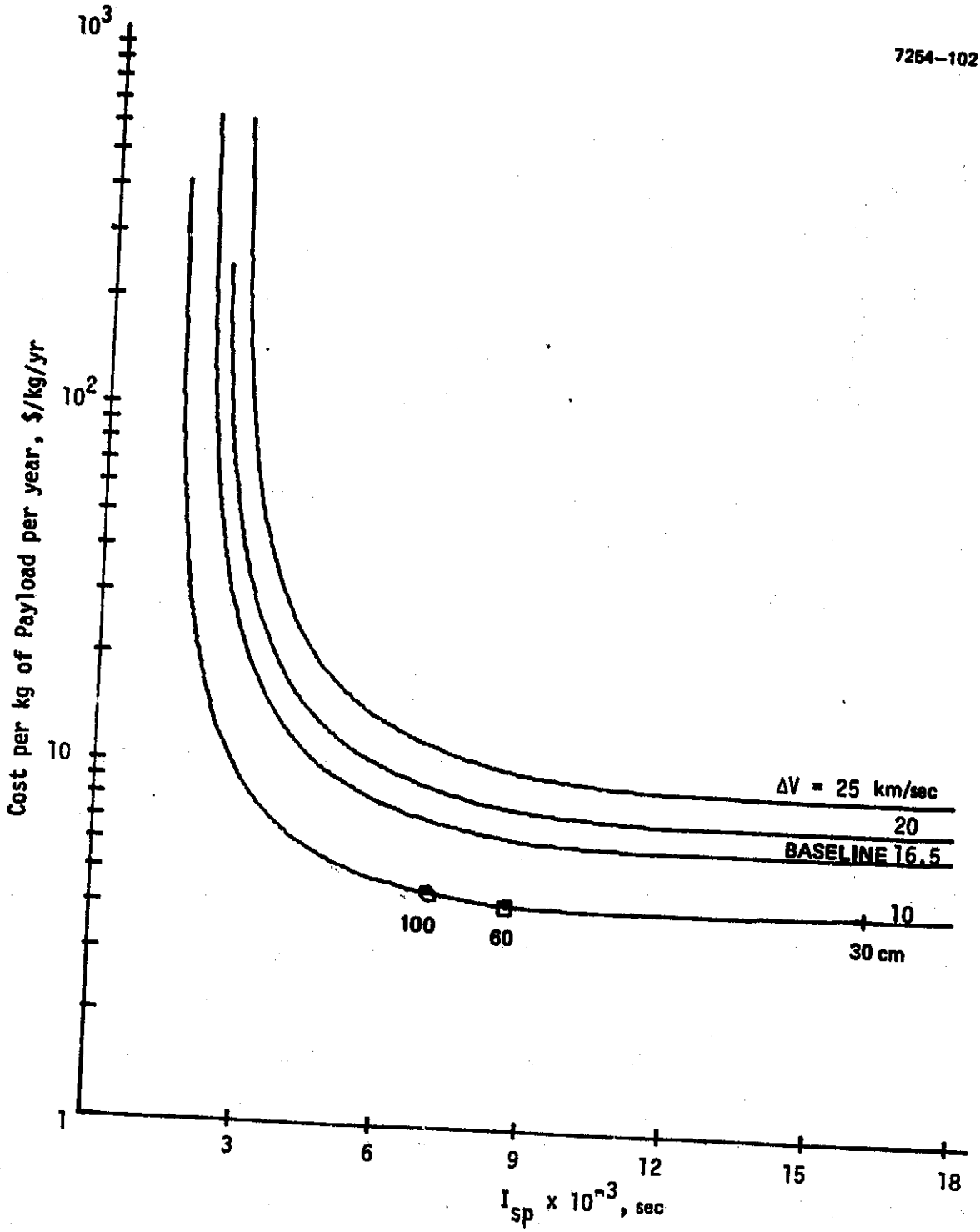

Figure 4-72. OO/LS effect of ΔV.

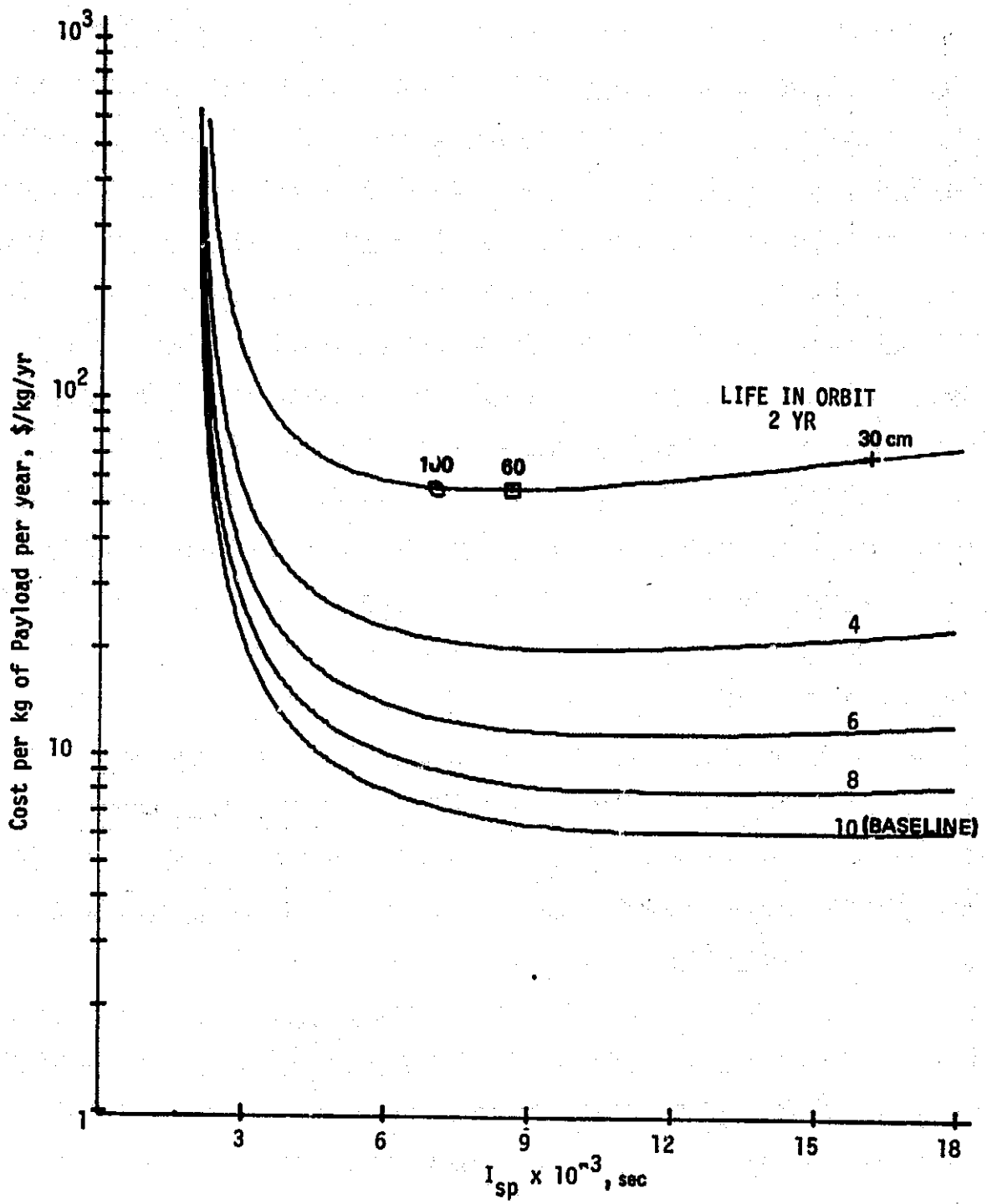

Figure 4-73. OO/LS effect of mission time.

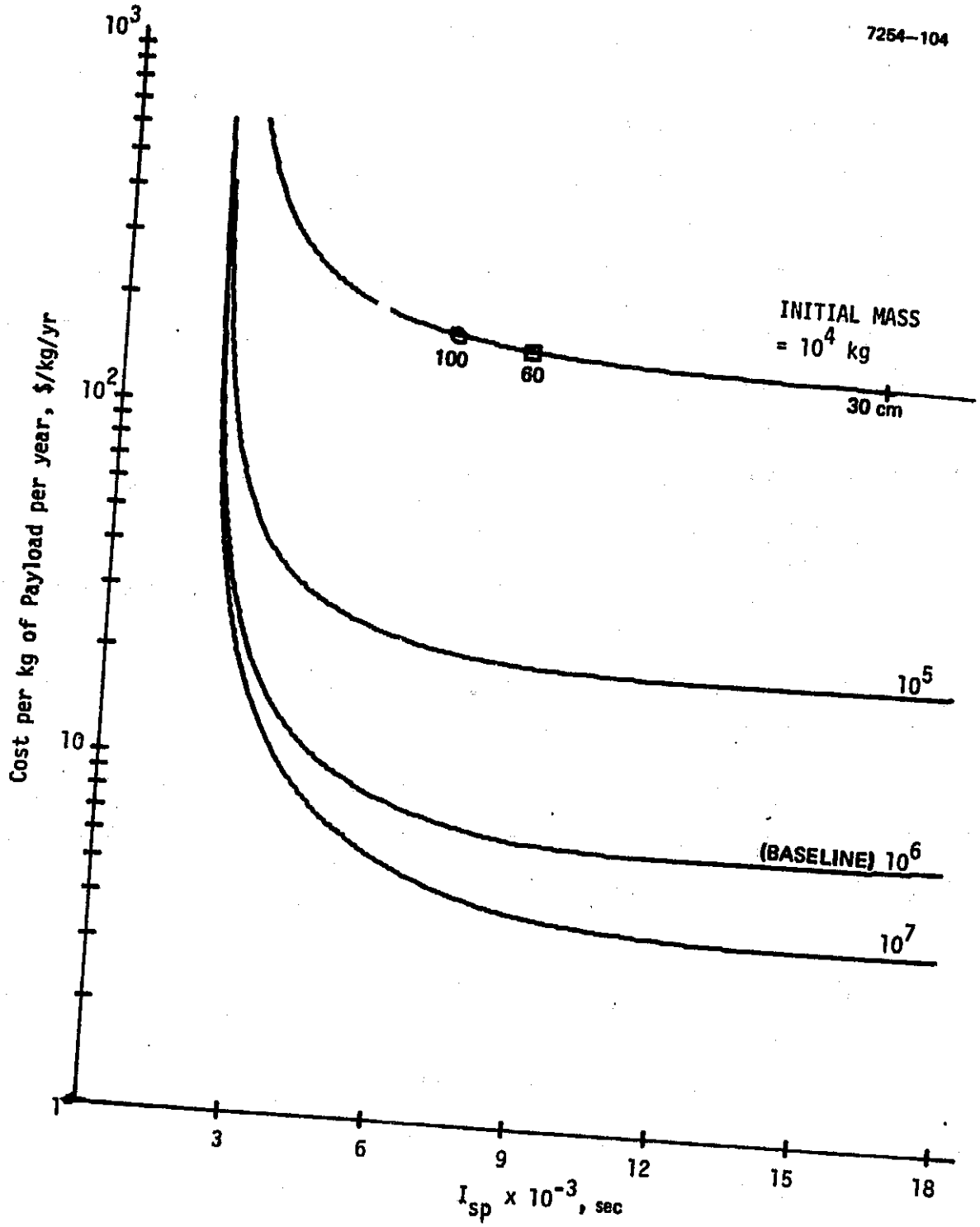

Figure 4-74. OO/LS effect of initial mass.

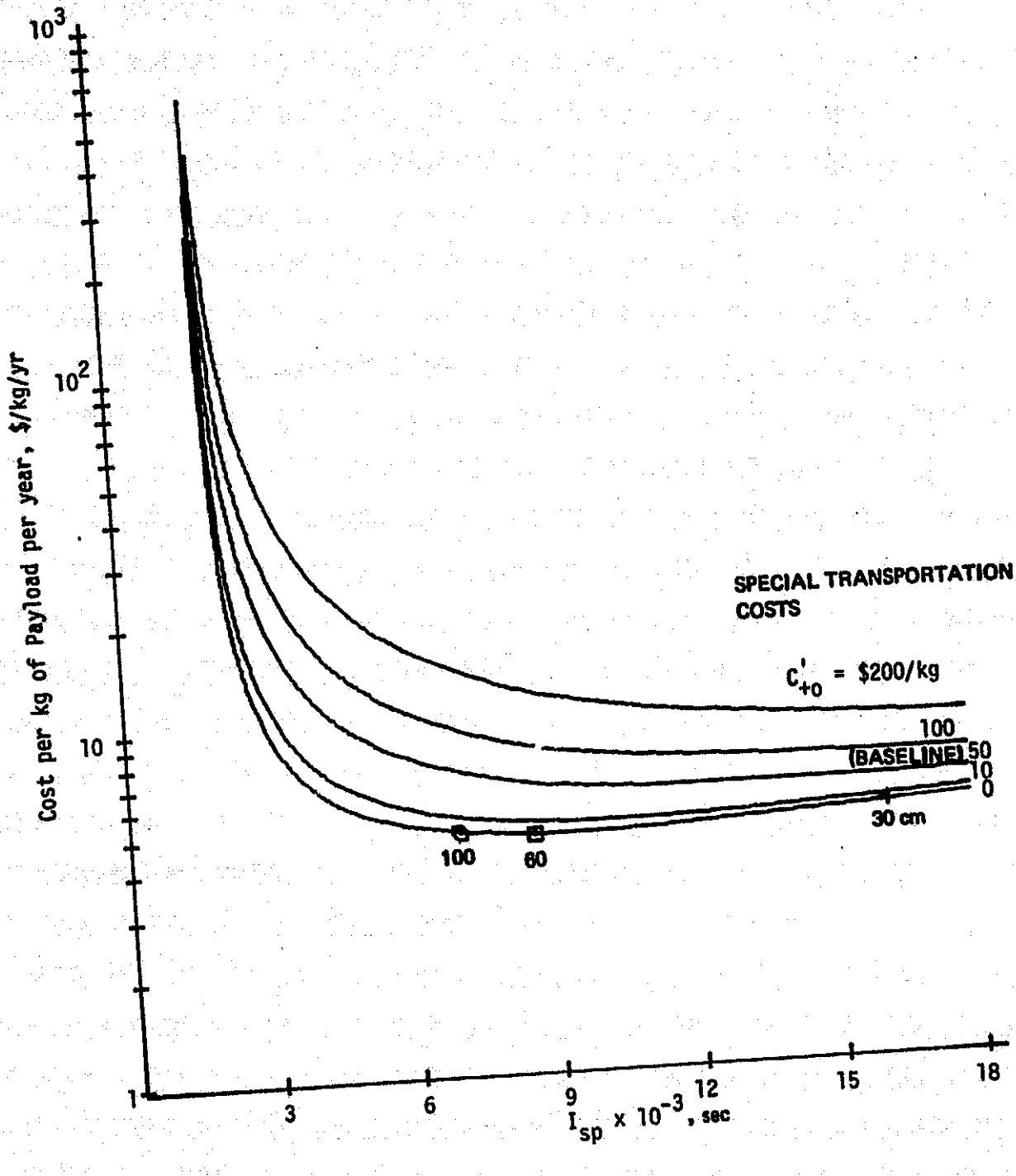

Figure 4-75. 00/LS effect of specific transportation cost from Earth to GEO.

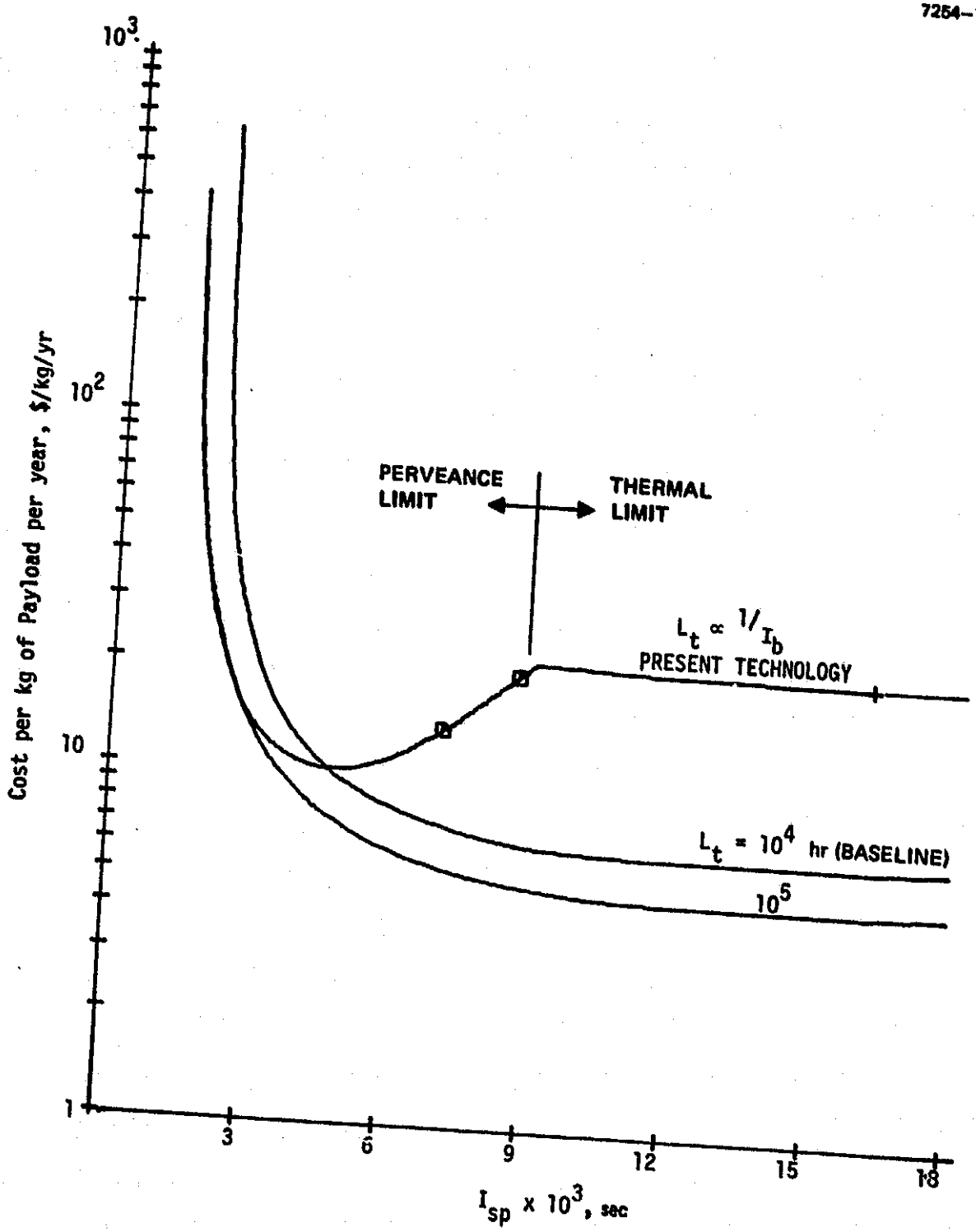

Figure 4-76. OO/LS effect of thruster life.

shorter life or a beam-current-dependent wearout characteristic would substantially increase specific cost. In addition, the sensitivity to I_{sp} becomes more pronounced for the variable life model. The optimum occurs between 3,000 and 6,000 sec and requires a large-diameter thruster (larger than 100 cm). However, if thruster diameter is limited to less than 60 cm, the cost sensitivity to I_{sp} is extremely small (for either life model).

(2) Thruster Efficiency — As shown in Figure 4-77, thruster efficiency variations over a reasonable range have little effect on specific cost. Efficiencies below 0.5 would have a larger impact since more modules would be needed.

(3) Thruster Mass — Thruster mass has only a moderate impact on cost, as Figure 4-78 shows. Only increases of several times would significantly change the cost level.

(4) Thruster Cost — The specific cost results are only moderately sensitive to thruster first unit cost as indicated in Figure 4-79. Again, increases of a factor of two or more would be required to change the specific on-orbit costs significantly.

(5) Thruster Redundancy — The baseline redundancy of 20 percent should provide a reasonable reliability. Even if a redundancy of 40 percent were used, the specific cost would not be strongly affected as Figure 4-80 shows.

e. Propellant Sensitivity

Based on the orbit-raising results, only propellant specific cost was considered here. The results are shown in Figure 4-81 for a range of propellant costs. Except around 6,000 to 9,000 sec, propellant cost has almost no influence on overall specific cost. Other propellants should produce similar results with only a shift in thruster diameters.

f. PPU Sensitivities

The sensitivities considered are indicated in Table 4-9 and include mass, cost, and redundancy.

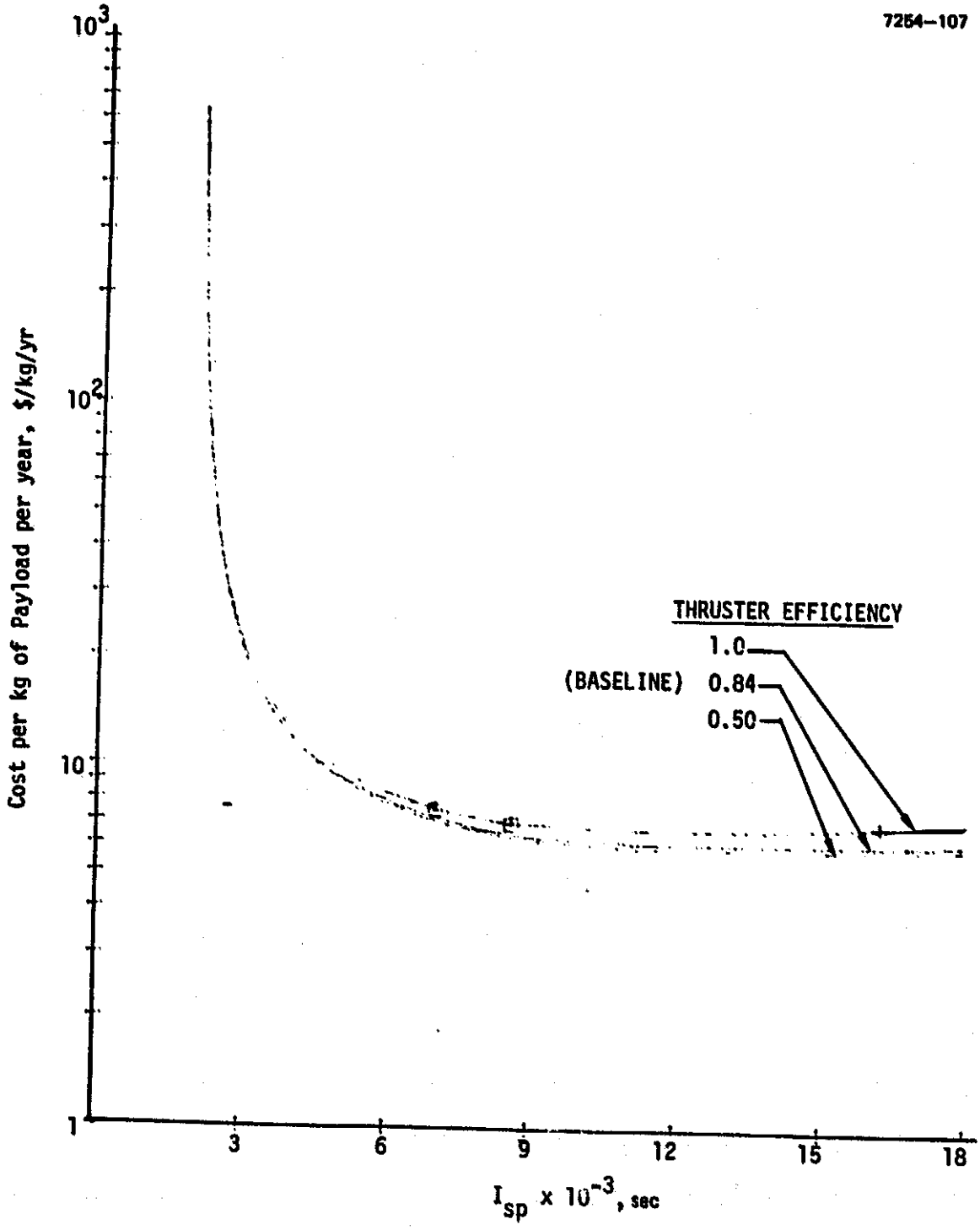

Figure 4-77. OO/LS effect of thruster efficiency.

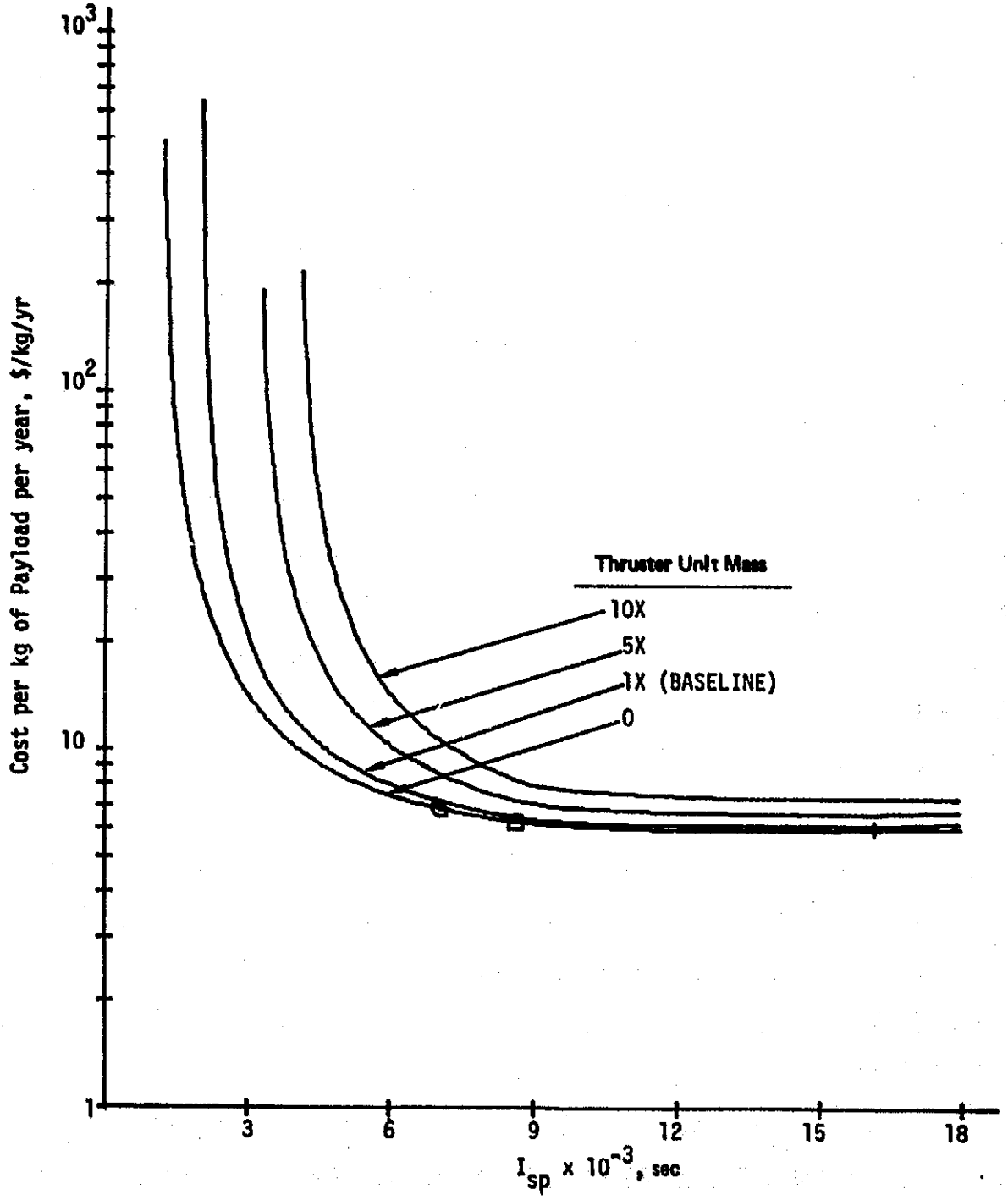

Figure 4-78. OO/LS effect of thruster mass.

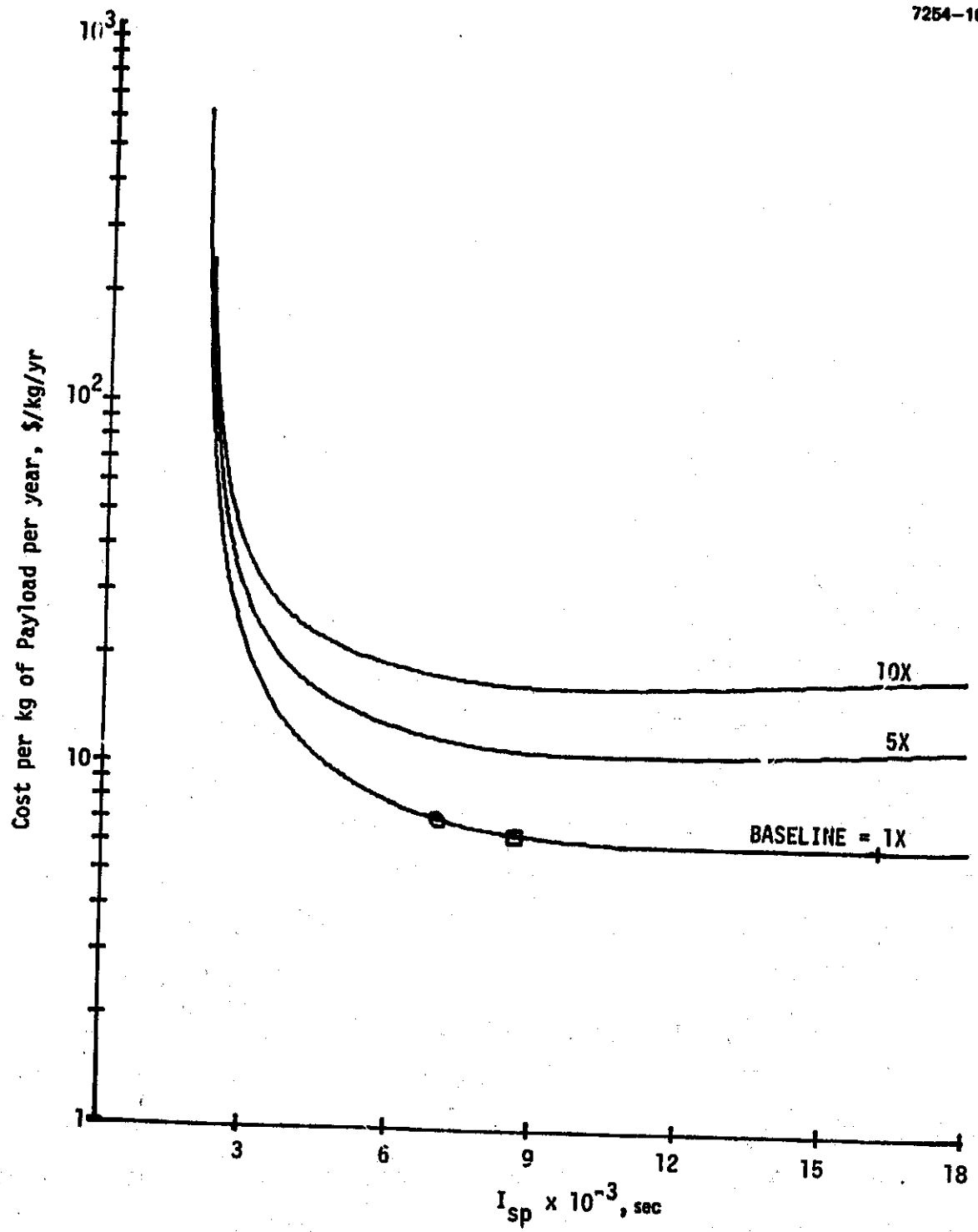

Figure 4-79. OO/LS effect of thruster first unit cost.

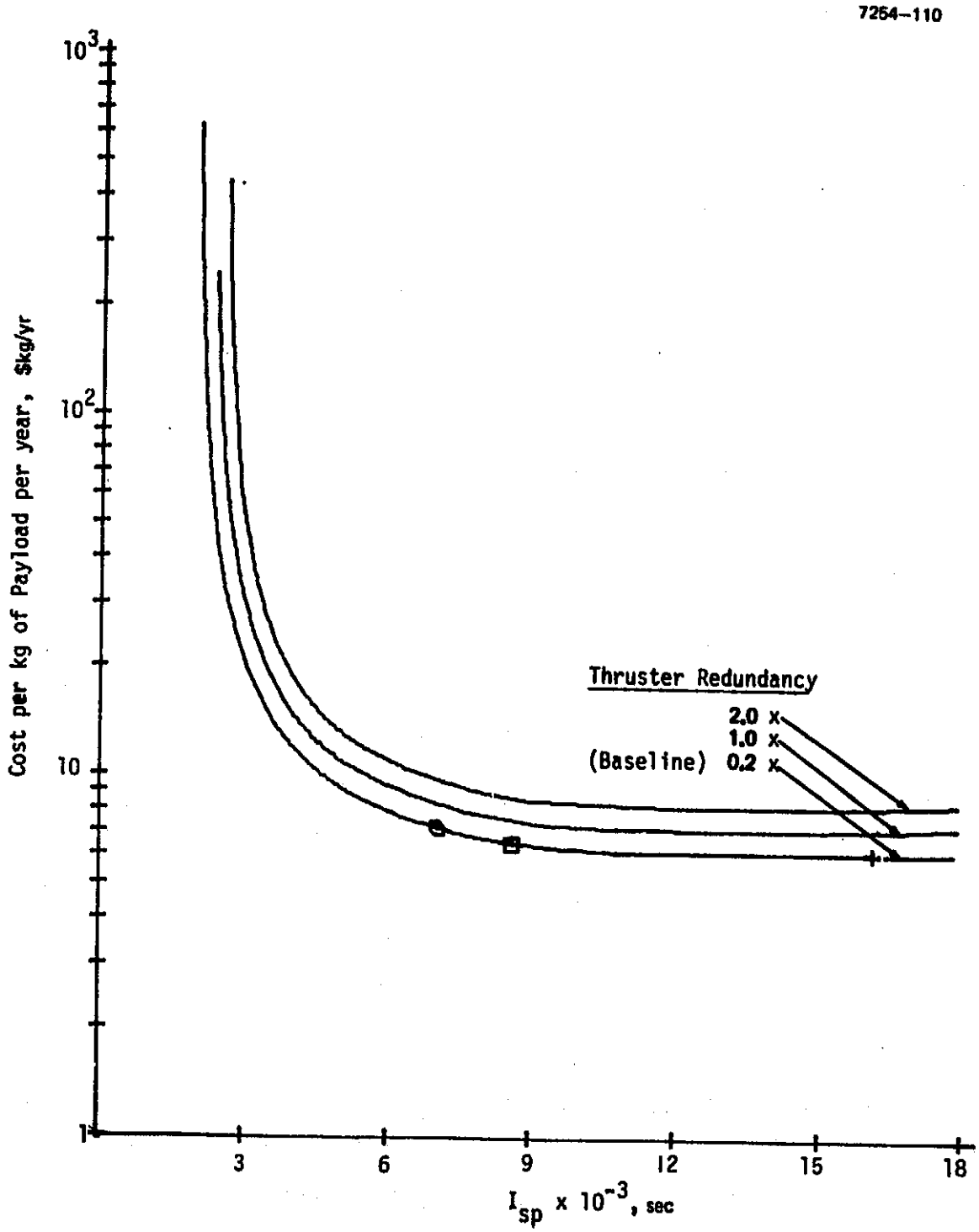

Figure 4-80. OO/LS effect of thruster redundancy.

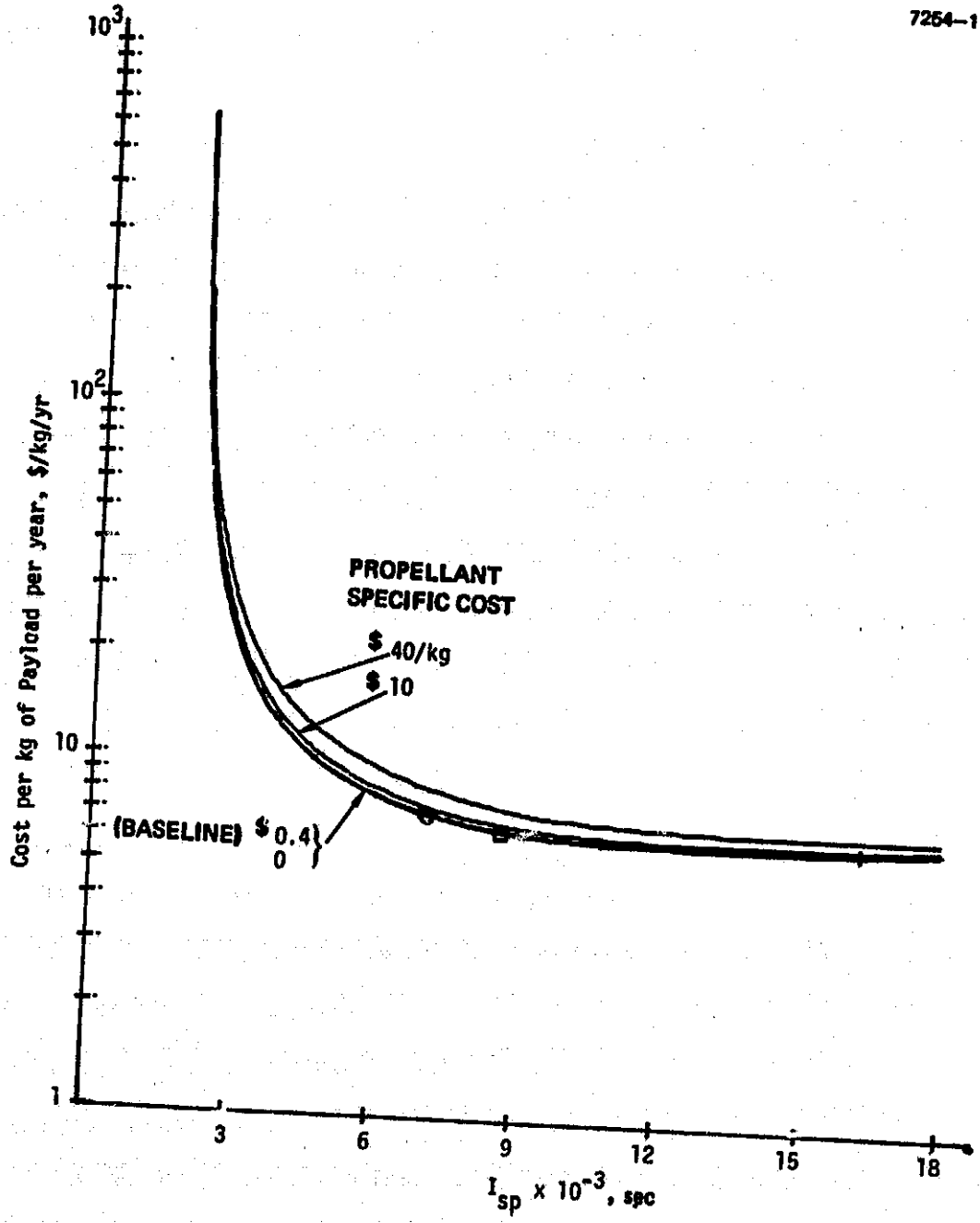

Figure 4-81. OO/LS effect of propellant specific cost.

(1) PPU Mass — As Figure 4-82 shows, PPU unit mass variations around the baseline have a small influence on cost.

(2) PPU Cost — PPU cost is somewhat more important as shown in Figure 4-83. However, modest variations around the baseline would not dramatically change the overall cost.

(3) PPU Redundancy — Results shown in Figure 4-84 indicate that PPU redundancy is also not too important in overall cost. A factor of two over the baseline should be an upper bound on the required redundancy.

g. Power Source Sensitivities

Results of the three major factors studies (Table 4-9) are shown in Figures 4-85 through 4-87. Power source specific mass (Figure 4-85) and degradation (Figure 4-87) show only small overall cost sensitivity. Power source specific cost ($/kW) is a more important factor, as Figure 4-86 shows. In addition to changing the overall cost level source, specific cost changes the curve shape and hence changes the I_{sp} optimum. At even higher power costs, this effect would be more pronounced.

h. OOP System Design Sensitivities

Representative system parameters (shown in Table 4-9) were investigated. Although many others could have been considered, the four selected should provide an indication of the sensitivity of overall cost to system factors.

(1) Structure and Mechanisms Sensitivity — As Figure 4-88 shows, structure costs below $\$10^5$/kg have little effect; costs of $\$10^6$/kg will increase the overall specific cost level but should not significantly influence thruster selection.

(2) Subsystems Sensitivity — The subsystems cost parameter essentially reflects complexity: the greater the complexity, the higher the cost. Figure 4-89 shows that any significant increase from the baseline ($\$10^4$/kg) will have a pronounced effect on overall cost.

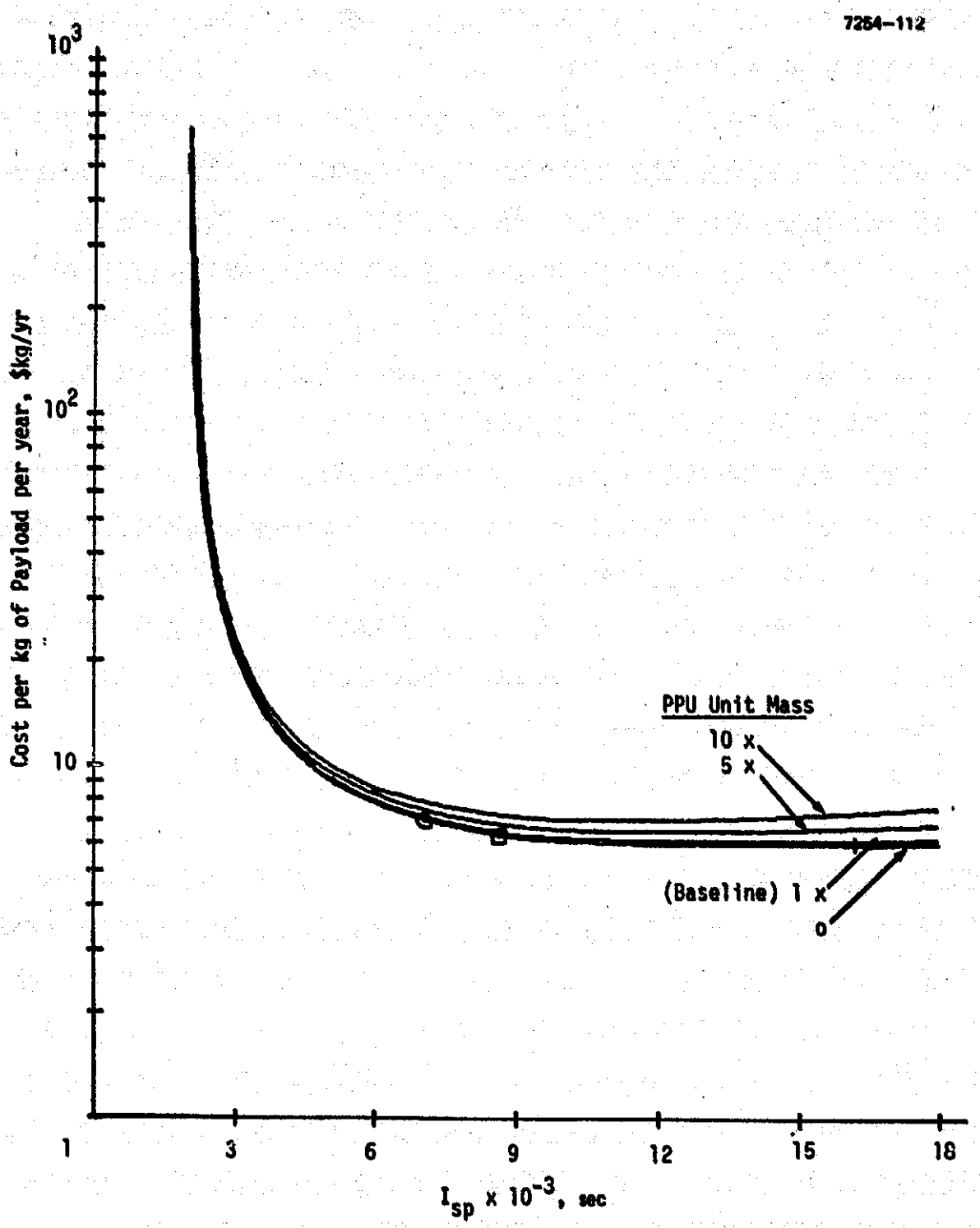

Figure 4-82. OO/LS effect of PPU mass.

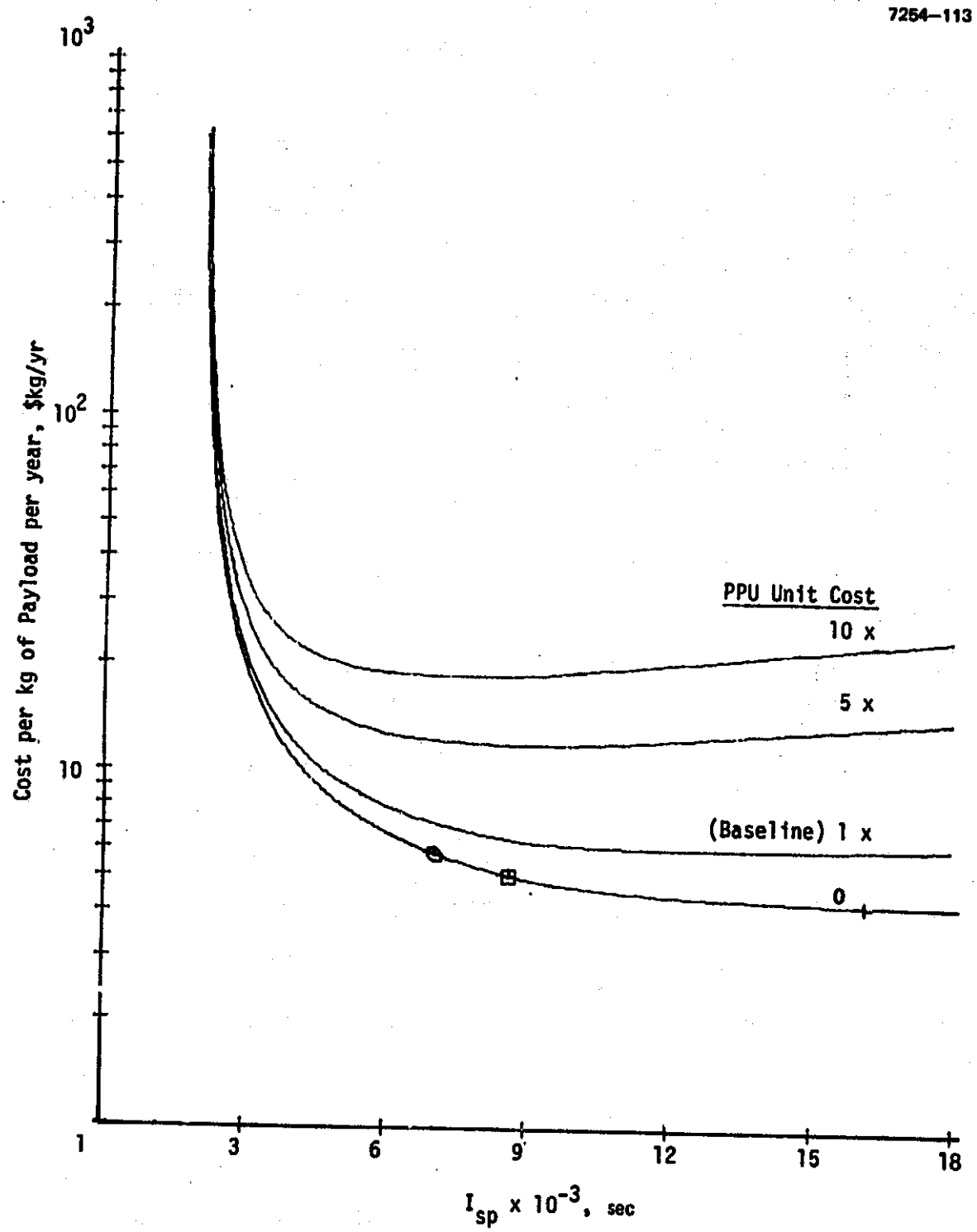

Figure 4-83. OO/LS effect of PPU cost.

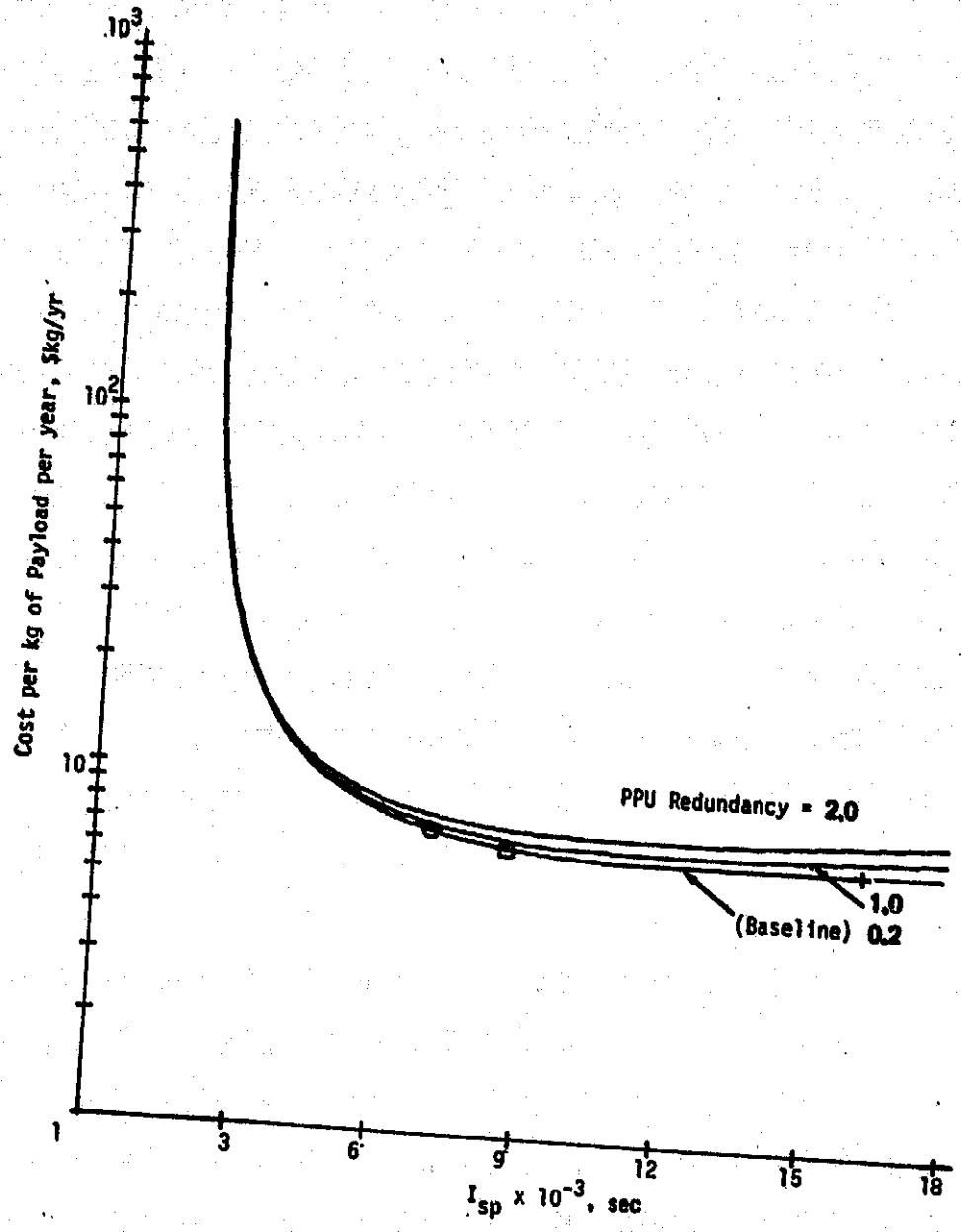

Figure 4-84. OO/LS effect of PPU redundancy.

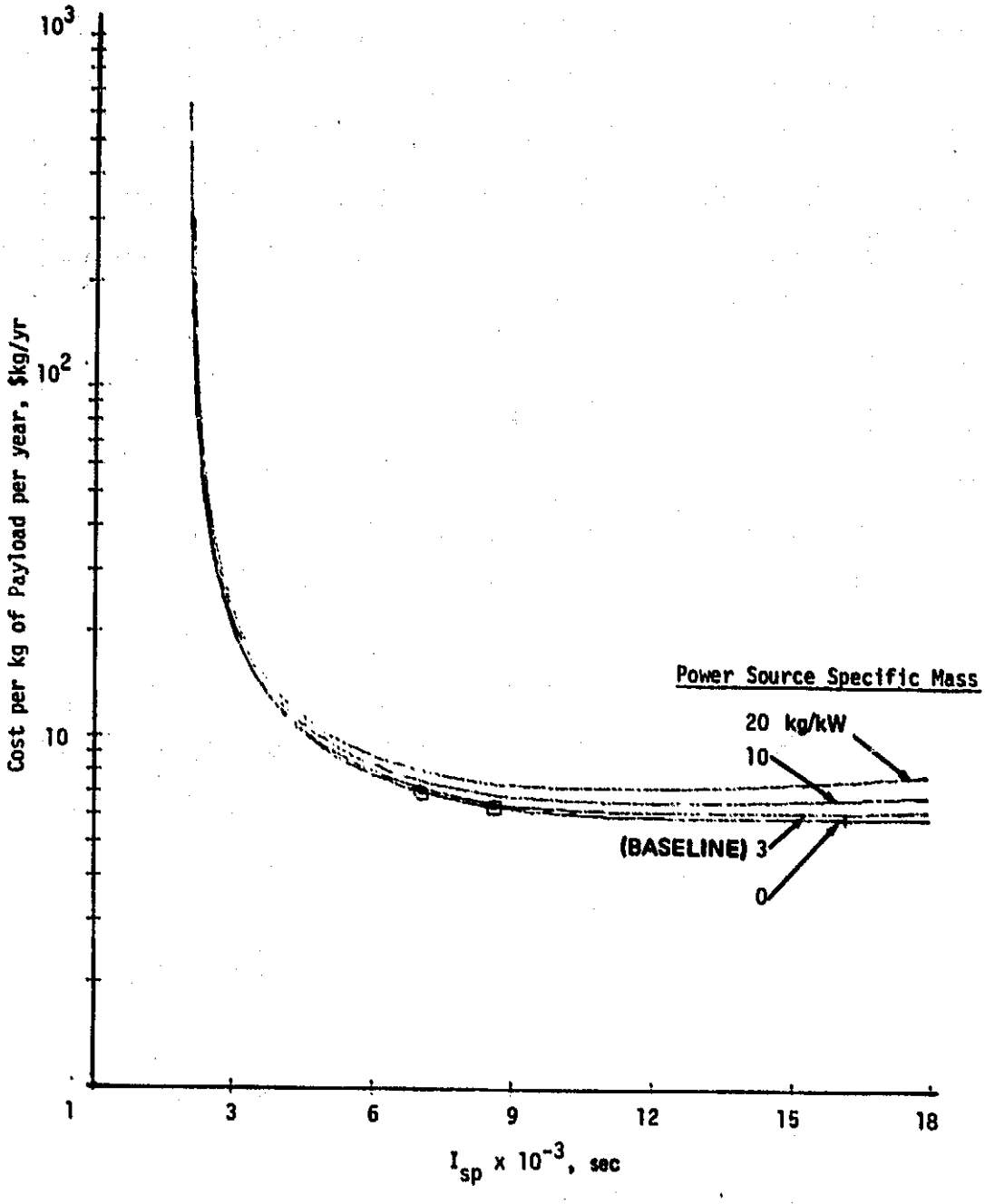

Figure 4-85. OO/LS effect of power source specific mass.

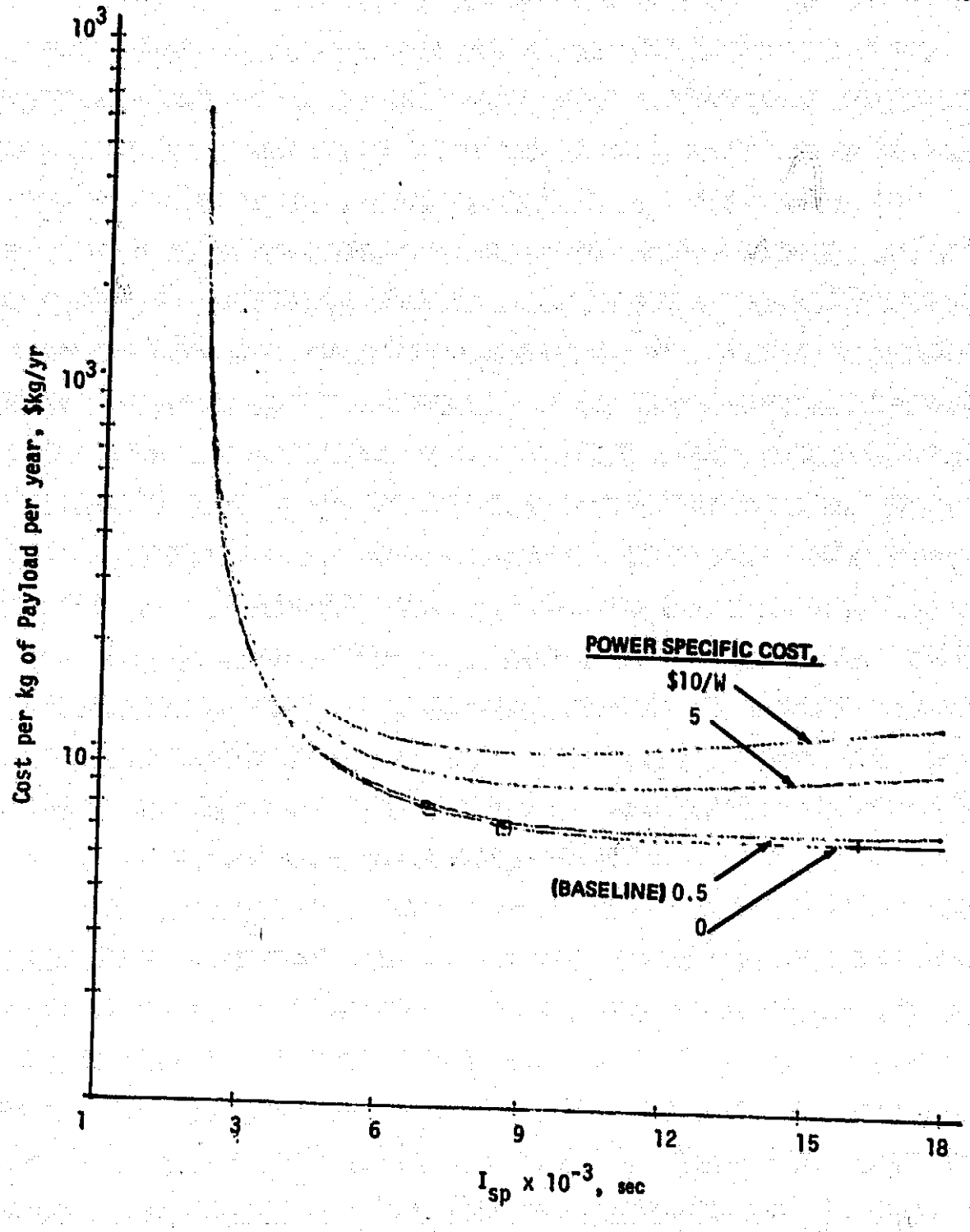

Figure 4-86. OO/LS effect of power source specific cost.

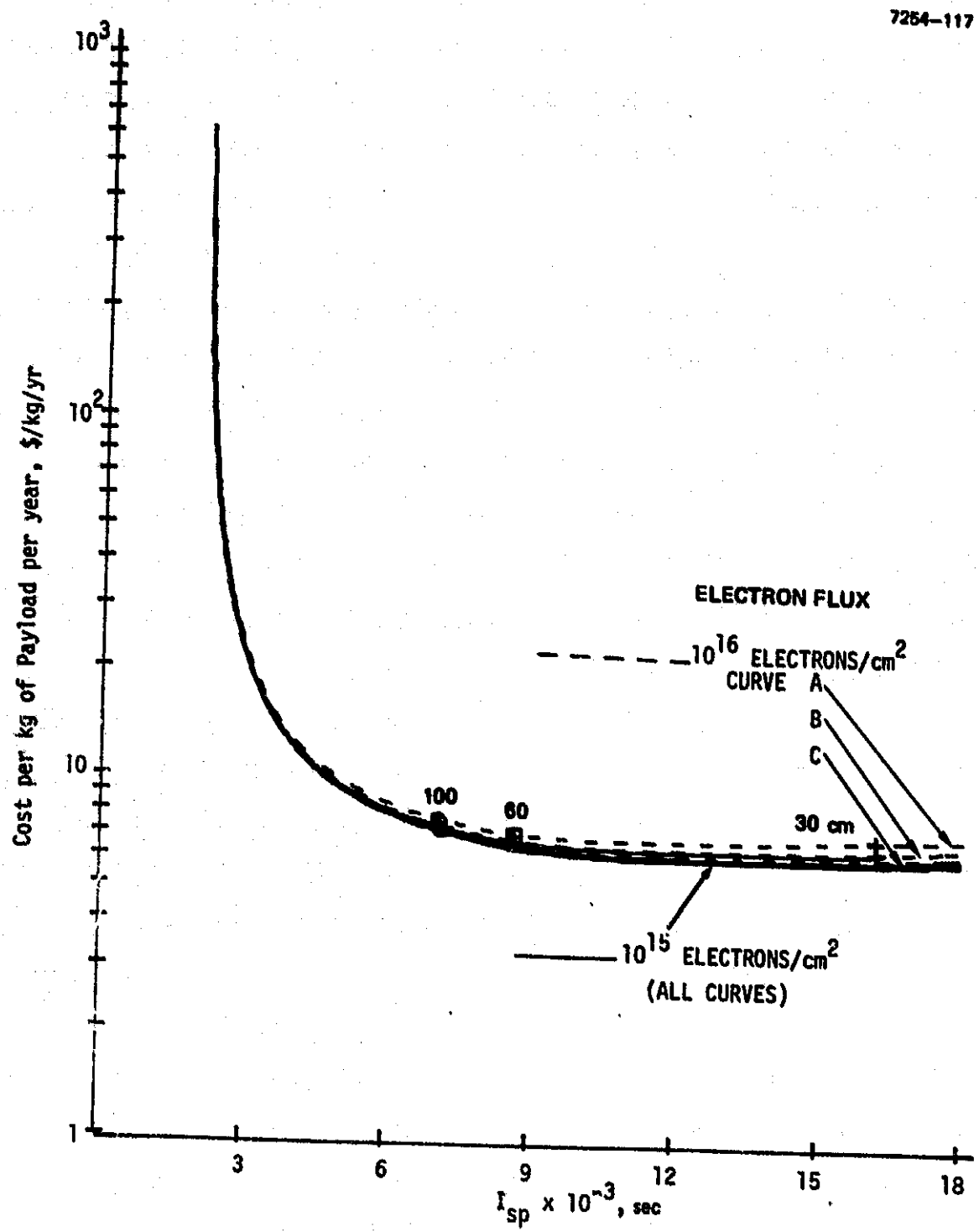

Figure 4-87. OO/LS effect of power source degradation.

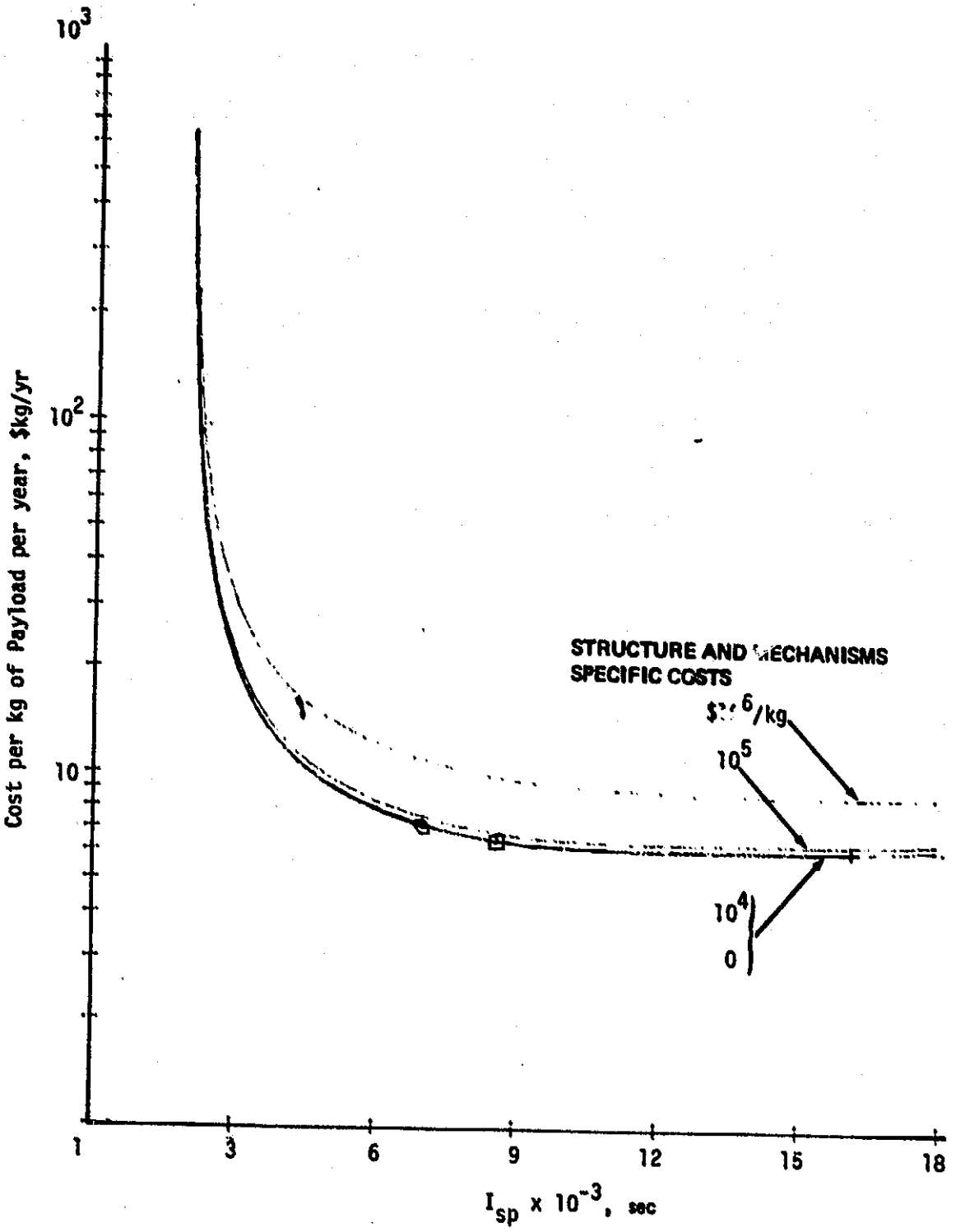

Figure 4-88. OO/LS effect of structure and mechanisms specific cost.

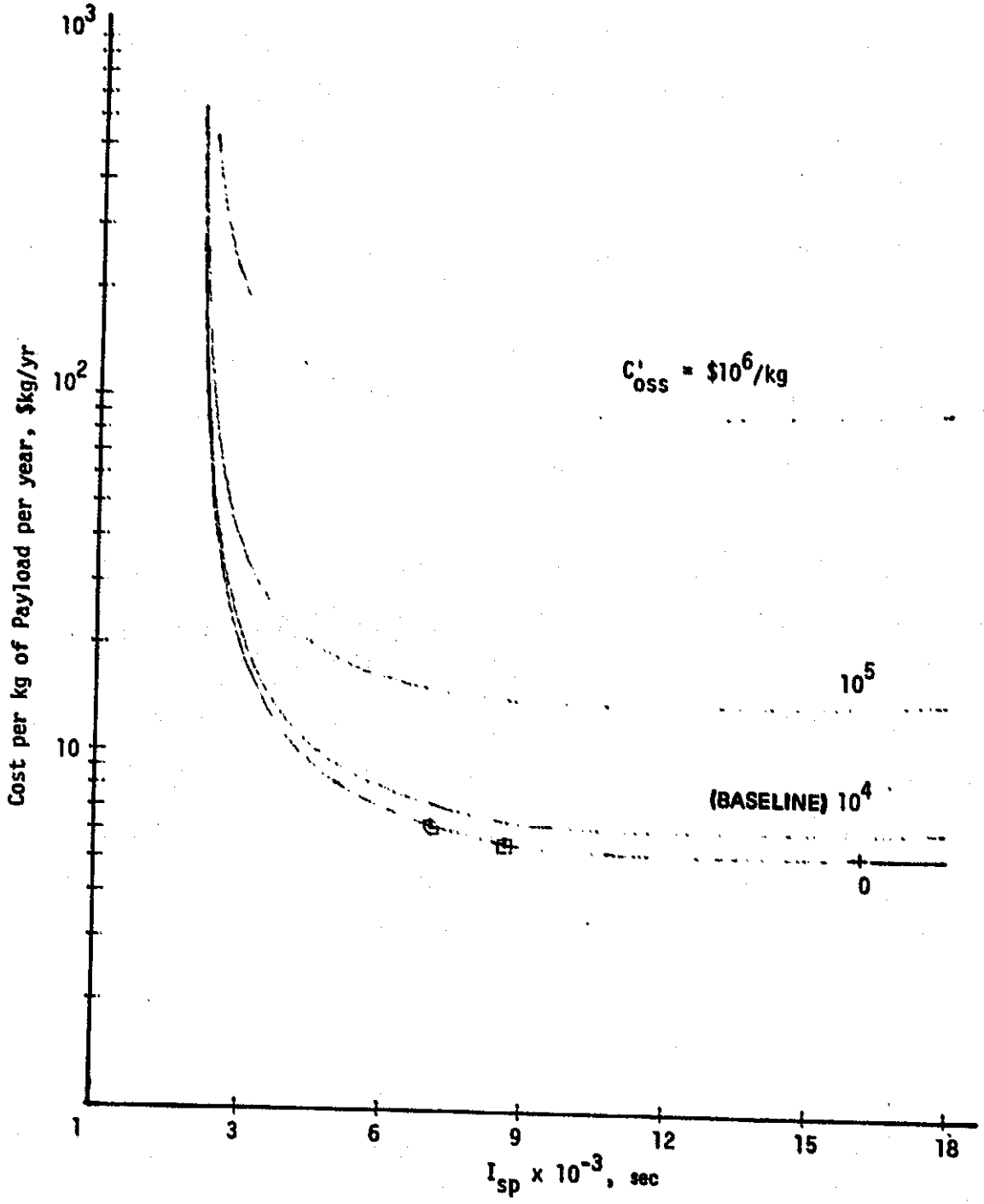

Figure 4-89. OO/LS effect of subsystems specific cost.

(3) Integration and Testing Sensitivity — The integration and test parameter illustrated in Figure 4-90 is also related to complexity. Costs above $10/kg shift the overall cost level and tend to influence thruster and I_{sp} selection.

(4) DDT&E Sensitivity — As shown in Figure 4-91, an increase from the baseline of more than an order of magnitude in DDT&E cost would be necessary to have much effect on overall cost. However, even higher DDT&E cost would not significantly influence thruster or I_{sp} selection.

6. On-Orbit/Matured Shuttle Era Baseline Mission Results

The on-orbit/matured Shuttle (OO/MS) baseline analyses used a philosophy similar to that discussed in Section 4.A.9. Baseline parameters that were changed from the large system baseline are shown in Table 4-10. Except for transportation cost, these are equivalent to the values shown in Table 4-5.

a. OO/MS General Results

Results for the OO/MS baseline are shown in Figures 4-92 through 4-95. In contrast with previous results, thruster diameters in the range of interest (30 to 100 cm) occur at I_{sp}'s below about 8,000 sec. Furthermore, as Figure 4-92 shows, the optimal I_{sp} results in small thruster diameters (i.e., less than 30 cm). The overall cost level is significantly higher (about 20 times) than that of the OO/LS baseline.

A cost breakdown and total cost as a function of I_{sp} are shown in Figure 4-93; a mass breakdown is presented in Figure 4-94. Specific cost and total cost are shown in Figures 4-94 and 4-95 as a function of net satellite mass. Although total cost is minimum at about 7,000 sec, the specific cost minimum occurs at about 10,000 sec for a payload mass of about 18,000 kg.

b. Power Source Sensitivites

The impacts of power source cost and mass are shown in Figures 4-96 and 4-97, respectively. Power source cost has a relatively large influence on overall specific cost. However, since thruster diameters less than 30 cm are of little interest, the sensitivity is

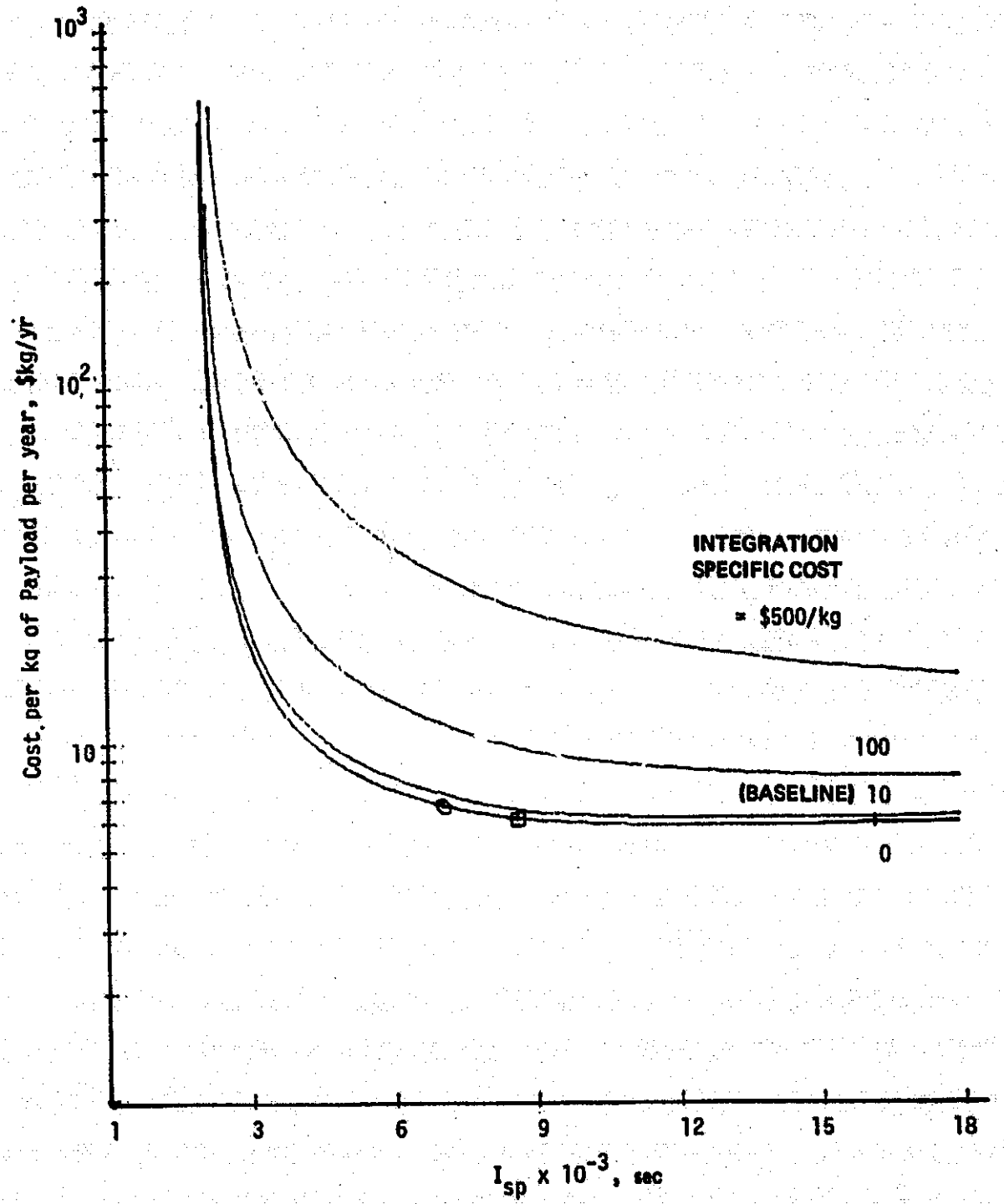

Figure 4-90. OO/LS effect of integration and test specific cost.

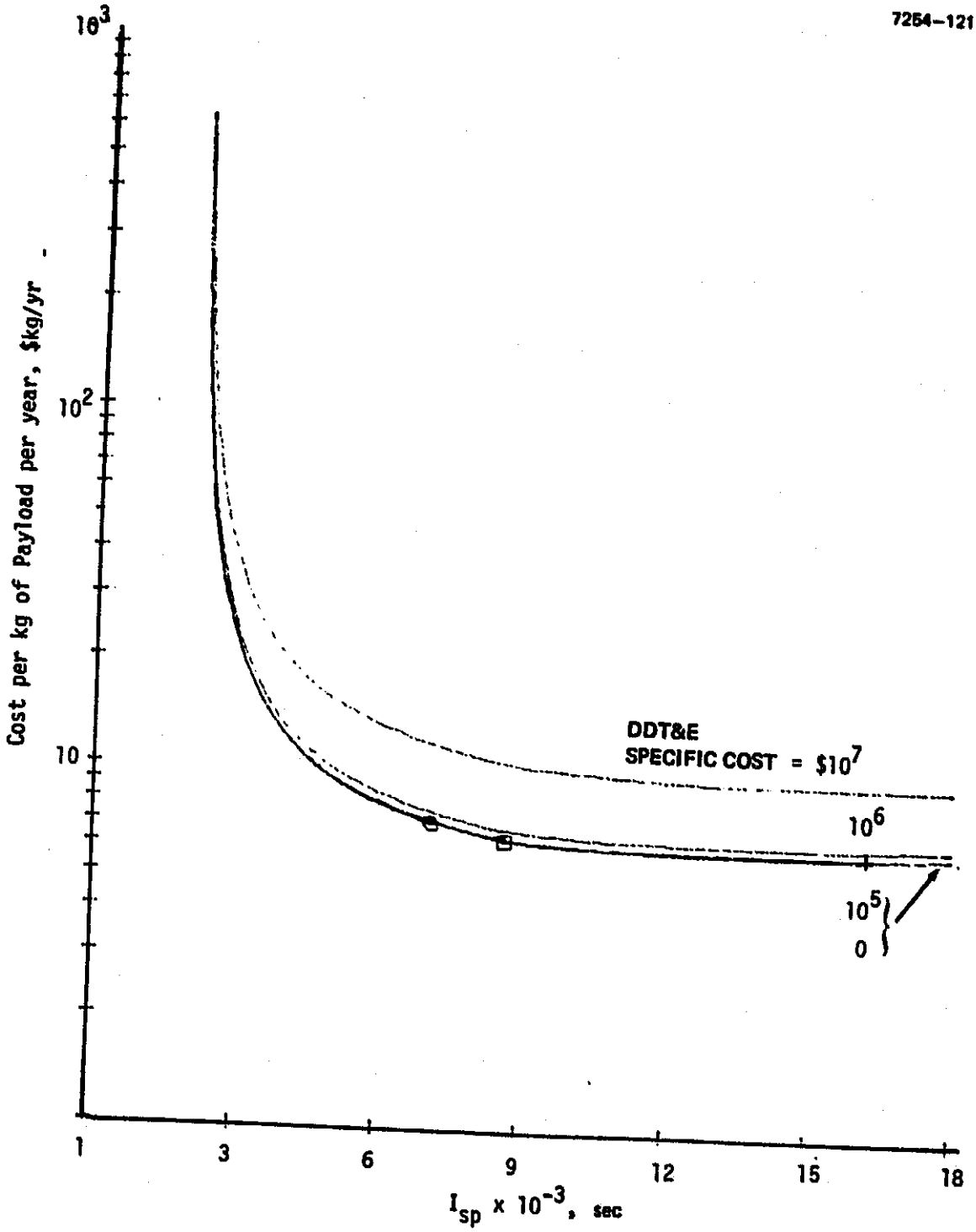

Figure 4-91. OO/LS effect of DDT&E specific cost.

Table 4-10. OO/MS Baseline Cost Model Parameters[a]

P_{mod}	= 20 kW	Module power
M_{os}	= 25×10^3 kg	Satellite initial mass
C'_{oi}	= \$40/kg	Integration and test cost
C'_{ow}	= \$100/W	Power source cost
α_{ps}	= 6 kg/kW	Power source specific mass
C'_{to}	= \$1,000/kg	Transportation cost
Propellant	= Xenon	

[a]All other cost model parameters are the same as those in Table 4-8.

6119

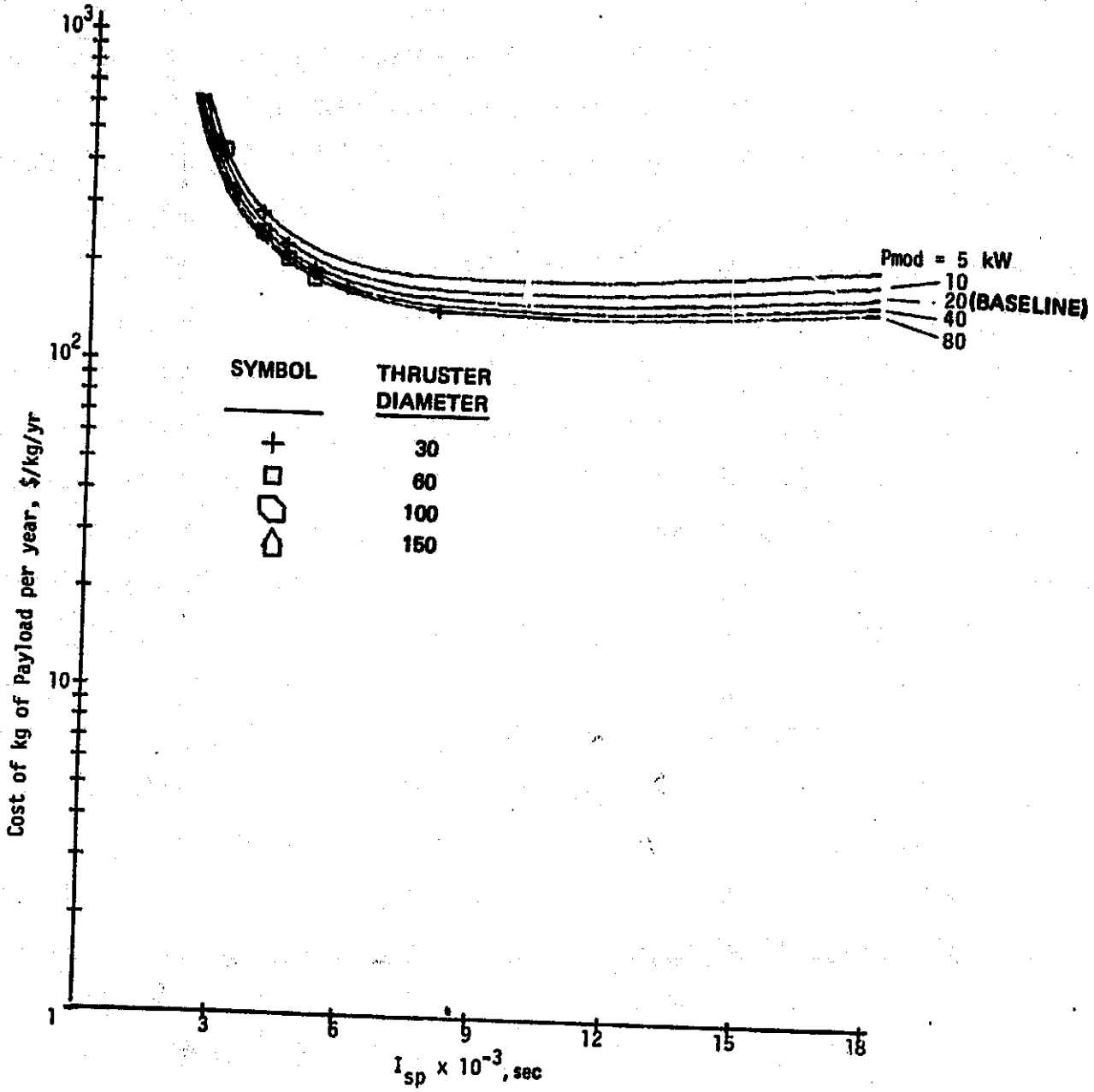

Figure 4-92. OO/MS effect of module power.

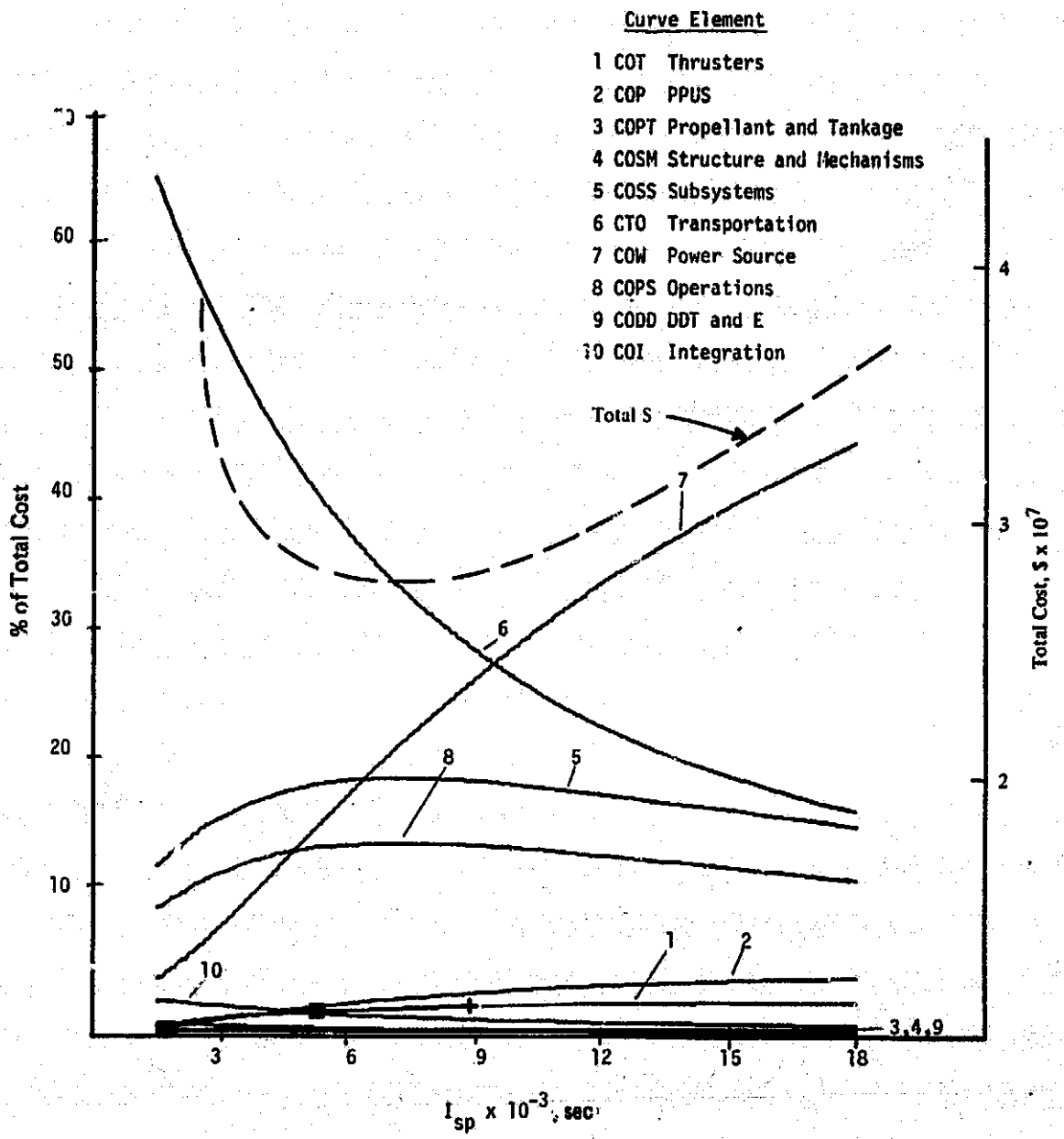

Figure 4-93. OO/MS cost breakdown.

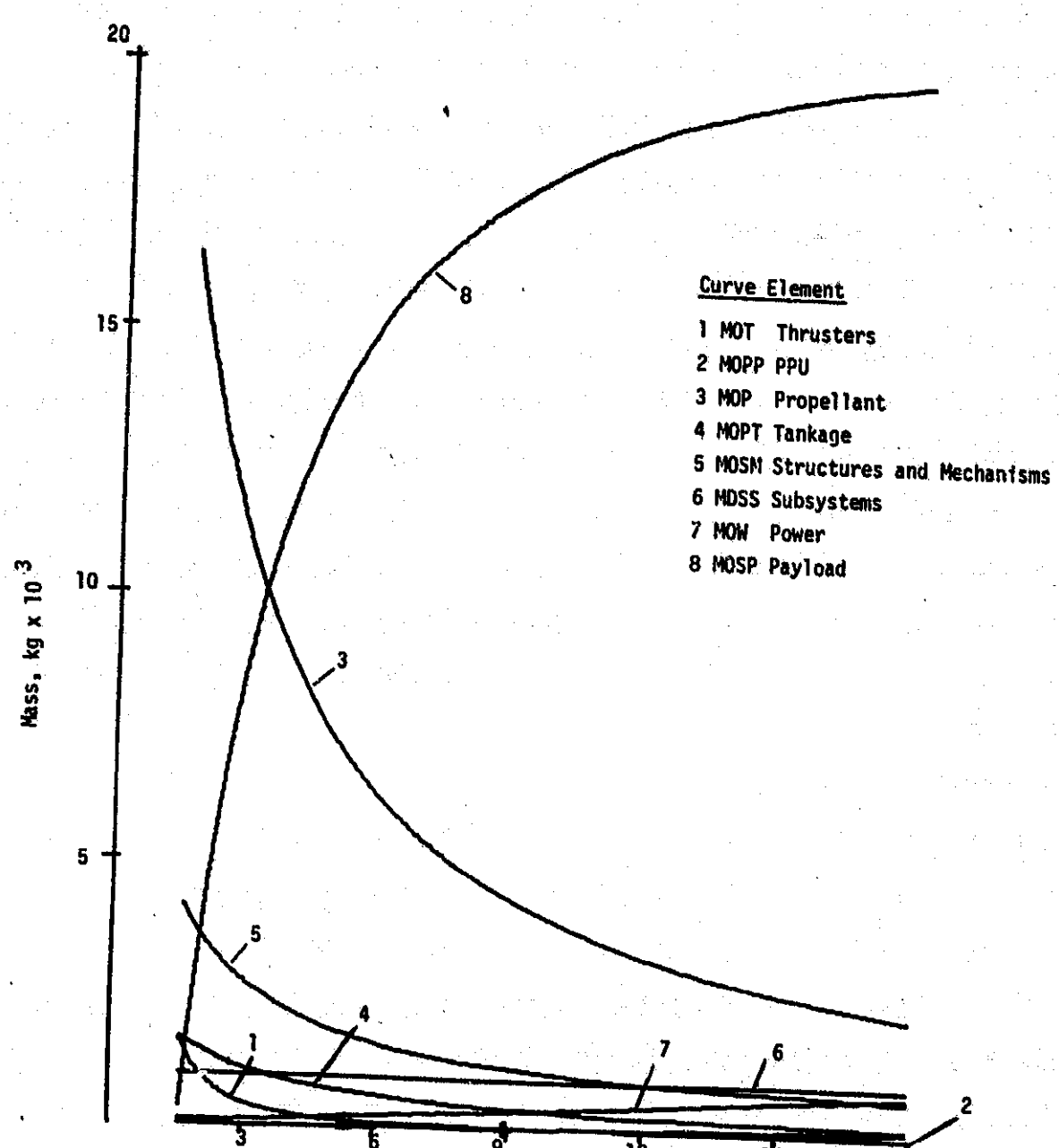

Figure 4-94. OO/MS mass breakdown.

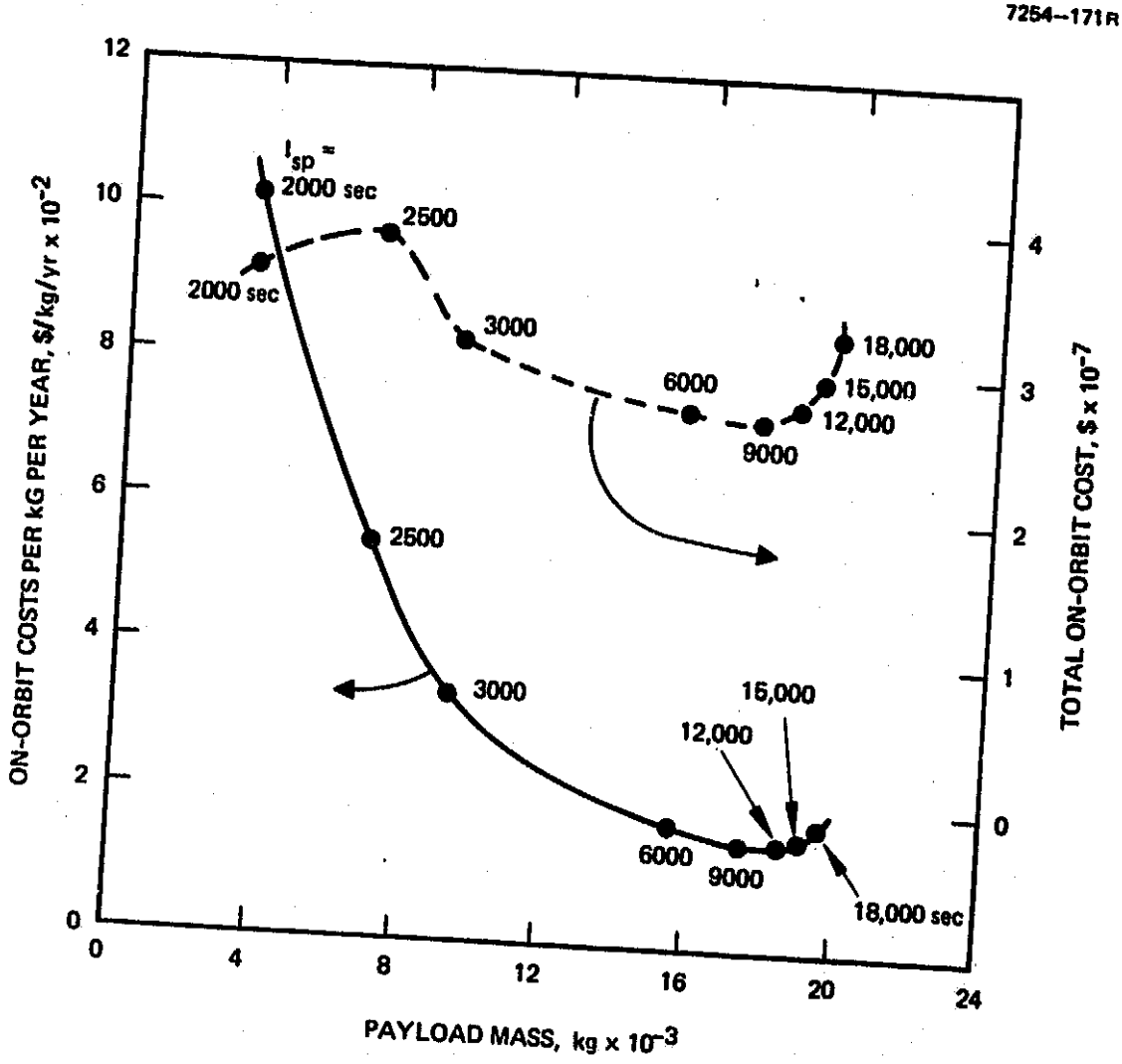

Figure 4-95. OO/MS cost versus payload mass.

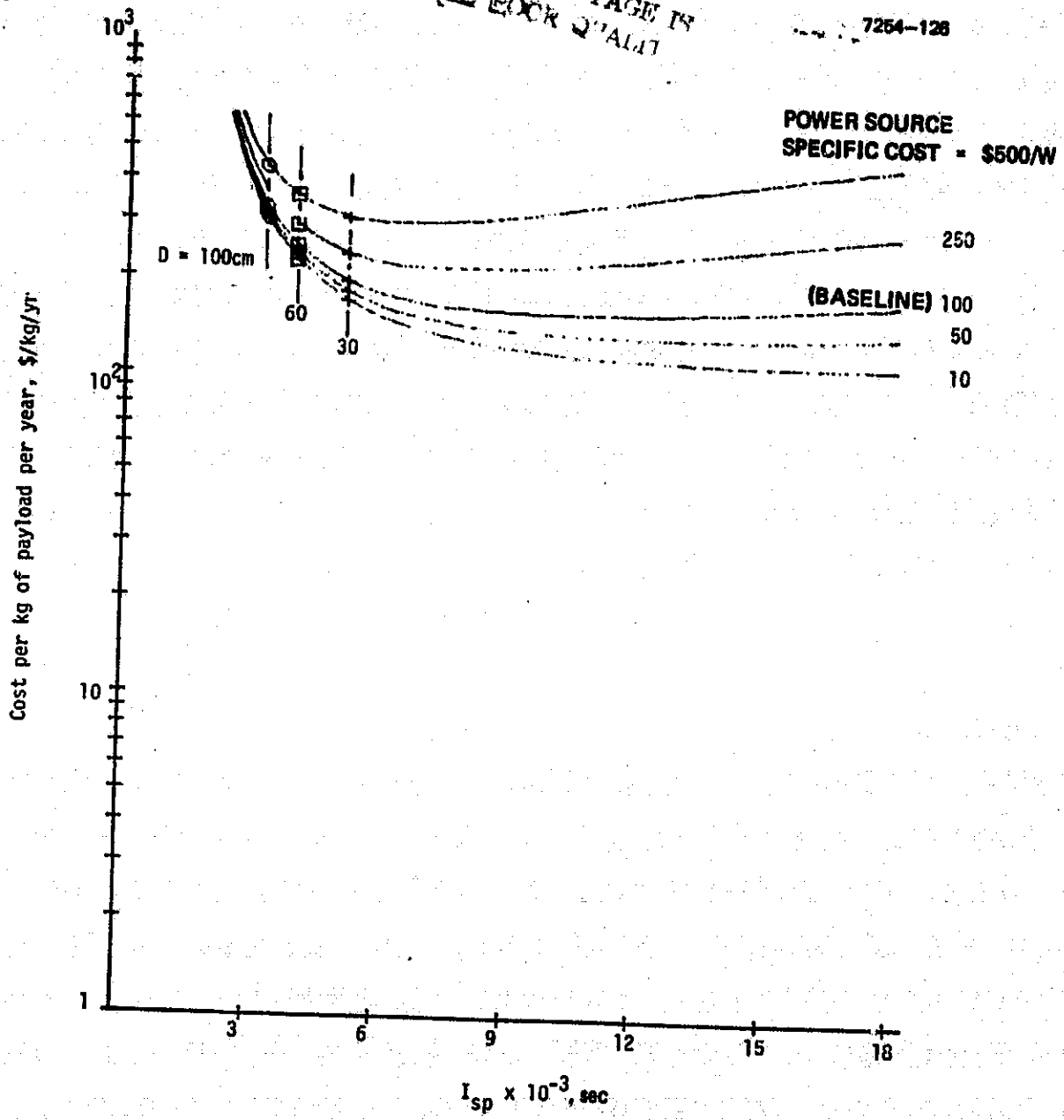

Figure 4-96. OO/MS effect of power specific cost.

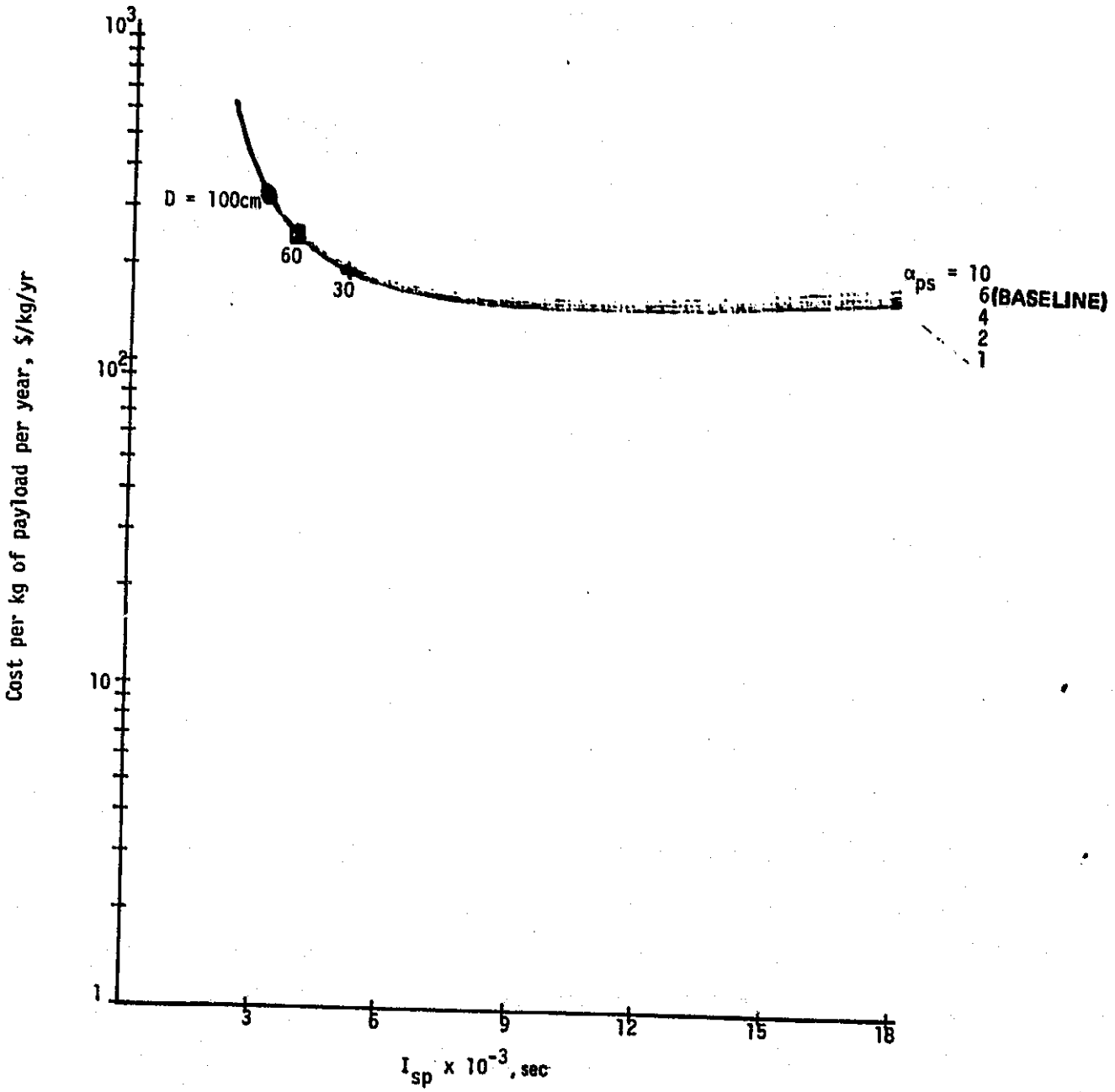

Figure 4-97. OO/MS effect of power specific mass.

somewhat reduced. An increase in power cost from the baseline is more significant than a decrease. The effect of power source specific mass is shown in Figure 4-97 to be of minor importance over a rather large range of α's.

c. Initial Mass Sensitivity

The effect of initial mass on overall cost is shown in Figure 4-98. On-orbit specific costs vary by about a factor of three (for a given I_{sp}) over the mass range considered. Higher mass results in lower cost (as before). Thus, there could be a cost advantage in building one large satellite rather than several smaller ones if such a situation occurred.

d. Transportation Cost Sensitivity

Within the range of thruster diameters of interest, specific cost is relatively sensitive to transportation cost. As shown in Figure 4-99, the $1,000/kg baseline is representative of the orbit raising results, but improvements in orbit raising costs would significantly benefit the on-orbit mission.

e. Integration and Testing Sensitivity

Integration costs are a small fraction of the total and even relatively large changes have essentially no effect on specific cost. This result is shown in Figure 4-100.

C. COST MODELING CONCLUSIONS

1. Thruster Size Recommendations

The results presented in Sections 4.A and 4.B were reviewed in terms of costs and thruster technology. A summary of general conclusions is shown in Table 4-11. The recommendations given reflect the ranges of key parameters that provide a reasonable compromise between system costs and thruster development difficulties. For example, under the OR/LS baseline, costs are minimized around 6,000 sec and with high module

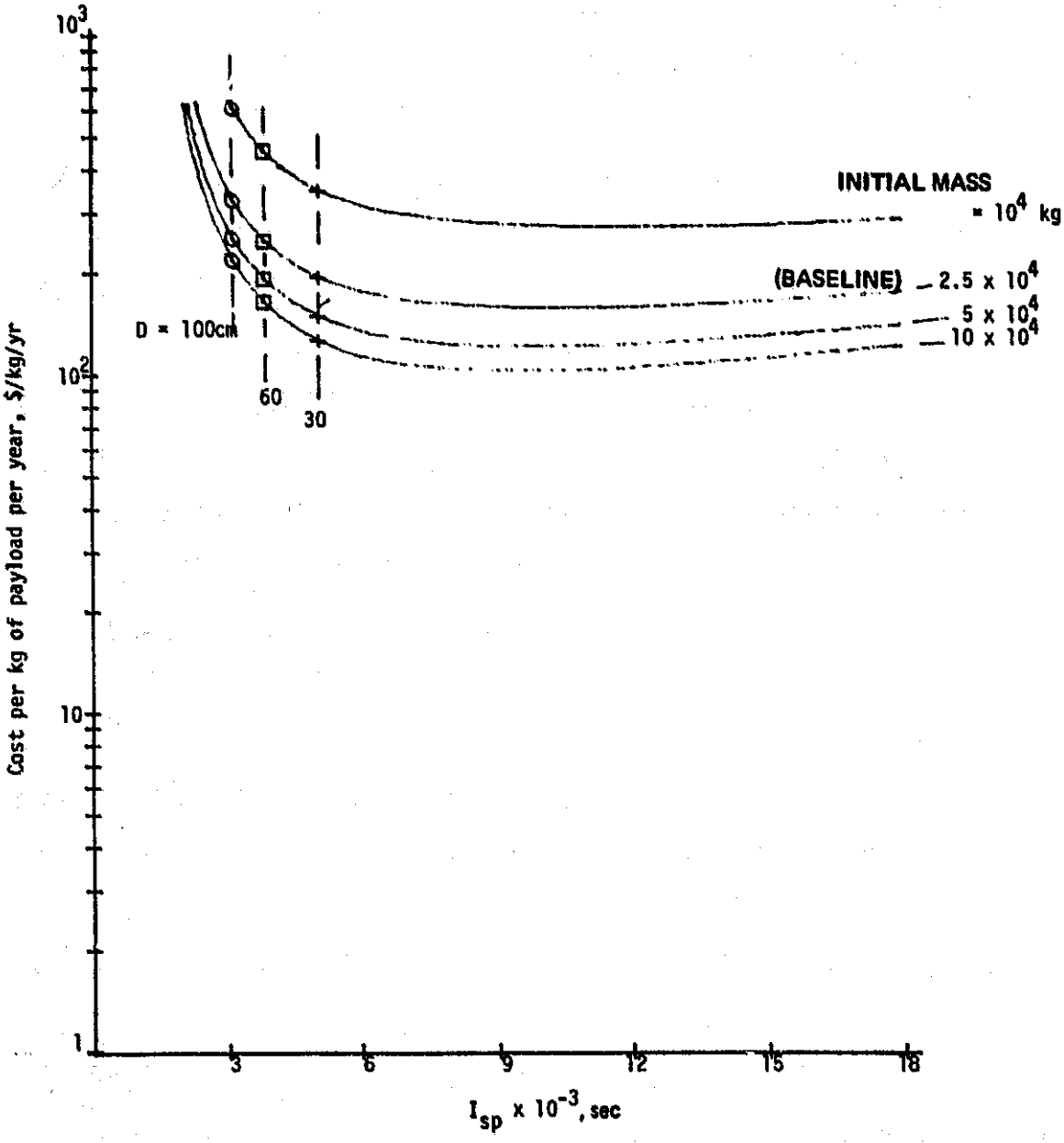

Figure 4-98. OO/MS effect of initial mass.

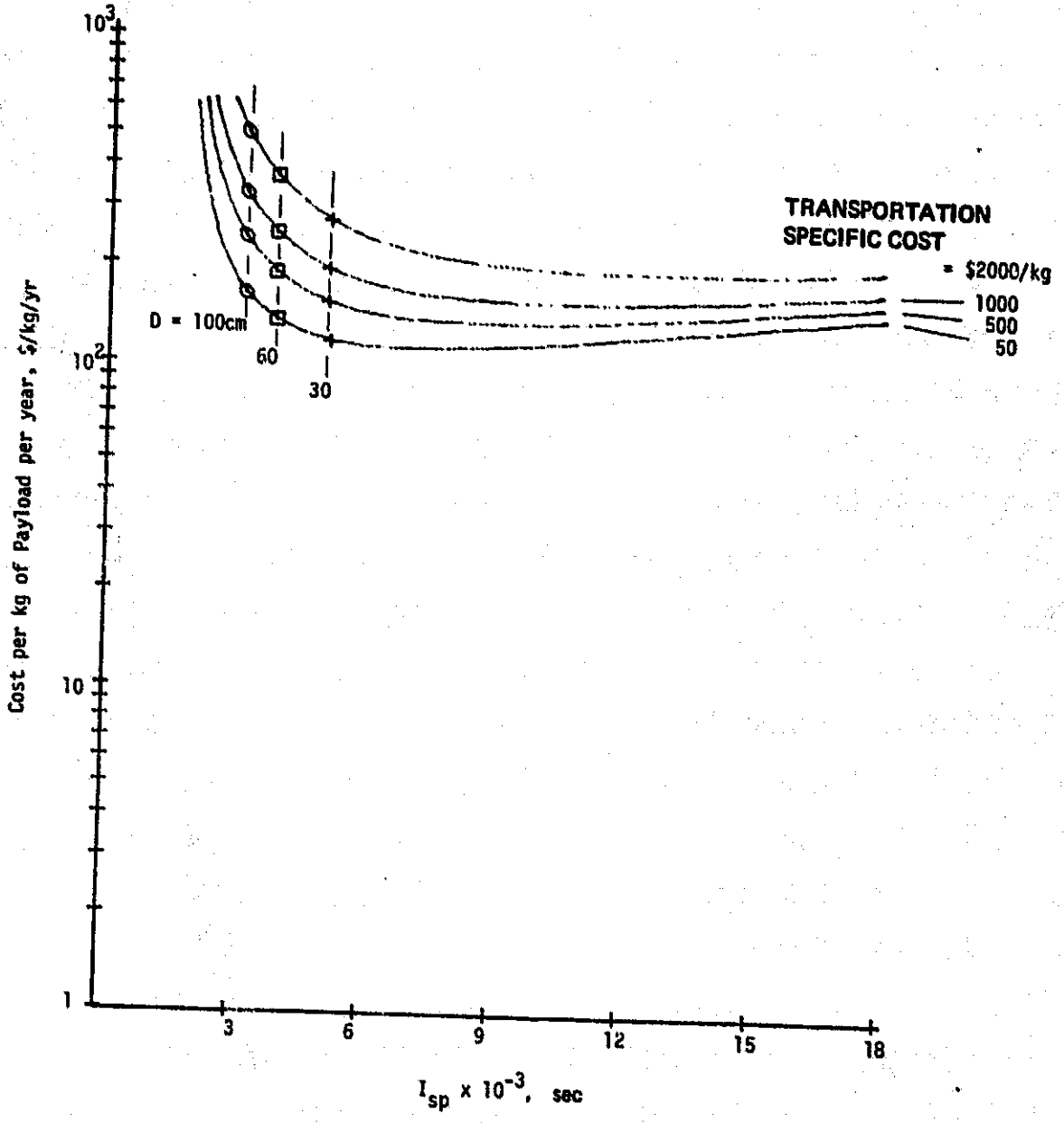

Figure 4-99. OO/MS effect of specific cost of transportation from Earth to GEO.

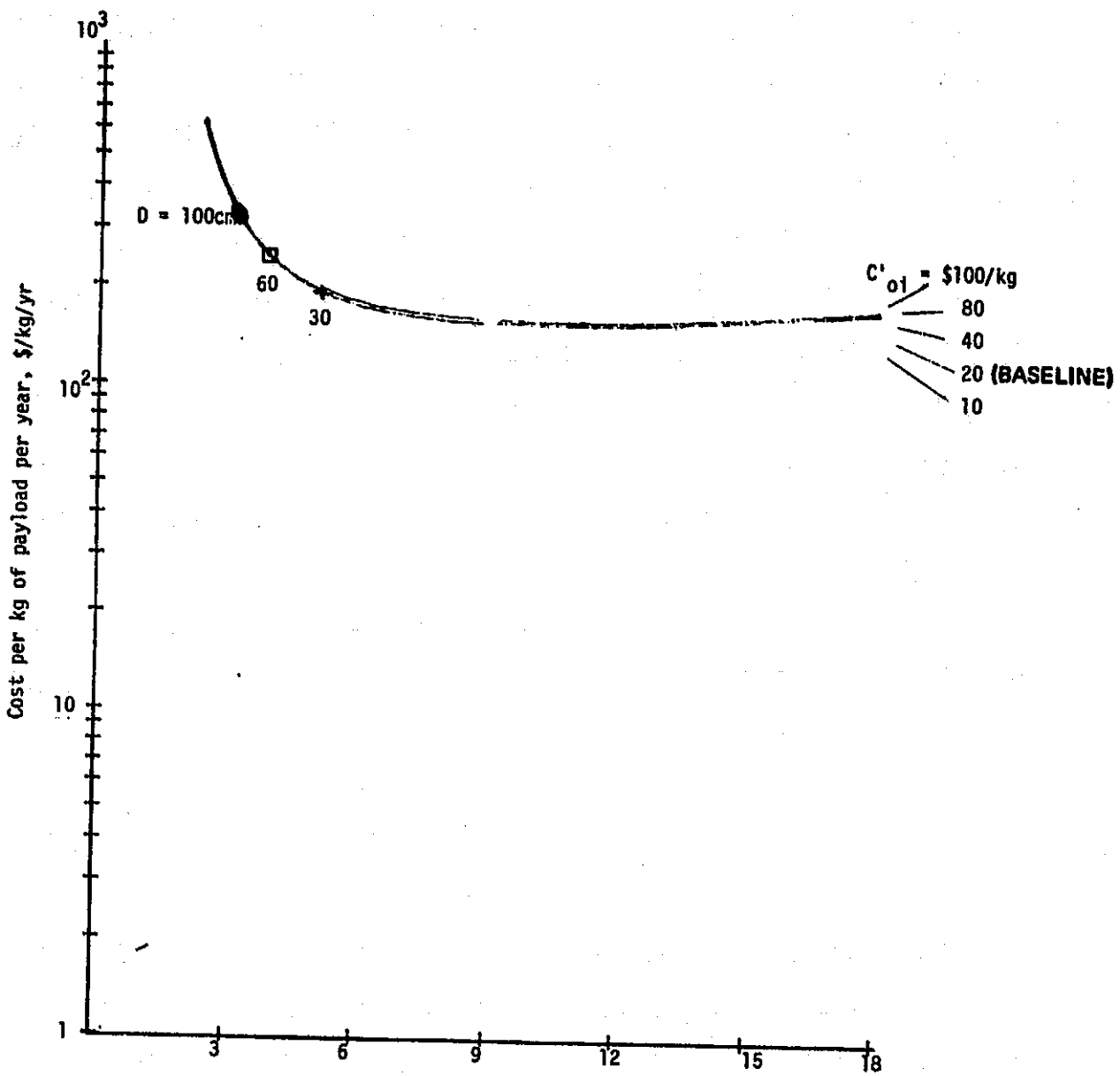

Figure 4-100. OO/MS effect of integration and testing cost.

Table 4-11. Summary of Cost Modeling Recommendations and Sensitivities

Parameter	Mission Option			
	OR/LS	OR/MS	OO/LS	OO/MS
Recommendations				
I_{sp}, sec	8,000-12,000	4,000-5,000	10,000-15,000	4,000-7,000
Thruster diameter, cm	40-70	30-70	40-70	30-60
Module power, kW	50-200	20-80	100-200	20-80
Propellant	Argon	Xenon	Argon	Xenon
Thruster sensitivities				
Module power	High	Moderate	High	Low
Life	Moderate	N/S	High	N/S
Efficiency	Moderate	N/S	Low	N/S
Mass	Low	N/S	Low	N/S
Unit cost	Low	N/S	Low	N/S
"R" ratio	Low	N/S	N/S	N/S
Redundancy	Low	N/S	Low	N/S
Propellant sensitivity				
Type	Low	N/S	N/S	N/S
Cost	Low	N/S	Low	N/S
PPU sensitivity				
Mass	Moderate	N/S	Low	N/S
Cost	High	N/S	High	N/S
Redundancy	Low	N/S	Low	N/S
Power source sensitivity				
Mass	High	Moderate	Low	Low
Cost	High	High	Moderate	Moderate
Degradation	Moderate	N/S	Low	N/S

Table 4-11. Summary of Cost Modeling Recommendations and Sensitivities (Continued)

Parameter	Mission Option			
	OR/LS	OR/MS	OO/LS	OO/MS
Mission design sensitivity				
ΔV	High	N/S	High	N/S
Mission time	Moderate	N/S	High	N/S
Initial mass	High	Moderate	High	High
Launch cost	High	High	High	High
System design sensitivity				
Struc. & mechs.	Low	N/S	Low	N/S
Subsystems	Moderate	N/S	Moderate	N/S
Integration	Moderate	Low	Moderate	Low
DDT&E	Moderate	N/S	Low	N/S
Flight ops	Low	N/S	N/S	N/S
Self powered sensitivity				
Power fraction	Moderate	N/S	N/A	N/A
One-way trip sensitivities				
ΔV	High	N/S	N/A	N/A
Free power	High	N/S	N/A	N/A
Trip time	Moderate	N/S	N/A	N/A
Initial mass	High	N/S	N/A	N/A
Launch cost	Moderate	N/S	N/A	N/A

N/A = Not applicable
N/S = Not studied

power. However, 6,000 sec results in large thruster diameters (or high cost). To stay within reasonable bounds (less than 100 cm) and retain low system costs, a minimum I_{sp} of about 8,000 sec is needed. With high module power, costs are not too strongly affected up to about 12,000 sec. With these bounds on I_{sp}, the range of thruster diameters and power are established. A similar rationale was applied to the other three mission options.

Having established the acceptable ranges of key parameters in Table 4-11, the results were reviewed with an eye to defining a single thruster "design" that would satisfy all four mission options. Thruster diameter is then bounded between 40 and 60 cm. To satisfy both large system baseline mission options, an I_{sp} in the range of 10,000 to 12,000 sec is needed. This I_{sp} range with argon corresponds to a thruster diameter range of about 50 to 40 cm, respectively, and a module power of about 100 kW (see Figures 4-4 and 4-6). A 40-cm thruster operating on xenon at 5,000 sec (the overlapping point for the MS baselines) would have a module power of about 30 kW; a 50-cm thruster would have a module power of about 45 kW.

The beam voltages for argon at 10,000 and 12,000 sec would be approximately 2,400 and 3,500 V, respectively. For xenon at 5,000 sec, the beam voltage would be about 2100 V. If a 50-cm thruster were designed for a beam voltage of 2400 V, it could be operated on argon to produce up to 100 kW of beam power or on xenon up to about 50 kW at 5400 sec. Thus, a 50-cm thruster is a good compromise for the four mission options and also allows for a common beam voltage.

A further consideration in selecting between a 40-cm and a 50-cm diameter thruster is the uncertainty of wearout life. Since module power is important to system cost effectiveness, if sufficient life could not be obtained with a 50-cm thruster, operation at lower beam current would be less significant than for a smaller thruster. At 50 cm, the options for maintaining high module power and some flexibility in wearout life are substantially greater than for a 40-cm design.

2. Sensitivity Conclusions

Results of the sensitivity studies are summarized qualitatively in Table 4-11. From a thruster standpoint, module power, life, and efficiency are most important. The importance of high power was reflected in the previous recommendations. Life is important, particularly for the on-orbit mission. To a certain extent, life can be compensated for through redundancy. However, a minimum life of less than about 5,000 hr would penalize the system. Higher efficiency than that used in the modeling would not significantly improve the cost picture; lower efficiency would not be desirable. The fact that thruster mass has a small influence indicates mass could be traded for life, efficiency, or cost. Although reliability is covered by redundancy assumptions, a trade of thruster mass for a simpler, more reliable thruster would also be prudent.

Somewhat unexpectedly, the type and cost of propellant is relatively unimportant. Propellant selection certainly influences thruster operating parameter selection, but the flexibility added by the availability of several propellants is quite significant.

PPU and power source cost and mass were found to be extremely important in overall system cost effectiveness. Costs of the magnitude used in the model should be sought at the possible expense of efficiency, reliability, or mass. (PPU efficiency was effectively included under thruster efficiency sensitivity.) Without light-weight, low-cost power sources, the overall system cost will be increased significantly.

From a system design point of view, this work verifies the fact that system complexity, as represented by subsystem, integration, and development costs, is relatively important. Although the parameter values are somewhat arbitrary, the point at which these parameters become important is defined.

Of the mission design parameters considered, it is clear that transportation cost is the most significant since the other parameters are determined by the mission selected. Since the orbit-raising mission cost is strongly dependent on launch cost, and on-orbit cost is dependent on orbit-raising cost, low-cost transportation to LEO is a fundamental requirement for a cost-effective near-Earth space transportation system.

SECTION 5

TECHNOLOGY ASSESSMENT

The source of the technology-related portions of the models described in Sections 3 and 4 was a thruster technology assessment study. The areas covered included ion optical systems, cathodes, thermal limitations, wearout life, thruster scaling, propellant type, and operational simplifications to reduce the required number of power supplies. These areas are discussed in this section.

A. ION OPTICAL SYSTEM

1. Perveance

Foremost among these technology tasks is the ion optics design. All other thruster design parameters are influenced by the selection of an ion optics design. Having specified the propellant, beam current, and beam voltage required to produce the required values of thrust and specific impulse, the first question that must be answered is that of the size of the thruster (grid area) necessary to generate these specifications. The ion thruster being considered uses a two-electrode system that has numerous aligned apertures that extract, accelerate, and focus the ion beam. Beam current and voltage are not independent quantities in that the maximum current that can be extracted is limited by space charge and is related to the electrode voltages by a form of Child's law. This limitation dictates the dimensions of the acceleration electrode assembly. Analysis of the extraction and acceleration processes has been performed by several workers and has been summarized and presented in well-referenced form by Kaufman.[66] Initially, the analysis here will be limited to obtaining equations for relating thruster (ion beam) diameter to beam voltage and current requirements.

First, the beam current I_B and voltage V_B are related by

$$I_b = P\, V_t^{3/2} \quad , \tag{5-1}$$

where

$$V_t = V_b + V_a \quad , \tag{5-2}$$

and V_a is the negative voltage applied to the accelerator electrode to prevent electron backstreaming from the neutralized ion beam into the interelectrode acceleration gap. The perveance P, constant for a given electrode design, is a function of aperture and interelectrode dimensions, and can be written

$$P = C_1\, N_a\, P_a \quad , \tag{5-3}$$

where N_a is the number of apertures in the acceleration electrodes, and P_a is individual aperture perveance. Figure 5-1 illustrates the aperture configuration and gives dimensions of the 700-900 series EMT design. In terms of the symbols used in Figure 5-1,

$$P_a = \frac{4.4 \times 10^{-9}}{\left(0.336 + \frac{\ell}{d_s}\right)^2} \left(AV^{-3/2}\right) \quad . \tag{5-4}$$

for singly charged mercury ions,[67] and

$$\ell = \ell_g + t_s \quad .$$

The dimensions shown in Figure 5-1 yield

$$P_a = 6.4 \times 10^{-9}\, AV^{-3/2} \quad .$$

The factor C_1 accounts for the variation in current as a function of beam radius that is a consequence of a radially varying discharge plasma density distribution. Essentially,

$$C_1 = \frac{4\int_o^R 2\pi r J\,(r)\,dr}{J_{max}\pi D^2} \quad , \tag{5-5}$$

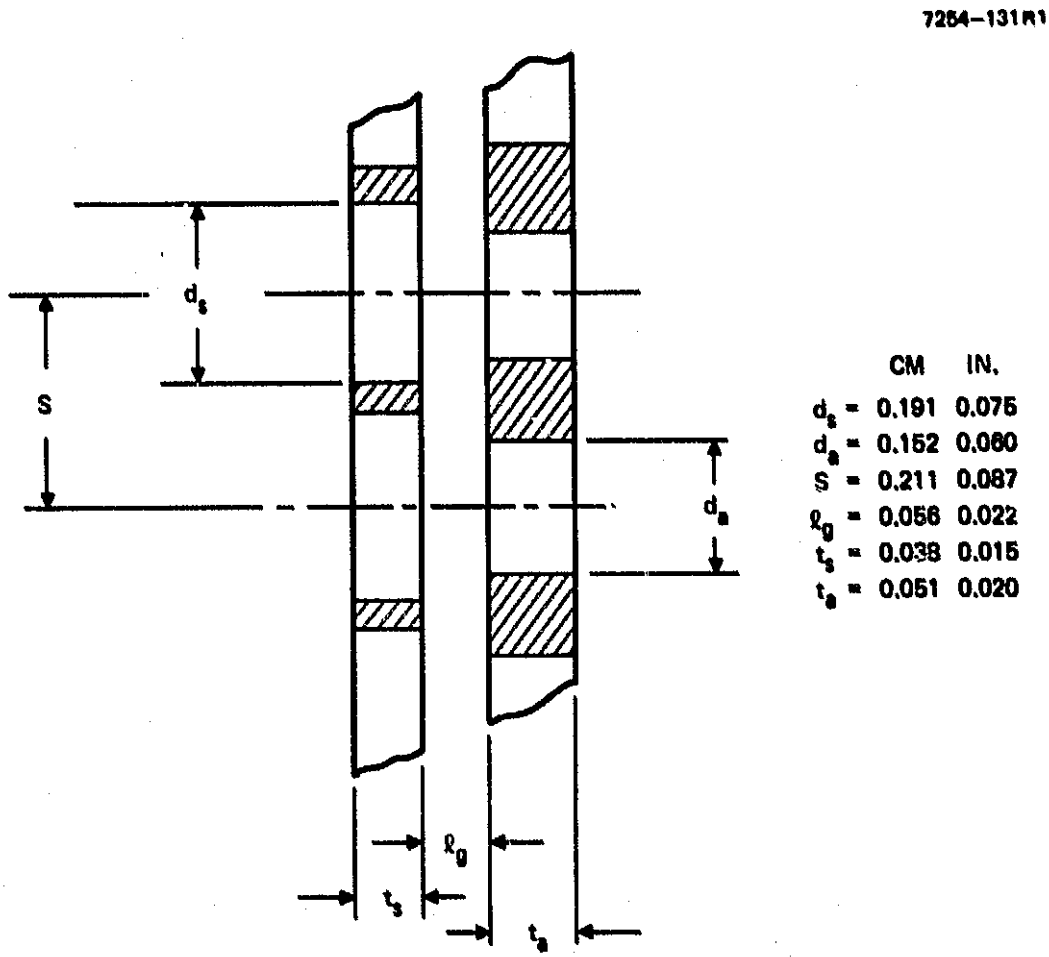

Figure 5-1. Aperture configuration for EMT ion optics.

and, for typical 30-cm operation, $C_1 = 0.52$. With the number of apertures set at 15,173 for the EM design, the perveance computed using Eq. 5-3 is $P = 5.1 \times 10^{-5}$. However, the maximum perveance measured experimentally with the EM ion optics design is only 4×10^{-5}, implying that the assumptions used in obtaining the analytic value of P may be slightly in error. To provide a realistic estimate of thruster size requirements, the empirical value can be used to determine an effective individual aperture perveance $\langle P_a \rangle$ by setting

$$\langle P_a \rangle = \frac{P}{N_a} = \frac{4 \times 10^{-5}}{15,173} = 2.6 \times 10^{-9} \, AV^{-3/2} \quad . \qquad (5\text{-}6)$$

For a hexagonal close-packed array of apertures,

$$N_a = 0.9 \, \frac{D^2}{S^2} \, , \qquad (5\text{-}7)$$

where D is the diameter of the array (beam diameter), and S is the center-to-center spacing of the apertures in the array. Eq. 5-3 can now be written

$$P = 2.34 \times 10^{-9} \, \frac{D^2}{S^2} \qquad (5\text{-}8)$$

and

$$I_b = 2.34 \times 10^{-9} \, \frac{D^2}{S^2} \, V_t^{3/2} \quad . \qquad (5\text{-}9)$$

Considering the extensive empirical parameter variation that has produced the EM ion optics design, the aperture parameters listed in Figure 5-1 are probably near optimum and are also a realistic basis for predicting beam diameter requirements. Therefore, Eq. 5-9 becomes

$$I_b = 4.79 \times 10^{-8} \, D^2 \, V_t^{3/2} \quad . \qquad (5\text{-}10)$$

Eq. 5-10 can now be used to illustrate the beam diameter requirements for a thruster operated on mercury as a function of beam current and total extraction voltage. Since it is the beam voltage that must really be specified, a further consideration is in order. Again, invoking empirical results from EM testing, electron backstreaming does not occur if

$$R = \frac{V_b}{V_b + V_a} = \frac{V_b}{V_t} \leq 0.7 \ . \tag{5-11}$$

Equation 5-11 is somewhat conservative in that thruster operation with R = 0.7 to 0.78 has been demonstrated without evidence of backstreaming; however, most testing has been done under the condition of Eq. 5-11. Hence, Eq. 5-10 can be written

$$I_b = 8.19 \times 10^{-8} D^2 V_b^{3/2} \tag{5-12}$$

and

$$D^2 = 1.22 \times 10^7 \ I_b \ V_b^{-3/2} \ . \tag{5-13}$$

Using Eq. 5-13, the beam requirements are illustrated graphically for mercury in Figure 5-2 and for argon in Figure 5-3. These curves are the basis for determining thruster technology requirements after translating thrust and specific impulse to beam current and voltage. Since there is a good technology base for ion optics designs up to 30-cm diameter, Figures 5-2 and 5-3 identify those ranges of beam current and voltage that require advanced technology. These curves are based on empirical perveance data obtained with state-of-the-art 30-cm thruster ion optics in the 0.5 to 4 A current range at beam voltages from 1000 to 1500 V. Consequently, the higher voltage curves should be considered valid only as a first-order estimate.

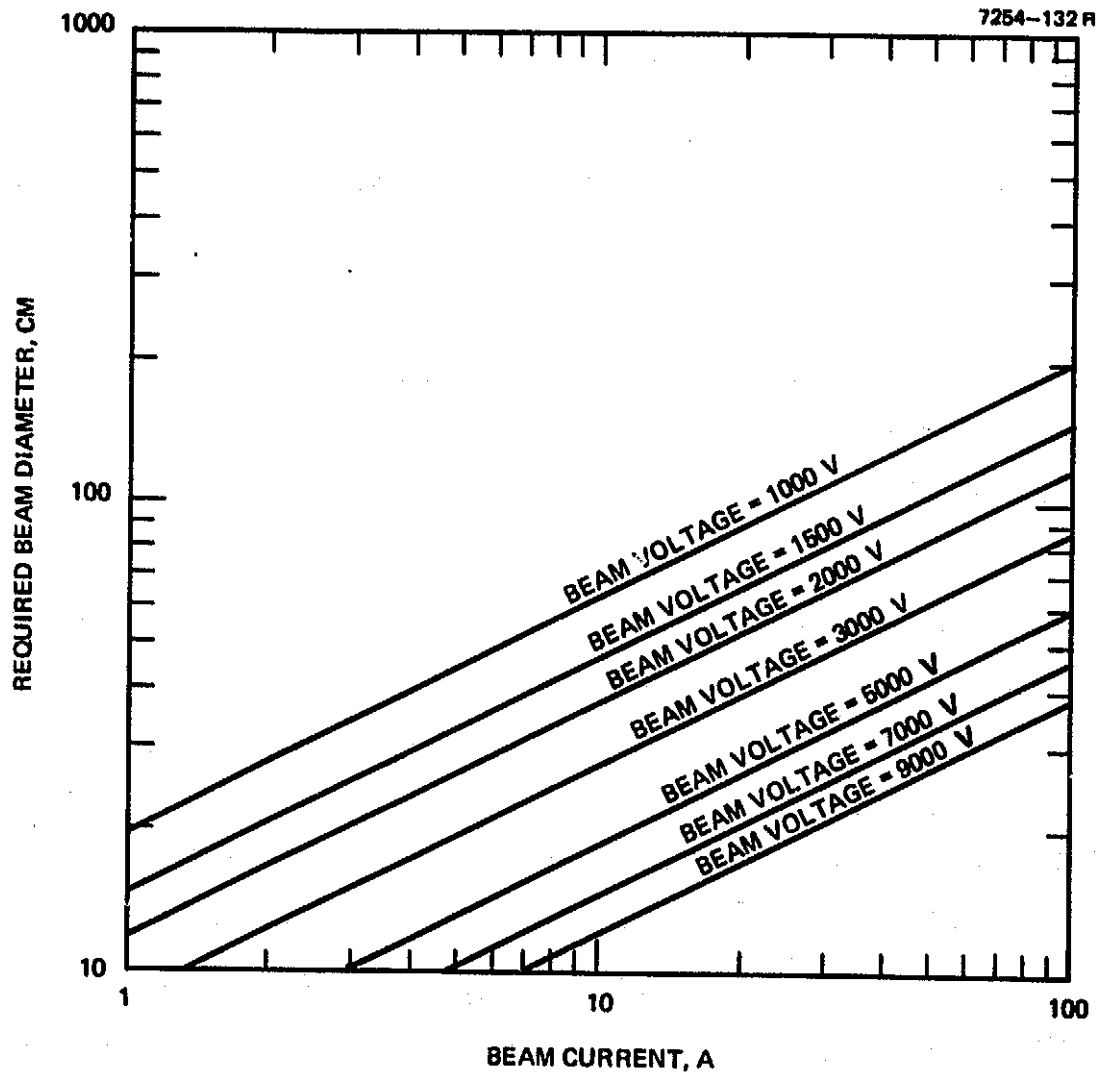

Figure 5-2. Beam diameter required to produce mercury ion beam current.

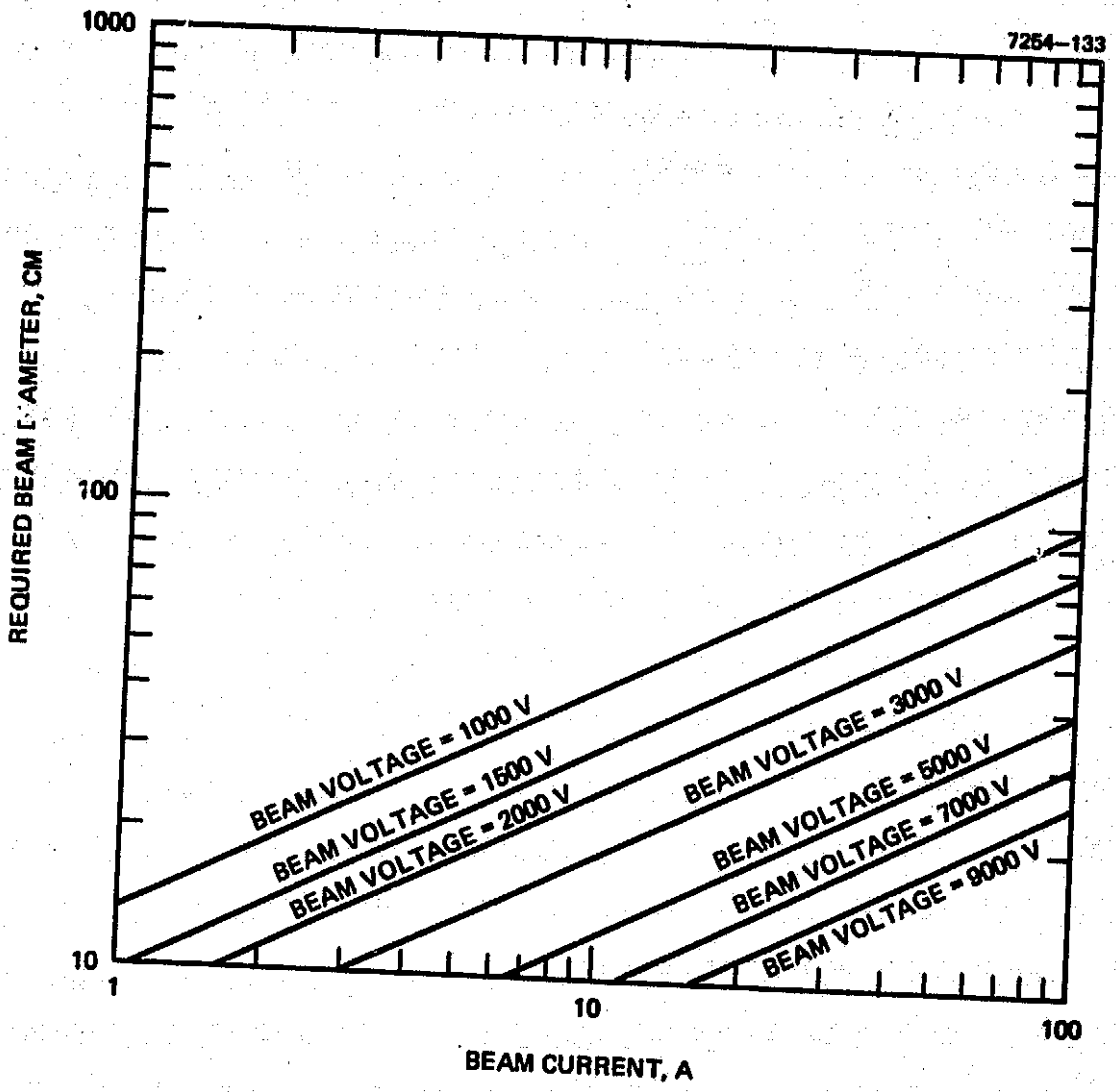

Figure 5-3. Beam diameter required to produce argon ion beam current.

2. Curved Electrode Thrust Losses

Since thruster diameters other than 30 cm are being considered in this study, the impact of grid curvature on thrust losses must be considered. Thrust loss was calculated as a function of thruster diameter, grid spacing, and radius of curvature (dish depth) for various dished grid geometries. For all these calculations, the compensation was limited to provide a maximum vectoring angle of 16°. Experimental results indicate that accelerator grid direct ion interception increases rapidly for angles greater than 16°. Although a relatively large dish depth (small radius of curvature) is desirable from a structural standpoint, the opposite is true from a thrust loss viewpoint. The results presented here show quantitatively the trade-off between thrust loss and dish depth (radius of curvature) as a function of thruster diameter. To all the thrust loss calculations presented here, the intrinsic beamlet divergence, which typically amounts to 1 to 2 percent, must be added.

a. Grid Compensation

Since thrust loss is a function of grid compensation, this parameter is discussed before the thrust loss calculations are made. Figures 5-4 and 5-5 show the geometrical parameters associated with a dished grid set. The basic compensation problem arises from the need to cancel (1) the effects of the dish angle and (2) the vectoring caused by the misalignment of the holes for noncompensated optics that occurs when the grids are separated. In the ideal case, the screen electrode hole pattern is "shrunk" an amount (compensated) such that all beamlets are vectored by an angle sufficient to exit parallel to the thruster axis, and, in that ideal case, the total compensation C_{tot} required to accomplish this can be broken into two parts:

$$C_{tot} = C(\ell_g) + C(\alpha) \quad . \tag{5-14}$$

Neglecting the electrode thicknesses, the compensation $C(\ell_g)$ required to align the holes is given by

$$C(\ell_g) = (2\ell_g/D) \tan \phi_{max} \quad , \tag{5-15}$$

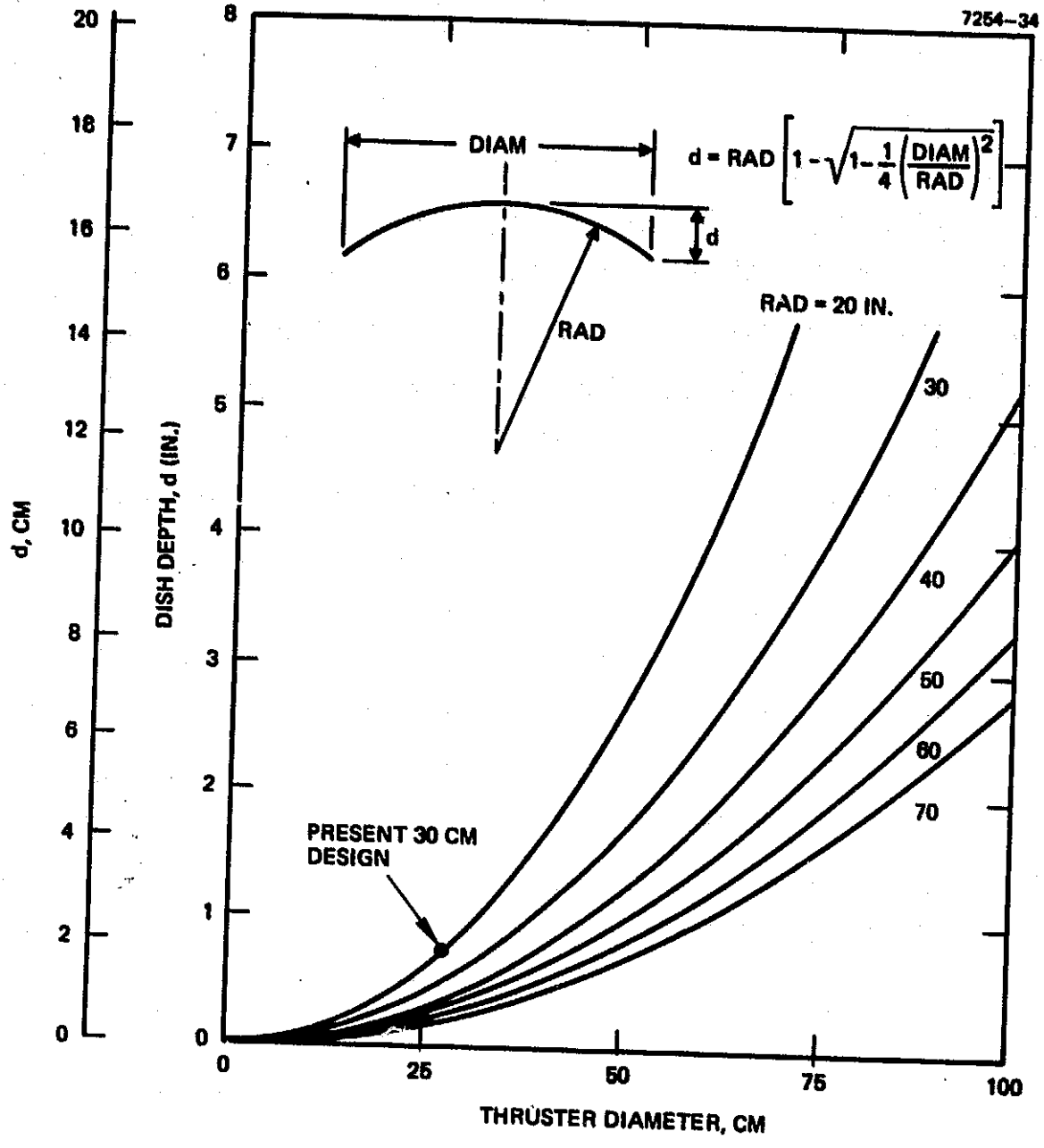

Figure 5-4. Dish depth as a function of thruster diameter with grid radius of curvature as a parameter.

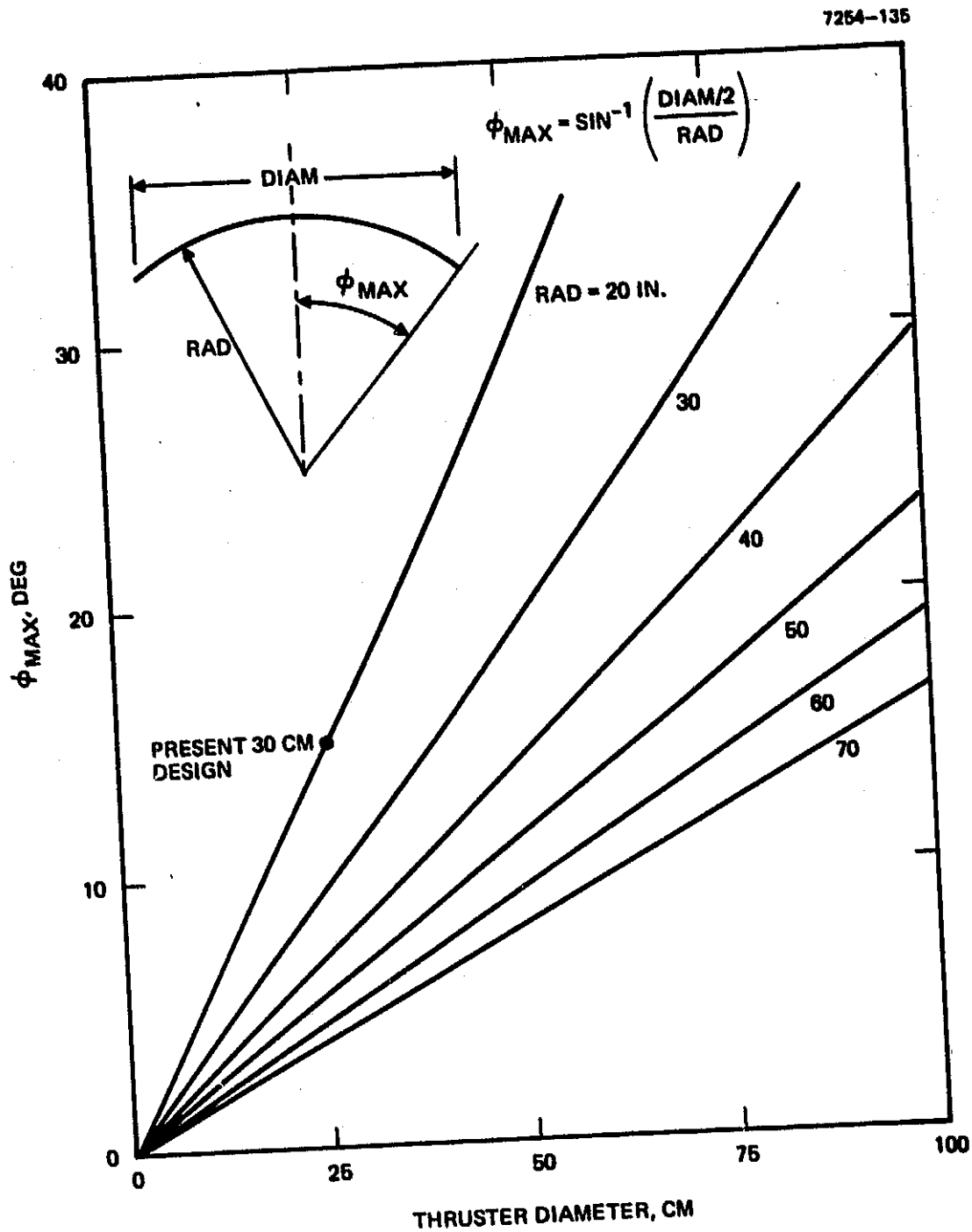

Figure 5-5. Maximum dish angle versus thruster diameter.

where ℓ_g is the grid spacing, D/2 is the beam radius, and ϕ_{max} is the dish semi-angle at the grid edge. For the present 30-cm dished grid, $\ell_g = 0.056$ cm, D = 29 cm, $\phi_{max} = 16°$, and therefore

$$C(\ell_g) = \frac{0.112}{29} \tan (16°) \simeq 0.11\% , \qquad (5.16)$$

which amounts to ∿25 percent of the total 0.4 percent compensation presently used. If thermal loading causes the grid spacing to decrease by causing the screen grid to move toward the accel grid, the compensation available for vectoring will be increased.

The compensation C(α) required to vector the beamlets an amount α depends on the vectoring sensitivity measured in degrees per normalized screen aperture offset. There have been efforts to determine this vectoring sensitivity using digital computer trajectory calculations, but the computed and experimental results did not agree very well. The basic problem is that the computer programs must be run with planar symmetry although the real problem has no symmetry. The approach taken here is to use the experimentally measured sensitivity for the present 30-cm grid set. Figure 5-6 shows some experimental data taken with the collimated ExB probe.[59] This data shows that there is a 2.4° difference between the r = 0 and r = 10.7 cm profiles. If the grid compensation were perfect, these profiles would be on top of each other. Since the dish semi-angle α at this radius is ∿12.4°, the net vectoring achieved was

$$\theta_{net} = 12.4 - 2.4 \simeq 10° .$$

For a grid compensation of 0.5 percent, the net grid offset at this radius is

$$\Delta_{net} = (.005)\ (10.7) - 0.06 \tan 12.4° = 0.04 \text{ cm} .$$

The measured vectoring sensitivity is thus

$$S_V = \frac{10°}{.04 \text{ cm}} = 250°/\text{cm} ,$$

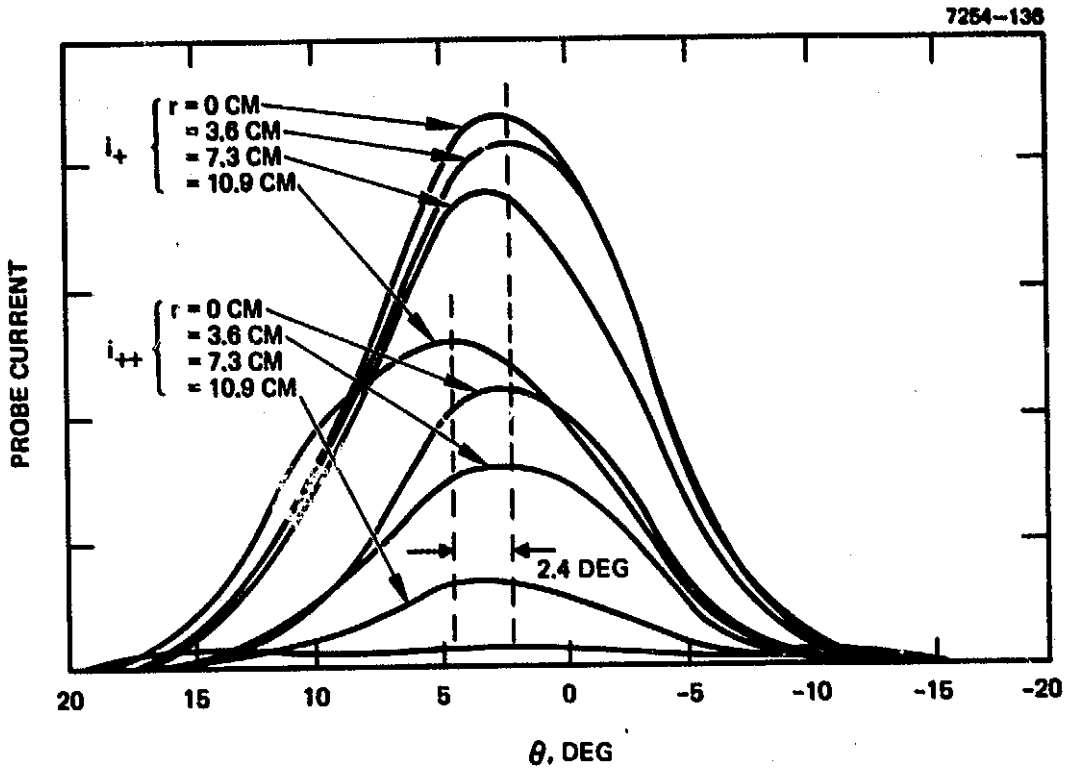

Figure 5-6. Beam profiles measured with ExB analyzer; 30-cm thruster using 0.5% compensation (Ref. 59).

or, in normalized form, since the screen aperture diameter is 0.1905 cm, S_{norm} = 1°/2.1 percent of screen aperture diameter offset. In comparison, the sensitivity obtained with the 5-cm thruster measured with a probe rake was 1°/1.6 percent; digital computer trajectory calculations predicted a sensitivity of ∿1°/1 percent. For the thrust loss calculations described in the following section, the sensitivity measured with the 30-cm EMT was used.

b. Thrust Loss Calculations

These calculations were made to aid in assessing the feasibility of new thruster design concepts. Several assumptions were used in making the thrust loss calculations:

- The current density across the grid varies as

$$J(r) = J_o \cos \frac{\pi r}{2r_o}$$

- A maximum beam vectoring of 16° at the beam edge
- Optics geometries for all cases are scaled from the present 30-cm design so that the normalized vectoring sensitivity = 1°/2.1 percent.

Using the first assumption, the grid thrust vector cos $\hat{\theta}$ and thrust loss T_{loss} (in percent) is given by

$$\cos \hat{\theta} = \int_o^{r_o} 2\pi r \cos \frac{\pi n}{2r_o} \cos \theta(r)\, dr \Big/ \int_o^{r_o} 2\pi r \cos \frac{\pi n}{2r_o}\, dr \quad , \quad (5\text{-}17)$$

where

$$T_{loss} = 100\,[1 - \cos \hat{\theta}]\ (\%) \quad , \quad (5\text{-}18)$$

and $\theta(r)$ is the difference between the dish angle α and the net vectoring angle. The net angle $\theta(r)$ used in evaluating the thrust loss in Eq. 5-16 is the difference between the dish angle and the net vectoring angle $\gamma(r)$:

$$\theta(r) = \alpha(r) - \gamma(r) \quad , \quad (5\text{-}19)$$

where

$$\gamma(r) = s[rC_{tot} - d \tan \alpha] \quad .$$

A maximum vectoring angle of 16° is assumed to prevent direct interception so that the $C(\alpha)$ compensation amounts to a maximum of 16 x 2.1 percent = 33.6 percent of the screen aperture diameter at the beam edge. Under this assumption, the compensation used for the thrust loss calculation was

$$C_{tot} = \frac{d}{r_o}\left[\frac{\theta}{s} + \tan \phi_{max}\right] , \qquad (5.20)$$

where $\theta = 16°$ if $\phi_{max} > 16°$, and $\theta = \theta_{max}$ if $\phi_{max} < 16°$. This expression is plotted in Figure 5-7 as a function of thruster diameter with radius of curvature as a parameter. The present 30-cm compensation should be increased to 0.6 percent to be perfectly compensated.

For $\phi_{max} \leq 16°$, $\gamma = 9°$ across the grid and $T_{loss} = 0$ (neglecting the intrinsic beamlet divergence, which typically amounts to 1 or 2 percent). The amount of thrust loss calculated using Eqs. 5.16, 5.17, and 5.19 is plotted in Figure 5-8 as a function of thrust diameter with grid radius of curvature as a parameter. Figure 5-8 shows that the present 20-in. grid curvature could be used up to a thruster diameter of ∿50 cm with less than 1 percent thrust loss. Figures 5-4 and 5-5 show that this diameter corresponds to a maximum dish angle of ∿30° and dish depth of ∿7 cm.

c. Practical Considerations

The calculations discussed above show the relationships between beam divergence, thrust loss, and grid compensation parameters for ideally spaced and aligned grids. In practice, ion optics electrodes cannot be spaced completely uniformly, and alignment to obtain the exact required offset in all radial directions presents a very difficult assembly task. If thrusters are required in very large numbers, requirements for such extremely high accuracies represent a costly

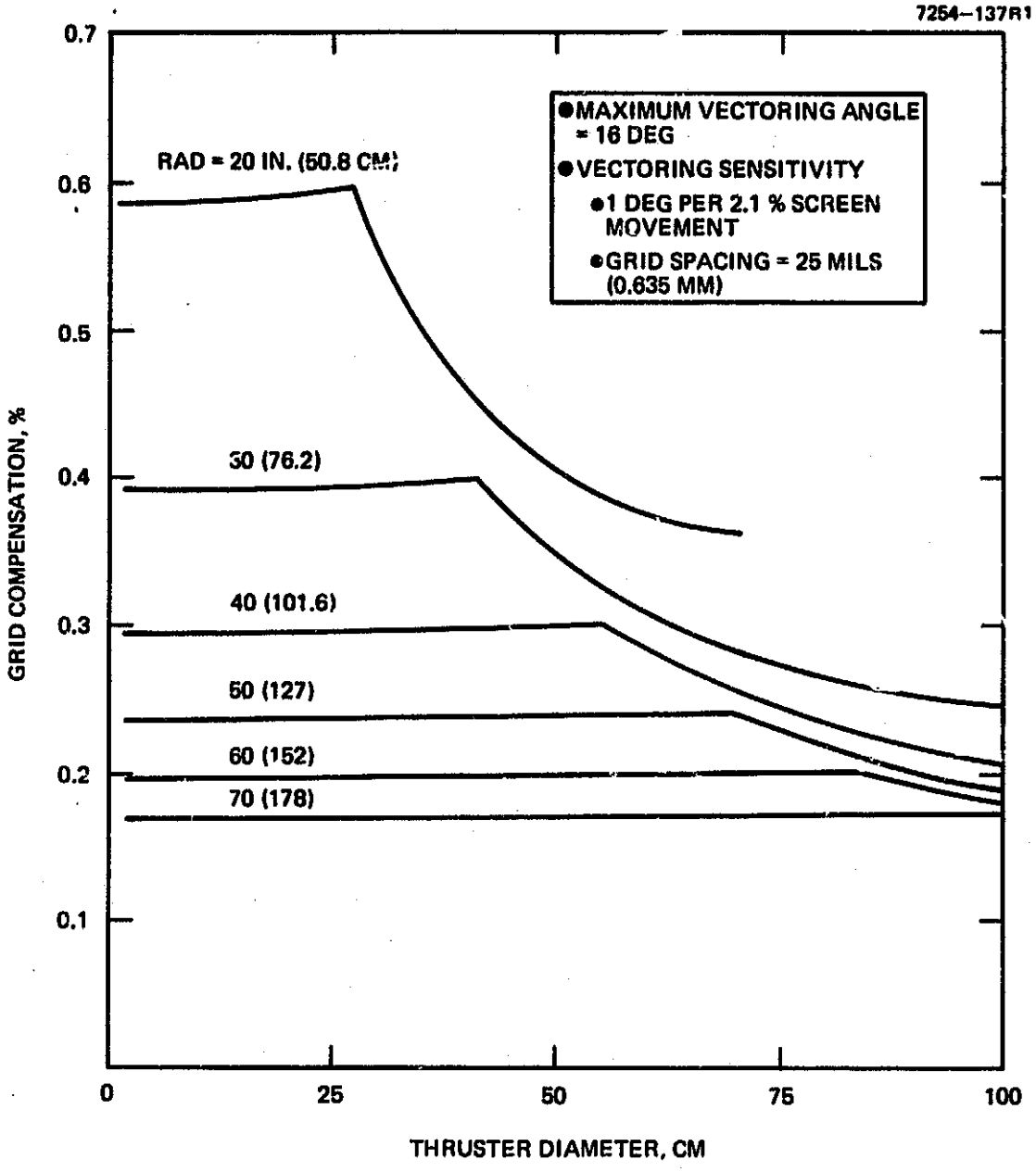

Figure 5-7. Grid compensation versus thruster diameter.

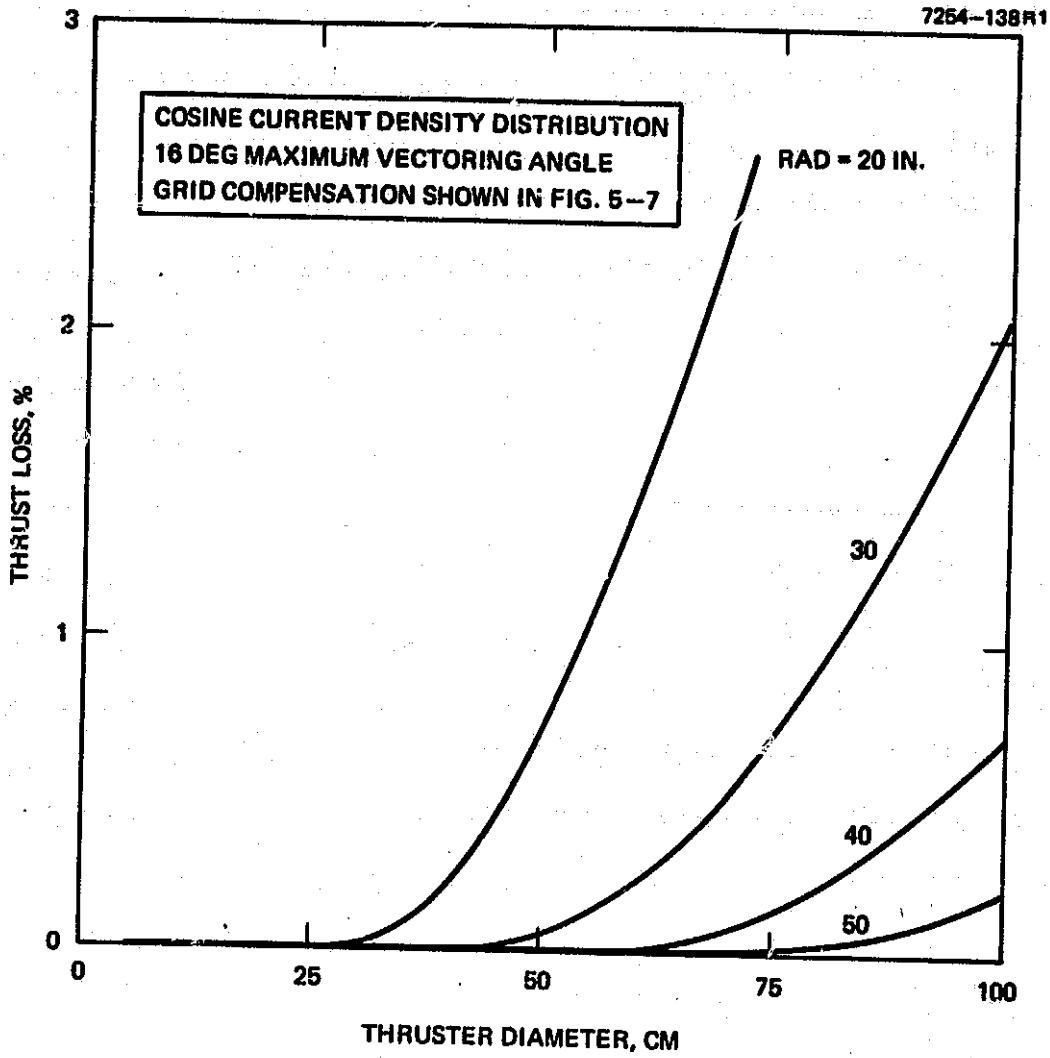

Figure 5-8. Thrust loss versus thruster diameter.

and formidable manufacturing obligation. Since 0.4 percent is considered the empirically determined practical limit for 30-cm thrusters, the calculations given above are only useful in a relative sense and show what could be achieved ideally. Achieving relatively small thrust losses would require developing fabrication processes to achieve adequate aperture alignment and electrode spacing.

B. CATHODES

The hollow cathode configuration shown in Figure 5-9 is the accepted cathode design for 30-cm thrusters. This cathode geometry has evolved from extensive development work at NASA LeRC and elsewhere and a complete referenced discussion of this development has been presented by Kaufman.[66] Essential features of this cathode design are

- A hollow tube with a gas-flow-limiting orifice
- An external heater to raise the tube and orifice temperature to 1300°K
- An internal source of BaO for providing a low-work-function surface
- An internal gas pressure of ~1 Torr during normal operating conditions
- Operational modes with characteristics that depend on gas flow and emission conditions.

Although several possible explanations of hollow-cathode physical processes are considered in Kaufman's review article, the discussion is by no means conclusive. Some conclusions for which there is general agreement are that

- Thermionic emission from the cathode orifice or interior is important to both ignition of the cathode discharge and its operation at low discharge (keeper) voltage.
- The hollow cathode plasma is characterized by an electron density, n_e, on the order of $10^{18}/m^3$ with a Maxwellian energy distribution that has an electron temperature, T_e, in the 0.5 to 2 eV range.

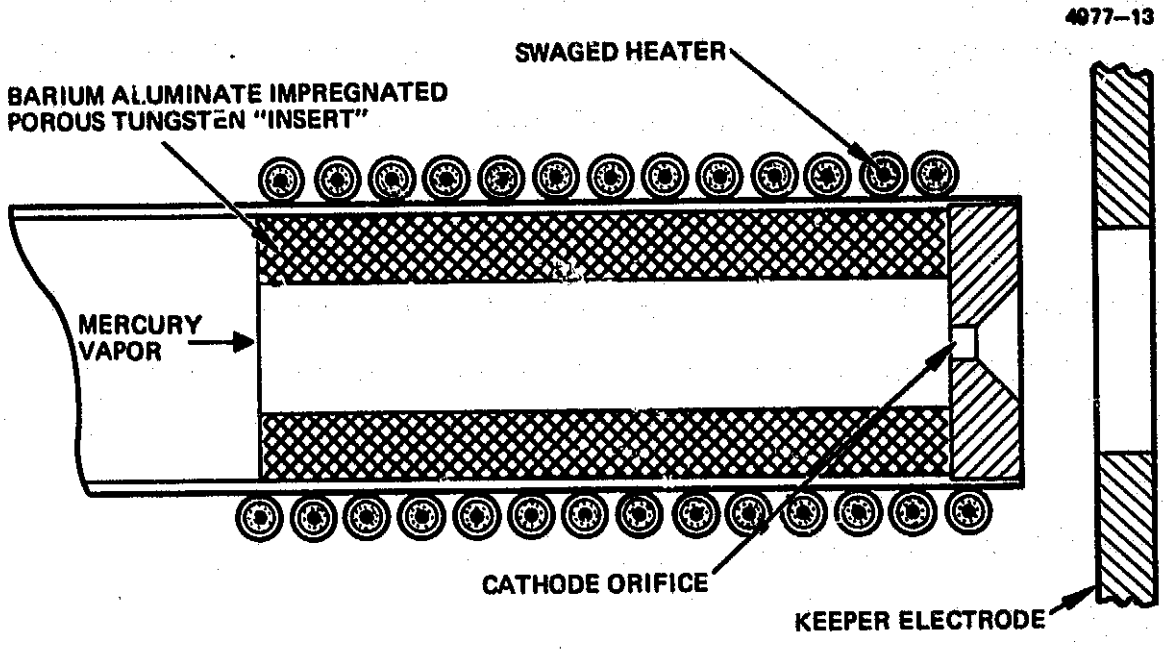

Figure 5-9. Hollow cathode configuration used in 30-cm EMT.

- Cathode orifice wear is proportional to emission current requirements and orifice dimensions.

The nominal emission current rating of the 30-cm thruster hollow cathode is 12 A for 2 A of beam current. Life tests have been conducted at this current that show negligible cathode wear for 18,000 hr of testing.[68] Since the 30-cm thruster cathode was scaled from the 15-cm thruster cathode (SERT II) on the basis of empirical results, we can suggest with some confidence that scaling a cathode for higher emission currents should not present a basic technology problem. In previous sections, beam currents as high as 15 A were considered a possibility, and such beam currents imply emission currents of 90 A. Emission currents of 20 A have been achieved without difficulty from the present 30-cm cathode design,[69] but extrapolation to higher currents would require experimental verification and probably some additional engineering to achieve the thermal environment considered to be a requirement for long lifetime.

The discussion presented above is relevant only for operation with mercury vapor as the propellant or working gas. Achieving the requisite low-voltage discharge conditions has not been adequately demonstrated with other gases, is not well documented empirically, and was not a subject of this investigation. Empirically, xenon appears most similar to mercury vapor with respect to discharge characteristics and cathode operation. Consequently, for operation with propellant other than mercury, a basic technology investigation and development program is considered to be a requirement.

C. THERMAL LIMITS

As discharge power is increased to obtain higher beam currents, the temperature distribution throughout the thruster changes. Power is not distributed uniformly, and some parts of the thruster will be heated more than others. To assess the relationship of thermal limits to beam current, a thermal modeling analysis was performed. An 11-node thermal model for the 30-cm thruster has been developed and has been used to predict the temperatures of critical thruster components for high beam

current operation. The starting point for this effort was a thermal model developed by Oglebay at NASA LeRC[70] for the 30-cm thruster. The nodal conductances, view factors, and power distribution for this model were received from NASA LeRC and were incorporated where applicable in the development of this simplified thermal model. A description and the results of this model are presented below.

1. Thermal Model

The thermal analysis was carried out by representing the 30-cm thruster as a lumped parameter network of 11 nodes with 22 radiation and conductor resistances. A schematic showing the thermal model and nodal numbering is shown in Figure 5-10. Each of the principal thruster components was represented by a node that was connected to adjacent nodes by radiation and conductance resistors. These parameters, along with the nodal area, view factor, and the emissivity assumed, are summarized in Table 5-1. The radiation exchange factors $\mathscr{F}_{ij}$ were calculated using

$$A_i \mathscr{F}_{ij} = \left[\frac{1}{A_i} \left(\frac{1}{e_i} - 1 \right) + \frac{1}{A_j} \left(\frac{1}{e_j} - 1 \right) + \frac{1}{A_i F_{ij}} \right]^{-1} \qquad (5\text{-}23)$$

and are also shown in Table 5-1.

2. Power Inputs

The nodal power inputs were calculated as a function of beam current on the basis of a discharge chamber efficiency of 185 eV/ion and a fixed loss of 21 W. The actual effective heating power produced by the discharge chamber efficiency was assumed to be reduced by (37 + 10) eV/ion to account for the kinetic energy and heat of ionization taken away by the beam ions. This results in an effective discharge heating power as a function of beam current of

$$P_{dis} = 138\ I_b + 21, \qquad (5\text{-}24)$$

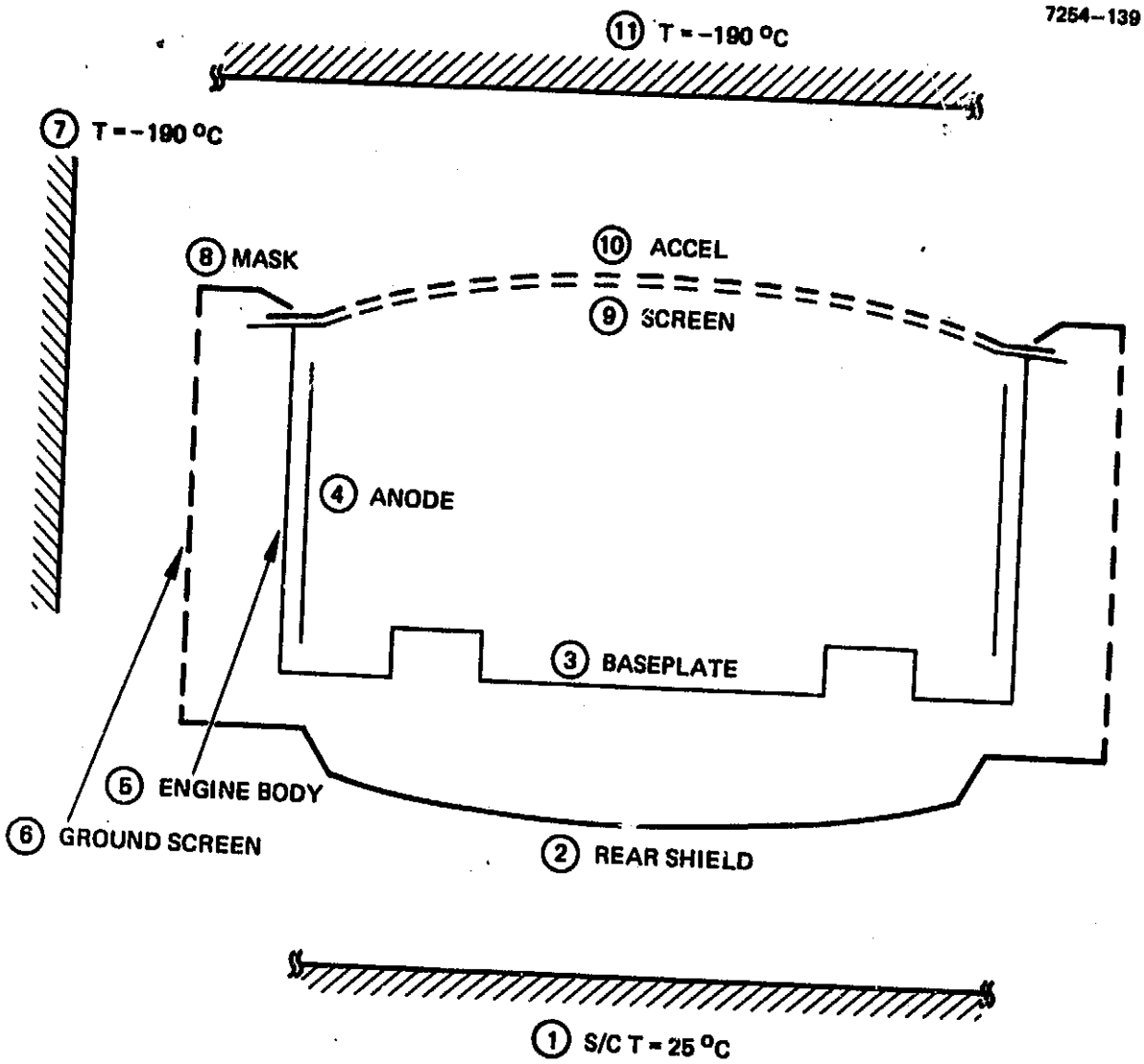

Figure 5-10. Thermal model node layout.

Table 5-1. Summary of Nodal Areas, View Factors, Emissivities and Form Factors Used in Thermal Model

Nodes Connected	Connector Number	A_i, $in.^2$	A_j, $in.^2$	e_i	e_j	F_{ij}	A_iF_{ij}, $in.^2$
2 and 1	1	231	195	0.15	1	0.5	30.1
3 and 2	2	120	231	0.20	0.20	0.47	14.6
3 and 6	3	120	74.4	0.15	0.15	0.03	2.5
5 and 7	4	352	396	0.15	1.0	0.175	30.9
6 and 7	5	396	396	0.15	1.0	0.50	51.6
8 and 11	6	81.1	81.1	0.15	1.0	0.50	10.6
10 and 11	7	111	195	0.15	1.0	0.50	14.5
9 and 11	8	91	195	0.15	1.0	0.235	9.2
4 and 11	9	171	120	0.25	1.0	0.05	7.4
3 and 11	10	155	120	0.25	1.0	0.16	16.8
4 and 3	11	171	120	0.25	0.15	0.17	10.1
4 and 9	12	171	114	0.25	0.15	0.06	6.07
4 and 10	13	171	113	0.25	0.15	0.06	6.05
4 and 5	14	171	352	0.25	0.15	0.50	22.05
5 and 6	15	215	396	0.15	0.15	0.325	18.2
5 and 8	16	215	81.1	0.15	0.15	0.02	3.0
9 and 10	17	114	114	0.15	0.15	0.265	7.5
2 and 6	18						0.05[a]
6 and 8	19						0.05[a]
3 and 5	20						0.095[a]
5 and 9	21						0.119[a]
3 and 9	22	155	114	0.25	0.15	0.053	5.06
3 and 10	23	155	114	0.25	0.15	0.056	5.27

[a]Conductances in W/°C

6119

where I_b is in amperes, and P_{dis} is in watts. This power was distributed to the screen, anode, and backplate nodes as follows. Assuming an effective screen grid open area of 70 percent, the wall flux of ions which strike this electrode produce an effective heating power of

$$P_{sc} = I_b \left(\frac{1 - 0.70}{0.70}\right) \left[37 + 10\right] \approx 20\ I_b\ , \qquad (5\text{-}25)$$

where we have neglected the cooling effect of the electrons that combine with ion wall flux.

By assuming that all the fixed losses are distributed to the backplate electrode, the power to this electrode was taken as

$$P_{back} = 13\ I_b + 21\ , \qquad (5\text{-}26)$$

where the coefficient of I_b was taken to agree with Oglebay's model at a 2-A beam current. The heat to the anode was found by subtracting Eqs. 5-25 and 5-26 from Eq. 5-24, resulting in an anode power

$$P_{anode} = 105\ I_b\ . \qquad (5\text{-}27)$$

The power distribution and the power taken away by the beam ions are summarized below:

$$P_{anode} = 105\ I_b$$

$$P_{screen} = 20\ I_b$$

$$P_{back} = 13\ I_b + 21$$

$$P_{lost} = 47\ I_b$$

$$\text{Total:} \quad 185\ I_b + 21.$$

The accelerator grid power ($I_{acc} V_{tot}$) was calculated as a function of beam current by linearly extrapolating the typically measured accelerator current at 1 and 2 A beam current. The total voltage V_t was found by solving:

$$I_b = P_x V_t^{3/2}$$

as a function of beam current and using a total thruster perveance of

$$P = 4.3 \times 10^{-5} A/V^{3/2} ,$$

which is typical of present close spaced optics. A complete summary of the resulting nodal powers as a function of beam current is shown in Table 5-2.

3. Results and Discussion

Table 5-3 summarizes the calculated temperatures as a function of beam current levels from 1 to 10 A. Also shown are some experimentally measured temperatures for the 1 and 2 A beam current levels; these results are in good agreement with the calculated values. The calculated temperatures are plotted in Figure 5-11 as a function of beam current.

To estimate the limiting beam current (temperature) for the present 30-cm thruster, we will assume that the magnet temperature must be less than 500°C and that the vaporizer temperature must be less than 300°C. We will also assume that the radial magnets operate at the baseplate temperature and that the lower limit to vaporizer temperature would be the rear shield temperature. Under these assumptions, it is clear from Table 5-3 or Figure 5-11 that the highest beam current is ∿9.5 A to maintain the radial magnet temperature at less than 500°C and must be less than ∿9 A to maintain vaporizer control. Assuming that these two limitations can be avoided by improved magnet material and the elimination of vaporizers with argon, the next temperature limit will probably be the ion optics (screen grid). If an upper limit of 700°C is chosen, the 30-cm thruster could probably be operated up to 15 A.

Clearly, the maximum beam current for any given size will be limited by a maximum operating temperature (probably ion optics). Results of a thermal analysis discussed previously were used to establish a temperature-limited beam current, as shown in Figure 5-12. Since a large fraction of the radiated heat is rejected through the ion optics, this

Table 5-2. Summary of Nodal Input Powers Used in Thermal Model

Node	Input Power, W					
	Beam Current, A					
	1	2	4	6	8	10
Accel (10)	1.8	6.4	21.5	46.5	77.5	114(W)
Screen (9)	20	40	80	120	160	200(W)
Anode (4)	105	210	420	630	840	1050(W)
Backplate (3)	34	47	73	99	125	151(W)

6119

Table 5-3. Summary of Calculated Temperatures for 30-cm Thruster. Values in ( ) Were Determined Experimentally.

Node		Calculated Temperature, °C					
		Beam Current, A					
		1	2	4	6	8	10
Rear shield	2	(120) 97	(153) 143	206	251	288	319
Base plate	3	(200) 189	(262) 258	(328) 348	411	462	504
Anode	4	271	372	492	574	638	691
Body	5	(174) 152	(230) 224	312	372	420	459
Ground Sc.	6	47	(96) 96	160	204	239	268
Mask	8	33	(62) 79	137	178	210	236
Screen	9	202	293	404	480	540	589
Accel	10	163	246	350	426	487	538

6119

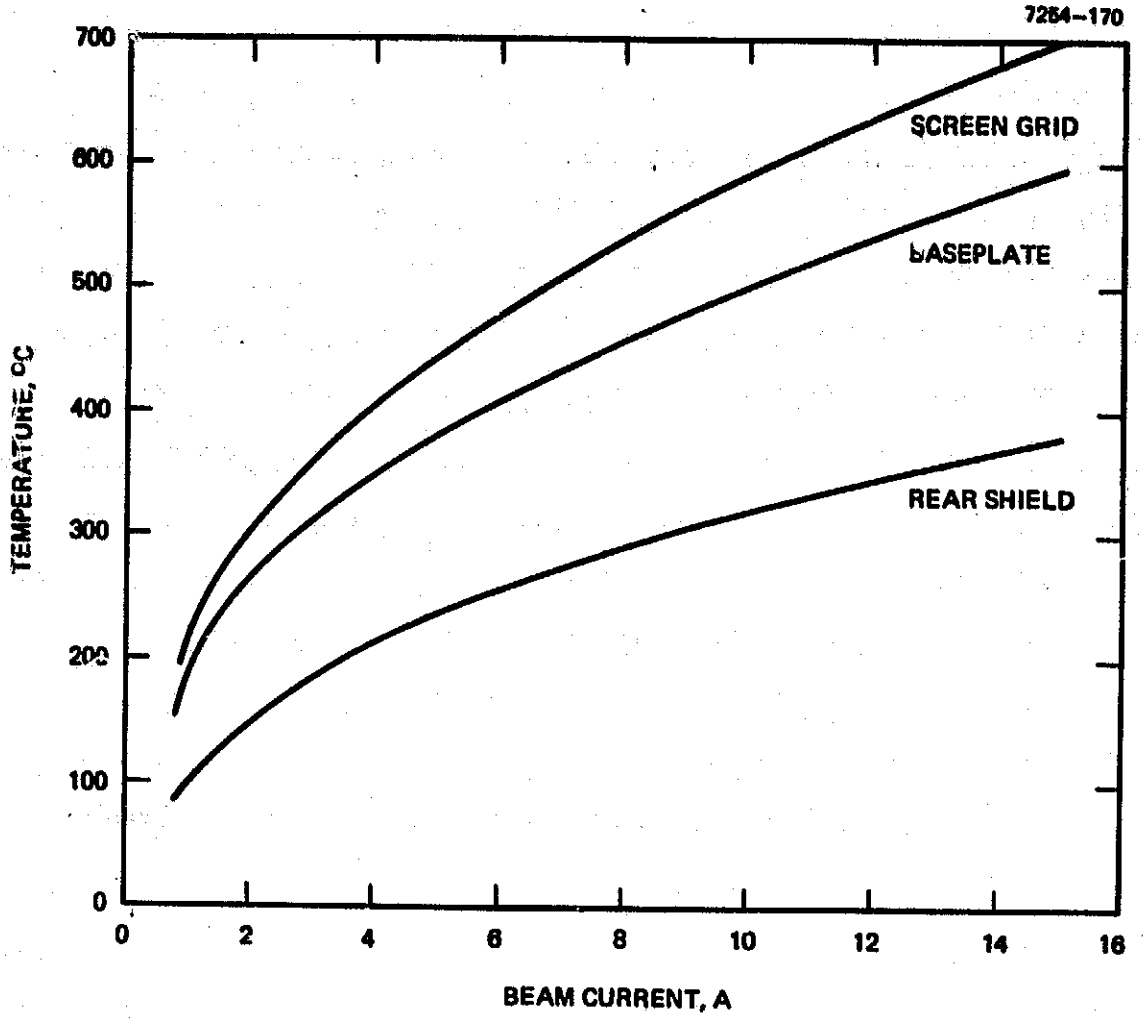

Figure 5-11. Calculated temperatures versus I_b.

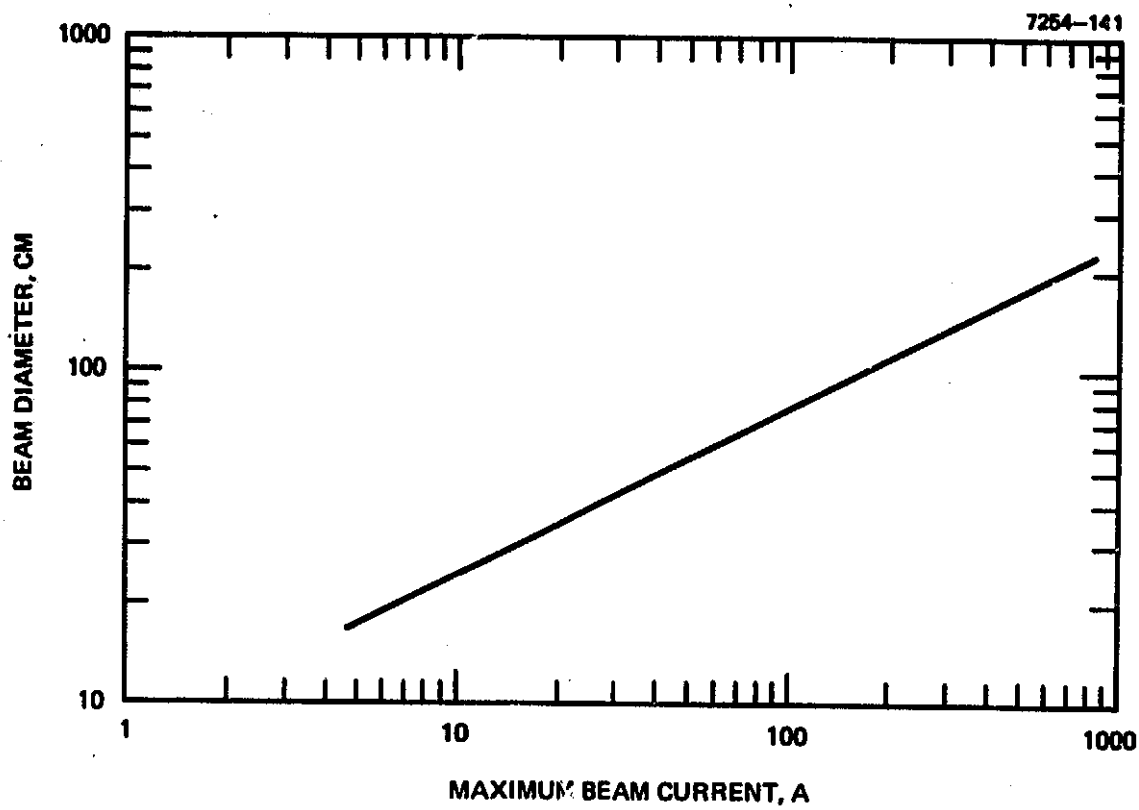

Figure 5-12. Estimated maximum beam current (limited by temperature) versus thruster diameter.

curve was derived by assuming that radiated power is proportional to beam diameter and beam current in the form

$$q_r = K_1 A_b T_{max}^4 = K_2 (I_b)_{max} . \quad (5\text{-}28)$$

Therefore,

$$A_b = \frac{K_2}{K_1} \frac{I_b}{T_{max}^4} = K_3 (I_b)_{max} \quad (5\text{-}29)$$

$$(I_b)_{max} = K_4 D^2 , \quad (5\text{-}30)$$

where the K's are constants,

T_{max} = maximum allowable temperature

D = beam diameter

$I_{b\ max}$ = maximum allowable beam current

K_4 = 0.0167 A/cm^2 .

The constant K_4 in Eq. 5-30 was evaluated for the 30-cm thruster assuming a maximum current of 15 A.

D. WEAROUT LIFE

In the preceding discussions, thruster diameter, or more properly ion beam diameter, was determined as a function of specified beam current (thrust) and voltage (I_{sp}) for both mercury and argon propellants on the basis of state-of-the-art ion extraction system capacity only. It is now appropriate to examine these results with respect to those practical constraints that are presently known and others that can be anticipated.

Consider first the operation of a 30-cm thruster at higher beam voltage to obtain higher beam current. With regard to the ion extraction system, results presented in Ref. 69 indicate that operation at increased beam voltage has relatively little impact on the design of this thruster component. If beam current is kept within the perveance

limitations, then beam current can also be increased without significantly affecting the ion optical properties of the extraction system. Similarly, operation at increased beam voltage is of little or no consequence to either discharge chamber or cathode operation or design. Propellant electrical isolators must be adapted to the appropriate voltage insulation, as must all the insulation used, but this is not a significant constraint unless extremely high voltages are specified (>10 kV).

Increasing the beam current at constant thruster diameter, however, requires an increase in beam current density and thus a proportional increase in plasma density and discharge current. Increasing plasma density at an approximately constant ionization fraction has been found to increase the double ionization percentage, and thus discharge chamber erosion rates increase at a rate somewhat greater than linear with increasing discharge current (beam current). An approximate dependence of erosion rate on beam current can be derived as follows. The number of particles q eroded from a unit area by a current density j impacting on that surface can be expressed as

$$q = \frac{1}{e}\left(j_+ S_+ + \tfrac{1}{2} j_{++} S_{++}\right) \qquad (5\text{-}31)$$

$$= \frac{1}{e} j_+ S_+ \left(1 + \tfrac{1}{2}\frac{j_{++}}{j_+}\frac{S_{++}}{S_+}\right) , \qquad (5\text{-}32)$$

where S is the sputtering coefficient for the appropriate ion species, and e is the electronic charge. The fraction j_{++}/j_+ is a function of the total current dentisy j_{tot}. On the basis of empirical data obtained with an EMT-like 700-series 30-cm Hg thruster,

$$\frac{j_{++}}{j_+} \approx 0.1 + \frac{I_b}{40} \quad , \quad \left(I_b \geq 1.0\text{A}\right) , \qquad (5\text{-}33)$$

where I_b is the total beam current, and the current densities are average values for the screen grid boundary. By setting j_+ proportional to total beam current, Eq. 5-32 becomes

$$q = C\, I_b S_+ \left[1 + \left(\frac{4 \cdot I_b}{40}\right)\frac{S_{++}}{S_+}\right] , \qquad (5\text{-}34)$$

C-4

where C is the proportionality constant between current density and total current. The sputtering coefficient for doubly charged ions is assumed to have the value measured for singly charged ions[71] at twice the ion energy (voltage). For the energy range of interest (30 to 40 V), the ratio S_{++}/S_{+} is approximately 15. Hence, Eq. 5-34 can be written

$$q \approx K I_b \left[1 + \left(\frac{I_b + 4}{5}\right)\right] = K I_b (0.2 I_b + 1.8) , \quad (5\text{-}35)$$

where K includes the appropriate considerations for relating current density to beam current, sputtering coefficient for the material being eroded, and to the energy of the eroding ions.

If a particular discharge chamber surface is now selected as the critical surface for material loss, it is possible to use Eq. 5-35 to relate useful lifetime to beam current. By specifying the allowable material loss in terms of atoms per unit area N, the lifetime, τ, is given by

$$q \tau = N = \text{constant}, \quad (5\text{-}36)$$

and hence

$$q_1 \tau_1 = q_2 \tau_2, \text{ etc.},$$

where the subscripts denote lifetimes and erosion fluxes for different current values; therefore,

$$q_1 K I_1 (0.2 I_1 + 1.8) = \tau_2 K I_2 (0.2 I_2 + 1.8)$$

or

$$\frac{\tau_2}{\tau_1} = \frac{I_1}{I_2} \left(\frac{1.8 + 0.2 I_1}{1.8 + 0.2 I_2}\right) . \quad (5\text{-}37)$$

Eq. 5-37 can now be used to extrapolate measured thruster lifetime for operation at lower currents to operation at higher current under the assumption that the conditions (particularly constant discharge voltage) stated in Eq. 5-33 are valid. Thus, conditions are thought to be satisfied for a 30-cm thruster of the 700-series EM design if the discharge

power input in watts per beam ampere (eV/ion) and the true propellant utilization efficiency are held constant. As an example, the screen grid lifetime was 60 percent consumed in the 10,000 hr endurance test of thruster S/N 701 (NASA CR-135011) and the average current was 1.4 A.[72] The lifetime τ at current I_b can be estimated by

$$\tau(I) = \frac{4.85 \times 10^4}{I_b(1.8 + 0.2\ I)} \qquad (5\text{-}38)$$

for operation at a discharge power input of 185 eV/ion and a corrected discharge propellant utilization efficiency of 88 percent (as shown graphically in Figure 5-13). Although the applicability of this curve to thruster operation in general may be quantitatively in question, this type of relationship between lifetime and beam current is considered to be qualitatively valid.

The ion extraction screen grid has been selected as the critical surface here because, as a discharge chamber component, the ion extraction screen grid thickness affects the efficiency of producing beam ions (eV/ion). Consequently, if one wishes to preserve thruster efficiency, one cannot simply increase the grid thickness to increase its lifetime, as is possible with some other discharge chamber components. Although the absolute value of the relationship shown in Figure 5-13 may be somewhat uncertain, it is possible to make the observation that, for short-term missions, existing 30-cm technology could produce high beam currents with useful lifetimes.

It is anticipated that operation at lower propellant utilization efficiency will change Eqs. 5-33 and 5-38 such that a family of curves will be generated that are shifted to higher lifetime. Again, drawing on empirical data, the relationship between j_{++}/j_{+} and corrected discharge chamber propellant utilization efficiency, shown in Figure 5-14, can be used to modify Eqs. 5-33 and 5-38 to obtain Figure 5-15. The applicability of the empirical data in Figure 5-14 in a general consideration is quantitatively questionable; however, the

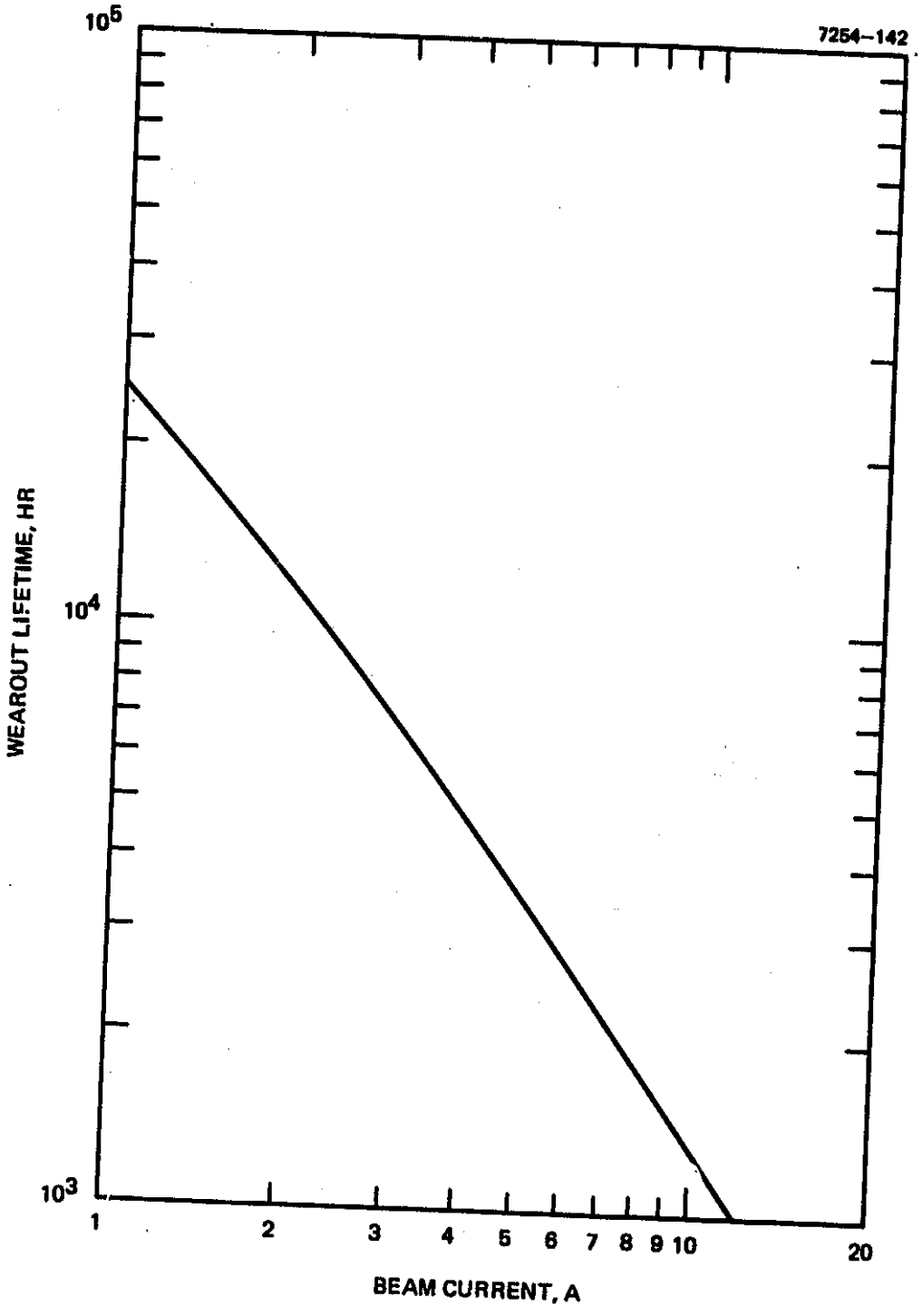

Figure 5-13. Estimated thruster wearout lifetime (700-series EMT, Hg, 37 V, η_u = 0.88).

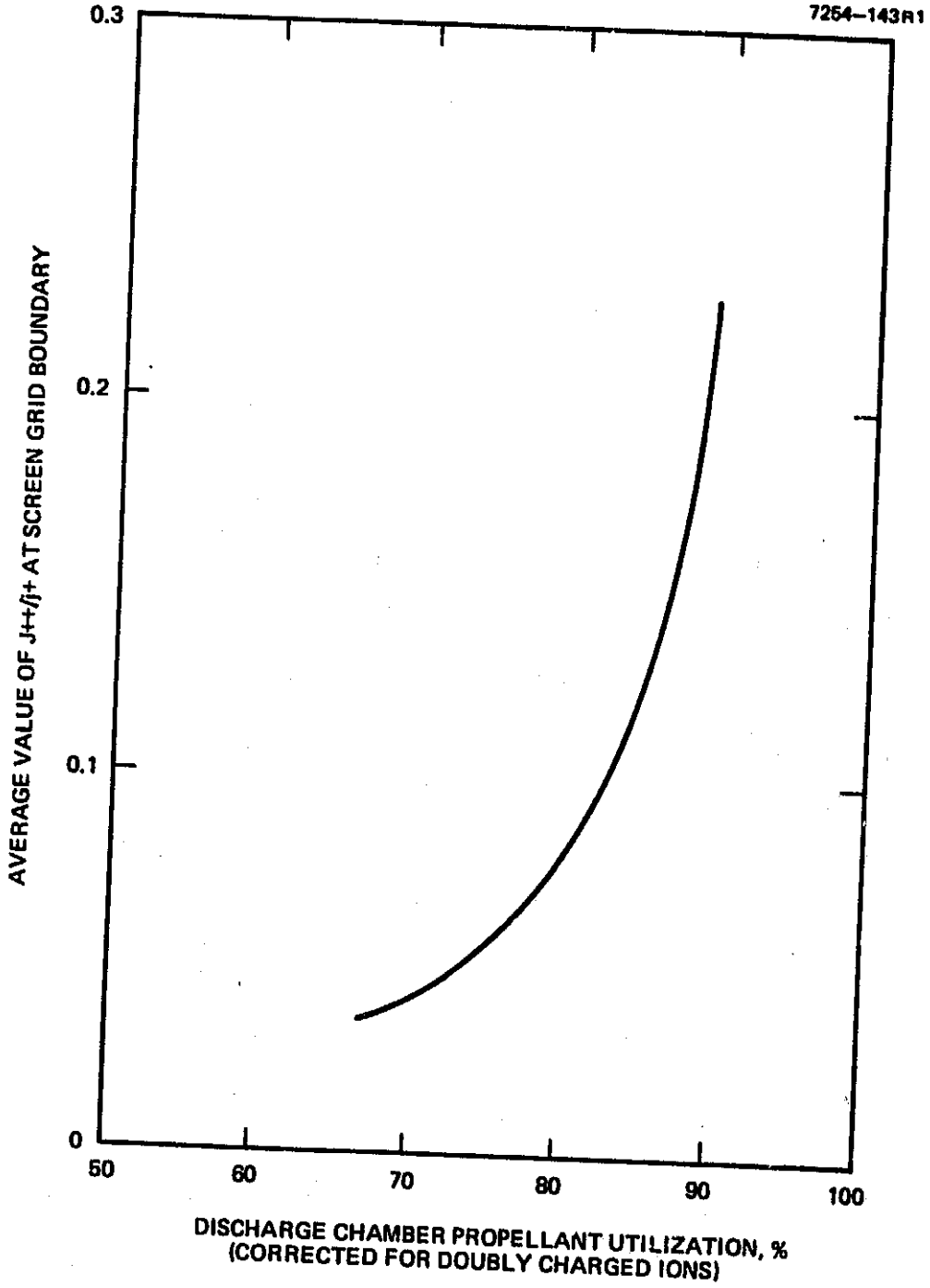

Figure 5-14. Relationship between (j_{++}/j_{+}) and discharge utilization efficiency (700-series EMT, Hg, 37 V).

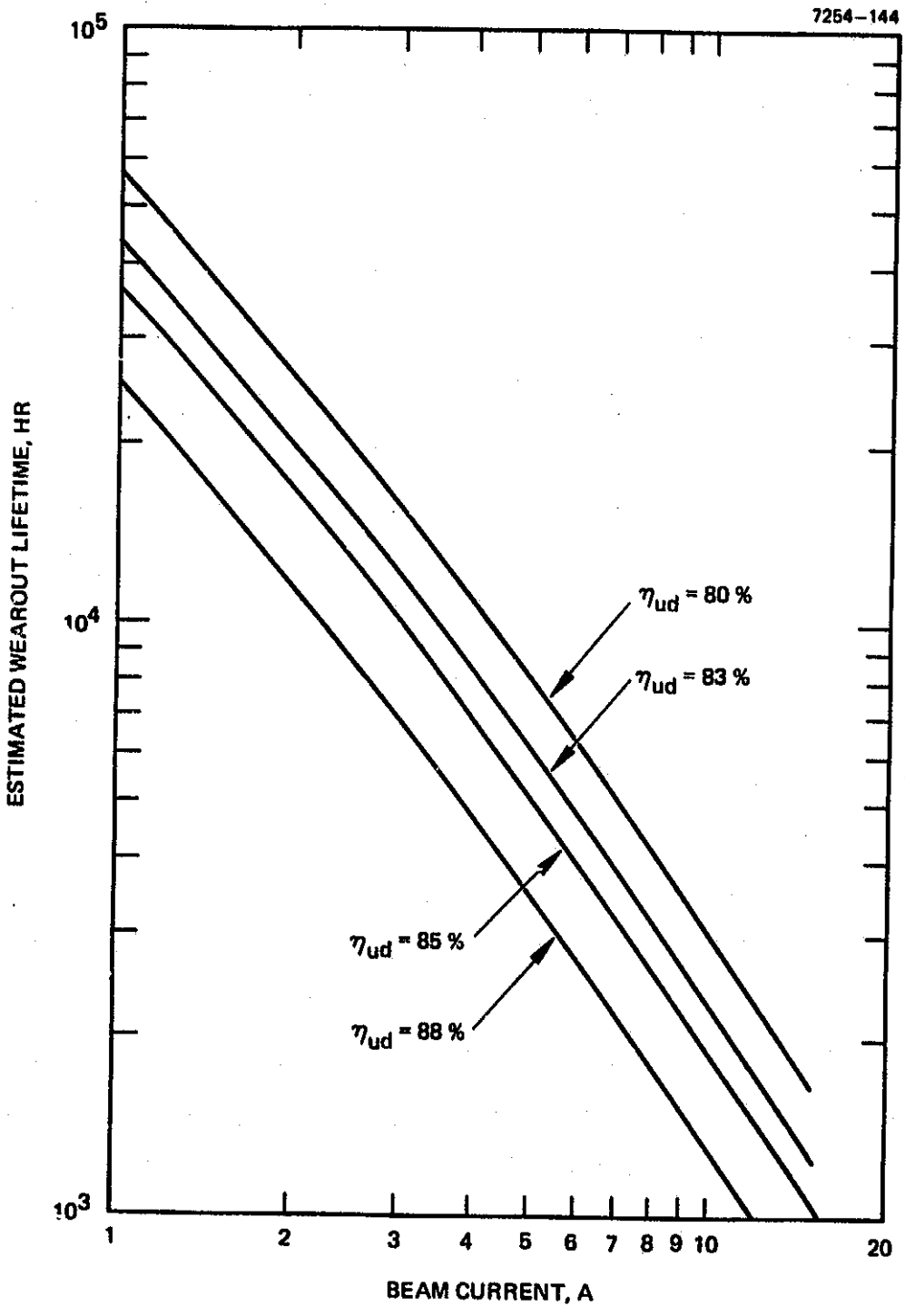

Figure 5-15. Estimated thruster wearout versus beam current, as a function of discharge utilization efficiency.

trends produced (as shown in Figure 5-15)should be valid. Consequently, the observation that a relatively small change in propellant utilization (5 percent) can produce a large change in screen grid wearout lifetime (100 percent) is considered valid (except for the absolute values of the changes).

It is useful at this point to consider the constraints placed on thruster design by the implications of Figure 5-15. If discharge chamber wearout lifetime is determined by the ion extraction screen thickness, unless the thruster configuration and operating characteristics are significantly changed, then Figure 5-15 can be used to restrict the relationship between beam current and beam diameter. Supposing that the wearout lifetimes shown in Figure 5-15 may be as much as a factor of two too low, the maximum beam current that can be considered practical for a minimal lifetime (3000 hr) is still only about 10 A. This limit is essentially independent of whether the propellant is argon or mercury, because the sputtering coefficients are essentially the same for both elements and doubly charged ions are formed in argon about as readily as in mercury. Extension of this limit would require new, advanced technology that is not directly identifiable from consideration of present 30-cm thruster development. Figure 5-16 shows the modifications of the beam-current/beam-diameter relationship with the current density limitation applied. The shaded areas of the charts are unavailable because the current densities required would not be consistent with lifetimes considered to be useful. The information in these relationships is applied as illustrated in the following example. If a given mission analysis indicated that a 40 A beam of argon ions at 2 kV beam voltage would be optimal for each thruster module, then Figure 5-16 indicates that the minimum beam diameter for useful lifetime would be 60 cm even though the ion optics could be designed to produce 40 A at 2 kV with a 50-cm-diameter beam.

E. THRUSTER SCALING

In the preceding sections, the factors that limit the power and thrust capacity of existing 30-cm mercury ion thrusters were discussed.

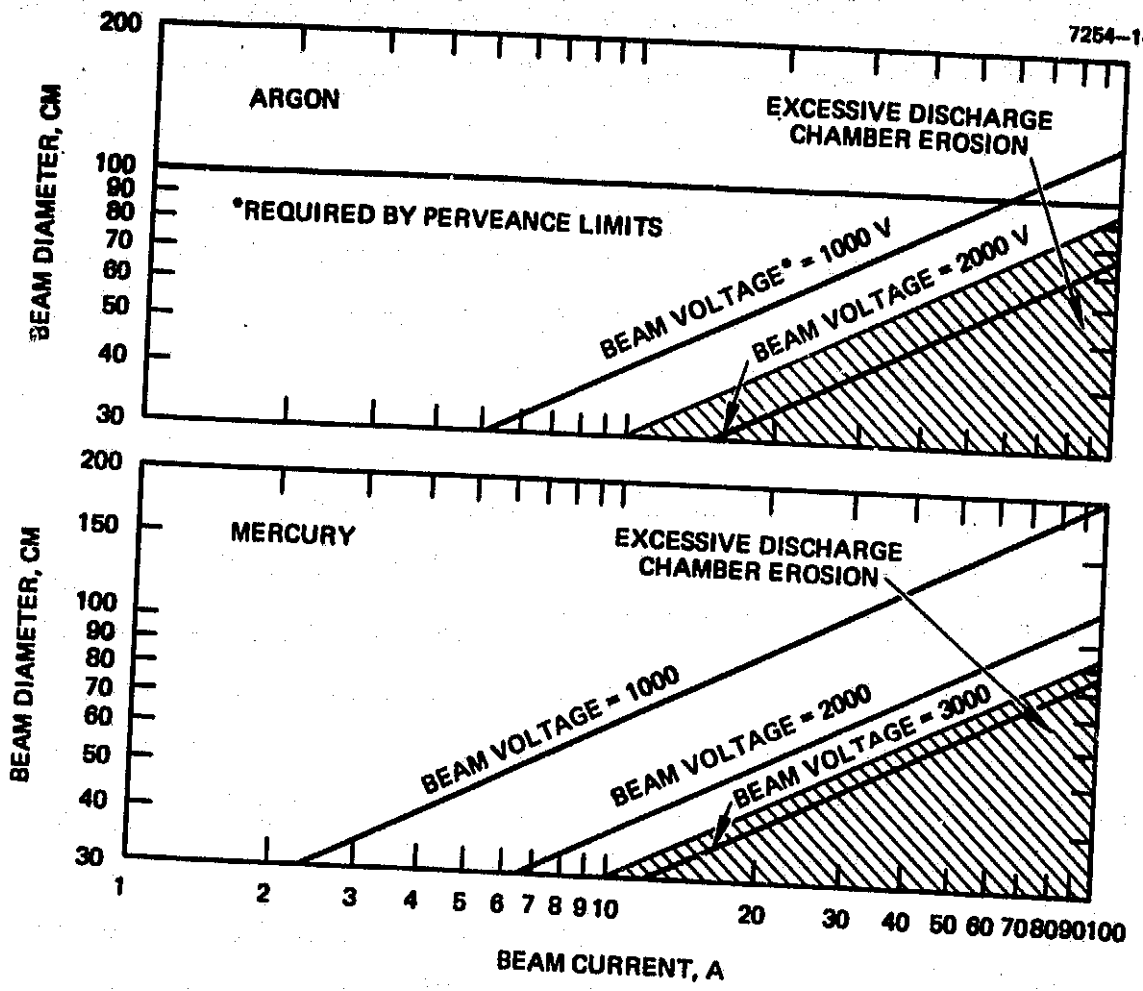

Figure 5-16. Beam diameter required to produce argon or mercury ion beams, including wearout limits.

It was shown that the upper limit on beam current is 10 or 15 A depending on whether wearout lifetime or thermal constraints are considered to be most important. For a mission of 125 days or more, screen grid wearout lifetime dominates and the current limit is 10 A. One option is to consider using several thruster modules with a single power processor to obtain the required lifetime. The ion optics thermal limit then becomes most important because any attempt to alleviate thermal problems in this component would constitute a major development task, whereas magnet temperature limitations might be alleviated by changes in magnet material or reduction of heat transfer to the magnets. Hence, 15 A would be the upper operational limit for a 30-cm-diameter thruster, based on the assumed ion optics thermal considerations. This limit is independent of propellant type or specific impulse since the discharge power input required per unit of beam current is essentially a constant and would be approximately 3 kW. Consequently, any improvement in 30-cm thruster capacity would have to address the problem of rejecting this order of thermal input without the temperature of the accelerating electrodes exceeding 700°C. An advanced concept 30-cm thruster would therefore depend on development of new technology capable of higher power density operation and designed specifically for heat rejection. Some of the fundamental requirements that can be predicted for specifying such a thruster concept are

- High specific impulse operation to permit adequate electrode thickness for heat rejection by conduction
- Improved beam and discharge plasma uniformity to distribute thermal inputs more evenly
- Incorporation of materials capable of higher temperature operation
- Efficient operation at low discharge voltage to minimize ion sputtering erosion.

Increasing the thruster beam area while keeping power (or thrust) densities at or below the limitations indicated above can be approached as an engineering problem rather than one requiring technology. As in

determining thruster limitations, the appropriate starting point in considering larger thruster modules is to examine the ion extraction system requirement.

One way to increase the beam area would be to increase the beam diameter. To maintain high current density at low beam voltage, the dimensions of the electrode thickness and interelectrode spacing must be kept as small as practical. This dimensional limitation implies the use of curved or dished electrodes to achieve mechanical stability. As discussed in Section 5.A.2, electrode curvature introduces a thrust loss because of non-axial beam trajectories. The technique used to vector the off-axis beamlets to "compensate" for electrode curvature approaches the direct interception limit at 30-cm beam diameter and therefore larger diameter thrusters might have to operate with uncompensated apertures at the periphery. Thrust losses resulting from this limitation were discussed in Section 5.A.2.b. An additional constraint to increasing beam diameter is the availability of electrode material. Molybdenum sheet is currently only available in widths up to 24 in. (61 cm), and at present no other material offers a viable substitute. Therefore, 50 cm is at present the practical fabrication limit on beam diameter.

F. PROPELLANT-TYPE CONSIDERATIONS

The 30-cm EMT has been developed primarily for operation using mercury as the propellant. It is a relatively straightforward matter to operate a thruster on other gases since the discharge mechanisms are not dependent on the mass or ionization potential of the gas used.[73,74] Performance characteristics are another matter, however, and the highly attractive characteristics of ion thrusters based on operation with mercury may not be maintained with an arbitrary choice of propellant. Because of the relatively large quantity of propellant required for some large earth orbital satellite applications ($\sim 10^6$ kg), an inert gas (e.g., argon) appears to be an attractive propellant possibility. The first consideration is the ionization potential: 15.75 V for argon as compared to 10.4 V for mercury. This means that more discharge energy goes into ionization of each argon ion and also that discharge voltage

must be higher to obtain the same number of ionizations per primary electron (cathode emitted). These facts present a trade-off between operating at increased discharge voltage (thereby increasing discharge chamber ion sputtering erosion) and limiting discharge voltage (thereby reducing propellant efficiency and increasing charge exchange ion sputtering erosion of the accel electrode). This trade in erosion rates will be assesed in more detail at a later time.

The mass of the argon atom is only 20 percent of the atomic mass of mercury, and therefore operation on argon implies higher specific impulse or higher power per unit of thrust. To approach the 30-cm EMT thrust and lifetime specifications (for mercury operation), an EMT design thruster operated on argon would have to be operated at a specific impulse of about 8000 sec and at a 12-kW power level (5500-V beam voltage at 2-A beam current). This power requirement could be prohibitive in some applications.

Next we consider some of the advantages and operational implications of using argon as the propellant. First, argon is a gas under anticipated operating conditions and no heaters or vaporizers are required for propellant supply. Flow rates can be accurately controlled using flow impedances and constant pressure regulators. This implies that thruster control must be established using only electrical parameters (not propellant flow) unless a variable flow impedance is developed. Thruster turn-on time can be essentially eliminated since no vaporizer warm-up is required. Because of reduced ionization efficiency, double ionization processes are not anticipated to be as important to thruster discharge chamber life in argon thrusters as in mercury thrusters. Thus, it may be possible to increase propellant utilization efficiency by increasing discharge voltage and yet maintain constant wearout life.

The more significant implication to advanced thruster technology, in so far as argon operation is concerned, is thruster lifetime and control. In applications where argon is nearly mandatory because of the quantity of propellant required, the number of thrusters will be large - even if the module size becomes significantly larger. Moreover, it

would be extremely desirable for an ion thruster to turn on and off with the simplicity of a fluorescent lighting fixture and to be capable of operating as long, or longer. Current hollow cathode technology provides long operating life but is relatively complex from the standpoint of cathode ignition and control. Advanced cathode technology has been investigated by personnel at NASA LeRC, Colorado State University, and HRL, but no results have been reported, at this time, that show possibilities of simplified long-life thruster operation on argon or other gaseous propellants. Thus, there is a clear opportunity for thruster/cathode technology innovation.

G. OPERATIONAL SIMPLIFICATIONS

The 30-cm mercury ion thruster, as presently developed, requires 12 power supplies, at least 8 of which are required to be more or less continuously variable in output. The 12 power supplies are

Variable output power supplies

- Beam or screen supply
- Discharge supply
- Accel supply
- Magnetic baffle coil supply
- Cathode vaporizer supply
- Main vaporizer supply
- Neutralizer vaporizer supply
- Neutralizer keeper supply

Fixed output power supplies

- Cathode tip heater supply
- Neutralizer cathode tip heater supply

- Isolator heater supply
- Cathode keeper power supply

Of the variable output power supplies, the only obvious possibility for simplification is the combination of beam and accelerator supplies. Feasibility of this combination was demonstrated under the 2.5-kW Advanced Technology Ion Thruster program (contract NAS 3-17831) during 1975. Similarly, all of the fixed power supplies listed, except the cathode keeper supply, are used only during start-up (or for very low power operation). Since the discharge power supply is variable and not in use during start-up until the heaters are no longer necessary, it can be used to supply heater power by appropriate heater design and interconnections of heaters. The power processor being developed for the 30-cm EMT uses the discharge supply for powering the isolator heaters prior to discharge ignition. This capability was also demonstrated during 1975 under the above-mentioned program for the cathode tip and the isolator heaters. Similarly, the cathode keeper discharge can be maintained after keeper ignition by using a dropping resistor from the anode, thereby eliminating the steady-state keeper supply requirement. The stability of the keeper discharge in this mode of operation has also been demonstrated for all anticipated transient conditions. Thus, it would be possible to eliminate one variable output and three fixed output power supplies without altering any of the steady-state control concepts now in use.

To identify further simplifications, it is appropriate to examine the function of each of the eight remaining power supplies as related to thruster operation requirements.

1. Beam (or Screen) Power Supply

This supply provides the voltage necessary to accelerate and focus the ion beam. It is operated as a constant-voltage supply with a current limit. Beam current is determined by discharge and vaporizer parameters.

2. Discharge Power Supply

This power supply ionizes the propellant and is operated as a constant current supply. Discharge current is an independent parameter determined by the beam current desired. Cathode propellant flow determines the discharge voltage.

3. Magnetic Baffle Coil Power Supply

This power supply excites the magnetic baffle coil and is an effective adjustment on the discharge voltage/cathode propellant flow characteristic. Variable output for this power supply is a convenience or flexibility option.

4. Cathode Vaporizer Heater Supply

This power supply provides cathode vaporizer propellant flow and its output is controlled in direct proportion to discharge voltage (closed loop), as compared with a reference voltage (independent parameter).

5. Main Vaporizer Heater Supply

This power supply provides main vaporizer propellant flow and its output is controlled in proportion to beam current (closed loop) and compared with a reference signal (independent parameter).

6. Neutralizer Keeper Power Supply

This power supply initiates and maintains the neutralizer hollow cathode plasma. The power supply is operated as a constant-current source with keeper current as an independent variable. Keeper power supply voltage varies with neutralizer vaporizer propellant flow rate. The neutralizer keeper current set-point is automatically changed when the beam current is turned off to maintain the total neutralizer emission current essentially constant.

7. Neutralizer Vaporizer Power Supply

This power supply provides neutralizer vaporizer propellant flow and is controlled in direct proportion to the keeper voltage (closed loop) in comparison to a reference voltage (independent variable).

8. Neutralizer Cathode Tip Heater

This power supply is used only during start-up periods to obtain initial neutralizer cathode ignition. Combining this function with the main cathode and isolator heater presents an insulation problem for steady state operation.

Finding further simplifications that would eliminate power supplies involves the defining of new control concepts or some loss of flexibility in parameter selection. For example, operation at a single beam current could reduce the discharge supply from a variable to a fixed-output power supply and reduce the complexity of the main vaporizer supply somewhat. Similarly, a thruster modification could eliminate the magnetic baffle coil requirements. Operation of the thruster with gaseous propellants would eliminate vaporizer power supplies.

SECTION 6

ADVANCED THRUSTER CONCEPTS

An initial objective of this study was to translate the thruster requirements defined by the mission studies into detailed hardware designs. However, the scope of the detailed design task was reduced to allow a greater emphasis on Earth orbit mission cost modeling. Although detailed designs were not developed, several advanced design options were considered. Three options are discussed in this section: (1) a 50-cm thruster scaled directly from the 30-cm EMT, (2) a 50-cm thruster using a new structural approach, and (3) an oval 30 x 90-cm thruster. Since these concepts were developed mainly for assessing first-order potential problems, the discussion is limited to describing salient features.

A. SCALED-UP 30-CM EMT CONCEPT

A 50-cm-diameter thruster concept, using the present 30-cm thruster components and structural approach, is shown in Figure 6-1. This particular diameter was chosen for several reasons:

- 50 cm is probably near the upper limit for straightforward ion optics development. Molybdenum sheets are currently available only up to about 60-cm widths. Thruster diameters larger than 50 cm would require expensive special mill runs or fabrication from joined sheets.
- Beam divergence thrust and efficiency losses start to become more important around 50 cm. If the grid radius of curvature must be maintained near that used for the 30-cm (50-cm radius), grid compensation cannot totally correct the divergence. Structural stability tests would be needed to establish confidence in a higher radius of curvature.
- Grid-to-grid hole alignment and spacing control become more difficult as the diameter increases.

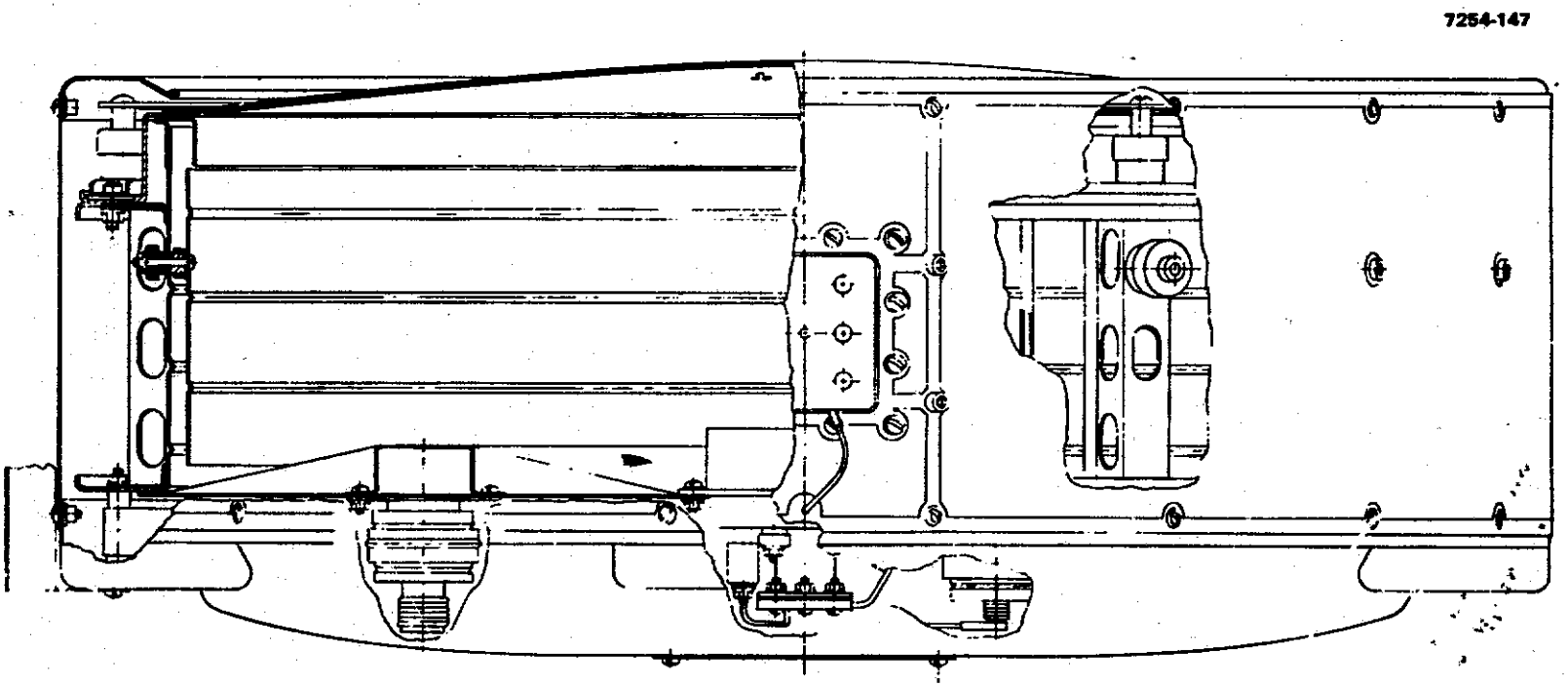

(a)

Figure 6-1. 50-cm-diameter thruster design scaled from 30-cm EMT: (a) side view, (b) front view.

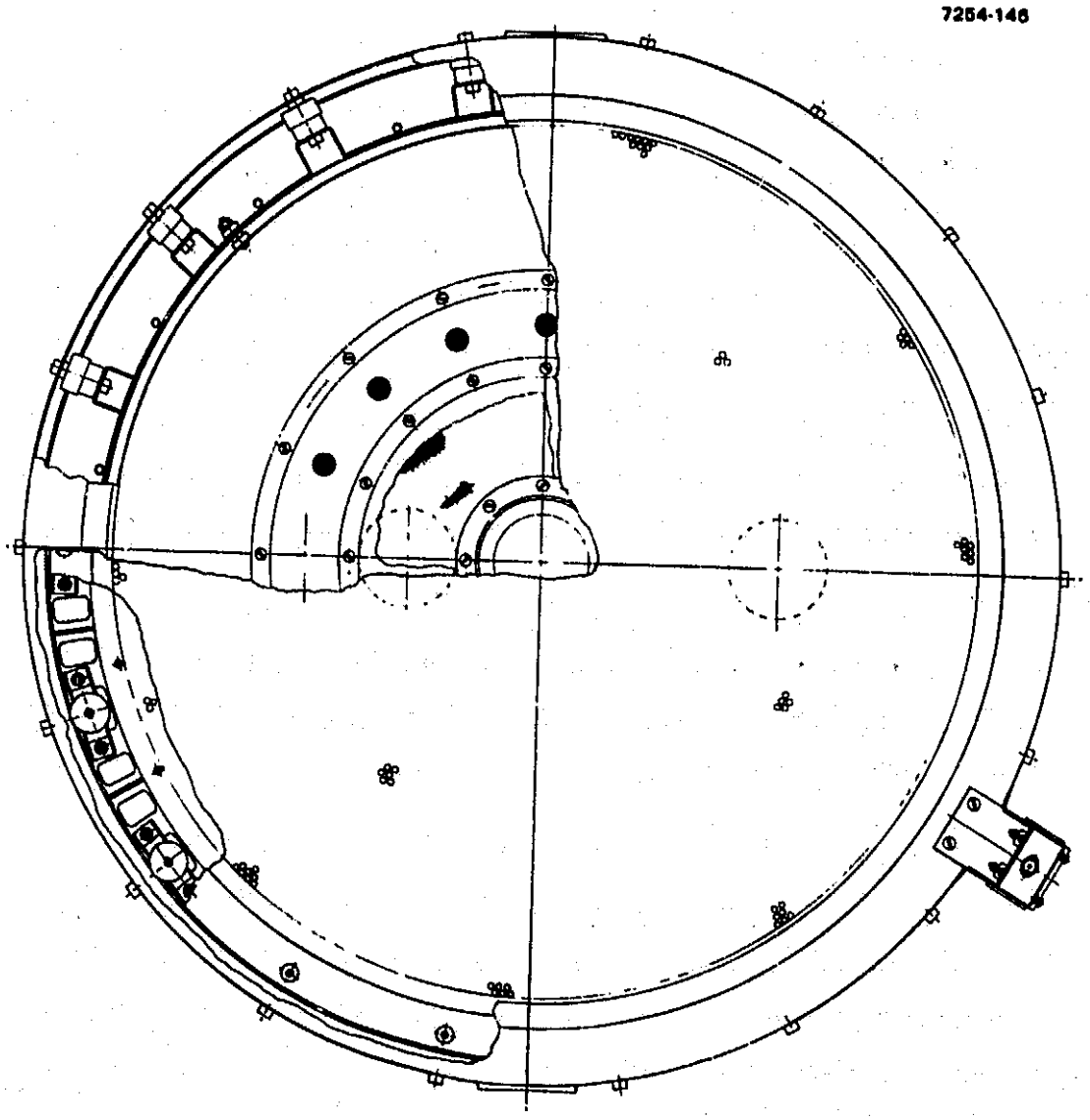

(b)

Figure 6-1. Continued.

- 50 cm is probably near the limit of high performance operation with a single cathode. At this size, plasma nonuniformity with a large central cathode might require extensive experiments for magnetic field shaping (e.g., cusped fields).

- A 50-cm thruster is in the region of interest for large vehicle missions in Earth orbit.

The design shown in Figure 6-1 utilizes the 30-cm thruster structural approach and the 30-cm thruster length. To a first approximation, the length need not be scaled since the neutral atom mean free path before ionization is less than the chamber length. Additional insulators and supports are provided for the optics and ground covers. With the two-point gimbal mount, the structure would probably require additional stiffening and thickness compared to the 30-cm design since loads are carried further. In addition, the fabrication tolerances and assembly procedures would be tighter than for the 30-cm thruster because of the greater difficulty of defining the ion beam axis relative to the gimbal pads.

The cathode and cathode pole shown are the 30-cm thruster design. The propellant plenum was arbitrarily placed at half the anode radius. Clearly, the final detailed designs of these and other parts would require prototype testing.

B. ADVANCED 50-CM THRUSTER CONCEPT

The 50-cm thruster design discussed in the previous section has several fabrication and structural weaknesses. The concept illustrated in Figure 6-2 should improve on these aspects of the design. Since a major portion of the thruster mass is associated with the optics assembly, use of the shell for structure is inefficient. By bridging around the shell at three locations, the optics loads can be transferred more directly to the gimbal mounts. In addition to improving the load path, the concept shown in Figure 6-2 simplifies the optics-gimbal tolerance problem.

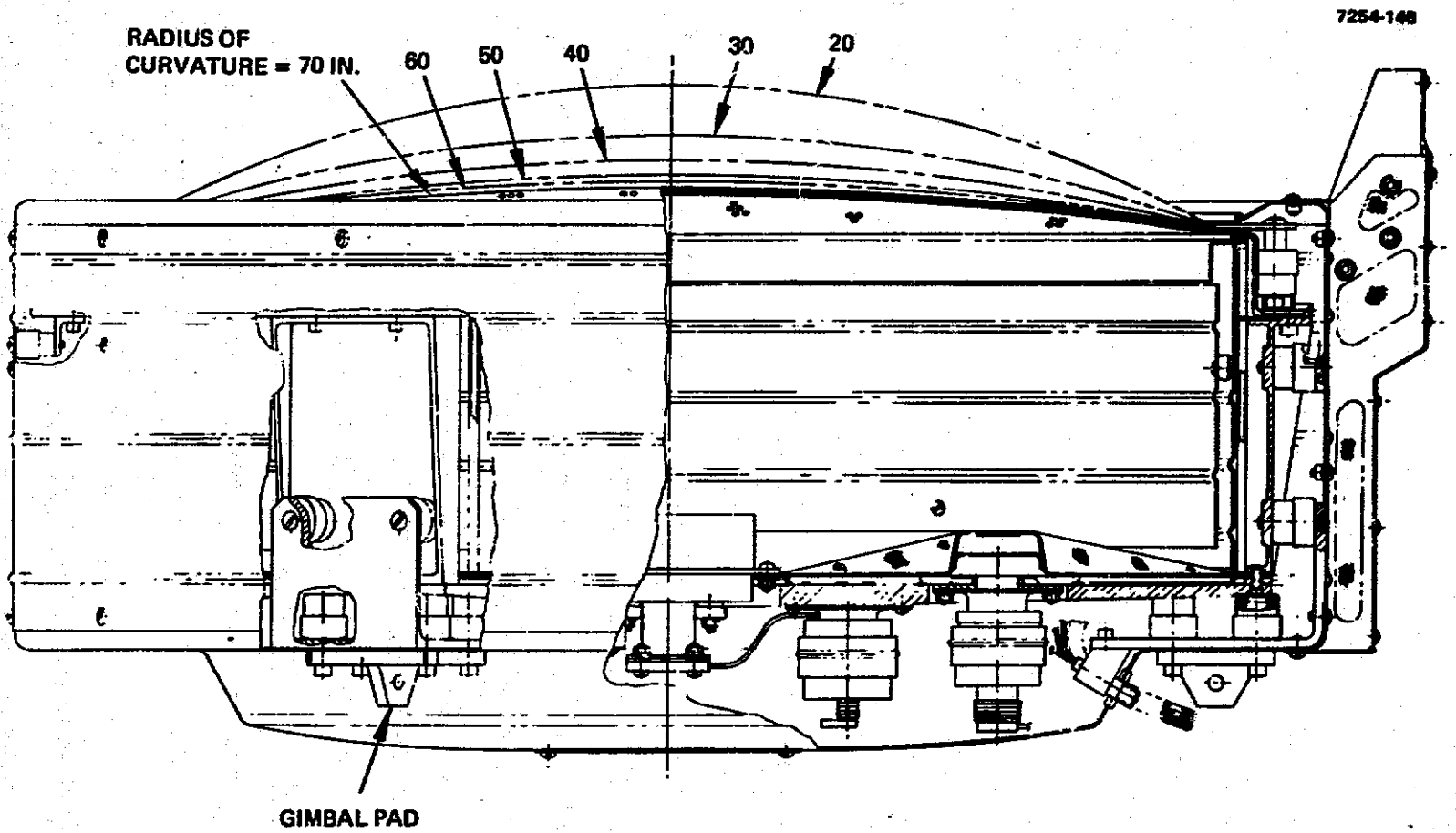

(a)

Figure 6-2. 50-cm diameter thruster design using new structural approach: (a) side view, (b) rear view.

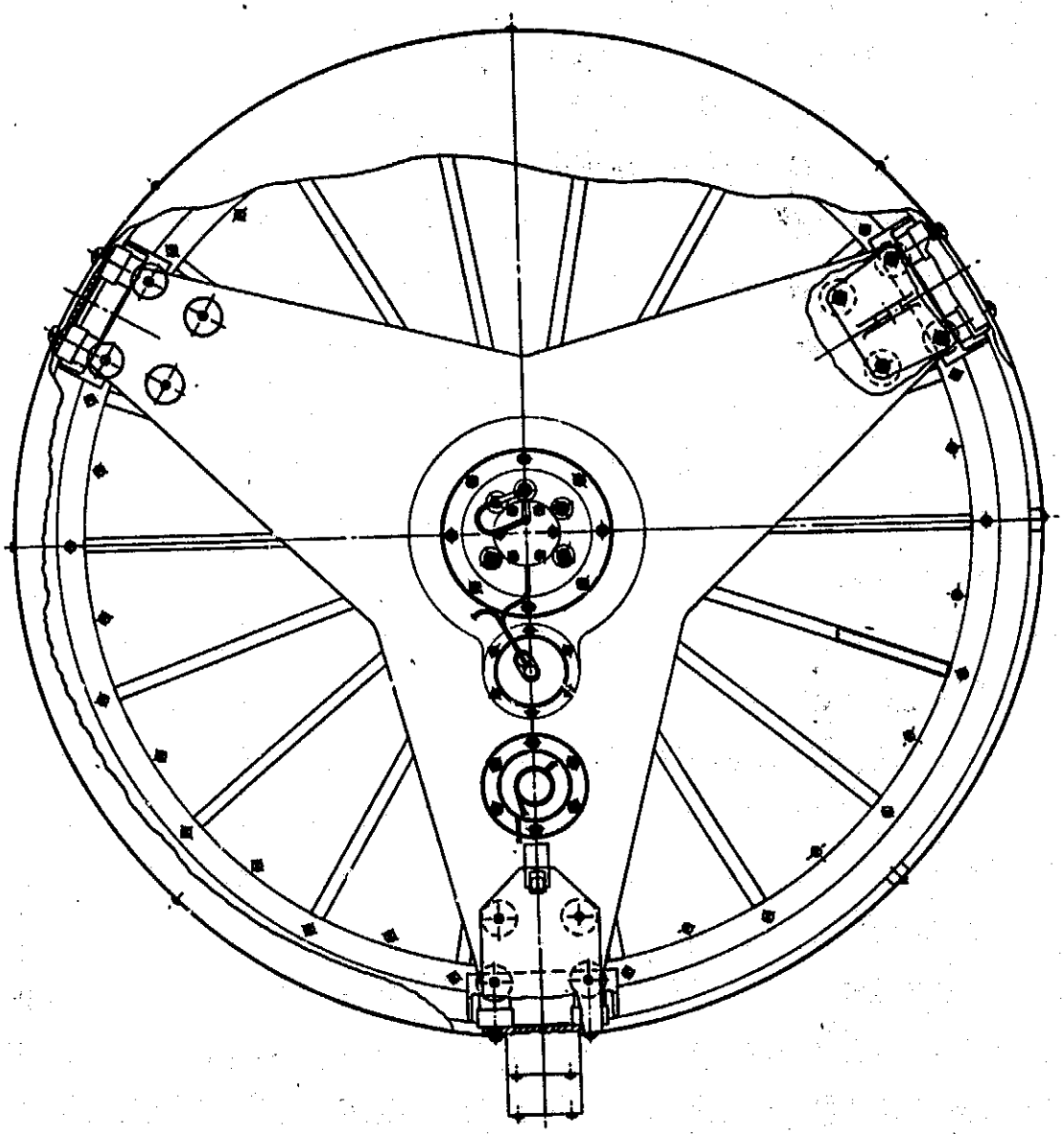

(b)

Figure 6-2. Continued.

The 30-cm EMT shell design resulted from a series of changes designed to make the thruster adequate dynamically without major redesign. However, if the shell design task were initiated anew, a concept more like that shown in Figure 6-2 would probably result. Avoidance of complex jigging, as currently required, should reduce assembly time and cost.

C. OVAL CROSS SECTION CONCEPT

An alternative to increasing the ion beam diameter is to increase the beam area by increasing one dimension only, thereby producing an oval cross section. An example of this approach is illustrated in Figures 6-3 and 6-4. The beam envelope becomes 30 cm x 90 cm and could be expected to perform at approximately three times the 30-cm thruster capacity with essentially the same lifetime and operational characteristics. Since molybdenum sheet is available in any desired length (at 60 cm widths), fabrication of the electrodes becomes a question of designing the proper hydroforming fixtures. Several main problems can be anticipated in developing such an advanced concept thruster:

- Achieving structural stability in the ion extraction electrodes and mounting assembly
- Achieving a relatively uniform discharge plasma in the elongated geometry
- Achieving adequate structural strength.

The structural questions present an engineering problem that is probably tractable if the weight constraints imposed are not too severe. The plasma uniformity problem is not so easily dismissed, however. The proposed solution to this problem makes use of two thruster cathodes and central propellant introduction. Integration and control of two hollow cathodes as shown represents a development task that has not been approached before; however, there should be no fundamental difficulty in such an approach. Solution of this problem will have to be primarily empirical because discharge modeling is not sufficiently analytical to permit design computations. Parameters to be explored would include:

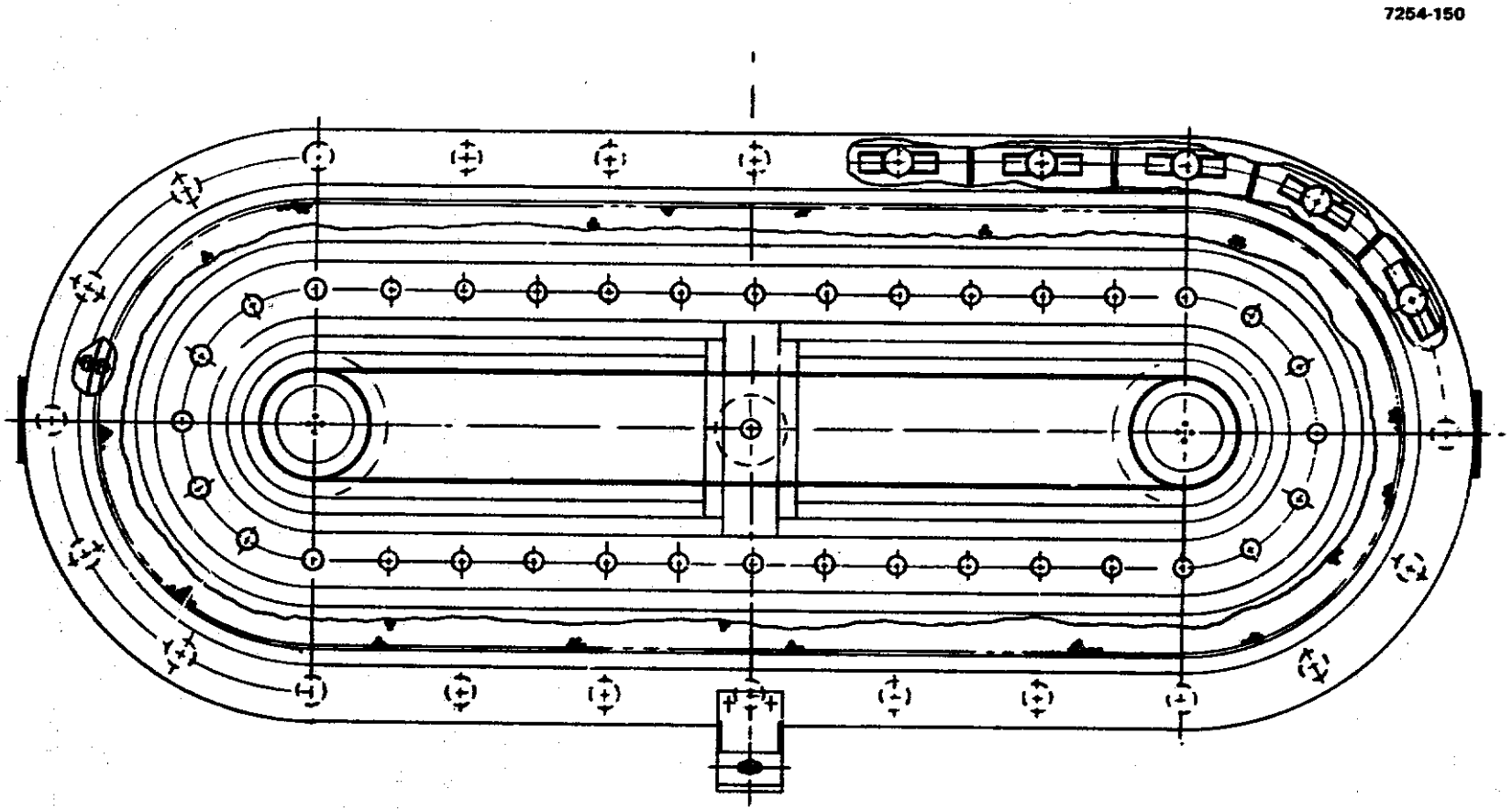

(a) DISCHARGE CHAMBER VIEW FROM FRONT

Figure 6-3. Oval, 30 x 90-cm thruster design.

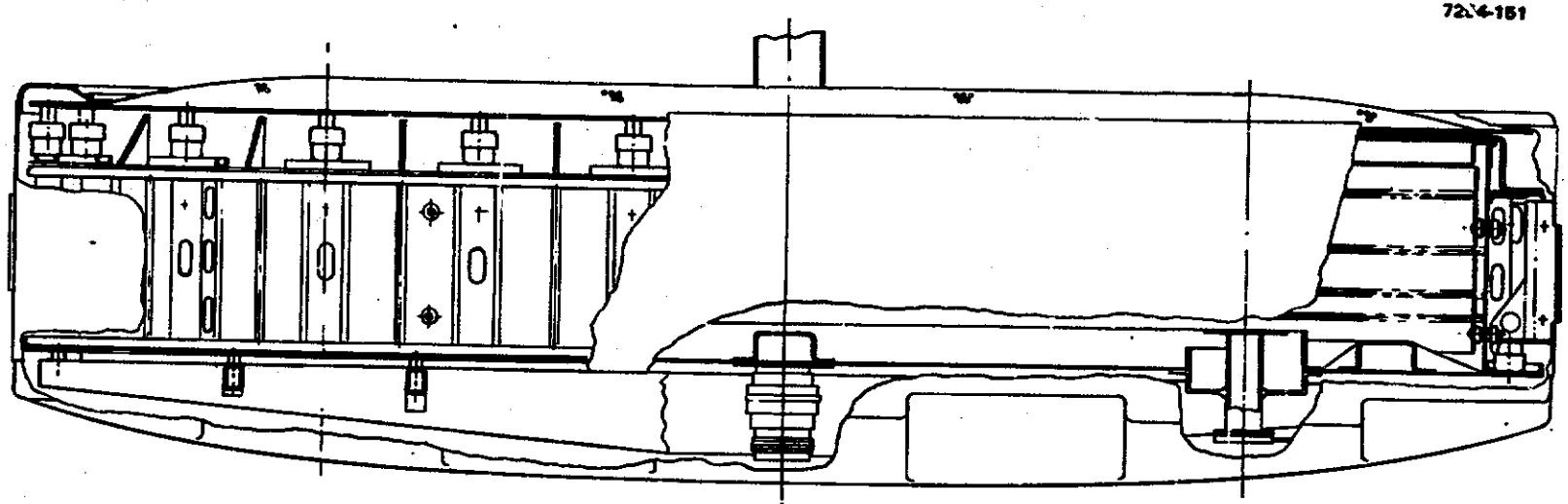

(b) SIDE VIEW

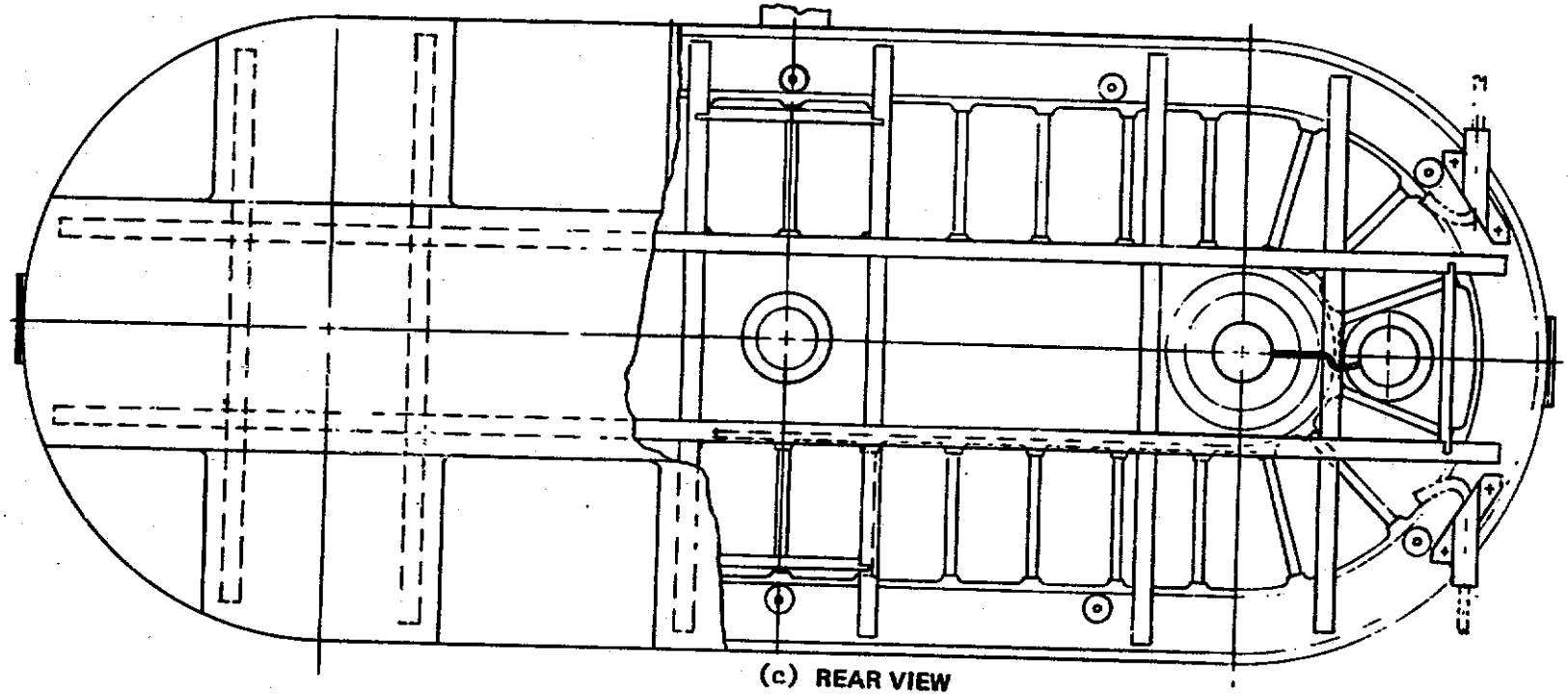

(c) REAR VIEW

Figure 4-3. Continued.

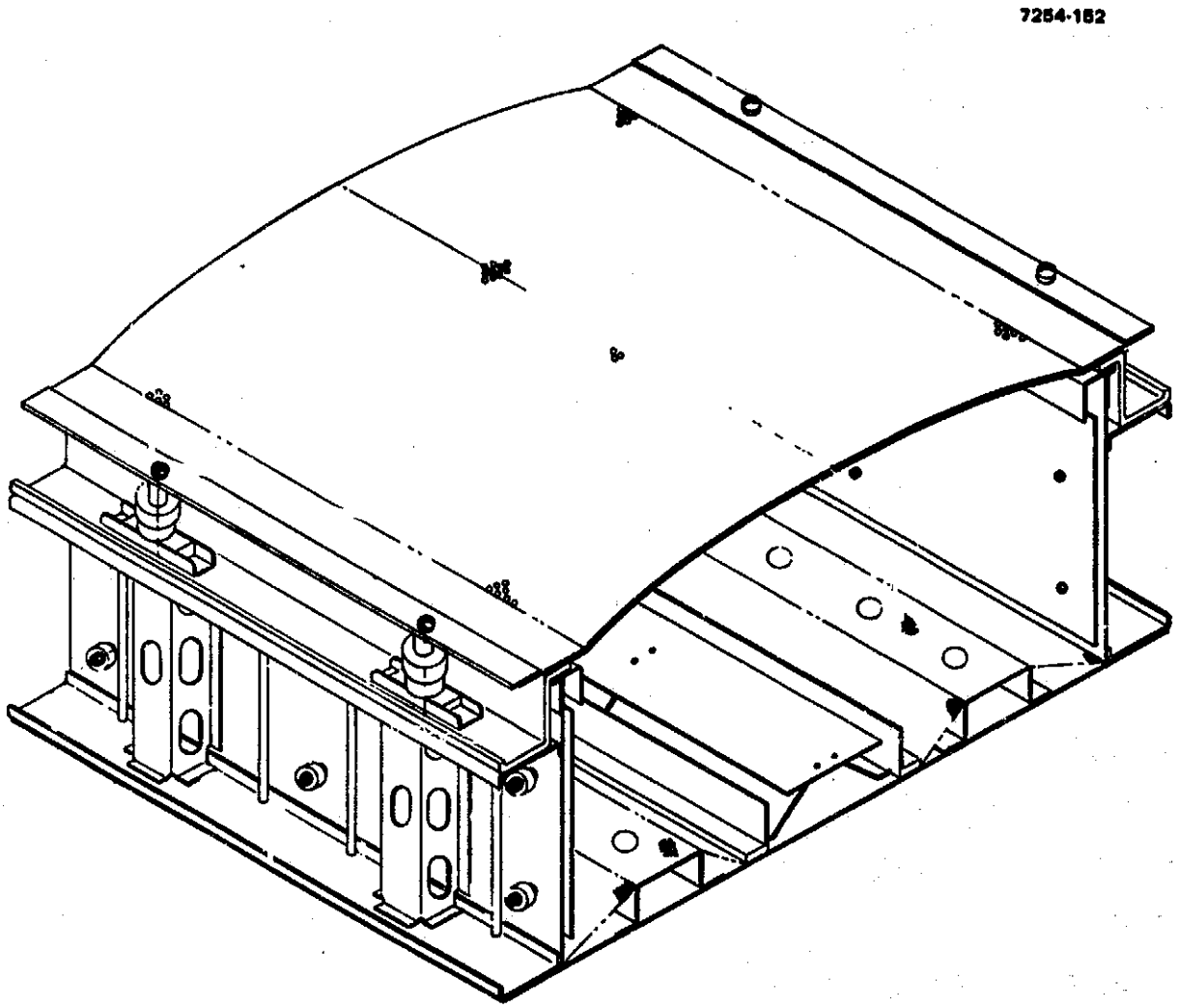

(d) ISOMETRIC CROSS SECTION VIEW

Figure 6-3. Continued.

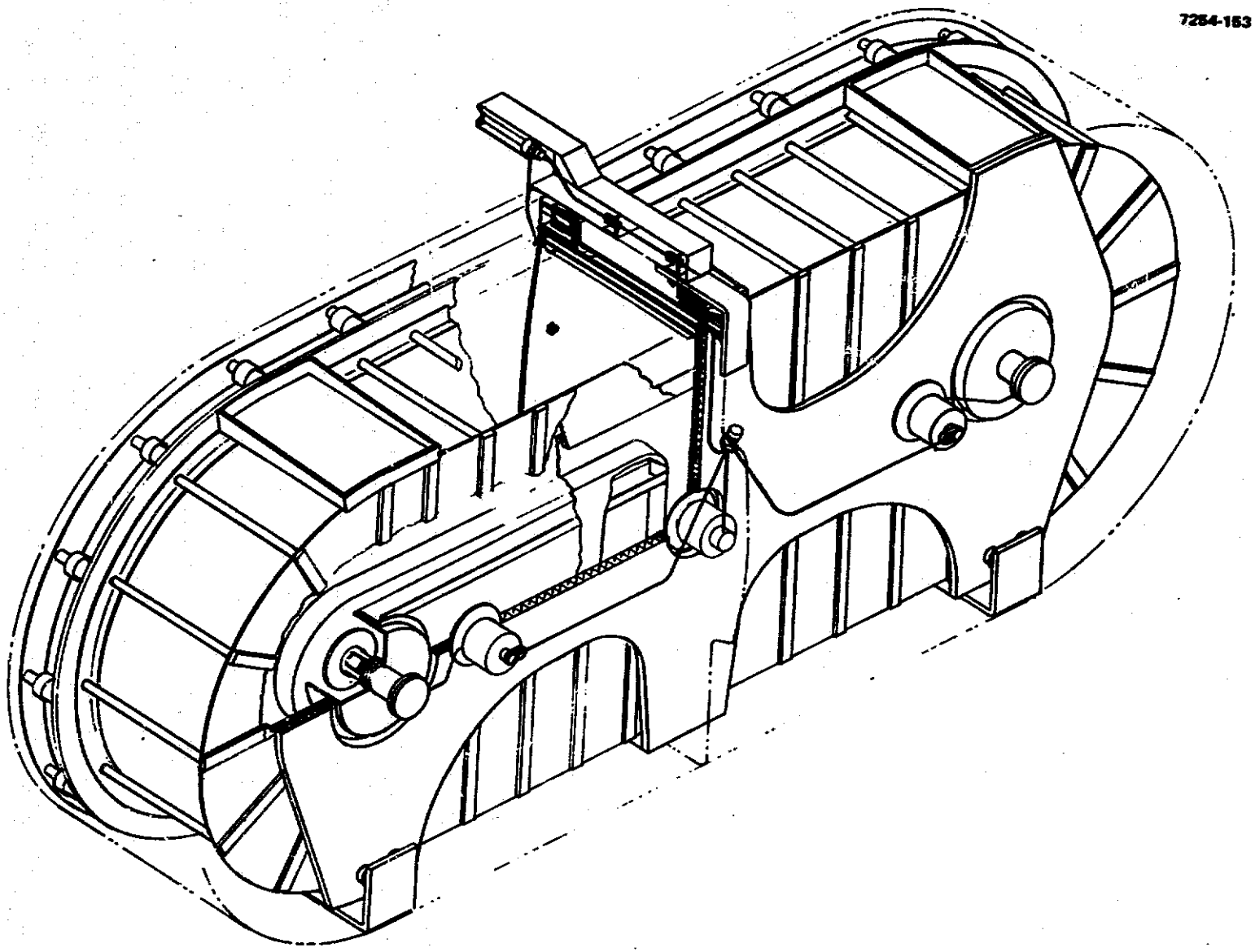

Figure 6-4. Isometric drawing of oval thruster design concept.

- Baffle size and shape
- Cathode location
- Pole piece geometry
- Propellant introduction
- Methods for controlling cathode propellant flow.

In the configuration shown in Figure 6-3, the magnetic field line geometry is still the divergent or SERT II type. Improved plasma uniformity has been obtained and reported by workers making use of boundary magnetic field geometries that have a cusped shape.[75,76] A single cusp configuration, as shown in Figure 6-5, is the most readily adapted to existing technology. In this configuration, the plasma volume is not entirely free of magnetic field, but improved plasma uniformity has been demonstrated. A multiple cusped geometry, shown in Figure 6-6, introduces considerably more complexity. Since the latter geometry might be operable with a single cathode, however, it cannot be ruled out a priori.

To examine some of the properties of an oval thruster in terms of EMT technology, two assumptions were made:

- An approximate thruster weight can be estimated by assuming that the weight of discharge chamber elements can be scaled in proportion to the circumference of the chamber, and that optics assembly and backplate weight scales in proportion to beam area.
- A plasma and beam current distribution can be established across the shorter beam dimension that matches the radial density distribution of a 30-cm thruster.

Given these assumptions, the scaled thruster mass would be about 2.4 times that of the 30-cm EMT, and the beam area ratio would be 3.55 times that of the 30-cm EMT. If one assumes a uniform beam current density, then the larger thruster could provide 7 A beam current with a lifetime of greater than 10^4 hr or a maximum beam current of 53 A for shorter lifetime.

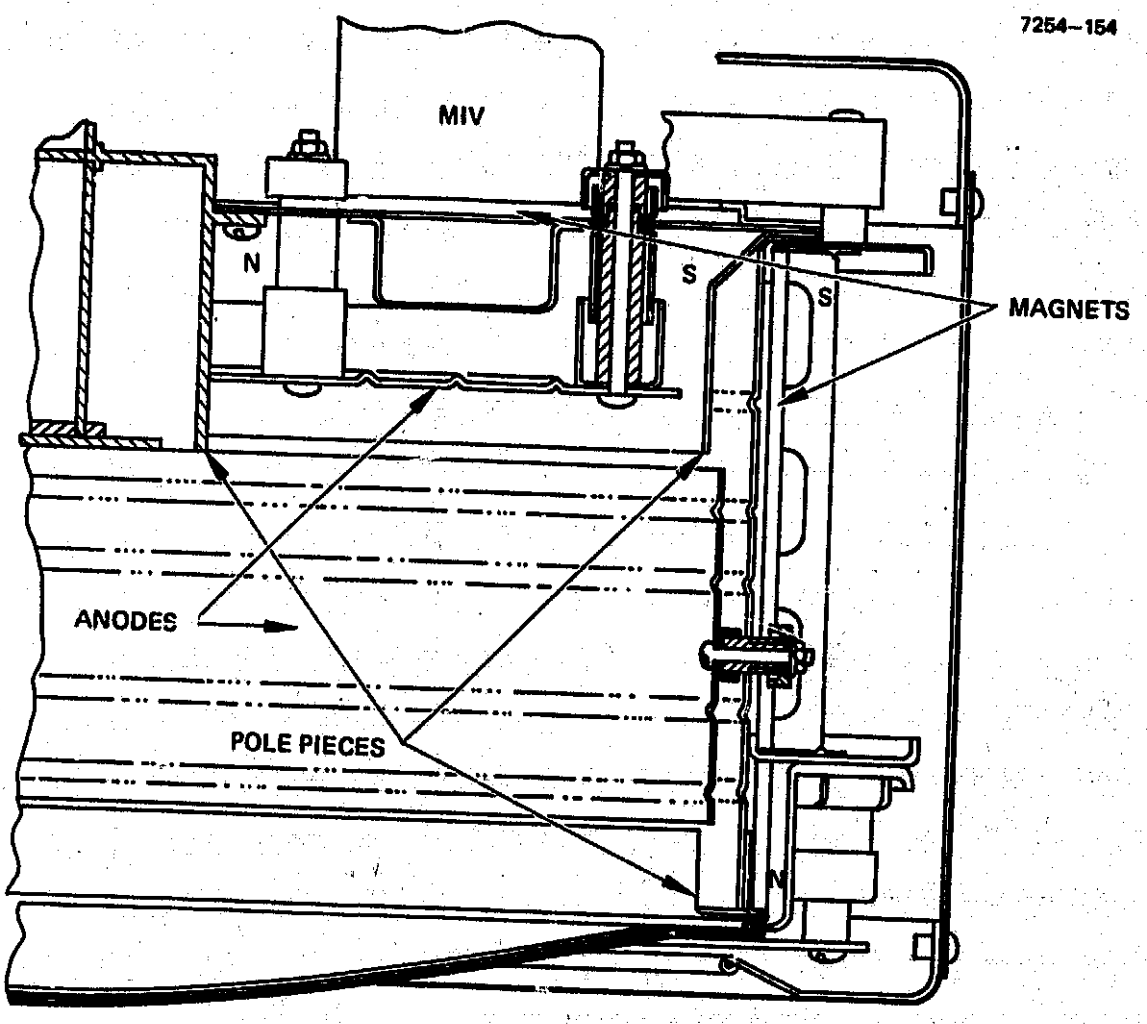

Figure 6-5. Single cusp magnetic field discharge chamber configuration.

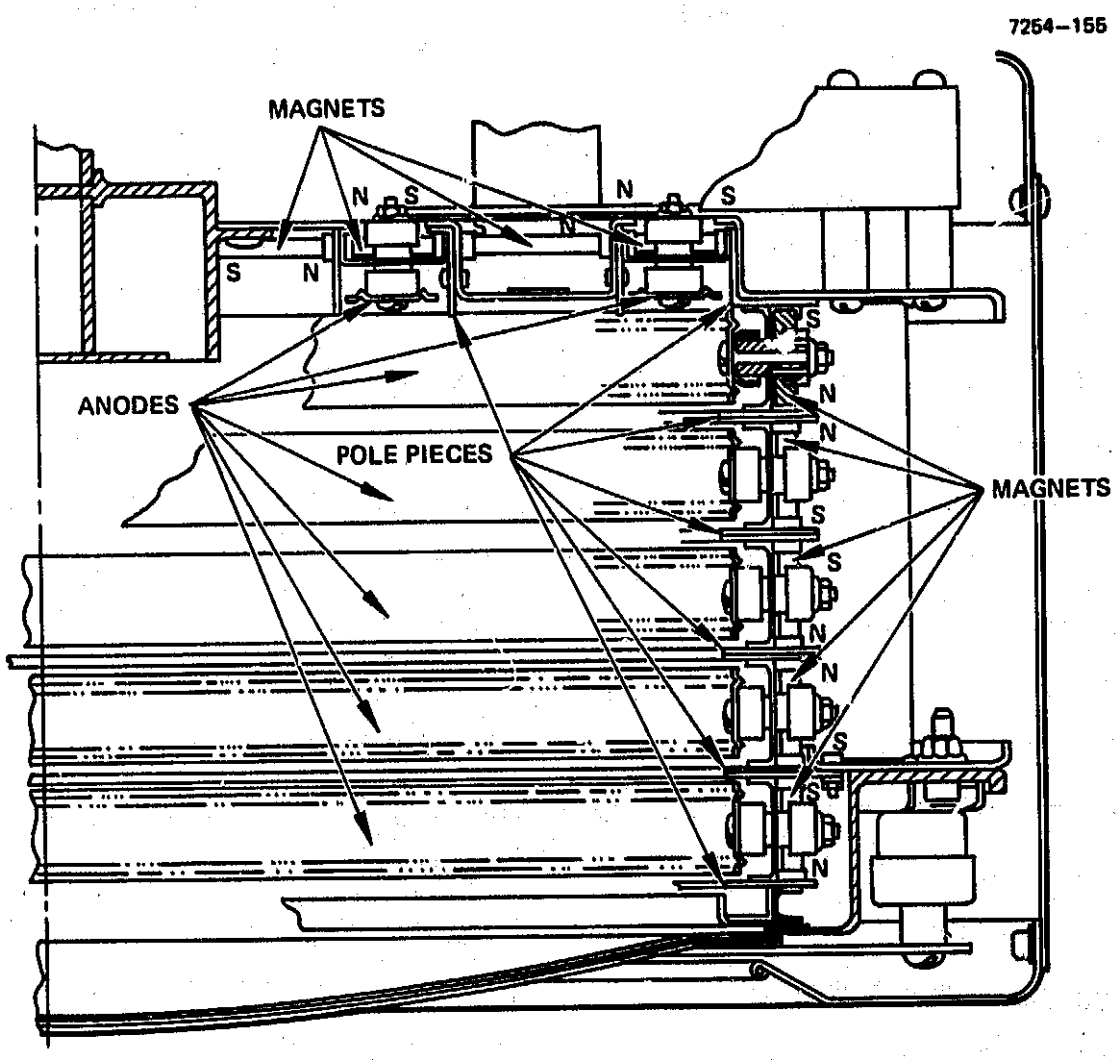

Figure 6-6. Multiple cusp magnetic field discharge chamber configuration.

If one assumes a current distribution that has the form

$$j(r) = j_o \cos \frac{\pi r}{D} ,$$

then the current capacity for the oblong thruster would be about 4.5 times that of the EMT, and, consequently, the thruster could provide 9-A beam current with greater than a 10^4-hr lifetime or a maximum beam current of 67 A for shorter periods. Thus, the scaled oval thruster configuration would have the following specifications:

- Thruster mass 18.5 kg
- Beam current 9 A (average)
- Beam current 67 A (maximum)
- Lifetime 10^5 (A-hr).

Preliminary assessment of the thermal characteristics of the "stretched" thruster shows no basis for estimating significant differences since the primary thermal process, radiation through the screen grid, has been scaled directly by area. Consequently, providing that discharge current and plasma density distributions can be established as assumed above, the scaled thruster configurations would have component temperatures essentially the same as those of the EMT. For an EMT-type magnetic confinement geometry, this may be a rather pessimistic assumption, and the cusped configurations may be more realistic for achieving a satisfactory plasma distribution in the oval geometry.

The cusped magnetic geometries may offer more promise for establishing a satisfactorily uniform plasma distribution, but they will also carry a weight penalty. We estimate that the additional anode and polepiece required for a single cusp geometry would add 1.2 kg (6%) to the thruster assembly.

Assuming a periodicity every 2.5 cm for the multiple cusp geometry, 6.5 kg (35%) additional weight would be added to the thruster. Since the 6.5 kg increase in weight could require heavier structural elements to satisfy launch requirements, this is probably a low estimate. Consequently, the single cusp may be the most promising alternative.

The most critical single element in this "stretched" configuration design is considered to be the ion optics assembly. The concerns are more practical than fundamental in that a fabrication process is required for manufacturing electrodes in the oblong shape with sufficient conformality that uniform interelectrode spacings can be achieved. Conceivably, the processes now used for hydroforming and chemically milling the circular, dished-grid electrodes can be adapted; however, this supposition remains to be demonstrated. Similarly, the electrode mounting structure becomes more vulnerable to distortion in the oblong configuration, and that possibility also affects the ability to achieve satisfactory interelectrode spacing. These two elements are the major concerns for increasing the longer dimension of the "stretched" thruster. If low I_{sp} (close grid spacing) is not a requirement, then the degree of difficulty is lessened. If these unproven factors can be adequately handled, the long dimension of the oval thruster can be extended or shortened to match thruster module requirements with a minimal impact on thruster design and performance characteristics.

An additional factor that should be mentioned is reliability. Although the oval concept may require multiple cathodes for best performance, operation with a failed cathode would be possible. Performance would probably be degraded with a failed cathode (e.g., one failed out of three), but mission options should be better relative to having a completely failed module.

SECTION 7

STUDY CONCLUSIONS

The most significant products of this work are the cost modeling methodology developed for Earth orbit missions, the generalized analysis approach for planetary missions, and the technology assessment results. Specific conclusions relative to the selection of an advanced thruster concept were also developed. These specific conclusions are important and necessary, but their value depends greatly on the input assumptions. Although the assumptions and resulting conclusions may be changed by additional study, the analysis tools developed here should provide a straightforward means of evaluating the assumption/conclusion relationship.

Earth orbit mission cost modeling results produced several reasonably clear conclusions. Under most conditions, module power is the key thruster parameter in producing low-cost transportation and on-orbit propulsion. The upper bound on module power is not a hard boundary, but thruster development considerations will probably restrict the power level to about 100 kW. Depending on the mission, thruster wearout life is the next most important parameter. When refurbishment is not included, wearout life is quite significant in the overall system cost picture. Other thruster parameters initially thought to be important (e.g., mass, unit cost, redundancy) appear to have only second-order effects on total cost. Power processor and power source parameters strongly influence total cost and should be carefully considered in selecting a vehicle design.

After evaluating the cost sensitivity of the transportation and on-orbit missions to a wide range of parameters, a 50-cm-diameter thruster was suggested. This thruster, operated at a beam voltage of about 2400 V, would satisfy a wide range of Earth orbit missions. For large systems (SPS size), the 50-cm thruster could be operated on argon with a beam power of about 100 kW. For somewhat smaller vehicles, xenon could be used effectively with a beam power of about 50 kW.

The generalized mission analysis approach was used to evaluate a broad range of planetary and small-body missions. For most of these missions, the existing 30-cm thruster is a good choice. However, payload performance for Encke's comet, Earth observatory, asteroid rendezvous, asteroid sample return, and out-of-the-ecliptic missions would be improved by higher thruster beam current. Beam currents of 4 A or more would significantly reduce the number of modules, reduce the propulsion system specific mass, and increase payload. This characteristic is similar to the module power dependence discussed previously. The primary difference between the Earth orbit and planetary missions is specific impulse. Planetary missions tend to demand lower specific impulse (e.g., 3000 sec) for high performance. Lighter and cheaper power sources would tend to remove this constraint and add some flexibility to increasing module power.

Several thruster design options were considered for thrusters in the 50-cm range. In addition to a simple scaling of the conventional circular cross section, an oval-shaped thruster was suggested. The oval cross section may increase the scaling range without significantly increasing the total technology effort.

SECTION 8

REFERENCES

1. K. L. Atkins, "U.S. Solar Electric Propulsion Planetary Mission Candidates: Out-of-Ecliptic, Small Bodies, and Orbiters of Mercury and Saturn," (JPL) NAS-7-100, III EEPC No. 74-243, October, 1974.

2. K. L. Atkins, "Mission Applications of Electric Propulsion," AIAA Paper No. 74-1085, AIAA/SAE 10th Propulsion Conf., San Diego, Calif., Oct. 21-23, 1974.

3. C. G. Sauer and K. L. Atkins, "Potential Advantages of Solar Electric Propulsion for Outer Planet Orbiters," AIAA Paper 72-423, AIAA 9th Electric Propulsion Conf., Bethesda, Md., April 1972.

4. Jet Propulsion Laboratory, "Solar Electric Multi-Mission Spacecraft (SEMMS), Phase A Final Report No. 617-4, March 17, 1972.

5. TRW Systems Group, "Study of a Solar Electric Multi-Mission Spacecraft," Final Report No. 09451-6001-RO-03, March 15, 1970.

6. TRW Systems Group, "Study of a Common Solar-Electric Propulsion Upper Stage for High Energy Unmanned Missions," Final Report No. 16552-6006-RO-00, July 14, 1971.

7. Rockwell International, "Feasibility Study for a Solar Electric Propulsion Stage and Integrated SEP Spacecraft," Final Report No. SD 72-SA-0011, March 27, 1972.

8. Rockwell International, "Extended Definition Feasibility Study for a Solar Electric Propulsion Stage," Final Report No. SD 73-SA-0177.

9. Rockwell International, "Concept Definition and Systems Analysis Study for a Solar Electric Propulsion Stage," Report No. SD 74-SA-0176, Feb., 1975.

10. Boeing Aerospace Co., "Concept Definition and Systems Analysis Study for a Solar Electric Propulsion Stage," Report No. D180-18553, Jan., 1975.

11. Boeing Aerospace Co., "Payload Utilization of SEPS," Final Report No. D180-19783-X, July, 1976.

12. Northrop Services, Inc., "Mission Roles for the Solar Electric Propulsion Stage (SEPS) with the Space Transportation System," Final Report on Contract NAS8-30742, 1975.

13. K. L. Atkins and C. Terwilliger, "Ion Drive: A Step Toward 'Star Trek'," AIAA Paper No. 76-1069, AIAA Inter. 12th Electric Propulsion Conf., Nov., 1976.

14. Hughes Aircraft Co., "Extended Performance Solar Electric Propulsion Thrust System Study," Final Report on Contract NAS 3-20395, Sept., 1977.

15. IIT Research Institute, Reports produced Under JPL Contract No. 952701, "Support Analysis for Solar Electric Propulsion Data Summary and Mission Applications," 1971/

16. D. R. Bartz and J. L. Horsewood, "Characteristics, Capabilities, and Costs of Solar Electric Spacecraft for Planetary Missions," AIAA Paper No. 69-1103, AIAA 6th Annual Meeting and Technical Display, Oct. 1969.

17. Hughes Aircraft Co., "Solar Powered Electric Propulsion Spacecraft Study," Final Report on JPL Contract 951144, Dec., 1965.

18. "Future Space Transportation Systems Analysis," Boeing Aerospace Co., Final Report on Contract NAS 9-14323, 1975.

19. "Space Based Solar Power Conversion and Delivery Systems Study," Grumman Aerospace Corp., Final Report on Contract NAS 8-31308, 1976.

20. "Space-Based Power Conversion and Power Relay Systems," Boeing Aerospace Co., Final Report on NAS 8-31628, 1976.

21. H. Davis, "Orbital Transportation in the 1980's and Beyond," AAS No. 75-141, 21st Annual Meeting - Space Shuttle Missions of the 80's, August, 1975.

22. "Outlook for Space," A Synopsis Report to the NASA Administrator, prepared by the Outlook for Space Study Group, January, 1976.

23. K. L. Atkins, private communication regarding Mars sample return mission, employing SEP, Oct., 1977.

24. R. O. Bartlett and F. J. Ceppolina, "The Multimission Modular Spacecraft for the '80's," AAS Paper No. 75-235, 21st Annual Meeting of the American Astronautical Society, August, 1975.

25. J. H. Duxbury, "Interplanetary Spacecraft Design Using Solar Electric Propulsion - A Circular 1.0 au Out-Of-The Ecliptic Mission," III EEPC Paper No. 74-242, October, 1974.

26. J. H. Duxbury and R. C. Finke, "A Candidate Mission Using The Shuttle and Solar Electric Propuslion," AAS Paper No. 75-163, 21st AAS Conf., August, 1975.

27. H. Meissinger, "Use of a Small SEP Spacecraft for High Inclination Extra-Ecliptic Mission."

28. W. Strack and F. Hrach, "Early Application of Solar Electric Propulsion to a 1-au Out-of-The Ecliptic Mission," AIAA Paper 78-1118, 8th Electric Propulsion Conf., Stanford, 1970.

29. E. Dazzo and R. Nagorski, "Trajectory Analysis for SEPS Planetary Missions," AIAA, 10th Electric Propulsion Conference, No. 73-1058, October 31 - November 2, 1973.

30. "A Study of Modifications to the Pioneer Venus Spacecraft for the Mercury Orbiter Mission," Hughes Aircraft Company, No. D6909, Contract No. 954556 (JPL), August, 1976.

31. V. Clark, Jr., personal communication regarding trajectories, for Mercury Orbiter, June, 1976.

32. L. Allen and P. Odom, "Evaluation of Comet and Asteroid Missions Potential of the Current SEP Stage Concept," AIAA 10th Electric Propulsion Conference, No. 73-1060, October 31 - November 2, 1973.

33. "Study of a 1980 Comet Encke-Asteroid Mission Using a Spin-Stabilized Spacecraft," Martin Marietta Corporation, NASA CR-114671, October, 1973.

34. J. Driver, "Encounter Trajectory Design for SEP Rendezvous with Low Mass Celestial Bodies," III EEPC, 72-424, prepared under JPL Contract NAS-7-100, October, 1974.

35. D. Bender and R. Bourke, "Asteroid Rendezvous Missions," 12th Colloquium of the IAU-Physical Studies of the Minor Planets, March, 1971.

36. A. Masay and J. Niehoff, "Sample Return Missions to the Asteroid Eros," 12th Colloquium of the IAU-Physical Studies of the Minor Planets, March, 1971.

37. H. Meissinger and E. Greenstadt, "Design and Science Instrumentation of an Unmanned Vehicle for Sample Return from the Asteroid Eros," 12th Colloquium of the IAU-Physical Studies of the Minor Planets, March, 1971.

38. J. Niehoff, "An Assessment of Comet and Asteroid Missions," AAS 17th Annual Meeting - The Outer Solar Systems, AAS 71-104, June, 1971.

39. "A Study of the Solar Electric Slow Flyby of Comet Encke in 1980," JPL, 760-90, January 25, 1974.

40. P. E. Hong, G. L. Shults, and R. J. Boain, "System Design Impact of Guidance and Navigation Analysis for a SEP 1979 Encke Flyby," AIAA Paper 73-1061, 10th Electric Propulsion Conf., October, 1973.

41. C. Sauer, Jr., "Trajectory Analysis and Performance for SEP Comet Encke Missions," AIAA 10th Electric Propulsion Conference, No. 73-1059, October 31 - November 2, 1973.

42. D. Bender and R. Bourke, "Multi-Asteroid Comet Missions Using Solar Electric Propulsion," III EEPC, (JPL) NAS-7-100, No. 72-429, October, 1974.

43. T. D. Masek, R. L. Poeschel, and C. R. Collett, "Evolution and Status of the 30-cm Engineering Model Ion Thruster," AIAA Paper 76-1006, AIAA Inter. Electric Prop. Conf., Nov., 1976.

44. J. J. Biess, L. Y. Inouye, andA. D. Schoenfeld, "Power Processor for the 30-cm Mercury Electric Propulsion Engine," AIAA Paper 76-992, AIAA Inter. 12th Electric Propulsion Conf., November, 1976.

45. R. V. Elms and L. E. Young, "SEP Full-Scale Wing Technology Program," IECEC Paper 779222, 12th Inter. Energy Conv. Engr. Conf., Wash. D.C., August, 1977.

46. V. A. Caluori, "Photovoltaic Solar Power Satellites," IECEC Paper 779231, 12th Inter. Energy Conv. Engr. Conf., Wash. D.C., August 1977.

47. T. D. Masek, "Solar Electric Propulsion Breadboard Thrust System Test Results," AIAA Paper No. 72-507, 9th Electric Prop. Conf., April, 1972.

48. B. G. Herron, J. Hyman, and D. J. Hopper, "Development of an 8-cm Engineering Model Thruster System," AIAA Paper 76-1058, AIAA Internat. 12th Electric Propulsion Conf., November, 1976.

49. D. J. Kerrisk, "Electric Propulsion System Design and Development for Primary Propulsion Applications," III EEPC Paper 74-219, October, 1974.

50. "A System Design Study of an Atmospheric Entry Probe for an Outer Planet Mission," Hughes Aircraft Proposal to NASA LRC, HAC Reference No. 76(44)-17131/D6358, October, 1976.

51. "Planetary Mission Summaries: Vol. 1 - Introduction and Overview," JPL, NASA CR 147093, August, 1974.

52. "Pioneer Jupiter Orbiter/Probe," Hughes Aircraft Study of Modified Pioneer Venus, Report No. 56284, June 24, 1975.

53. "Pioneer Jupiter Orbiter With Entry Probe, PJOP," TRW, NAS-2-8532, 31 March, 1975.

54. "Titan Exploration Study (Science, Technology, and Missing Planning Options)," Hughes Aircraft Company Proposal No. 75(44)-02146/D4669, February 7, 1975.

55. "Advanced Propulsion Comparison Study, Phase II, Planetary Program Evaluations," JPL, April 4, 1972.

56. "Mariner Encke 1980 Study Report," JPL, 660-7, June 20, 1975.

57. C. Cohen, "Requirements and Considerations in Selecting Space Tug Propulsion Systems," AAAS No. 75-160, 21st Annual Meeting - Space Shuttle Missions of the 80's, August, 1975.

58. "Shuttle Performance Curves," Informal Communication from JPL, June 1977.

59. R.L. Poeschel, and R.P. Vahrenkamp, "Performance Mapping of a 30-cm Engineering Model Thruster," AIAA Paper 75-342, AIAA Inter. 11th Electric Prop. Conf., March, 1975.

60. R.P. Vahrenkamp, "An Experimental Investigation of Multiple Ion Processes in Mercury Bombardment Thrusters," AIAA Paper 75-397, AIAA Inter. 11th Electric Prop. Conf., March 1975.

61. R. R. Peters, P. J. Wilbur, and R. P. Vahrenkamp, "A Doubly Charged Ion Model for Ion Thrusters," AIAA Paper No. 76-1010, Key Biscayne, Fla., November, 1976.

62. R. P. Vahrenkamp, "Characteristics of a 30-cm Thruster Operated with Small Hole Accelerator Grid Ion Optics," AIAA Paper No. 76-1030, Key Biscayne, Fla., November, 1976.

63. J. L. Power, "Solutions for Discharge Chamber Sputtering and Anode Deposit Spalling in Small Ion Thrusters," AIAA Paper No. 75-399, New Orleans, La., March 1975.

64. M. A. Mantenieks and V. K. Rawlin, "Sputtering Phenomena of Discharge Chamber Components in a 30-cm Diameter Hg Ion Thruster," AIAA Paper No. 76-988, Key Biscayne, Fla., 1976.

65. "Solar Cell Space Manual," Centralab, Semiconductor Products, Electronics Division, Globe Union, Inc.

66. H. R. Kaufman, "Technology of Electron-Bombardment Ion Thrusters," Advances in Electronics and Electron Physics, Vol. 36, Academic Press, San Francisco, 1974.

67. N. B. Kramer and H. J. King, "Extraction of Dense Ion Beams From Plasmas," J.A.P. 38, 10 p. 4021, September, 1967.

68. M.J. Mirtich and W.R. Kerslake, "Long Lifetime Hollow Cathodes for 30-cm Mercury Ion Thrusters," AIAA Paper No. 76-985, Key Biscayne, Fla., 1976.

69. Hughes Research Labs, "High Power and 2.5 kW Advanced Technology Ion Thruster," NASA CR-135,163, Feb, 1977.

70. J. Oglebay, "A Thermal Analytic Model of a 30 cm Engineering Model Mercury Ion Thruster," AIAA Paper 75-344, New Orleans, La., March, 1975.

71. S. G. Askerov and L. A. Sena, "Cathode Sputtering of Metals by Slow Mercury Ions," Soviet Physics - Solid State 11, 1288 (1969).

72. C. R. Collett and R. L. Poeschel, "A 10,000 Hour Endurance Test of a 700 Series 30-cm Engineering Model Thruster," AIAA Paper No. 76-1019, AIAA Inter. 12th Electric Prop. Conf., November, 1976.

73. J. S. Sovey, "A 30-cm Diameter Argon Ion Source," AIAA Paper No. 76-1017, AIAA Inter. Electric Prop. Conf., November, 1976.

74. D. C. Byers and P. D. Reader, "Operation of an Electron Bombardment Ion Source Using Various Gases," NASA TN D-6620, 1971.

75. W.D. Ramsey," 12 Centimeter Magneto-Electrostatic Containment Argon/Xenon Ion Source Development," AIAA Paper No. 78-681, AIAA Inter. Electric Prop. Conf., April, 1978.

76. G.R. Longhurst and P.J. Wilbur, "Multipole Mercury Ion Thruster," AIAA Paper No. 78-682, AIAA Inter. Electric Prop. Conf., April, 1978.

SECTION 9

DEFINITIONS AND NOMENCLATURE

A. ABBREVIATIONS

SEP	=	solar electric propulsion
EMT	=	engineering model thruster
LEO	=	low Earth orbit
GEO	=	geosynchronous Earth orbit
ORV	=	orbit raising vehicle
OOP	=	on-orbit propulsion system
LS	=	large space system era
MS	=	matured shuttle era
OR	=	orbit raising
OO	=	on-orbit
ORS	=	orbit raising self-powered
ORP	=	orbit raising payload powered
ORO	=	orbit raising one way trip
PS	=	propulsion system
AU	=	astronautical unit
PPU	=	power processing unit

B. PROPULSION SYSTEM PERFORMANCE

I_{sp}	=	True specific impulse (corrected for multiply charged ions, beam divergence, and propellant utilization efficiency)
T	=	thrust
P_{ps}	=	propulsion system input power (after degradation)
P_{pp}	=	power processor input power
P_t	=	thruster input power
P_j	=	total propulsion system jet power
P_{mod}	=	thruster beam power (jet power)
P_{tot}	=	total installed power (before degradation)
I_b	=	beam current
I_n	=	neutral flowrate equivalent current
V_b	=	beam voltage
m_i	=	ion mass

g_o	=	gravitational constant
e	=	electronic charge
E_j	=	ion beam jet energy
v_i	=	ion velocity
v	=	average beam velocity
η_{ps}	=	propulsion system total efficiency
η_t	=	thruster total efficiency
η_{pp}	=	power processor efficiency
η_c	=	cabling efficiency
η_{pd}	=	power source degradation factor
η_u	=	thruster measured propellant utilization efficiency
η_e	=	thruster electrical efficiency
η_1	=	mass fraction of singly charged ions
η_2	=	mass fraction of doubly charged ions
γ	=	thrust loss of efficiency correction parameter
β	=	parameter defined by Eq. 3-32
μ	=	atomic mass unit
W	=	atomic weight
λ	=	atomic weight ratio
AH	=	ampere-hours
A_o	=	vehicle initial acceleration
ΔV	=	vehicle velocity change associated with trajectory
C_3	=	launch energy parameter
t_f	=	mission propulsion time
L_t	=	thruster life
ω	=	thruster life parameter, Eq. 4-20
D	=	thruster beam diameter
TOTRIP	=	orbit raising mission round trip propulsion time
I_{eq}	=	equivalent 30-cm thruster beam current
I_{mod}	=	beam current associated with a single thruster module
P	=	perveance for an electrode design
P_a	=	perveance for a single aperture
V_t	=	total accelerating voltage
V_a	=	accelerator voltage

N_a	=	number of apertures
C_1	=	ion optics parameter defined by Eq. 5-5
ℓ	=	ion optics dimension
ℓ_g	=	screen grid to accelerator grid spacing
d_s	=	screen grid aperture diameter
d_a	=	accelerator grid aperture diameter
S	=	aperture center-to-center spacing
t_s	=	screen grid thickness
t_a	=	accelerator grid thickness
J(r)	=	beam current density as a function of radius r
J_o	=	beam current density on centerline
R	=	"R" ratio defined by Eq. 5-11
C_{tot}	=	ion optics aperture "total compensation"
$C(\ell_g)$	=	compensation required to correct for grid curvature
$C(\alpha)$	=	compensation required to correct for aperture offset
α	=	electrode curvature semi-angle at edge
θ_{net}	=	beam vectoring angle
Δ_{net}	=	aperture offset distance
r_o	=	radius parameter used in defining beam current profile
ϕ_{max}	=	beam maximum vectoring angle allowable without direct interception
d	=	grid dish depth
T_e	=	electron temperature
n_e	=	electron density
F_{ij}	=	thermal model parameter, Eq. 5-23
A_i	=	thermal model parameter, Eq. 5-23
e_j	=	thermal model parameter, Eq. 5-23
P_{dis}	=	discharge power
P_{sc}	=	screen grid heating power by plasma
P_{back}	=	back plate heating power by plasma
P_{anode}	=	anode heating power by plasma
P_{lost}	=	power radiated through apertures
q_r	=	total power radiated from thruster
K_1, K_2	=	constants, Eq. 5-28
K_3	=	constant, Eq. 5-29

K_4 = constant, Eq. 5-30

A_b = beam area

T_{max} = maximum allowable temperature

q = number of particles eroded per unit area by ion sputtering

j, j_+, j_{++} = ion current density

S_+, S_{++} = sputtering coefficients

C = constant used in Eq. 5-34

K = constant used in Eq. 5-35

N = allowable material loss in atoms per unit area

τ = lifetime used in Eq. 5-36

C. MASS DEFINITIONS

M_o = vehicle initial mass

M_f = vehicle final mass

M_p = propellant mass (general analysis)

$\dot{M}_p$ = propellant mass flowrate

$M_{p\ell}$ = payload mass

M_{ps} = propulsion system mass

MF = payload mass fraction, Eq. 3-5

MFR = required payload mass fraction

M_{sp} = satellite net mass

M_{oop} = on-orbit vehicle mass

M_{rt}, M_{ot} = thruster unit mass

M_{orp}, M_{op} = propellant mass

M_{rpt}, M_{opt} = propellant tankage mass

α_{rpt} = propellant tankage fraction of propellant

M_{rpp}, M_{opp} = power processor mass

α_{pp} = power processor specific mass

M_{rw}, M_{ow} = power source mass

M_{rss}, M_{oss} = subsystems mass

M_{rsm}, M_{osm} = structure and mechanisms mass

α_{sm} = structure and mechanisms mass fraction

α_{ps} = propulsion system specific mass

R_t = thruster redundancy

R_p = power processor redundancy

N_{ot} = number of thrusters (with redundancy)

N_{op} = number of power processors (with redundancy)

N_{mod} = number of operating modules (thrusters)

N_{ow} = number of thrusters required by wearout

T_{used} = mass of thrusters worn out during one round trip

D. COST DEFINITIONS

C_{or} = total orbit raising cost

C_{oef} = ORV utilization cost factor

C_l = ORV hardware cost

C_{rt}, C_{ot} = cost of thrusters

C'_{rt} = thruster unit cost

C_{orp}, C_{op} = propellant cost

C'_{orp} = propellant cost per unit mass

C_{rpt}, C_{opt} = propellant tankage cost

C'_{rpt} = tankage cost per unit mass

α_{pt} = tankage factor

C_{rpp}, C_{opp} = cost of power processors

C'_{rpp}, C'_{opp} = power processor unit cost

C_{opf} = flight operations fixed cost

C_{opt} = flight operations time dependent cost

C_ℓ = launch cost to LEO

C'_ℓ = launch cost per unit mass

r = interest rate

C_{rsm}, C_{osm} = structure and mechanisms cost

C_{rss}, C_{oss} = subsystems cost

C_{rw}, C_{ow} = power source cost

C'_{rw} = power cost per unit power

C_{ori}, C_{oi} = ORV integration and testing

C'_{ori}, C_{oi} = integration cost per unit of ORV or OOP dry mass

C_{ord} = cost of design, development, test, and evaluation (DDT&E)

C'_{ord} = DDT&E cost coefficient

α	=	learning curve parameter, Eq. 4-30
N_r	=	number of ORV's over which DDT&E costs are amortized
C'_{rss}	=	subsystems cost coefficient
C'_{rsm}	=	structure and mechanisms cost coefficient
C_{oop}	=	cost of on-orbit propulsion
C_{to}	=	transportation cost, earth to final orbit
C'_{to}	=	transportation cost per unit mass
C_{ops}	=	on-orbit operations cost
C'_{ops}	=	operations cost per unit time

APPENDIX A

DOCUMENT LIST

The following document list was provided by NASA LeRC as an initial guide in mission selection and analysis. Although most of these reports were consulted in the course of the study, not all were used directly. Reports referenced directly in the text were presented in Section 8.

1. Future Space Transportation Systems Analysis Study Space Program Optics and Transportation Requirements Interum Report 11 December 1974 Contract NAS9-14323

2. Outlook for Space - A Forecast of Space Technology 1980-2000 NASA 15 July 1975

3. Orbital Transportation in the 1980's and Beyond H. P. Davis paper no. AAS 75-141

4. Requirements and Considerations in Selecting Space Tug Propulsion Systems C. J. Cohan AAS Paper no. 75-160

5. Preliminary Technology Assessment Satellite Power System Concepts W. B. Lenoir and R. E. Currie, Jr., February 1975

6. Mission Roles for the Solar Electric Propulsion Stage (SEPS) with the Space Transportation System Northrup Services, Inc. Final Review Presentation, January 1975 NAS8-30742

7. Solar Electric Propulsion Thrust Subsystem Description JPL TM 701-209, 1 February 1975

8. Concept Definition and System Analysis for Solar Electric Propulsion Stage Vols. 1-5, Boeing, NAS8-30921, January 1975

9. A Study of the Solar Electric Slow Flyby of Comet Encke in 1980 JPL TM 760-90 Rev. A, 25 January 1974

10. Interplanetary Spacecraft Design Using Solar Electric Propulsion - A Circular 1.0 AU Out-of-the-Ecliptic Mission
J. H. Duxbury (JPL) NAS7-100
III EEPC Paper no. 74 - October 1974

11. U. S. Solar Electric Propulsion Planetary Mission Candidates: Out-of-the-Ecliptic, Small Bodies, and Orbiters of Mercury and Saturn
K. L. Atkins (JPL) NAS7-100
III EEPC Paper no. 74-243 October 1974

12. Mission Applications of Electric Propulsion
K. L. Atkins, AIAA Paper no. 74-1085 October 1974

13. Cometary Exploration: A Case for Encke
K. L. Atkins and J. W. Moore, AIAA Paper no. 73-596
10 July 1973

14. Solar Electric Spacecraft for the Encke Slow Flyby Mission
J. H. Duxbury, AIAA Paper 73-1126, November 1973

15. A Study of the Compatibility of Science Instruments with the Solar Electric Propulsion Space Vehicle
JPL TM 33-641 15 October 1973

16. Feasibility Study for a Solar Electric Propulsion Stage and Integrated SEP Spacecraft
NAS8-27360, 18 January 1973 and 27 March 1972

17. Thermoelectric Outer Planets Spacecraft (TOPS) Advanced Systems Technology Project
JPL TM 33-589 1 April 1973

18. Solar Electric Propulsion System Integration Technology (SEPSIT)
JPL TM 33-583, 15 November 1972, Vol. 1, 2, 3

19. Solar Electric Propulsion/Instrument Subsystems Interaction Study
TRW NAS2-6940 Final 30 March 1973 and Mid-Term 19 September 1972

20. Solar Electric Multimission Spacecraft (SEMMS) Phase A
JPL 617-2, 30 July 1971 and 617-4 3 March 1972

21. Study of a Common Solar-Electric-Propulsion Upper Stage for High-Energy Unmanned Missions
Vol. 1, 2, 3, TRW NAS2-6040 14 July 1971

22. Feasibility Study for a Multi-Mission Electric Propulsion Spacecraft (Pioneer Concept)
TRW NAS2-6287, 18 June 1971

23. Study of a Solar Electric Multi-Mission Spacecraft, Vol. 1A, 1B, 11 TRW, JPL Contract 952394, 15 March 1970

24. Solar Electric Propulsion Asteroid Belt Mission Study
JPL Vol. 1 5070-21-1, Vol. 11 5070-21-2, Vol. III 5070-21-3
JPL Contract 952566 19 January 1970

25. 1975 Jupiter Flyby Mission Using a Solar Electric Spacecraft
JPL ASD 760-18, 1 March 1968

26. Evaluation of Comet and Asteroid Missions Potential of the Current SEP Stage Concept
AIAA Paper no. 73-1060, L. C. Allen and P. R. Odom, 31 October 1973

27. Solar Electric Propulsion Mission and Spacecraft Capabilities for Outer Planet Exploration
K. L. Atkins and J. H. Duxbury AIAA Paper 75-1158

28. A Candidate Mission Using the Shuttle and Solar Electric Propulsion
J. L. Duxbury and R. C. Finke, AAS Paper no. 75-163, 26 August 1975

29. System Definition for "Cometary Explorer," Goddard Space Flight Center

30. Thermionic Spacecraft Design Study 120 kW Nuclear Electric Propulsion System
Final Report GESP-648 June 1971, Under JPL Contract 952381

31. Solar Electric Grand Tour Missions to the Outer Planets
G. A. Flandro, Final Report NASA Grant no. NGR 45-003-050, April 1970

32. Solar Electric Propulsion - A Survey - Technology Status and Mission Applications, IIT Research Institute Report no. M-21, March 1970

33. Solar Electric Propulsion for Jupiter and Saturn Orbiter Missions
I.I.T.R.I. Report no. M-24, July 1970

34. Halley's Comet Flythrough and Rendezvous Missions via Solar Electric Propulsion
I.I.T.R.I. Report no. T-28, May 1971

35. Mars Surface Sample Return Missions via Solar Electric Propulsion
I.I.T.R.I. Report no. T-29, August 1971

36. Report on the Status and Prospects of the NASA Space Power and Propulsion Research and Technology Program
Ad Hoc Working Group on Space Power and Propulsion, Vol. 1, 2, 3, 30 May 1975

37. OAST Workshop Report, 1975

38. HRL Proposal to RFP 3-740634

39. Feasibility Study for Solar Electric Propulsion Stage, Rockwell, NAS-8-27360

40. S.P.S. Study, LeRC, Fall 1975

41. Earth Observatory Satellite (E.O.S.), TRW, NAS-5-20519

42. E.O.S., GE, NAS-5-20518

43. E.O.S., Grumman, NAS-5-20520

44. Status of N.E.P., Stearns, AAS-75-164

45. Thermionic S/L Design Study, 120 kW N.E.P.S. JPL 952381

46. Mission Concepts for S.E.P. Test Flight, Meissenger Presentation, 1-18-74

APPENDIX B

MISSION STUDY DETAILED RESULTS

In Section 3 all mission work was condensed into a specific format, called the "generalized analysis approach." However, several analyses were conducted in more detail with trajectory runs. The missions analyzed included (1) Mercury orbiter, (2) Comet Encke, (3) Comet Halley, and (4) out-of-the-ecliptic. The basic results for the last of these four missions were adequately discussed in Section 3. Additional detailed results for the other three missions are discussed here.

A. MERCURY ORBITER (MO) MISSION

The MO mission was analyzed to clarify certain characteristics that bear on thruster requirements. Specifically, efforts were directed toward evaluating trajectories that would eliminate potentially severe thruster thermal requirements. By constraining the nominal thrust vector to be directed 90° to the sun line, thruster thermal loading should be controllable well within present thruster limits. Since a mission "penalty" might be expected from such a constraint, this analysis was initiated to estimate the order-of-magnitude of the effect of the constraint on payload and/or flight time.

Two series of trajectory calculations were made to bound the required acceleration levels with thrust attitude constrained to be 90° from the sun line:

- Low Power, Low Acceleration. This case is similar to previous JPL results, with a high launch energy (C_3 = 25 kM^2/sec^2), power of 16.1 kW (maximum of 21.7 kW), injected mass of 3827 kg, but with a constrained thrust angle and acceleration level of 1.6×10^{-5} g.

- High Power, High Acceleration. For this case, low thrust propulsion is traded for launch energy. The launch mass was raised to 5720 kg for a C_3 of 4 km^2/sec^2, power level was 28.4 kW (38.3 kW maximum), and acceleration of 2.07×10^{-5} g.

Figure B-1 presents the approach velocities for these two cases. Although the low acceleration runs are connected by a dotted line, they are actually discrete solutions which do not exist at intermediate points. Each solution represents a discrete number of orbit revolutions. The low acceleration level, with constrained thrust attitude, can give similar flight times to the unconstrained JPL case but at a cost of higher approach velocities. Allowing flight times to increase (utilizing coast periods) can greatly reduce the approach velocity. Approach velocity is important because it strongly influences retro requirements.

Figure B-2 depicts both the approach mass to Mercury and the net orbited mass. A 500 km by 6 hr orbit was plotted for comparison of trajectories. All cases use the same high thrust retro propulsion assumptions after ejecting a propulsion system rated at 55.3 kg/kW. (This is the value used by JPL). The results show that although the higher acceleration and power can orbit about 1250 kg, it is possible to orbit 1190 kg for a much lower power if flight time is increased. The relatively small difference probably does not justify the added propulsion system expense, unless flight time must be constrained to low values. Also, comparing Figures B-1 and B-2 shows that reducing the approach velocity to below about 1 km/sec reduces net orbited mass because the total velocity starts to be more effectively delivered with an impulsive high thrust retro.

The total number of thrusters required is shown in Figure B-3. The purpose of the figure is only to determine whether the 30-cm thruster is adequate for the mission. It is not intended to be used to select a mission profile or nominal

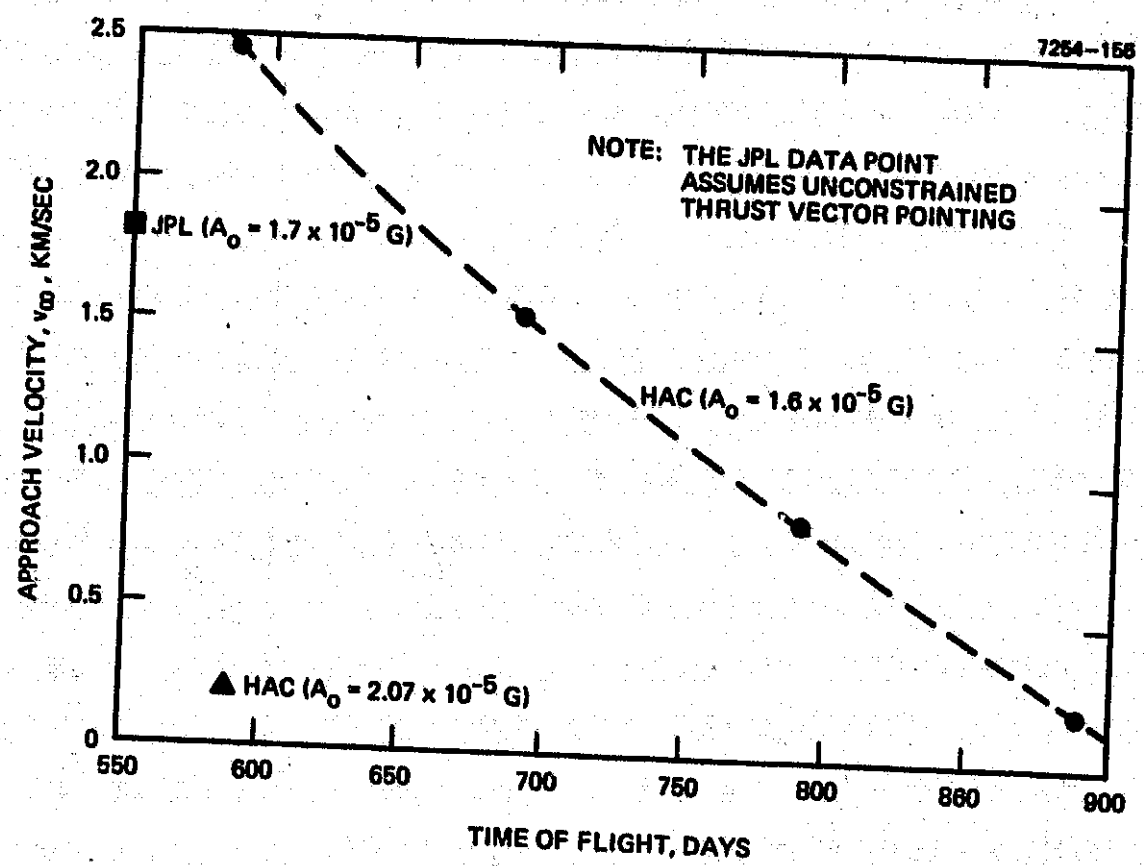

Figure B-1. Mercury approach velocity versus time of flight for MO mission.

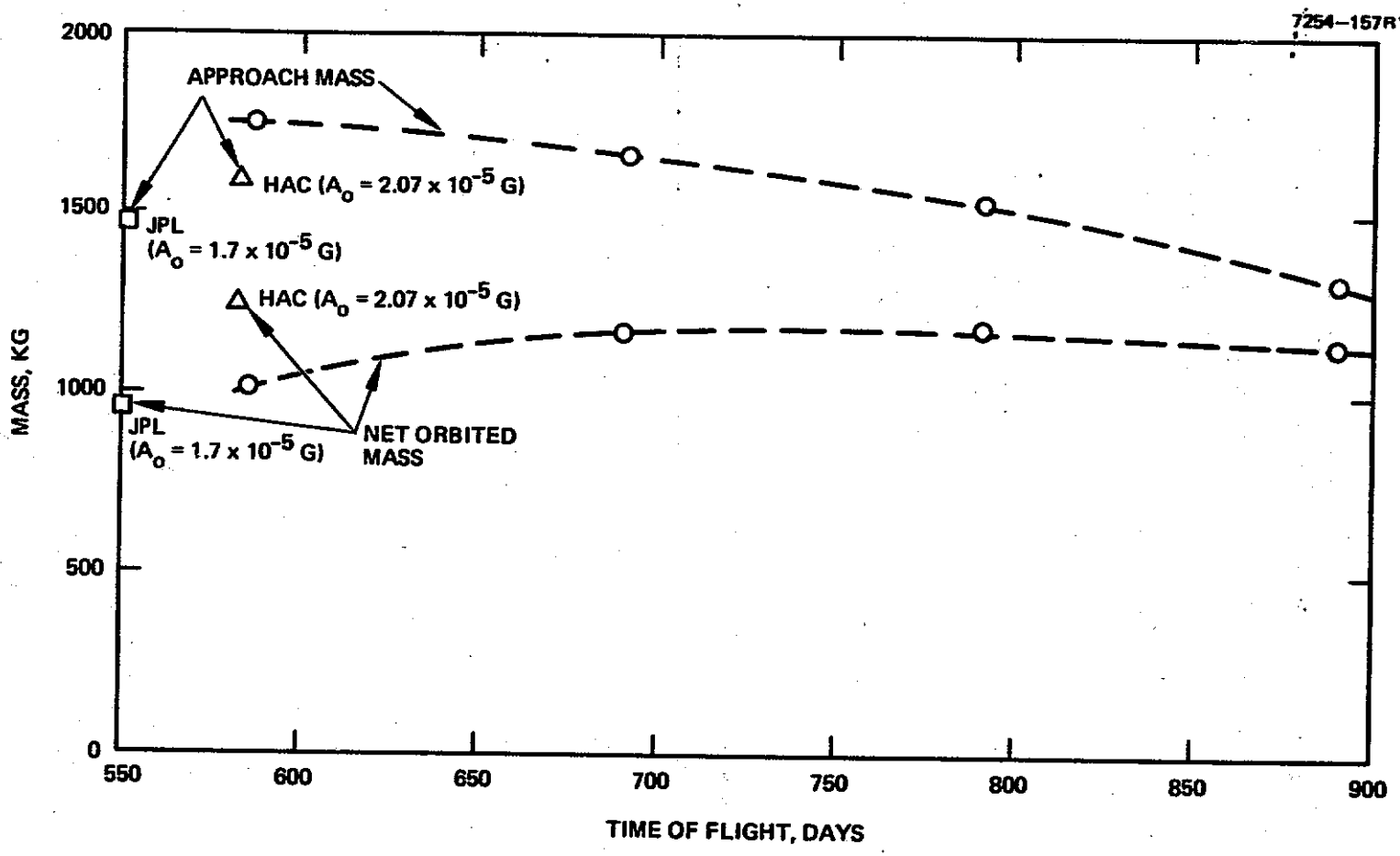

Figure B-2. Delivered mass versus time of flight, MO mission.

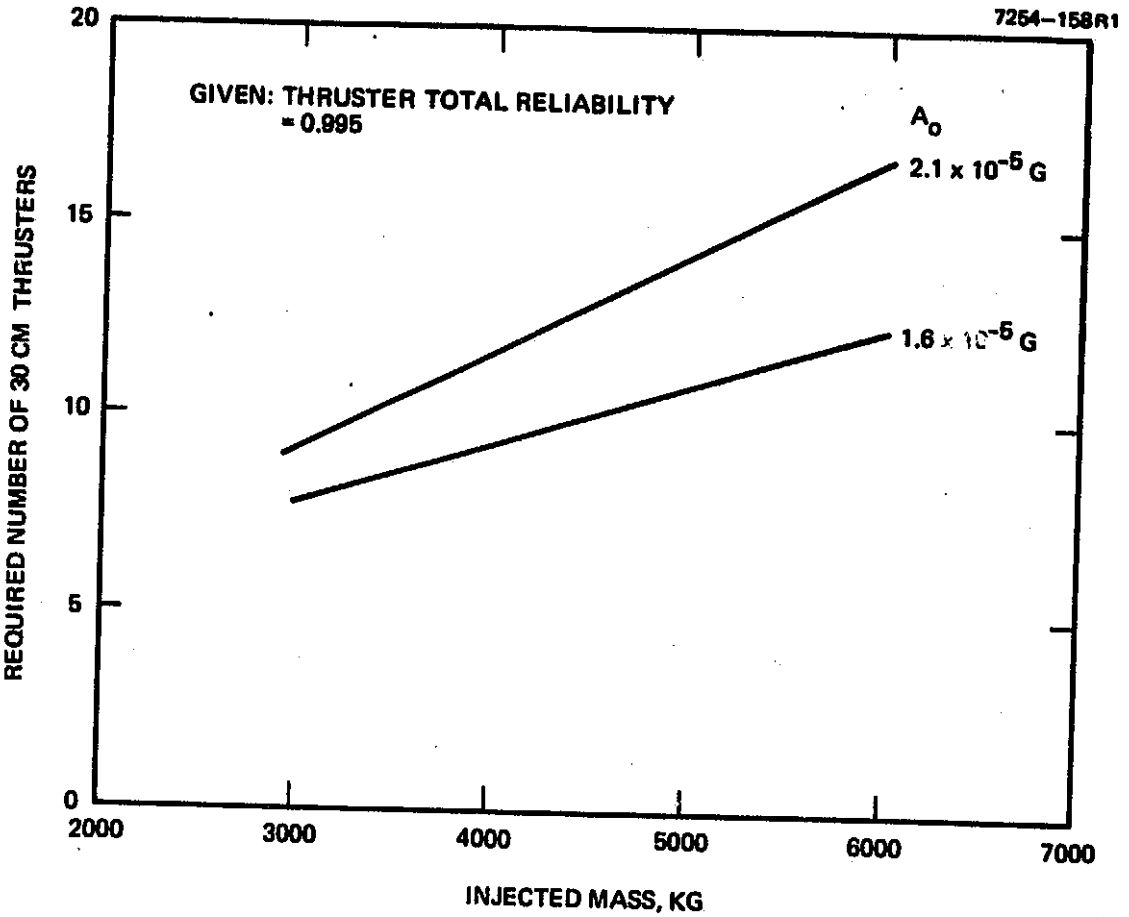

Figure B-3. Required number of thrusters versus injected mass (at Earth); MO mission.

power level. The range of injected masses adequate for a Mercury orbiter mission was found to be 3000 to 6000 kg from literature surveys and other HAC studies. The acceleration levels appeared to be bounded between 1.6 and 2.1 x 10^{-5} g. HAC EPSTOP computer runs were also made to determine the required number of 30-cm thrusters and spares using the reliability computations with acceptable thruster reliability greater than 0.995. The results, presented in Figure B-3, show that a maximum of 16 thrusters would be required for the seemingly least desirable missions with high power levels (though these missions may still be acceptable). The lower power profiles would probably require 8 to 10 30-cm thrusters, depending on reliability requirements. For these calculations, only thruster reliability was considered since the intent was to define thruster requirements.

From this work, we concluded that the existing 30-cm thruster can adequately support a range of seemingly acceptable MO missions. The 90° thrust attitude constraint significantly reduces the thruster thermal level that would be experienced in the unconstrained case. The impact of this constraint is mainly reflected in slightly increased flight times.

The Mercury orbiter mission was also used to illustrate the sensitivity of mission performance to propulsion system specific mass. The variation of propulsion system mass with thruster lifetime is shown in Figure B-4, which uses detailed trajectory computations from EPSTOP. The propulsion system mass (see Section 3.B) is plotted versus thruster lifetime. The Mercury orbiter mission is a fairly long duration mission and typically would require 32,000 A-hr wearout lifetime for a 2 A thruster. If the actual lifetime of the 2 A thruster is greater than that value, no savings in propulsion system

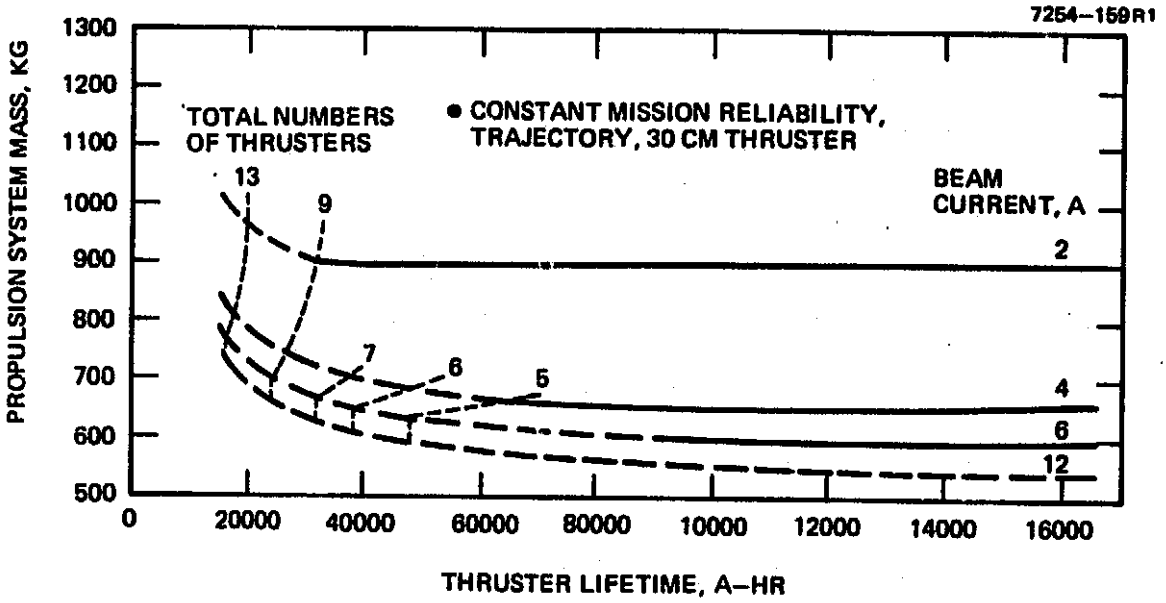

Figure B-4. Variation in propulsion system mass (Mercury Orbiter mission).

mass over that shown in Figure B-4 would occur. On the other hand, if the lifetime is less than 32,000 A-hr, spare thrusters must be carried to replace those that wear out. Every point on any of these curves in Figure B-4 has similar reliability (at least 0.995) and flies basically the same trajectory.

Assuming 20,000 A-hr as a representative thruster lifetime, Figure B-4 indicates a small mass savings (4 thrusters or 68 kg) obtained by increasing the thruster lifetime to 32,000 A-hr. Alternatively, if the beam current is increased to 4 A, with a wearout lifetime of 20,000 A-hr, the propulsion system mass would decrease by almost 200 kg. The relative mass savings from increasing beam current from 4 A to 12 A is less than 80 kg, which indicates that most of the beneift could be obtained from raising beam current from 2 A to 4 A.

The total number of thrusters is indicated by the dashed lines in Figure B-4. These lines are not straight vertical lines because of the favorable tradeoff in reliability at higher beam currents when each thruster operates for a shorter period. Thus, a large decrease in propulsion system mass (and a correspondingly large increase in net payload) is obtained by raising beam current if thruster lifetime (in terms of ampere-hours) can be maintained relatively constant. Increasing the lifetime of the thruster helps somewhat, but results in a far less dramatic mass improvement even for relatively large changes in lifetime.

B. COMET ENCKE SLOW FLYBY MISSION

During the study, interest was focused on the relationship between mission performance and thruster throttling characteristics. Comet Encke was chosen as a typical mission for assessing this sensitivity.

An Encke slow flyby (4.5 km/sec) trajectory was simulated; the results are shown in Table B-1. The reference trajectory was that obtained with the EMT power varied at constant beam voltage. For all options except the last two (which incorporate a two-fold increase in module power), the resulting performance variation is less than 10 kg. These results suggest that a small performance gain and a reduction in power may be obtained by operating near the perveance limit. It is not surprising that performance is improved by increasing efficiency or decreasing thruster mass.

On the other hand, the large performance increase caused by increasing maximum beam current is important, and this is the primary result of this portion of the study. The large performance increase is not due to improved thruster efficiency but rather to propulsion system mass reductions due to using this operating condition. This option could also be compared to increasing specific impulse, which also yields a substantial gain in net spacecraft mass. The last cases in Table B-1 were chosen to yield the same module power (5.2 kW at 4100 sec and 2 A) as for the 4 A, 3000 sec case. Both cases give a large payload improvement, but the higher I_{sp} requires a 35% increase in power.

C. COMET HALLEY MISSION

This effort was performed at a time when the Comet Halley mission was being actively considered by NASA. Since it is quite late to start the program, this information is only for the record.

1. Comet Science

The next appearance of comet Halley has an estimated perihelion date of February 5-9, 1986; the uncertainty is due to the postulated presence of non-gravitational decelerating

Table B-1. Effect of Various Thruster Operating Conditions on Encke Slow Flyby Trajectory

Condition	Total Thruster Power at 1AU, kW	Relative Net Mass, kg
Constant I_{sp} = 3000	19.8	0.0
Constant I_{sp} = 2850	19.0	+.2
Constant I_{sp} = 2700	18.2	-.3
"Perveance Limit Throttling" $I_B \leq 2$ A	18.2	+5.5
Variable I_{sp}	18.8	-2.5
Constant Utilization Efficiency and Beam Divergence	19.4	+8.8
Total Efficiency Increased 1%	19.6	+3.4
Thruster Mass Decreased 1 kg	19.8	+10.0
Maximum Beam Current = 4 A	18.4	+267.2
Constant I_{sp} = 4100 sec	26.8	+64.6

6119

forces (mass ejection under the influence of solar radiation heating). Earth-based sightings will recover Halley's comet when the nuclear brightness is about 20th magnitude, which may occur in 1983 and could refine the estimate of when the perihelion will occur. Unfortunately, the along track distance will be the least sensitive to optical measurements, so considerable ephemeris uncertainty will probably exist.

The Whipple icy congolmerate model of cometary behavior is currently most widely accepted; it views comets as "small, fragile, low-density structures of frozen gases, well mixed with dust and larger debris. Approaching the sun, the gases begin to vaporize from this nucleus, forming an extended atmosphere of dust and gas (seen as the coma) which streams back under the influence of solar pressure and the solar wind to form tails." The burst of activity noticed at about 3 AU from the sun may be caused by water vaporization, which is thought to be the major volatile component of most comets.

Imaging the nucleus has a high priority because a nucleus has never been seen, only postulated. Mass spectroscopy and dust analysis also have high priority in studies of the origin of comets and of the composition of the nucleus. Measurements of the existence, location, and physical properties of the solar wind and bowshock interactions (with potential contact surfaces) is of great interest to plasma physicists.

The desired mission scenario, a spatial survey, would probably satisfy most science objectives. The spacecraft would enter the bowshock, traverse the coma, and then image the nucleus. Then it would fly slowly through the tail in a manner that would maximize the data collection time and distance from the nucleus.

Tradeoffs among science return, instrument development requirements and costs, and approach velocity (trip time

and propulsion system technology) are complex but most probably favor a slow fly-through of 1 to 2 km/sec (if possible).

b. Trajectory Analysis

Figure B-5 illustrates the retrograde nature of Halley's comet and the comet's motion in the near perihelion region. Rendezvous is preferred before perihelion as indicated in the JPL "ion drive" trajectories in Figures B-6 and B-7. The 1982 launch opportunity has rendezvous just outside of 1 AU at 50 days prior to closest approach. The trajectories in the following analysis leave the arrival data unconstrained (but less than 3 AU). Fixing the arrival date could affect the minimum flyby opportunities for the later launch dates.

Typical propulsion system requirements are given in Figure B-8 for launch dates between 1982 and 1985. The curves are called "typical" since a small range of accelerations and SEP velocity additions could produce similar approach velocities. Slight trajectory deviations exist due to the differing acceleration time histories of the various propulsion systems modeled. The chief cause is varying propellant utilization with I_{sp}, but the exact trajectories are also a function of launch energy (C_3, or, equivalently, initial mass), intial power, and technology level specific mass of the propulsion system. The trends clearly show the increased propulsion system requirements needed to decrease approach velocity. A rendezvous, if possible, must take place with an early 1982 launch. As late as 1985 would not be improved by an SEP system.

Tradeoffs of net spacecraft mass and power requirements for a spectrum of technology levels and launch opportunities are shown in Figures B-9 to B-14. These launch opportunities occur early in each launch year for the pre-perihelion Comet Halley fly-throughs. Four thruster and system technology levels

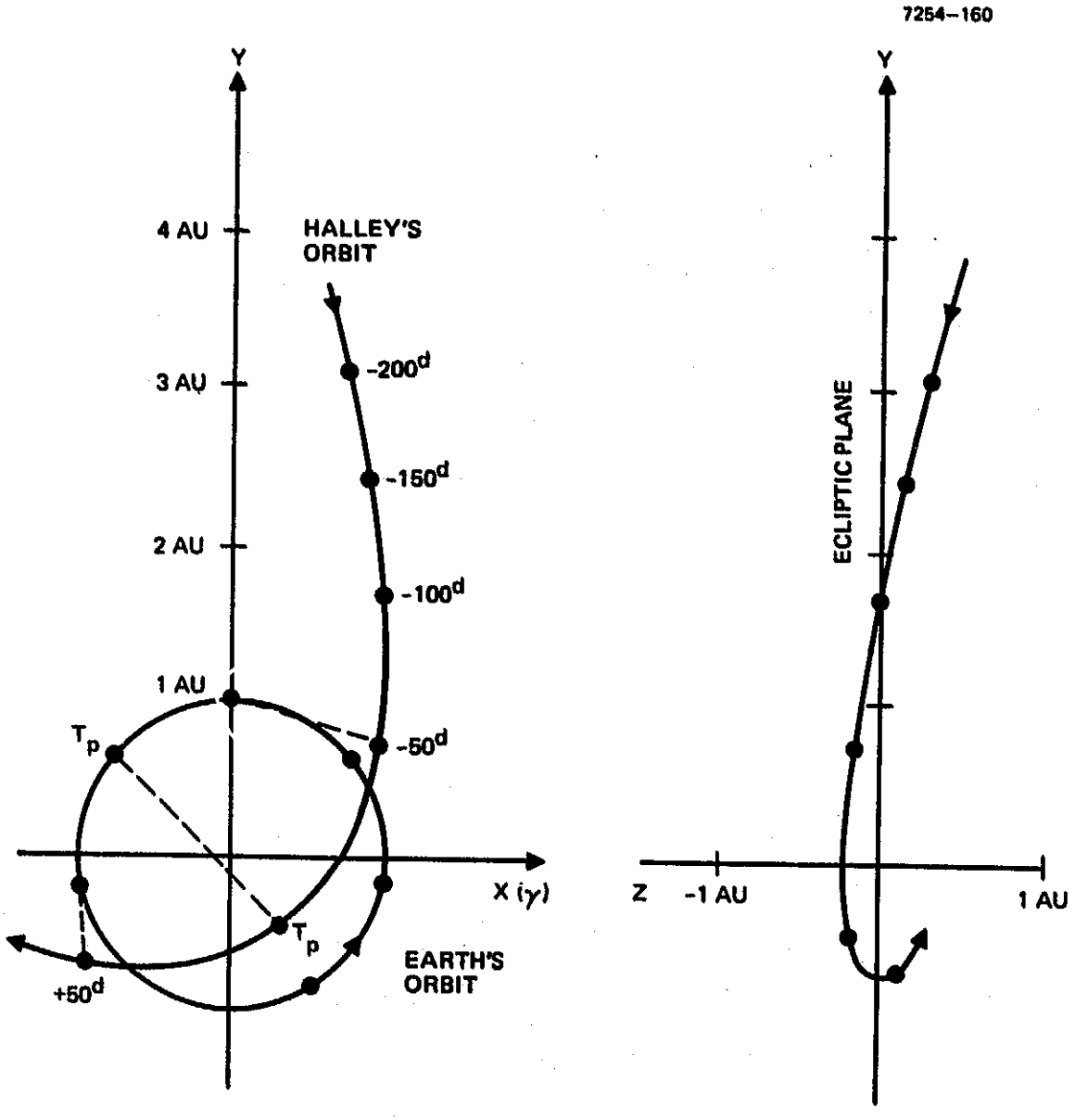

Figure B-5. Orbit of comet Halley near perihelion.

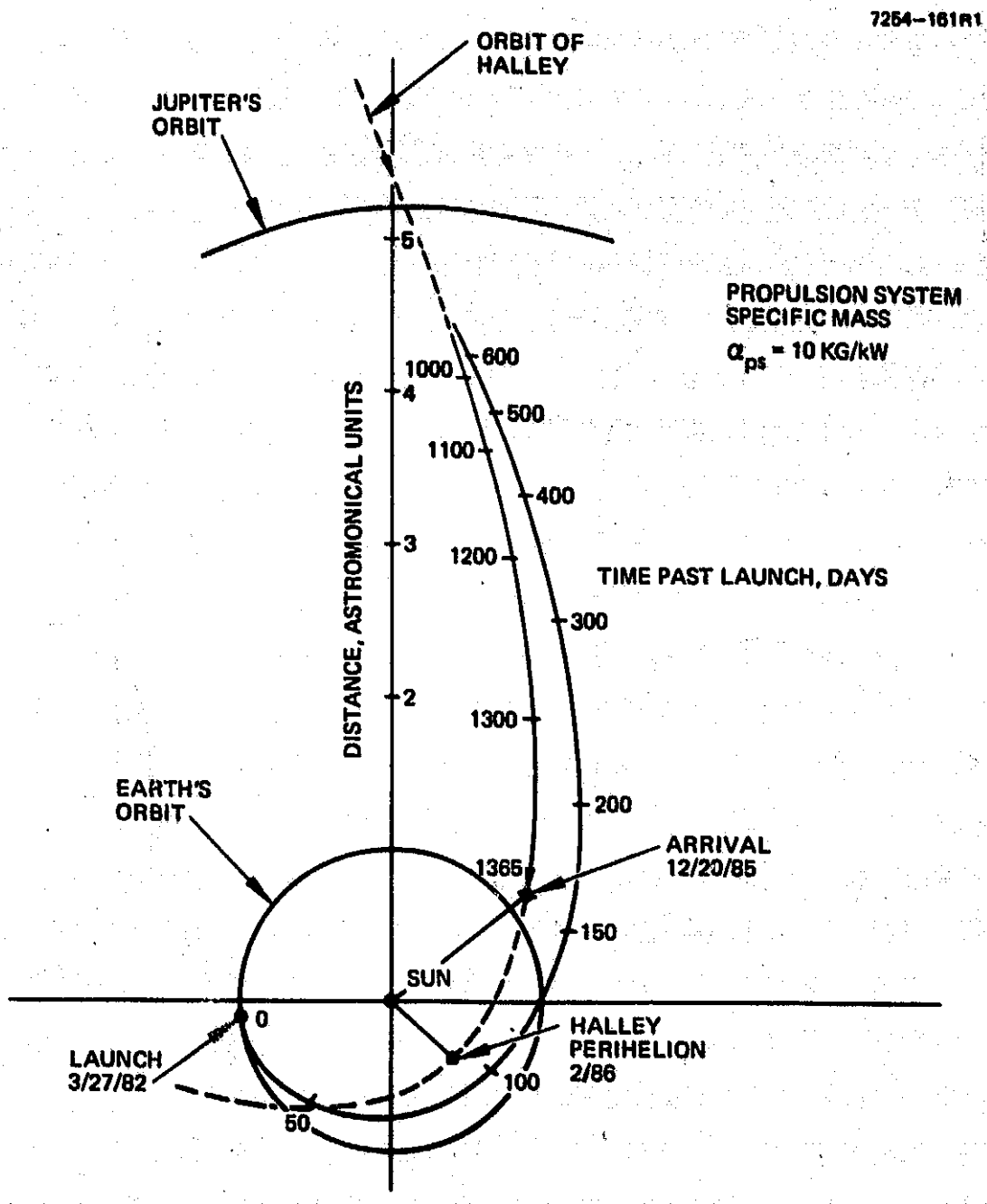

Figure B-6. Ion drive flight path to Comet Halley.

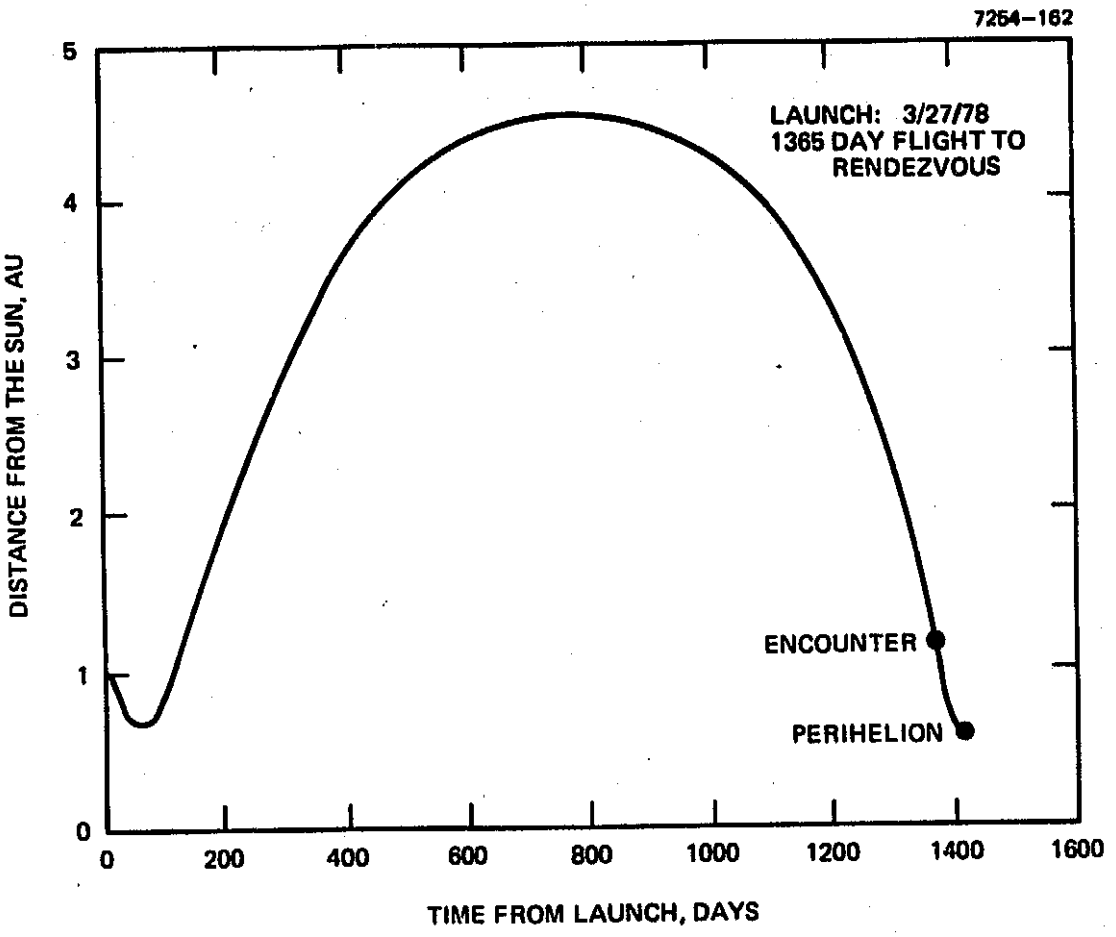

Figure B-7. Ion drive "baseline" trajectory.

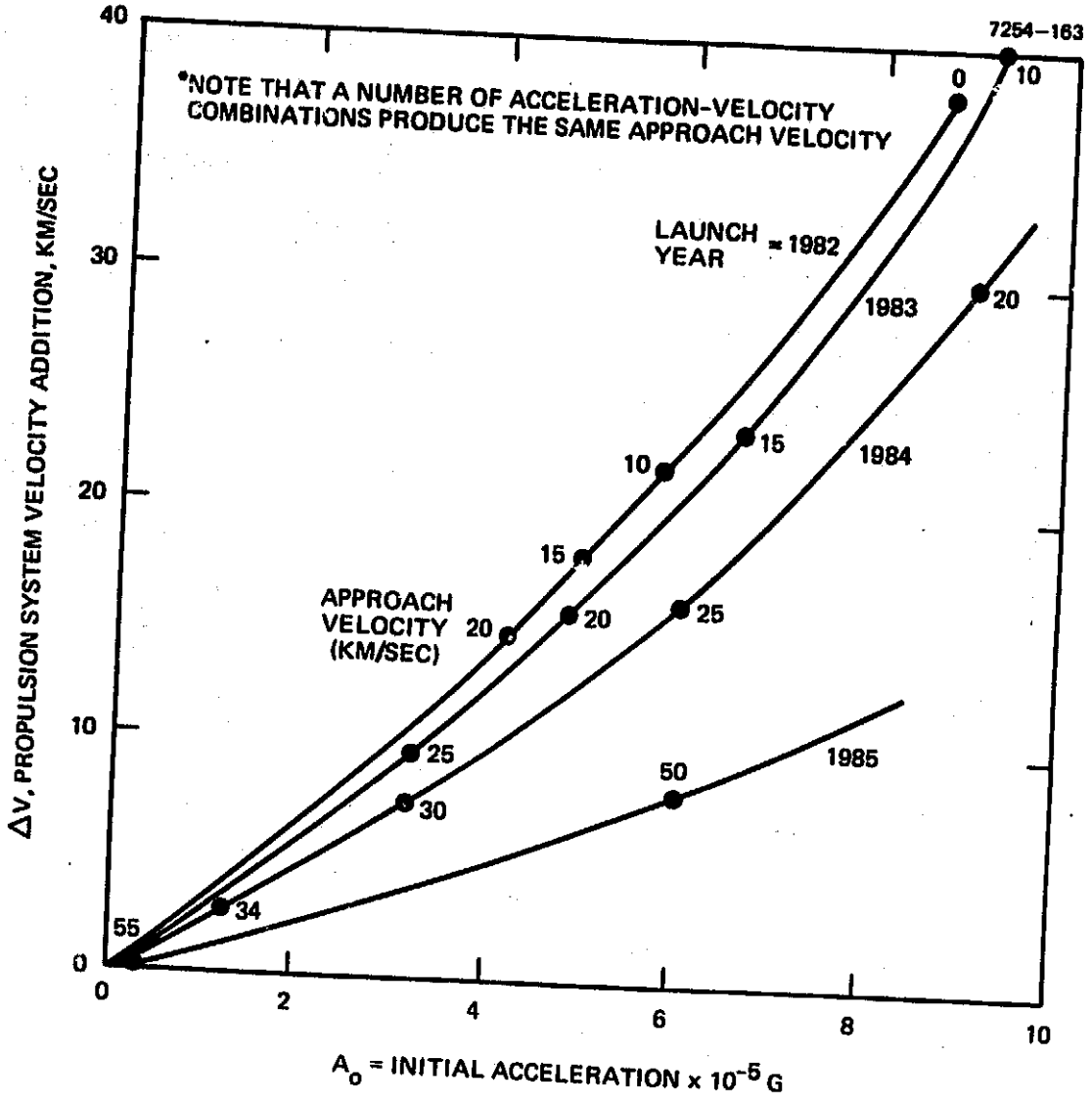

Figure B-8. Typical propulsion system requirements.

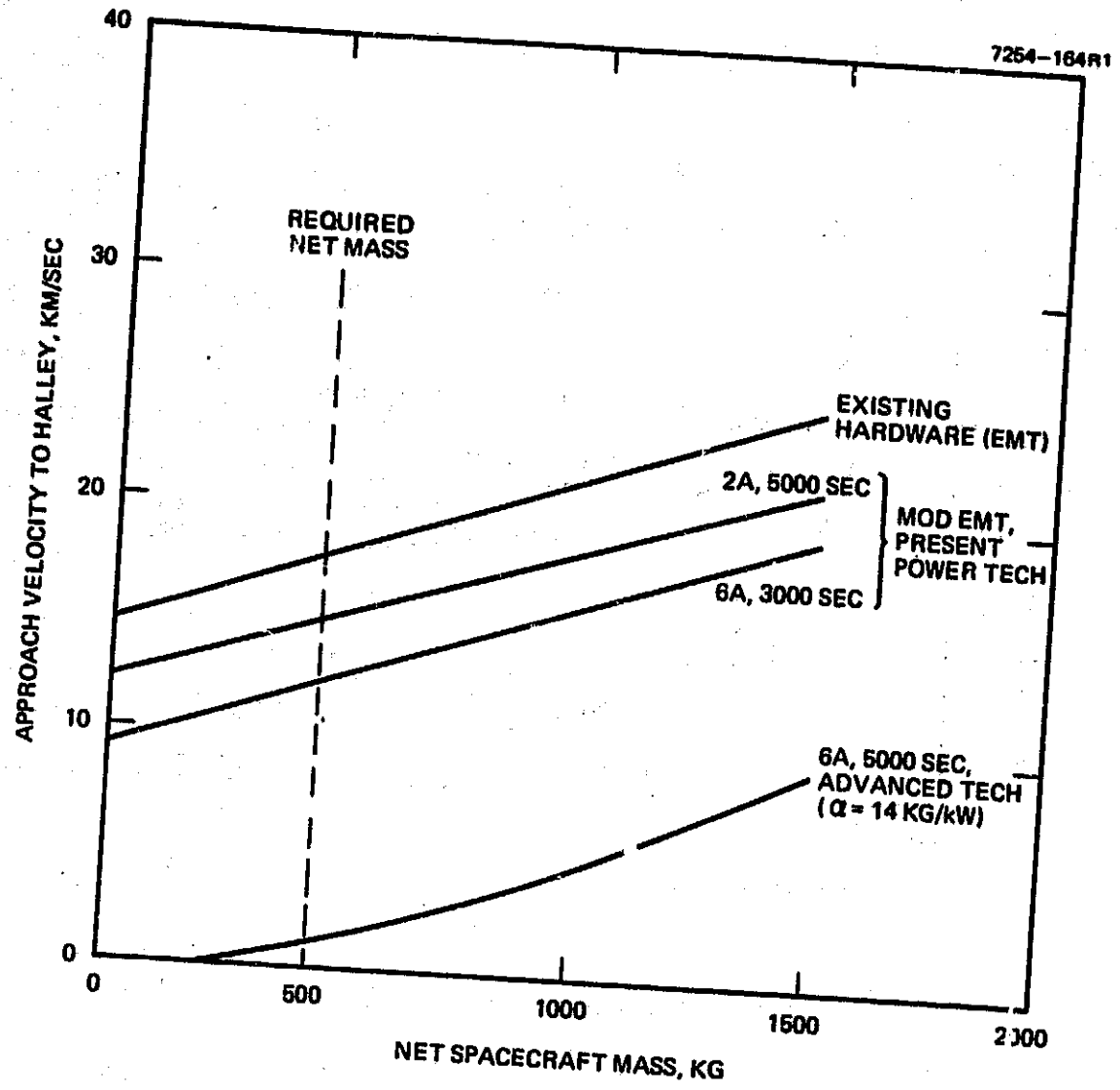

Figure B-5. Comet Halley mission performance analysis, 1982 launch date.

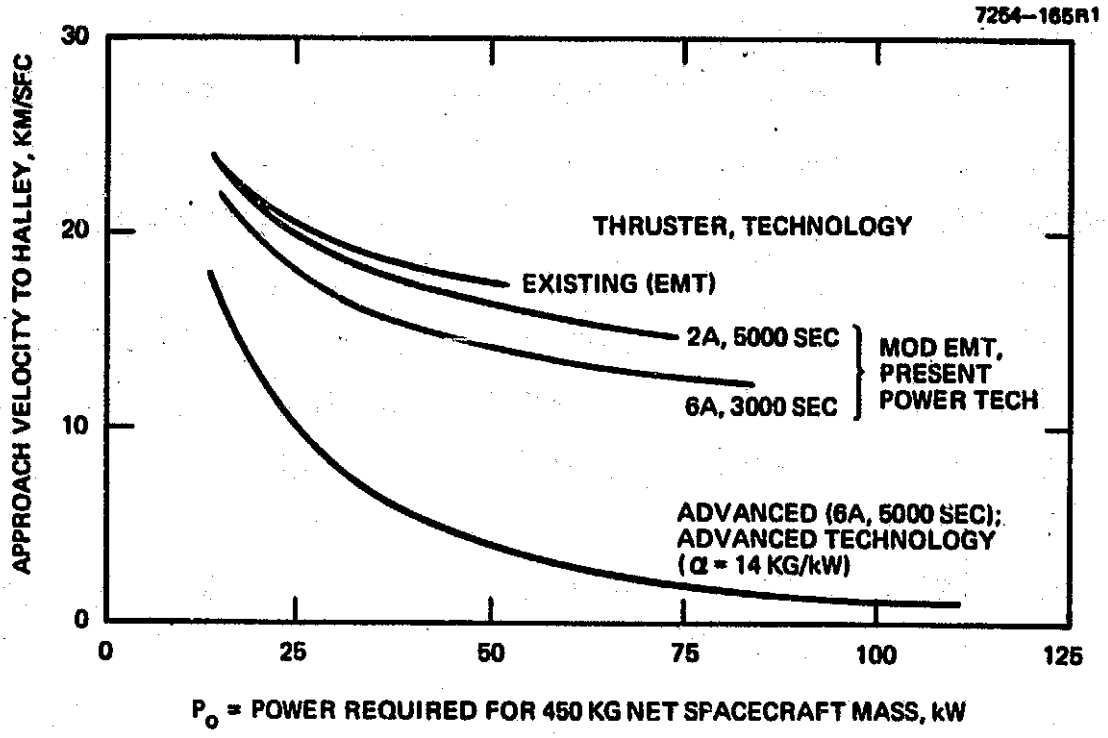

Figure B-10. Power requirements, 1982 launch date.

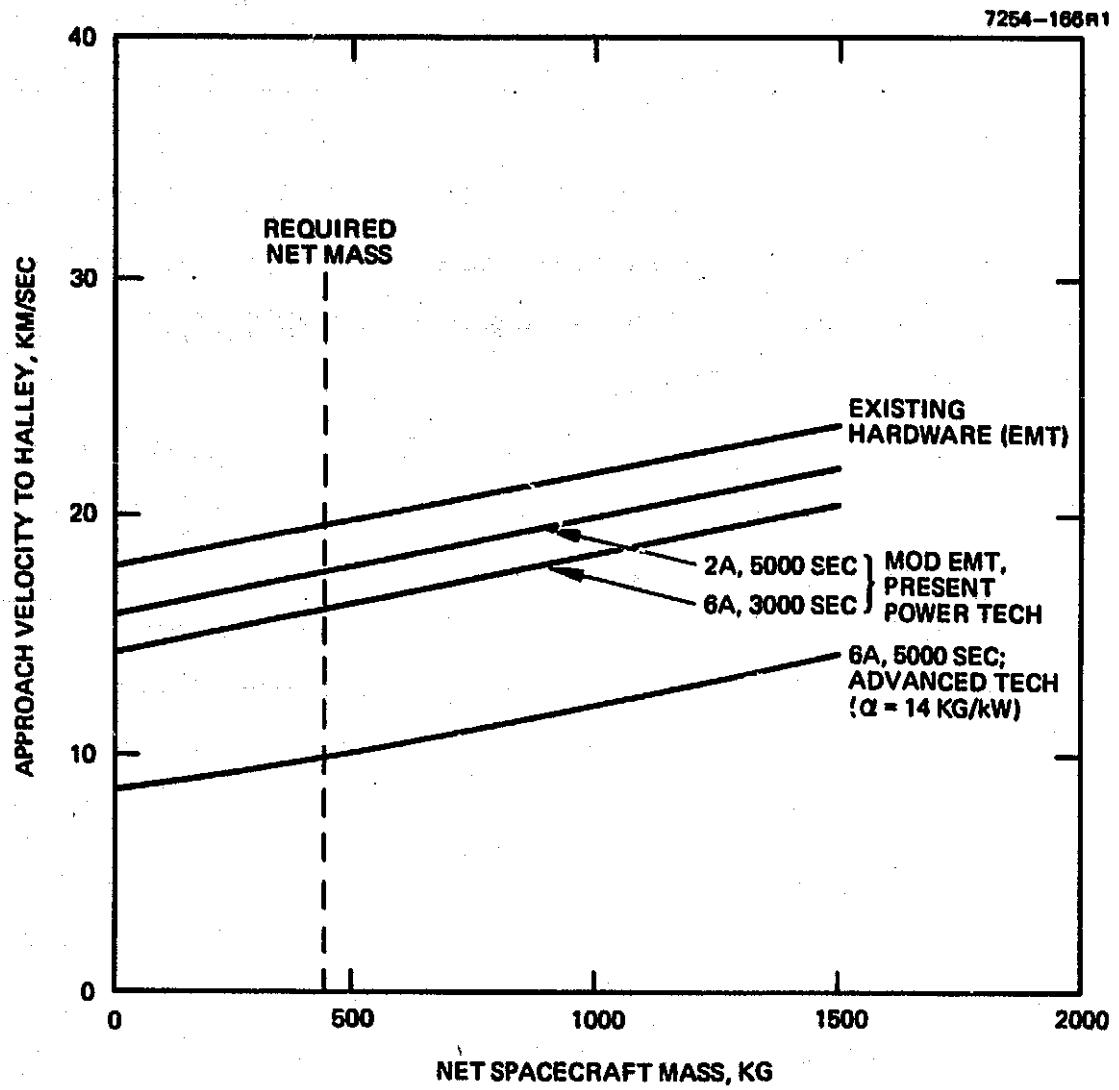

Figure B-11. Performance analysis, 1983 launch date.

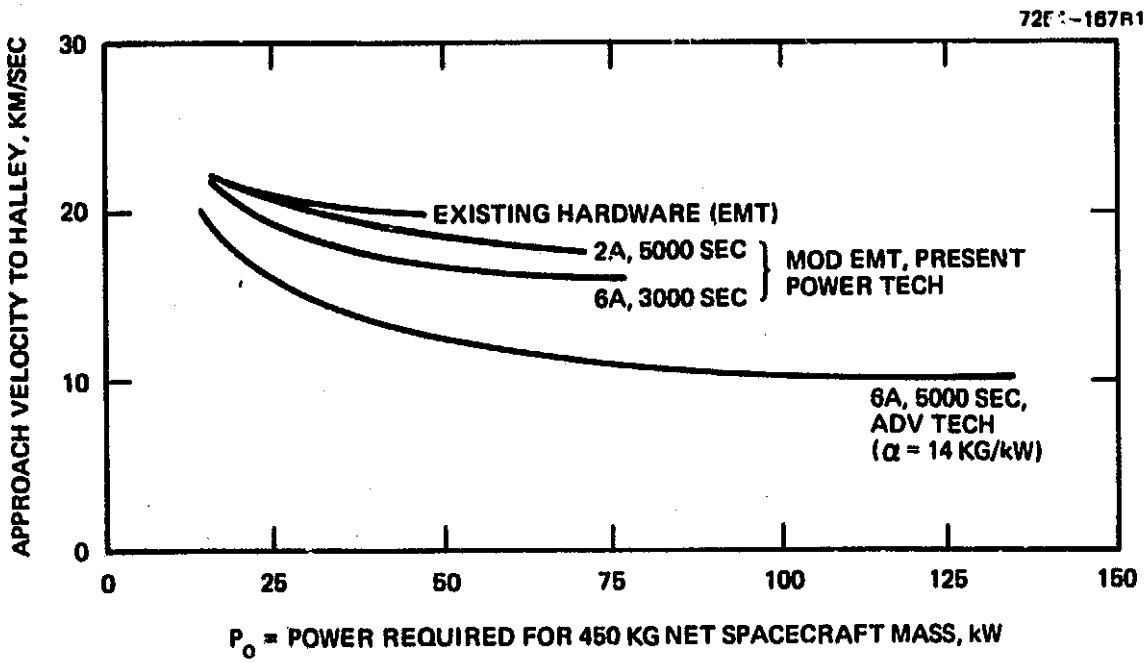

Figure B-12. Power requirements, 1983 launch date.

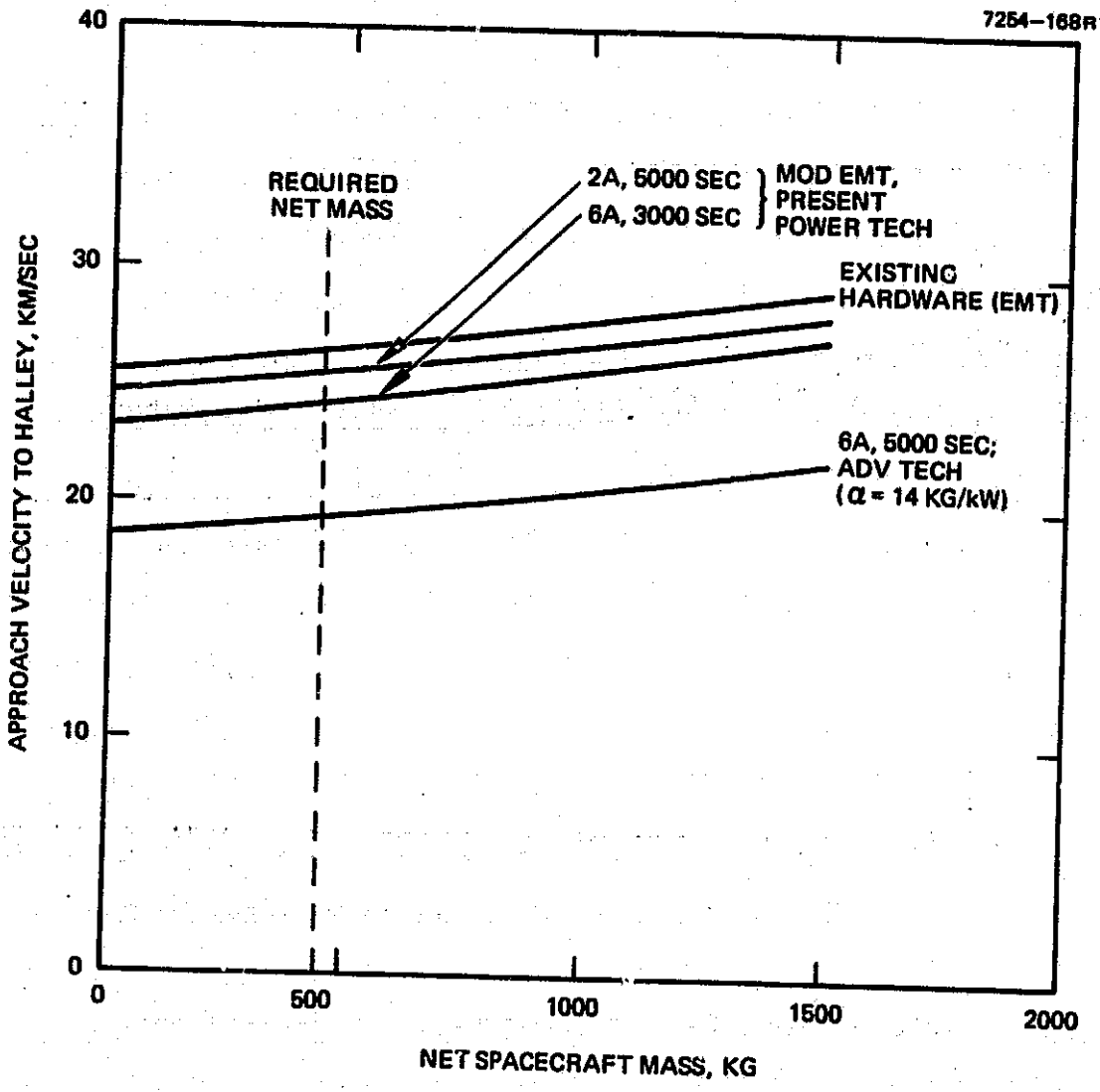

Figure B-13. Performance analysis, 1984 launch date.

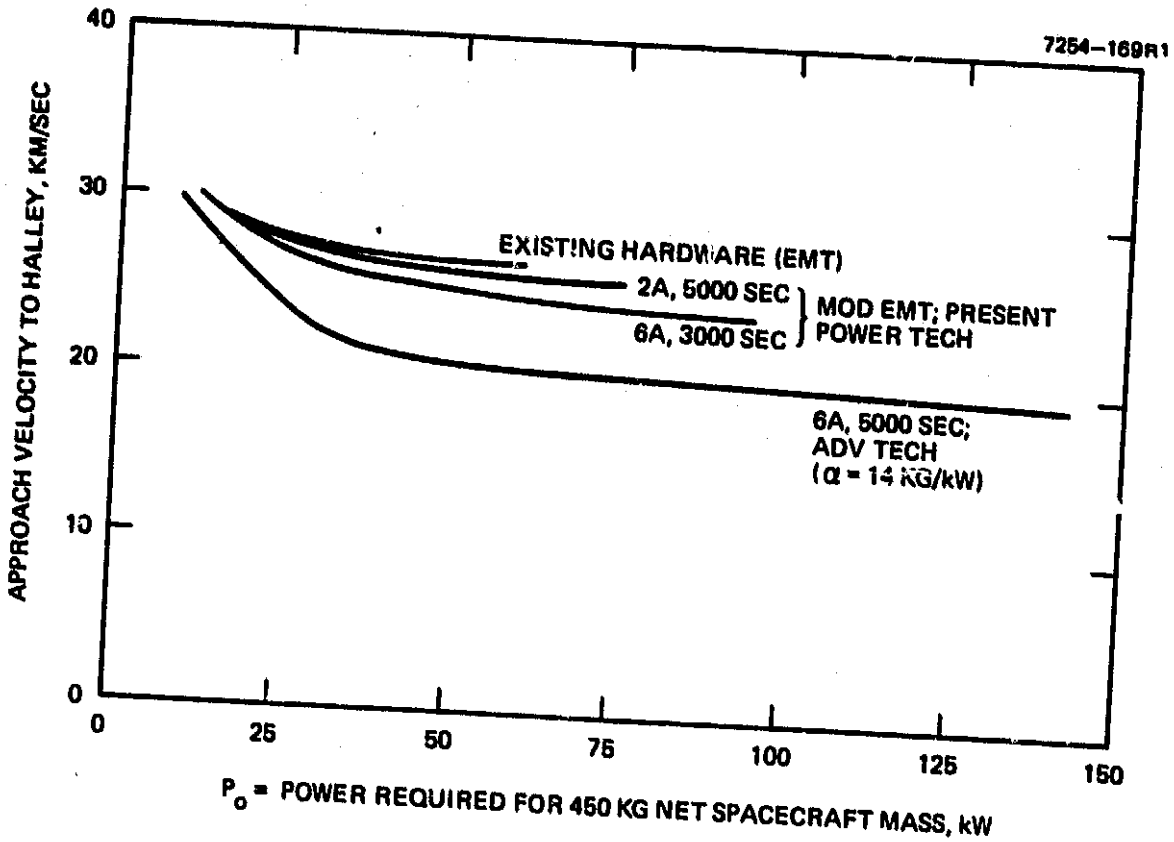

Figure B-14. Power requirements, 1984 launch date.

are presented. The first is the present engineering model thruster (EMT) with present technology power conditioning and solar panels. The EMT operates at 2 A and 3000 sec I_{sp}. When spares are added, the propulsion system specific mass α_{ps} becomes 45.5 kg/kW.

The next two systems have modified EMTs. The first assumes an I_{sp} of 5000 sec; the second assumes a beam current of 6 A. Power conditioners are modeled according to present technology estimates of masses. In the second case, increased wearout rate of higher beam current thrusters necessitates thruster replacement due to wearout. As one thruster wears out, a replacement thruster is connected to the power conditioner in a manner similar to that occuring in a thruster failure. Specific masses of the two systems are 33 and 29 kg/kW, respectively.

The final system modeled contains an advanced concept thruster operating at high beam current (6 A) and high I_{sp} (5000 sec). This thruster is assumed lighter and more efficient than the EMT. Corresponding breakthroughs occur in power conditioning and solar panel masses to yield an extremely light system having α_{ps} of only 14 kg/kW. This α_{ps} is still somewhat higher than the ion drive[3] system with a value of only 10 kg/kW (a 4 kg/kW difference).

Figures B-9 and B-10 present the results of the March 1982 launch opportunity. The net spacecraft mass is given in Figure B-9 as a function of desired approach velocity and technology level and compared to an estimated mass of 450 kg required for this type of mission. None of the technology levels is capable of rendezvous with the required mass, but the advanced technology comes very close (≈ 1 km/sec). In fact, the extra payload delivered by the ion drive system with its 4 kg/kW difference at about a 100 kW power level

could achieve the rendezvous. The three present power technology levels do show some approach velocity improvements with thruster changes at 450 kg (18 km/sec to 12 km/sec), but, as seen in Figure B-10, higher power is required. Figure B-10 depicts the same trades as Figure B-9 in terms of power required for a 450 kg net spacecraft. Whenever a technology's performance is greater than 450 kg (in Figure B-9), the Shuttle payload is scaled to decrease the power requirements (i.e., initial mass), but acceleration, ΔV, and propulsion system characteristics are kept constant. The penalty for the 6 km/sec decrease in approach velocity is now clear — over 30 kW of increased power is required (i.e., from 50 to 84 kW). At a potential $500,000/kW of solar panel, the cost for the 33% extra science time is very high. Similarly, the power/cost for reducing the approach velocity towards zero is extraordinary for even the advanced technology. Reducing the approach velocity from 4 to 1 km/sec more than doubles P_o (from 50 to 110 kW). These values are consistent with the ion drive results when efficiency differences (0.74 versus 0.76), acceleration levels, and α_{ps} are taken into account. Small technology changes require large power jumps because of the asymptotic nature of the curves. For each curve in Figure B-10, the last few km/sec changes in approach velocity (above the 450 kg limit) causes high relative changes in power level. A clear message is that the trajectory requirements are barely satisfied, and any slight change in technology will be extremely costly.

The 1983 opportunity is depicted in Figures B-11 and B-12, in which trends similar to the 1982 launch are exhibited. The basic difference is the minimum approach velocity, which is now about 10 km/sec for the unconstrained arrival date. The three present technology curves (EMT and modified EMT) are also closer to each other in approach velocity

performance (<4 km/sec) but still differ significantly in power requirments (>30 kW in Figure B-12). Again the lower regions of approach velocity for each technology implies large increases in power levels. For example, decreasing the advanced technology from 21 to 19 km/sec raises power required from 35 to 115 kW, a threefold increase.

The curves for the 1984 opportunity (Figures B-13 and B-14) exhibit a still further decrease in the difference between technology levels. Above 20 km/sec, large increases in net spacecraft mass result from small increases in approach velocity, which show that technology level is important.

APPENDIX C

EARTH ORBIT COST MODEL PROGRAM LISTING

Computer programs were written to model the cost methodology for both the orbit-rising and on-orbit cost models described in Section 4 of this report. These programs were developed and used with the DEC System-10 time-sharing service and were written in FORTRAN IV. Copies of the listings for the three principal versions of the orbit-raising and the on-orbit programs are presented in Tables C-1 through C-6. These listings are for Shuttle era baseline cases run using Xe propellant and an initial mass of 25,000 kg.

The three versions of each cost model produce outputs which calculate

- Cost per net payload ($/kg)
- Normalized cost breakdown for each major subsystem
- Mass breakdown (kg) for each major subsystem

Each of these programs plots the chosen variable (e.g., cost per net payload) as a function of I_{sp} with any of the other input variables as a parameter. Since most of the equations are common to all of the programs, only the orbit-raising version is discussed here. The nomenclature used for the various parameters follows that used in the computer listings in which all the program variables use only capital letters. In the listings, multiple statements on a line are separated by semi-colons.

The computer program uses specific impulse (XISP) as the independent variable, over the range from 3000 to 18,000 sec. For argon, the beam voltage VB is given in terms of the specific impulse XISP as

$$VB = \left[XISP/199 \right]^2 \quad . \qquad (C\text{-}1)$$

TABLE C-1.

```
C   <HWARD>ORVPLT.FOR;8    FRI 20-JAN-78 1:17PM                    PAGE
C   ORBIT RAISING COST MODEL
      REAL NMOD,IMOD,LT,NOP,NOT,MOOP,MOSP,LORV,MSP,IEN,MPDWN
      REAL MORV,MRT,MRPP,MORP,MRPT,MRSS,MRM
      DIMENSION A(5),P(5),VCOEF(4),RATIO(4),VCRIT(4)
      DATA VCOEF/5.2,3.0,2.88,2.33/
      DATA RATIO/1.,2.098,3.267,5.022/
      DATA VCRIT/2026.,2590.,3005.,3462./
      DATA P/5.,10.,20.,40.,80.,160./
      DATA A/50.,300.,600.,800.,1600./
      M1=22;M2=0;M3=1;M4=2
C     ORBIT RAISING COST MODEL WRITTEN BY BILL WARD AT MRL - 1977
CC    MODIFIED DEC 77 FOR NEW BASELINE IE. XE ETC
C     FOR THIS LISTING PMOD IS VARIED FROM 5KW TO 80KW
C     CALL PLOTS(30);CALL PLOT(0.,0.,-3)
      LIFE OF LORV AND PPU,THRUSTER AND PPU REDUNDANCYS
      LORV=2000.;ROT=.2,ROP=.2
      DO 6 JCASE=1,1
C  INITIAL CONDITIONS
      DELV=6.;XMO=25.E3;TIME=150.
      DO 5 J=1,5
      RATIOX=RATIO(3);VCRITX=VCRIT(3);VCOEFX=VCOEF(3)
      IPEN=3;DOWN=.5*TIME
      PMOD=P(J)*1000.
      FLUX=1.E15;XFLUX=ALOG10(1.E-15*FLUX)
      ICURVE=3
      IF(ICURVE.EQ.1) SOLEFF=-.1912*XFLUX+.75
      IF(ICURVE.EQ.2) SOLEFF=-.1775*XFLUX+.9
      IF(ICURVE.EQ.3) SOLEFF=-.129*XFLUX+.
      DO 5 I=1,1000
      XISP=17.*FLOAT(I-1)+1000.
      GISP=.0098*XISP
      VB=RATIOX*XISP/199.*XISP/194.
      IMOD=PMOD/VB
      IF(VB.LT.VCRITX) GO TO 20
      D=30.*SQRT(IMOD/15.)
      GO TO 33
20    D=30.*SQRT(IMOD/VCOEFX*(VB/1000.)**-1.5)
33    CONTINUE
      XMASS=.078*D**1.35
      BETA=DELV/GISP
      XMF=XMO/EXP(BETA)
      XMP=XMO-XMF
      SEC=TIME/100.*8.64E6
      PJET=XMP*GISP*GISP*.5E6/SEC
      ALPTHR=XMASS/P(J)
      EXPONX=-.505*ALOG10(P(J))+1.153
      ALPPU=10.**EXPONX
      EFF=.84*VB/(VB+220.);TOTEFF=EFF*SOLEFF*.95
      PTOT=PJET/TOTEFF
      NMOD=PJET/PMOD
      IEN=IMOD*900./(D*D)
      IEM=-1.27*ALOG10(IEN)+4.4
      LT=10.**IEM
C  TAKE OUT NEXT LINE FOR VARIABLE THRUSTER LIFE
      LT=1.E4
79    TOTRIP=TIME+DOWN
      FACTOR=TOTRIP*24./LT;FACT=FACTOR;IF(FACTOR.LT.1.) FACTOR=1.
      NOT=NMOD*FACTOR*(1.+ROT)
      NOP=NMOD*(1.+ROP)
      MRT=2.*XMASS*NOT;MRPP=.001*ALPPU*PTOT;MORP=XMP;MRPT=.1*MORP
      MRSS=100.*(1.+1.E-6*PTOT)+100.*(NOT/NOP-1.);MRSS=MRSS*(1+.1)
      MRSM=.2*(MRT+MRPP+MORP+MRPT+MRSS)
      MRM=6.*.001*PTOT;MORV=MRT+MRPP+MORP+MRPT+MRSM+MRSS+MRM
      IF(MORV.GT.XMO) GO TO 5
      MOP=XMO-MORV;POUT=MORV*(1.-EXP(-DELA))
      XTIME=TIME*MPLAN/XMP;DEL=ABS(XTIME-DOWN)
      IF(DEL.LT. 2) GO TO 37
      DOWN=XTIME;GO TO 79
37    TOTRIP=TIME+XTIME
```

TABLE C-1 (Continued)


```
C  <BWARD>ORVPLT.FOR;6    FRI 20-JAN-78 1:17PM                    PAGE 1:1

C  THRUSTER COST USING 80% RULE
C   ONLY PAY FOR THRUSTER LIFE USED
      USENOT=NOT;IF(FACT.LT.1.) USENOT=FACT*NOT
      COST=42.E3*ALOG10(D);CRT=2.*COST*USENOT**.68/.68
C  PPU COSTS AT ASSUMED PPU EFF OF 95%
      PPUPWR=P(J)/TOTEFF
      UNIT=4.5E5*PPUPWR**.12;CRP=UNIT*NOP**.68/.68
C  INCLUDE DOWN PROPELLANT IN CPROP AND CORRECT PAYLOAD
      CPROP=(XMP+MPDWN)*10.;CTANK=.1*100.*(XMP+MPDWN);MSP=MSP-MPDWN
C  USED THRUSTER WEIGHT
      USED=XMASS*NMOD*FACT*(1.+ROT);CRSM=1.E4*MRSM**.5
      CRSS=1.E4*MRSS**.9;CORT=40.*(MORV-MORP+USED);COPF=1.E5
      CORD=1.E5/10.*(MORV-MORP)**.5;CRM=100.*PTOT
      COPT=1.E3*TOTRIP;CL=300.*(XMO+USED)
      COST1=CORT+CRT+CRP+CTANK+CRSM+CRSS+CRM+CORD
      COEFF=TOTRIP/MORV+2.7E-4*TOTRIP
      COST=COEFF*COST1+COPF+COPT+CL+CPROP;AVGCST=COST/MSP
      X=XISP/5000.;Y=AVGCST;IF(Y.LT.10) GO TO 5
      Y=2.5*ALOG10(.1*Y);IF(Y.GE.7.) GO TO 5
      CALL PLOT(X,Y,IPEN)
      IPEN=2
      D1=ABS(50.-D);D2=ABS(60.-D);D3=ABS(100.-D);D4=ABS(150.-D)
      IF(D1.LT..10) CALL SYMBOL(X,Y,.1,M1,0.,-1)
      IF(D2.LT..24) CALL SYMBOL(X,Y,.1,M2,0.,-1)
      IF(D3.LT..24) CALL SYMBOL(X,Y,.1,M3,0.,-1)
      IF(D4.LT..24) CALL SYMBOL(X,Y,.1,M4,0.,-1)
    5 CONTINUE
    6 CONTINUE
      CALL PLOT(0.,0.,-3);DO 51 JX=1,10
      Y=FLOAT(JX);Y=2.5*ALOG10(Y)
   51 CALL SYMBOL(0.,Y,.1,24,0.,-1)
      DO 63 JX=20,100,10
      Y=FLOAT(JX);Y=2.5*ALOG10(Y)
   63 CALL SYMBOL(0.,Y,.1,24,0.,-1)
      DO 64 JX=200,1000,100
      Y=FLOAT(JX);Y=2.5*ALOG10(Y)
   64 CALL SYMBOL(0.,Y,.1,24,0.,-1)
      DO 52 JX=1,6
      X=FLOAT(JX)
   52 CALL SYMBOL(X,0.,.1,15,0.,-1)
      CALL PLOT(0.,0.,-3);CALL POFF
      STOP;END
```

6119

```
C   <HWARD>ORVCST.FOR;4    FRI 20-JAN-78 1:26PM

C   ORBIT RAISING NORMALIZED COST BREAKDOWN
      REAL NMOD,IMOD,LT,NOP,NOT,MOOP,MOSP,LORV,MSP,IEQ,MPOWR
      REAL MORV,MRT,MORP,MORP,MRPT,MRSM,MRSS,MRA
      DIMENSION A(5),P(6),VCUEF(3),VCRIT(3)
      DATA VCUEF/2.68,12.04,3.57/
      DATA VCRIT/3005.,1154.,2605./
      DATA P/20.,50.,100.,200.,500.,1000./
      DATA A/50.,100.,150.,200.,0./
      M1=22;M2=0;M3=1;M4=2
C     ORBIT RAISING COST MODEL WRITTEN BY BILL WARD AT DRL - 1977
C     MODIFIED FOR XE LOWER POWER ETC IN DEC
C     CALL PLOTS(50);CALL PLOT(0.,0.,-3)
C     LIFE OF LORV ,THRUSTER AND PPU REDUNDANCYS
      LORV=2000.;ROT=.2;ROP=.2
      DO 6 JCASE=1,1
C   INITIAL CONDITIONS
      DELV=6.;XMO=25.0;TIME=150.
      DO 5 J=1,12
      CALL POFF
      READ(5,*) ZZZZ;WRITE(5,*) ZZZZ
      CALL PON
      P(J)=20.;VCRITX=VCRIT(1);VCUEFX=VCUEF(1)
      IFFX=3;DOWN=.5*TIME
      PMOD=P(J)*1000.
      FLUX=1.E15;XXFLUX=ALOG10(1.E-15*FLUX)
      ICURVE=3
      IF(ICURVE.EQ.1) SOLEFF=-.1912*XXFLUX+.73
      IF(ICURVE.EQ.2) SOLEFF=-.1775*XXFLUX+.9
      IF(ICURVE.EQ.3) SOLEFF=-.129*XXFLUX+.995
      DO 5 I=1,1000,5
      XISP=17.*FLOAT(I-1)+1000.
      GISP=.0098*XISP
      VB=3.287*XISP/199.*XISP/199.
      IMOD=PMOD/VB
      IF(VB.LT.VCRITX) GO TO 20
      D=30.*SQRT(IMOD/15.)
      GO TO 33
   20 D=30.*SQRT(IMOD/VCUEFX*(VB/1000.)**4-1.5)
   33 CONTINUE
      XMASS=.076*D**1.35
      BETA=DELV/GISP
      XMF=XMO/EXP(BETA)
      XMP=XMO-XMF
      SEC=TIME/100.*8.64E6
      PJET=XMP*GISP*GISP*.5E6/SEC
      ALPTHR=XMASS/P(J)
      EXPONX=-.503*ALOG10(P(J))+1.153
      ALPPU=10.**EXPONX
      EFF=.84*VB/(VB+220.);TOTEFF=EFF*SOLEFF*.95
      PTOT=PJET/TOTEFF
      PMOD=PJET/PMOD
      IEQ=IMOD*900./(VB*D)
      TEM=-1.27*ALOG10(IEQ)+4.4
      LT=10.**TEM
C   TAKE OUT NEXT LINE FOR VARIABLE THRUSTER LIFE
      LT=1.E4
   79 TOTRIP=TIME+DOWN
      FACTOR=TOTRIP*24./LT;FACT=FACTOR;IF(FACTOR.LT.1.) FACTOR=1.
      NOT=PMOD*FACTOR*(1.+ROT)
      NOP=PMOD*(1.+ROP);MOPP=.001*ALPPU*PTOT*(1.+ROP)
      MRT=2.*XMASS*NOT;MORP=XMF;MRPT=.1*MORP
      MRSS=100.*(1.+1.E-6*PTOT)+100.*(NOT/NOP-1.);MRSS=MRSS*(1+.1)
      MRSM=.2*(MRT+MORP+MOPP+MORV=MRT+MOPP+MORP+MRPT+MRSM+MRSS+MRA
      MRA=6.*.001*PTOT;MORV=MRT+MOPP+MORP+MRPT+MRSM+MRSS+MRA
      IF(MORV.GT.XMO) GO TO 5
      MSP=XMO-MORV;MPOWR=MORV*(1.-EXP(-BETA))
      XTIME=TIME*MPOWR/XMP;DEL=ABS(XTIME-DOWN)
      IF(DEL.LT. 2) GO TO 37
      DOWN=XTIME;GO TO 79
   37 TOTRIP=TIME+XTIME
```


6119

TABLE C-2 (Continued)

```
C   <BWARD>UNVCST.FOR;-    FRI 20-JAN-78 1:20PM                    PAGE 1:1

C   THRUSTER COST USING 0.6 RULE
C    ONLY PAY FOR THRUSTER LIFE USED
        USEFNOT=NOT;IF(FACT.LT.1.) USEFOUT=FACT*NOT
        COST=4P.E5*ALOG10(D);CPT=2.*COST*USEFOUT**.66/.66
C   PPU COSTS AT ASSUMED PPU FRF OF 95%
        PPUPWR=P(J)/TLEFF
        UNIT=4.5E5*PPUPWR**.12;CPP=UNIT*NUP**.66/.66
C   INCLUDE LOAN PRINCIPLE AMT IN CPNOP AND CUSTREL1 PAYLOAD
        CPROP=(XMF+MPL*.5)*10.;CTANK=.1*100.;MSP=MSP+MPLOAD
C   USED THRUSTER WEIGHT
        USED=XMASS*NMOD*FACT(1.*NOT);CRSM=1.E4*MFSM**.5
        CRSS=1.E4*MRSS**.9;CORI=4E.*(MORV-MLOP+USED);COPF=1.E5
        CORD=1.E5/10.*(MORV-MOPP)**.3;CRP=100.*PTOT
        COPT=1.E5*TOTRIP;CL=300.*(XMO+USED)
        COST1=CORI+CRP+CTANK+CRSM+CRSS+CRM+CLOAD
        COEFF=TOTRIP/LORV+2.7E-4*TOTRIP
        COST=COEFF*COST1+CRT+COPF+COPT+CL+CPROP;AVGCST=COST/MSP
        XXF=COEFF*10./COST;XYZ=10./COST
        X=XISP/3000.
        IF(J.EQ.1) Y=CORI*XXF;IF(J.EQ.2) Y=CRI*XXF
        IF(J.EQ.3) Y=XXF*CRP;IF(J.EQ.4) Y=XXF*CTANK
        IF(J.EQ.5) Y=XXF*CRSM;IF(J.EQ.6) Y=XXF*CRSS
        IF(J.EQ.7) Y=XXF*CRM;IF(J.EQ.8) Y=XXF*CORD
        IF(J.EQ.9) Y=XYZ*COPF;IF(J.EQ.10) Y=XYZ*COPT
        IF(J.EQ.11) Y=XYZ*CL;IF(J.EQ.12) Y=XYZ*CPROP
        CALL PLOT(X,Y,IPEN)
         IPEN=2
        IF(J.GT.1) GO TO 5
        D1=ABS(50.-D);D2=ABS(60.-D);D3=ABS(100.-D);D4=ABS(150.-D)
        IF(D1.LT..10) CALL SYMBOL(X,Y,.1,M1,0.,-1)
        IF(D2.LT..24) CALL SYMBOL(X,Y,.1,M2,0.,-1)
        IF(D3.LT..24) CALL SYMBOL(X,Y,.1,M3,0.,-1)
        IF(D4.LT..24) CALL SYMBOL(X,Y,.1,M4,0.,-1)
        IPEN=2
 5      CONTINUE
 6      CONTINUE
        DO 52 JX=1,6
        X=FLOAT(JX)
 52     CALL SYMBOL(X,0.,.1,13,0.,-1)
        CALL PLOT(0.,0.,-3);CALL PUFF
        STOP;END
```

6119

TABLE C-2 (Continued)

```
C   <BWARD>OKVMS1.FOR;1    FRI 20-JAN-78 1:55PM                    PAGE 1:1

C   THRUSTER COST USING 80% RULE
C    ONLY PAY FOR THRUSTER LIFE USED
        USEDOT=NOT;IF(FACT.LT.1.) USEDOT=FACT*NOT
        COST=42.E3*ALOG10(D);CRT=2.*COST*USEDOT**.66/.66
C   PPU COSTS AT ASSUMED PPU EFF OF 95%
        PPUPWR=P(J)/TOTEFF
        UNIT=4.3E5*PPUPWR**.12;CRT=UNIT*NOP**.68/.66
C   INCLUDE DOWN PROPELLANT IN CPROP AND CORRECT PAYLOAD
        CPROP=(XMP+MPDWN)*10.;CTANK=.1*100.;MSP=MSP-MPDWN
C   USED THRUSTER WEIGHT
        USED=XMASS*NMOD*FACT*(1.+ROT);CRSM=1.E4*MRSM**.5
        CRSS=1.E4*MRSS**.9;CORT=40.*(MORV-MORP+USED);COPF=1.E5
        CORD=1.E5/10.*(MORV-MORP)**.3;CRW=100.*PTOT
        COPT=1.E3*TOTRIP;CL=300.*(XMO+USED)
        COST1=CORT+CRP+CTANK+CRSM+CRSS+CRW+CORD
        COEFF=TOTRIP/LORV+2.7E-4*TOTRIP
        COST=COEFF*COST1+CRT+COPF+COPT+CL+CPROP;AVGCST=COST/MSP
        XXF=10./XMO
        X=XISP/3000.
        IF(J.EQ.1) Y=MRT*XXF;IF(J.EQ.2) Y=MRPP*XXF
        IF(J.EQ.3) Y=XXF*MORF;IF(J.EQ.4) Y=XXF*MRPT
        IF(J.EQ.5) Y=XXF*MRSM;IF(J.EQ.6) Y=XXF*MRSS
        IF(J.EQ.7) Y=XXF*MPDWN;IF(J.EQ.8) Y=XXF*MPDWN
        IF(J.EQ.9) Y=MSP*XXF
        IF(Y.LT.0) GO TO 5
        CALL PLOT(X,Y,IPEN)
         IPEN=2
        IF(J.GE.1) GO TO 5
        D1=ABS(30.-D);D2=ABS(60.-D);D3=ABS(100.-D);D4=ABS(150.-D)
        IF(D1.LT..10) CALL SYMBOL(X,Y,.1,M1,0.,-1)
        IF(D2.LT..24) CALL SYMBOL(X,Y,.1,M2,0.,-1)
        IF(D3.LT..24) CALL SYMBOL(X,Y,.1,M3,0.,-1)
        IF(D4.LT..24) CALL SYMBOL(X,Y,.1,M4,0.,-1)
        IPEN=2
    5   CONTINUE
    6   CONTINUE
        DO 52 JX=1,6
        X=FLOAT(JX)
   52   CALL SYMBOL(X,0.,.1,15,0.,-1)
        CALL PLOT(0.,0.,-3);CALL PUFF
        STOP*END
```

6119

TABLE C-3.

```
C   <BWARD>ORVMST.FOR;1    FRI 20-JAN-78  1:35PM                    PAGE 1

C    ORBIT RAISING MASS BREAKDOWN
       REAL NMOD,IMOD,LT,NOP,NOT,MOOP,MOSP,LORV,MSP,IEG,MPDWN
       REAL MORV,MRT,MRPP,MORP,MRPT,MRSM,MRSS,MRW
       DIMENSION A(5),P(6),VCUEF(3),VCRIT(3)
       DATA VCUEF/2.85,12.04,3.57/
       DATA VCRIT/3005.,1156.,2605./
       DATA P/20.,50.,100.,200.,500.,1000./
       DATA A/50.,100.,150.,200.,0./
       M1=22;M2=0;M3=1;M4=2
C      ORBIT RAISING COST MODEL WRITTEN BY BILL WARD AT HRL - 1977
C      MODIFIED TO USE XF,LOWER XMO ETC DECEMBER 77
       CALL PLOTS(30);CALL PLOT(0.,0.,-3)
C      LIFE OF LORV AND PPU,THRUSTER AND PPU REDUNDANCYS
       LOPV=2000.;ROT=.2;ROF=.2
       DO 6 JCASE=1,1
C   INITIAL CONDITIONS
       DELV=6.,XMO=25.E3,TIME=150.
       DO 5 J=1,9
       CALL POWF
       READ(5,*) ZZZZ;WRITE(5,*) ZZZZ
       CALL POW
       P(J)=20.;VCRITX=VCRIT(1);VCUEFX=VCUEF(1)
       IPEN=3;DOWN=.5*TIME
       PMOD=P(J)*1000.
       FLUX=1.E15;XXFLUX=ALOG10(1.E-15*FLUX)
       ICURVE=3
       IF(ICURVE.EQ.1) SOLEFF=-.1912*XXFLUX+.73
       IF(ICURVE.EQ.2) SOLEFF=-.1775*XXFLUX+.9
       IF(ICURVE.EQ.3) SOLEFF=-.129*XXFLUX+.995
       DO 5 I=1,1000,5
       XISP=17.*FLOAT(I-1)+1000.
       GISP=.0098*XISP
       VB=3.287*XISP/199.*XISP/199.
       IMOD=PMOD/VB
       IF(VB.LT.VCRITX) GO TO 20
       D=30.*SQRT(IMOD/15.)
       GO TO 33
  20   D=30.*SQRT(IMOD/VCUEFX*(VB/1000.)**-1.5)
  33   CONTINUE
       XMASS=.076*D**1.35
       BETA=DELV/GISP
       XMF=XMO/EXP(BETA)
       XMP=XMO-XMF
       SEC=TIME/100.*8.64E6
       PJET=XMP*GISP*GISP*.5E6/SEC
       ALPIHK=XMASS/P(J)
       EXPONX=-.503*ALOG10(P(J))+1.153
       ALPPU=10.**EXPONX
       FFF=.84*VB/(VB+220.);TOTEFF=EFF*SOLEFF*.95
       PTOT=PJET/TOTEFF
       NMOD=PJET/PMOD
       IEG=IMOD*900./(D*D)
       TEM=-1.27*ALOG10(IEG)+4.4
       LT=10.**TEM
C   TAKE OUT NEXT LINE FOR VARIABLE THRUSTER LIFE
       LT=1.E4
  79   TOTRIP=TIME+DOWN
       FACTOR=TOTRIP*24./LT;FACT=FACTOR;IF(FACTOR.LT.1.) FACTOR=1.
       NOT=NMOD*FACTOR*(1.+ROT)
       NOP=NMOD*(1.+ROP);MRPP=.001*ALPPU*PTOT*(1.+ROP)
       MRT=2.*XMASS*NOT;MORP=XMF;MRPT=.1*MORP
       MRSS=100.*(1.+1.E-6*PTOT)+100.*(NOT/NOP-1.);MRSS=MRSS*(1+.1)
       MRSM=.2*(MRT+MRPP+MORP+MRPT+MRSS)
       MRW=6.*.001*PTOT;MORV=MRT+MRPP+MORP+MRPT+MRSM+MRSS+MRW
       IF(MORV.GT.XMO) GO TO 5
       MSP=XMO-MORV;IPOWN=MORV*(1.-EXP(-BETA))
       XTIME=TIME*MPDWN/XMP;DEL=ABS(XTIME-DOWN)
       IF(DEL.LT. 2) GO TO 37
       DOWN=XTIME;GO TO 79
  37   TOTRIP=TIME+XTIME
```

TABLE C-4.

```
C   <BWARD>MASS.FOR;6    FRI 20-JAN-78  3:54PM                    PAGE 1

C     ON ORBIT COST MODEL
        REAL NMOD,IMOD,LT,NOP,NUT,MOOP,MOSP,MOA,IEM
        REAL MOSS,MOT,MOPP,MOP,MOPT,MOSS,MOPM,MOS
        DIMENSION A(5),P(6)
        DATA P/5.,10.,20.,40.,80.,100./
        DATA A/1.,2.,4.,6.,10./
C   ON ORBIT COST PROGRAM WHICH PLOTS COST/KG/YEAR AS FUNC(ISP)
C    WRITTEN BY BILL WARD AT DRL IN 1977
C    CHANGED DEC 77 TO USE XE ETC
        M1=22;M2=0;M3=1;M4=2
        YRS=10.;RUT=.2;ROP=.2
        DELV=16.5;TIME=365.*YRS
        CALL PLOTS(30)
        XMO=25.E3;ICURVE=3
        DO 6 JCASE=1,1;CPEN=2
        IF(JCASE.EQ.2) CPEN=5
        DO 5 J=1,5
        P(J)=20.;RGOO=A(J)
        IPEN=3;ICURVE=3
C   SOLAR CELL DEGRADATION:INPUT FLUX AND CURVE CHOSEN
        FLUX=1.E15;XXFLUX=ALOG10(1.E-15*FLUX)
        IF(ICURVE.EQ.1) SOLEFF=-.1912*XXFLUX+.73
        IF(ICURVE.EQ.2) SOLEFF=-.1775*XXFLUX+.90
        IF(ICURVE.EQ.3) SOLEFF=-.129*XXFLUX+.995
        PMOD=P(J)*1000.
        CXX=1/.
        DO 5 I=1,1000
          XISP=CXX*FLOAT(I-1)+1000.
        GISP=.0098*XISP
        VB=5.287*XISP/199.*XISP/199.
        IMOD=PMOD/VB
        IF(VB.LT.3005.) GO TO 20
        D=30.*SQRT(IMOD/15.)
        GO TO 53
20      D=30.*SQRT(IMOD/2.58*(VB/1000.)**-1.5)
53      CONTINUE
        XMASS=.078*D**1.35
        BETA=DELV/GISP
        XMF=XMO/EXP(BETA)
        XMP=XMO-XMF
        SEC=TIME/100.*8.64E6
        PJET=XMP*GISP*GISP*.5E6/SEC
        EXPONX=-.503*ALOG10(P(J))+1.193
C     INCREASE PPU WEIGHT BY REDUNDANCY FACTOR
        ALPPU=(1.+ROP)*10.**EXPONX
        EFF=.84*VB/(VB+220.)
C     ASSUME PPU EFF=CONSTANT=.95
        TOTEFF=EFF*SOLEFF*.95;PIOI=PJET/TOTEFF
        NMOD=PJET/PMOD;IEG=IMOD*900./(D*D)
        TLM=-1.2/*ALOG10(IEG)+4.4;LI=10.**IEM
C   TAKE OUT NEXT LINE FOR VARIABLE THRUSTER LIFE
        LI=1.E4
        FACTOR=TIME/(LT/24.)
        IF(FACTOR.LT.1.) FACTOR=1.
        NUT=NMOD*FACTOR*(1.+RUT)
        NOP=NMOD*(1.+ROP)
C       COMPUTE THRUSTER COST=UNIT*(1+1/2**4+1/3**ALPHA....)ETC
C       COST=42.E3*ALOG10(D);COT=2.*COST*NOT**.66/.66
C     COMPUTE PPU COSTS
        PPUPAR=P(J)/TOTEFF
C     IN THIS EXAMPLE POWER SPECIFIC MASS IS VARIED FROM 1 TO 10KG/KW
C
C     INITIALIZE ARRAY WITH PROPER DATA FOR PARAMETRIC CHANGES
        UNIT=4.3E3*PPUPAR**.12;COP=UNIT*NOP**.68/.68
        MOT=2.*XMASS*.001;MOPP=.001*ALPPU*PJET/TOTEFF;MOP=XMP;MOPT=.1*MOP
        MOSS=100.*(1.+1.E-6*PIOI)+100.*(MOT/NOP-1.);MOSS=MOSS*(1+.1)
        MOSM=.2*(MOT+MOPP+MOP+MOPT+MOSS)
        MOP=RGOO*.001*PIOI;MOOP=MOSM+MOT+MOPP+MOP+MOPT+MOSS+MOM
        MOSP=XMO-MOOP
```

TABLE C-4 (Continued)

```
C   <HWARD>MASS.FOR;6    FRI 20-JAN-78 5:54PM                          PAGE 1:1

        COPT=XMOP*(10.+.1*100.)
        COSM=1.64*MOSM**.5;COOD=1.E5/10.*(MOOP-MOP)**.3
        COSS=1.64*MOSS**.9;CTO=1000.*MOOP
        COI=40.*MOOP;COA=100.*PILOT;COPS=1.E5*TIME
        COST=COI+COP+COPT+COSM+COSS+CTO+COI+COA+COPS+COOD
        MOSP=XMO-MOOP;AVGCST=COST/(MOSP*YRS)
        X=XISP/5000.;Y=AVGCST;IF(Y.LT.1.) GO TO 5
         Y=2.5*ALOG10(Y);IF(Y.GE.7.) GO TO 5
        CALL PLOT(X,Y,IPEN)
        IPEN=OPEN
         D1=ABS(30.-D);D2=ABS(60.-D);D3=ABS(100.-D);D4=ABS(150.-D)
        IF(D1.LT..1) CALL SYMBOL(X,Y,.1,M1,0.,-1)
        IF(D2.LT..24) CALL SYMBOL(X,Y,.1,M2,0.,-1)
        IF(D3.LT..24) CALL SYMBOL(X,Y,.1,M3,0.,-1)
        IF(D4.LT..24)  CALL SYMBOL(X,Y,.1,M4,0.,-1)
  5     CONTINUE
  8     CONTINUE
C  WRITE LOG TIC MARKS
        CALL PLOT(0.,0.,-3);DO 51 JX=1,10
         Y=FLOAT(JX);Y=2.5*ALOG10(Y)
  51    CALL SYMBOL(0.,Y,.1,24,0.,-1)
        DO 63 JX=20,100,10
        Y=FLOAT(JX);Y=2.5*ALOG10(Y)
  63    CALL SYMBOL(0.,Y,.1,24,0.,-1)
        DO 64 JX=200,1000,100
        Y=FLOAT(JX);Y=2.5*ALOG10(Y)
  64    CALL SYMBOL(0.,Y,.1,24,0.,-1)
         DO 52 JX=1,6
         X=FLOAT(JX)
  52    CALL SYMBOL(X,0.,.1,15,0.,-1)
        CALL PLOT(0.,0.,-3);CALL POFF
        STOP;END
```

6119

TABLE C-5.

```
C   <BOARD>MASCS1.FOR;1    FRI 20-JAN-78  3:37PM                    PAGE 1

C     ON ORBIT COST BREAKDOWN
        REAL NMOD,IMOD,LT,NOP,NOT,MOOP,MOSP,MOW,IEQ
        REAL MOSM,MOI,MOPP,MOM,MOPT,MOSS,MOPM,MOS
        DIMENSION A(5),P(6),MES(3),YYY(101)
        DATA P/20.,50.,100.,200.,500.,1000./
        DATA A/5.,10.,20.,0.,0./
C     ON ORBIT COST MODEL WRITTEN BY BILL WARD  AT HRL 1977
C     MODIFIED DEC 77 FOR XE, ETC
        M1=22;M2=0;M3=1;M4=2
C     INITIALIZE VARIOUS CONSTANTS
        YRS=10.;ROT=.2;ROP=.2
        DELV=10.5;TIME=365.*YRS
        CALL PLOTS(30)
        XMO=25.E3;ICURVE=3
        DO 6 JCASE=1,1;CPEN=2
        IF(JCASE.EQ.2) CPEN=5
        DO 5 J=1,10
          CALL PUFF
C     NEXT LINE SLOWS DOWN PLOTTER SO YOU CAN NUMBER THE CURVES
        READ(5,*) ZZZ;WRITE(5,*) ZZZ,FACTOR
        CALL PLOT(P(1)=20.

        FLUX=1.E15;XXFLUX=ALOG10(1.E-15*FLUX)
        IF(ICURVE.EQ.1) SOLEFF=-.1912*XXFLUX+.73
        IF(ICURVE.EQ.2) SOLEFF=-.1775*XXFLUX+.90
        IF(ICURVE.EQ.3) SOLEFF=-.129*XXFLUX+.995
        IPEN=3
        PMOD=P(1)*1000.
        CXX=17.
        IVVV=5
        IF(J.EQ.1) IVVV=1
        DO 5 I=1,1000,IVVV
          XISP=CXX*FLOAT(I-1)+1000.
        GISP=.009d*XISP
        VB=3.267*XISP/199.*XISP/199.
        IMOD=PMOD/VB
        IF(VB.LT.3005.) GO TO 20
        D=30.*SQRT(IMOD/15.)
        GO TO 33
   20   D=30.*SQRT(IMOD/2.88*(VB/1000.)**-1.5)
   33   CONTINUE
        XMASS=.078*D**1.35
        BETA=DELV/GISP
        XMF=XMO/EXP(BETA)
        XMP=XMO-XMF
        SEC=TIME/100.*8.64E6
        PJET=XMP*GISP*GISP*.5E6/SEC
        EXPONX=-.503*ALOG10(P(1))+1.153
        ALPPU=10.**EXPONX
        EFF=.64*VB/(VB+220.)
C     ASSUME PPU EFF=CONSTANT=.95
        TOTEFF=EFF*SOLEFF*.95;PJOT=PJET/TOTEFF
        NMOD=PJET/PMOD;IEQ=IMOD*900./(D*D)
        IEM=-1.27*ALOG10(IEQ)+4.4;LT=10.**IEM
C     TAKE OUT NEXT LINE FOR VARIABLE THRUSTER LIFE
        LT=1.E4
        FACTOR=TIME/(LT/24.)
        IF(FACTOR.LT.1.) FACTOR=1.
        NOT=NMOD*FACTOR*(1.+ROT)
        NOP=NMOD*(1.+ROP)
C       COMPUTE THRUSTER COST=UNIT*(1+1/2**A+1/3**ALPHA....)ETC
        COST=42.E3*ALOG10(D);COT=2.*COST*NOT**.68/.68
   80   FORMAT(1X,'TOTAL COST=',E12.4,'AVG COST=',E12.4)
C     COMPUTE PPU COSTS
        PPUPWR=P(1)/TOTEFF
        UNIT=4.365*PPUPWR**.12;COP=UNIT*NOP**.68/.68
        MOT=2.*XMASS*NOT;MOPP=.001*ALPPU*PJOT;MOP=XMP;MOPT=.1*MOP
        MOSS=100.*(1.+1.E-6*PJOT)+100.*(NOT/NOP-1.);MOSS=MOSS*(1+.1)
        MOSM=.2*(MOI+MOPP+MOP+MOPT+MOSS)
```

TABLE C-5 (Continued)

```
C   <BWARD>MASCST.FOR;1    FRI 20-JAN-78  5:57PM                    PAGE 1:1

      MOW=6.*.001*PIOT;MOOP=MOSM+MOI+MOPP+MOP+MOPT+MOSS+MOW
      IF(MOOP.GT.XMO) GO TO 5
      MOSP=XMO-MOOP
      COPI=XMP*(10.+.1*100.)
      COSM=1.E4*MOSM**.3;COOD=1.E5/10.*(MOOP-MOP)**.3
      COSS=1.E4*MOSS**.9;CTO=1000.*MOOP
      COT=40.*MOOP;COW=100.*PIOT;COPS=1.E5*TIME
      COSI=COI+COP+COPI+COSM+COSS+CTO+COT+COW+COPS+COOD
      MOSP=XMO-MOOP;AVGCST=COST/(MOSP*YRS)
      X=XISP/5000.;XXF=10./COSI
       IF(J.EQ.1) Y=XXF*COI;IF(J.EQ.2) Y=XXF*COP
       IF(J.EQ.3) Y=XXF*COPI;IF(J.EQ.4) Y=XXF*COSM
       IF(J.EQ.5) Y=XXF*COSS;IF(J.EQ.6) Y=XXF*CTO
      IF(J.EQ.7) Y=XXF*COW;IF(J.EQ.8) Y=XXF*COPS
      IF(J.EQ.9) Y=XXF*COOD;IF(J.EQ.10) Y=XXF*COI
      IF(Y.GT.9.) GO TO 5;IF(Y.LT.0.) GO TO 5
      CALL PLOT(X,Y,IPEN)
      IPEN=2;IF(J.GE.2) GO TO 5
      D1=ABS(50.-D);D2=ABS(60.-D);D3=ABS(100.-D);D4=ABS(150.-D)
      IF(D1.LT..24) CALL SYMBOL(X,Y,.1,M1,0.,-1)
      IF(D2.LT..24) CALL SYMBOL(X,Y,.1,M2,0.,-1)
      IF(D3.LT..24) CALL SYMBOL(X,Y,.1,M3,0.,-1)
      IF(D4.LT..24)  CALL SYMBOL(X,Y,.1,M4,0.,-1)
      IPEN=CPEN
5     CONTINUE
6     CONTINUE
30    FORMAT(10E10.3)
77    FORMAT(1X,'D=',F10.2,'P=',F10.7,'I=',I7)
      CALL PLOT(0.,0.,-3);CALL POFF
      STOP;END
```

6119

TABLE C-6.

```
C   <BWARD>MAS1.FOR;1    FRI 20-JAN-78 3:56PM                    PAGE 1

C    ON ORBIT MASS BREAKDOWN
       REAL NMOD,IMOD,LI,NOP,NOT,MOOP,MOSP,MOD,IEQ
       REAL MOSM,MOT,MOPP,MOP,MOPT,MOSS,MOPN,MOS
       DIMENSION A(5),P(6),MES(3),YYY(101)
       DATA P/20.,50.,100.,200.,500.,1000./
       DATA A/5.,10.,20.,0.,0./
C   ON ORBIT COST MODEL WRITTEN BY BILL WARD AT HRL 1977
C   MODIFIED DEC 77 FOR AE,EIC.
       M1=22;M2=0;M3=1;M4=2
C    INITIALIZE VARIOUS PARAMETERS
       LI=2.;YRS=10.;ROT=.2;ROP=.2
       DELV=16.5;TIME=365.*YRS
       CALL PLOTS(30)
       XMO=25.E3;ICURVE=3
       DO 6 JCASE=1,1;CPEN=2
       IF(JCASE.EQ.2) CPEN=5
       DO 5 J=1,6
         CALL POPP
       READ(5,*) ZZZ;WRITE(5,*) ZZZ,FACTOR
       CALL POP;P(1)=20.

       FLUX=1.E15;XXFLUX=ALOG10(1.E-15*FLUX)
       IF(ICURVE.EQ.1) SOLEFF=-.1912*XXFLUX+.75
       IF(ICURVE.EQ.2) SOLEFF=-.1775*XXFLUX+.90
       IF(ICURVE.EQ.3) SOLEFF=-.129*XXFLUX+.995
       IPEN=5
       PMOD=P(1)*1000.
       CXX=17.
       IVVV=5
       IF(J.EQ.1) IVVV=1
       DO 5 I=1,1000,IVVV
         XISP=CXX*FLOAT(I-1)+1000.
       GISP=.0098*XISP
       VB=5.287*XISP/199.*XISP/199.
       IMOD=PMOD/VB
       IF(VB.LT.3005.) GO TO 20
       D=30.*SQRT(IMOD/15.)
       GO TO 35
   20  D=30.*SQRT(IMOD/2.88*(VB/1000.)**-1.5)
   35  CONTINUE
       XMASS=.078*D**1.35
       BETA=DELV/GISP
       XMF=XMO/EXP(BETA)
       XMP=XMO-XMF
       SEC=TIME/100.*8.64E6
       PJET=XMP*GISP*GISP*.5E6/SEC
       EXPONX=-.503*ALOG10(P(I))+1.153
C    RAISE PPU MASS BY REDUNDANCY FACTOR
       ALPPU=(1.+ROP)*10.**EXPONX
       EFF=.68*VB/(VB+220.)
C    ASSUME PPU EFF=CONSTANT=.95
       TOTEFF=EFF*SOLEFF*.95;PIOT=PJET/TOTEFF
       NMOD=PJET/PMOD;IEQ=IMOD*900./(D*D)
       TEM=-1.67*ALOG10(IEQ)+4.4;LI=10.**IEM
       LI=2.E4
       FACTOR=TIME/(LI*24.)
       IF(FACTOR.LT.1.) FACTOR=1.
       NOT=NMOD*FACTOR*(1.+ROT)
       NOP=NMOD*(1.+ROP)
C      COMPUTE THRUSTER COST=UNIT*(1+1/2**A+1/3**ALPHA....)EIC
       COST=42.E3*ALOG10(D);COT=2.*COST*NOT**.68/.68
   80  FORMAT(1X,'TOTAL COST=',E12.4,'AVG COST=',E12.4)
C     COMPUTE PPU COSTS
       PPUPWR=P(I)/TOTEFF
       UNIT=4.5E5*PPUPWR**.12;COP=UNIT*NOP**.68/.68
       MOT=2.*XMASS*NOT;MOPP=.001*ALPPU*PIOT;MOP=XMP;MOPT=.1*MOP
       MOSS=100.*(1.+1.E-6*PIOT)+100.*(NOT/NOP-1.);MOSS=MOSS*(1+.1)
       MOSM=.2*(MOT+MOPP+MOP+MOPT+MOSS)
       MOM=6.*.001*PIOT; MOOF=MOSM+MOT+MOPP+MOP+MOPT+MOSS+MOM
```


6119

TABLE C-6 (Continued)

```
C  <BWARD>MAS1.FOR;1    FRI 20-JAN-78 5:56PM                    PAGE 1:1

      IF(MUOP.GT.XMU) GO TO 5
      MOSP=XMU-MOOP
      COPT=XMP*(10.+.1*100.)
      COSM=1.E4*MOSM**.5;COOD=1.E5/10.*(MUOP-MOP)**.3
      COSS=1.E4*MOSS**.9;CTO=1000.*MOOP
      COT=40.*MOOP;COW=100.*PIOT;COPS=1.E3*TIME
      COST=COT+COP+COPT+COSM+COSS+CTO+COT+COW+COPS+COOD
      MOSP=XMU-MOOP;AVGCST=COST/(MOSP*YRS)
      X=XISP/5000.;XXF=10./XMU
       IF(J.EQ.1) Y=XXF*MOT;IF(J.EQ.2) Y=XXF*MOPP
       IF(J.EQ.3) Y=XXF*MOP;IF(J.EQ.4) Y=XXF*MOPT
       IF(J.EQ.5) Y=XXF*MOSM;IF(J.EQ.6) Y=XXF*MOSS
      IF(J.EQ.7) Y=XXF*MOW;IF(J.EQ.8) Y=XXF*MOSP
      IF(Y.GE.9.) GO TO 5;IF(Y.LT.0.) GO TO 5
      CALL PLOT(X,Y,IPEN)
      IPEN=2;IF(J.GE.2) GO TO 5
      D1=ABS(30.-D);D2=ABS(60.-D);D3=ABS(100.-D);D4=ABS(150.-D)
      IF(D1.LT..24) CALL SYMBOL(X,Y,.1,M1,0.,-1)
      IF(D2.LT..24) CALL SYMBOL(X,Y,.1,M2,0.,-1)
      IF(D3.LT..24) CALL SYMBOL(X,Y,.1,M3,0.,-1)
      IF(D4.LT..24)  CALL SYMBOL(X,Y,.1,M4,0.,-1)
      IPEN=CPEN
5     CONTINUE
6     CONTINUE
50    FORMAT(10E10.3)
77    FORMAT(1X,'D=',F10.2,'P=',F10.7,'I=',I7)
      CALL PLOT(0.,0.,-3);CALL PUFF
      STOP;END
```

6119

This relation is derived from the expression

$$I_{sp} = \bar{v}/g = \left[\frac{\eta_1 + \eta_2}{g}\right] \sqrt{\frac{2eVB}{M}} \quad \gamma \ , \tag{C-2}$$

where

$$\begin{aligned} \eta_1 &= 0.81 \\ \eta_2 &= 0.067 \\ \gamma &= 0.958 \\ M &= 6.63 \times 10^{-26} \text{ kg} \ . \end{aligned} \tag{C-3}$$

For Hg, Xe, or Kr propellants, the expression on the right hand side of Eq. C-1 should be multiplied by the mass ratios listed below:

Propellant	M/M Argon
Hg	5.022
Xe	3.287
Kr	2.098

For example, at 4000 sec, VB = 404 V for Ar and 2029 V for Hg (assuming the same η_1, η_2, and γ). After the program calculates the beam voltage, the beam current per module I_{MOD} is calculated from the assumed module (beam) power as

$$I_{MOD} = PMOD/_{VB} \ . \tag{C-4}$$

The thruster diameter D is then calculated by assuming an optics perveance equivalent to the 30-cm thruster. Experimentally, using mercury propellant, it is found that at a beam voltage of 1000 V and a net to total ratio of 0.7, a beam current of 2.33 A can be extracted from a 30-cm-diameter thruster. Or, in general, at R = 0.7,

$$I_{MOD} = VCOEF\left(\frac{VB}{1000}\right)^{3/2} \cdot \left(\frac{D}{30}\right)^2 \ , \tag{C-5}$$

where the VCOEF for different propellants is listed below:

Propellant	VCOEF, A	VCRIT, V
Hg	2.33	3462
Xe	2.88	3005
Kr	3.60	2590
Ar	5.20	2026

6119

The parameter VCRIT is the voltage at which the extracted beam current is the maximum possible for a given thruster diameter because of thermal limitations. For the 30-cm-diameter thruster, a thermal analysis predicted a maximum possible beam current of 15 A; in general

$$I_{MOD} = 15 \left(\frac{D}{30}\right)^2 . \qquad \text{(C-6)}$$

The computer program solves for the thruster diameter at a given VB and I_{MOD} using Eq. C-5 for VB < VCRIT and Eq. C-6 for VB> VCRIT. The parameters VCRIT and VCOEF for Ar^+ become 12.04 A and 1,158 V for R = 0.4 and 3.57 A and 2,605 V for R = 0.9.

After the thruster diameter is calculated, the thruster mass XMASS is calculated using the empirical formula

$$XMASS = 0.078\ D^{1.35}\ (kg) , \qquad \text{(C-7)}$$

and the PPU specific mass (kg/kW) is calculated from the empirical formula

$$ALPPU = 10^{\left[-.503 \log (PMOD) + 1.153\right]}\ (kg/kw) , \qquad \text{(C-8)}$$

where PMOD is in kW.

From the assumed velocity change DELV and initial mass XMO, the final mass XMF and propellant mass XMP are calculated using the rocket equation. The jet power PJET is then calculated from the propellant mass and trip time SEC as follows:

$$PJET = \frac{XMP \left[g * XISP\right]^2}{2\ (SEC)} . \qquad \text{(C-9)}$$

The total input power PTOT is calculated by dividing the jet power by the product of the thruster, solar cell, and the PPU efficiencies. PPU efficiency is assumed to be constant at 0.95. Thus,

$$PTOT = PJET\ (EFF * SOLEFF * .95)^{-1}, \qquad (C\text{-}10)$$

where the thruster efficiency is given by

$$EFF = \frac{0.84\ VB}{(VB + 220)} . \qquad (C\text{-}11)$$

Eq. C-11 assumes a discharge power of 200 eV/ion and a fixed loss of 20 eV/ion. The 0.84 factor in Eq. C-11 results from using the same mass efficiency and loss factors as for the 30-cm thruster at 2 A of Hg^+ beam current. The solar cell efficiency is determined from the total electron flux (input) and a degradation model.

The number of operating modules NMOD is calculated from the jet power by dividing the latter by the assumed module beam power,

$$NMOD = PJET/_{PMOD} . \qquad (C\text{-}12)$$

Stand-by redundancy for both the thrusters (ROT) and power processors (ROP) is included in the modeling. Thus NOP, the total number of PPU modules, is given by

$$NOP = NMOD\ [1 + ROP] , \qquad (C\text{-}13)$$

which assumes that the life of the PPU is much greater than that of the mission. The number of thruster modules, NOT, is calculated from the thruster lifetime LT and the total trip time TOTRIP as

$$NOT = NMOD \left(\frac{TOTRIP}{LT}\right) (1 + ROT) . \qquad (C\text{-}14)$$

For most cases, thruster lifetime is taken as a constant equal to 10^4 hr. However, the computer program has an optional empirical formula that calculates thruster lifetime as a function of the beam current

density. In Eq. C-14, the total trip time is obtained from the sum of the down time (DOWN) and the up trip time (TIME). This calculation is done iteratively since the down time depends on the down propellant mass, MPDWN, which is not known until the vehicle mass, MORV, is calculated for the up trip. Thus,

$$\text{MPDWN} = \text{MORV}\left[1 - e^{-\text{DELV}/\text{GISP}}\right] . \qquad \text{(C-15)}$$

In Eq. C-15, it is assumed that the same GISP, DELV, and PTOT are used for the down trip and for the up trip.

After the above calculations are made, it is a straightforward algebraic calculation to calculate the other system masses and costs. Since these formulas are in the computer listings and have been discussed in the text of this report, they are not repeated here. A summary of the mass and cost nomenclature used for both the orbit-raising and on-orbit models is shown in Table C-7.

Table C-7. Summary of Nomenclature for Cost Models

MASS DEFINITIONS

Orbit Raising	On Orbit	
MRT	MOT	Thrusters, Gimbals, etc.
MRPP	MOPP	PPU
MORP	MOP	Proppellant (up)
MPDWN	-----	Propellant (down)
MRPT	MOPT	Tankage
MRSM	MOSM	Structures and Mechanisms
MRSS	MOSS	Subsystems
MRW	MOW	Power
MORV	MOOP	Vehicle
MSP	MOSP	Payload

COST DEFINITIONS

Orbit Raising	On Orbit	
CRT	COT	Thruster Costs
CRP	COP	PPU Costs
-----	COPT	Propellant and Tankage
CPROP	-----	Propellant
CTANK	-----	Tank
CRSM	COSM	Structures and Mechanisms
CRSS	COSS	Subsystems
CRW	COW	Power
CORD	CODD	DDT and E Cost
COPT	COPS	Time Dependent Cost
CORI	COI	Integration and Testing
COPF	-----	Costs not associated with electric ORV
C1	-----	Launch Cost
-----	CTO	Earth to Orbit Cost

6119

APPENDIX D

RELIABILITY AND REDUNDANCY

Calculations were made to determine if the redundancy factors presently used in the cost model were consistent with good reliability practices and if different system designs were being properly compared. The analysis that follows shows that the PPU and thruster redundancy factors should be approximately 0.15 to 0.20 to assure high reliability. However, changes in redundancy factors produce only a small change in the cost per kilogram of payload calculated by the cost model.

A. ANALYSIS

Standby redundancy is the technique considered here for increasing the reliability of the thruster and PPU systems. As shown below, the reliability of these systems can be increased to any desired level if enough standbys are used. It is shown in Ref. D-1 that if the failure rate of a single unit is λ (failures/hour), then the reliability of a single unit operating for t hours will be

$$R(t) = e^{-\lambda t} \quad . \tag{E-1}$$

This exponential law is derived on the assumption that the failures are random (i.e., chance failures) and that their statistics are given by the Poisson process. Mathematically, this means that the probability of exactly n failures occurring in a device during a time interval τ is

$$P(n, \tau) = e^{-\lambda\tau}\frac{(\lambda \tau)}{n!} \tag{E-2}$$

and that the early and wearout failures have been eliminated. It is also shown in Ref. D-1 that the reliability of a redundant system consisting of m operating modules and n standby units is given by

$$R_{m,n} = e^{-m\lambda t}\sum_{r=o}^{n} \frac{(m\lambda t)}{r!} \quad . \tag{E-3}$$

Figure D-1 shows eq. D-3 plotted as a function of the number of operating units m for a redundancy of 0.15 so that the number of standbys was given by

$$n = 0.15\ m \quad \text{(integer part)} \quad . \tag{D-4}$$

The sawtooth behavior in the computed reliability is caused by the step function changes in the number of standby units. For example, as m varies from 14 to 19, the PPU reliability decreases because the number of standbys (two) remains constant while at m = 20 the standbys increase to three, producing a sudden jump in reliability.

The results shown in Figure D-1 were computed for $t = 10^4$ hr and an assumed λ of 10^{-5} and 5×10^{-6} for the thruster and PPU, respectively. We are also assuming the reliability of the switching necessary to turn on a standby is included in these failure rates. Figure E-1 shows that above approximately 200 units the total thruster reliability is greater than 0.99, while for the PPU this reliability is achieved at about 40 units.

Reference to Table D-1 or D-2 shows the number of operating units for a wide range of module power and I_{sp} and indicates that the number of operating modules varies from $\sim$ 2,000 to $\sim$ 25 depending on the module power and I_{sp}. The results shown in Figure D-1 imply a higher redundancy than 0.15 would be needed for the lower number of modules. However, comparing the data in Tables D-1 and D-2 shows that the cost/kg changes less than 1% for more than a 100% change in PPU/thruster redundancy. Thus, the use of a constant redundancy factor produces a total thruster and PPU reliability which varies depending on the module power level and beam current density. Henceforth, a PPU and thruster reliability of 0.2 will be assumed that will provide a worst case reliability of > 0.99 for nearly all cases.

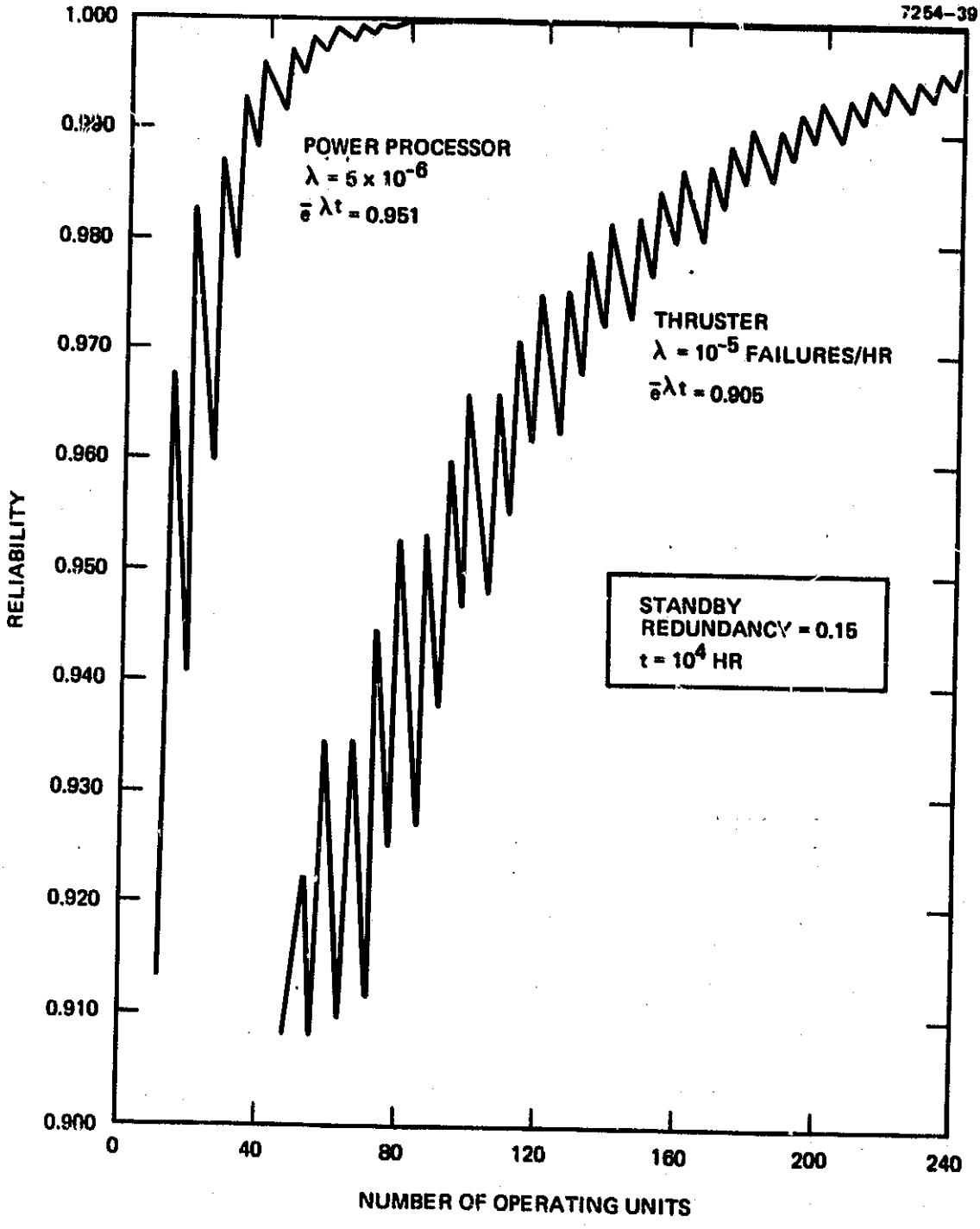

Figure D-1. Reliability/redundancy results.

Table D-1. Tabulation of Orbit Raising Cost Model Parameters as a Function of I_{sp} with Module Power as a Parameter.

$Mo = 10^6$ kg ΔV = 6 km/sec
Δt = 100 days Lorv = 1000 days

Thruster redundancy = 0.10
PPU redundancy = 0.05

I_{sp}, sec	Number of Operating Units	Total Number of Thrusters	Thruster Diameter, cm	Thruster Life, hr	$\bar{P}_{total}$ MW	Payload Mass, 10^{-3} x kg	Payload Cost, $/kg
PMOD= 20KW							
4000.	631	957	182.6	17396.3	23.2	467.4	228.7
6000.	970	6903	66.3	3711.5	28.7	463.3	286.4
8000.	1310	27890	32.3	1240.3	35.4	403.1	422.0
10000.	1650	54052	21.8	806.1	42.7	320.9	637.5
12000.	1990	65191	18.2	806.1	50.3	228.9	1001.6
PMOD= 50KW							
4000.	252	383	288.8	17396.3	23.2	505.5	192.9
6000.	388	2761	104.8	3711.5	28.7	505.6	234.0
8000.	524	11156	51.1	1240.3	35.4	453.8	327.7
10000.	660	21621	34.5	806.1	42.7	381.4	465.8
12000.	796	26076	28.7	806.1	50.3	299.9	665.4
PMOD=100Kw							
4000.	126	191	408.4	17396.3	23.2	525.2	177.
6000.	194	1380	148.2	3711.5	28.7	527.1	211.
8000.	262	5578	72.2	1240.3	35.4	479.4	288.
10000.	330	10810	48.7	806.1	42.7	411.9	398.
12000.	398	13038	40.6	806.1	50.3	335.7	551.
PMOD=200Kw							
4000.	63	95	577.6	17396.3	23.2	539.3	166.
6000.	97	690	209.6	3711.5	28.7	542.3	196.
8000.	131	2789	102.1	1240.3	35.4	497.5	263.2
10000.	165	5405	68.9	806.1	42.7	433.5	357.
12000.	199	6519	57.4	806.1	50.3	360.9	484.0
PMOD=500KW							
4000.	25	36	913.2	17396.3	23.2	552.2	157.6
6000.	38	276	331.4	3711.5	28.7	556.0	184.3
8000.	52	1115	161.4	1240.3	35.4	513.5	242.9
10000.	66	2162	109.0	806.1	42.7	452.6	325.0
12000.	79	2607	90.8	806.1	50.3	383.4	432.6

Table D-2. Tabulation of Orbit Raising Cost Model Parameters as a Function of I_{sp} with Module Power as a Parameter.

Same input data as Table I, except:

Thruster redundancy = 0.2
PPU redundancy = 0.2

I_{sp}, sec	Number of Operating Units	Total Number of Thrusters	Thruster Diameter, cm	Thruster Life, hr	P_{total} MW	Payload Mass 10^{-3} x kg	Payload Cost, $/kg
PMOD= 20Kw							
4000.	631	1044	182.6	17396.3	23.2	467.4	231.8
6000.	970	7530	66.3	3711.5	28.7	463.3	291.2
8000.	1310	30425	32.3	1240.3	35.4	403.2	429.8
10000.	1650	58966	21.8	806.1	42.7	321.1	649.6
12000.	1990	71118	18.2	806.1	50.3	229.0	1020.3
PMOD= 50Kw							
4000.	252	417	288.8	17396.3	23.2	505.5	194.6
6000.	388	3012	104.8	3711.5	28.7	505.6	236.6
8000.	524	12170	51.1	1240.3	35.4	453.9	331.6
10000.	660	23586	34.5	806.1	42.7	381.6	471.6
12000.	796	28447	28.7	806.1	50.3	300.0	674.0
PMOD=100KW							
4000.	126	208	408.4	17396.3	23.2	525.2	178.1
6000.	194	1506	148.2	3711.5	28.7	527.1	212.8
8000.	262	6085	72.2	1240.3	35.4	479.4	290.6
10000.	330	11793	48.7	806.1	42.7	412.1	402.2
12000.	398	14223	40.6	806.1	50.3	335.8	555.6
PMOD=200Kw							
4000.	63	104	577.6	17396.3	23.2	539.3	167.2
6000.	97	753	209.6	3711.5	28.7	542.3	197.4
8000.	131	3042	102.1	1240.3	35.4	497.5	264.6
10000.	165	5896	68.9	806.1	42.7	433.6	359.6
12000.	199	7111	57.4	806.1	50.3	361.1	486.5
PMOD=500KW							
4000.	25	41	913.2	17396.3	23.2	552.2	150.9
6000.	38	301	331.4	3711.5	28.7	556.0	184.8
8000.	52	1217	161.4	1240.3	35.4	513.6	243.4
10000.	66	2358	109.0	806.1	42.7	452.8	325.7
12000.	79	2844	90.8	806.1	50.3	383.5	433.6

APPENDIX D

REFERENCES

1. "Solar Electric Propulsion Spacecraft Study" Final Report JPL cont. 951144, Hughes Aircraft Space Systems, DC. 1965.

APPENDIX E

ON-ORBIT MISSION ΔV MODEL

As part of the on-orbit mission cost modeling analysis, it was necessary to estimate ΔV requirements. Thrust is required for both station-keeping (orbit perturbations) and for attitude control. Obviously, the magnitude of these forces and torques is highly dependent on satellite mass and shape. Based on a review of space power satellite (SPS) studies, the following equation for total impulse per year (N-sec/yr) was developed:

$$\text{Impulse} = 50\ M_s + 150\ A_s + 6 \times 10^6 \left(\frac{K}{R_s^3}\right) M_s\ A_s^{1/2}, \qquad \text{(E-1)}$$

where M_s = satellite total mass, kg

A_s = satellite area exposed to sunlight, m^2

K = earth gravitational parameter

$= 4 \times 10^5\ km^3/sec^2$

R_s = satellite orbit radius.

The first term represents north-south stationkeeping, the second term accounts for solar pressure (orbit and attitude perturbations), and the third term accounts for gravity gradient torques. The sole purpose of this equation is to estimate the magnitude of the ΔV requirements for a range of satellite sizes and is not considered to be more than a rough estimate. The details involved in obtaining this equation are discussed in this section.

A. STATIONKEEPING PERTURBATIONS

Of the many possible perturbations that might affect a satellite orbit, four were considered: (1) east-west forces, caused by "triaxiality;" (2) north-south forces, caused by solar and lunar perturbations; (3) solar pressure; and (4) microwave emission from an

antenna. East-west forces and microwave radiation were neglected as being small compared with others.

The north-south forces result in a ΔV requirement of about 50 m/sec per year. Using the relationship between average thrust and ΔV,

$$T = M_s \frac{\Delta V}{\Delta t} \tag{E-2}$$

and

$$\text{Impulse} = T \, \Delta t \quad . \tag{E-3}$$

Thus, the first term in Eq. E-1 is simply $50 \, M_s$.

Solar pressure force on typical arrays is approximately 55% of that for a perfect reflector. This translates into a pressure of

$$P_{sp} = (0.55) \; (2) \; (4.4 \times 10^{-6}) = 4.7 \times 10^{-6}, \; N/m^2. \tag{E-4}$$

The force associated with solar pressure is

$$F_{sp} = 4.7 \times 10^{-6} \, A_s \; , \; N \; , \tag{E-5}$$

and the annual impulse needed to balance this force is approximately

$$I_{sp} = 150 \, A_s, \; N \cdot sec/yr. \tag{E-6}$$

B. ATTITUDE CONTROL PERTURBATIONS

The two major attitude perturbations considered were gravity gradients and solar-pressure/CG-misalignment. Gravity gradient torques are important if the moments of inertia of the satellite are unequal. Since sun-line orientation and antenna pointing place several limitations on satellite configuration, the moments of inertia for large-area satellites (e.g., SPS) are significantly different. In addition, when large masses and large dimensions are involved, the gravity gradient torques are high.

Clearly, without a given satellite design, gravity gradient torques can only be grossly estimated. The order of magnitude of this torque was assumed to be

$$\text{Torque} = \frac{1}{12} M_s W_o^2 A_s \quad , \tag{E-7}$$

where

$$W_o = \text{satellite orbit rotational frequency}$$
$$= \left(\frac{K}{R_s^3}\right)^{1/2}$$
$$= 7.3 \times 10^{-5} \text{ rad/sec at synchronous altitude.}$$

The angular momentum per year associated with this torque is approximately

$$\text{Momentum (GG)} = 3 \times 10^6 \left(\frac{K}{R_s^3}\right) M_s A_s, \text{ N•m•sec/yr} \quad . \tag{E-8}$$

The impulse required to compensate this momentum can be estimated by assuming propulsion forces are applied with a lever arm (LA) length equal to

$$LA = 1/2 A_s^{1/2} \quad , \tag{E-9}$$

such that

$$\text{Impulse (GG)} = 6 \times 10^6 \left(\frac{K}{R_s^3}\right) M_s A_s^{1/2} \quad . \tag{E-10}$$

Solar pressure torque results from a misalignment of the center of pressure and the satellite center of mass. If the misalignment is 1% of a typical satellite dimension (i.e., $0.01\ A_s^{1/2}$), the momentum imparted would be

$$\text{Momentum (sp)} = 1.5 A_s^{1/2} \text{, N•m•sec/yr} \quad . \tag{E-11}$$

Since misalignments probably could be kept to a few percent of typical dimensions, this perturbation would be small compared with others.

C. ΔV ESTIMATE

An estimate of the propulsion ΔV requirement can be obtained from Eq. E-1. Using an $M_s = 10^6$ kg and an $A_s = 10^7 m^2$, the total impulse requirement per year at synchronous altitude is

$$\text{Impulse} = 1.65 \times 10^9 \text{ , N·sec/yr} \quad , \tag{E-12}$$

or

$$\Delta V = 1.65 \times 10^3 \text{ , m/sec/yr.} \tag{E-13}$$

This ΔV value was used in the on-orbit cost model calculations.